

API Standard Paragraphs Rotordynamic Tutorial: Lateral Critical Speeds, Unbalance Response, Stability, Train Torsionals, and Rotor Balancing

API RECOMMENDED PRACTICE 684
SECOND EDITION, AUGUST 2005

REAFFIRMED, NOVEMBER 2010



AMERICAN PETROLEUM INSTITUTE

API Standard Paragraphs Rotordynamic Tutorial: Lateral Critical Speeds, Unbalance Response, Stability, Train Torsionals, and Rotor Balancing

Downstream Segment

API RECOMMENDED PRACTICE 684
SECOND EDITION, AUGUST 2005

REAFFIRMED, NOVEMBER 2010



AMERICAN PETROLEUM INSTITUTE

SPECIAL NOTES

API publications necessarily address problems of a general nature. With respect to particular circumstances, local, state, and federal laws and regulations should be reviewed.

API is not undertaking to meet the duties of employers, manufacturers, or suppliers to warn and properly train and equip their employees, and others exposed, concerning health and safety risks and precautions, nor undertaking their obligations under local, state, or federal laws.

Information concerning safety and health risks and proper precautions with respect to particular materials and conditions should be obtained from the employer, the manufacturer or supplier of that material, or the material safety data sheet.

Nothing contained in any API publication is to be construed as granting any right, by implication or otherwise, for the manufacture, sale, or use of any method, apparatus, or product covered by letters patent. Neither should anything contained in the publication be construed as insuring anyone against liability for infringement of letters patent.

Generally, API standards are reviewed and revised, reaffirmed, or withdrawn at least every five years. Sometimes a one-time extension of up to two years will be added to this review cycle. This publication will no longer be in effect five years after its publication date as an operative API standard or, where an extension has been granted, upon republication. Status of the publication can be ascertained from the API Standards department telephone (202) 682-8000. A catalog of API publications, programs and services is published annually and updated biannually by API, and available through Global Engineering Documents, 15 Inverness Way East, M/S C303B, Englewood, CO 80112-5776.

This document was produced under API standardization procedures that ensure appropriate notification and participation in the developmental process and is designated as an API standard. Questions concerning the interpretation of the content of this standard or comments and questions concerning the procedures under which this standard was developed should be directed in writing to the Director of the Standards Department, American Petroleum Institute, 1220 L Street, N.W., Washington, D.C. 20005. Requests for permission to reproduce or translate all or any part of the material published herein should be addressed to the Director, Business Services.

API standards are published to facilitate the broad availability of proven, sound engineering and operating practices. These standards are not intended to obviate the need for applying sound engineering judgment regarding when and where these standards should be utilized. The formulation and publication of API standards is not intended in any way to inhibit anyone from using any other practices.

Any manufacturer marking equipment or materials in conformance with the marking requirements of an API standard is solely responsible for complying with all the applicable requirements of that standard. API does not represent, warrant, or guarantee that such products do in fact conform to the applicable API standard.

All rights reserved. No part of this work may be reproduced, stored in a retrieval system, or transmitted by any means, electronic, mechanical, photocopying, recording, or otherwise, without prior written permission from the publisher. Contact the Publisher, API Publishing Services, 1220 L Street, N.W., Washington, D.C. 20005.

FOREWORD

API publications may be used by anyone desiring to do so. Every effort has been made by the Institute to assure the accuracy and reliability of the data contained in them; however, the Institute makes no representation, warranty, or guarantee in connection with this publication and hereby expressly disclaims any liability or responsibility for loss or damage resulting from its use or for the violation of any federal, state, or municipal regulation with which this publication may conflict.

Suggested revisions are invited and should be submitted to the standardization manager, American Petroleum Institute, 1220 L Street, N.W., Washington, D.C. 20005, standards@api.org.

CONTENTS

	Page
1 OVERVIEW	1-1
1.1 Introduction	1-1
1.2 Organization	1-1
1.3 Standard Paragraphs	1-1
1.4 Definitions and References	1-1
1.5 Fundamental Concepts Of Rotating Equipment Vibrations	1-1
2 LATERAL ROTORDYNAMICS	
2.1 Introduction	2-1
2.2 Rotor Bearing System Modeling	2-1
2.3 Rotor Modeling Methods and Considerations	2-1
2.4 Support Stiffness Effects	2-13
2.5 Journal Bearing Modeling	2-22
2.6 Seal Types and Modeling	2-43
2.7 Elements of a Standard Rotordynamics Analysis	2-58
2.8 Machinery Specific Considerations	2-71
2.9 API Testing and Results	2-97
2.10 Standard Paragraph Sections for Lateral Analysis	2-105
3 STABILITY ANALYSIS	3-1
3.1 Introduction	3-1
3.2 Rotor Modeling	3-4
3.3 Journal Bearings	3-5
3.4 Seals	3-25
3.5 Excitation Sources	3-36
3.6 Support Stiffness Effects	3-43
3.7 Experience Plots	3-48
3.8 Machinery Specific Considerations	3-51
3.9 Solving Stability Problems	3-67
3.10 Identifying Fluid Induced Instabilities	3-72
3.11 Stability of Testing Machinery	3-73
3.12 Standard Paragraph Sections for Stability Analysis SP6.8.5 – SP6.8.6	3-78
4 TORSIONAL ANALYSIS	4-1
4.0 Introduction and Scope	4-1
4.1 Modeling	4-2
4.2 Machinery Specific Modeling Considerations	4-15
4.3 Reciprocating Machinery	4-20
4.4 Torsional Analysis Calculations	4-27
4.5 Torsional Excitation Sources from Rotating Machinery	4-42
4.6 Fatigue Analysis	4-49
4.7 Contents of a Torsional Report	4-52
4.8 Field Testing to Determine Torsional Response	4-54
4.9 Torsional—Lateral Vibration Coupling	4-57
4.10 API Document Paragraphs on Torsional Vibration	4-57
5 BALANCING OF MACHINERY	5-1
5.1 Scope	5-1
5.2 Introduction	5-1
5.3 Balancing Machines	5-7
5.4 Balancing Procedures	5-11

	Page
Figures	
1-1 Simple Mass-spring-damper System	1-2
1-2 Amplitude Ratio Versus Excitation Frequency (Rotation Speed)	1-3
1-3 Phase Angle Versus Excitation Frequency	1-3
1-4 Response of a Spring-mass System to Transient (Stable)	1-4
1-5 Response of a Spring-mass System to Transient (Unstable)	1-4
1-6 Jeffcott Form for Rotor Model	1-5
1-7 Simplified Model of a Beam-type Rotating Machine	1-5
1-8 Simplified Model of a Beam-type Rotating Machine with Damping	1-5
1-9 Spring-Mass-Damper Model of Beam Type Rotating Machine	1-6
1-10 Synchronous Response of Beam Type Machine for Various Shaft Stiffness Values	1-6
2-1 Schematic of a Lumped Parameter Rotor Model	2-3
2-2 3D Finite Element Model of a Complex Geometry Rotating Component	2-5
2-3 Elastic Modulus vs. Temperature	2-7
2-4 Rotor Model Cross-section of an Eight-Stage 12 MW (16,000 HP) Steam Turbine	2-7
2-5 Turboexpander with Curvic Coupling Fits	2-8
2-6 Turbocompressor with Rabbet and Curvic Coupling Fits	2-8
2-7 Modeling of Curvic Coupling Joints	2-8
2-8 Train Lateral Model	2-10
2-9 Train Lateral Guideline Diagram (W_{jnl} = Static Bearing Reaction)	2-10
2-10 Train Lateral Mode Shapes	2-11
2-11 Equivalent Coupling Model	2-12
2-12 Steam Turbine Support Schematic	2-14
2-13 Journal Bearing Fluid Film and Flexible Support Model	2-15
2-14 Single Degree of Freedom Flexible Support Model	2-15
2-15 Dynamic Stiffness Analysis Diagram	2-16
2-16 Exhaust End Dynamic Compliance Plots	2-17
2-17 Steam End Test Stand Response	2-18
2-18 Exhaust End Test Stand Response	2-18
2-19 Exhaust End Constant Stiffness Support Model	2-19
2-20 Steam End Dynamic Compliance Support Model	2-20
2-21 Steam End Analytical Results, Dynamic Compliance Model	2-21
2-22 Journal Bearing Hydrodynamic Film	2-23
2-23 Two Axial Groove Bearing	2-23
2-24 Spring Stiffness	2-24
2-25 Journal Bearing Stiffness and Damping	2-24
2-26 Pressure Dam Bearing	2-25
2-27 Pressure Dam Bearing—Top and Bottom Pads	2-26
2-28 Elliptical Bearing	2-27
2-29 Offset Half Bearing	2-27
2-30 Taper Land Bearing with Three Tapered Pockets	2-28
2-31 Multi-Lobe Bearing with Three Preloaded, Offset Lobes	2-28
2-32 5-Pad Tilting Pad Bearing Schematic	2-30
2-33 Zero Preloaded Pad	2-31
2-34 Preloaded Pad	2-31
2-35 Negative Preloaded Pad	2-32
2-36 Stiffness and Damping vs. Preload and Bearing Clearance, 4-pad Bearing	2-33
2-37 Stiffness and Damping vs. Preload and L/D Ratio, 4-pad Bearing	2-34
2-38 Lund's Data vs. Experimental	2-35
2-39 Jones and Martin Data vs. Experimental	2-35
2-40 Actual Test Stand Response, 3-axial Groove Bearings	2-36
2-41 Analytically Predicted Response	2-37
2-42 Actual Test Stand Response, 4-pad Tilting Pad Bearings	2-38
2-43 Analytically Predicted Response, Various Bearing Designs	2-39
2-44 Induction Motor Test Stand Response, Tilting Pad Bearings	2-39

	Page
2-45 Induction Motor Analytical Response, Tilting Pad Bearings	2-40
2-46 Induction Motor Analytical Response, Elliptical Bearings	2-40
2-47 Induction Motor Test Stand Response, Elliptical Bearings	2-41
2-48 Oil Bushing Breakdown Seal	2-45
2-49 Pressures Experienced by the Outer Floating Ring Seal	2-45
2-50 Mid-span Rotor Unbalance Response of a High Pressure Centrifugal Compressor for Different Suction Pressures at Start-Up	2-46
2-51 Mechanical (Contact) Shaft Seal	2-47
2-52 Liquid-film Shaft Seal with Cylindrical Bushing	2-47
2-53 Liquid-film Shaft Seal with Pumping Bushing	2-48
2-54 Compressor Labyrinth Seals	2-49
2-55 Typical Turbine Shaft Seal Arrangement—HP End	2-49
2-56 Honeycomb Seal	2-50
2-57 Pocket Damper Seal	2-50
2-58 Segmented-ring Shaft Seal	2-51
2-59 Self-acting Gas Seal	2-52
2-60 Swirl and Thrust Brakes Used in High-Pressure Compressors [27]	2-52
2-61 Measured Natural Frequency and Damping Showing a Drop of the First Bending Mode of the Shaft [27]	2-54
2-62 Change in First Critical Speed Frequency Due to Influential Gas Seals	2-55
2-63 Change in Separation Margin From Unbalance Response Calculation	2-55
2-64 Labyrinth Seal Bulk Flow Control Volume Approaches	2-56
2-65 Undamped Critical Speed Map	2-60
2-66 Mode Shape Examples for Soft and Stiff Bearings Relative to Shaft	2-61
2-67 Typical Undamped Modes Shapes for a Between Bearing Machine with Different Values of Support Stiffness	2-62
2-68 Typical Bode Plot for Asymmetric System with Split Critical Speeds	2-64
2-69 Example Compressor with Probes Rotated to True Horizontal and Vertical	2-65
2-70 Evaluating Amplification Factors (AFs) from Speed-amplitude Bode Plots	2-67
2-71 Rotor Response Shape Plots in 2D and 3D Form	2-68
2-72 Motion of a Stable System Undergoing Free Oscillations	2-69
2-73 Motion of an Unstable System Undergoing Free Oscillations	2-70
2-74 Steam Turbine Support Schematic	2-71
2-75 Typical Resultant Bearing Load Vector Including Partial Admission Steam Forces	2-73
2-76 Resolution of Partial Admission Forces into Journal Bearing Reactions	2-73
2-77 Gear Set	2-75
2-78 Gear Force Schematic	2-75
2-79 Gear Load Angles at Partial and Full Load	2-76
2-80 Accumulated Pitch Error Chart	2-77
2-81 FCC Expander Critical Speed Map	2-78
2-82 FCC Expander Cross-section	2-80
2-83 FCC Expander Rotor-bearing-support Model	2-80
2-84 Axial Compressor Rotor Construction: Disc-on-shaft Shrink Fit	2-81
2-85 Axial Compressor Rotor Construction: Stacked Discs with Tie Bolts	2-82
2-86 Axial Compressor Rotor Construction: Drum Rotor with Studs	2-82
2-87 Axial Compressor Rotor Construction: Drum Rotor with Tie Bolts	2-83
2-88 Typical Multi-stage Compressor	2-85
2-89 Soft Support Undamped Mode Shapes—Multi-stage Compressor	2-85
2-90 Stiff Support Undamped Mode Shapes—Multi-stage Compressor	2-86
2-91 Typical Unbalance Distributions for Multi-Stage Compressors	2-87
2-92 Unbalance Response of 1st and 3rd Critical Speeds	2-88
2-93 Rotor Response Shape @ 4500 rpm	2-88
2-94 Unbalance Response of 2nd Critical Speed	2-89
2-95 Rotor Response Shape @ 12,800 rpm	2-89
2-96 Typical Overhung Compressor	2-90

	Page
2-97 Overhung Compressor Assembly	2-90
2-98a Soft Support Undamped Mode Shapes—Overhung Compressor	2-91
2-98b Stiff Support Undamped Mode Shapes—Overhung Compressor	2-91
2-99 Undamped Critical Speed Map—Overhung Compressor	2-92
2-100 Typical Unbalance Distribution—Overhung Compressors	2-93
2-101 Impeller Unbalance Response—Overhung Compressor	2-94
2-102 Rotor Response Shape at 4,300 rpm	2-94
2-103 Coupling Unbalance Response—Overhung Compressors	2-95
2-104 Typical Pinion Rotors from an Integrally Geared Compressor	2-95
2-105 Pinion Rotor Model—Integrally Geared Compressor	2-96
2-106 Typical Rigid and Flexible Body Mode Shapes & Unbalances Used to Excite Each	2-96
2-107 Baseline Vibration Reading (Graphically)	2-99
2-108 Readings After the Addition of the Unbalance Weight	2-99
2-109 Influence of the Unbalance Weight	2-100
2-110 Bode Plot for Eight-Stage Compressor	2-101
2-111 Unbalance Weight Influence (... Predicted ___ Test)	2-101
2-112 Bode Plot for Three-Stage Compressor	2-102
2-113 Unbalance Weight Influence (... Predicted ___ Test)	2-102
2-114 Bode Plot of Example #3	2-103
2-115 Unbalance Weight Influence (...Predicted ___ Test)	2-103
SP-1 Rotor Response Plot	2-105
SP-2 Undamped Critical Speed Map	2-106
SP-3 Typical Mode Shapes	2-108
3-1 Definition of Log Dec Based on Rate of Decay	3-1
3-2 Stability Analysis Flow Chart	3-3
3-3 Fixed Geometry Bearing Schematic	3-6
3-4 High-Speed, Lightly-Loaded, Unstable Bearing	3-7
3-5 Low-Speed, Heavily-Loaded, Stable Bearing	3-7
3-6 Bearing-Induced Shaft Whip and Oil Whirl	3-8
3-7 Frequency Spectrum, Power Turbine Test, 3-Axial Groove Bearings	3-9
3-8 Rotor Bearing System Stability, Power Turbine $N = 5,000$ rpm	3-10
3-9 Frequency Spectrum, Power Turbine Test, Double Pocket Bearings	3-11
3-10 Frequency Dependent Stiffness and Damping	3-12
3-11 Full Coefficient vs. Synchronous Reduced Tilting Pad Bearing Stability Sensitivity	3-13
3-12 Waterfall Showing Self-excited Instability	3-14
3-13 High Speed Balance Vacuum Pit Oil Atomization Resulting in Subsynchronous Vibration	3-15
3-14 Single Housing Orifice Design Resulting in Subsynchronous Vibration	3-16
3-15 Button Spray Design Resulting in Subsynchronous Vibration	3-16
3-16 Spray Bar Evacuated Housing Design	3-16
3-17 Squeeze Film Damper Schematic	3-17
3-18 Typical End Seal Arrangements	3-18
3-19 Axial Pressure Profiles of Various Damper Arrangements [Enrich, 10]	3-19
3-20 Squeeze Film Damper Coefficients vs. Eccentricity Ratio: Short Bearing Theory (Cavitated) [Enrich, 10]	3-20
3-21 Idealization of Bearing-damper-support Characteristics	3-21
3-22 O-ring Supported Squeeze Film Damper Schematic	3-22
3-23 Mechanical Arc Spring Supported Squeeze Damper	3-23
3-24 Squeeze Film Damper Stability Map	3-24
3-25 Re-excitation of Rotor First Critical from Oil Seal Excitation	3-26
3-26 Rotor Tracking Instability from Low-pressure Oil Seal Test	3-27
3-27 Rotor Tracking Instability from Distorted Oil Seal Lip Contact Area	3-27
3-28 Typical Configuration for the Last Stage of a Series Flow Compressor Showing the Impeller Eye Seal, the Inter Stage Seal and a Typical Balance Piston Seal	3-29
3-29 Typical Shunt Line Schematic to Reduce Entry Swirl	3-30

	Page
3-30 Typical Swirl Brake Schematic to Reduce Entry Swirl	3-31
3-31 Compressor on Full Load Test: With Inert Gas Showing no Instability at Rotor First Critical Frequency, With Process Gas Showing Instability from Balance Piston Excitation, [5,20].....	3-31
3-32 Honeycomb Seal Arrangement	3-33
3-33 Comparison of Honeycomb and Hole Pattern Seals	3-34
3-34 Various Hole Pattern Surface Areas Relative to Honeycomb	3-34
3-35 Pocket Seal Arrangement	3-35
3-36 Blade Forces Due to Centerline Displacement	3-37
3-37 Shrink Fit Internal Friction and Shaft Material Hysteresis Destabilizing Force	3-39
3-38 Dry Friction Rub Backward Whirl Excitation	3-40
3-39 Entrapped Fluid Cross-Coupled Force	3-41
3-40 Differential Heating at Bearing Journal for Synchronous Forward Whirl	3-42
3-41 Simple Bearing—Support Model	3-44
3-42 System for Measuring Support Compliance	3-45
3-43 Horizontal Dynamic Compliance of the Bearing Supports	3-45
3-44 Experimental Flexible Rotor with Flexible Supports	3-46
3-45 Predicted Response at the Rotor Center with and without Bearing Support	3-47
3-46 Predicted Response at the Bearings with and without Bearing Support Models	3-47
3-47 Predicted and Measured Stability Threshold with and without Bearing Support Models ..	3-48
3-48 Sood's General Rotor Stability Criteria	3-49
3-49 Sood/Fulton Empirical Stability Criteria	3-50
3-50 Kirk's Compressor Design Map	3-50
3-51 Sheffield's Compressor Experience Using Fulton's Criteria	3-51
3-52 Steam Turbine Leakage Path	3-52
3-53 Aerodynamic Labyrinth Seal Forces	3-53
3-54 Typical Resultant Bearing Load Vector Including Partial Admission Steam Forces	3-54
3-55 Resolution of Partial Admission Forces into Journal Bearing Reactions	3-54
3-56 FCC Expander Critical Speed Map	3-57
3-57 FCC Expander Cross-section	3-58
3-58 FCC Expander Rotor-bearing-support Model	3-59
3-59 Axial Compressor Rotor Construction: Disk-on-shaft Shrink Fit	3-60
3-60 Axial Compressor Rotor Construction: Stacked Disks with Tie Bolts	3-60
3-61 Axial Compressor Rotor Construction: Drum Rotor with Studs	3-61
3-62 Axial Compressor Rotor Construction: Drum Rotor with Tie Bolts	3-61
3-63 High-speed Gearbox Pressure Dam Pinion Bearing	3-63
3-64 High-speed Gearbox Pressure Dam Bull Gear Bearing	3-63
3-65 Typical Multi-stage High-pressure Centrifugal Compressor Rotor	3-65
3-66 Overhung Compressor Rotor	3-65
3-67 Pinion Rotors from an Integrally Geared Compressor	3-66
3-68 Forces Exerted on a Whirling Shaft	3-68
3-69 Mode Shapes for Various Support/Rotor Stiffnesses	3-68
3-70 Half Spectrum Plot	3-72
3-71 Fluid Induced Instability Orbit Plots	3-74
3-72 Shaft Centerline Plot	3-75
3-73 Typical Subsynchronous Rub Orbits	3-75
3-74 Forward Precession Vibration	3-76
3-75 Reverse Precession Vibration	3-76
3-76 Full Spectrum—Reverse Precession of 0.5X	3-77
3-77 Calculating Logarithmic Decrement from Test Data	3-77
SP-4 Typical Plot of Applied Cross-coupled Stiffness vs. Log Decrement	3-82
SP-5 CSR Plot to Determine Analysis Level	3-82
3-78 Process Compressor Cross-Section	3-85
3-79 Gas Injection Compressor Cross-Section	3-85
Sheet 3-1 Modified Alford's Force—Processor Compressor	3-86

	Page
Sheet 3-2 Modified Alford's Force—Gas Injection Compressor	3-87
3-80 Process Compressor Stability Plot	3-88
3-81 Gas Injection Compressor Stability Plot	3-88
3-82 Process and Gas Injection Compressors on Experience Plot	3-89
4-1 Diagram of a Shaft Undergoing Torsional Elastic Deflection	4-1
4-2 Side View of a Typical Motor/Gear/Compressor Train	4-3
4-3 Modeling a Typical Motor/Gear/Compressor Train	4-3
4-4 Schematic Lumped Parameter Model for the Motor/Gear/Compressor Train	4-4
4-5 Side View of a Typical Steam Turbine Driven Compressor Train	4-4
4-6 Modeling a Typical Steam Turbine Drive Compressor Train	4-5
4-7 Schematic Lumped Parameter Model for the Steam Turbine Driven Compressor Train	4-5
4-8 Typical Non-linear Stiffness vs. Torque for an Elastomeric Coupling	4-6
4-9 A Typical Twin-Pinion Integrally-geared Centrifugal Compressor That Should be Modeled as a Branched System	4-8
4-10 Effective Penetration of a Smaller Diameter Shaft Section into a Larger Diameter Shaft Section	4-9
4-11 Examples of Shrunk on Sleeves With and Without Relieved Fits	4-10
4-12 A Reduced Moment Gear Coupling	4-11
4-13 A Marine-style Diaphragm Coupling	4-11
4-14 A Reduced Moment Disc Coupling	4-11
4-15 Coupling Spacer Torsional Stiffness Model	4-12
4-16 Two Mass Torsional System with Damping	4-13
4-17 An Elastomeric Hybrid Coupling (w/Disc Type)	4-14
4-18 Temperature Dependent Shear Modulus Curve	4-14
4-19 Cross-sectional View of a Parallel Shaft Speed Increaser	4-16
4-20 Torsional Model of a Parallel Shaft Speed Increaser	4-17
4-21 Cross-section of the Shaft Under the Windings of a Typical Induction Motor	4-18
4-22 View of Typical Screw Compressor Rotor Pair	4-20
4-23 Typical System Model of a Dry Screw Compressor Train	4-21
4-24 Typical System Model of a Flooded Compressor Train	4-21
4-25 Portion of a Typical Crankshaft Throw	4-22
4-26 Finite Element Models Used to Calculate Torsional Stiffness of Crankshaft Sections	4-23
4-27 Untuned Damper	4-24
4-28 Campbell Diagram for a Motor-gear-compressor System	4-28
4-29 Campbell Diagram for a Steam Turbine Driven Compressor System	4-29
4-30 Torsional Mode Shapes for a Typical Motor-gear-compressor Train	4-30
4-31 Torsional Mode Shapes for a Typical Motor-gear-compressor Train (Continued)	4-33
4-32 Campbell Diagram for a Motor-gear-compressor Train After Tuning	4-34
4-33 Torsional Mode Shapes for a Typical Steam Turbine Driven Compressor Train	4-35
4-34 3rd Torsional Natural Frequency of a Motor-gear-compressor System	4-36
4-35 1st Torsional Natural Frequency of a Motor	4-36
4-36 A Typical Magnification Factor Plot of a Torsional Synchronous Response Analysis	4-38
4-37 Transient Torsional Motor Fault Analysis Plot	4-39
4-38 Speed Torque Curve for a Synchronous Motor.	4-39
4-39-1 Plot of Synchronous Motor Transient Response Analysis With Motor Torque Shaft Torques, Motor Speed And Torque Dependent Damping of an Elastomeric Coupling	4-40
4-39-2 Crossover Points on Torque Residual Curves.....	4-42
4-40 Transient Torque Associated with a Single Line to Line to Line Fault	4-48
4-41 High Cycle Fatigue for Continuous Excitation Sources	4-48
4-42 Plot of a Shaft Operating Stress as a Function of Shaft Operating Speed	4-50
4-43 Transient Torsional Simulation of a Synchronous Motor-Driven Compressor Train	4-51
4-44 Typical Speed Torque Curve for a Synchronous Motor with Laminated Pole Construction.....	4-52
4-45 Typical Speed Torque Curve for a Synchronous Motor with Solid Pole Construction	4-53
4-46 Displacement Measurement Considerations	4-55

	Page
4-47 Torsional Measurements Using a Toothed Wheel and Sensors	4-56
4-48 Torsional Vibration Measurements with a Laser	4-56
5-1 Unbalance Expressed as the Product of Weight and Distance	5-3
5-2 Static Unbalance	5-4
5-3 Couple Unbalance	5-4
5-4 Quasi-Static Unbalance	5-5
5-5 Dynamic Unbalance	5-5
5-6 Unbalance Distribution Resolution	5-6
5-7 ISO Unbalance Tolerance Guide for Rigid Rotor	5-8
5-8 Shaft Centerline Unbalance Orbits (Based on ISO and API Standards)	5-9
5-9 Unbalance Versus Speed for API Limits and Balance Machine Limit (Calculated at $w=1$ pound)	5-9
5-10 Applicable Speed Ranges for Hard-bearing and Soft-bearing Balancing Machines	5-10
5-11 Fit Eccentricity Related Unbalance	5-13
5-12 Unbalance Correction to Fit Eccentricity	5-13
5-13 Initial Reading of the Index Balancing Method	5-14
5-14 Indexed Component Relative to the Shaft	5-15
5-15 Vector Representation of R_{11} and R_{12}	5-15
5-16 Results of Adding and Subtracting Vectors R_{11} and R_{12}	5-16
SP-6 Rotor Response Plot	5-22
SP-7 Undamped Critical Speed Map	5-23
SP-8 Typical Mode Shapes	5-25
SP-9 Typical Plot of Applied Cross-coupled Stiffness vs. Log Decrement	5-29
SP-10 Level I Screening Criteria	5-29
 Tables	
2-1 Typical Units for Material Properties	2-6
2-2 Computer Model Generated for the Eight-stage Steam Turbine Rotor	2-9
2-3 General Synchronous Behavior and Requirements of Oil and Gas Seals	2-44
2-4 Rotordynamic Characteristics of Axial Compressors	2-84
2-5 Summary of the Results of the Tests	2-104
3-1 Formula for Squeeze Film Damper Stiffness and Damping Coefficients	3-20
3-2 Rotordynamic Characteristics of Axial Compressors	3-62
3-3 Level I Stability Results for Process and Gas Injection Compressor	3-89
3-4 Minimum Log Decrement for Gas Injection Compressor	3-89
4-1 Penetration Factors for Selected Shaft Step Ratios	4-9
4-2 Comparison of Exact and Approximate Results for Torsional Rigidity (Simple Geometric Cross-sectional Shapes)	4-17
5-1 Relationship Between Balancing Machine Pedestal Stiffness, Rotor Weight and Operating Speed (for one manufacturer)	5-18

API Standard Paragraphs Rotordynamic Tutorial: Lateral Critical Speeds, Unbalance Response, Stability, Train Torsionals, and Rotor Balancing

SECTION 1—OVERVIEW

1.1 INTRODUCTION

This document is intended to describe, discuss, and clarify the API Standard Paragraphs (SP) Section 6.8 which outlines the complete lateral and torsional rotordynamics and rotor balancing acceptance program designed by API to ensure equipment mechanical reliability. Background material on the fundamentals of these subjects (including terminology) along with rotor modeling utilized in this analysis is presented for those unfamiliar with the subject.

The standard paragraphs are introduced with references to the appropriate background material to enhance the understanding. This information is intended to be a primary source of information for this complex subject and is offered as an introduction to the major aspects of rotating equipment vibrations that are addressed during a typical lateral dynamics analysis. It is not intended to be a comprehensive guideline on the execution of rotordynamics analyses but is intended to:

- a. Provide guidance on the requirements for analysis;
- b. Aid in the interpretation of rotordynamics reports; and,
- c. Provide guidance in judging the acceptability of results presented.

1.2 ORGANIZATION

The document is divided into four sections:

1. Lateral Dynamic Analysis
2. Stability Analysis
3. Torsional Analysis
4. Balancing of Machinery

The individual sections have been prepared in a stand alone manner. As a result, necessary material may be repeated in a succeeding section to provide sufficient clarity to the discussion.

The first three (analysis) sections have a parallel organization:

- Modeling criteria
- Analysis techniques and results
- Machine specific considerations
- Testing
- Applications and Examples

1.3 STANDARD PARAGRAPHS

In order to aid turbomachinery purchasers, the American Petroleum Institute's Subcommittee on Mechanical Equipment has produced a series of specifications that define mechanical acceptance criteria for new rotating equipment. Experience accumulated by turbomachinery purchasers over the past ten years indicates that if the API standards are properly applied, the user can be reasonably assured that the installed unit is fundamentally reliable and will, barring problems with the installation and operator misuse, provide acceptable service over its design life.

An integral component of these individual equipment specifications is contained in the API Standard Paragraphs, those specifications that are generally applicable to all types of rotating equipment. The criteria associated with lateral and torsional rotordynamics and balancing have been categorized as standard paragraphs. In rotating equipment specifications published by API (for example, API Standard 617—*Axial and Centrifugal Compressors and Expander-compressors for Petroleum, Chemical and Gas Industry Services*) there is a section on rotordynamics and balancing. The backbone of those sections are the standard paragraphs augmented by additional information that is applicable only to the type of unit considered in the standard.

The Standard Paragraphs relevant to each section of the document are introduced at the end of each section. Limited comments are made to explain the individual paragraphs. Reference is made to the appropriate discussion in the tutorial to describe the background, justification, or application of the paragraph. The complete text of the Standard Paragraphs is included at the end of the document.

1.4 DEFINITIONS AND REFERENCES

Definitions are incorporated into each section of the document. Due to very large number of references employed, they are identified at the end of each relevant section.

1.5 FUNDAMENTAL CONCEPTS OF ROTATING EQUIPMENT VIBRATIONS

In order to understand the results of a rotordynamics design analysis, it is necessary to first gain an appreciation for the physical behavior of vibratory systems. Begin by noting that all real physical systems/structures (such as buildings, bridges, and trusses) possess natural frequencies. Just as a tuning fork has a specific frequency at which it will vibrate most violently when struck, a rotor has specific frequencies at

which it will tend to vibrate during operation. Each resonance is essentially comprised of two associated quantities: the frequency of the resonance and the associated deflections of the structure during vibration at the resonance frequency. Resonances are often called modes of vibration or modes of motion, and the structural deformation associated with a resonance is termed a mode shape.

The modes of vibration are important only if there is a source of energy to excite them, like a blow to a tuning fork. The natural frequencies of rotating systems are particularly important because all rotating elements possess finite amounts of unbalance that excite the rotor at the shaft rotation frequency (synchronous frequency) and its multiples. When the synchronous rotor frequency equals the frequency of a rotor natural frequency, the system operates in a state of resonance, and the rotor's response is amplified if the resonance is not critically damped. The unbalance forces in a rotating system can also excite the natural frequencies of non-rotating elements, including bearing housings, supports, foundations, piping, and the like.

Although unbalance is the excitation mechanism of greatest concern in a rotordynamics analysis, unbalance is only one of many possible lateral loading mechanisms. Lateral forces can be applied to rotors by the following sources: impeller aerodynamic loadings, misaligned couplings and bearings, rubs between rotating and stationary components, and so on. A more detailed list of rotor excitation mechanisms of particular interest is found in the API Standard Paragraphs, 6.8.1.1. This subject is discussed in detail in 3.5, as well as scattered in the appropriate sections of this document.

The vibration behavior of a rotor can be described with the aid of a simple physical model. Assume that a rotor-bearing system is analogous to the simple mass-spring-damper system presented in Figure 1-1.

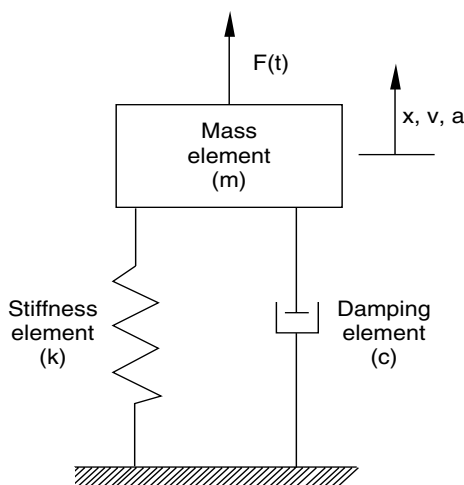


Figure 1-1—Simple Mass-spring-damper System

From physics, the governing equation of motion for this system can be written as Equations 1-1 and 1-2:

$$ma + cv + kx = F(t) \quad 1-1$$

$$m\ddot{x} + c\dot{x} + kx = F(t) \quad 1-2$$

where

m = mass of the block, kg (lbm),

$a = \ddot{x}$ = acceleration, m/s² (in./s²),

c = viscous damping coefficient, N-s/m (lbf-s/in.),

$v = \dot{x}$ = velocity, m/s (in./s),

k = stiffness of the elastic element, N/m (lbf/in.),

x = displacement of the block, m (in.),

$F(t)$ = force applied to the block (time-dependent function), N (lbf).

In this example, the displacement response of the block to the applied force is counteracted by the block's mass and the support's stiffness and damping characteristics. The undamped natural frequency of this system is calculated by determining the eigenvalue of the second order homogeneous ordinary differential equation ($F = 0$) for the case where the damping term is neglected ($c = 0$) as seen in Equation 1-3.

$$\omega = \sqrt{\frac{k}{m}} \quad 1-3$$

where

ω = undamped natural frequency, rad/s.

Since real, physical systems include damping, this needs to be included in the analysis. The damped natural frequency of the homogeneous system ($F = 0$) is defined in Equation 1-4.

$$\omega_d = \sqrt{\frac{k}{m} - \left(\frac{c}{2m}\right)^2} \quad 1-4$$

where

ω_d = frequency of oscillation, rad/s.

If the system was excited (hit by a hammer), this damped natural frequency is the frequency of vibration that would be seen as the system responds. Note that the oscillatory frequency of the damped system, ω_d , is equal to the undamped natural frequency of the system only when system damping is negligible. In a practical sense, this occurs in turbomachinery only when the mode shape indicates that the journal motion in the bearing is less than 5% of the shaft midspan displacement. This observation underscores the fact that an undamped critical speed analysis should, in general, not be used to define the critical speeds of a rotating machine.

If the exciting force is sinusoidal, i.e.,

$$F(t) = A \sin(\omega t) \quad 1-5$$

The response will be:

$$x(t) = B \sin(\omega t + \theta) \quad 1-6$$

where

$$\left(\frac{B}{A}\right) = \text{Amplitude ratio,}$$

$$\theta = \text{Phase angle, rad.}$$

In the case of a rotor with unbalance, the unbalance force is defined in Equation 1-7:

$$F_{UB} = me_u \omega^2 \quad 1-7$$

where

$$m = \text{mass of rotor, kg (lbm),}$$

$$e_u = \text{mass eccentricity, m (in.),}$$

$$\omega = \text{rotational speed, rad/s,}$$

$$F_{UB} = \text{unbalance force, N (lbf).}$$

This result is called a forced response analysis and is analogous to the unbalance response analysis performed in rotordynamics studies. The amplitude ratio depends upon frequency of the excitation and the damping in the system. Figure 1-2 shows the amplitude ratio versus the excitation frequency. Maximum amplitude ratio is seen where the excitation frequency equals the natural frequency of the system. Amplitude ratio also increases as damping decreases with the amplitude becoming infinite at zero damping (a situation which is not physically practical).

There is a phase difference between the excitation and response. This phase difference is a function of damping and reaches 90 degrees at the natural frequency. Figure 1-3 shows the phase angle versus excitation frequency.

If a transient rather than a sinusoidal excitation excites the system, the actual response normally look like that shown in Figure 1-4.

In this case, the response is at the natural frequency. It decays with time based on the amount of damping. This response is called “stable”. In Figure 1-5, the response grows with time. In this configuration, the damping causes the response to grow with time. This response is called “unstable”.

While the simple, single degree of freedom system described above is useful for examining the general concepts of vibration theory, this system is clearly not representative of a turbomachine. A more accurate representation of a rotating assembly is comprised of lumped masses that are connected by elastic springs. Once the mathematical model of the rotating element is generated, it is connected to ground through elastic stiffness and viscous damping elements that represent the fluid film support bearings, seals, and supports. The major contributor to this analysis occurred in the early 1900’s with the development of the Jeffcott model as shown in Figure 1-6.

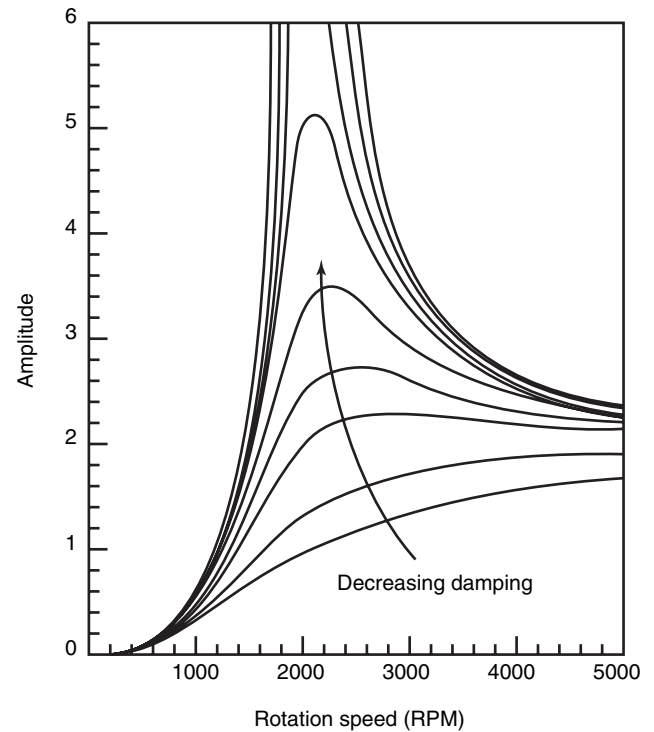


Figure 1-2—Amplitude Ratio Versus Excitation Frequency (Rotation Speed)

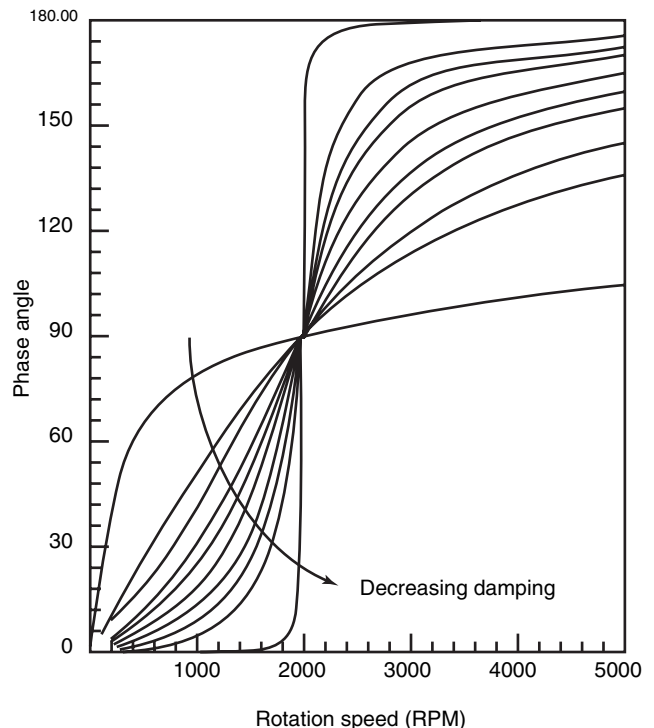


Figure 1-3—Phase Angle Versus Excitation Frequency

This system is comprised of a massive, rigid disk that is held between two identical elastic bearings/supports by a massless shaft. If the shaft is assumed rigid or extremely stiff relative to the bearings/supports, then the primary sources of flexibility in the system are the two bearing support systems. This model had three degrees of lateral freedom (x , y , and z) and one degree of rotation. Considerable analysis of this

model was performed which ultimately led to much of our current methodology.

Further modeling considerations will use a simplified undamped system (damping is considered zero for simplicity), similar in appearance to a beam rotating machine to represent the Jeffcott Model. The representation is presented in Figure 1-7.

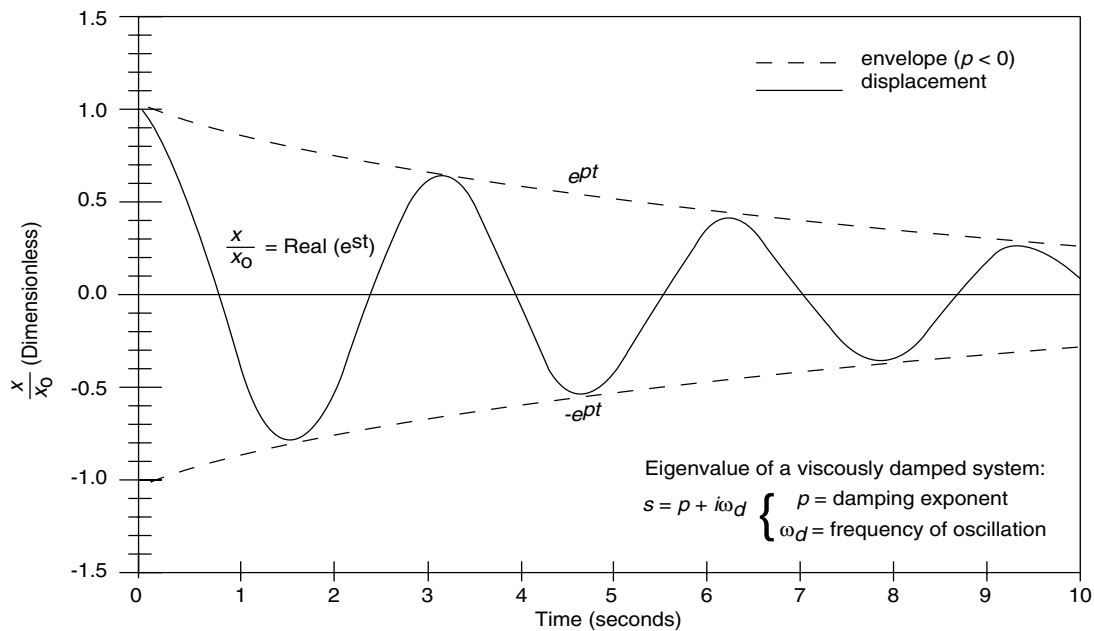


Figure 1-4—Response of a Spring-mass System to Transient (Stable)

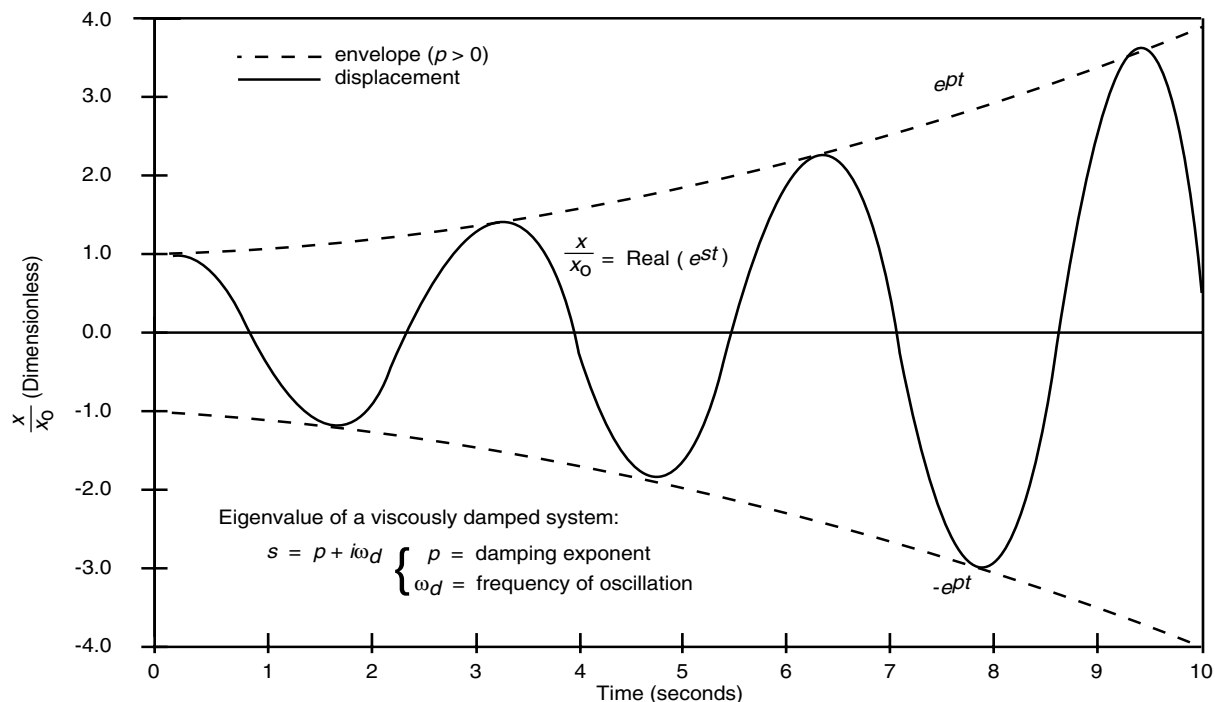


Figure 1-5—Response of a Spring-mass System to Transient (Unstable)

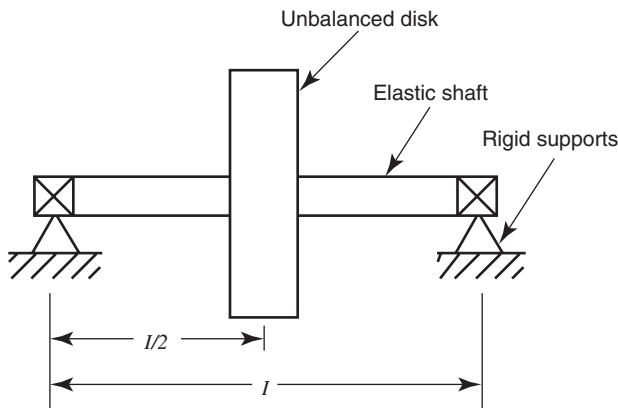


Figure 1-6—Jeffcott Form for Rotor Model

In order to consider the effect of the combined shaft and bearing stiffness, we need to review the effective combined stiffness as shown in the second set of drawings in the figure. As shown, the effective stiffness, K_{eq} , is the result of the individual stiffnesses added. The equation that describes this is:

$$K_{eq} = \frac{2}{\left(\frac{2}{K_{shaft}}\right) + \left(\frac{1}{K_{brg}}\right)} \quad 1-8$$

$$K_{shaft} = \frac{48EI}{L^3} \quad 1-9$$

where

E = Young's modulus for shaft material, N/m^2 (lbf/in.²),

L = shaft section length, m (in.),

K_{shaft} = shaft thickness, N/m (lbf/in.).

$$I = \frac{\pi D^4}{64} \quad 1-10$$

where

D = shaft diameter, m (in.),

I = area moment of inertia, m^4 (in.⁴).

This equation indicates that the stiffness of the combined shaft-bearing system will be less than the stiffness of the single most flexible element. In this example, the shaft is the single most flexible element ($k_{shaft} = 8756.5 \text{ N/mm}$ or $50,000 \text{ lbf/in.}$). According to Equation 1-8, the effective stiffness of the combined shaft-bearing spring system is only 7297.7 N/mm ($41,670 \text{ lbf/in.}$).

To carry this analysis one step higher in complexity, consider the sketch of a rotordynamic system displayed in Figure 1-8. Figure 1-9 shows the model with masses, springs, and dampers.

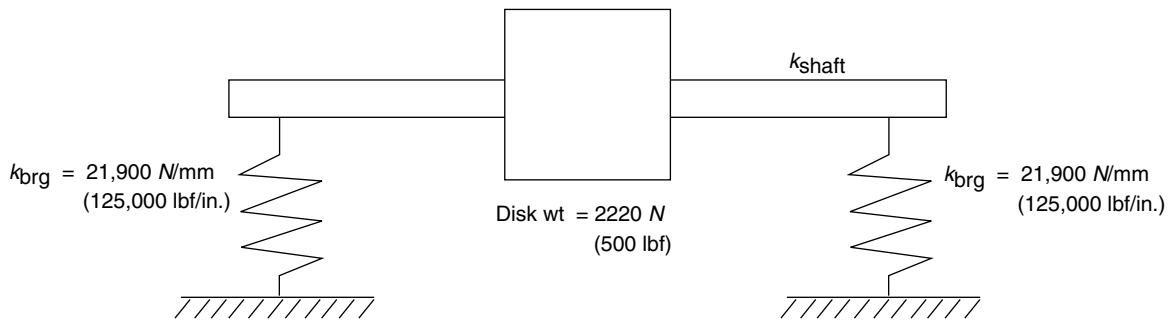


Figure 1-7—Simplified Model of a Beam-type Rotating Machine

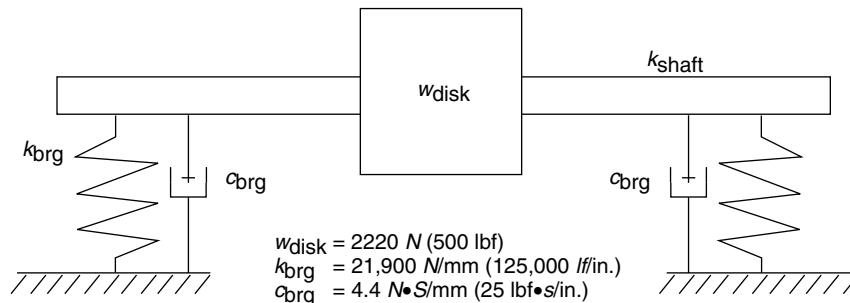


Figure 1-8—Simplified Model of a Beam-type Rotating Machine with Damping

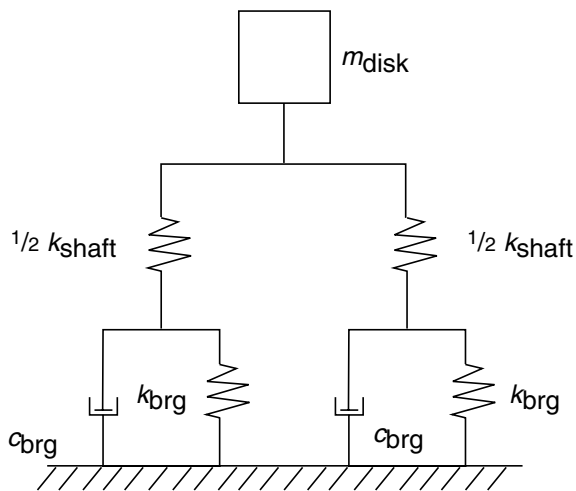


Figure 1-9—Spring-mass-damper Model of Beam Type Rotating Machine

Note that this system is identical to the system just discussed except that viscous damping elements have been added to the bearing model. All oil film bearings generate significant viscous damping forces. Figure 1-10 displays the calculated response of the disk to a harmonic load acting at the disk for various values of shaft stiffness

Note that as the shaft stiffness decreases, the peak response frequency decreases while the amplitude of the peak response and the sharpness of the peak both increase. These observations are understood by noting that the decrease in shaft stiffness decreases the relative deflection of the shaft in the bearings and diminishes the magnitude of the damping forces provided by the bearings. Thus, one may conclude that the effect of damping provided by the bearings is maximized when the shaft stiffness is large relative to the bearing stiffness.

These general concepts of vibrations will be demonstrated in considerably more detail in the sections that follow.

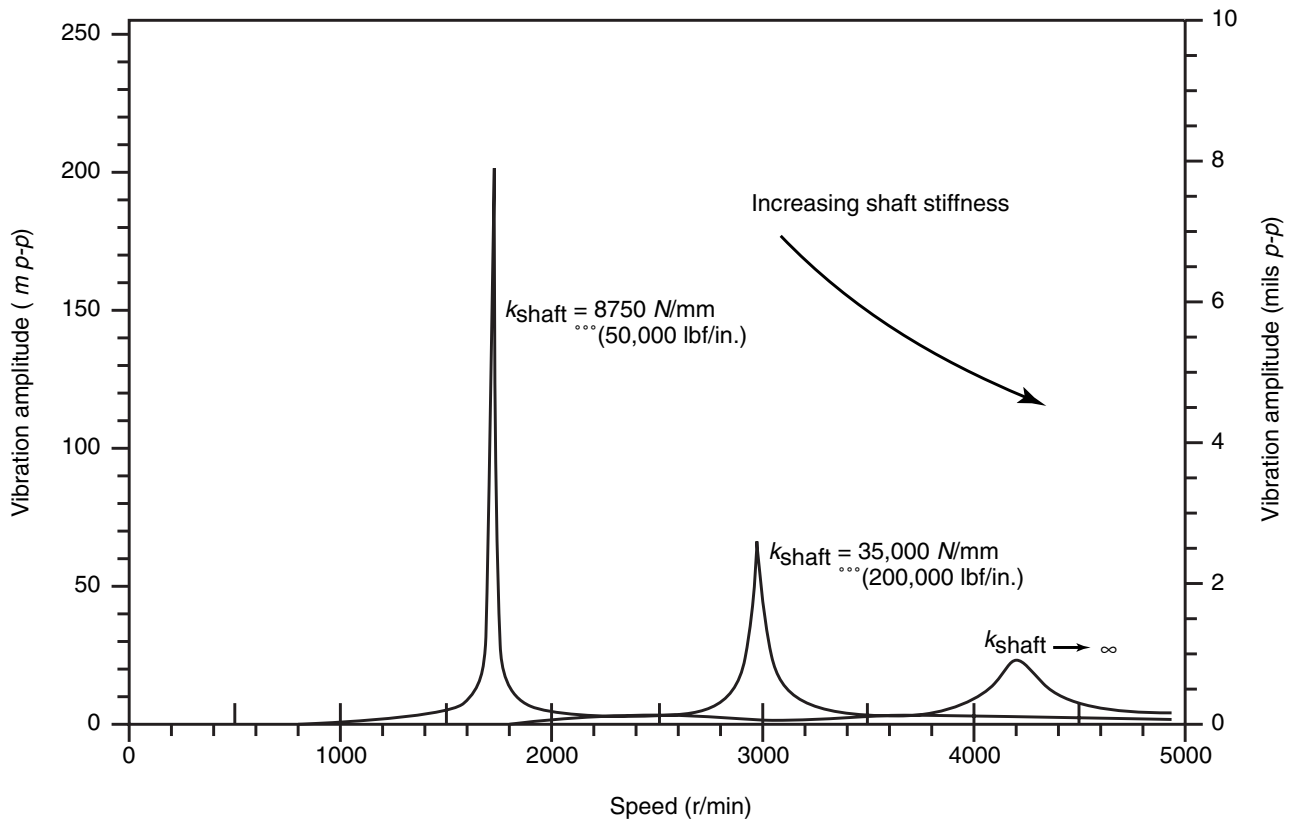


Figure 1-10—Synchronous Response of Beam Type Machine for Various Shaft Stiffness Values

SECTION 2—LATERAL ROTORDYNAMICS

2.1 INTRODUCTION

The ultimate mechanical reliability of rotating equipment depends heavily upon decisions made by both the purchaser and vendor prior to equipment manufacture. Units that are designed using the appropriate application of sophisticated computer-aided engineering methods will be less problematic than units designed without the benefit of such analysis. Even with performance of mechanical acceptance tests prior to delivery and installation, the discovery of design-related problems during these tests may compromise the planned cost of the unit and/or its delivery schedule.

For this reason, rotordynamics analysis tools have been developed and are continuing to evolve. In the late 19th century, there was a wide spread belief that machines could not be operated above the first critical speed and designs focused on machines that operated below that critical. Once it was proven that operation above the first critical was possible, it was still difficult to execute the designs due to the complexity of the analysis and the limits of computational power (i.e., pen and paper). In the mid 20th century, critical breakthroughs were made in the analytical tools. Once this was coupled with the explosion of computational power, analysis methodology took off. Today, very comprehensive analyses may be performed on the desk top and analysts are continuing to develop finer and more accurate modeling and analysis techniques. In addition, improved measurement capabilities are providing the opportunity to prove and improve this work.

Today, these analysis tools and procedures have become a standard fundamental design tool for a class of turbomachinery that includes centrifugal and axial compressors, centrifugal pumps, steam turbines, gas turbines, electric motors, expander turbines, and gears. Application of this technology requires communication between the purchaser and manufacturer to be most effective. This document has been prepared to facilitate this communication by providing the means to achieve a common understanding or platform upon which to hold meaningful discussion. This document identifies the analysis requirements as well as providing an aid to interpret and understand results of that analysis.

The general class of machines to which this document applies are primarily custom designed, i.e., while they belong to a machine class, the specific design features like bearing span, rotor weight, operating speed, etc. fall within design ranges selected for the specific application. This is different from “standard design” turbomachinery, e.g., aircraft gas tur-

bines which are complex but which have many identical machines built. Most of the principles identified in this document apply to those machines but the details have not been directed at that class of machine.

This edition of RP 684 has been considerably expanded over the First Edition. In addition to addressing the changes which have been incorporated into the Standard Paragraphs basis the growth in understanding and experience with this technology, this document has an extensive coverage on stability analysis. A comprehensive section on stability analysis has been incorporated in the current version of the Standard Paragraphs. This document addresses those standard paragraphs in its discussion.

2.2 ROTOR BEARING SYSTEM MODELING

Modeling is the single most important process in performing any engineering analysis of a physical system. Several checks should be incorporated into the modeling procedure in order to assure the designer that the model accurately simulates the dynamic behavior of the design. If the model does not accurately simulate the proposed design, the sophisticated analysis and evaluation of the design will do little good. The five steps taken to model rotating equipment are listed in sequence below:

- a. Generate a mass-elastic lateral model of the unit's rotating assembly.
- b. Calculate the static bearing reactions (including miscellaneous static load mechanisms such as gear loading, loads resulting from partial arc steam admission, and so forth).
- c. Calculate the linearized fluid film bearing coefficients.
- d. Calculate the linearized floating ring oil seal coefficients (if present).
- e. Calculate all other excitation mechanisms (such as aerodynamic effects and labyrinth seal effects).

These steps will be discussed in greater detail in the following pages.

2.3 ROTOR MODELING METHODS AND CONSIDERATIONS

2.3.1 General

It has become axiomatic to engineers wishing to perform an accurate computer simulation of physical systems that only accurate models generate accurate results. This section will describe some of the methods that have been

successfully employed over a period of many years to model the important elements of a solid shaft rotor-bearing system. The reader is cautioned that tie-bolt rotors are potentially subject to greater modeling complications than solid shaft rotor designs. For example, the rotor bending stiffness characteristics may be related to the tie-bolt stretch. The non-linear axial face friction forces between rotor segments may become significant if the segments move relative to each other during rotor operation. Finally, small high speed built-up rotors may simply not be adequately represented by direct application of cylindrical beam elements. In such cases, sophisticated finite element analysis of the rotating element may be necessary to build an equivalent beam element model that permits accurate prediction of results.

An accurate model of a rotor system is a model that permits accurate calculation of the actual rotor system's dynamic characteristics. This occurs when the rotor's mass elastic (mass-inertia-stiffness) properties are adequately represented. For the purpose of performing a basic rotordynamics design audit, two simple building blocks are joined together to form a complete model of the rotating assembly. These elements are the shaft lumped mass-inertia elements and the disk lumped mass-inertia elements. Shaft elements contribute mass, inertia and stiffness to the global model; whereas, disk elements contribute mass and inertia only. More complicated element types can be used at the cost of introducing complexity to the model. In general, however, most turbomachinery can be adequately modeled using the lumped mass-inertia shaft and disk elements presented in this tutorial.

Once the type of elements to be used in the analysis has been established, it simply remains for the engineer to generate a description of the subject rotor's geometry using a sufficient number of the selected elements. Schematics of a rotor and its associated lumped parameter model are displayed in Figure 2-1. Some general constraints must be placed on the use of the lumped mass-inertia shaft elements, however, to ensure that accurate rotor models emerge from the process. Clearly, if too few elements are used the resulting model may not possess sufficient resolution to accurately capture some of the detailed mass-elastic properties of the rotating assembly. If a large number of elements are used to model the rotor, then numerical problems may result. A secondary benefit of minimizing the number of elements used to produce a rotor model is a reduction of the amount of time needed by the engineer to generate data files and for the computer to perform calculations.

2.3.2 Division of Rotor into Discrete Sections

The modeling process starts with the analyst's dividing the rotor into a series of stations connected by shaft elements that

begin and end at step changes in the outside diameter (OD) or inside diameter (ID). The stations are chosen to coincide with the axial locations of the concentrated mass or shrunk on members, such as impellers, turbine disks, thrust collars, balance pistons spacer sleeves, couplings, dry gas seal rotors etc. Also, stations are located at the journal bearing centerlines, sometimes at the centerlines of seals, monitoring radial probe locations and at the ends of the rotor.

The number of stations needed to represent the physical rotor depends on the number and shape of modes to be examined [9]. Stations are also chosen to adequately approximate the curvature of the rotor modes. It is suggested that the number of stations should be at least four times the number of desired modes to be calculated if the rotordynamic programs used in the study are based on the transfer matrix method. Once initial division of the rotor has been accomplished, further refinement of the model is almost certainly required. The following simple guidelines are proposed for modeling a long uniform shaft segment:

- a. The length to diameter ratio of any section should not exceed 1.0 (0.5 is preferred).
- b. The length to diameter ratio of any section should not be less than 0.10.

The first guideline is proposed to ensure that the model possesses sufficient resolution to permit accurate calculation of the undamped critical speeds. The number of critical speeds calculated should be sufficient that the next undamped critical speed above maximum continuous speed or trip is identified. The second guideline is proposed to ensure that large length changes in adjacent shaft elements are avoided as this practice may generate numerical calculation problems. When a large length difference exists between adjacent shaft elements, a large difference in the resulting shaft stiffness is created that can cause numerical round-off errors to accumulate when these stiffnesses are added together during the model assembly process. It should be noted that some transfer matrix based programs are capable of modeling well outside these guidelines without any significant degradation of model accuracy. In general, however, the guidelines provide a safe modeling procedure for those cases where sufficient program benchmarking has not been performed.

Whenever the analyst is unsure of how to model a given feature in the rotating element, he or she may always proceed by determining the sensitivity of calculated results to various ways of modeling the feature in question. For example, if one strictly adheres to the two modeling guidelines proposed above, a short circumferential groove machined into the shaft cannot be modeled. Such grooves are often found on compressor shafts to locate split rings at the ends of the aerodynamic assembly and to lock thrust collars onto the shaft. The authors generally ignore such design features when analysis

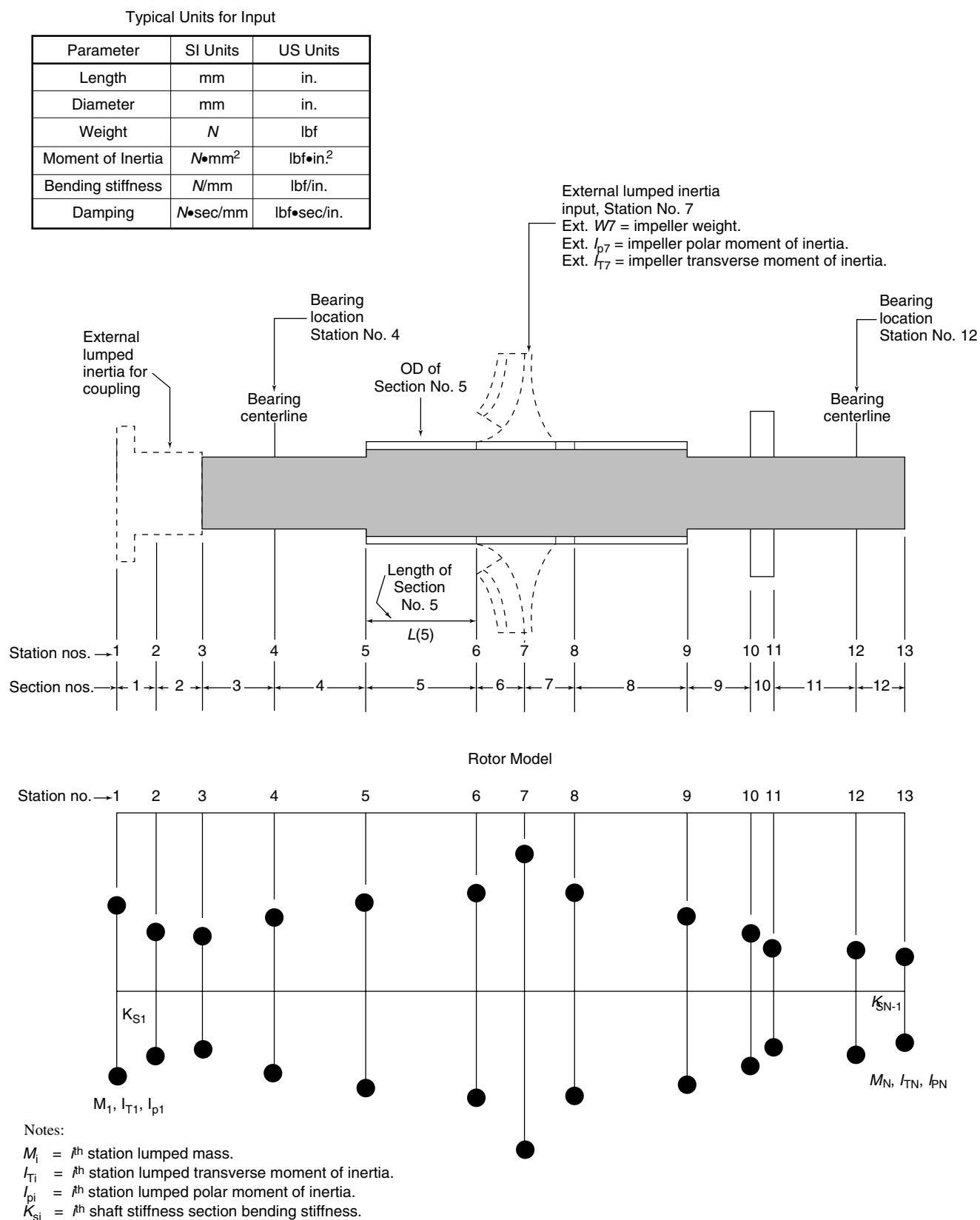


Figure 2-1—Schematic of a Lumped Parameter Rotor Model

indicates that decreasing the diameter of the entire element encompassing the groove does not affect the criticals of concern or the associated modeshapes. When a given geometric feature possesses a strong influence on calculated results, the designer must examine the possibility that the rotor's design may be fundamentally flawed.

On those occasions when the analyst has difficulty modeling a rotating assembly because the rotor geometry cannot be readily described using rudimentary shaft elements, then an equivalent model can be formulated from more sophisticated analysis. For example, the bending characteristics of a stub shaft bolted to the second stage impeller on an overhung gas pipeline compressor have been determined using a finite element analysis of the shaft and impeller sections. The finite element mesh is displayed in Figure 2-2. Note that the large counter-bored bolt holes dramatically decrease that stub shaft's lateral bending stiffness. Once the static bending analysis of the component is accomplished, an equivalent lumped parameter beam-type model of the type used in rotordynamics analysis can be formulated that possesses identical bending stiffnesses at the lumped mass and inertia locations.

2.3.3 Addition of External Masses and Inertial Loadings

Sometimes components that are shrunk on turbomachinery shafts (impellers, sleeves, thrust collars, and so on) affect the bending stiffness of the rotating element. The amount of shrink fit determines the amount of contribution to the bending stiffness of the rotor. The model used to predict the unit's critical speeds may have to be refined according to data collected during mechanical testing of the actual machine if the critical speeds differ by more than 5%.

Components shrunk or fitted onto the shaft affect the mass and inertia characteristics of the rotating assembly, and must be added to the model. This is most often accomplished by adding lumped masses and inertias at the mass centers of the shrunk-on components. It is occasionally necessary, as in the case of motor cores, to generate detailed inertia distributions of the shrunk-on component. Most rotors will include at least several of the following additional masses:

- a. Impeller/disks.
- b. Couplings.
- c. Sleeves.
- d. Balance pistons.
- e. Thrust collars.
- f. Gas seals.

In the rotor lateral model, a station located at the center of gravity of coupling hub should be specified for the coupling associated with the distributed coupling weight and moment of inertia. Coupling vendors provides the location of the center of gravity of each half of the assembled coupling and the

weight distribution on the drawings. If the coupling drawing is not available, coupling half weight and moments of inertia can be approximately specified in the rotor model by using information from coupling vendor publications or web sites. When the center of gravity of coupling hub is beyond the shaft end, an equivalent shaft diameter can be estimated from more sophisticated analysis to provide the same bending stiffness. This can also be done by including an element with very low mass and very high modulus of elasticity where the center of gravity can be located.

Particular machines will have specific masses that must be added, including the following:

- a. Armature windings in electric motors.
- b. Shrunk-on gear meshes.
- c. Wet impeller mass and inertia in pumps.

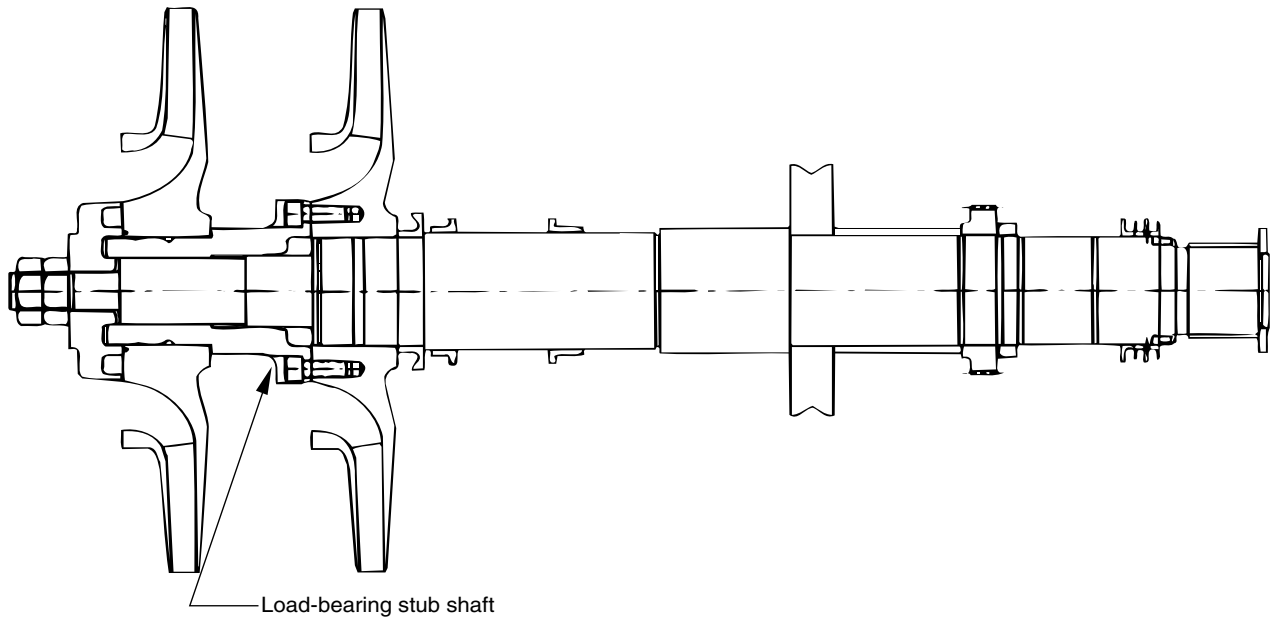
It is imperative that the rotor model properly account for these masses and any additional rotating masses that may be peculiar to a particular system.

2.3.4 Addition of Stiffening Due to Shrink Fits and Irregular Sections

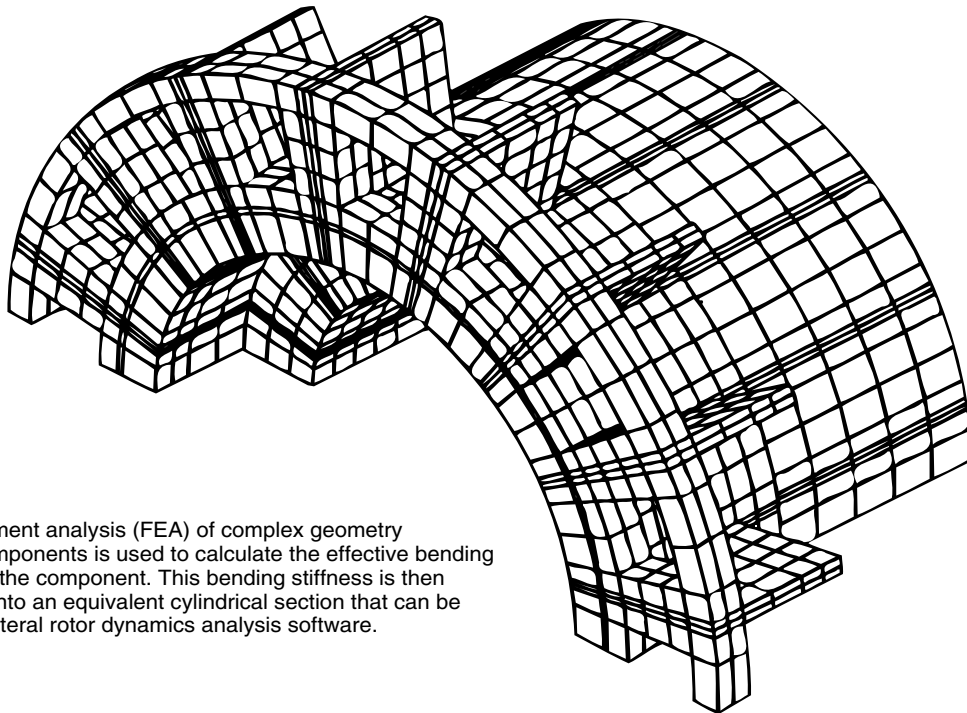
Most rotating assemblies have non-integral collars, sleeves, impellers, and so forth that are shrunk onto the shaft during rotor assembly. If the amount and length of the shrink fit and the size of the shrunk-on component are sufficiently large, then the shrunk-on component must be modeled as contributing to the shaft stiffness. The vendor must determine the importance of shrink fits for particular cases. Often, this can be accomplished only by experience with units of similar type. A modal test of a vertically hung rotor will give some indication of the stiffening effect of shrunk-on components, but such measurements will likely exaggerate such effects because the fits will tend to be relieved as a result of centrifugal growth at normal operating speeds.

In some cases, a shaft segment consists of a series of short grooves and steps. Such segments are often found on turbine shafts at main labyrinth packing locations. Since the decrease in the diameter of the shaft segment encompassing the grooves does not affect the rotor critical speeds and the associated mode shapes, the stepping segment is usually simplified as one element using the average shaft diameter to evaluate the mass and bending stiffness of the stepping shaft segment.

Non-circular rotor cross-sections are common in the midspan areas of electric motors and generators. These electrical machines frequently possess integral or welded-on arms in the midspan area to support the rotor core. These structures add significant stiffening to the rotor midspan. This contribution to the lateral bending stiffness of the rotating assembly must be accounted for, as it is incorrect to model the stiffness of motor rotors using the base shaft only. Older steam turbines of built-up construction may also possess non-circular midspan rotor cross-sections.



**Cross-Section of Rotating Element
with Complex Geometry Component**



A finite element analysis (FEA) of complex geometry rotating components is used to calculate the effective bending stiffness of the component. This bending stiffness is then converted into an equivalent cylindrical section that can be input into lateral rotor dynamics analysis software.

3D Finite Element Model of Stub Shaft

Figure 2-2—3D Finite Element Model of a Complex Geometry Rotating Component

2.3.5 Location of Bearings, Seals, and Radial Probes

It is well understood that bearings and seals can dramatically alter the vibration behavior of a rotating machine. It follows that these coefficients must be accurately placed in the rotor model for the numerical simulation to generate accurate results. Each fluid film support bearing and floating ring oil seal is typically represented using a set of eight linearized dynamic coefficients. The linearized models of the bearings and oil seals are assumed to act at the centerlines of the associated bearing and sealing lands.

A dry gas seal only adds lumped external mass and inertia to the shaft station located at the center of gravity of the dry gas seal. The principle stiffness and damping of gas seals are relatively small, and are typically not included in the rotordynamics model for lateral critical speed and unbalance response analyses. Under certain conditions labyrinth seals have been identified to be a major source of destabilizing forces, which cause subsynchronous vibration problems in compressors and turbines. The labyrinth seal and its replacement, such as honeycomb seal, hole pattern seal, and pocket damper seal, have to be included in the lateral model for stability analyses. The linearized models of labyrinth seals are assumed to act at the centerlines of the associated sealing lands.

The locations of the radial bearing probes are included in the rotor model, as this is where the vibration of the rotating machine will be measured.

2.3.6 Determination of Material Properties

The material properties required to generate the model are presented in Table 2-1.

Table 2-1—Typical Units for Material Properties

Quantity	Typical SI Units	Typical US Customary Units
Gravitational acceleration (g)	9.88m/s ²	386.1 in./s ²
Mass density (ρ)	kg/m ³	lbf·s ² /in. ⁴
Weight density (ρg)	N/m ³	lbf/in. ³
Young's modulus (E)	N/m ²	lbf/in. ²
Shear/Rigidity modulus (G)	N/m ²	lbf/in. ²

The shafts of most rotating machinery are made of carbon and low-alloy steels, such as AISI 4340 and ASTM A 470. The properties of carbon and low-alloy steels change considerably over the temperature range from 0°F to 650°F. Manufacturers must determine the importance of temperature on shaft material properties for particular applications. For high-

temperature cases, vendors should be aware of the influence of temperature on the elastic modulus of shaft materials in the rotor lateral models. Sometimes, an apparent variation of temperature exists along the shaft, which would result in a change in the elastic modulus along the axial length. Figure 2-3 shows the trends of the changes in elastic modulus with temperature for several low-alloy steels, including AISI 4340, which are determined during “static” tensile loading and dynamic loading (from Reference 8 in 2.3.9).

Results of the complete modeling process are displayed for an eight-stage 12-megawatt (16,000-horsepower) steam turbine rotor. A larger version of this drawing was used to describe shaft geometry. The measured rotor weight was used to check the results of the modeling process. The resulting tabular description of the model is presented in Table 2-2. Note that the translational and rotational inertias shown in this table are formed by the sum of externally applied inertias (from turbine blades and disks) and shaft inertias calculated for each of the shaft sections. A cross-section of the rotor model is displayed in Figure 2-4.

2.3.7 Built-up Rotors

Some rotors are constructed of axially segmented sections, which are stacked and bolted together. The turboexpander in Figure 2-5 and the turbocompressor in Figure 2-6 are examples of built-up rotors. The segments are radially located by either rabbet or spline fits and are held together axially by through bolts. When properly designed, the joints are very stiff, and can be approximated as being an integral piece of metal.

Rotor modeling of a joint is illustrated in Figure 2-7. The hatched areas represent the elements used to model the rotor stiffness while the unhatched areas are modeled as masses and inertias only. These methods have been shown to be sufficiently accurate when the rotor is properly designed, and assembled with appropriate preloading of the stacked components. While a more precise joint model can be obtained by using finite element methods or by verifying through modal analysis testing; such methods are typically unnecessary.

2.3.8 Train Lateral

Most machinery trains consist of a series of two-bearing rotors connected by spacer-type flexible couplings as shown in Figure 2-8. Individual units are typically isolated from each other by the coupling such that they can be treated as separate units. A lateral rotordynamic analysis of the entire coupled system (train lateral analysis) is therefore rarely required. There are, however, unique circumstances in which the train lateral analysis can be considered:

1. The coupling spacer natural frequency is within the region shown in Figure 2-9 [1] as ‘train lateral recommended’.

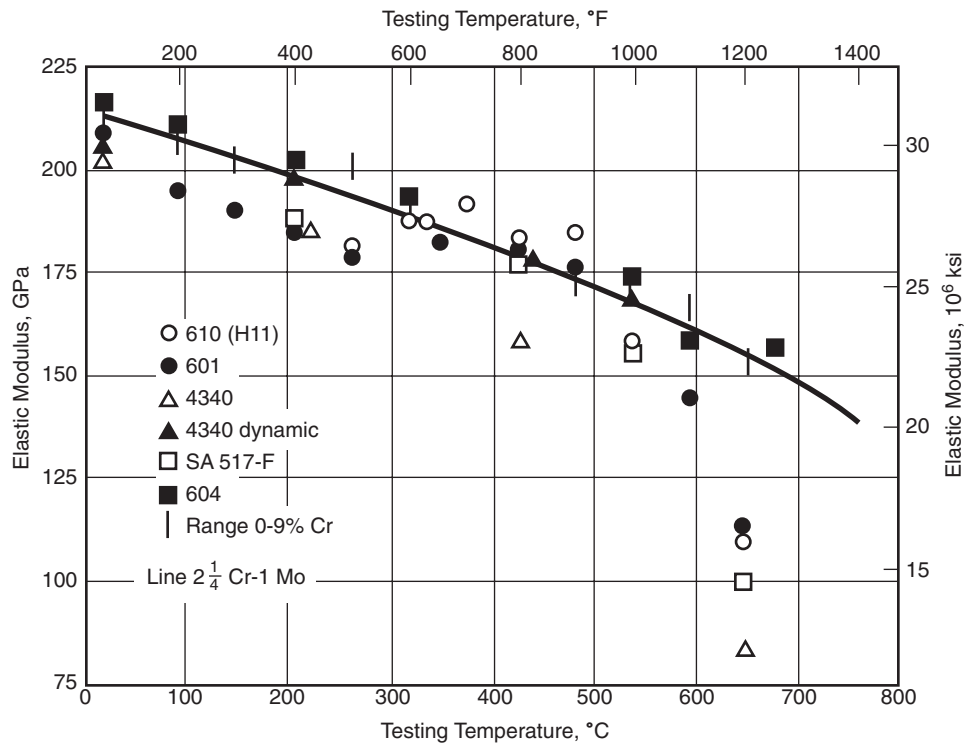


Figure 2-3—Elastic Modulus vs. Temperature

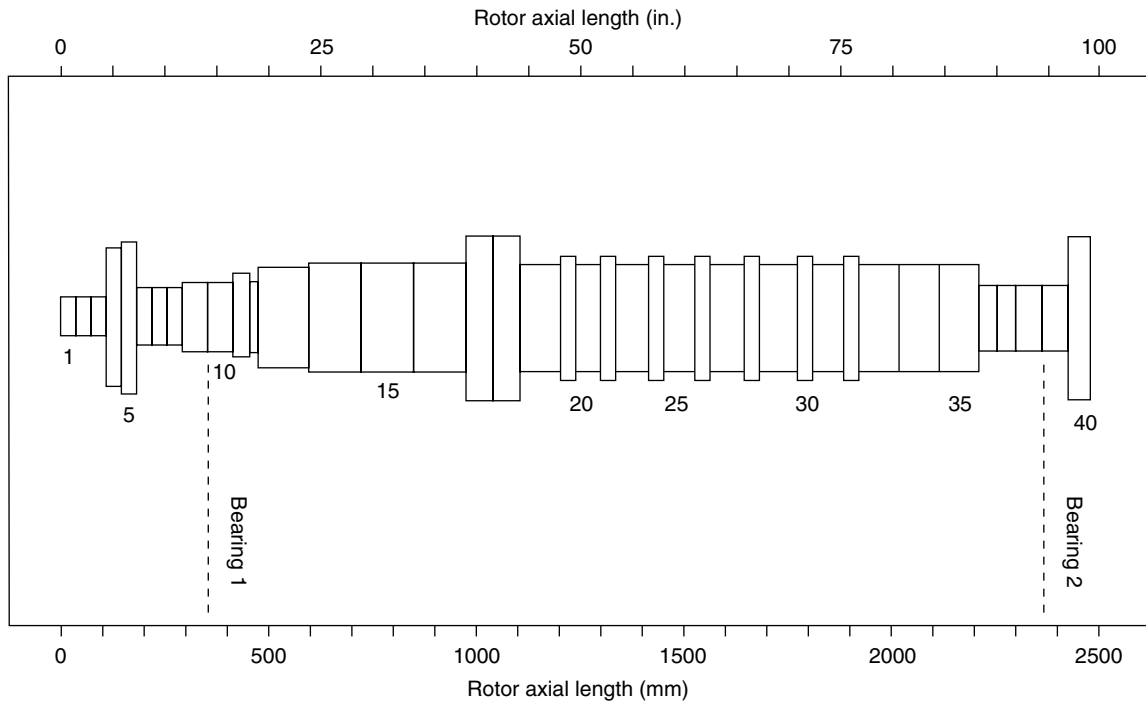


Figure 2-4—Rotor Model Cross-section of an Eight-sage 12 MW (16,000 HP) Steam Turbine

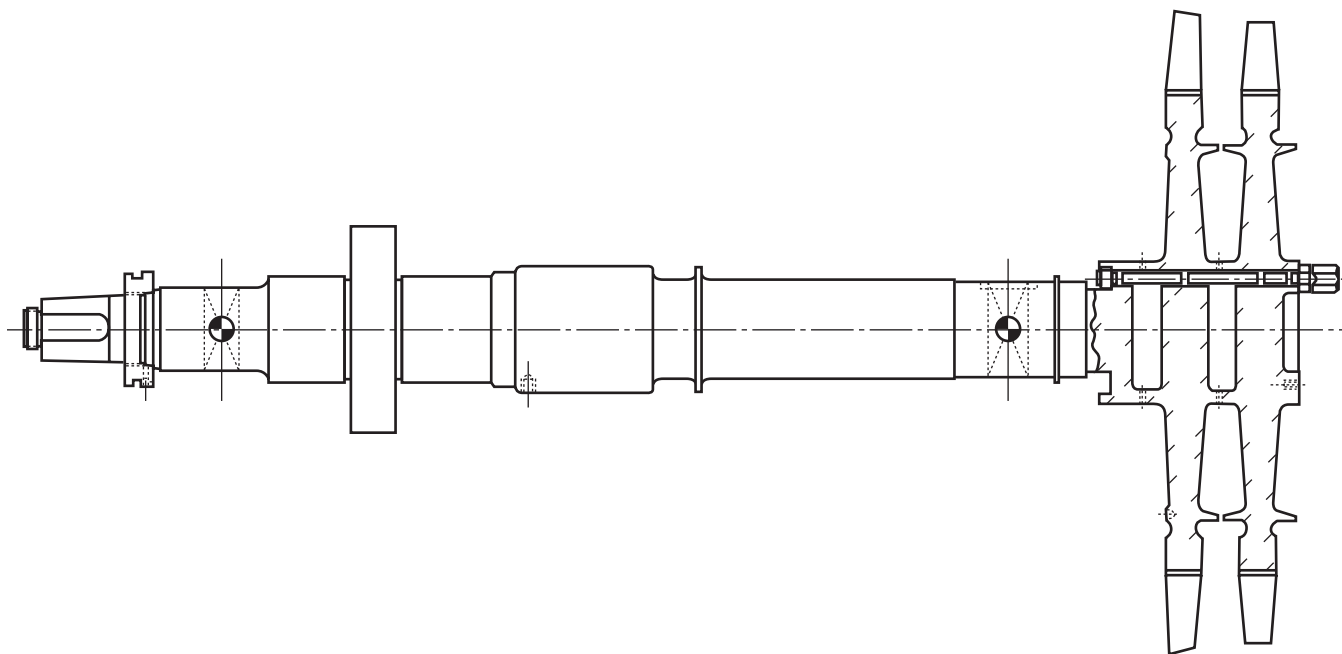


Figure 2-5—Turboexpander with Curvic Coupling Fits

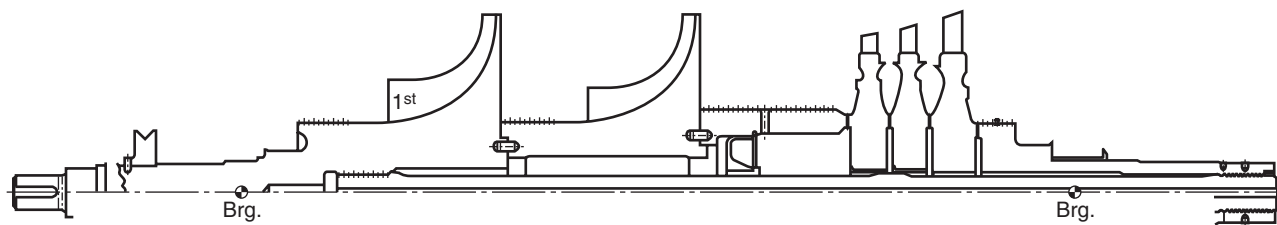


Figure 2-6—Turbocompressor with Rabbet and Curvic Coupling Fits

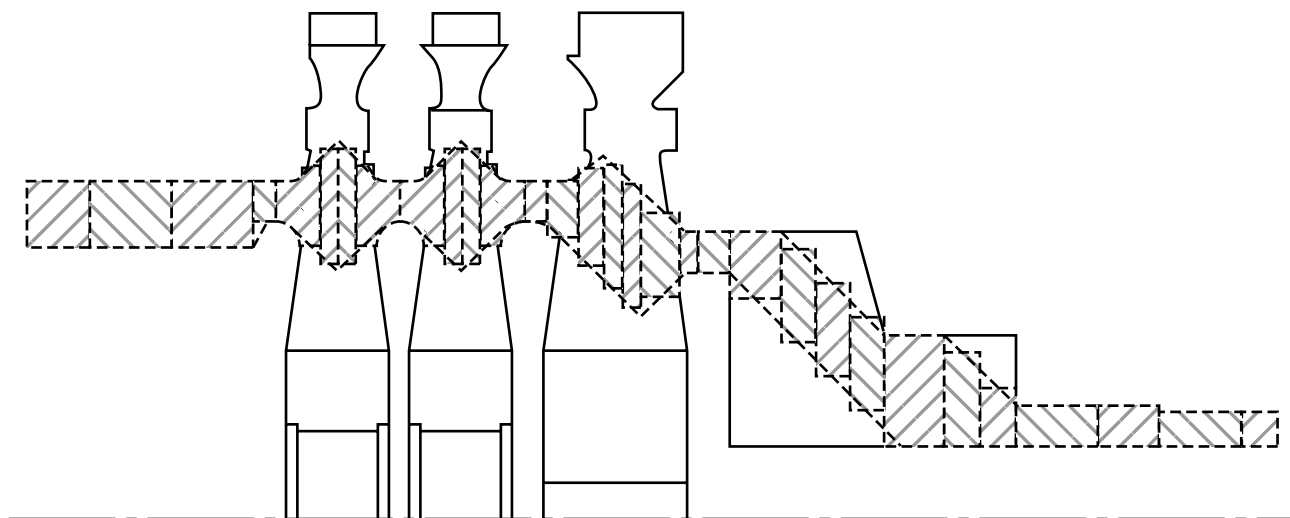


Figure 2-7—Modeling of Curvic Coupling Joints

Table 2-2—Computer Model Generated for the Eight-Stage Steam Turbine Rotor

Station No.	Axial Disp. (in.)	Wt. (lbm)	Length (in.)	Shaft OD (in.)	Shaft ID (in.)	I (in. ⁴)	IP (lbm-in. ²)	IT (lbm-in. ²)	E*10 ⁻⁶ (lb/in. ²)
1	0.00	1.762	1.500	3.25	0	5.48	2.321	1.491	28.7
2	1.50	3.523	1.500	3.25	0	5.48	4.652	2.991	28.7
3	3.00	3.523	1.500	3.25	0	5.48	4.652	2.991	28.7
4	4.50	23.786	1.300	12.35	0	1140.08	421.909	214.386	28.7
5	5.80	47.029	1.200	13.69	0	1724.18	1005.320	508.760	28.7
6	7.00	29.793	1.723	5.00	0	30.68	600.712	304.538	28.7
7	8.72	9.579	1.723	5.00	0	30.68	29.941	17.336	28.7
8	10.45	9.579	1.723	5.00	0	30.68	29.941	17.336	28.7
9	12.17	13.195	2.100	6.00	0	63.62	52.789	30.671	28.7
10	14.27	17.970	2.390	6.00	0	63.62	80.869	48.077	28.7
11	16.66	17.007	1.190	7.50	0	155.32	95.364	53.119	28.7
12	17.85	12.185	1.010	6.50	0	87.62	77.377	39.974	28.7
13	18.86	43.105	4.260	9.00	0	322.06	413.466	265.154	28.7
14	23.12	117.719	5.680	10.00	0	490.87	906.536	563.578	28.7
15	28.80	109.175	4.910	10.00	0	490.87	1364.690	901.689	28.7
16	33.71	109.172	4.910	10.00	0	490.87	1364.650	901.648	28.7
17	38.62	515.401	2.500	15.00	0	2485.05	1402.150	811.401	28.7
18	41.12	515.404	2.500	15.00	0	2485.05	2629.720	1316.590	28.7
19	43.62	59.702	3.570	10.00	0	490.87	1215.930	650.785	28.7
20	47.19	138.463	1.250	11.25	0	786.28	9424.440	4816.280	28.7
21	48.44	127.568	2.590	10.00	0	490.87	9288.250	4722.120	28.7
22	51.03	157.523	1.570	11.57	0	879.64	12322.200	6252.180	28.7
23	52.60	158.524	2.680	10.00	0	490.87	12334.700	6260.170	28.7
24	55.28	162.368	1.560	11.56	0	876.60	13086.000	6636.280	28.7
25	56.84	165.258	2.940	10.00	0	490.87	13122.200	6660.060	28.7
26	59.78	170.604	1.570	11.57	0	879.64	14030.000	7115.410	28.7
27	61.35	171.937	3.060	10.00	0	490.87	14046.700	7126.750	28.7
28	64.41	174.432	1.570	11.57	0	879.64	14517.900	7362.870	28.7
29	65.98	177.100	3.300	10.00	0	490.87	14551.300	7386.300	28.7
30	69.28	177.100	1.570	11.57	0	879.64	14551.300	7386.290	28.7
31	70.85	170.763	2.730	10.00	0	490.87	14472.100	7332.250	28.7
32	73.58	197.509	1.880	11.88	0	977.77	17066.500	8649.220	28.7
33	75.46	211.795	4.015	10.00	0	490.87	17245.100	8779.610	28.7
34	79.47	146.058	4.785	10.00	0	490.87	1115.940	677.903	28.7
35	84.26	32.353	2.240	9.00	0	322.06	423.397	220.752	28.7
36	86.50	27.875	1.640	6.50	0	87.62	244.917	132.617	28.7
37	88.14	15.406	1.640	6.50	0	87.62	81.369	44.136	28.7
38	89.78	19.540	2.520	6.50	0	87.62	103.196	59.591	28.7
39	92.30	24.801	2.760	6.50	0	87.62	130.976	79.978	28.7
40	95.06	111.748	2.000	21.62	0	10724.00	314.579	165.750	28.7
41	97.06	77.957	0.000	21.62	0	0.00	4554.850	2292.050	28.7
		4475.292	97.059						

Bearing Reactions: 2190.92 lbm at Station 10
2284.38 lbm at Station 39

For trains with more than two bodies, a partial train lateral analysis consisting only of the bodies meeting the specified criteria is acceptable since other units in the train, connected by couplings with adequate spacer natural frequencies, would be sufficiently isolated and have little effect on the rotordynamic characteristics of the remaining train. Figure 2-10 displays the first seven mode shapes of a three body string. The first unit is a three bearing gas turbine. The second unit is a

two bearing compressor, and the third unit is a three bearing motor. The turbine and compressor are joined by a coupling with spacer natural frequency 1.67 times running speed. The compressor and motor are joined by a coupling with spacer natural frequency 10.28 times running speed. By the criteria listed, a partial train lateral analysis of the turbine and compressor is sufficient.

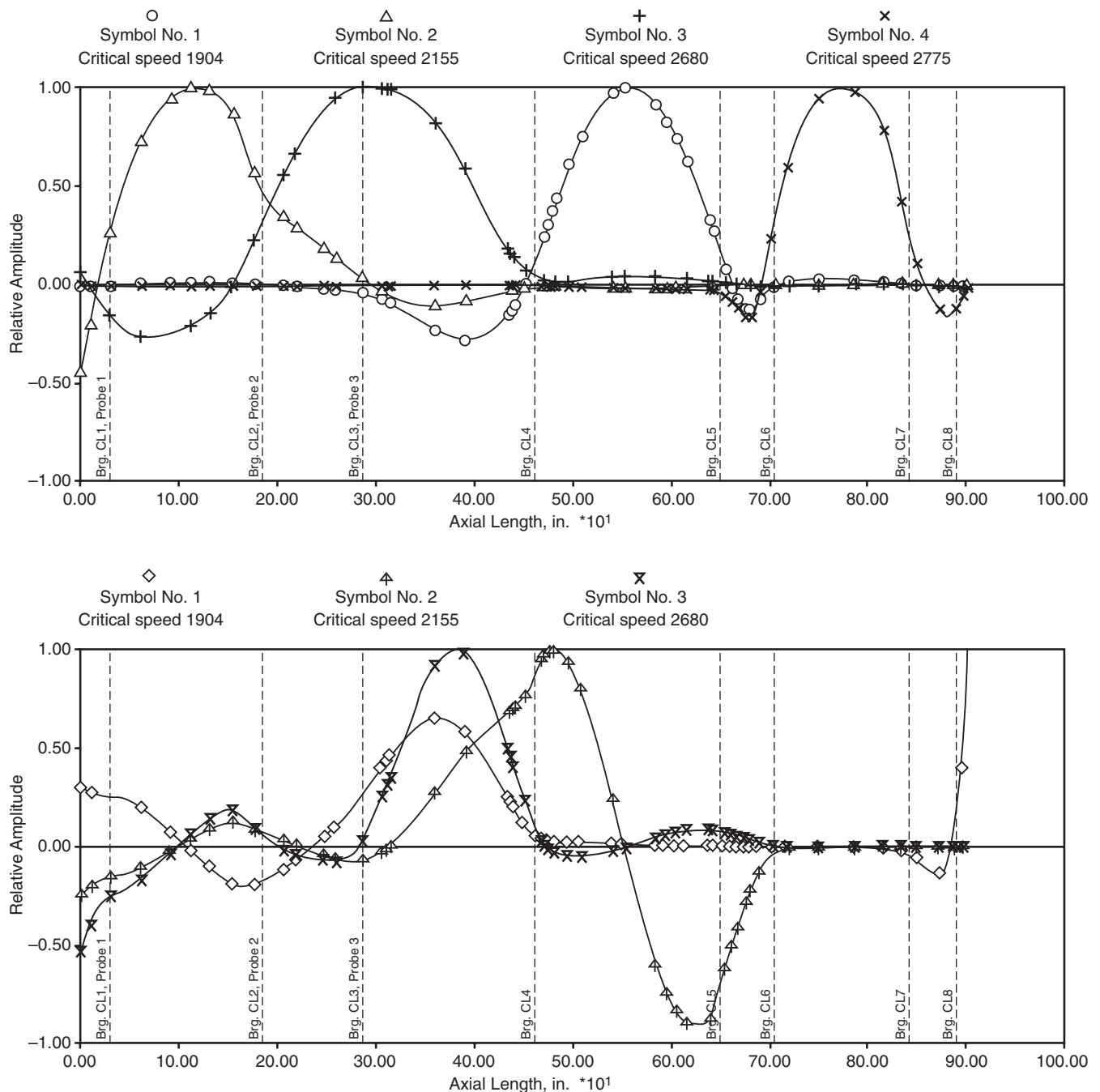


Figure 2-10—Train Lateral Mode Shapes

The lateral train analysis of geared train, if performed shall be divided into two subsystems:

1. Driver – Coupling – Gear
2. Pinion – Coupling – Driven Machine(s)

The bearing analyses of the gear and pinion are normally at the rated conditions.

Prior to performing a train lateral rotordynamic analysis, each of the unit rotordynamic analyses should be completed and acceptable. The modeling of the train consists of coupling the unit models together through the coupling. The half inertia properties as used in the unit model are no longer valid and the entire coupling including the hubs, flexible joints, and spacer are modeled instead.

2.3.8.1 Coupling Models

For flexible couplings, the hubs are assumed to be integral with the shaft ends while the flexible joints are modeled as either bending springs or equivalent beam elements. The bending stiffness is to be supplied by the coupling vendor or calculated [2,3]. The spacer is modeled as a hollow shaft (tube) using the techniques described in 2.3.2. A model using equivalent beam elements is illustrated in Figure 2-11.

Gear type couplings are modeled the same as flexible couplings except that the joints are assumed to have no bending moment transfer, and can be modeled with either zero or very low bending stiffness.

Solid flange couplings do not correspond to API 671 standards. For these couplings, the coupling hubs are assumed integral to the shaft end, and the flange portions are modeled as an equivalent beam element or bending spring. This data is either supplied by the coupling vendor, derived by finite element analysis or calculated based on either analytical or empirical methods [3,4,5,6].

Spline type couplings are typically modeled with separate radial and torsional stiffnesses at the joints [7].

2.3.8.2 Static Bearing Loads

The static bearing loads of the string are handled by superposition. That is, the load at each bearing would be the same as the uncoupled case for a multi-span system where each span is supported by two bearings. For three bearing systems, the loads are considered to be distributed as if the rotor were hinged at the center bearing, such that there is no bending moment force on the rotor at the center bearing location.

2.3.9 References:

1. Kirk R. G., Mondy R. E., Murphy R. C., “Theory and Guidelines to Proper Coupling Design for Rotor Dynamics Considerations”, *Journal of Vibration, Acoustics, Stress, and Reliability in Design*, 106, 1, pp 129-138.
2. Rothfuss N. B., “Design and Application of Flexible Diaphragm Couplings to Industrial-Marine Gas Turbines”, ASME paper 73-GT-75.
3. Johnson S. G., Rothfuss N. B., “Contoured Flexible Diaphragm Couplings”, International Conference on Flexible Couplings, 1977, Paper D1.
4. Bannister, R. H., 1980, “Methods for Modeling Flanged and Curvic Couplings for Dynamic Analysis of Complex Rotor Constructions”, *Journal of Mechanical Design*, Vol. 102, pp 130-139.
5. Young, Warren C., *Formulas for Stress and Strain*, 6th edition, McGraw-Hill Book Company, 1989, pp 434-435.
6. Tondl, A., *Some Problems of Rotordynamics*, 1965, Chapman & Hall, London.
7. Marmol, R. A., Smalley, A. J. and Tecza, J. A., “Spline Coupling Induced Nonsynchronous Rotor Vibrations”, *Journal of Mechanical Design*, Vol. 102, pp 168-176.
8. American Society for Metals, *Metals Handbook*, 9th edition, Vol. 1, pp.641
9. Childs, Dara, “Turbomachinery Rotordynamics”, John Wiley & Sons Inc., 1993, pp. 126-127.

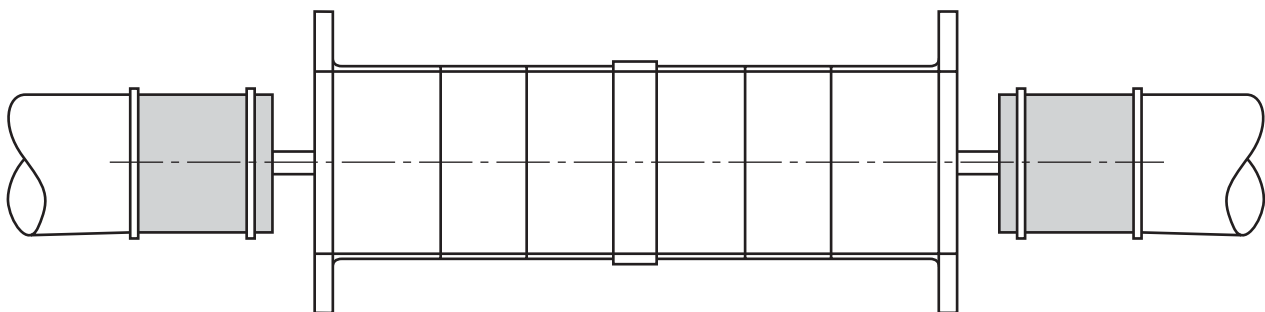


Figure 2-11—Equivalent Coupling Model

2.4 SUPPORT STIFFNESS EFFECTS

2.4.1 Introduction

The flexibility of the bearing support beyond the fluid film can dramatically alter the effective bearing stiffness and damping properties acting on the rotating shaft [1–6]. The analysis of machine vibration response based on rigid bearing supports predict critical speeds that are substantially higher than actual values [1–4]. Nicholas and Barrett [3] found that for the four rotors analyzed, neglecting support flexibility resulted in predicted first critical errors that range from 14% to 21% high and second critical errors that range from 40% to 88% high. Since rotating machinery is designed, marketed and sold, for the most part based on analytical predictions, an accurate method of easily incorporating the support flexibility effect into rotordynamic analyses is of paramount importance.

To this end, several researchers have included the effects of support flexibility into rotordynamic analyses. The method usually used is to model the supports with stiffness and damping coefficients which are constant over the entire speed range [3,7]. In most cases, the support stiffness is based on static deflections of the bearing pedestal (experimentally and/or analytically calculated). While this approach can be successfully utilized to predict both the location and amplification of rotor critical speeds [3], it will not show more than a single support or foundation resonance.

Recently, detailed models of support structures have been incorporated into rotordynamic analyses in an effort to predict the support-rotor resonance interactions. The usual approach has been to use a modal model from a finite element analysis of the structure [8,9]. Li and Gunter [8] use a component mode synthesis technique whereas Queitzsch [9] uses analytical frequency response functions (FRF) to represent the supporting structure. These methods have been proven successful, but they are time-consuming and costly.

The method proposed by Nicholas, Whalen and Franklin [1] utilizes experimental FRF data to represent the bearing support structure. The experimental data is determined from modal analysis techniques where the response of the structure to a known force is recorded. The resulting FRF data are plotted as a function of frequency. If the magnitude of the FRF function is displacement divided by the force, the resulting data is called dynamic compliance [10].

The application of experimental FRF data to rotordynamic analyses has been discussed previously [1,2,4,11]. One of the biggest advantages of this method is that the support mass is included implicitly in the FRF data along with the support stiffness [1]. The FRF data can easily be incorporated into the rotordynamic support model used in References [1,2,3,7], either as a constant dynamic stiffness over a narrow speed range or as a speed dependent dynamic stiffness over the entire speed range [1].

The modal analysis technique used in determining the dynamic compliance data is detailed herein and in Reference [1]. The data can then be employed in a forced response rotordynamic analysis, using various levels of flexible support model sophistication. Example results are compared to actual test stand speed amplitude plots from a steam turbine running on the test stand with a known midspan unbalance.

2.4.2 Flexible Support Model

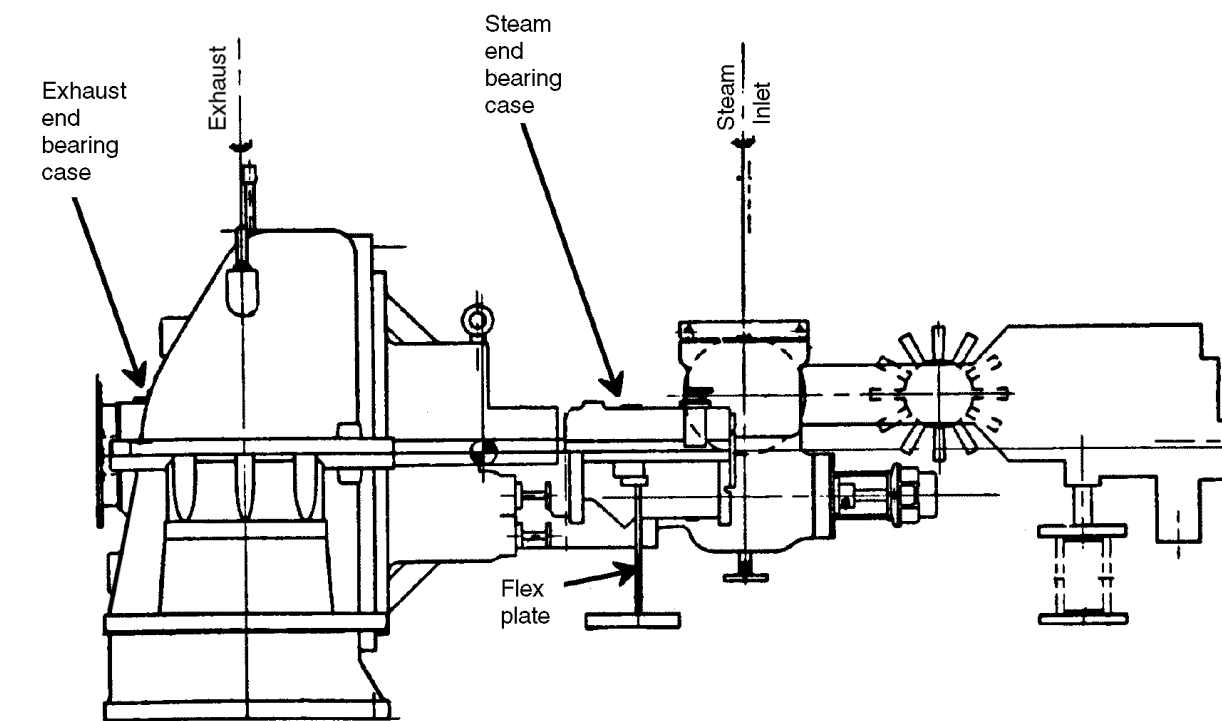
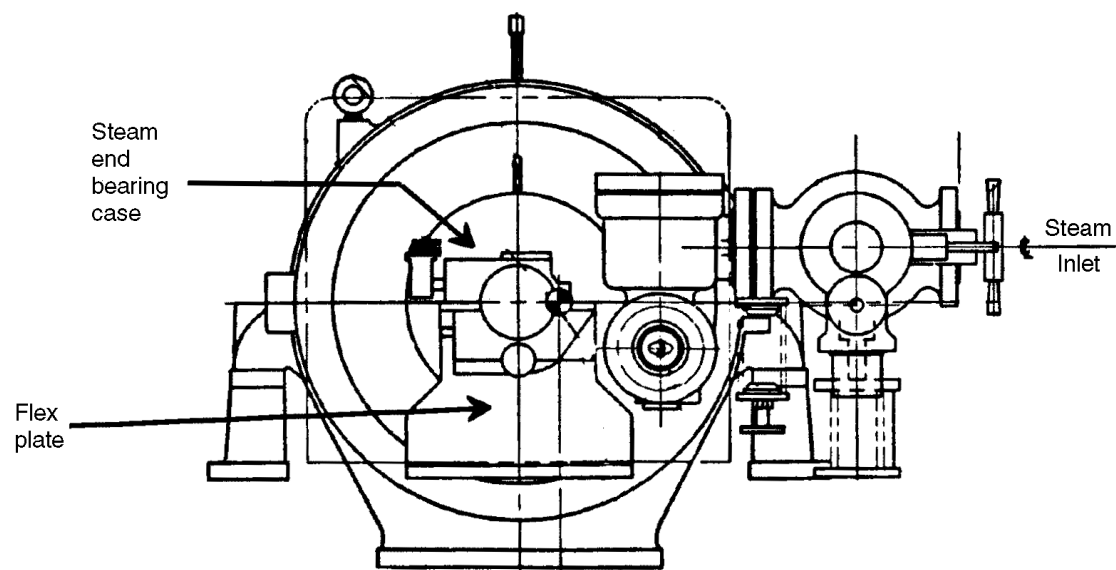
A typical outline drawing of a steam turbine case is shown in Figure 2-12. The steam end bearing is housed in a bearing case that is supported by a flex plate to allow for axial thermal expansion. The exhaust end bearing case is supported within the exhaust casing which sits on two sets of thick horizontal plates with gussets for added stiffness. These plates along with the flex plate are attached to the baseplate.

A model for this complex support is illustrated in Figure 2-13. The first level of flexibility is the bearing fluid film which is represented by eight principal (xx,yy) and cross-coupled (xy,yx) stiffness and damping coefficients. For tilting pad bearings, the second level of flexibility is the pad [6] and the pad pivot [12]. This effect may be accounted for in the tilting pad bearing analysis [3,6,11,12]. The next level of flexibility is everything past the pad pivot. This includes the bearing case, the supporting plates and the baseplate. Again, the support may be modeled by eight principal and cross-coupled stiffness and damping coefficients along with the support mass.

Further support model simplification for tilting pad journal bearings is shown in Figure 2-14. The single support mass with two degrees of freedom model illustrated in Figure 2-13 is reduced to two single degrees of freedom (SDOF) support spring-mass-damper systems in both the horizontal X and vertical Y directions. The X and Y direction equations are uncoupled since the cross-coupled terms are zero or near zero for tilting pad bearings. For illustrative purposes, only the Y direction is considered in Figure 2-14, but an identical system also exists in the X direction.

The Y displacement shown in Figure 2-14 is the absolute rotor response; Y_1 is the support or pedestal response and $Y - Y_1$ is the relative rotor response. Since most vibration probes are mounted on the bearing case to monitor shaft motion, it is the relative response that is of primary importance for correlation purposes.

From Figure 2-14, the bearing stiffness and damping are combined with the support mass, stiffness and damping to yield an equivalent support model. In this model, the bearing stiffness and damping, K_b and C_b , are functions of the shaft rotational speed, ω . The equivalent support properties are also speed dependent while the support stiffness and damping, K_s and C_s , may be constant or speed dependent. The details of combining the support and bearing properties for tilt pad bearing with no cross-coupling terms are shown in [1,3].

**Side View****View from Steam End****Figure 2-12—Steam Turbine Support Schematic**

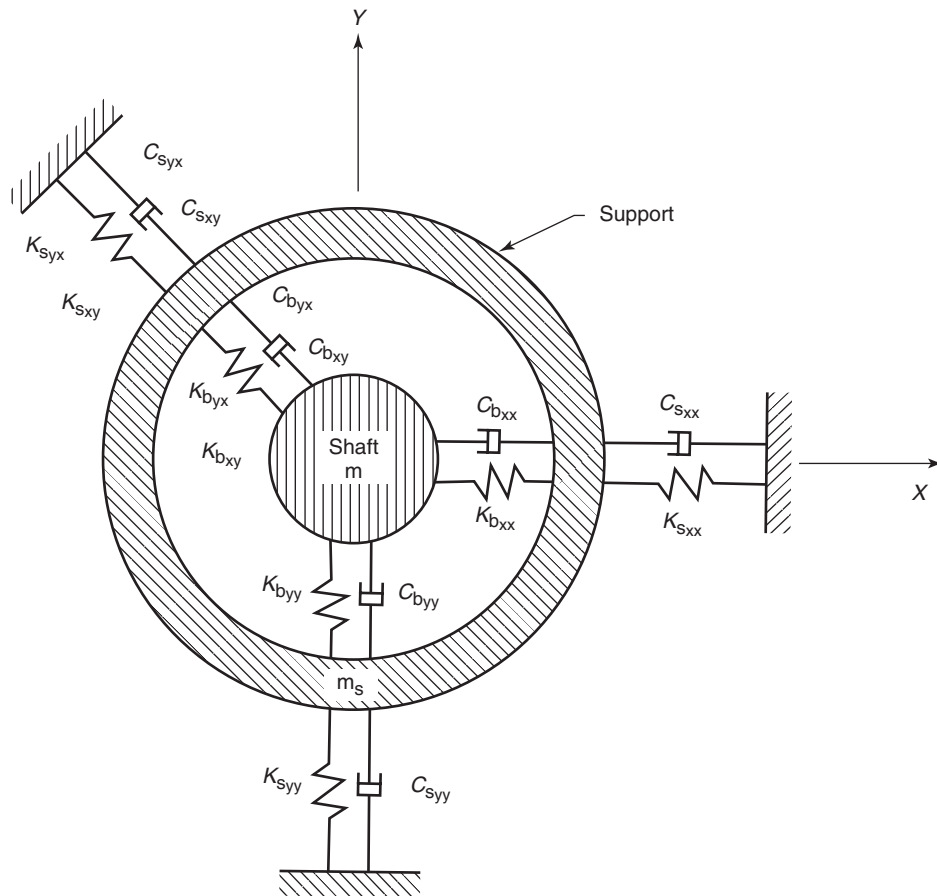


Figure 2-13—Journal Bearing Fluid Film and Flexible Support Model

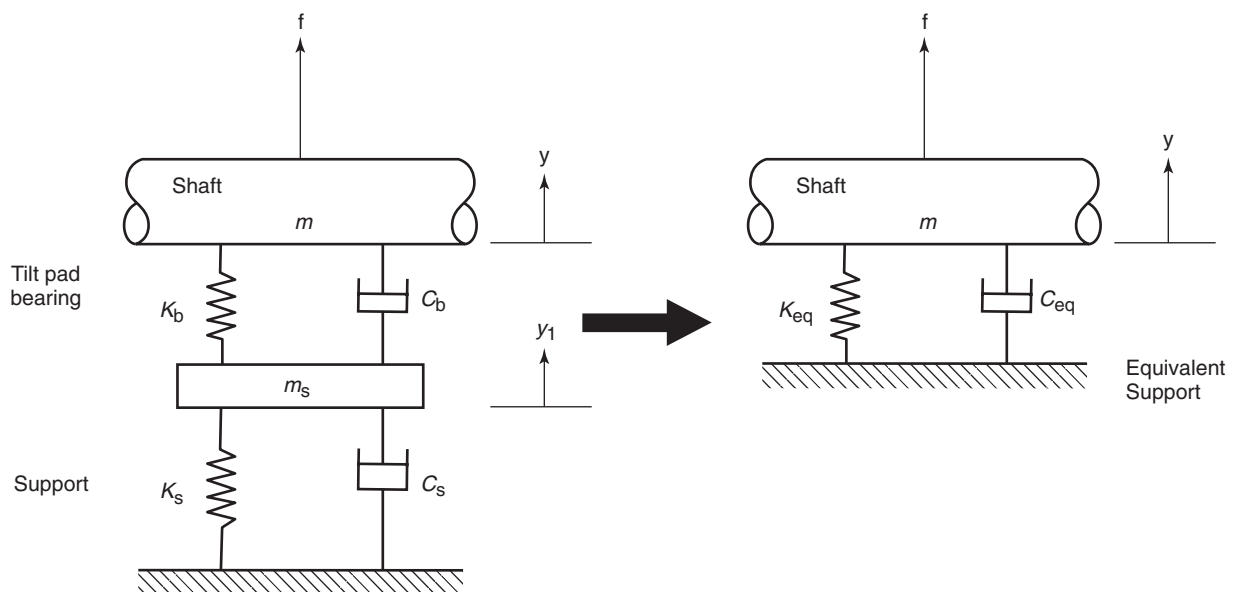


Figure 2-14—Single Degree of Freedom Flexible Support Model

However, bearing cross-coupling can easily be incorporated into the model. Furthermore, support cross-coupling is usually set to zero. However, the modeling techniques outlined by Barrett, Nicholas and Dhar [4] or by Vazquez, Barrett and Flack [5] can easily consider support cross-coupling in the horizontal and vertical directions as well as cross-coupling from one support to another.

To summarize, the bearing oil film stiffness and damping properties are calculated with or without the effect of pad and/or pivot flexibility. These characteristics are then combined with the SDOF support systems' stiffness, mass, and damping properties via the equations in References [1] and [3]. These calculations yield equivalent stiffness and damping coefficients that may then be used directly in rotordynamic response and stability computer programs.

2.4.3 Dynamic Support Stiffness

In order to determine the stiffness and damping properties of an actual bearing support, a frequency or spectral analyzer may be utilized. A block diagram of the test system is illustrated in Figure 2-15. An impact hammer is used to

excite the bearing case at the bearing centerline. An internal load cell registers the force imparted on the bearing case by the hammer.

Mounted on the case at the bearing centerline is an accelerometer that senses the case motion that results from the impact force. The acceleration is double integrated and the resulting displacement is divided by the force from the impact hammer. This integration and division, calculated over a specified frequency range, is the compliance FRF, which is complex, containing both amplitude and phase information.

An example compliance FRF plot is shown in Figure 2-16 for a steam turbine case. The exhaust end vertical compliance results from a vertically mounted accelerometer sensing vertical acceleration from a vertical excitation (principal compliance). Two different excitation sources are shown: an impact hammer and an electromagnetic exciter or shaker. Note that for frequencies below 200 Hz (12,000 cpm), both excitation sources give very nearly identical results. The impact hammer offers the advantage of being significantly quicker to set up and conduct the actual dynamic compliance testing.

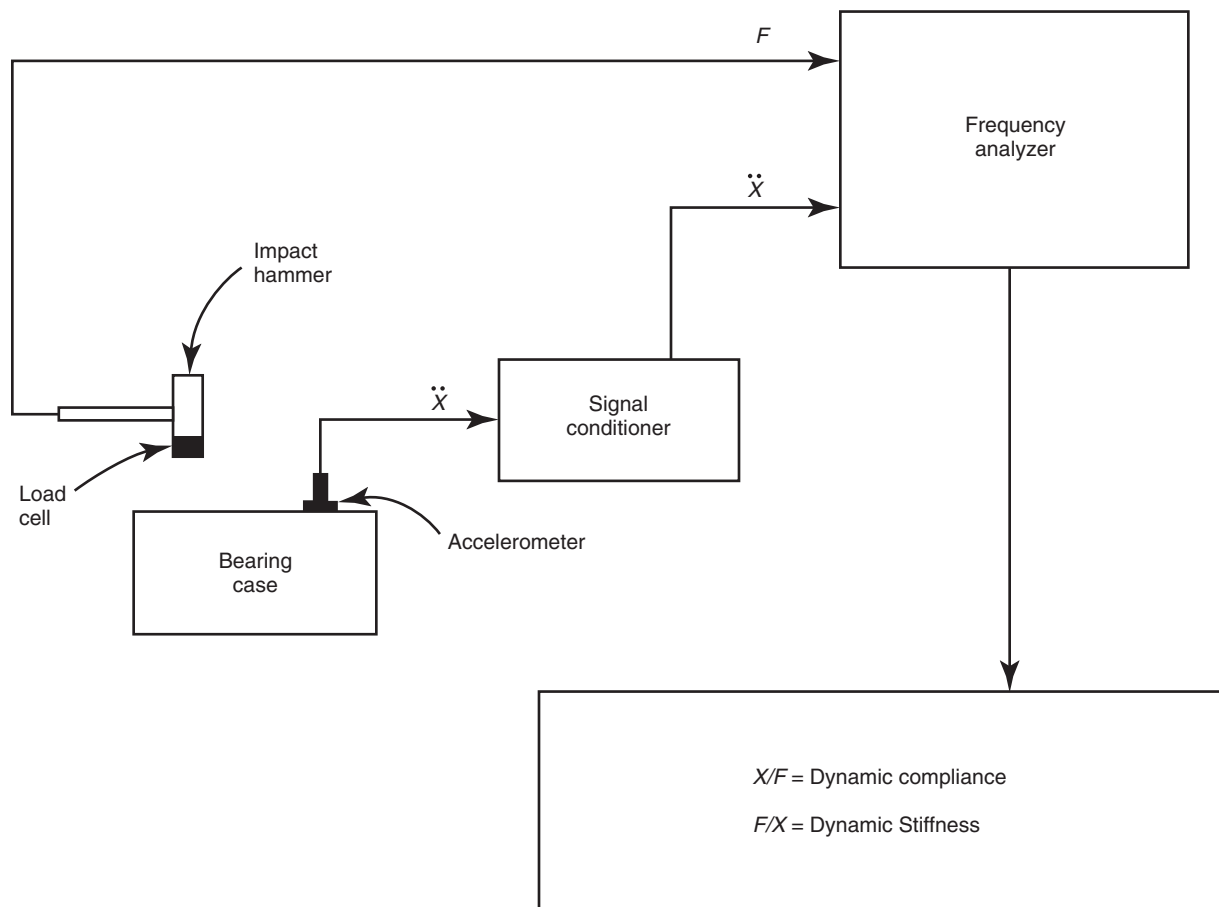


Figure 2-15—Dynamic Stiffness Analysis Diagram

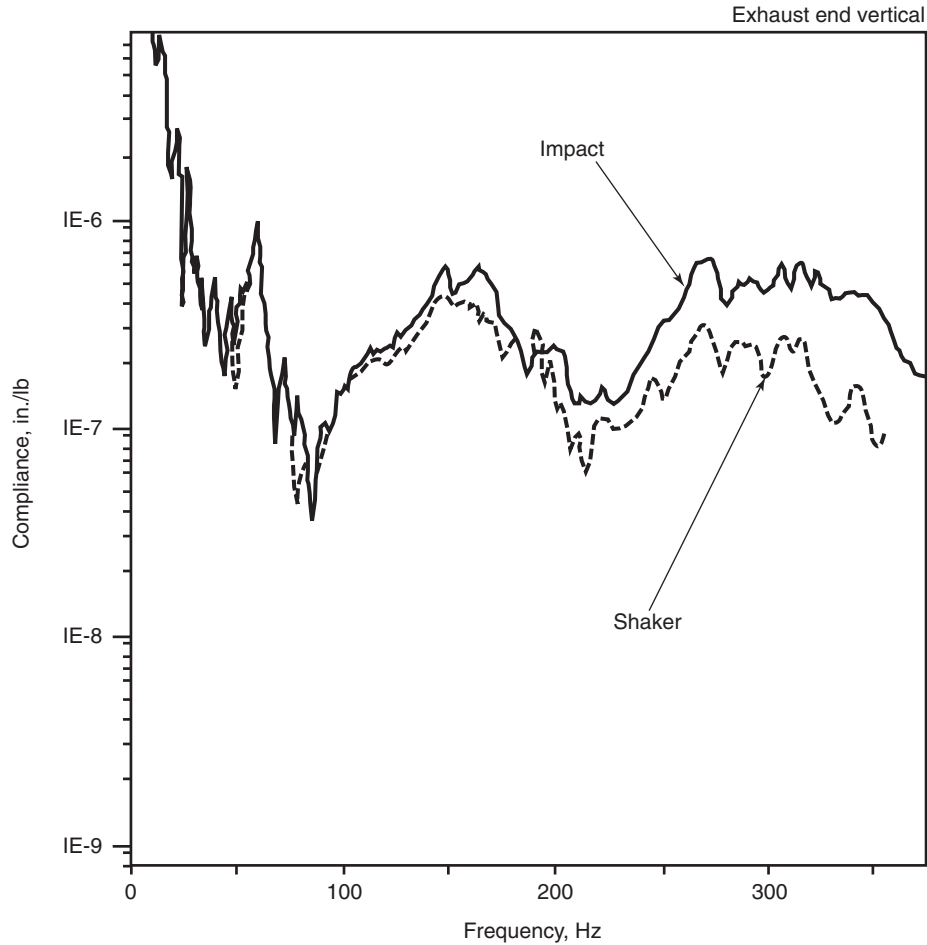


Figure 2-16—Exhaust End Dynamic Compliance Plots

The compliance plot in Figure 2-16 plots the *magnitude* of the complex compliance FRF. Since the support model discussed previously (Figure 2-14) uses two SDOF spring-mass-damper systems per bearing case, it is appropriate to examine the compliance FRF for a SDOF system [1,10].

The magnitude of the complex compliance is

$$|\alpha(\omega)| = \frac{|X|}{|F|} = \frac{1}{\sqrt{(K_s - m_s\omega^2)^2 + (C_s\omega)^2}} \quad 2-1$$

where

F = applied force, N (lbf),

X = resulting displacement, m (in.).

Inverting

$$K_D = \frac{|F|}{|X|} = \sqrt{(K_s - m_s\omega^2)^2 + (C_s\omega)^2} \quad 2-2$$

Thus, for small support damping, the dynamic stiffness becomes:

$$K_D = K_s - m_s\omega^2 \quad 2-3$$

2.4.4 Forced Response Correlation

A nine stage 1,097 kg (2,418 lbm) steam turbine rotor was tested with 16,560 g-mm (23 oz-in.) of unbalance placed at the center wheel rim. The rotor, operating on 5-pad tilting pad bearings with 127 and 102 mm (5.0 and 4.0 in.) diameter journals on the exhaust and steam ends respectively, was run up to a trip speed of 6,150 rpm.

The resulting speed-amplitude plot is shown in Figure 2-17 for the steam end probes (see Reference [1] for the exhaust end probe plots). The probes, which are mounted on the bearing case, are clocked 45° from top-dead-center and are referred to as “right probe” and “left probe.” From Figure 2-17, both probes exhibit split or dual first critical speed peaks. Split critical speeds often indicate strong support interaction with the rotor-bearing system. Figure 2-18 shows a phase-amplitude plot for the exhaust end right probe. The inner loop at 2,872 rpm also indicates strong support interaction.

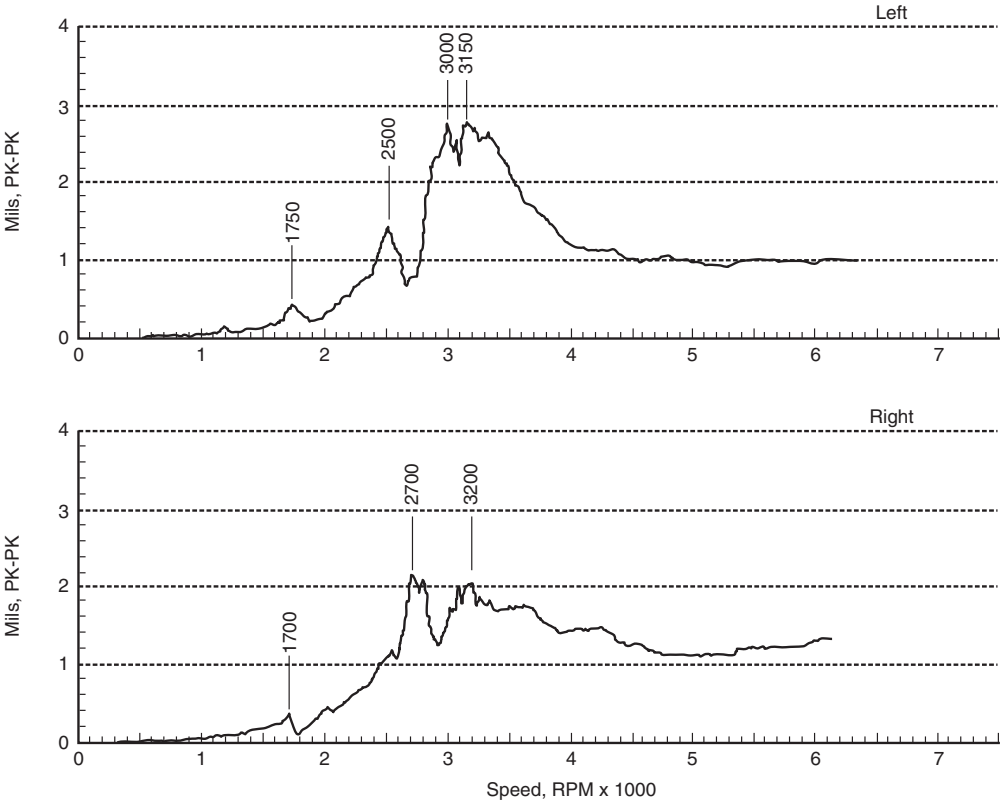
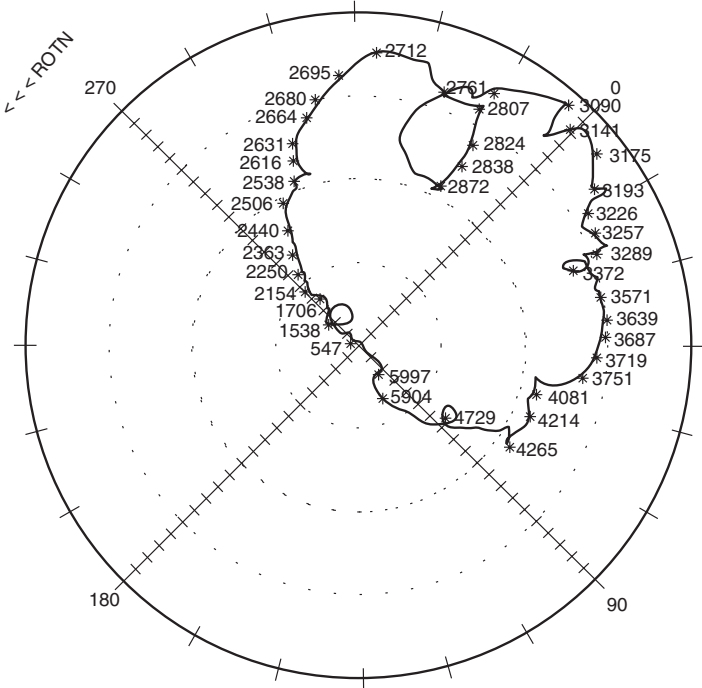


Figure 2-17—Steam End Test Stand Response



POLAR PLOT—EXHAUST END RIGHT PROBE

Full Scale Amp = 2 Mils, PK-PK Amp per Div = 0.1 Mils, PK-PK

Figure 2-18—Exhaust End Test Stand Response

In an effort to accurately predict the actual turbine response plot of Figure 2-17, inclusion of the dynamic support flexibility is required. The simplest flexible support model that can be employed is to use the identical spring-mass-damper support system over the entire speed range, for both bearing cases and for both the horizontal and vertical directions [1,2,3]. Values for the spring-mass-damper system can be calculated from the compliance FRF plots. A plot for the exhaust end bearing case, horizontal direction, is shown in Figure 2-19. From Equation 2-3, with small support damping, the dynamic stiffness contains not only the support stiffness, K_s , but also the support mass, m_s . However, K_s and m_s need not be determined explicitly as the value for K_d may be used directly in the equivalent support equations [1].

The dynamic stiffness, K_d , for the exhaust end horizontal location is picked off of Figure 2-19 at 3,000 cpm (near the critical speed in question). The dynamic stiffness for the steam end horizontal, steam end vertical and exhaust end vertical locations may be determined in the same manner. Thus, the constant stiffness model is employed by using the actual K_d values from each of the four dynamic compliance plots.

While it is not necessary, for simplicity, a single, average value for the four locations may be used. This type of constant stiffness model has been successful in accurately predicting the location and amplification of the first and second critical speeds [2,3]. Different models should be used for each critical in question as the dynamic compliance can be significantly different in the vicinity of the first critical speed compared to the second or the third critical speeds. Thus, separate forced response runs should be made with the different SDOF support models to locate each critical speed.

In an attempt to predict the split critical peak frequencies of Figure 2-17, a more sophisticated model is devised where multiple SDOF spring-mass-damper systems are used to represent the supports over the entire speed range. The model approximations are illustrated in Figure 2-20 on the steam end horizontal compliance FRF curve. As indicated in the figure, the dynamic compliance curve is approximated as a series of straight lines. The dynamic stiffness along with the frequency is tabulated for all points where the straight lines intersect. These data are then used as flexible support input parameters in the forced response computer program.

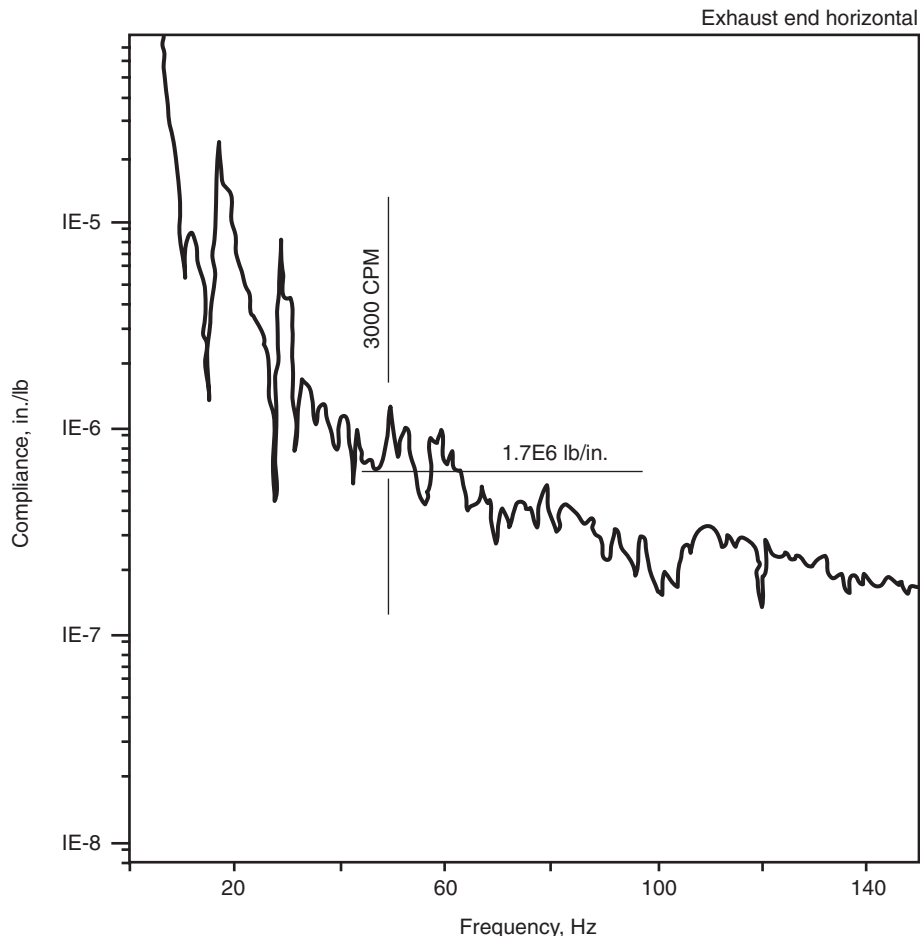


Figure 2-19—Exhaust End Constant Stiffness Support Model

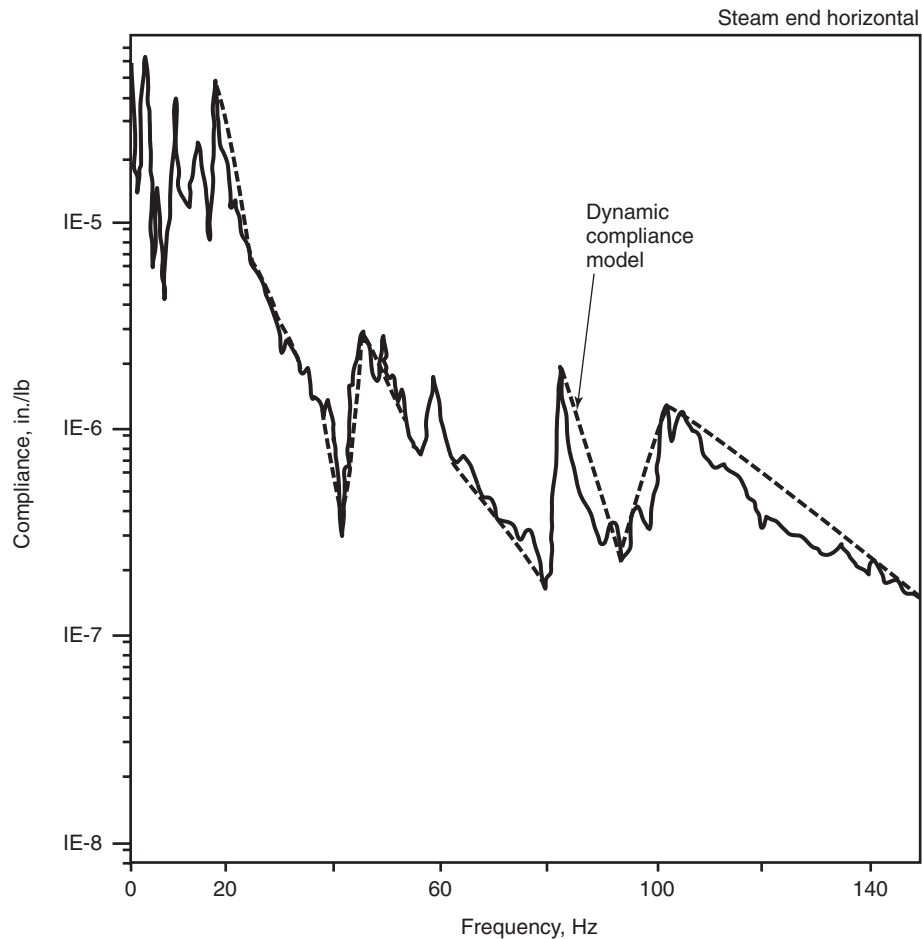


Figure 2-20—Steam End Dynamic Compliance Support Model

Thus, a different SDOF spring-mass-damper support system is used for every speed increment in the response program. Linear interpolation is used for all speeds between the input speeds.

The *relative* probe-to-shaft forced response plot for the steam end probes using this dynamic compliance model is shown in Figure 2-21. (see Reference [1] for the exhaust end probe plots). Figure 2-21 predicts a split critical for the left probe at 2,925 cpm and 3,100 cpm, which correlates very closely to the actual values of 3,000 cpm and 3,150 cpm from Figure 2-17. The predicted right probe split critical peaks are at 2,700 cpm and 3,225 cpm, with a support resonance peak at 3,675 cpm. Actual right probe split critical peaks are at 2,700 cpm and 3,200 cpm. The predicted 3,675 cpm support resonance is more evident on the right exhaust end probe, where the actual support resonance speed is 3,600 cpm [1].

In conclusion, for the example presented, modeling each bearing support as two SDOF systems and utilizing impact hammer compliance FRF data produces excellent analytical

forced response correlation with actual test stand results. Using the constant stiffness model, the location of the first critical speed is accurately predicted. However, the split critical peaks are not evident. Using many SDOF spring-mass-damper systems over the operating speed range (dynamic compliance model) results not only in an accurate first critical speed prediction, but the split critical peaks are also evident along with one of the support resonances.

2.4.5 References

1. Nicholas, J. C., Whalen, J. K. and Franklin, S. D., 1986, "Improving Critical Speed Calculations Using Flexible Bearing Support FRF Compliance Data," *Proceedings of the Fifteenth Turbomachinery Symposium*, Texas A&M University, College Station, Texas, pp. 69-78.
2. Nicholas, J. C., 1989, "Operating Turbomachinery on or Near the Second Critical Speed in Accordance with API Specifications," *Proceedings of the Eighteenth Turboma-*

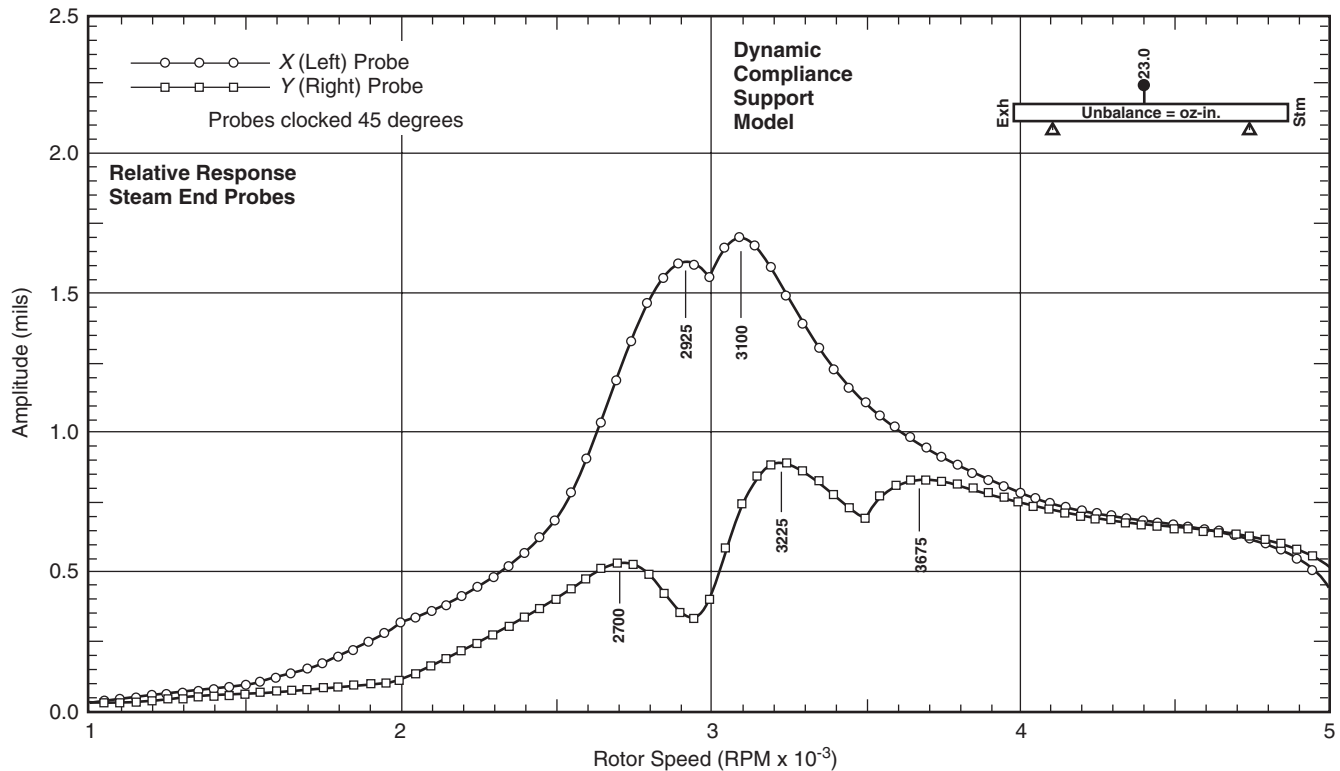


Figure 2-21—Steam End Analytical Results, Dynamic Compliance Model

- chinery Symposium, Texas A&M University, College Station, Texas, pp. 47-54.
3. Nicholas, J. C. and Barrett, L. E., 1986, "The Effect of Bearing Support Flexibility on Critical Speed Prediction," *ASLE Transactions*, 29 (3), pp. 329-338.
4. Barrett, L. E., Nicholas, J. C. and Dhar, D., 1986, "The Dynamic Analysis of Rotor-Bearing Systems Using Experimental Bearing Support Compliance Data," *Proceedings of the 4th International Modal Analysis Conference*, Union College, Schenectady, New York, II, pp. 1531-1535.
5. Vazquez, J. A., Barrett, L. E. and Flack, R. D., 2001, "A Flexible Rotor on Flexible Bearing Supports: Stability and Unbalance Response," *ASME Journal of Vibration and Acoustics*, 123 (2), pp. 137-144.
6. Lund, J. W. and Pedersen, L. B., 1986, "The Influence of Pad Flexibility on the Dynamic Coefficients of a Tilting Pad Journal Bearing," *ASME Journal of Tribology*, 109 (1), pp. 65-70.
7. Kirk, R. G. and Gunter, E. J., 1972, "The Effect of Support Flexibility and Damping on the Synchronous Response of a Single Mass Flexible Rotor," *ASME Journal of Engineering for Industry*, 94 (1), pp. 221-232.
8. Li, D. F. and Gunter, E. J., 1982, "Component Mode Synthesis of Large Rotor Systems," *ASME Journal of Engineering for Power*, 104 (2), pp. 552-560.
9. Queitzsch, G. K., 1985, "Forced Response Analysis of Multi-Level Rotor Systems with Substructure," Ph.D. Dissertation, University of Virginia.
10. Ewins, D. J., 1984, *Modal Testing: Theory and Practice*, Letchworth, Hertfordshire, England, Research Studies Press.
11. Caruso, W. J., Gaus, B. E. and Catlow, W. G., 1982, "Application of Recent Rotor Dynamics Developments to Mechanical Drive Turbines," *Proceedings of the Eleventh Turbomachinery Symposium*, Texas A&M University, College Station, Texas, pp. 1-17.

12. Nicholas, J. C. and Wygant, K. D., 1995, "Tilting Pad Journal Bearing Pivot Design for High Load Applications," *Proceedings of the Twenty-Fourth Turbomachinery Symposium*, Texas A&M University, College Station, TX, pp. 33-47.

2.5 JOURNAL BEARING MODELING

2.5.1 Introduction

Fluid film journal bearings play a key role in determining the rotordynamic characteristics of rotating machinery. Their stiffness and damping properties influence the location and severity of the rotor's critical speeds and the stability characteristics of the rotor-bearing system. Because of this key role, bearing modeling is critical in accurate rotordynamic predictions.

Furthermore, accurate bearing modeling is essential in determining the bearing's oil flow requirements as well as its operating temperatures. Designing a bearing to perform dynamically is not good enough as it is also necessary that the bearing operate at reasonable temperatures for prolonged life.

Determining the static or steady state (temperature and oil flow) and dynamic (stiffness and damping) properties of a fluid film bearing is difficult as the governing hydrodynamic pressure equation, Reynold's equation, is a second order nonlinear differential equation which must be solved using numerical methods such as the finite difference or the finite element methods. However, computer codes are readily available that perform these calculations along with, in some advanced codes, solving the energy equation and the elasticity equation (see 2.5.4.1). Additionally, computational results have been compared to experimental results with a fair degree of accuracy (see 2.5.4.8).

In the following sections, many different journal bearing designs are discussed along with some of the key parameters available to the bearing designer that have a profound affect on rotordynamics. Several popular fixed geometry sleeve bearing designs are included (see 2.5.3). Tilting pad journal bearings are addressed in detail including a comprehensive discussions of many of the important tilting pad bearing geometric variables that are available to the bearing designer for improved rotordynamic behavior (see 2.5.4.2).

2.5.2 Stiffness and Damping Properties

Figures 2-22 and 2-23 display exaggerated views of an operating fixed geometry journal bearing. Note that the operating position of the journal is located below the bearing centerline. In most of the top half of the bearing, the oil film is cavitated because the thickness of the oil film is divergent (increases in the direction of shaft rotation) in this area. In most of the bottom half of the bearing, the film thickness converges (decreases in the direction of shaft rotation) so a pressurized oil film wedge forms to support the rotating journal.

Note that for the journal to attain a steady state equilibrium position in the bearing, the oil film forces (integrated pressures) must balance in both the horizontal and vertical directions. For this reason, for fixed geometry journal bearings the rotating shaft does not displace solely in the vertical downward ($-Y$) direction but also displaces sideways in the positive horizontal ($+X$) direction. The steady state operating position is most often measured by analyzing the DC gap of local eddy current displacement probes.

The displacement of the journal from the center of the bearing is a nonlinear function of the applied load and journal speed. Thus, the bearing's oil film stiffness coefficients (rate change of force with displacement), K_{xx} , K_{xy} , K_{yx} and K_{yy} , are also nonlinear functions of the journal's equilibrium position. The bearing's damping coefficients (rate change of force with velocity) generated by the bearing are similarly nonlinear functions of the journal's equilibrium position. Thus, the bearing's damping coefficients, C_{xx} , C_{xy} , C_{yx} and C_{yy} , are not solely dependent on the bearing geometry, but also on the applied bearing load and the rotational speed of the journal. The differences in the bearing dynamic characteristics with bearing type and applied load can make a great difference in the lateral rotordynamic characteristics of a given machine.

In order to establish the influence that bearings have on the dynamic characteristics of a rotor system, the linearized bearing dynamic coefficients are calculated based on small perturbations in displacement and velocity from the journal's equilibrium position. Many effects must be considered including the effect of heat generation due to fluid shearing in the film, fluid turbulence, variation in oil supply temperatures, and so on.

Linearized stiffness is examined in Figure 2-24 using a simple spring-mass system. Perturbing the mass by a small $+X$ displacement results in a restoring force in the $-X$ direction. If the spring stiffness, K , is linear, then $K = -F/x$ for all values of the displacement, x . If the spring stiffness is nonlinear, then $K = -F/x$ only holds for small values of x since F was initially determined via a small $+X$ displacement.

Expanding this concept to a fluid film bearing becomes somewhat more complicated. From Figure 2-25, a small $+X$ displacement or perturbation not only results in a $-X$ restoring force called the direct horizontal stiffness, K_{xx} , but it also creates a force in the vertical Y direction resulting in a cross-coupled stiffness, K_{yx} . The net modeling result is a set of eight (four stiffness and four damping) linearized hydrodynamic bearing coefficients. They are linear as it is assumed that the stiffness value remains proportional to the displacement regardless of the magnitude of the displacement. In truth, these forces are nonlinear. Thus, the resulting dynamic coefficients are said to be good for "small displacements about equilibrium." In other words, these linearized coefficients are valid for small vibrational motion about the steady state operating position. For large shaft displacements or shaft

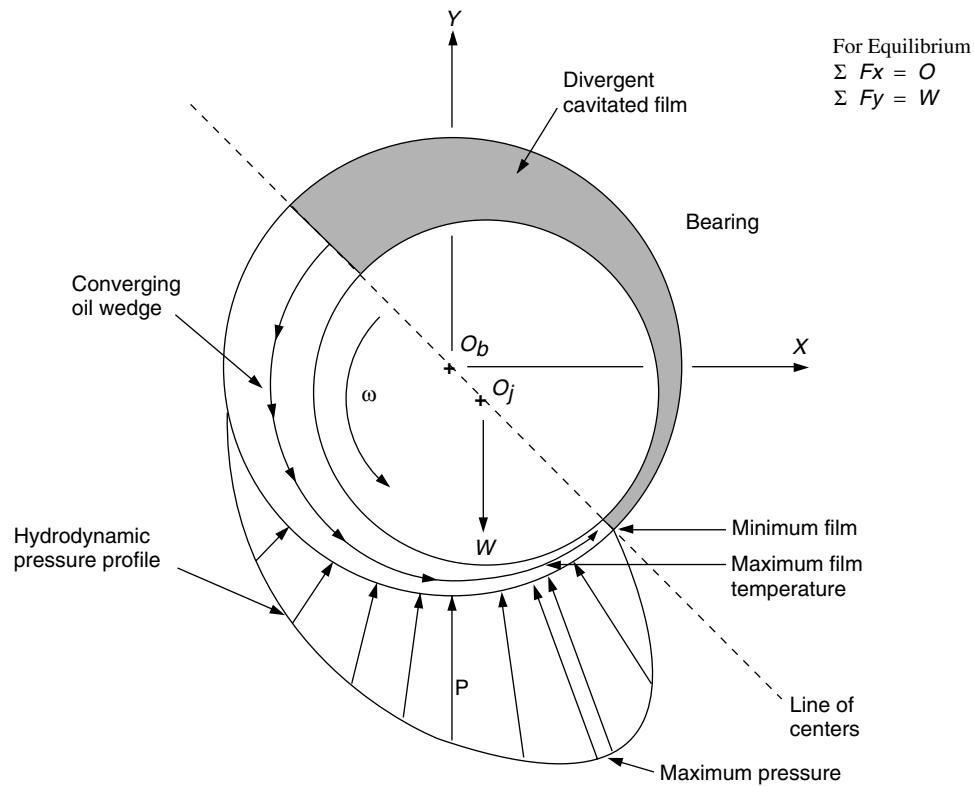


Figure 2-22—Journal Bearing Hydrodynamic Film

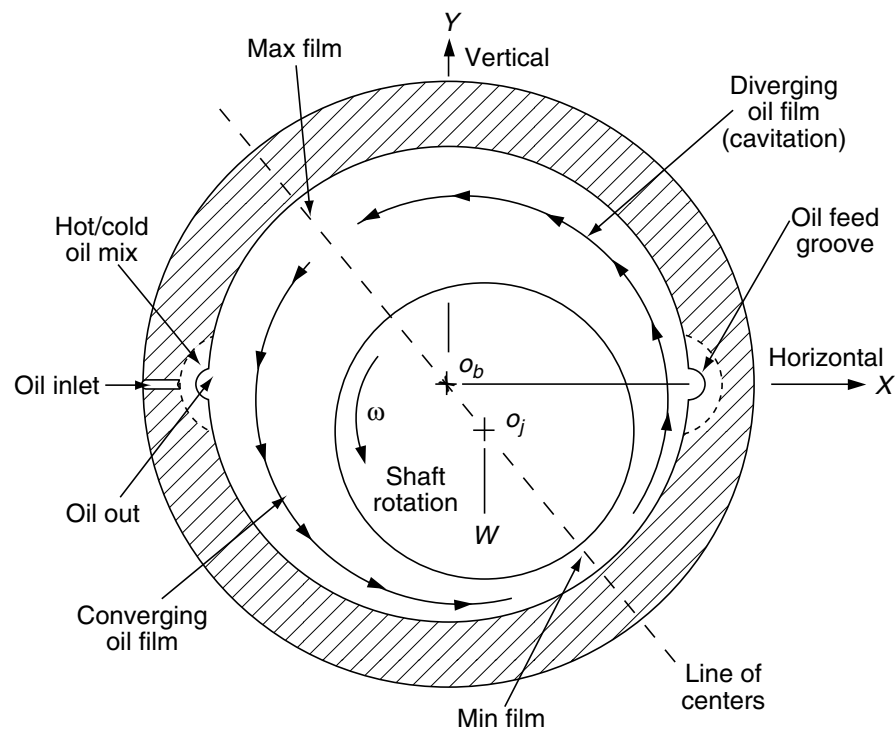


Figure 2-23—Two Axial Groove Bearing

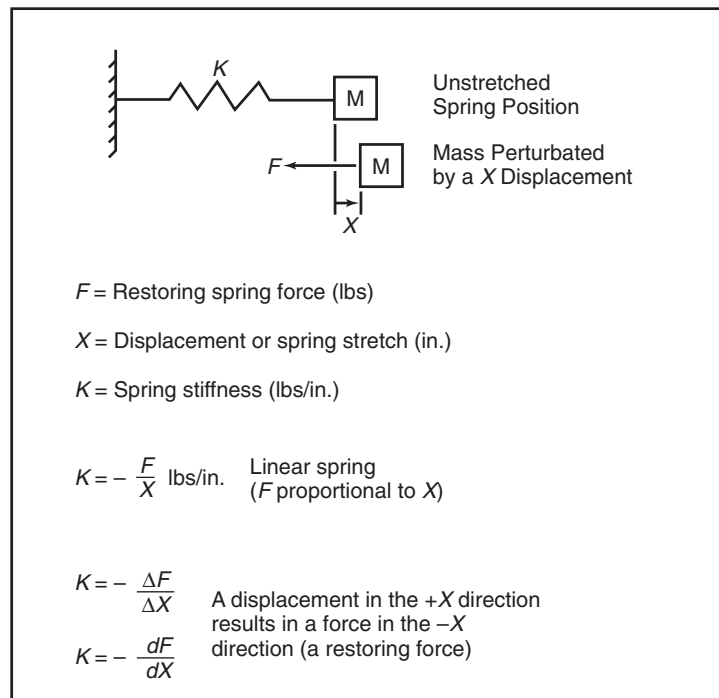


Figure 2-24—Spring Stiffness

vibration (roughly above 80% of the bearing clearance) the bearing's nonlinear effects would become important.

2.5.3 Fixed Geometry Journal Bearings

2.5.3.1 Introduction

Fixed geometry or sleeve bearings have the annoying property of creating an excitation force that can drive the rotor unstable by creating a subsynchronous vibration. This phenomena usually occurs at relatively high rotor speeds and/or light bearing loads, or, more generally, at high Sommerfeld Numbers (see 3.2.1). The problem is that sleeve bearings (i.e., all journal bearings excluding tilting pad bearings) support a resultant load with a displacement that is not directly in line with the resultant load vector but at some angle with rotation from the load vector. This angle can approach 90° for light loads and high speed which results in high cross-coupling forces that may drive the rotor unstable. This subject is discussed in detail in 3.3.2.

2.5.3.2 Axial Groove Bearings

Axial groove bearings, sometimes called plain sleeve bearings, have a cylindrical bore with typically 2-to 4-axial oil feed grooves. Figure 2-23 illustrates a 2-axial groove design. These bearings are very popular in relatively low speed equipment. For a given bearing load magnitude and orientation, the stability characteristics of axial groove bearings are primarily controlled by the bearing clearance. Tight clearances produce higher instability thresholds but tight clearance

bearings present other problems that make them undesirable. For example, as clearance decreases, the bearing's operating oil temperature increases. Furthermore, babbitt wear during repeated start-ups will increase the bearing's clearance thereby degrading stability. In fact, many bearing induced instabilities in the field are caused by bearing clearances that have increased due to wear from oil contamination, repeated starts or slow-rolling with boundary lubrication.

One method of increasing the instability threshold speed of a 2-axial groove bearing is to place a circumferential oil relief track or groove in the bottom half of the bearing (see the bottom pad in Figures 2-26 and 2-27). The relief track removes some of the bearing's load carrying capacity thereby forcing the bearing to operate at a higher eccentricity ratio. While adding a circumferential groove to the lower half of a 2 axial groove bearing is a popular field fix for a bearing induced instability, care must be taken before this is attempted. This fix should not be attempted for large bearing unit loads (above $L_u = 100$ psi).

2.5.3.3 Pressure Dam Bearings

Because of the limitations of grooving the lower half of an axial groove bearing to increase stability, another fixed-bore anti-whirl bearing design is desirable that is easily manufactured, relatively insensitive to design tolerances, and available for quick retrofits in existing 2-axial groove bearing inserts. The pressure dam bearing falls into this category (Figures 2-26 and 2-27, Nicholas and Allaire [1]). The details of the surface inside the pocket are of secondary importance since the

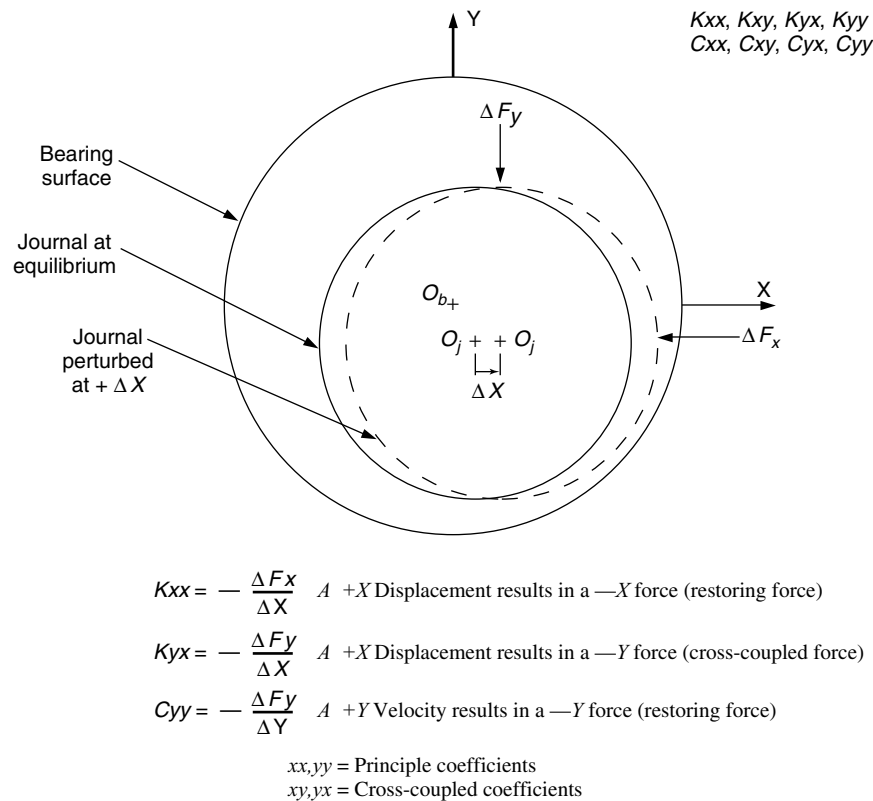


Figure 2-25—Journal Bearing Stiffness and Damping

side lands hold the flow and the pressure. The hydrodynamic load created by the pocket provides the increased margin of stability for step bearings compared to plain bearings. Finally, the tolerance on the pocket depth is not as critical as lobe clearance tolerances for multi-lobe bearings.

Pressure dam or step journal bearings have long been used to improve the stability of turbomachinery as replacements for plain journal or axial groove bearings. In many cases, these bearings provide a quick and inexpensive fix for machines operating at high speeds near or above the stability threshold. For example, a plain cylindrical axial groove bearing can easily be removed from a machine displaying subsynchronous vibration. Milling a step in the top pad of the proper size and location may be all that is necessary to eliminate the stability problem. This is much less expensive and faster than installing tilting pad bearings that may require a change in the bearing housing.

Most pressure dam bearings have two oil supply grooves located in the horizontal plane as shown in Figure 2-26. For a downward directed load (negative y-direction) corresponding to a portion of the rotor weight, a pocket is cut in the upper half of the bearing with the end of the pocket (the step or dam) located in the second quadrant for counter-clockwise

shaft rotation. The pocket has side lands to hold the pressure and flow as shown in Figure 2-27. A circumferential relief groove or track is sometimes grooved in the bottom half of the bearing as illustrated in Figures 2-26 and 2-27. Both of these effects (dam and relief track) combine to increase the operating eccentricity of the bearing compared to a plain cylindrical bearing.

At high Sommerfeld numbers (light loads and/or high speeds), the axial groove journal bearing's eccentricity ratio approaches zero and the journal runs centered in the bearing. This condition leads to unstable operation. However, the pressure dam bearing eccentricity either approaches some minimum value or increases as the Sommerfeld number increases due to the effect of the stepped pocket. At high speeds and/or light loads, the step creates a loading that maintains a minimum operating eccentricity. That is, as speed is increased, the bearing eccentricity does not approach zero as it would for axial groove bearings. The eccentricity approaches some minimum value or may even increase with increasing speed due to the step loading. Thus, a properly designed step bearing would operate at a moderate eccentricity ratio even at high Sommerfeld numbers. This condition helps to stabilize the pressure dam bearing in the high Sommerfeld number range.

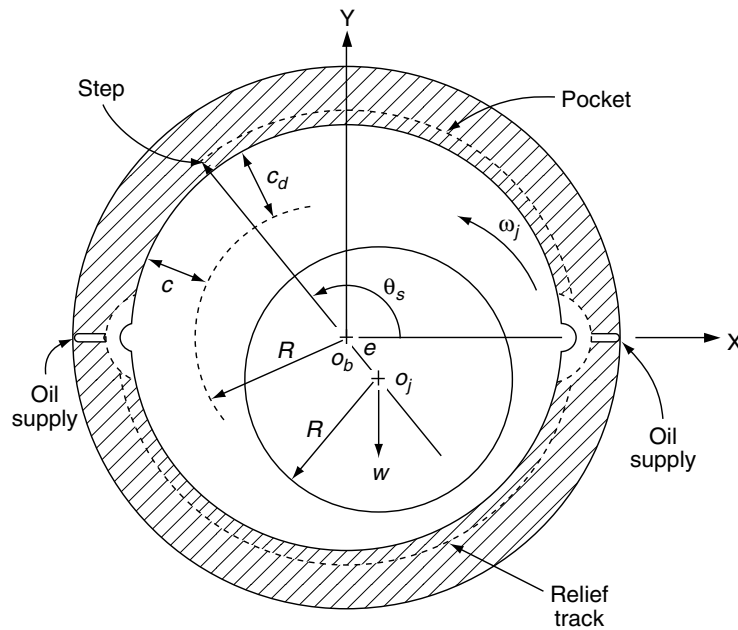


Figure 2-26—Pressure Dam Bearing

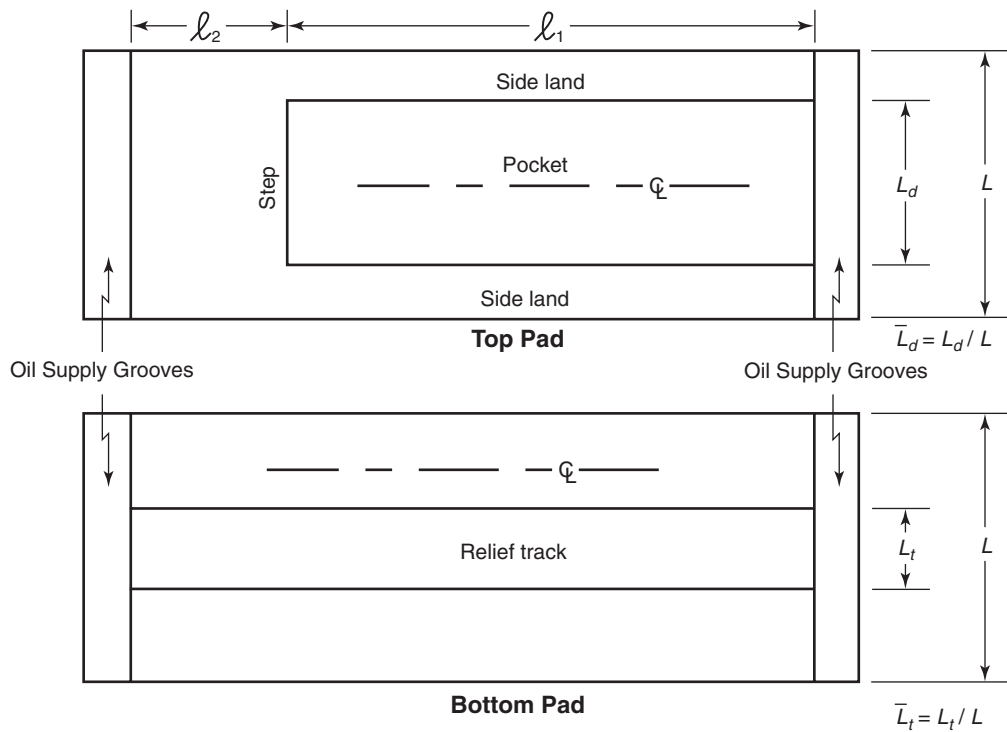


Figure 2-27—Pressure Dam Bearing—Top and Bottom Pads

Many rotors used in the rotating equipment industry operate on vendor installed or retrofitted pressure dam bearings. The most common applications are steam turbines and gear boxes. In high speed gear boxes, the gear loading may vary from several thousand pounds at 100% load to only a few

hundred pounds at partial load. This large variance in load is often accompanied by a change in load direction. A pressure dam bearing example in gearbox application may be found in 3.8.5.

While the pressure dam or step journal bearings will not solve all rotordynamic instability problems, it remains an extremely effective, low cost anti-whirl bearing. If near optimum clearance ratios and step locations are used [1], many oil whirl instabilities may be eliminated with pressure dam bearings.

2.5.3.4 Elliptical Bearings

A popular field fix for an unstable sleeve bearing is to elliptize a circular bore by placing a 1.0, 2.0 or even a 3.0 mil shim at top-dead-center between the bearing insert and housing. This has the effect of crushing the insert and reducing the vertical bearing clearance thereby increasing the bearings instability threshold speed. Note that if there is 1.0 mils of looseness between the existing insert and the bearing housing, a 2.0 mil shim is necessary for 1.0 mils of insert of crush.

Two axial groove bearings are also machined elliptical and supplied in new equipment often with their horizontal clearance equal to twice the vertical clearance. An elliptical or “lemon bore” bearing is illustrated in Figure 2-28. It is essentially a 2-axial groove bearing with a slightly tighter vertical clearance and a more open horizontal clearance. This type of bearing is very popular in Europe and is the standard sleeve bearing design of at least one major European compressor manufacturer. It is also used in the United States with at least one large domestic motor-generator manufacturer utilizing this design. Elliptizing a pressure dam bearing for improved stability characteristics is also possible, Mehta, et. al. [2].

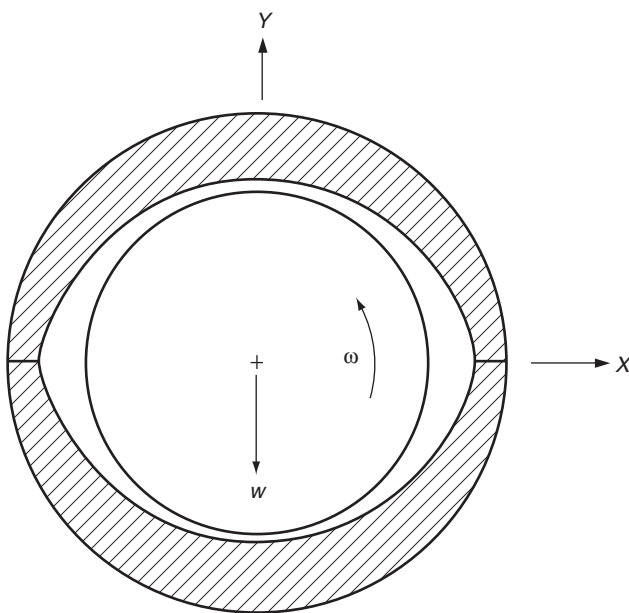


Figure 2-28—Elliptical Bearing

2.5.3.5 Offset Half Bearings

Another method to stabilize a 2-axial groove bearing is to offset the bore usually at the horizontal split. An offset half bearing is shown in Figure 2-29. This bearing is also very popular in Europe. Offsetting a pressure dam bearing is also possible for improved stability, Mehta, et. al. [3].

2.5.3.6 Taper Land Bearings

Taper land bearings (Figure 2-30) are also very popular sleeve bearings that are successful in increasing the instability threshold speed compared to cylindrical sleeve bearings. The taper land bearing has side lands similar to a pressure dam and thus is a pocket bearing. Care must be taken when using this design in heavy load applications as load capacity may be a problem, Nicholas and Kirk [4]. Taper land bearings are very frequently utilized in small, light rotors operating at high speeds such as small turbo-expanders, cryogenic expanders and turbochargers.

2.5.3.7 Multi-Lobe Bearings

Multi-lobe bearings, Flack and Lanes [5,6], do not have side lands. The elliptical bearing is a 2-lobe multi-lobe bearing. The lobes are always preloaded as a zero preloaded multi-lobe bearing is simply an axial groove bearing. Note that for fluid film journal bearings, preload relates the geometric ratio of bore radius to pad radius, not to an actual preload force. Preloading each lobe provides a converging film thus producing a hydrodynamic force regardless of bearing

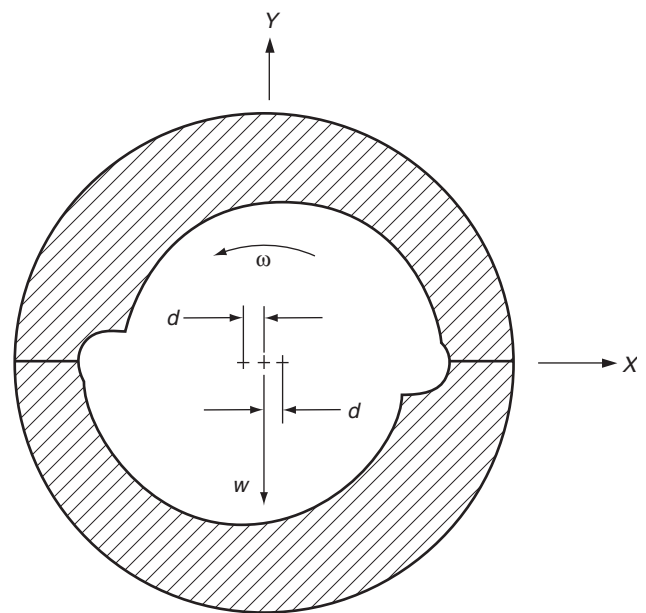


Figure 2-29—Offset Half Bearing

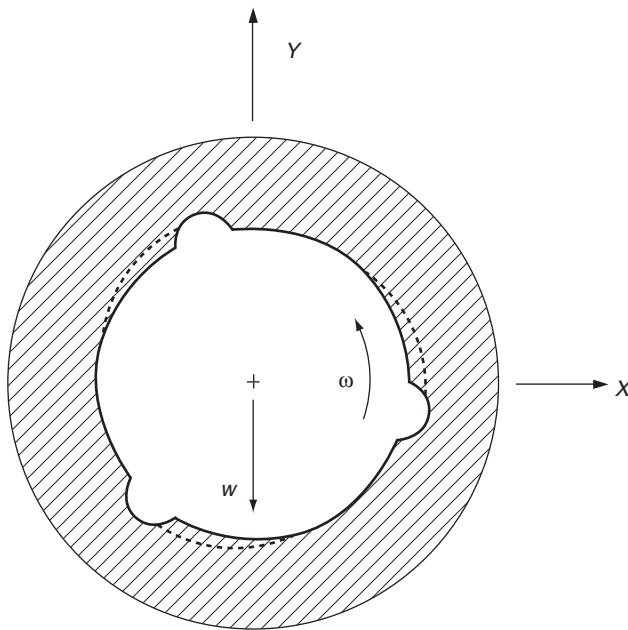


Figure 2-30—Taper Land Bearing with Three Tapered Pockets

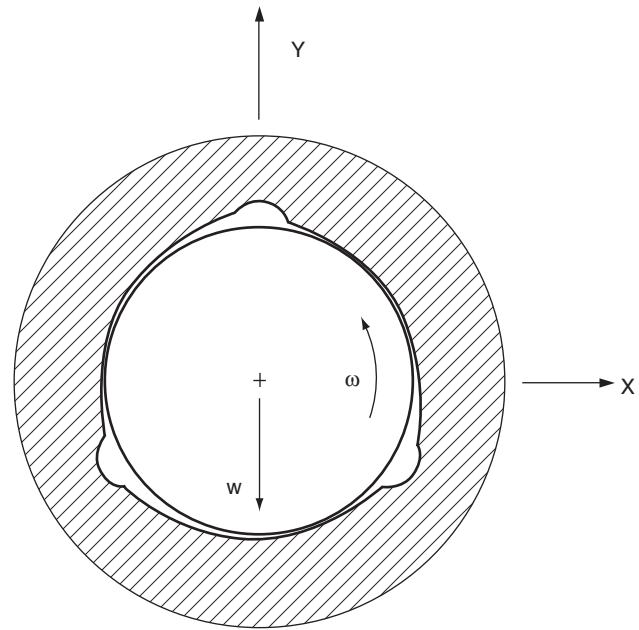


Figure 2-31—Multi-Lobe Bearing with Three Preloaded, Offset Lobes

load or journal operating position. Preload is discussed in detail in 2.5.4.2. The lobes can also be offset with the minimum lobe clearance located at some angle with rotation from the center of the lobe as in Figure 2-31.

2.5.3.8 References

1. Nicholas, J. C. and Allaire, P. E., 1980, "Analysis of Step Journal Bearings—Finite Length, Stability," *ASLE Transactions*, 23 (2), pp. 197-207.
2. Mehta, N. P., Singh, A., Gupta, B. K., 1981, "Stability of Finite Elliptical Pressure Dam Bearings with Rotor Flexibility Effects", *ASLE Transactions*, 24 (2), pp. 269-275.
3. Mehta, N. P. and Singh, A., 1986, "Stability Analysis of Finite Offset-Halves Pressure Dam Bearings", *ASME Journal of Tribology*, 108 (2), pp. 270-274.
4. Nicholas, J. C. and Kirk R. G., 1981, "Theory and Application of Multi-Pocket Bearings for Optimum Turborotor Stability," *ASLE Transactions*, 24 (2), pp. 269-275.
5. Flack, R. D. and Lanes, R. F., 1982, "Effects of Three-Lobe Bearing Geometries on Rigid-Rotor Stability", *ASLE Transactions*, 25 (2), pp. 221-228.
6. Lanes, R. F. and Flack, R. D., 1982, "Effects of Three-Lobe Bearing Geometries on Flexible Rotor Stability", *ASLE Transactions*, 25 (3), pp. 377-385.

2.5.4 Tilting Pad Journal Bearings

2.5.4.1 Historical Perspective

The state-of-the-art in tilting pad journal bearing design and analysis has advanced tremendously in the last 50 years, spawned by the landmark paper by Jorgen Lund in 1964 [1]. Lund's paper, *Spring and Damping Coefficients for the Tilting-Pad Journal Bearing*, was the first major published document that contained tilting pad journal bearing stiffness and damping coefficients. Furthermore, his paper presented the innovative analytical methodology that Lund used to determine these dynamic characteristics. His analytical procedure is commonly known as "Lund's pad assembly method."

Prior to 1964, tilting pad journal bearing studies consisted of steady-state analyses which were limited to determining load capacity and power loss. For many years, the only analysis available was detailed in a 1953 paper by Boyd and Raimondi [2]. A pivoted flat slider on a flat runner was used to determine results which roughly approximated the special case of the bearing assembled clearance equal to the tilting pad machined-in clearance (i.e., zero pad preload). With no knowledge of the dynamic characteristics, they concluded that tilting pad bearings offer "No striking advantages over plain journal bearings...." A second paper by the same authors in 1962 expanded their analysis in an attempt to include preloaded pads by approximating the actual pad radius of curvature by adding a crown to the pivoted slider [3].

Lund's pad assembly method calculates the stiffness and damping contribution of each individual pad of a tilting pad journal bearing by considering each pad as a partial arc bearing. "A summation over all pads results in the combined spring and damping coefficients for the complete tilting-pad journal bearing" [1]. The inertia of the pad was included in the analysis. Lund utilized the finite difference method for the partial arc Reynolds equation solution. Stiffness and damping design curves were presented for assembled tilting pad journal bearings with 4, 5, 6 and 12 centrally pivoted pads.

Orcutt [4] extended the work of Lund with the inclusion of turbulence in a paper published in 1967. Using Lund's pad assembly method, a 4-pad tilting pad journal bearing was analyzed and design plots presented.

Nicholas, Gunter and Allaire, 1979 [5], employing the finite element method to determine the single pad dynamic data, utilized Lund's pad assembly method to present stiffness and damping design curves for assembled 5-pad tilting pad bearings of varying pad preloads, pivot offsets and pivot load orientations. Nicholas, Gunter and Barrett, 1978 [6], used the data in [5] to show the effects of pad preload, pivot offset and pivot loading on the stability of an 11 stage centrifugal compressor.

Jones and Martin, 1979 [7], also utilized the pad assembly method along with the finite difference method to produce steady state and dynamic properties of 5-pad centrally pivoted bearings including the effects of turbulence. Furthermore, while using an isoviscous solution for the partial arc single pad analysis, their model allowed for different temperatures on each pad. They compared their results to experimental data and to the analytical results from [5] and from Shapiro and Colsher, 1977 [8].

In Reference [8], the authors discuss the fact that, since the pads of a tilting pad journal bearing tilt, each pad adds a degree of freedom to the journal bearing system. Thus, for a 5-pad bearing, there are 7 degrees of freedom (the x,y journal motion and the 5 tilt modes of the pads). This results in a 7×7 stiffness and a 7×7 damping matrix. These 7×7 matrices may be reduced to standard 4×4 matrices by assuming a pad excitation frequency. The design curves presented in Lund's 1964 paper [1] are based on synchronous frequency as does the reduced data in References [4, 5, 6, 7]. Reference [8] presents two sets of full 7×7 stiffness and 7×7 damping matrices for a 5-pad bearing with zero and 50% pad preload along with the reduced 4×4 data for a synchronous frequency, called synchronously reduced coefficients. The authors also present the equations for reducing full stiffness and damping matrices that include pad tilt degrees of freedom to reduced 4×4 matrices.

Other authors [9–12] have investigated the frequency dependency of the reduced tilting pad bearing characteristics starting with Parsell, Allaire and Barrett in 1983 [9] and

continuing with Wygant in 2001 [12]. This subject is addressed in detail in 3.3.3.1.

Also starting in the late 1980s, more advanced tilting pad journal bearing codes were developed which did not treat the pads as independent partial arc bearings. Instead, the steady state and dynamic operating characteristics were determined with a global, fully assembled analysis [13–18].

The first example of this development was presented by Knight and Barrett, 1988 [13]. They solved Reynolds equation using the finite element method for a fully assembled tilting pad bearing assuming a parabolic axial pressure profile. Their methodology includes the solution of a first order energy equation with constant axial and approximate radial temperature profiles. The authors found the journal equilibrium position by iterating on the imposed load, leading edge boundary conditions, journal temperature, pad rotation angles and the coupled pressure (Reynolds) and energy equations.

Branagan, 1988 [14], used similar axial pressure and temperature approximations but included pad and pivot elasticity effects when solving for the dynamic properties of a fully assembled tilting pad journal bearing including pad tilt. Other authors followed in the 1990s solving the Reynolds equation with the energy equation and the elasticity equation for the assembled bearing [15–18]. All three equations are iteratively coupled. For example, Kim, Palazzolo and Gadangi [17] check the convergence on the pad tilt angles, journal eccentricity, shaft temperature, fluid film temperature, pad temperatures, pad deformations and drain temperature at each iterative step.

A more detailed discussion concerning the historical development of tilting pad journal bearing analytical tools may be found in Nicholas [19].

2.5.4.2 Geometric Properties

One advantage of tilting pad bearings is the many design parameters that are available for variation [6, 20, 21]. These including pad load orientation, pivot offset, pad preload and pad axial length.

2.5.4.3 Pad Orientation

First, consider pivot or pad load orientation. The load between pivot configuration is shown in Figure 2-32. Directing the resultant loading between pivots provides more symmetric stiffness and damping coefficients, Nicholas and Kirk [20]. Symmetric support properties provide circular orbits whereas asymmetric supports cause elliptical orbits. Circular orbits are preferable for synchronous response attenuation since, in general, their vibration amplitudes are smaller going through a critical compared to the major axis of an elliptical orbit. However, the asymmetry associated with the load on pivot configuration often provides superior stability characteristics.

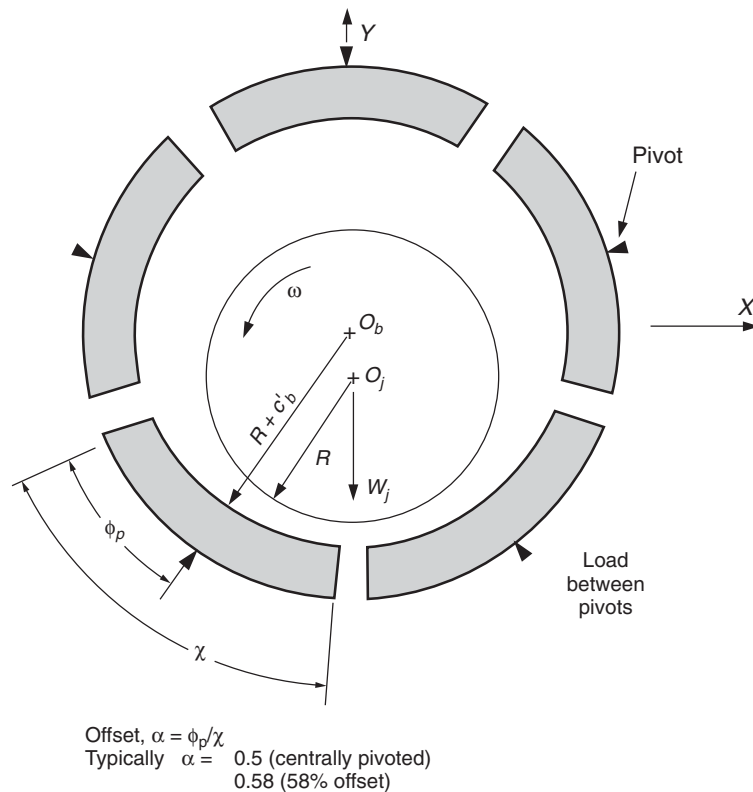


Figure 2-32—Five-pad Tilting Pad Bearing Schematic

2.5.4.4 Pad Pivot Offset

Another tilting pad parameter available to the bearing designer is pad pivot offset. Referring to Figure 2-32, the pad pivot offset is defined as

$$\alpha = \frac{\phi_p}{\chi} \quad 2-4$$

For centrally pivoted pads, $\alpha = 0.5$ (50% offset). Typical offset pivot values range from $\alpha = 0.55$ to $\alpha = 0.6$ (55 to 60% offset).

Offset pivots are very popular with thrust bearings as offsetting the pivot increases the operating film thickness thereby decreasing the operating temperature (i.e., offset pivots increase bearing load capacity). For tilt pad journal bearings, offset pivots also increase load capacity [5,21] which results in lower journal bearing operating temperatures. Also, offset pivots increase bearing stiffness, especially K_{xx} , compared to centrally pivoted pads [5]. Finally, offsetting the pad pivot makes the tilting pad journal bearing unidirectional.

2.5.4.5 Pad Preload

Possibly the most important tilting pad bearing parameter available to the bearing designer is tilting pad bearing preload

[6,19–21]. A geometric parameter, not an actual load, tilting pad bearing preload is defined as

$$m = 1 - \left(\frac{c_b}{c_p} \right) \quad 2-5$$

For zero preload, the pad machined-in clearance equals the assembled bearing clearance ($c_p = c_b$). When the bearing and journal centers coincide, the journal-to-pad radial clearance at any circumferential location along the pad is constant and equal to the bearing radial clearance (Figure 2-33).

For a preloaded pad, the pad clearance is greater than the bearing clearance ($c_p > c_b$). Typical preload values range from 0.0 to 0.5 (0% to 50%). When a pad is preloaded, a converging film section exists even if the journal runs centered in the bearing (Figure 2-34). Thus, the pad will continue to produce hydrodynamic forces as the bearing load approaches zero. A pad with a negative preload is illustrated in Figure 2-35.

The biggest advantage of reducing the tilting pad preload to near zero is illustrated in Figure 2-36 [20]. For this tilt pad bearing example, as preload decreases, bearing damping increases while bearing stiffness remains approximately constant. Both of these trends help in increasing the bearing's effective damping. This trend generally holds for a majority of turbomachinery applications.

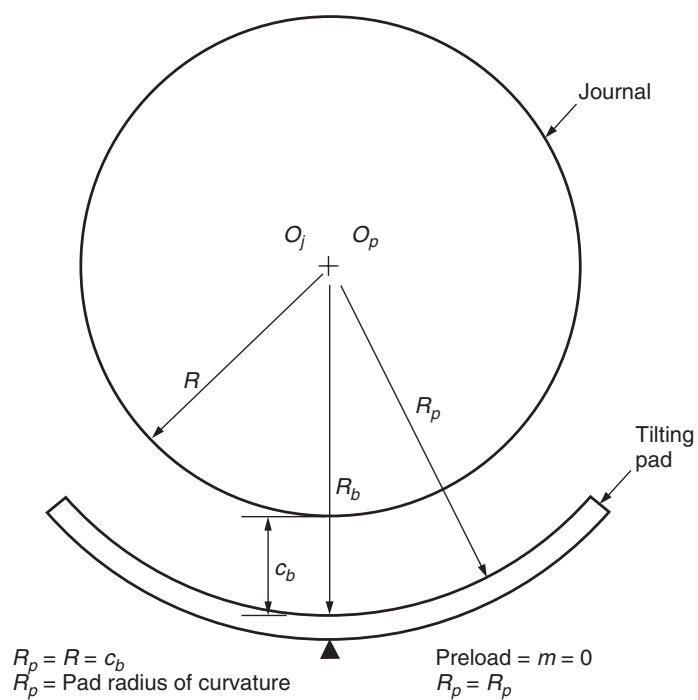


Figure 2-33—Zero Preloaded Pad

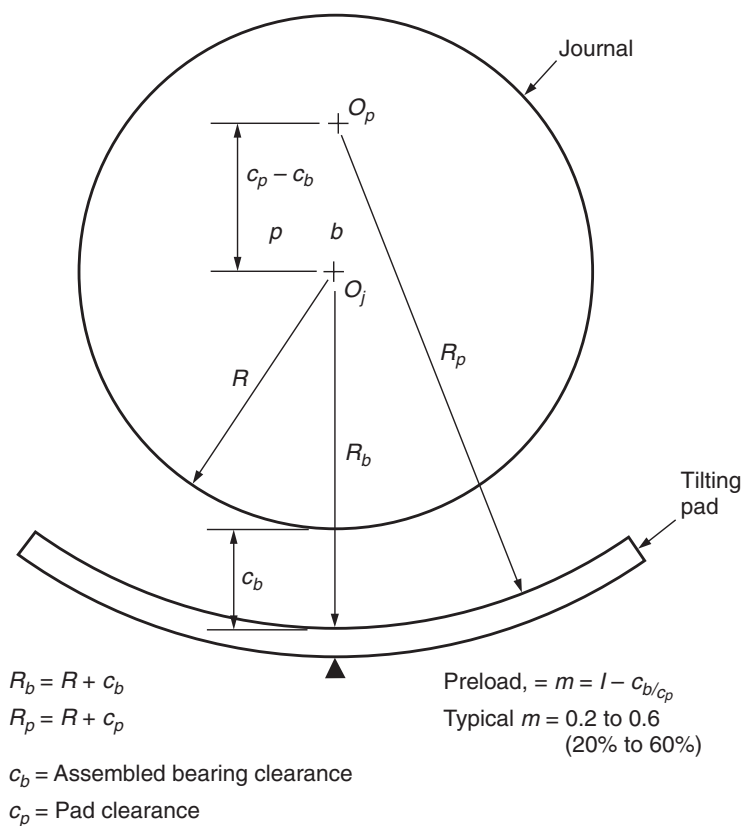


Figure 2-34—Preloaded Pad

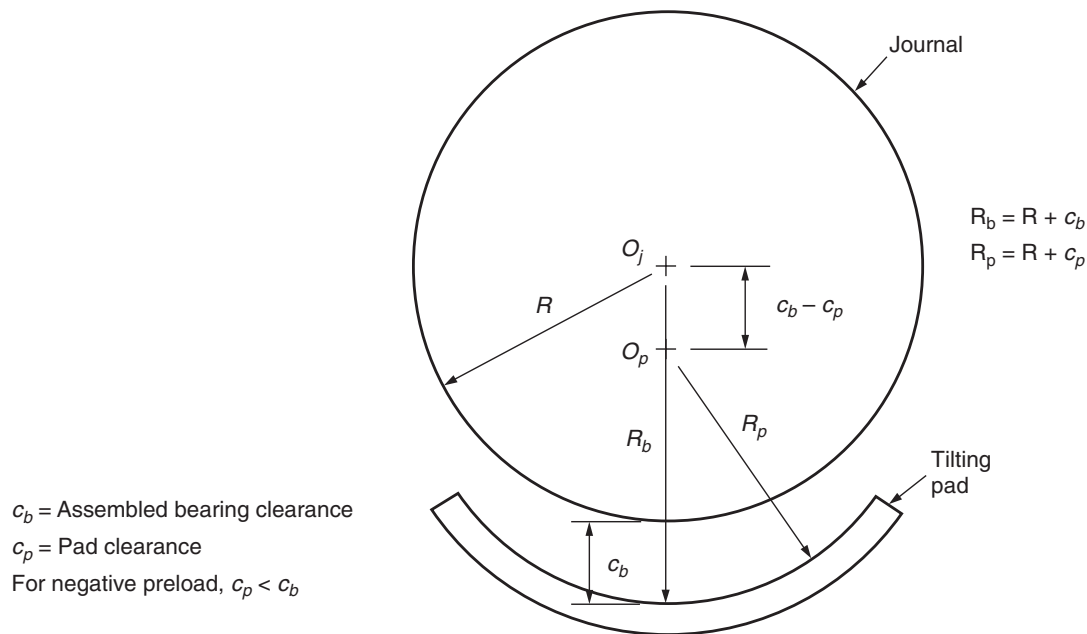


Figure 2-35—Negative Preloaded Pad

Effective damping is a measure of how much bearing damping is effective in shaft vibration suppression. As effective damping increases, shaft vibration decreases. Bearing stiffness has a big influence on the amount of effective damping that a bearing produces. Normally, as bearing damping increases, bearing stiffness also increases. This trend can also be seen from Figure 2-36. As bearing assembled clearance decreases for a constant preload, bearing stiffness and damping both increase. Even though bearing damping increases, the effective damping decreases because the corresponding increase in bearing stiffness makes the bearing damping less effective. The increased bearing stiffness restricts the shaft from moving in the bearing thereby reducing the effectiveness of the oil film produced damping.

Since the decreasing pad preload, increasing effective damping trend is a typical characteristic of many rotor bearing systems, the temptation to decrease tilting pad preload to near zero to improve machine stability is strong. However, there are several major disadvantages to low preload pads. First, there may be a drastic decrease in horizontal stiffness and damping (K_{xx} and C_{xx}) as the pad preload becomes negative (Figure 2-35). This trend is shown analytically and discussed in detail in Nicholas [21] for a centrifugal compressor on 5-pad tilting pad bearings with on pivot loading where the negative preload results from a rather generous machining tolerance range. If zero preload is desired, the tolerance range on the journal diameter, the pad radius of curvature and the assembled bearing clearance can all contribute to producing a negative preload.

The second problem with light preload is the loss of damping when the top pads become unloaded. Top unloaded pads

also flutter since there does not exist a tilt angle at which the pad can seek equilibrium. Fluttering pads may cause rotor vibration and excessive pivot wear [21].

A third problem is the frequency dependent effect. As preload decreases, and as the whirl frequency decreases from synchronous, damping decreases and stiffness increases [9,19].

2.5.4.6 Bearing Length-to-Diameter Ratio

Another powerful design parameter available to the tilting pad bearing designer is pad length-to-diameter, L/D , ratio. An example where increasing the pad L/D ratio *increases* bearing damping but *decreases* bearing stiffness is shown in Figure 2-37 [20]. Again, both changes contribute to the increase in effective damping.

Of course, it is usually more practical to increase the pad length as opposed to decreasing the journal diameter. For this reason, longer pad lengths have become more popular recently with bearing designers. The old standard pad $L/D = 0.5$ is often replaced by $L/D = 0.75$ or, in some cases, with $L/D = 1.0$.

2.5.4.7 Summary

As with many journal bearing design trends, a design change that results in improved synchronous response attenuation may adversely affect stability performance. In the same manner, a journal bearing design change to improve stability may often increase synchronous response vibration when passing through a critical speed. Thus, when contemplating a bearing redesign, synchronous response and stability must both be considered.

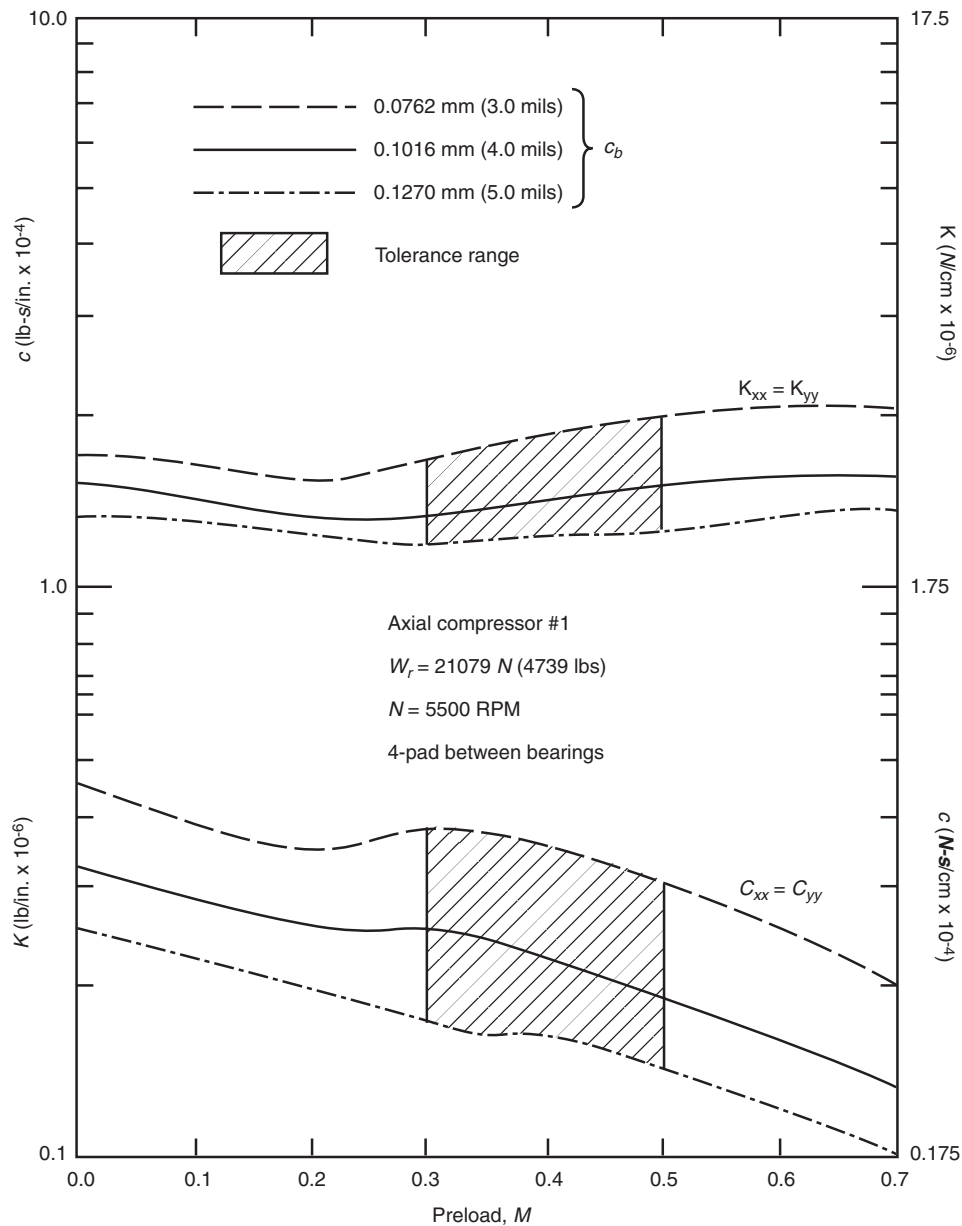


Figure 2-36—Stiffness and Damping vs. Preload and Bearing Clearance, 4-Pad Bearing

2.5.4.8 Experimental Verification

The earliest comparison of analytical and experimental tilting pad journal bearing dynamic coefficients was made by Lund [1]. Lund compares his theoretical data to some experimental data from Hagg and Stankey [22]. His comparison plot for a load between pivot 4-pad bearing is included here as Figure 2-38. It should be noted that Lund's coordinate system is defined as: y-axis horizontal to the right, x-axis vertically downward with counter-clockwise rotation. Another early comparison may be found in Jones and Martin [7]. They compared their analytical data to the experimental data in Yamauchi and Someya [23]. The comparison plot is illus-

trated in Figure 2-39. Both of these figures show reasonable correlation.

Since then, many other researchers have conducted tilting pad journal bearing experimental testing. For example, eccentricity measurements are presented in Tripp and Murphy [24] for a 5-pad tilting pad bearing showing, for the first time, a slight attitude angle with rotation from bottom dead center.

Other examples include Brockwell, et al. [25]. The authors measured the stiffness and damping characteristics for a 76 mm diameter (3.0 in.) 5-pad tilting pad bearing and compared his results to theoretical calculations. They conclude that, while "... there is reasonable agreement between theory and

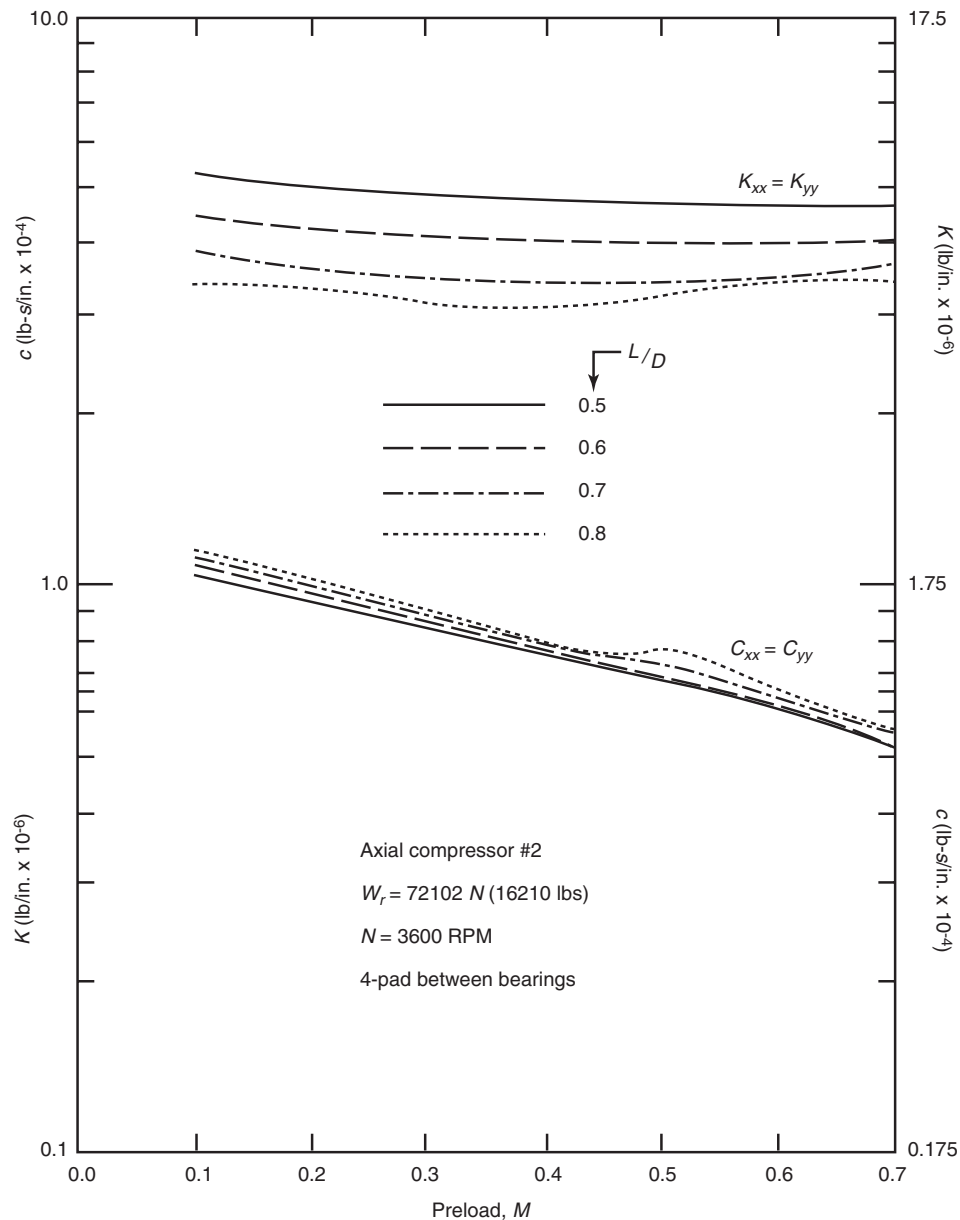


Figure 2-37—Stiffness and Damping vs. Preload and L/D Ratio, 4-Pad Bearing

experiment ...”, the theoretical model “... overestimates the damping characteristics of the bearing” even with the inclusion of pad pivot stiffness.

Dmochowski and Brockwell [26] also considered a 76 mm diameter (3.0 in.) 5-pad tilting pad bearing. Their data includes an uncertainty analysis based on the work of Koszrzewsky and Flack [27,28]. Dmochowski and Brockwell conclude that the “... uncertainty analysis of the measured coefficients has shown that the error associated with the stiffness coefficients is in the range $\pm 5\%$ to $\pm 11\%$, while that for the damping coefficients is in the range $\pm 5\%$ to $\pm 17\%$.”

Wygant et al. [29] presents measured dynamic coefficients for a 70 mm diameter (2.75 in.) 5-pad tilting pad bearing with

on-pivot loading. The authors present stiffness and damping coefficients for their test bearing with “rocker-back” and “spherical seated” pad pivots. Their data also includes an uncertainty analysis. “Uncertainty levels ranged from 8 to 42% for K_{xx} , from 5 to 45% for K_{yy} , from 9 to 28% for C_{xx} from 6 to 82% for C_{yy} ...”

Pettinato and De Choudhury [30] tested a 127 mm diameter (5.0 in.) 5-pad tilting pad bearing with between-pivot loading. The authors present stiffness and damping coefficients including an uncertainty analysis for their test bearing with “key-seat” and “spherical seated” pad pivots. Theoretical data is also included and compared to the test data.

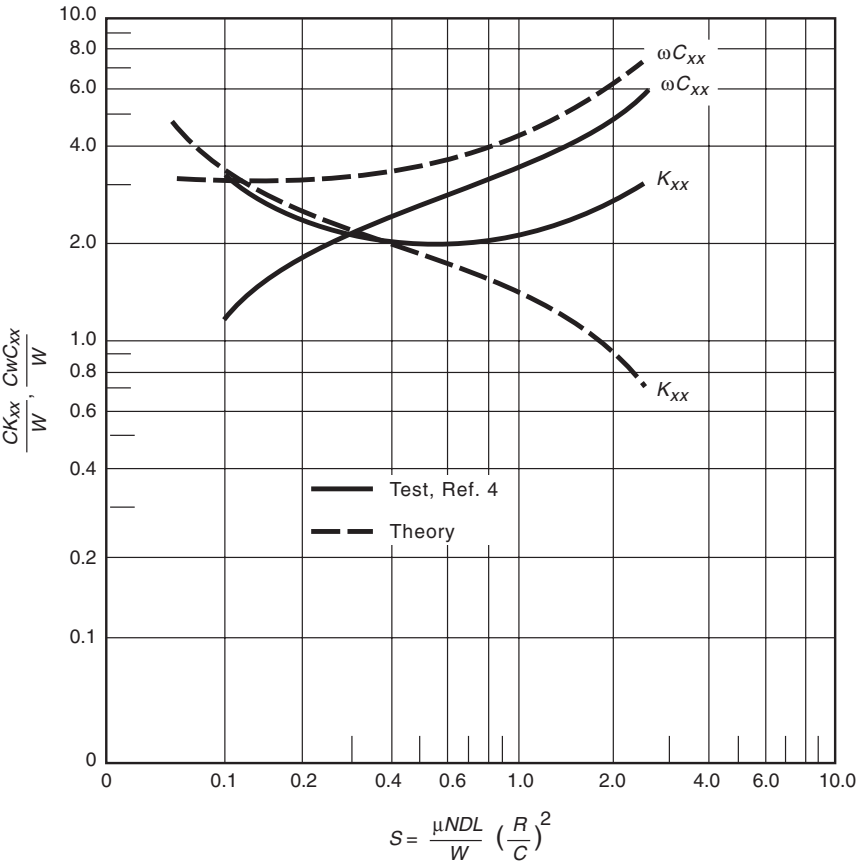


Figure 2-38—Lund's Data vs. Experimental

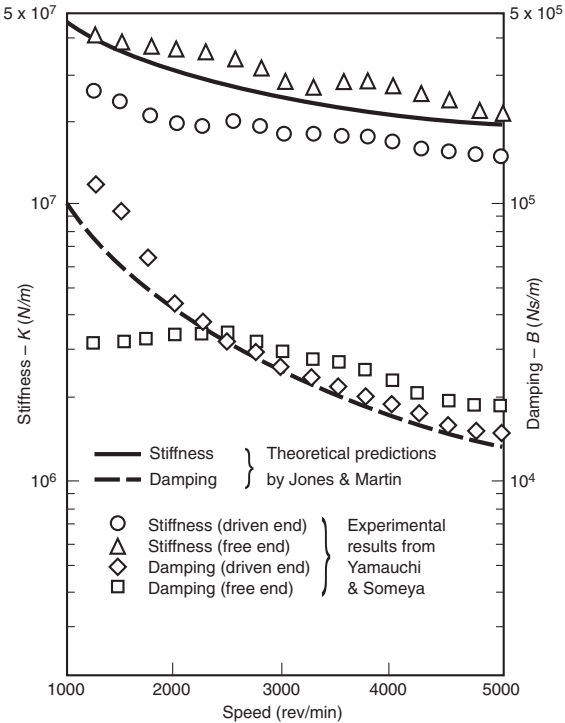


Figure 2-39—Jones and Martin Data vs. Experimental

Steady state tilting pad bearing test data is also available [31-34]. Simmons et al. [31] present temperature data for a 200 mm (7.87 in.) 5-pad tilting pad bearing for unit loads up to 600 psi and surface velocities up to 345 f/s for centrally pivoted pads. Offset pivoted pads are considered in [32] where temperature comparisons are made showing a significant pad operating temperature reduction for offset pivots.

Brockwell et al. [33] presents pad operating temperature data for a 152 mm (6.0 in.) 5-pad tilting pad bearing, comparing offset pivoted to centrally pivoted pads for unit loads up to 318 psi and surface velocities up to 279 f/s. The authors concluded that “In terms of bearing operating temperatures, there does seem to be an advantage in switching from LOP to LBP. This advantage improves at higher shaft speeds.” Note that LOP is load on pivot and LBP is load between pivots. They also conclude that “In all test conditions, the offset pivot bearing ran cooler than the center pivot bearing. In some cases the difference was as much as 20°C.”

DeCamillo and Brockwell [34] tested a 6.0-in., 5-pad tilting pad bearing comparing “... the effects of pivot offset, oil flow, load orientation, method of lubrication, and oil discharge configuration.” Unit bearing loads ranged up to 320 psi with surface velocities up to 393 f/s. Most of their data was for 288 f/s, however. Among their conclusions are that “Reducing flow rate to the offset pivot bearing by 50% reduced power losses 10 to 20%.”

2.5.5 Journal Bearing Retrofits

Probably the most powerful design tool available to bearing and rotordynamic designers concerns the stiffness and damping asymmetry of sleeve bearings such as axial groove, pressure dam, elliptical or multi-lobe bearings. These asymmetric properties often result in split first critical speeds [20,35]. That is, since the horizontal stiffness and damping are much softer than the vertical, a horizontal first critical speed may appear several hundred to several thousand revolutions per minute lower than the vertical critical.

Tilting pad bearings, however, produce more symmetric bearing properties especially when loaded between pivots. In fact, the stiffness and damping values for a 4-pad tilting pad bearing loaded between pivots are exactly equal [20]. This symmetry often results in a single un-split critical that is located approximately midway between the sleeve bearings split peaks [20,35].

As an example, consider the design and retrofit application of a 4-pad tilting pad bearing for a relatively heavy (16,210 lb), low speed (3,600 rpm) axial compressor [20]. The compressor was originally designed to operate on plain, cylindrical, 3-axial groove sleeve bearings with a unit load of $L_u = 179$ psi. The actual test stand results for the compressor with 3-axial groove bearings is shown in Figure 2-40. A peak response is evident at 3,750 rpm which is unacceptably close to the 3,600 rpm operating speed.

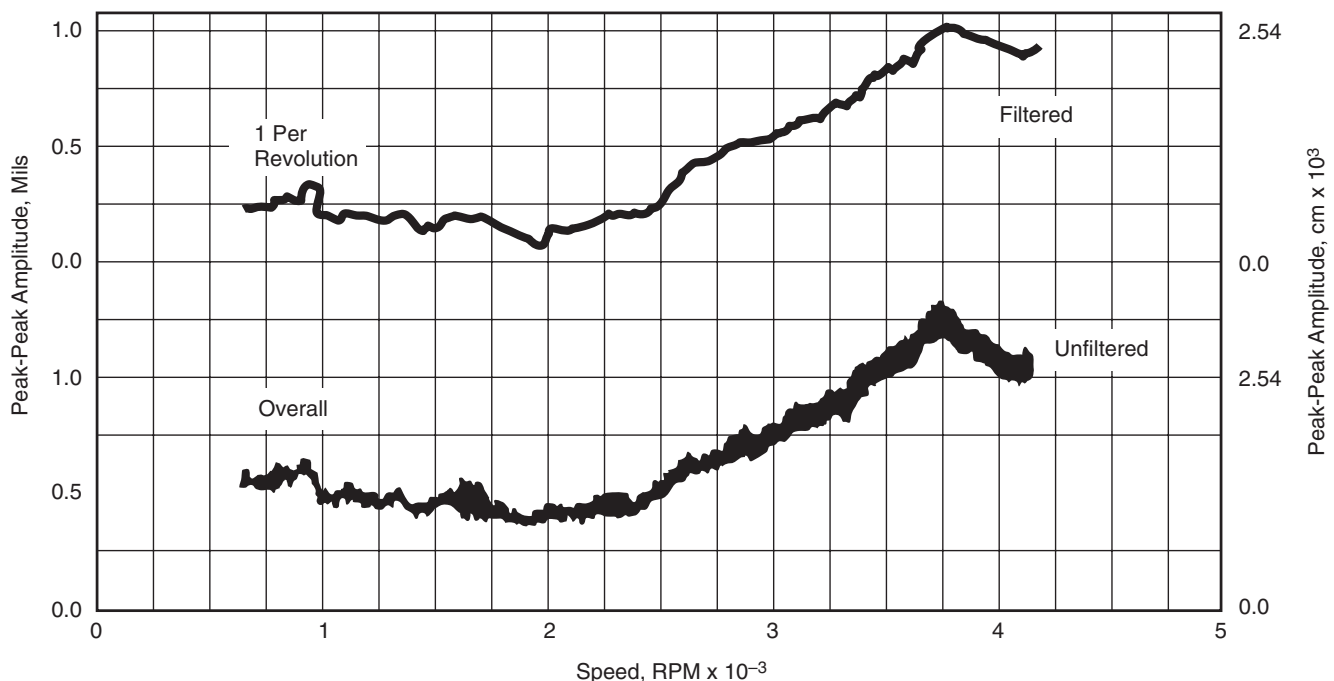


Figure 2-40—Actual Test Stand Response, 3-Axial Groove Bearings

The high unit load on the 3-axial groove bearings produces bearing properties that are extremely asymmetric. This asymmetry results in two distinct peaks for the first critical speed. The lower, horizontal peak is non-responsive in Figure 2-40 and the peak at 3,750 rpm is the higher, vertical first critical. This is illustrated in Figure 2-41 where an analytical response curve is shown for the axial compressor with the original 3-axial groove bearings. The 3-axial groove predicted response shows two peaks at 2,000 and 3,500 rpm. Close examination of the mode shapes and critical speed map indicates that both peaks are first mode criticals due to the asymmetry in the axial groove bearings.

The major advantage of a 4-pad tilting pad bearing is the symmetric stiffness and damping properties that result when loaded between pivots [20]. With symmetric dynamic characteristics, the split first mode no longer exists. It is replaced by a single peak located approximately midway between the sleeve bearing split peaks. Figure 2-41 also shows the predicted response for the axial compressor with a proposed retrofit: a 4-pad tilting pad bearing design with load between pivots. The 4-pad tilting pad bearing with between pivot loading is symmetric and results in only one peak at 2,800 rpm.

Test results for the compressor operating on 4-pad tilting pad bearings with between pivot loading is shown in Figure 2-42. The critical is now located between 2,850 and 3,000 rpm, 16.7 to 20.8% below operating speed.

Figure 2-43 illustrates a similar trend for a smaller axial compressor operating at 5,500 rpm, comparing three different tilting pad bearing designs to the original 3-axial groove bearing with split first critical peaks.

In another example, a two-pole 5,000 HP induction motor was designed and built as a rigid shaft machine [35]. That is, it was to operate with the first critical speed located at least 20% above the synchronous operating speed of 3,600 rpm. Thus, the first critical speed had to be above 4,320 rpm. The motors relevant mass-elastic rotordynamic properties include a rotor weight of 4,430 lb, a bearing span of 69.4 in. and a journal diameter of 5.5 in.

The resulting test stand response plot is illustrated in Figure 2-44 for the induction motor operating on the original 4-pad tilting pad bearings. Clearly, the first critical speed, N_1 , is located at 3,900 rpm with an associated amplification factor of $A_1 = 5.7$. With 10 oz.-in. of unbalance placed in-phase at each fan inboard of the bearings, the resulting vibration is 2.5 mils peak-to-peak (pk-pk).

The corresponding analytical response plot is shown in Figure 2-45 with 10 oz.-in. of unbalance in-phase at each fan. The resulting predicted first critical speed is 3,900 rpm with an amplification factor of 6.4 and 2.6 mils of pk-pk vibration. Unfortunately, the initial analysis assumed an unreasonably high support stiffness (see 2.4). Thus, the first critical was initially erroneously predicted above 4,320 rpm.

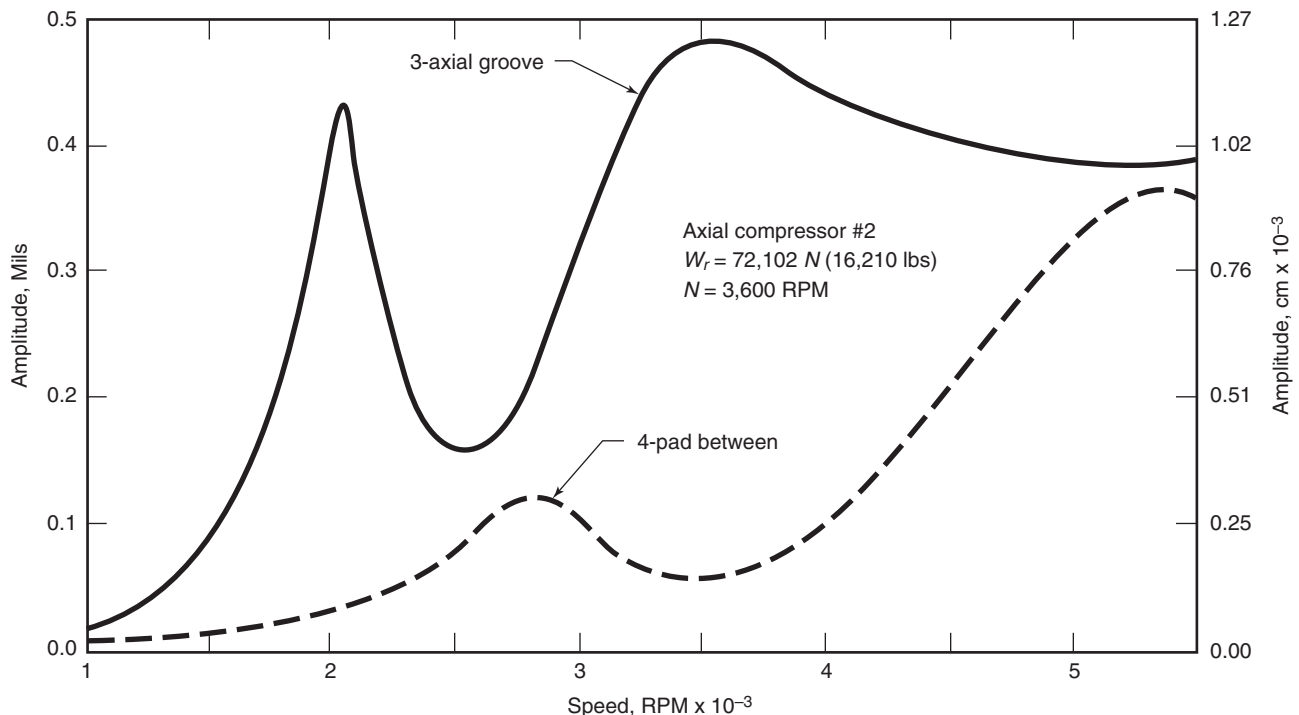


Figure 2-41—Analytically Predicted Response

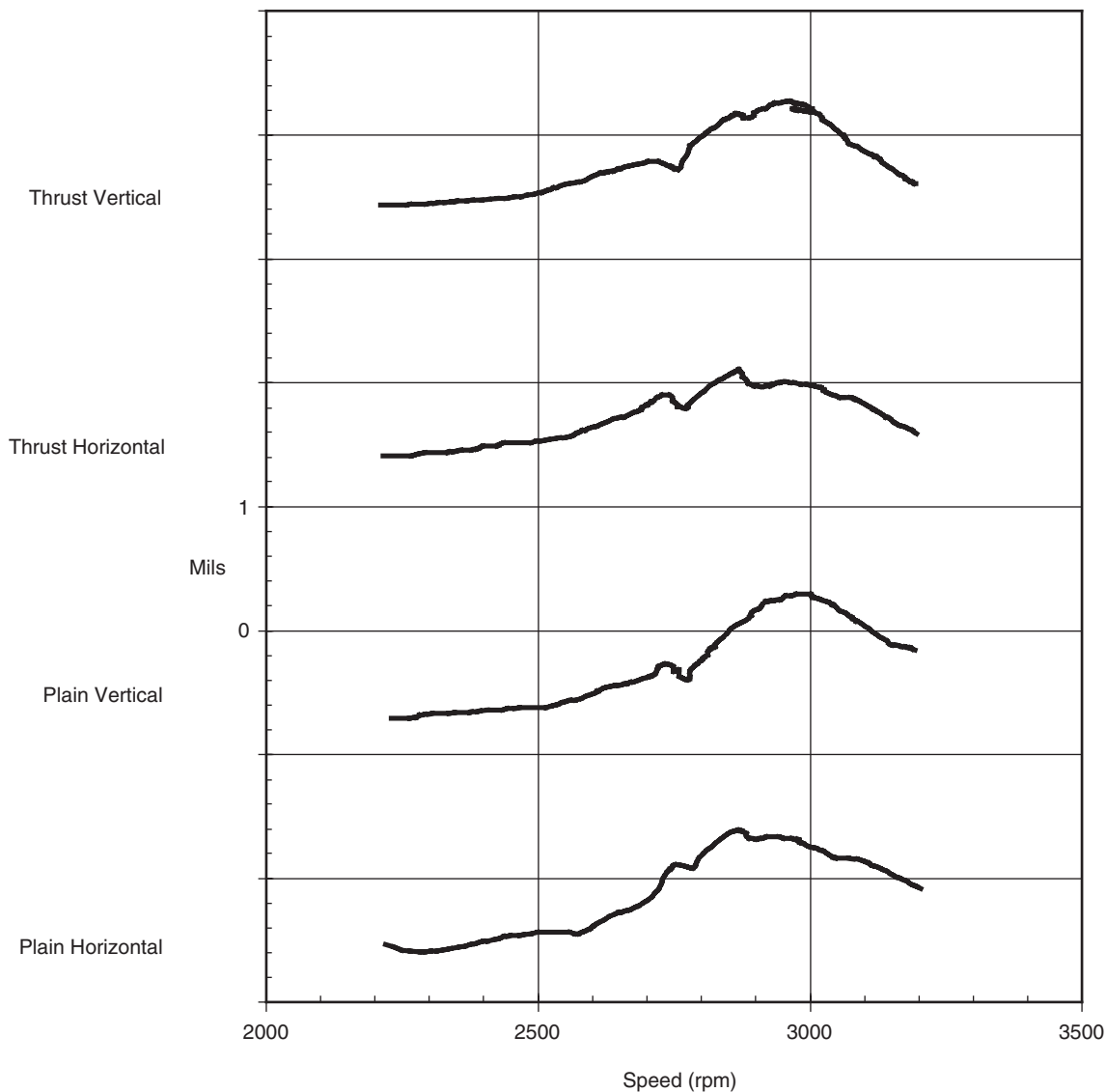


Figure 2-42—Actual Test Stand Response, 4-Pad Tilting Pad Bearings

Numerous failed attempts were made to raise the first critical speed by stiffening the bearing support. For example, stiffeners were added to the bearing brackets and the motor was moved around the test floor seeking the least flexible location.

After these and other design efforts were exhausted short of a complete rotor redesign, an analysis was conducted replacing the original tilting pad bearings with elliptical sleeve bearings. The resulting analytical response plot is shown in Figure 2-46. Again with 10 oz.-in. of unbalance at the fan locations, two distinct first criticals are evident. The lower or horizontal first critical, N_h , is located at 2,350 rpm with $A_h = 2.2$ and with 1.6 mils of pk-pk vibration. The higher, or vertical, first critical, N_v , is at 4,550 rpm with $A_v = 3.8$. Both criticals now meet the required separation margin.

The resulting test stand plot for the motor with elliptical bearings and with 10 oz.-in. of in-phase unbalance at the fans is shown in Figure 2-47. The vibration level is 1.6 mils pk-pk with $N_h = 2,740$ rpm and $A_h = 1.5$. Compared to the predicted results, the vibration magnitude and amplification factor are quite close, but the actual location of the critical is 390 rpm higher than predicted. The motors were commissioned with the elliptical bearings and have been operating free of vibration problems since 1993.

2.5.6 Viscosity Units

Although kinematic viscosity is more commonly used in fluid mechanics, dynamic or absolute viscosity is the key viscosity for hydrodynamic lubrication. Probably the least used unit of dynamic or absolute viscosity in defining lubricants is

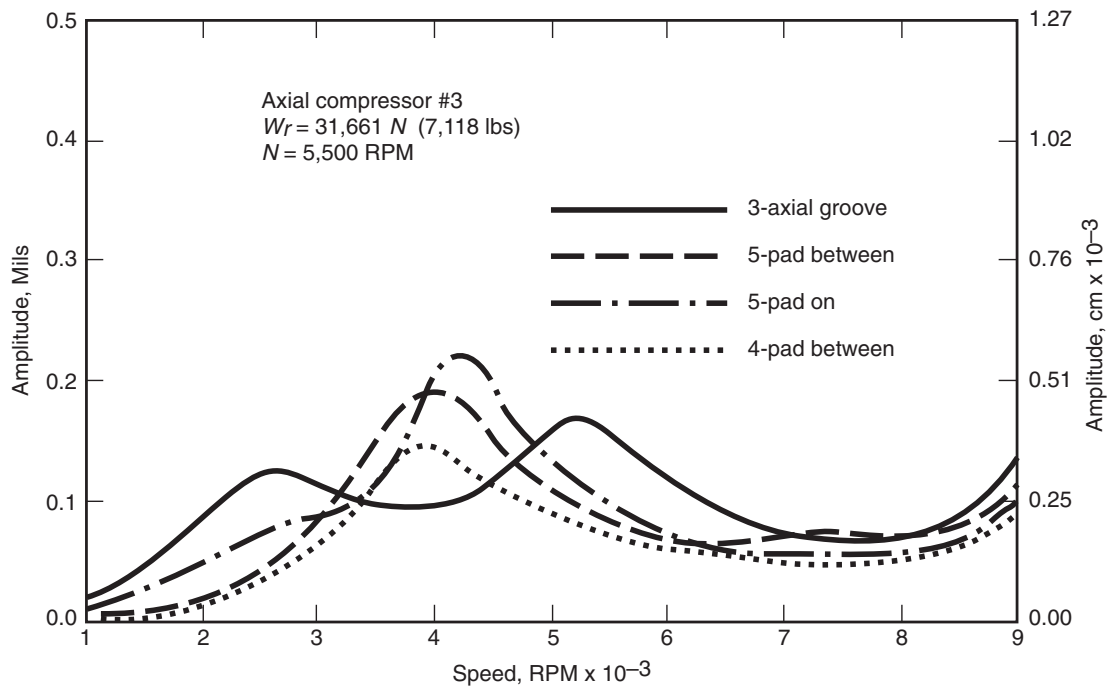


Figure 2-43—Analytically Predicted Response, Various Bearing Designs

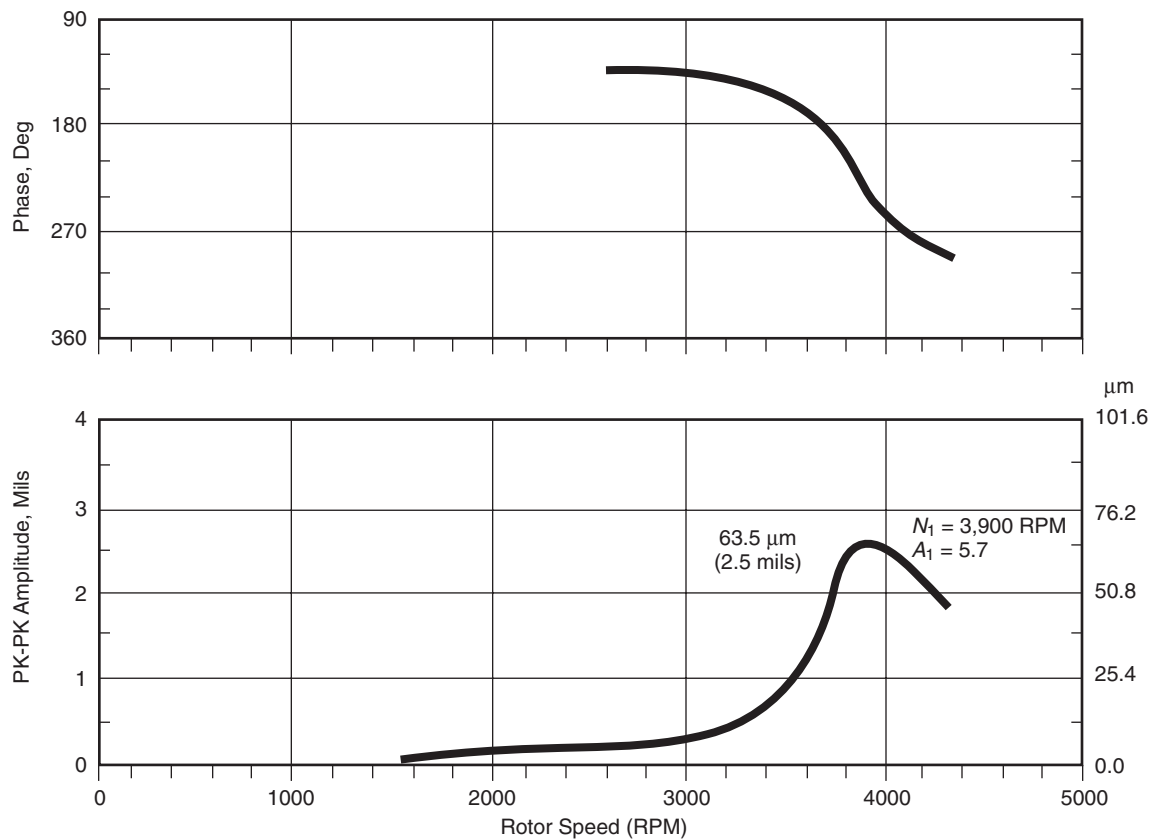


Figure 2-44—Induction Motor Test Stand Response, Tilting Pad Bearings

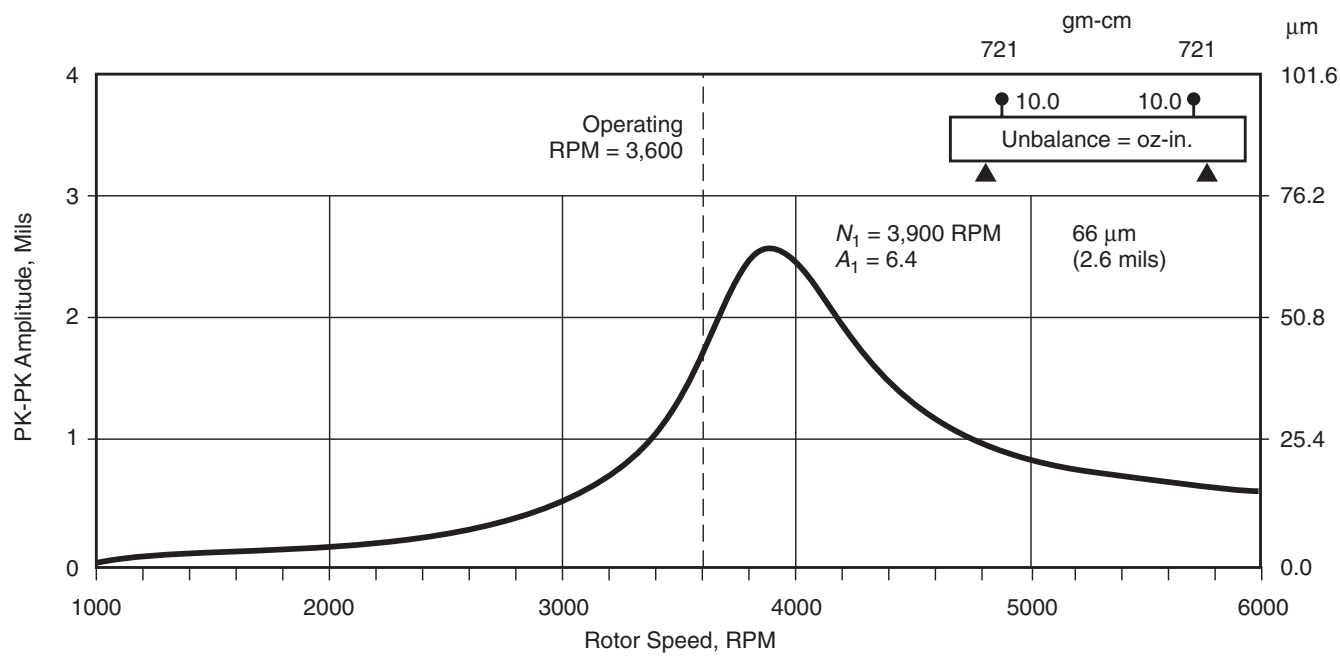


Figure 2-45—Induction Motor Analytical Response, Tilting Pad Bearings

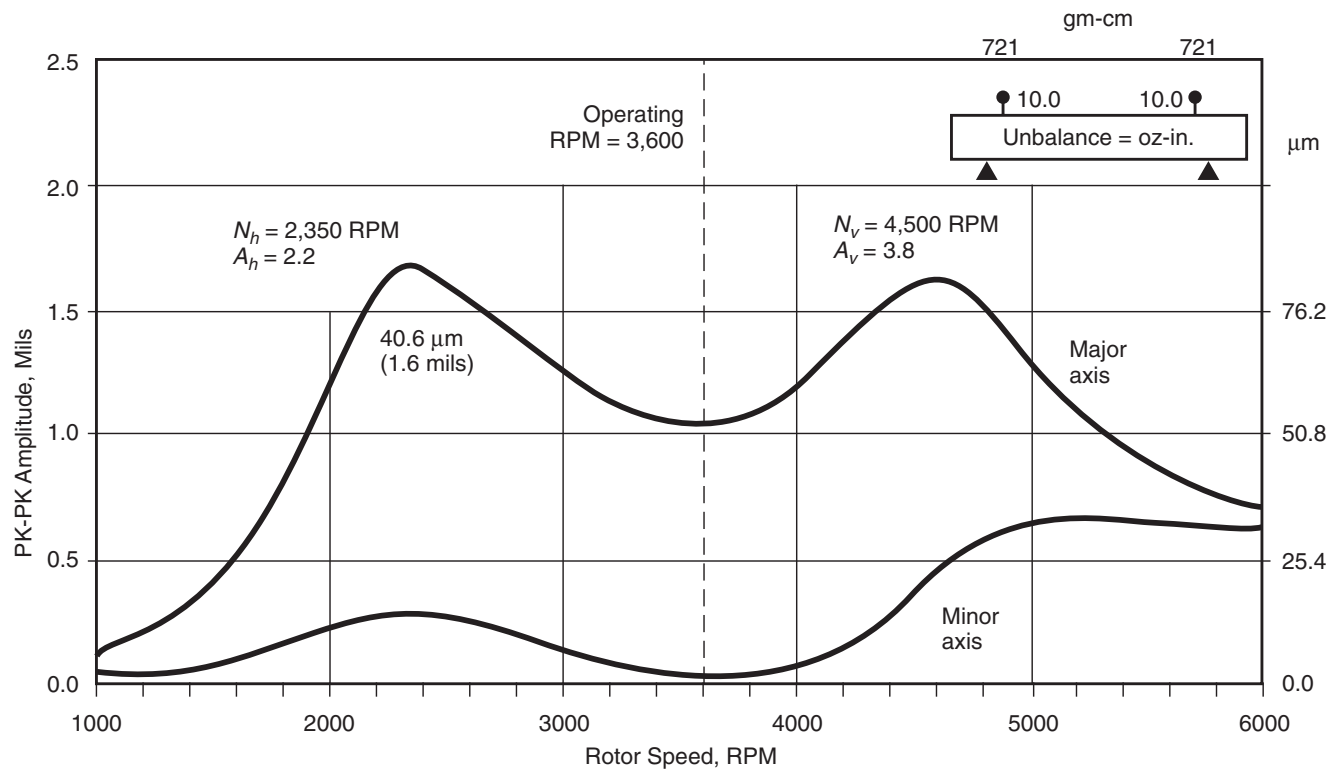


Figure 2-46—Induction Motor Analytical Response, Elliptical Bearings

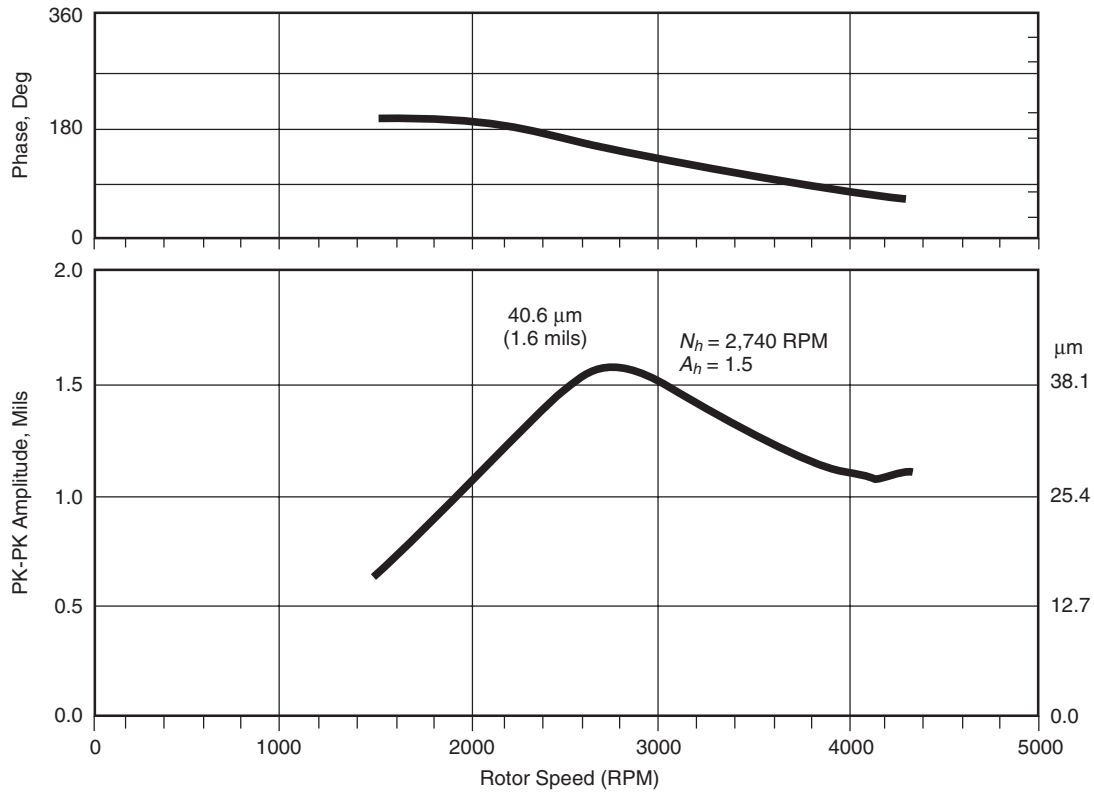


Figure 2-47—Induction Motor Test Stand Response, Elliptical Bearings

the reyn, named in honor of Sir Osborne Reynolds. The reyn, however, is a key viscosity unit as it is the required unit for the dynamic pressure equation (Reynolds equation). A reyn is defined as [36]

$$\mu_r = \frac{\text{lbf} \cdot \text{s}}{\text{in.}^2} = \text{reyn} \quad 2-6$$

Another viscosity unit is the poise, named in honor of the physician, Doctor Poiseuille [36]

$$\mu_p = \frac{\text{dyne} \cdot \text{s}}{\text{cm}^2} = \text{poise} \quad 2-7$$

where 1 lbf = 448,000 dynes. Likewise, a centipoise is equal to 10^{-2} poise

$$\mu_{cp} = \mu_p \times 10^{-2} = \text{centipoise} \quad 2-8$$

The relationship between a reyn and a centipoise is

$$\mu_r = \mu_{cp} \times 1.45^{-7} \quad 2-9$$

In the metric system, the dynamic viscosity unit is the pascal-second

$$\mu_{pa} = \frac{N \cdot s}{m^2} = Pa \cdot s \quad 2-10$$

The relationships between a pascal-second to a reyn and to a centipoise are

$$\mu_{pa} = \mu_r \times 6.894^3 \quad 2-11$$

$$\mu_{pa} = \mu_{cp} \times 10^{-3} \quad 2-12$$

The kinematic viscosity is the dynamic viscosity divided by the lubricant density. Convenient to measure, the kinematic viscosity is a common parameter given for lube oil characteristics. The metric unit for kinematic viscosity is the stoke which is defined as

$$\nu_s = \frac{\text{cm}^2}{s} = \text{stoke} \quad 2-13$$

Also, a centistoke is equal to 10^{-2} stokes

$$\nu_{cs} = \nu_s \times 10^{-2} = \frac{\text{mm}^2}{s} = \text{centistoke} \quad 2-14$$

Most lubricants are now defined by a viscosity unit called Saybolt Seconds Universal, SSU. This unit is simply the time in seconds required for the lubricant to empty out of a cup in a Saybolt viscometer through a capillary opening. For high flow times (high viscosity lubricants), the Saybolt viscosity is proportional to the kinematic viscosity. For low viscosity lubricants (values below 70 centistokes, 325 SSU), turbulence and other effects influence the efflux time making the relationship nonlinear [37].

An approximate equation relating centistokes to Saybolt viscosity is

$$v_{cs} = 0.22 \times \mu_{ssu} - \frac{180}{\mu_{ssu}} \quad 2-15$$

A detailed discussion of this equation and its limitations may be found in Reference [37].

2.5.7 References

1. Lund, J. W., 1964, "Spring and Damping Coefficients for the Tilting-Pad Journal Bearing," *ASLE Transactions*, 7, pp. 342-352.
2. Boyd, J., and Raimondi, A. A., 1953, "An Analysis of the Pivoted-Pad Journal Bearing," *Mechanical Engineering*, 75, No. 5, pp. 380-386.
3. Boyd, J., and Raimondi, A. A., 1962, "Clearance Considerations in Pivoted Pad Journal Bearings," *ASLE Transactions*, 5, No. 2, pp. 418-426.
4. Orcutt, F. K., 1967, "The Steady-State and Dynamic Characteristics of the Tilting-Pad Journal Bearing in Laminar and Turbulent Flow Regimes," *ASME Journal of Lubrication Technology*, 89, No. 3, pp. 392-404.
5. Nicholas, J. C., Gunter, E. J., and Allaire, P. E., 1979, "Stiffness and Damping Coefficients for the Five Pad Tilting Pad Bearing," *ASLE Transactions*, 22, No. 2, pp. 112-124.
6. Nicholas, J. C., Gunter, E. J., and Barrett, L. E., 1978, "The Influence of Tilting Pad Bearing Characteristics on the Stability of High Speed Rotor-Bearing Systems," *Topics in Fluid Film Bearing and Rotor Bearing System Design and Optimization*, an ASME publication, pp. 55-78.
7. Jones, G. J., and Martin, F. A., 1979, "Geometry Effects in Tilting-Pad Journal Bearings," *ASLE Transactions*, 22, No. 3, pp. 227-244.
8. Shapiro, W. and Colsher, R., 1977, "Dynamic Characteristics of Fluid Film Bearings," *Proceedings of the Sixth Turbomachinery Symposium*, Texas A&M University, College Station, Texas, pp. 39-53.
9. Parsell, J. K., Allaire, P. E. and Barrett, L. E., 1983, "Frequency Effects in Tilting-Pad Journal Bearing Dynamic Coefficients," *ASLE Transactions*, 26, pp. 222-227.
10. Barrett, L. E., Allaire, P. E. and Wilson, B. W., 1988, "The Eigenvalue Dependence of Reduced Tilting Pad Bearing Stiffness and Damping Coefficients," *ASLE Transactions*, 31, pp. 411-419.
11. Ha, H. C., and Yang, S. H., 1999, "Excitation Frequency Effects on the Stiffness and Damping Coefficients of a Five-Pad Tilting Pad Journal Bearing," *ASME Journal of Tribology*, 121 (3), pp. 517-522.
12. Wygant, K. D., 2001, "The Influence of Negative Preload and Nonsynchronous Excitation on the Performance of Tilting Pad Journal Bearings," Ph.D. Dissertation, University of Virginia, Charlottesville, Virginia.
13. Knight, J. D., and Barrett, L. E., 1988, "Analysis of Tilting Pad Journal Bearing with Heat Transfer Effects," *ASME Journal of Tribology*, 110, No. 1, 128-133.
14. Branagan, L. A., 1988, "Thermal Analysis of Fixed and Tilting Pad Journal Bearings Including Cross-Film Viscosity Variations and Deformation," Ph.D. Dissertation, University of Virginia, Charlottesville, Virginia.
15. Ettles, C. M., 1992, "The Analysis of Pivoted Pad Journal Bearing Assemblies Considering Thermoelastic Deformation and Heat Transfer Effects," *STLE Tribology Transactions*, 35, No. 1, pp. 156-162.
16. Parkins, D. W. and Horner, D., 1993, "Tilting Pad Journal Bearings—Measured and Predicted Stiffness Coefficients," *STLE Tribology Transactions*, 36, No. 3, pp. 359-366.
17. Kim, J., Palazzolo, A., and Gadangi, R., 1995, "Dynamic Characteristics of TEHD Tilt Pad Journal Bearing Simulation Including Multiple Mode Pad Flexibility Model," *ASME Journal of Vibration and Acoustics*, 117, No. 1, pp. 123-135.
18. Fillon, M., Desbordes, H., Frene, J., and Wai, C. C. H., 1996, "A Global Approach of Thermal Effects Including Pad Deformation in Tilting-Pad Journal Bearings Submitted to Unbalance Load," *ASME Journal of Tribology*, 118, No. 1, pp. 169-174.
19. Nicholas, J. C., 2001, "Lund's Pad Assembly Method for Tilting Pad Journal Bearings," ASME Paper No. DETC2001/VIB-21371, *Proceedings of DETC'01*, ASME 2001 Design Engineering Technical Conferences and Computers and Information in Engineering Conference, Pittsburgh, Pennsylvania, September 9-12, 2001.
20. Nicholas, J. C. and Kirk R. G., 1982, "Four Pad Tilting Pad Bearing Design and Application for Multi-Stage Axial Compressors," *ASME Journal of Lubrication Technology*, 104, No. 4, pp. 523-532.

21. Nicholas, J. C., 1994, "Tilting Pad Bearing Design," *Proceedings of the Twenty-Third Turbomachinery Symposium*, Texas A&M University, College Station, Texas, pp. 179-194.
22. Hagg, A. C. and Stankey, G. O., 1958, "Elastic and Damping Properties of Oil-Film Journal Bearings for Applications to Unbalance Vibration Calculations," *ASME Journal of Applied Mechanics*, 25, No. 1, pp. 141-143.
23. Yamauchi, S. and Someya, T., 1977, "Balancing of a Flexible Rotor Supported by Special Tilting-Pad Bearings," CIMAC Twelfth International Congress on Combustion Engines, Tokyo, Japan.
24. Tripp, H. and Murphy, B., 1984, "Eccentricity Measurements on a Tilting-Pad Bearing," *ASLE Transactions*, 28, pp. 217-224.
25. Brockwell, K., Kleinbub, D. and Dmochowski, W., 1990, "Measurement and Calculation of the Dynamic Operating Characteristics of the Five Shoe Tilting Pad Journal Bearing," *STLE Tribology Transactions*, 33 (4), pp. 481-492.
26. Dmochowski, W. and Brockwell, K., 1995, "Dynamic Testing of the Tilting Pad Journal Bearing," *STLE Tribology Transactions*, 38 (2), pp. 261-268.
27. Kostrzewsky, G. J. and Flack, R. D., 1990, "Accuracy Evaluation of Experimentally Derived Dynamic Coefficients of Fluid Film Bearings Part I: Development of Method," *STLE Tribology Transactions*, 33 (1), pp. 105-114.
28. Kostrzewsky, G. J. and Flack, R. D., 1990, "Accuracy Evaluation of Experimentally Derived Dynamic Coefficients of Fluid Film Bearings Part II: Case Studies," *STLE Tribology Transactions*, 33 (1), pp. 115-121.
29. Wygant, K. D., Barrett, L. E. and Flack, R. D., 1999, "Influence of Pad Pivot Friction on Tilting-Pad Journal Bearing Measurements—Part II: Dynamic Coefficients," *STLE Tribology Transactions*, 42 (1), pp. 250-256.
30. Pettinato, B. and De Choudhury, P., 1999, "Test Results of Key and Spherical Pivot Five-Shoe Tilt Pad Journal Bearings—Part II: Dynamic Measurements," *STLE Tribology Transactions*, 42 (3), pp. 675-680.
31. Simmons, J. E. L. and Dixon, S. J., 1994, "Effect of Load Direction, Preload, Clearance Ratio, and Oil Flow on the Performance of a 200 mm Journal Pad Bearing," *STLE Tribology Transactions*, 37 (2), pp. 227-236.
32. Simmons, J. E. L. and Lawrence, C. D., 1996, "Performance Experiments with a 200 mm, Offset Pivot Journal Pad Bearing," *STLE Tribology Transactions*, 39 (4), pp. 969-973.
33. Brockwell, K., DeCamillo, S. and Dmochowski, W., 2001, "Measured Temperature Characteristics of 152 mm Diameter Pivoted Shoe Journal Bearings with Flooded Lubrication," *STLE Tribology Transactions*, 44 (4), pp. 543-550.
34. DeCamillo, S. and Brockwell, K., 2001, "A Study of Parameters that Affect Pivoted Shoe Journal Bearing Performance in High-Speed Turbomachinery," *Proceedings of the Thirtieth Turbomachinery Symposium*, Texas A&M University, College Station, Texas, pp. 9-22.
35. Nicholas, J. C. and Moll, R. W., 1993, "Shifting Critical Speeds Out of the Operating Range by Changing from Tilting Pad to Sleeve Bearings," *Proceedings of the Twenty-Second Turbomachinery Symposium*, Texas A&M University, College Station, Texas, pp. 25-32.
36. Fuller, D. D., 1984, *Theory and Practice of Lubrication for Engineers*, John Wiley & Sons, New York.
37. Wilcock, D. F. and Booser, E. R., 1957, *Bearing Design and Application*, McGraw Hill Book Company, New York.

2.6 SEAL TYPES AND MODELING

2.6.1 Introduction

For convenience in rotordynamic modeling, seals can be categorized into two groups: liquid and gas. The effect these seals have on the rotordynamic differs according to the type of seal and analysis being considered. The impact on turbomachine stability of all seals is significant. Whether positive or negative, nearly every seal needs to be accounted for when performing a stability analysis. How the seals are modeled may vary from a CFD analyses to empirical relations. Section 3.4 covers the role that seals play in the rotordynamic stability in detail.

For unbalance response analysis, the API requirement is to include oil seals only. Oil is specified since the use of liquid film seals with fluids other than oil is rare in the equipment discussed in this tutorial. The distinction made between oil and other liquid seals, such as water, is a result of the viscosity of the sealing liquid. In journal bearings and oil film seals, the film forces produced by the oil viscosity supports the journal load and creates the dynamic coefficients. The fluid dynamics are modeled using Reynolds equation. For inviscid fluids, annular seals under large pressure gradients are highly turbulent and require a different analytical approach. This section will focus more on oil seals reflecting their use in the equipment.

The unbalance response analysis involves forces and vibratory motion at the synchronous frequency. At this frequency, the oil seal's damping improves the rotor response. However, the destabilizing aspects of these seals at subsynchronous frequencies are one factor that has led to their replacement with dry gas seals. The trade-off is an increase in synchronous response; the magnitude of which is dependent on the rotor/bearing design.

Table 2-3—General Synchronous Behavior and Requirements of Oil and Gas Seals

	Oil Seals	Gas Seals
Inclusion in Unbalance Response Analysis	API requirement	Not required but may be needed for accurate analyses
Inclusion in Stability Analysis	API requirement	Effects need to be accounted for
Strong Principle Stiffness Terms	Yes	No (See exceptions)
Strong Effective Damping ($\omega C - k$) Terms	Yes (Can be positive or negative)	Yes (Can be positive or negative)
Positive Damping at Synchronous Whirl Frequency	Yes	Yes and no

Gas seals (this includes dry gas seals, labyrinths, balance pistons, etc.) are basically neutral in their behavior at synchronous frequencies due to several factors. First, their principle stiffness terms are normally several orders of magnitude less than the bending stiffness of the shaft or the rotor support stiffness. With lower principle stiffness terms, they have little influence on the location of the critical speeds. Additionally, the effective damping ($\omega C - k$) is approximately zero or slightly positive at the synchronous frequency, ω_{synch} , and their influence on the response magnitude tends to be insignificant. However, there are exceptions. The gas seal section, 2.6.4, will discuss these exceptions further.

We can summarize the general synchronous behavior and requirements of oil and gas seals in Table 2-3.

2.6.2 Oil Seals

One major application of oil seals is the pressure containment in centrifugal compressors. It is in these applications that the seals play a major role in the dynamic behavior of the rotor/bearing system. Oil seals are designed to keep process fluids from discharging into the atmosphere by placing a barrier between the process gas and the atmosphere. A typical single breakdown liquid-film shaft seal with cylindrical bushings is shown in Figure 2-48. A diagram of the outer sealing ring is presented in Figure 2-49, showing key dimensions and the general oil pressure distribution.

Optimally, the sealing ring floats keeping nearly concentric with the rotating shaft. In this condition, the dynamic characteristics produced by the seal ring are low. The extent to which these rings can float (i.e., track the shaft motion) is determined by balancing the radial forces generated by the oil film, with the radial friction load stemming from the unbalanced axial pressure. The axial force is obtained from integrating the pressure distribution on the radial faces. This force determines the contact pressure at the lapped sealing face on the left side of the ring, Figure 2-49. The coefficient of friction between the lapped face and the housing produces a radial holding force that inhibits the seal from moving. The magnitude of the axial force can be affected by relocating the

dimension, D_o . Since a certain lapped surface area is required for sealing and to prevent distortion of the face, the axial force can only be minimized and not eliminated.

During eccentric operation of the seal ring, the oil film between the ring and shaft will produce a restoring force similar to that found in journal bearings. In bearings, the force supports the shaft load. In seals, the radial force will attempt to overcome the holding force and restore the ring to a centered position. Equilibrium is achieved when the restoring force is equal to or is less than the holding force. In this “locked” position, dynamic coefficients of the ring can be obtained and applied to rotor/bearing system. Highly eccentric operation of the ring has been shown to be detrimental to both the rotor stability and unbalance response. Allaire et al. [1] describes a case history involving the balancing of a seal’s pressure distribution, modification of the seal restoring force and subsequent impact on the rotor’s dynamic behavior.

For synchronous response, locking of the seal position may occur when the machinery is started up. The locked position is determined by the pressure distribution axially and the oil film characteristics. While modifying the sealing diameter, D_o , can affect the holding force, so can varying the suction pressure during start-up. For example, the damped response of the hydrogen recycle compressor rotor to a general unbalance distribution has been calculated for various start-up sealing pressures. The mid-span response of this compressor through the first critical speed is displayed in Figure 2-50 for three start-up sealing pressures. Note that as the sealing pressure increases, the influence of the oil seals increases due to an increase in the damping generated by the seals. In general, the damping provided by oil seals tends to reduce the amplification associated with the fundamental critical and to raise the frequency of the critical speed.

Although the effect of oil seals on unbalance rotor response characteristics is extremely positive, oil seals may prove quite detrimental to the unit’s rotor stability at operating speed and cause large amplitude subsynchronous vibrations. Much design effort has focused on minimizing the destabilizing effect of the seals. Oil seals are generally pres-

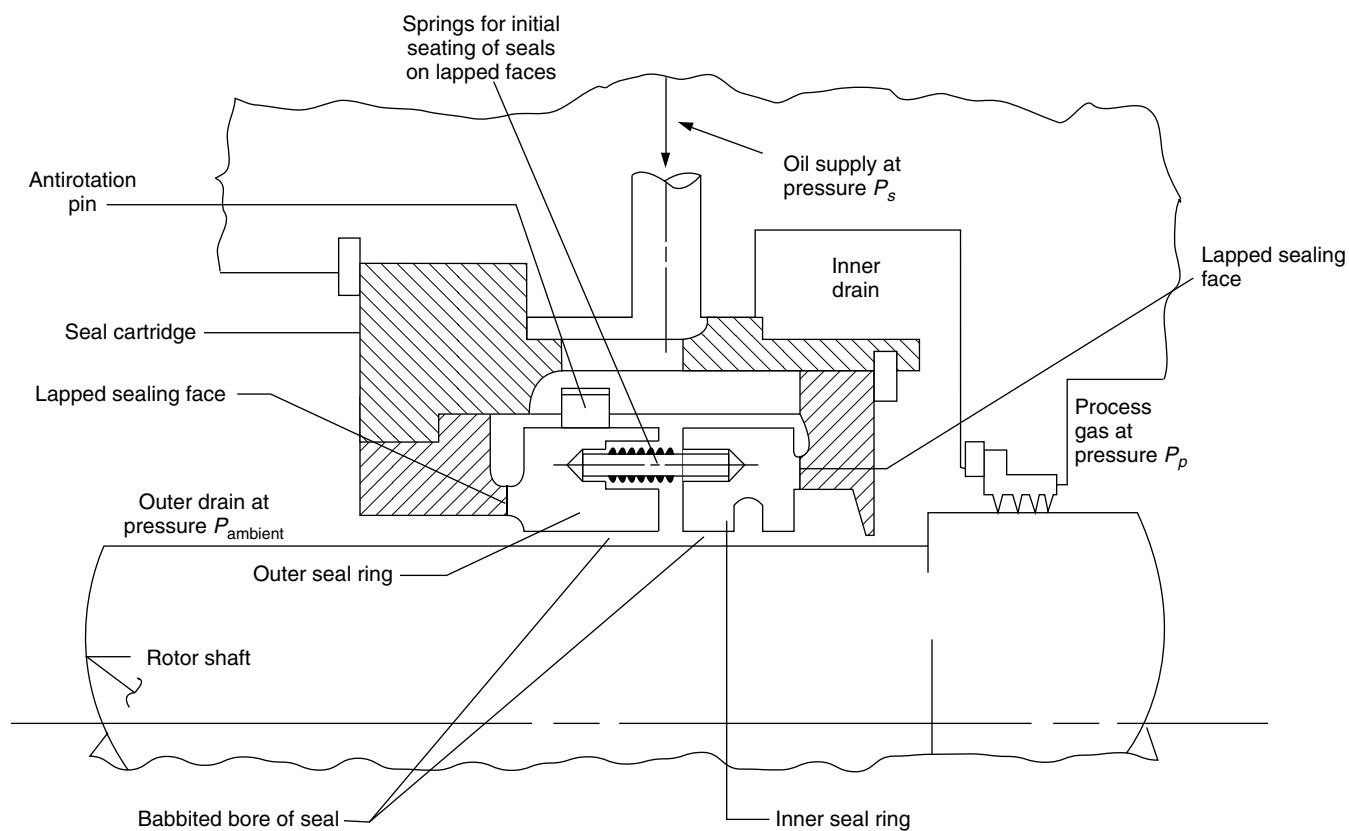


Figure 2-48—Oil Bushing Breakdown Seal

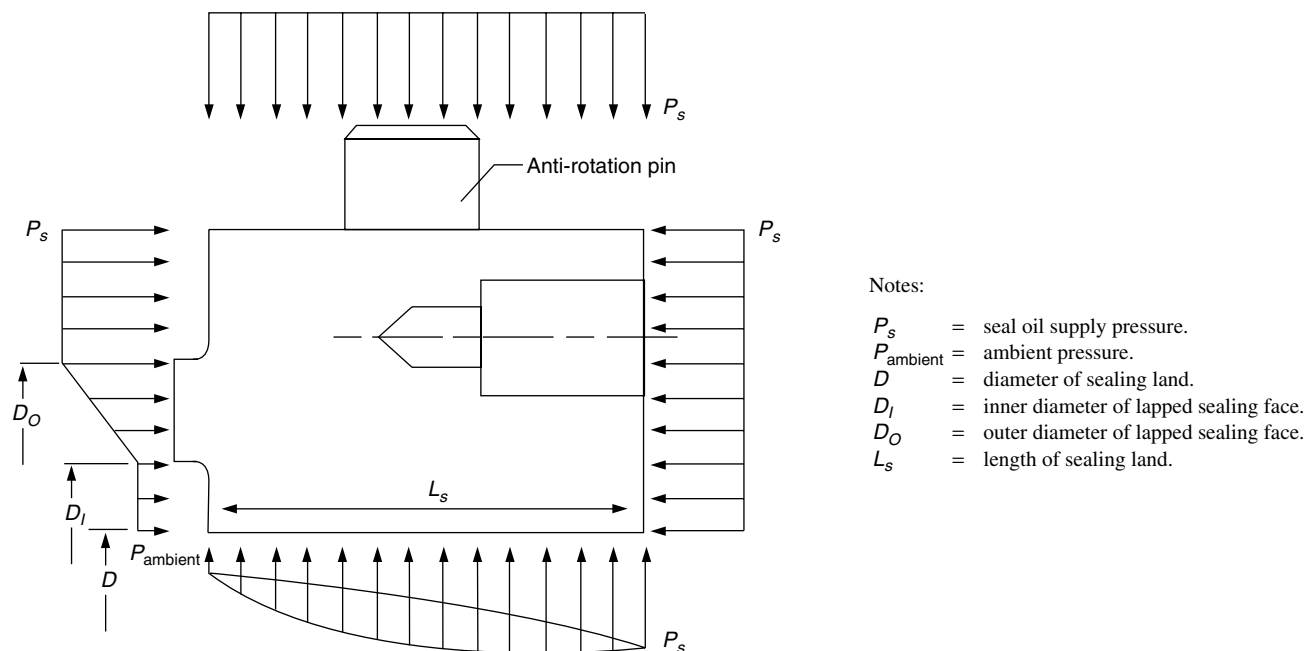


Figure 2-49—Pressures Experienced by the Outer Floating Ring Seal

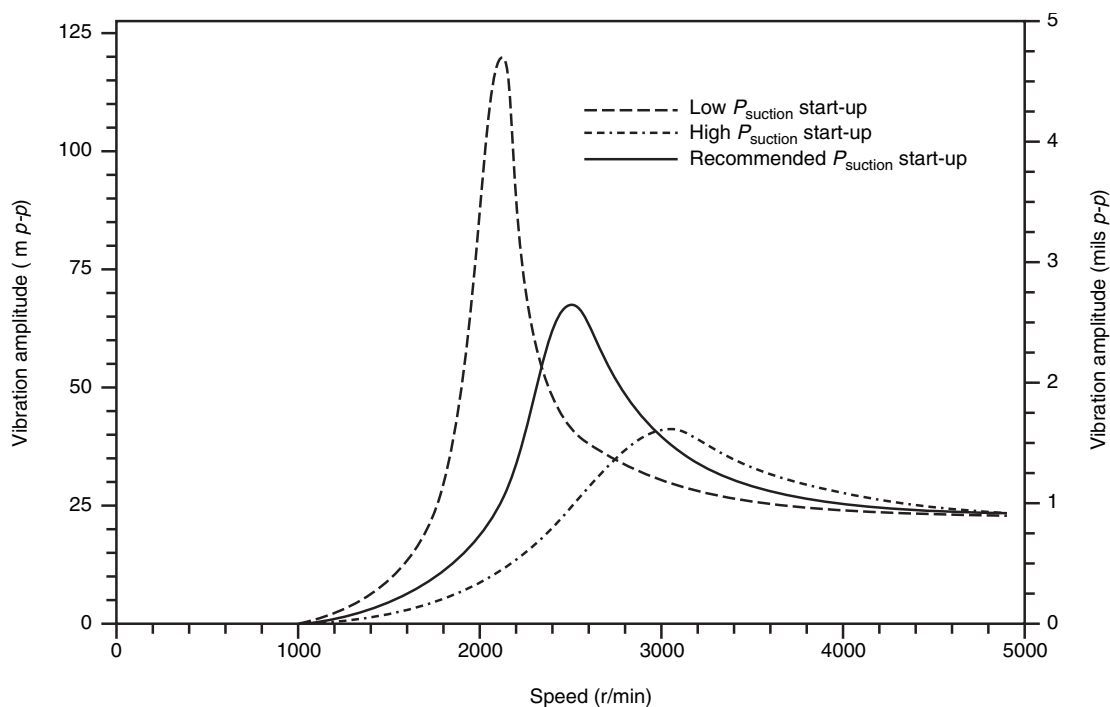


Figure 2-50—Mid-Span Rotor Unbalance Response of a High Pressure Centrifugal Compressor for Different Suction Pressures at Start-up

sure balanced to minimize axial forces; the sealing lands are frequently grooved in order to diminish hydrodynamic load capacity; and various centering mechanisms are used to reduce the eccentricity of the ring, relative to the shaft during operation.

Kirk [2] presents an excellent description of the pressure balance on both the inner and outer rings. A case study is described where grooving is used to eliminate the destabilizing aspects of the outer ring. While this achieved the desired results, it was also noted that the accompanying decrease in damping increased the unbalance response of the first critical speed. Grooving greatly reduces the hydrodynamic effects of the oil film with the resulting decrease in effective damping. The rule of thumb is that the cross-coupled stiffness and direct damping vary with the length cubed. Thus, adding two grooves reduces the land length by a factor of 3, but triples the number of lands, so the net reduction in coefficients is 9, Allaire [1].

Cerwinski et al. [3] also presents a case study describing the influence of high-pressure bushing seals on the rotordynamic characteristics of a centrifugal compressor. An analysis of the floating ring to determine the locked position of the ring and its affect on the stability is described. As with Kirk [2], the author states the importance of analyzing not only the stability but the change in the unbalance response of the rotor as well.

Lastly, the determination of the oil film characteristics of the locked ring is dependent on many factors: the sealing pressure and temperature, eccentricity of the locked ring, geo-

metric data and lubricant properties. The pressure field of the oil film in the seals is described using similar differential equations employed to describe the oil film pressures in hydrodynamic journal bearings. The principal difference between the numerical methods used to analyze bearings and seals lies in part due to the pressure differential across the axial length of the seal. Additionally, turbulence and fluid inertia may not be negligible especially in water film seal. Baheti and Kirk [4] present a finite-element method of floating ring seals using a thermo-hydrodynamic solution that takes into account many of these factors. A list of factors include:

- a. Journal diameter.
- b. Shaft speed.
- c. Sealing pressure and temperature.
- d. Axial length of seal ring.
- e. Number of grooves.
- f. Radial seal clearance.
- g. Inner and outer diameter of sealing face or lip.
- h. Coefficient of friction between ring and housing.
- i. Oil viscosity, density and thermal properties.

Various configurations of oil seals are presented in Figures 2-51 – 2-53. Some have fixed breakdown rings, others have a floating outer ring and some have multiple floating rings. All have an oil film between the rotating assembly and stationary components that affect the rotordynamic characteristics of centrifugal compressors in the manner described above.

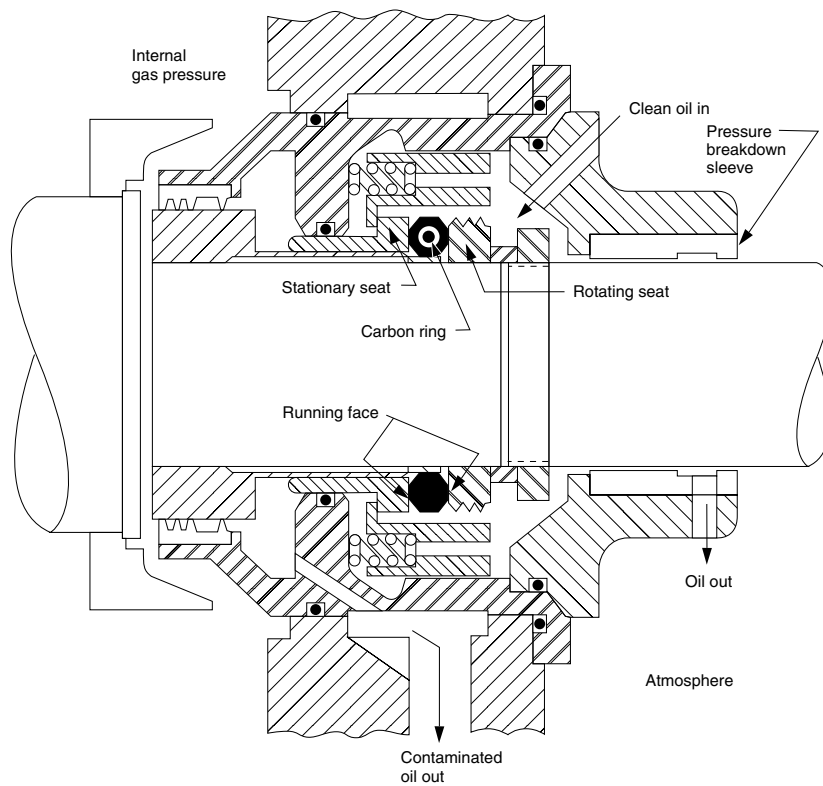


Figure 2-51—Mechanical (Contact) Shaft Seal

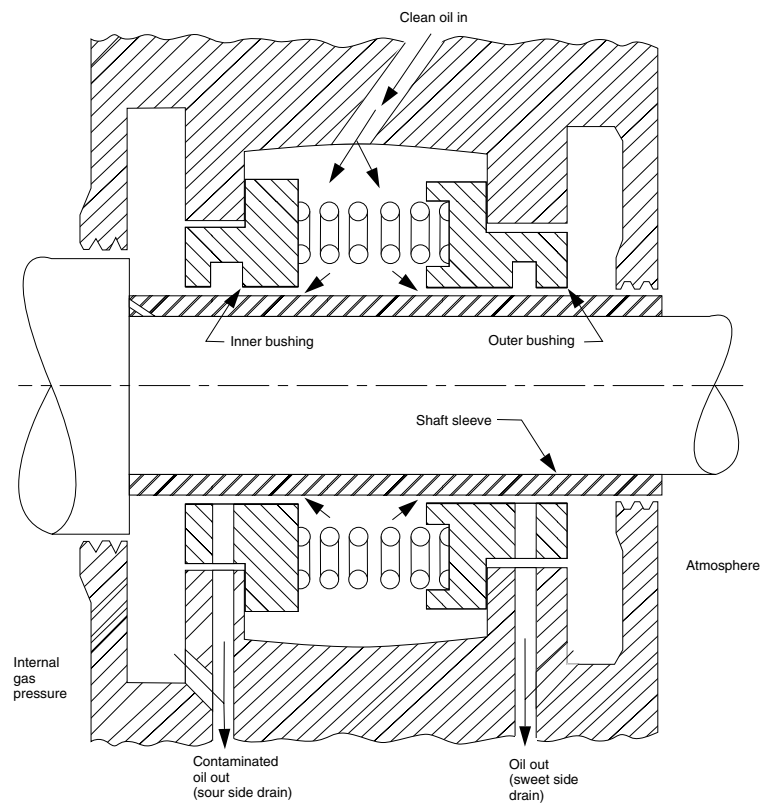


Figure 2-52—Liquid-film Shaft Seal with Cylindrical Bushing

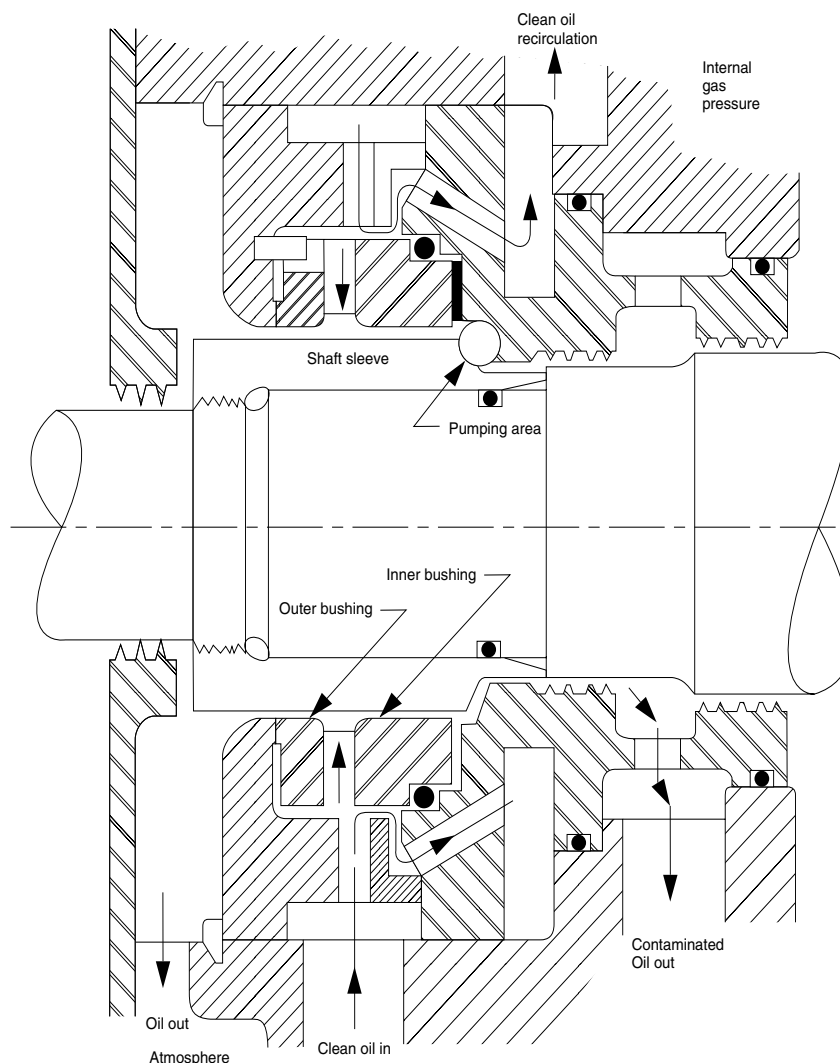


Figure 2-53—Liquid-film Shaft Seal with Pumping Bushing

2.6.3 Oil Seal Modeling & Testing

The modeling of liquid film seals got a significant start with Black [5,6]. In this work, the influence of high axial flow seals with Reynolds numbers > 2000 on the rotordynamic behavior of pumps was explained. Light viscosity liquids, large axial pressure gradients and large clearance to radius ratio characterized these seals. This work brought into attention how dramatically different seal flow was from conventional circular journal bearing flow.

The bulk of the work that followed examined various aspects of modeling turbulent flow. Hirs' bulk flow model [7] was applied to the turbulent flow seals by Childs [8,9]. Hirs' theory assumes the friction factor is a function of Reynolds number only. This was found restrictive when analyzing seals with rough surfaces. Moody's equation, which assumes that friction factor is a function of both Reynolds number and rel-

ative roughness, provided closer agreement with experimental results [10,11].

Dietzen and Nordmann [12] applied fully three-dimensional flow methods using a κ - ϵ turbulence model. Turbulence models applied to CFD codes attempt to model the turbulence flow. (Hirs' model treats the turbulence effects as a change in viscosity.) Large centered whirl amplitudes were included by Tam et al. [13]. In both cases, the additional computational effort produced marginal benefits over bulk flow models. Other research included variable properties [14] and fluid inertia effects [15].

Experimental results were largely obtained by Childs at Texas A&M. Childs et al. measured damper seals with different surface roughness [16] and tapered seals [17]. Grooved seals [18,19] and hole-pattern damper seals [20] were also tested.

As noted earlier, annular seals with inviscid fluids tend to be highly turbulent requiring a specialized analytical

approach. In some cases, these solutions can be applied to the lower Reynolds number axial flow found in oil seals but may not include the lock-up analysis that is unique with floating ring seals. Kirk and Miller [21] developed an approach based on Reynolds lubrication equation including the locking mechanism. This approach was extended to include a thermal heat balance [22] and later to include multiple floating rings [23].

Kirk [3] shows the importance of determining the locked position by stating that cross coupled stiffness can increase by tenfold with increasing eccentricity. A quasi-static method for estimating the lock-up eccentricity was presented by Allaire et al. [24]. Static measurements of these holding forces were made by Kirk and Browne [25].

2.6.4 Gas Seals

The inclusion of gas seals in lateral analysis (excluding stability) is not a requirement of the API specifications. In general, gas seals are treated as a second order effect in unbalance response analysis. Principle stiffness and effective damping terms are usually small in comparison to oil film seals and journal bearings. However, there are configurations of gas seals that do produce significantly large principle stiffness and damping terms. In these situations, an accounting of their effect would be needed for an accurate response analysis. These exceptions are discussed later in this section. Some examples of gas seals found in turbomachinery are illustrated in Figures 2-54 – 2-60.

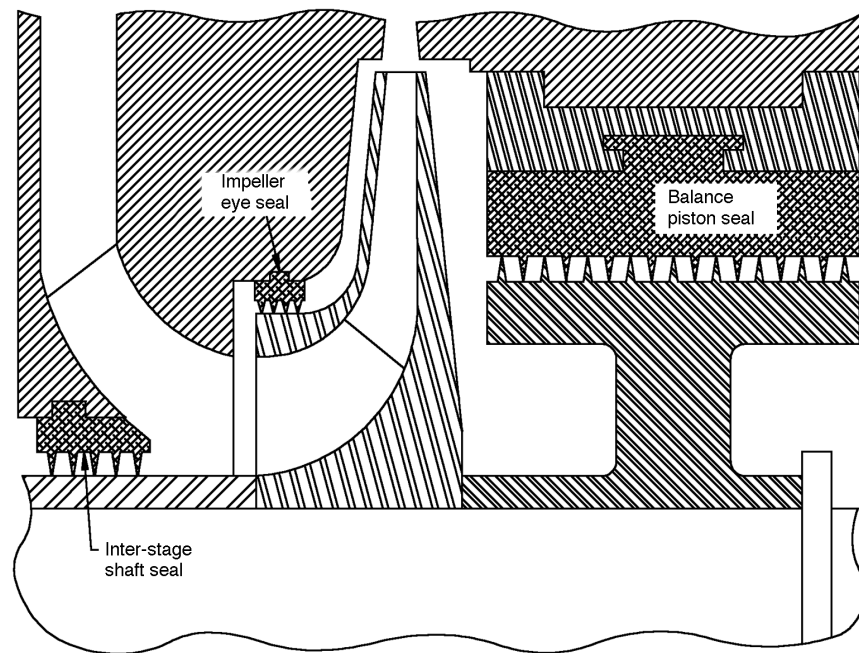


Figure 2-54—Compressor Labyrinth Seals

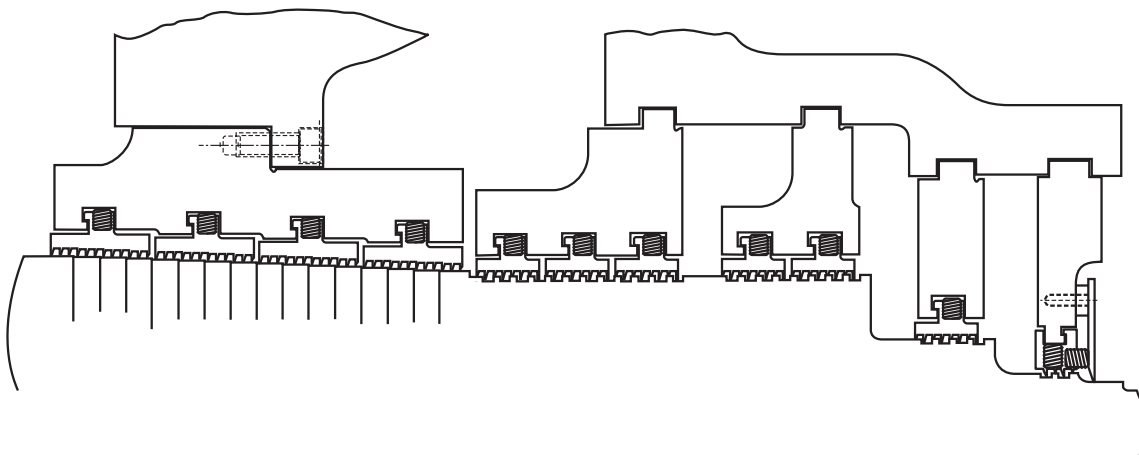


Figure 2-55—Typical Turbine Shaft Seal Arrangement—HP End

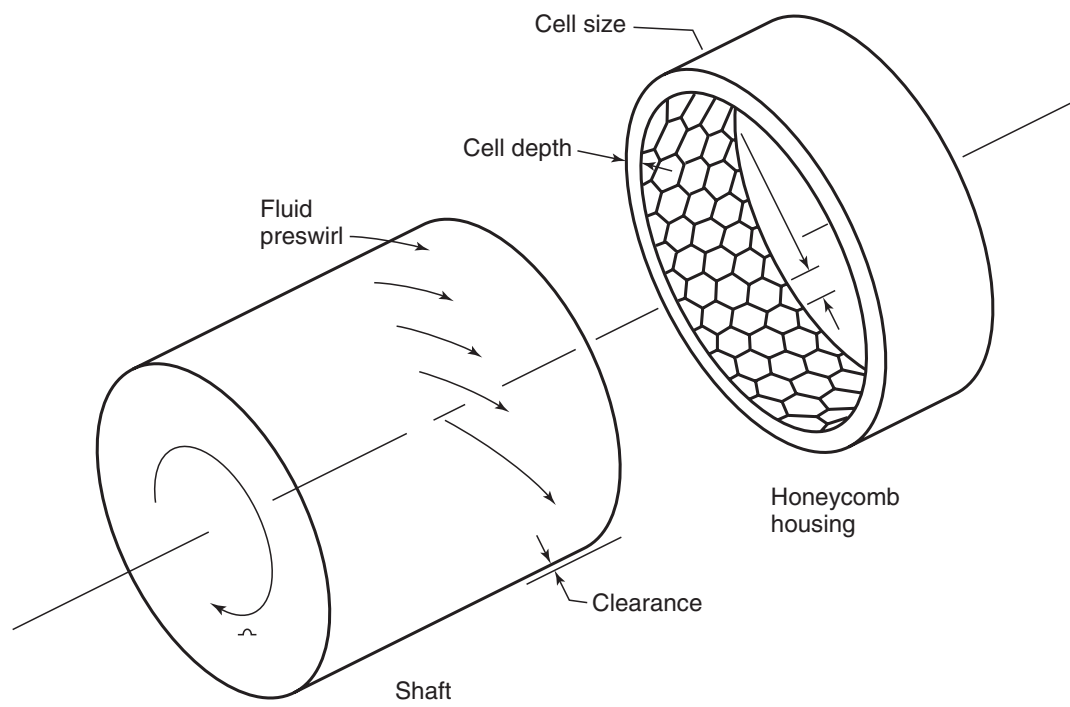


Figure 2-56—Honeycomb Seal



Figure 2-57—Pocket Damper Seal

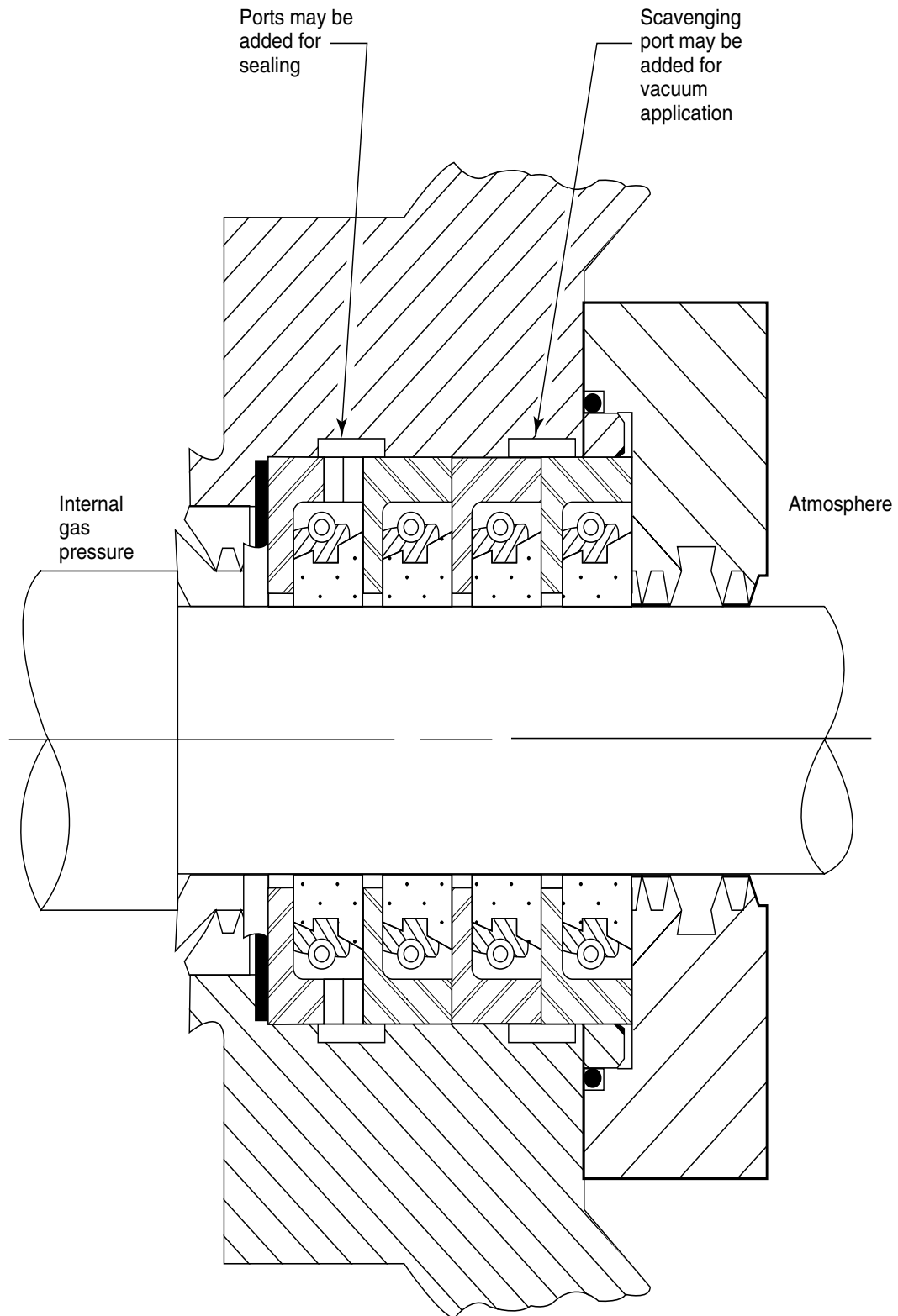


Figure 2-58—Segmented-ring Shaft Seal

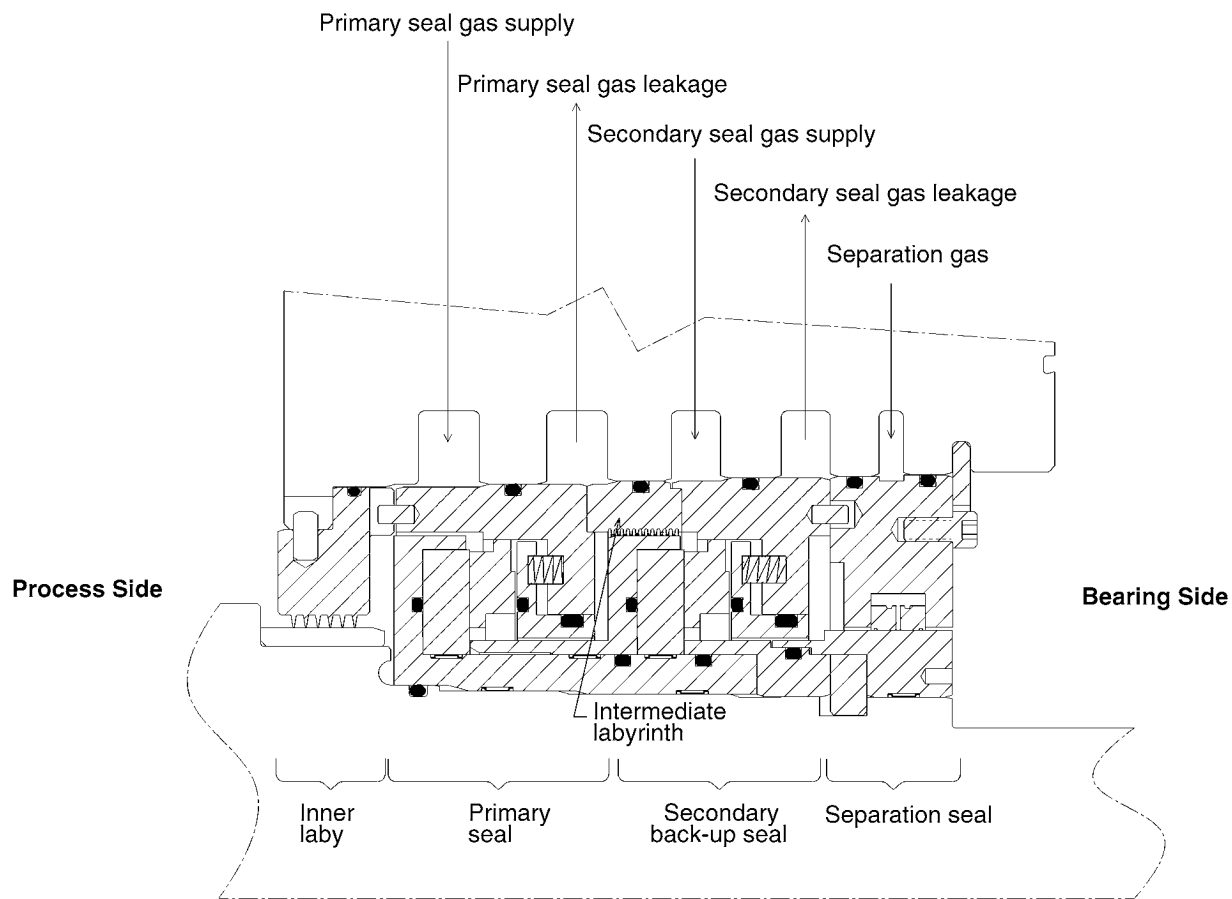


Figure 2-59—Self-acting Gas Seal

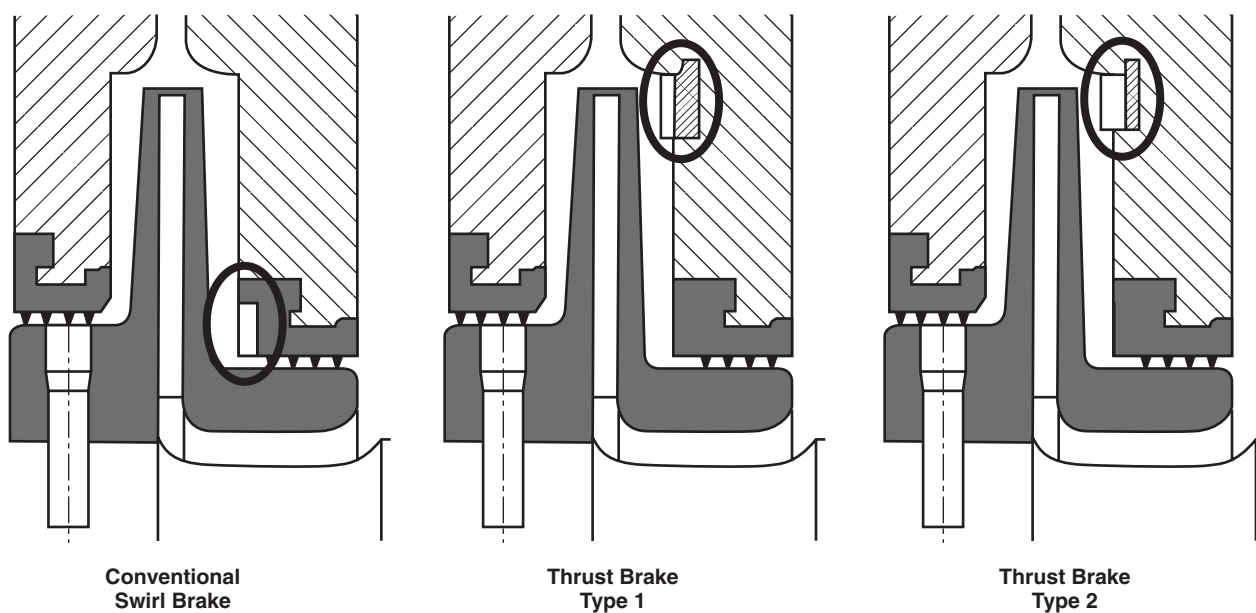


Figure 2-60—Swirl and Thrust Brakes Used in High-pressure Compressors [27]

Of the gas seals listed, the self-acting gas seal and the segmented-ring shaft seal are basically neutral dynamically. The segmented-ring seal is frequently applied as a barrier seal as well. Their contributions to the unbalance or stability analyses are added mass and inertia to the rotor model (if sleeves are used in conjunction with the segmented-ring seal).

The labyrinth seal has drawn considerable attention in rotordynamics concerning rotor stability. Over the last 30 years, many articles have recognized the importance of the labyrinth seal on rotor stability in a variety of rotating equipment, centrifugal compressors, aircraft gas turbines and cryogenic rocket turbopumps to name a few. However, little attention has been paid to the effect on synchronous vibrations. This can be attributed to several factors:

- a. Early analytical methods predicted negative principle stiffness terms especially for the balance piston seal in centrifugal compressors. Analytically, a major impact on the location of the rotor critical speeds would be predicted. However, this was not experienced during operation. The lack of agreement led many analysts to stop using the principle stiffness terms predicted for the labyrinth seal. Recently, experimental results have indicated the principle stiffness to be nearly zero and have a smaller than predicted effect on the critical speed frequency.
- b. The whirl frequency ratio for a typical labyrinth seal with no swirl brakes or re-injection is close to unity. The inlet swirl ratio (the ratio of circumferential flow rate to the shaft surface speed) is typically in the order of 0.6 to 0.8 for many applications without special inlet flow treatments. In this range, analytical predictions and testing results indicate a whirl frequency ratio of approximately 1.0. Obviously many factors affect this value and the deviation can be significant on the plus or minus side. But whirl frequency values around one would be neutral in terms of damping or exciting synchronous vibrations.

Exceptions to any rule will inevitably occur over time. For gas seals, the exceptions are in the form of the honeycomb seal, gas damper seal and labyrinth seals with inlet flow treatment. Published material has recently become available that suggests that these configurations of gas seals may have a significant effect on response levels and critical speed locations.

Memcott [26] reported on a 7 stage back-to-back compressor that underwent modification to eliminate a vibration problem. The center labyrinth was replaced with a honeycomb balance piston. This increased the frequency of the subsynchronous vibration to 94% of running speed indicating that the location of the first critical speed was affected. Subsequent inclusion of shunt holes eliminated the subsynchronous vibration.

Baumann [27] presents experience with swirl brakes of various configurations used on high-pressure compressors. One interesting and unexplained phenomena was a significant drop in the natural frequency of several compressors with increased discharge pressure, in some cases by nearly 40%. This occurred in compressors where swirl brakes were placed at several locations throughout the machine. Figures 2-60 and 2-61 are taken from that report showing the swirl brake arrangements and the reported loss in frequency of the first bending mode.

Even though these gas seals demonstrate the capability of changing the location and behavior of the rotor critical speeds, one important factor still exists; a pressure drop is required to produce the dynamic coefficients. Why is this important? Most flexible rotors will have their first critical speed around 50% \pm 15% of design speed. Assuming that discharge pressure (and pressure gradient) is developed as the square of speed, at 50% of the design speed only $1/4$ of the design pressure gradient has been achieved. At this level, gas seals dynamics will be greatly reduced accordingly and thus, their affect on the rotordynamics of the shaft.

While the synchronous behavior of the first critical speed may only be affected in a minor fashion by gas seals, it is becoming apparent that the subsynchronous location of the first critical may change significantly. Whether it is an increase in frequency that Memcott [26] reported or the drop that Baumann [27] noted, a change is possible and in some cases likely. This will alter the true separation margin of the critical speed in question. In these cases, the separation margin calculated by the unbalance response can be misleading.

The variation of support stiffness as a function of discharge pressure (and thus rotor speed) can result in a phenomenon called critical speed tracking. This is the situation where the critical speed location tracks the running speed. Increasing shaft speed does not relate to an increase in the separation margin of the mode. In most rotating equipment with gas as the working fluid, the critical speed frequency may remain unchanged or vary only slightly over the operating range. For the cases noted above, the variations can become significant. Graphically, this can be shown as Figure 2-62.

In a case where the first natural frequency was raised to 94% of running speed at MCS, the separation could be affected as shown on Figure 2-63. In this hypothetical case, the unbalance response predicts a peak response of the first critical speed at 5,000 rpm. As speed is increased and the gas seals (in this case a mid-span honeycomb) have a greater influence on the rotordynamics, the frequency of the first critical speed increases as well. This continues until MCS is reached. At this point, the actual separation margin between the running speed and first natural frequency is only 6%. This represents the critical speed tracking phenomenon mentioned earlier. This behavior is seen on cryogenic turbopumps incorporating hydrostatic bearings. In this application, the principle support stiffness of the bearings is tied to pressure being

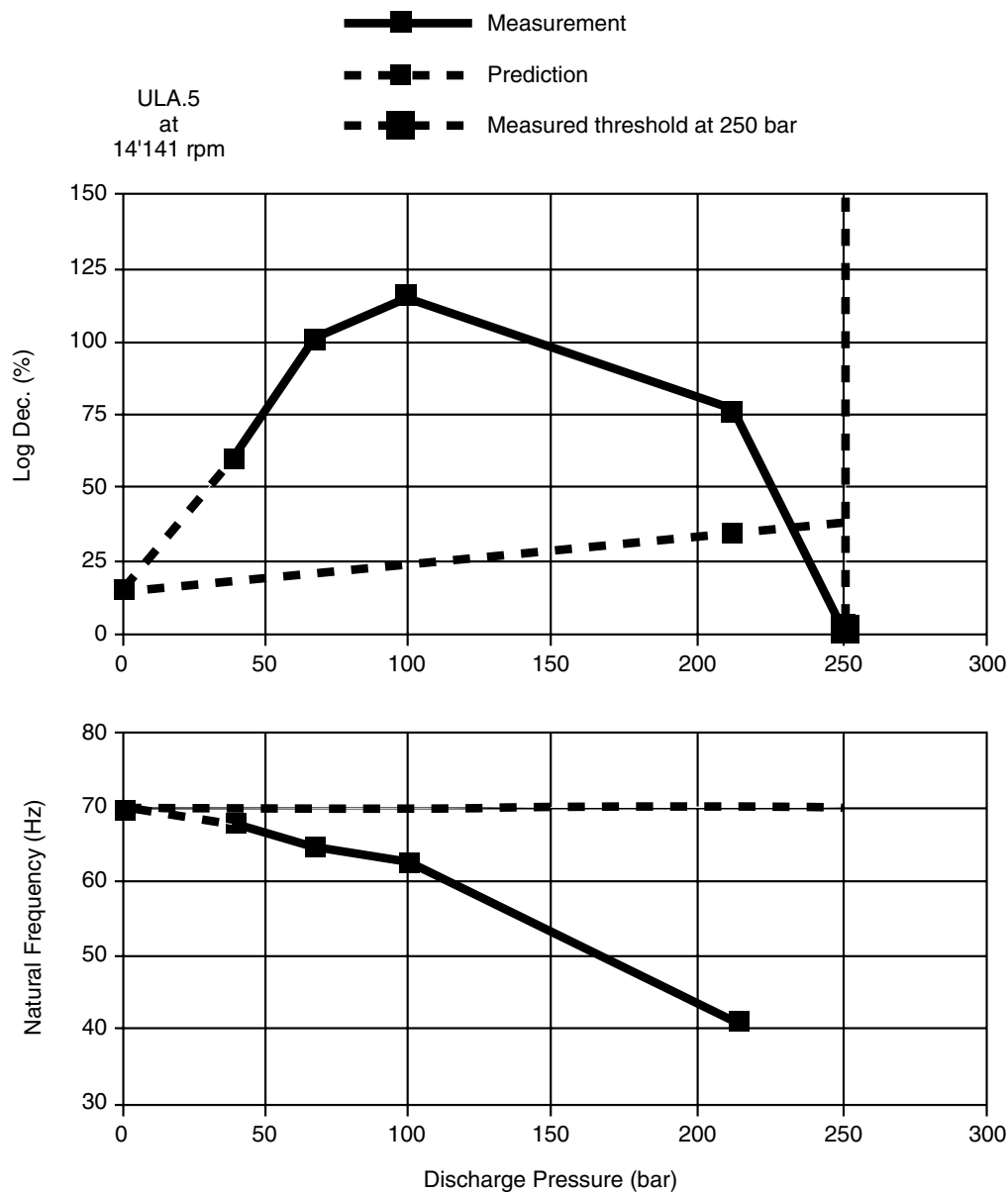


Figure 2-61—Measured Natural Frequency and Damping Showing a Drop of the First Bending Mode of the Shaft [27]

developed in the pump. As discharge pressure increases with speed, so does the rotor support stiffness producing an effect similar to that shown on Figure 2-63.

2.6.5 Gas Seal Modeling

Section 3.4.2 presents an excellent background on the analysis and testing of labyrinth seals in the literature. Some of that information is repeated here. In addition, Childs [28] provides an excellent overview of modeling techniques, analytical methods and testing results for various types of gas seals from smooth to interlocking labyrinths. A brief summary of Childs' chapter dealing with gas seals is included here.

Labyrinth seals have been modeled using bulk flow models with various control volumes. A single volume was investigated by Childs and Scharrer [29] and extended to eccentric shaft positions by Kurohashi et al. [30] and stepped labyrinths by Scharrer [31]. A two-control volume model was proposed by Wyssman et al. [32]. The model has one volume in the cavity between teeth and one covering the through-flow region. A three-control volume model has been studied by Nordmann and Weiser [33]. The control volume are illustrated in Figure 2-64. In addition, Nordmann and others have investigated the use of Navier-Stokes CFD models to analyze gas seals.

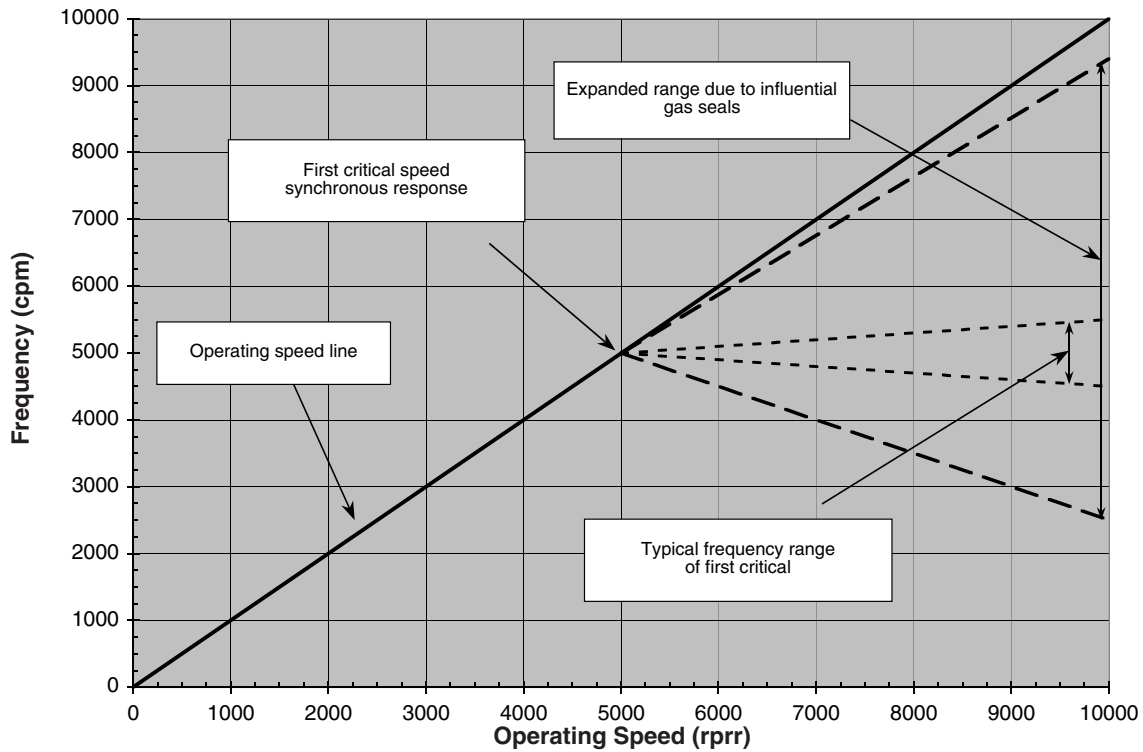


Figure 2-62—Change in First Critical Speed Frequency Due to Influential Gas Seals

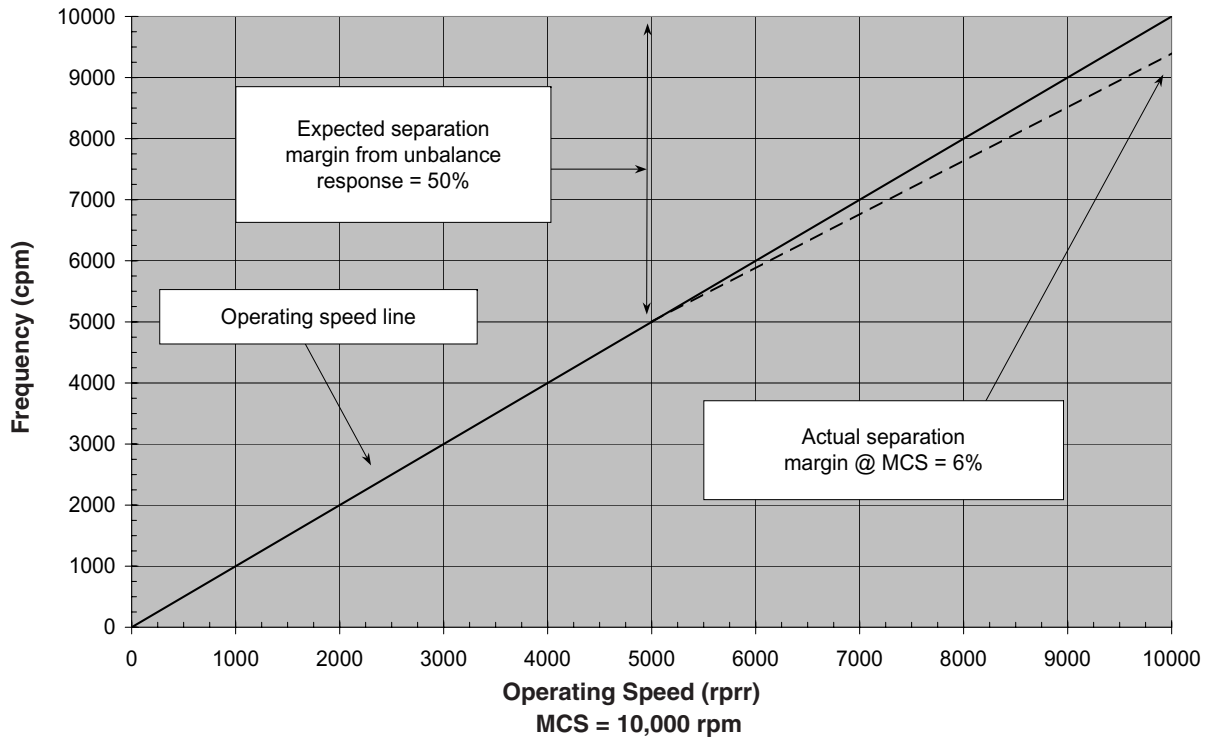


Figure 2-63 Change in Separation Margin From Unbalance Response Calculation

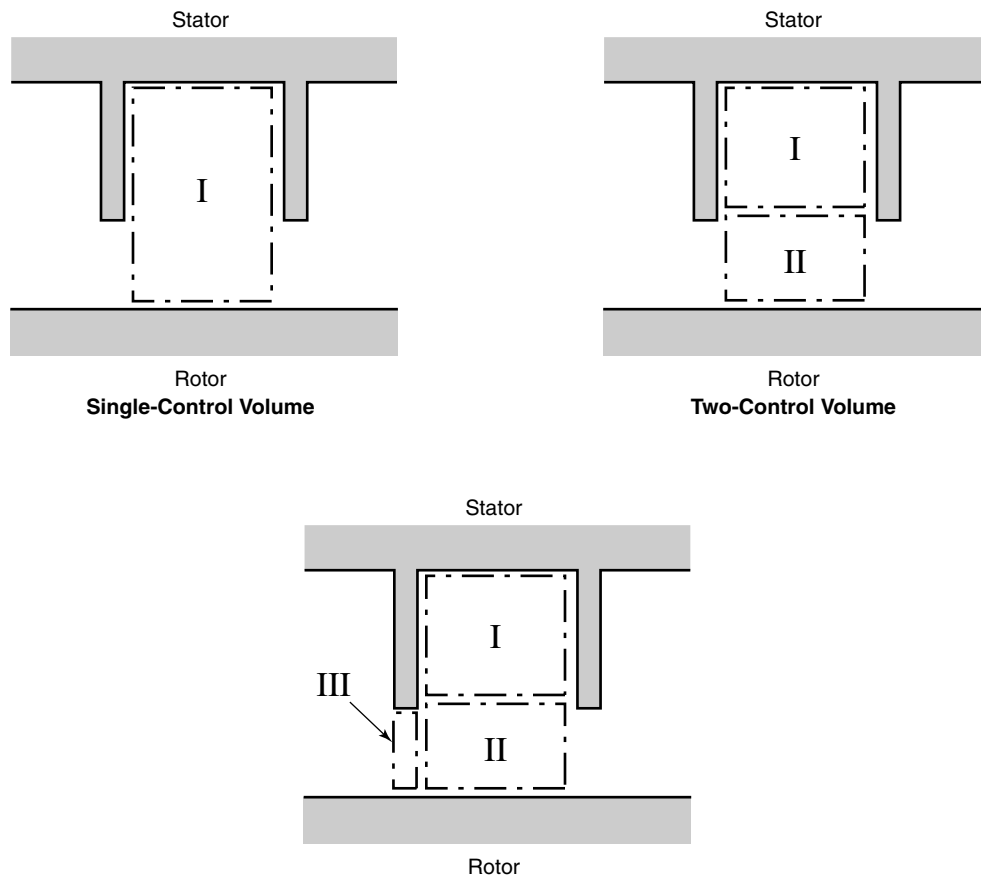


Figure 2-64—Labyrinth Seal Bulk Flow Control Volume Approaches

The research summarized in Childs [28] provided the first measurements of the stiffness and damping coefficients. While the results gave the first comprehensive basis for comparison against predictions, Childs and Ramsey [34] revealed the importance of testing at or near the application conditions. The test rig was extended toward this goal by Childs and Scharrer [35] and then again by Elrod, et al. [36]. Teeth-on-stator, teeth-on-rotor, and interlocking configurations were tested.

Wagner and Steff [37] developed a test rig supported by magnetic bearings. The intent of the rig was to further expand the existing knowledge database to geometries and gas conditions matching industrial applications, namely, pressure differential, size and speed. The magnetic bearings made it possible to set the eccentricity and superimpose circulatory movement independent of speed. The rig permitted the inlet pressure and the backpressure to be set independently of one another. Pressures of 70 bar (115 psi) were possible at surface speeds up to 157 m/s (515 fps).

Finally, predictions and test results for honeycomb seals are relatively recent and still preliminary in their depth. Modeling techniques of the honeycomb seal include those based on bulk flow analysis using a friction factor to model the hon-

eycomb surface, Ha and Childs [38]. The friction factor has been defined using a Blasius- or Moody-equation. The weakness of these models stems from origin of the friction factors. Literature has shown that these must be obtained experimentally to provide reasonable predictions of the dynamic behavior of honeycomb seals.

Unfortunately, the bulk of the honeycomb test results are proprietary. However, some testing is available in the open literature. Recent tests have indicated a “resonance” condition in the honeycomb seal. This is related to the fundamental acoustic resonance in the cavity, Kleynhans and Childs [39]. It is accompanied by an abrupt change in the friction factor and dynamic coefficients of the seal.

Experimental results have confirmed the beneficial aspects of the honeycomb seal, Yu and Childs [40]. These advantages include low whirl frequency ratios, less leakage than comparable clearance tooth-on-stator labyrinths, and ruggedness. Manufacturing costs and times can be reduced when a hole-pattern configuration is employed without loss in dynamic behavior, Holt and Childs [41]. Experimental data also indicates principle stiffness and damping terms on the order of smooth seals and significantly higher than labyrinth seals especially in heavy gases.

2.6.6 References

1. Allaire, P. E., Stroh, C. G., Flack, R. D., Kocur, Jr., J. A. and Barrett, L. E., 1987, "Subsynchronous Vibration Problem and Solution in Multistage Centrifugal Compressor," Proceedings of the 16th Turbomachinery Symposium, Turbomachinery Laboratory, Texas A&M University, College Station, Texas, pp. 65-73.
2. Kirk, R. G., 1986, "Oil Seal Dynamics: Considerations for Analysis of Centrifugal Compressors," Proceedings of the 15th Turbomachinery Symposium, Turbomachinery Laboratory, Texas A&M University, College Station, Texas, pp. 25-34.
3. Cerwinski, T. J., Nelson, W. E. and Salamone, D. J., 1986, "Effects of High Pressure Oil Seals On the Rotordynamic Response of a Centrifugal Compressor," Proceedings of the 15th Turbomachinery Symposium, Turbomachinery Laboratory, Texas A&M University, College Station, Texas, pp. 35-51.
4. Baheti, S. K. and Kirk, R. G., 1994, "Thermo-Hydrodynamic Solution of Floating Ring Seals for High Pressure Compressors Using the Finite-Element Method," *STLE Tribology Transactions*, Volume 37, No. 2, pp. 336-346.
5. Black, H. F., 1969, "Effects of Hydraulic Forces on Annular Pressure Seals on the Vibration of Centrifugal Pump Rotors," *Journal of Mechanical Engineering Science*, Vol. 11, No. 2, pp. 206-213.
6. Black, H. F. and Jenssen, D. N., 1971, "Effects of High Pressure Ring Seals on Pump Rotor Vibrations," ASME Paper 71-WA/FF-38.
7. Hirs, G. G., 1973, "A Bulk Flow Theory for Turbulence in Lubricating Films," *ASME Journal of Lubrication Technology*, Vol. 95, No. 2, pp. 137-146.
8. Childs, D. W., 1983, "Dynamic Analysis of Turbulent Annular Seals Based on Hirs Lubrication Equation," *ASME Journal of Lubrication Technology*, Vol. 105, pp. 429-436.
9. Childs, D. W., 1983, "Finite Length Solutions for Rotordynamic Coefficients of Turbulent Annular Seals," *ASME Journal of Lubrication Technology*, Vol. 105, pp. 437-444.
10. Nelson, C. C. and Nguyen, D. T., 1987, "Comparison of Hirs' Equation with Moody's Equation for Determining Rotordynamic Coefficients of Annular Pressure Seals," *ASME Journal of Tribology*, Vol. 109, pp. 144-148.
11. Nelson, C. C. and Nguyen, D. T., 1988, "Analysis of Eccentric Annular Incompressible Seals: Part 1 – A New Solution Using Fast Fourier Transforms for Determining Hydrodynamic Forces," *ASME Journal of Tribology*, Vol. 110, pp. 361-366.
12. Dietzen, F. J. and Nordmann, R., 1988, "A Three-Dimensional Finite-Difference Method for Calculating the Dynamic Coefficients of Seals," Proceedings of the Rotordynamics Instability Problems in High-Performance Turbomachinery, NASA Publ. 3026, pp. 211-228.
13. Tam, L. T., et. al., 1988, "Numerical and Analytical Study of Fluid Dynamics Forces in Seals and Bearings," *ASME Journal of Vibration, Acoustics, Stress and Reliability Design*, pp. 315-325.
14. San Andres, L. A., 1991, "Analysis of Variable Fluid Properties, Turbulent Annular Seals," *ASME Journal of Tribology*, Vol. 113, pp. 694-702.
15. Simon, J. and Frene, J., 1990, "Rotordynamic Coefficients of Turbulent Annular Misaligned Seals," 3rd International Symposium on Transport Phenomena and Dynamics of Rotating Machinery (ISROMAC-3), Vol. 2: Dynamics, pp. 124-143.
16. Childs, D. W. and Kim C.-H., 1985, "Analysis and Testing for Rotordynamic Coefficients of Turbulent Annular Seals with Different, Directionally-Homogenous Surface Roughness Treatment for Rotor and Stator Elements," *ASME Journal of Tribology*, Vol. 107, No. 3, pp. 296-306.
17. Childs, D. W. and Dressman, J. B., 1985, "Convergent-Tapered Annular Seals: Analysis and Testing for Rotordynamic Coefficients," *ASME Journal of Tribology*, Vol. 107, No. 3, pp. 307-317.
18. Childs, D. W. and Kim C.-H., 1986, "Testing for Rotordynamic Coefficients and Leakage: Circumferentially Grooved Seals," Proceedings of the Second IFTOMM International Conference on Rotordynamics, Tokyo, Japan, pp. 609-618.
19. Childs, D. W., Nolan, S. and Kilgore, J., 1990, "Test Results for Turbulent Annular Seals Using Smooth Rotors and Helically-Grooved Stators," *ASME Journal of Tribology*, Vol. 112, pp. 254-258.
20. Childs, D. W., Nolan, S. and Kilgore, J., 1990, "Additional Test Results for Round Hole-Pattern Damper Seals: Leakage, Friction Factors and Rotordynamic Force Coefficients," *ASME Journal of Tribology*, Vol. 112, pp. 365-371.
21. Kirk, R. G. and Miller, W. H., 1979, "The Influence of High Pressure Oil Seals on Turbo-Rotor Stability," *ASLE Transactions*, Vol. 22, No. 1, pp. 14-24.
22. Kirk, R. G. and Nicholas, J. C., 1980, "Analysis of High Pressure Oil Seals for Optimum Turbocompressor Dynamic Performance," Vibrations in Rotating Machinery 2nd International Conference, Institution of Mechanical Engineers, Cambridge, pp. 125-134.

23. Reedy, S. W. and Kirk, R. G., 1992, "Advanced Analysis of Multi-Ring Liquid Seals," *ASME Journal of Vibration and Acoustics*, Vol. 114, pp. 42-46.
24. Allaire, P. E., Kocur, J. A. and Stroh, C. G., 1986, "Oil Seal Effects and Subsynchronous Vibrations in High Speed Compressors," Proceedings of the Rotordynamics Instability Problems in High-Performance Turbomachinery, NASA Publ. 2409, pp. 205-223.
25. Kirk, R. G. and Browne, D. B., 1990, "Experimental Evaluation of Holding Forces in Floating Ring Seals," Proceedings of the International Federation for Theory of Machinery and Mechanical International Conference, pp. 319-323.
26. Memmott, E. A., 1994, "Stability of a High Pressure Centrifugal Compressor Through Application of Shunt Holes and a Honeycomb Labyrinth," Presented at the 13th Machinery Dynamics Seminar, CMVA, Toronto, Canada, September 12-13.
27. Baumann, U., 1999, "Rotordynamic Stability Tests on High-Pressure Radial Compressors," Proceedings of the 28th Turbomachinery Symposium, Turbomachinery Laboratory, Texas A&M University, College Station, Texas, pp. 115-122.
28. Childs, D. W., 1993, *Turbomachinery Rotordynamics: Phenomena, Modeling, and Analysis*, John Wiley & Sons, Inc., New York.
29. Childs, D. and Scharrer, J., 1986, "An Iwatsubo-Based Solution for Labyrinth Seals: Comparison to Experimental Results," *ASME Journal of Engineering for Gas Turbines and Power*, Vol. 108, pp. 325-331.
30. Kurohasi, M., Inoue, Y., Abe, T. and Fujikawa, T., 1980, "Spring and Damping Coefficients of the Labyrinth Seals," *Proceedings ImechE – 2nd International Conference on Vibrations in Rotating Machinery*, Cambridge, England, pp. 215-222.
31. Scharrer, J., 1988, "Rotordynamic Coefficients for Stepped Labyrinth Gas Seals," *ASME Transactions, Journal of Tribology*, Vol. 111, pp. 101-107.
32. Wyssman, H., Pham, T. and Jenny, R., 1984, "Prediction of Stiffness and Damping Coefficients for Centrifugal Compressor Labyrinth Seals," *ASME Journal of Engineering for Gas Turbines and Power*, Vol. 106, pp. 920-926.
33. Nordmann, R. and Weiser, H., 1990, "Evaluation of Rotordynamic Coefficients of Look-Through Labyrinths by Means of a Three Volume Bulk Model," *Rotordynamic Instability Problems in High-Performance Turbomachinery*, NASA CP-3122, pp. 141-157.
34. Childs, D. W. and Ramsey, C., 1990, "Seal-Rotordynamic-Coefficient Test Results for a Model SSME ATD-HPFTP Turbine Interstage Seal With and Without a Swirl Brake", *Rotordynamic Instability Problems in High-Performance Turbomachinery*, NASA CP-3122, pp. 179-190.
35. Childs, D. W. and Scharrer, J. K., 1986, "Experimental Rotordynamic Coefficient Results for Teeth-on-Rotor and Teeth-on-Stator Labyrinth Gas Seals", *ASME 86-GT-12*.
36. Elrod, D. A., Pelletti, J. M. and Childs, D. W., 1995, "Theory Versus Experiment for the Rotordynamic Coefficients of an Interlocking Labyrinth Gas Seal," *ASME paper 95-GT-432*, presented at the International Gas Turbine and Aeroengine Congress and Exposition, Houston, Texas, June 5-8.
37. Wagner, N. G. and Steff, K., 1996, "Dynamic Labyrinth Coefficients From a High-Pressure Full-Scale Test Rig Using Magnetic Bearings," *Rotordynamic Instability Problems in High-Performance Turbomachinery*, NASA CP-3344, pp. 95-111.
38. Ha, T. W., and Childs, D.W., 1994, "Annular Honeycomb-Stator Turbulent Gas Seal Analysis Using a New Friction-Factor Model Based on Flat Plate Tests," *ASME Journal of Tribology*, Vol. 116, pp. 352-360.
39. Kleynhans, G.F., and Childs, D.W., 1996, "The Acoustic Influence of Cell Depth on the Rotordynamic Characteristics of Smooth-Rotor/Honeycomb-Stator Annular Gas Seals," *ASME Journal of Engineering for Gas Turbines and Power*, Vol. 119, pp. 949-956.
40. Yu, Z., and Childs, D.W., 1998, "A Comparison of Experimental Rotordynamic Coefficients and Leakage Characteristics Between Hole-Pattern Gas Damper Seals and a Honeycomb Seal," *ASME Journal of Engineering for Gas Turbines and Power*, Vol. 120, pp. 778-783.
41. Holt, C.G., and Childs, D.W., 2002, "Theory Versus Experiment for the Rotordynamic Impedances of Two Hole-Pattern-Stator Gas Annual Seals," *ASME Journal of Tribology*, Vol. 124, pp. 137-143.

2.7 ELEMENTS OF A STANDARD ROTORDYNAMICS ANALYSIS

2.7.1 Introduction

The purpose of a standard rotordynamic analysis and design audit is to enable an engineer to characterize the lateral dynamics design characteristics of a given design. One might compare such analysis to the routine physical in which a doctor seeks to determine a patient's general health rather than specifically testing for the source of a known problem or developing a comprehensive treatment plan for a specific disease. While analysis of some rotating equipment may require analysis specific to the unit, a general method has emerged

for performing the standard lateral analysis. With modeling of the individual components (rotor, bearings, seals, etc.) completed and described in the previous sections, the standard lateral analysis is composed of three parts: (a) undamped critical speed analysis, (b) damped unbalance response analysis, and (c) stability (damped eigenvalue) analysis.

The analysis of the lateral dynamics of rotating shafts began in 1869 [1] when Rankine identified the existence of critical speeds. Dunkerley [2] showed that the problem of calculating these critical speeds was equivalent to the problem of finding the natural frequencies of the shaft, treating it as a flexible beam on simple supports (rigid bearings). Based on Rankine's and Dunkerley's conclusions about the destructive nature of operating near or above the first critical speed, manufacturers focused on simply calculating the first critical speed and designed their machines to operate well below it [3]. This design approach was eventually found to be overly conservative through the experimental steam turbine work of De Laval and the landmark analysis of Jeffcott [4].

Possessing no knowledge of the bearings' stiffness and damping characteristics, for many years, rotordynamic analysis focused on accurately modeling the rotor's mass/elastic properties for critical speed prediction assuming rigid bearings. Without the computational power available today, approximating the first critical speed of a shaft with variable cross-section was a serious challenge. Several methods gained popularity. These included Rayleigh's quotient where the first critical speed was estimated by assuming the first mode shape, and Stodola's graphical technique [5] which was more widely used. These were replaced by the transfer matrix method of Myklestad [6] and Prohl [7], which was a variation of Holzer's technique for torsional dynamic analysis. This method allowed the mass/elastic properties of a variable cross-section rotor to be more accurately represented. It also made use of the growing accuracy of computers [8]. For almost 20 years after Prohl's publication, most machines were designed using this method to predict the critical speeds assuming rigid bearings with no oil film flexibility or damping.

With a greater availability of computational power in the early 1970's, manufacturers began applying the latest fluid film bearing models for the stiffness and damping characteristics, negating the need to assume rigid supports. This allowed for improved estimates of the critical speeds based on an undamped critical speed analysis. At the same time, manufacturers began performing unbalanced response analysis as a standard machine design calculation. In this analysis, the predominant technique was (and still is) the Lund and Orcutt algorithm [9] which expanded the transfer matrix method and allowed for actual vibration levels to be predicted along with the critical speeds and amplification factors. This algorithm also incorporated the full dynamic (stiffness and damping) characteristics of the machine's bearings.

Lund [10] also provided industry with a complete stability analysis algorithm in 1974. Also based on the transfer matrix method, this analysis technique was, for many years, only used by manufacturers on a selective basis for machines where stability would be of concern. See 3.1.1 for a complete historical review of stability analysis.

Today with the availability of high-speed computers, a complete dynamic picture of the machine can be obtained using advanced bearing/seal codes along with forced response and stability analysis codes.

2.7.2 Undamped Critical Speed Analysis

Serving as the primary analysis technique for many years, the undamped critical speed analysis is still performed today for the preliminary estimation of critical speeds and mode shape characteristics. It is deemed preliminary because this analysis excludes any damping in the system as well as any forces such as unbalance; items that determine the machine's actual dynamics. However, the undamped critical speed analysis can be of great value in rapidly assessing the general dynamic behavior of the machine.

The critical speeds and their associated mode shapes are most influenced by the support (bearing and pedestal structure) stiffness magnitudes, the support locations, and the rotor's mass and stiffness properties. Aimed at defining this influence for the specific machine, the undamped critical speed analysis applies a varying amount of stiffness at the support locations to the rotor model. The critical speeds and mode shapes of the system are then calculated for each support stiffness level. The primary result is the undamped critical speed map, for which a typical map is shown in Figure 2-65. This plot typically presents the first four undamped, forward-whirling modes as a function of total bearing/support stiffness. Both the abscissa (support stiffness) and ordinate (frequency of the critical speed) axes of the critical speed map are generally log scales. The important relationship that governs the overall characteristics of the critical speed map is the one between the shaft's stiffness and the support stiffness. Although not shown in Figure 2-65, the natural frequencies with zero support stiffness, or free-free condition, are governed by the shaft stiffness, with the first two natural frequencies being zero due to rigid body movement. When the stiffness of the bearings are small relative to the shaft's bending stiffness, the stiffness of the bearings and the rotor mass govern the frequency of the unit's lowest critical speed. The mode shapes affirm this behavior with little bending of the shaft. Conversely, when the bearings are much stiffer than the bending stiffness of the shaft, the frequency of the unit's undamped critical speeds will principally be governed by the mass and bending stiffness of the rotor (refer to Equation 1-8). Under this condition, the bearing supports become node points and a high degree of shaft bending occurs in the mode shape. This mode shape behavior is shown in Figure 2-66.

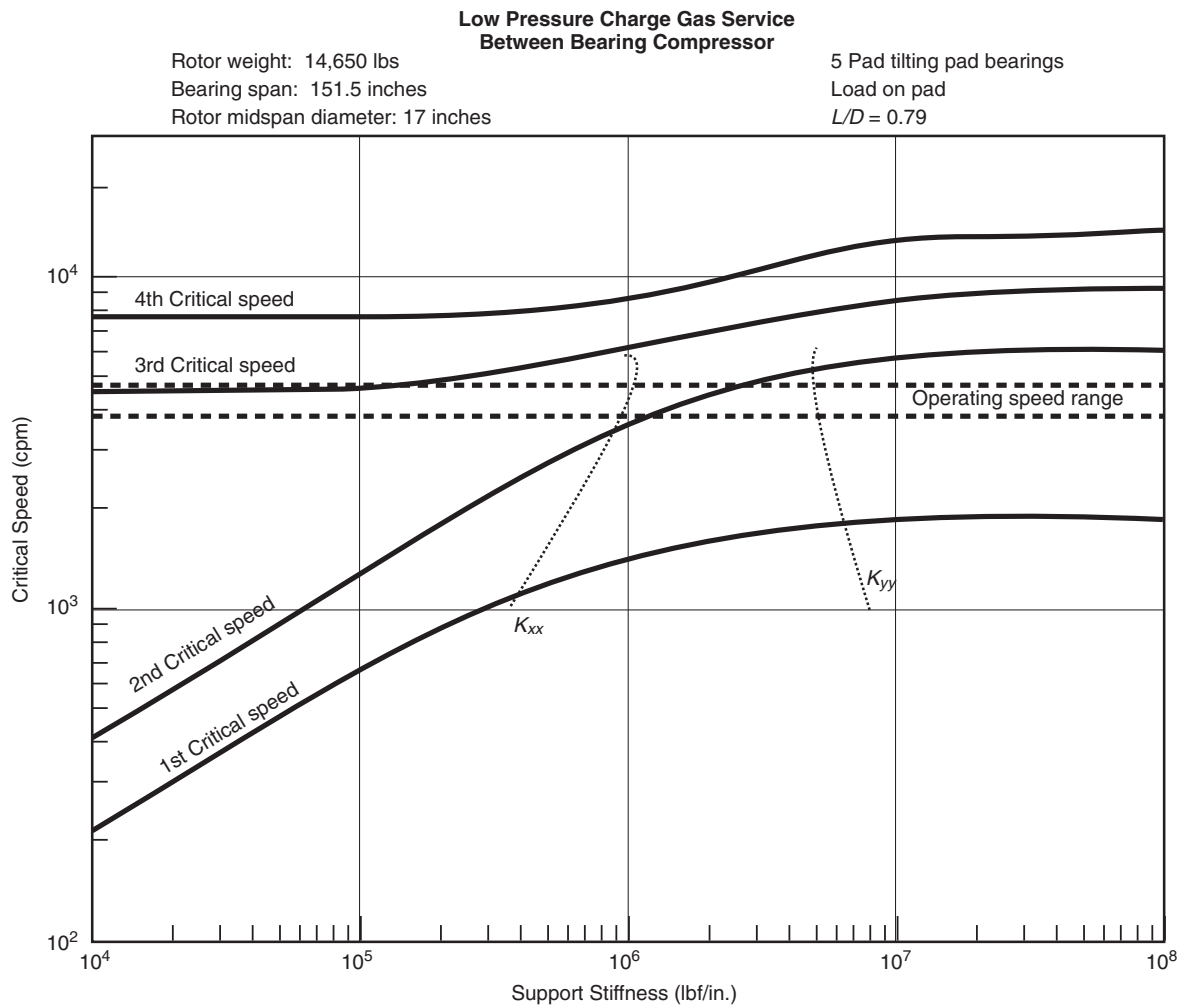


Figure 2-65—Undamped Critical Speed Map

The undamped critical speed map summarizes these relationships for the particular rotor being analyzed. Focusing our attention on the first two critical speed lines as displayed in Figure 2-65, there lies a region of bearing stiffness where the slope of these two lines is positive and approximately constant. This area is called the stiff rotor part of the critical speed map because the bending stiffness of the rotor is appreciably greater or the same order of magnitude as the bearing stiffness. On the right hand side of the undamped critical speed maps lies an area where the critical speeds do not change with increasing bearing stiffness. Referred to as the stiff bearing part of the critical speed map, the curves have reached asymptotic values because the shaft stiffness is dominating the system stiffness (refer to Equation 1-8). The asymptotic values of the critical speed lines are often referred to as the rigid bearing critical speeds. Since both are governed by the shaft properties, the “rigid criticals” and the “free-free criticals” are sometimes measured experimentally to verify and improve the mathematical model of the rotor [11,12].

With the critical speed map defined, the final step in the analysis is to define what the actual support characteristics are in order to estimate the critical speeds. Using the results from bearing and support analysis techniques, speed-dependent total bearing/support principal stiffnesses (K_{xx} , K_{yy}) are cross-plotted on the map like that displayed in Figure 2-65. Speeds where the support coefficient curves intersect the critical speed curves are the potential critical speeds of the system. For highly asymmetric bearings, like the one shown in this example, these intersections may be at substantially different speeds for the same mode indicating a critical speed associated with the horizontal direction and one for the vertical direction, i.e., a “split critical”. Note that in beam-type machines (no overhung wheels or stages), the difference in bearing static loads often does not vary significantly from end to end. Consequently, the calculated bearing coefficients often are nearly equal on both ends of the unit. For this reason, only one set of a bearing’s coefficients typically appears on a critical speed map. For machines where the bearings’

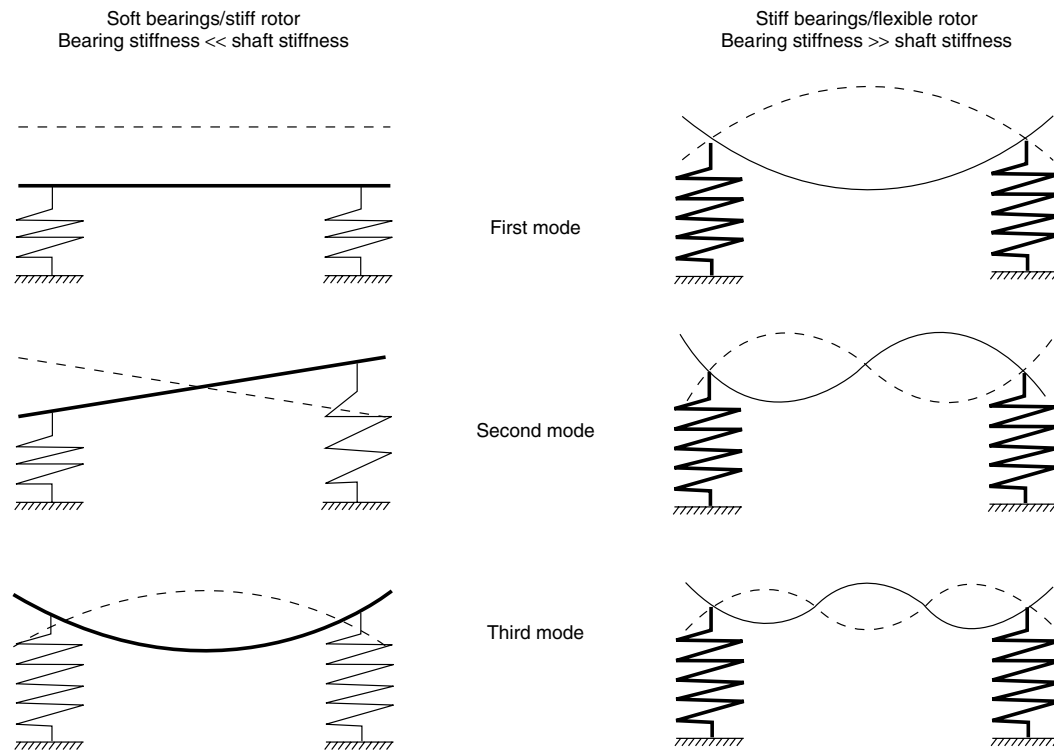


Figure 2-66—Mode Shape Examples for Soft and Stiff Bearings Relative to Shaft

static loads differ substantially, the undamped critical speed map and the overall undamped analysis are more difficult to interpret. See the later sections of this tutorial for how to handle specific machines which fall into this category. The discussions here focus on between bearing machines.

Cross-plotting the calculated bearing coefficients on undamped critical speed maps allows one to infer the general damped unbalance response characteristics of a rotor-bearing system. If the bearing stiffness intersects a critical speed line in the stiff rotor part of the undamped critical speed map, then the amplification factor associated with the critical will be small (less than 8), and the rotor's response to unbalance during operation near the critical speed will be well-damped. For the compressor example map shown in Figure 2-65, the horizontal stiffness intersects in the stiff rotor part of the critical speed map. If, however, the bearing/support stiffnesses intersect a critical speed line on the flat part of the critical speed line, the amplification factor associated with the critical speed will be large (probably greater than 8). The rotor's response to unbalance will be highly amplified during operation near the critical speed. Referring to our example map, this compressor would be expected to have a large amplification factor in the vertical direction.

The relationship between the undamped critical speed map and the results of other lateral dynamics analysis, such as the damped unbalance response analysis, may be better understood if the undamped mode shapes associated with the first

few undamped critical speeds are examined for the soft and stiff bearing cases (Figure 2-66). Note in the case of soft bearings (relative to shaft bending stiffness) that shaft deflections are small relative to the bearing deflections. The damping generated by the bearings will be used to attenuate rotor vibrations caused by potential rotor exciting forces such as unbalance. On the other hand, when the bearings are stiff relative to the shaft bending stiffness, the shaft deflections are large relative to the bearing deflections. In this case, even if the bearing damping coefficients are large, the damping forces provided by the bearings will be small because the rotor motion at the bearings is small. Thus, rotor vibrations caused by unbalance and other forces will be highly amplified at critical speeds if the bearings are much stiffer than the rotor bending stiffness.

Mode shapes associated with the undamped lateral natural frequencies should be calculated as part of the undamped critical speed analysis and presented as shown in Figure 2-67. This figure shows the typical mode shapes for a between bearing rotor. Other machine types will have fundamentally different mode shapes and the reader should consult the machine specific consideration sections which follow. Mode shapes are usually calculated using bearing principle stiffnesses which bracket the predicted bearing stiffness range. These plots display the rotor's normalized free (unforced) rotor deflections associated with the lateral undamped natural

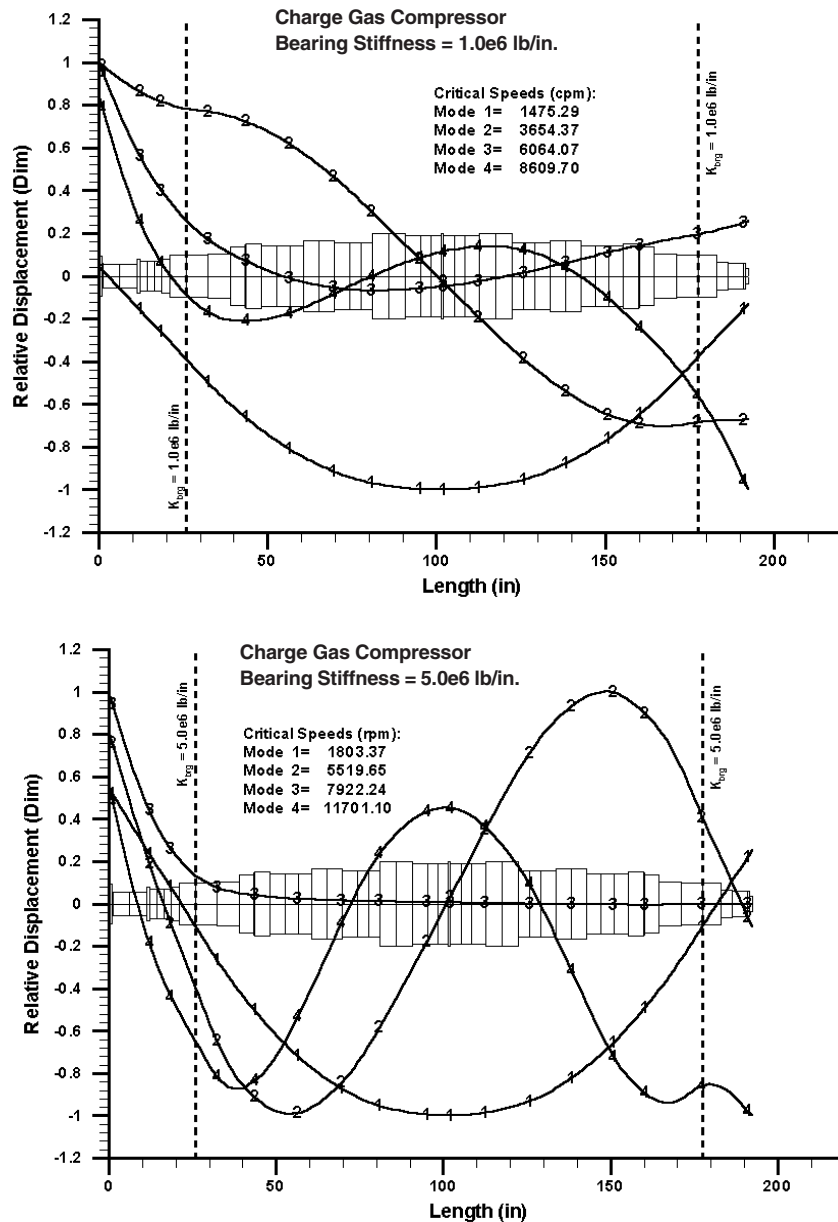


Figure 2-67—Typical Undamped Modes Shapes for a Between Bearing Machine with Different Values of Support Stiffness

frequencies. The undamped mode shapes are useful for the following reasons:

- The undamped mode shapes are planar or two dimensional; undamped mode shapes do not possess the complex three dimensional bending experienced by the rotor due the presence of damping.
- The undamped mode shapes provide an approximate indication of the relative displacements that the shaft undergoes when the rotor operates in the vicinity of the associated critical speed. Thus, given a vibration amplitude at a probe location during operation near a critical speed, one may esti-

mate the vibration amplitude at other locations on the rotating element.

- An undamped mode shape gives an indication of what unbalance distribution will be necessary to excite the associated critical speed. This is information is vital for determining the unbalance locations that are needed for the damped unbalance response analysis where unbalance must be specified at certain locations along the rotor.
- Undamped mode shapes can be used to determine unbalance response and stability through modal analysis techniques. Using the undamped mode shapes, the rotor sys-

tem can be simplified (known as model reduction [8]) allowing for quicker computations of response and stability. When these modal analysis techniques are employed, most often the rotor's undamped free-free mode shapes are utilized where no bearings or supports are present.

2.7.3 Damped Unbalanced Response Analysis

With the undamped critical speed analysis providing some knowledge of the critical speeds and their sensitivity, it does not provide any information regarding the actual vibrational amplitudes expected. This is accomplished by conducting an unbalance response analysis with damping included. Its objective is to determine whether the machine will meet the required separation margins and vibration limits. The API standard paragraphs establish the following unbalance response performance requirements for the machine:

- a. Adequate separation margin between critical speeds and operating speeds
- b. The probe vibration limit is not exceeded within the specified operating speed range even with twice the maximum allowable residual unbalance present.
- c. No rubbing will occur even if the rotor's balance state degrades to the probe vibration limit.

The unbalance response analysis determines whether or not these performance requirements are achieved.

Given the criticality of this analysis, an accurate model is imperative and this accuracy is obviously dependent upon the level of detail incorporated. The model must incorporate the speed dependence of bearings', seals', and support pedestals' dynamic properties for the machine's entire speed range including trip speed. Furthermore, as discussed earlier, these properties are highly dependent on clearances, loads, and other parameters likely to vary throughout a machine's life span. The analysis must cover the wide spectrum of these possible component variations in order to bracket the expected range of critical speeds and vibration amplitudes.

With the machine's governing dynamics defined by the mass, stiffness and damping properties of the components in the model, the rotor unbalance forces must also be defined to determine the predicted vibrational amplitudes. The response at any location depends on both the amount of unbalance as well as its axial and phase distribution along the rotor. The amount of unbalance to be applied analytically is prescribed by the API standard paragraphs. This amount is based on the unbalance allowable under API following final balancing, with the design intent being that the rotor should not exceed probe vibration limits with twice this level of unbalance present. The distribution of this unbalance becomes just as important as its amount. This is due to the fact that to excite a natural frequency of any system, the forces must not be at node points of the natural frequency's mode shape. For example, unbalance at the midspan of the compressor in Figure 2-67 would excite the first mode

but would not excite the second mode because the midspan is a node point for the second mode. Examining the second mode shape, it will be excited by any out-of-phase unbalances at opposite ends of the rotor. Likewise, to excite this example compressor's third mode, Figure 2-67 indicates that any unbalance present at the rotor's left end would accomplish this. For most between bearing machines, unbalance at the shaft ends where coupling hubs and thrust collars typically exist are effective in exciting the third mode, a mode usually having high deflections at the shaft ends.

The actual unbalance distribution along a rotor following balancing is unknown. Therefore, to insure that the vibration limits are not exceeded and the critical speeds are accurately identified, different distributions must be applied which most adversely excite the critical speeds of concern. While the API standard paragraphs prescribe some appropriate generic distributions, the mode shapes from the undamped critical speed analysis can provide better information toward the selection of unbalance distributions for a specific machine.

Much of the unbalance response analysis performed today is based on the landmark work of Lund and Orcutt [7] who provided the first comprehensive algorithm for conducting this type of analysis. While the analysis techniques have remained essentially the same, significant advancements have been made in modeling various components such as bearings and seals. These advancements have helped to improve the overall accuracy of the predictions. Even though an accurate model is vital, several other factors must also be considered when performing the analysis. These include the following:

- a. Probe orientation and mounting: For accurate comparison with test data, the predicted response at probe locations should account for the probe angular orientation. Furthermore, when probes are mounted, care must be taken to ensure they are well damped with low peak response and low amplification factor.

As required by the API standard paragraphs, the main products of the unbalance response analysis are the Bode response plots, critical speed locations including their amplification factors and separation margins, and rotor deflection shapes at these critical speeds. The Bode plots and rotor deflection shapes are the primary outputs used to determine whether the machine meets the unbalance response performance requirements. Displaying the calculated vibration amplitude and phase resulting from a particular unbalance distribution as a function of operating speed, Bode plots are normally provided only for probe locations. Each plot should clearly indicate the identifying parameters used to create the plot, i.e., response location, unbalance distribution, bearing condition, etc.

Sample Bode plots are shown in Figure 2-68, displaying the X and Y response at a probe location and its adjacent journal bearing of the example compressor. The level of unbalance is the API allowable residual unbalance applied at the rotor's midspan, in a static unbalance configuration. This distribution was chosen to excite the first critical speed as sug-

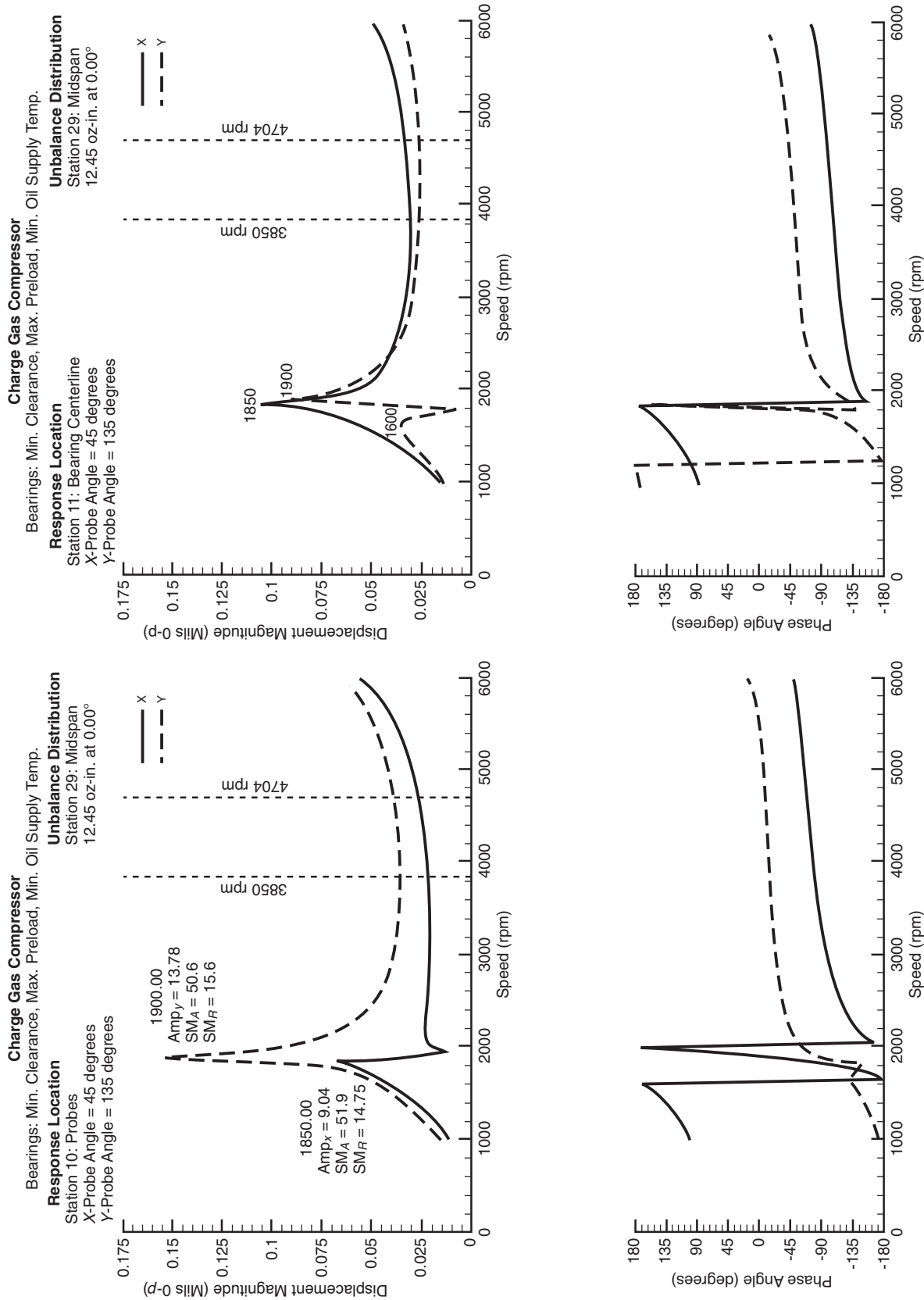


Figure 2-68—Typical Bode Plot for Asymmetric System with Split Critical Speeds

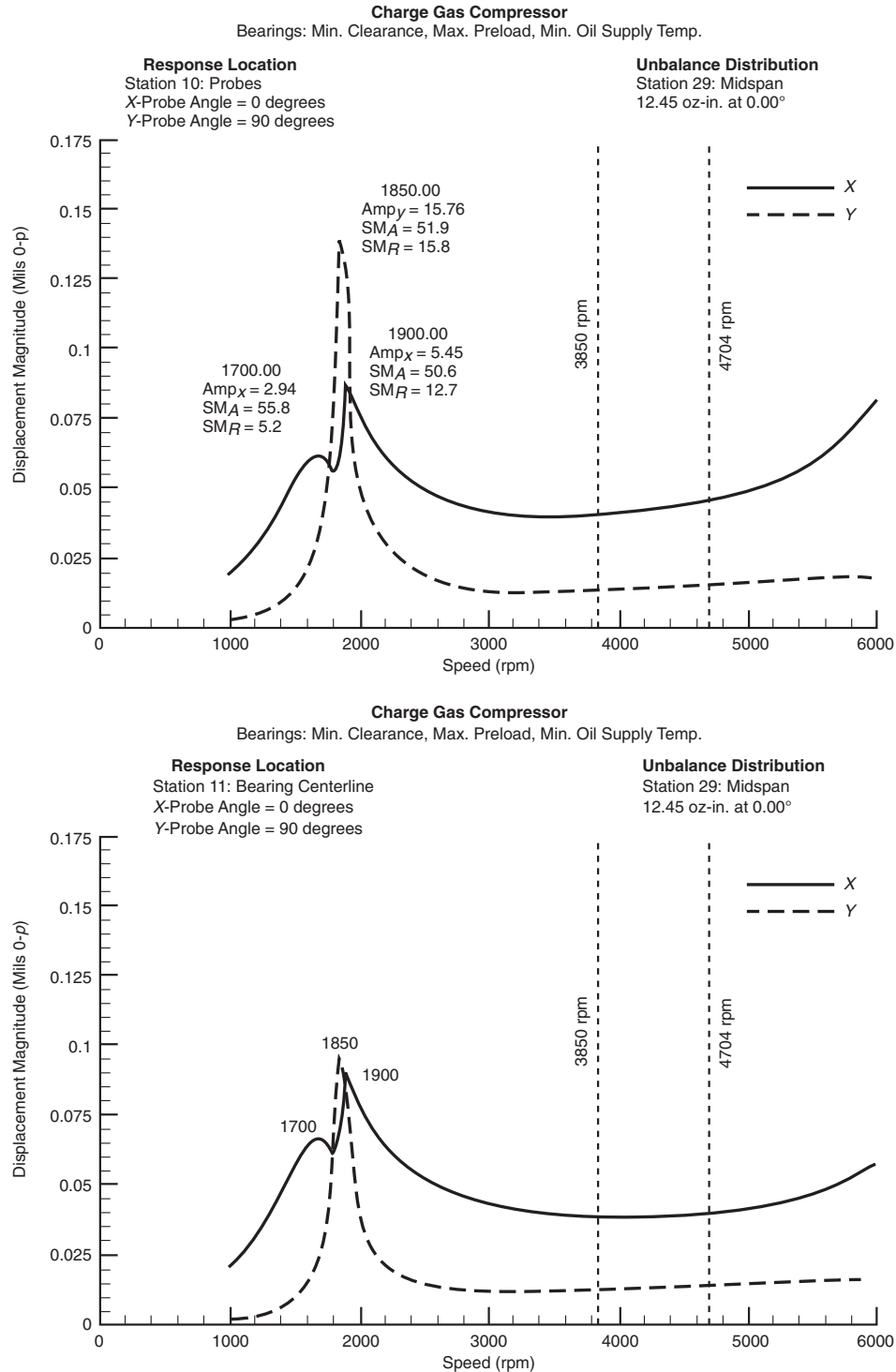


Figure 2-69—Example Compressor with Probes Rotated to True Horizontal and Vertical

gested by the undamped mode shapes in Figure 2-67. Comparing the probe to the bearing response, it is clear that the probes “see” more vibration than the bearing and that the unbalance distribution has indeed excited some sort of resonance. Examining the bearing Bode plot, it appears that three

resonances are present at 1600, 1850 and 1900 cpm, while the probes only show two peaks. This situation highlights the difficulties in interpreting Bode plots that sometimes occur. Since the undamped critical speed map (Figure 2-65) indicated very asymmetric load on pad bearings, a split critical

speed can be expected. To verify whether these three peaks are actually a split critical, it is often helpful to analytically rotate the probes from 45° and 135° to observe the true horizontal and vertical response. Figure 2-69 displays the magnitude Bode plots for the true horizontal and vertical (virtual probes at 0° and 90°) response. A split critical is clearly present with the horizontal direction experiencing a well damped resonance at 1700 cpm and then peaking again as part of the poorly damped critical at 1850 cpm which is predominantly in the vertical direction. The peaks at 1850 and 1900 are the same resonance. This figure illustrates the influence that probe orientation has on the presented results. One must always keep in mind that the X and Y response are spatially fixed while observing an orbit that can dramatically change in shape from circular to very elliptical.

The various unbalance distributions are meant to excite the critical speeds of concern for their accurate determination. For the example compressor, the midspan distribution excites a split critical speed with the highly amplified critical speed at 1900 being of primary concern. Based on the minimum operating speed, this critical has a separation margin of roughly 50%. To determine whether this margin is adequate, the amplification factor must be calculated as outlined in Figure 2-70. The amplification factor is a simplified measure of the amount of damping available to a natural frequency. When considering the amplification factor for use in determining the separation margin, several considerations must be kept in mind. First, not only will the amplification factors vary with bearing clearance and other variations, it will also vary depending on the probe response location and the unbalance distribution. For a given unbalance distribution and model, an amplification factor calculated at one end of the machine may be different than the one calculated based on the other end. Second, the amplification factor should be determined based on the individual probe responses. Using the major axis to calculate the amplification factor can result in liberal values (low amplification factor, high damping) especially when significant support asymmetry exists creating split critical speeds.

For this particular machine, the highly amplified first critical meets the separation margin requirements, yet, extensive shop balancing effort was made to help insure that this critical speed was not excited in actual operation. As emphasized earlier, to insure overall acceptability of the design, all of the calculated output must be duplicated for expected changes in components' operation, i.e., bearing clearance variation, etc.

Continuing to examine this midspan unbalance distribution, the analysis must next address whether the vibration amplitude design objectives are achieved. First, one must verify that at operating speed, the vibration limit at the probes will not be exceeded when twice the allowable residual unbalance is present. This question can easily be answered by utilizing the fact that this unbalance response analysis is linear. Recalling that the unbalance applied at the midspan of the example compressor was only the API allowable, the

response with twice the allowable unbalance is simply twice the response already calculated. More specifically, taking the maximum probe amplitude at 3,850 rpm from Figure 2-68,

$$Y_{1U} = 1.793\mu\text{m}(0.0706\text{ mils})p-p$$

$$Y_{2U} = 2Y_{1U} = 3.586\mu\text{m}(0.1412\text{ mils})p-p$$

$$L_{\text{vibe limit}} = 25.4 \sqrt{\frac{12,000}{4,704}} = 40.564\mu\text{m}(1.597\text{ mils})p-p$$

Therefore, at 3,850 rpm and twice the allowable unbalance (2×12.45 oz.-in.) at the midspan, the maximum response at the probes is 0.1412 mils $p-p$, well below the vibration limit of 1.597 mils $p-p$. One should notice that the probe vibration limit is based upon the maximum continuous speed. A proper analysis would perform a similar verification at the other probe axial location(s) as well as for other speeds within the specified operating range.

The second vibration limit requirement ensures that rubbing at critical clearance locations will not occur even if the vibration limit is reached at the bearing probes. Once again utilizing the analysis' linearity, the unbalance level required to cause the probes to reach the vibration limit can be determined. Here the unbalance sensitivity for the particular unbalance distribution is applied. Using the Bode plot response at the first critical speed (Figure 2-68), the midspan unbalance needed to achieve the vibration limit is calculated accordingly:

$$S = \frac{0.304\text{ mils } p-p}{12.45\text{ oz-in}} = 0.0244 \frac{\text{mils } p-p}{\text{oz-in}}$$

Unbalance Sensitivity @ 1st Critical Speed

$$U_{\text{vibe limit}} = \frac{L_v}{S} = \frac{1.597}{0.0244} = 64.45\text{ oz-in}$$

As previously stated, a similar calculation would need to be performed at the other probe location(s). The unbalance sensitivities determined are only applicable for a particular unbalance distribution and speed. Therefore, the sensitivities would need to be calculated for each unbalance distribution. As a side note, the unbalance sensitivities are equivalent to influence coefficients measured during balancing procedures.

With this calculated level of unbalance applied, the response at all the critical clearance locations must be determined. The results are typically displayed using a rotor deflection plot at the critical speed of concern. For the example compressor, Figure 2-71 presents the rotor deflection plot with the rotor at 1,850 rpm in both two and three-dimensional views. As with a Bode plot, the identifying parameters to create the plot should be shown. The three-dimensional plot illustrates the orbital response at the individual stations across the entire rotor. As concluded earlier, this critical speed at 1,850 rpm is dominated by response in the vertical direction and Figure 2-71 reaffirms this. Here one can also see that the response at the bearings is not indicative of the rest of the

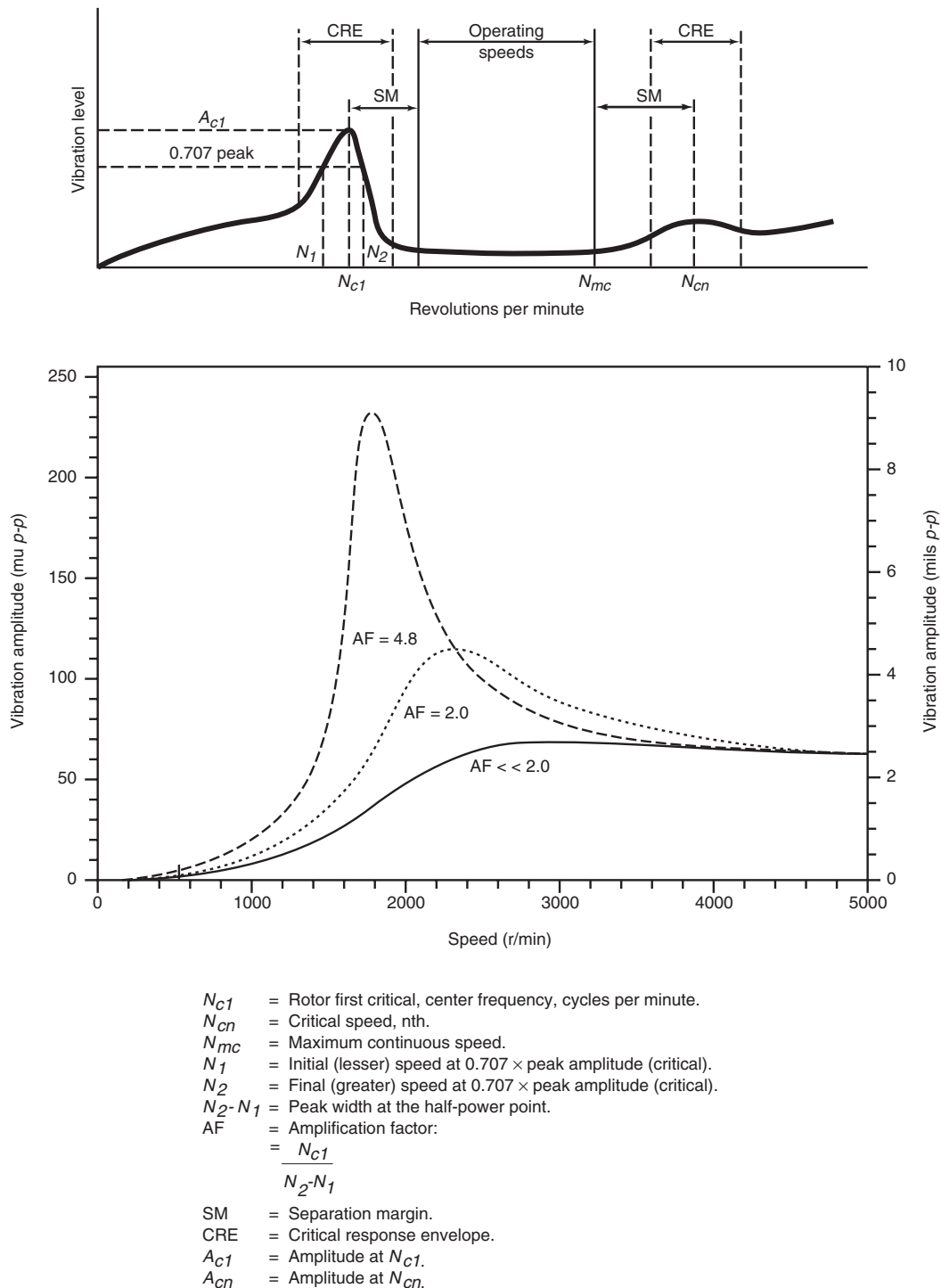


Figure 2-70—Evaluating Amplification Factors (AFs) from Speed-amplitude Bode Plots

rotor. In fact, relative to the rest of the rotor, the bearings are close to being node points having almost no amplitude, causing their damping to be ineffective, and resulting in the very amplified critical speed seen in the Bode plot. Comparing these levels to the available clearances along the rotor, the designer can determine whether this unbalance distribution

causes vibration amplitudes to exceed the 75% clearance limit established by the API standard paragraphs.

This entire process is repeated for each unbalance distribution as well as for the expected changes in the components during the operational life of the machine, such as bearing clearances or load variation, oil seal pressures, etc. When

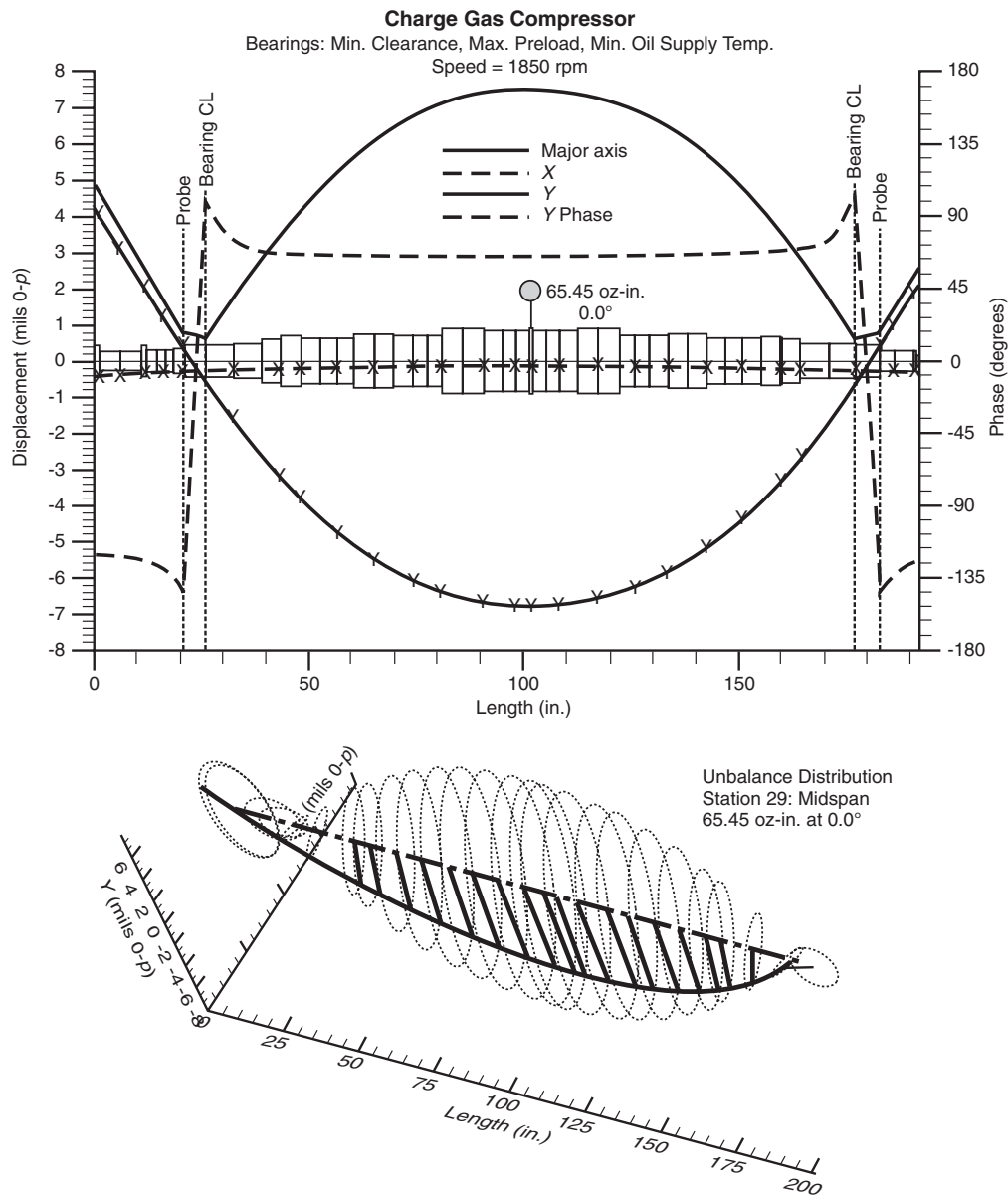


Figure 2-71—Rotor Response Shape Plots in 2D and 3D Form

investigating such variations, it is important to maintain the same unbalance distributions for accurate comparison.

Poor unbalance response performance can be exhibited in many different ways. A highly amplified first critical may cause significant damage to tight clearance areas during start-up or shutdown. Increased bearing clearance or variations in oil supply temperature may reduce a separation margin. The machine may be prone to fouling problems at locations that have high unbalance sensitivities with respect to the probes. While each machine design is unique, solving poor unbalance response performance, typically, involves optimizing the rotor characteristics with its support structure characteristics. Introducing more damping is not always the solution. Section

2.5.5 discusses how journal bearing design can be used to improve response performance. References [13,14] are also important fundamental papers examining this rotordynamic design problem.

2.7.4 Stability Analysis

Current technology identifies the damped eigenvalue, evaluated at the rotor's operating speed, as the principal measure of rotor stability. Each damped eigenvalue is a complex number of the form $s = p \pm i\omega_d$ where p is the damping exponent, ω_d is the frequency of oscillation, and $i = \text{square root } (-1)$. The effect of the sign of the damping exponent on the motion of the rotor is presented in Figures 2-72 and 2-73. As previ-

ously noted, if the damping exponent of an eigenvalue is negative, then the rotor vibrations associated with this mode will be stable (envelope of vibrations decreases with time). If the damping exponent of an eigenvalue is positive, then the rotor vibrations associated with the mode will be unstable (envelope of vibrations increases with time) and a frequency component matching ω_d will be expected to appear in the machine's response spectrum.

Although the real part of the complex eigenvalue is the direct result of rotor stability calculations, API specifications evaluate rotor stability using a derived quantity called log decrement. The log decrement, δ , is calculated as follows:

$$\delta = \frac{-2\pi p}{|\omega_d|} \quad 2-16$$

The log decrement is a measure of how quickly the free vibrations experienced by the rotor system decay. When the log decrement is positive, the system is stable. Conversely, when the log decrement is negative, the system is unstable. The log decrement has proven to be a useful measure of rotor stability because it is a non-dimensional quantity allowing easy comparison of different machines and may be interpreted using general design rules.

A rotor stability analysis can be used to estimate critical speeds and their amplification factors using a damped eigenvalue map [10]. However, an unbalance response analysis

cannot determine the stability characteristics of a machine. Some qualitative relationships do exist between the two analyses, namely, a first critical speed with a high amplification factor may suggest a sensitive machine in terms of stability. Only a stability analysis can confirm such an estimation.

Up until recently, the lack of nonuniform guidelines for evaluating a design led to the absence of the stability topic in API standards. Experience with stability problems, improvements in modeling capabilities, and consensus around appropriate methodologies, however, have finally resulted in some new stability requirements defined in the API standard paragraphs. These requirements are discussed in Section 3 which contains an extensive state of the art tutorial on stability.

2.7.5 References

1. Rankine, W.J.M., (1869) "On the Centrifugal Force of Rotating Shafts," *The Engineer*, London, 27, pp. 249.
2. Dunkerley, S., (1895) "On the Whirling and Vibration of Shafts," *Proceedings of the Royal Society*, London, Series A, 185, pp. 279 – 360.
3. Gunter, E.J., (1966) d, NASA SP-113.
4. Jeffcott, H.H., (1919) "The Lateral Vibration of Loaded Shafts in the Neighborhood of a Whirling Speed—The Effect of Want of Balance," *Philosophical Magazine*, Series 6, 37, pp. 304 – 314.

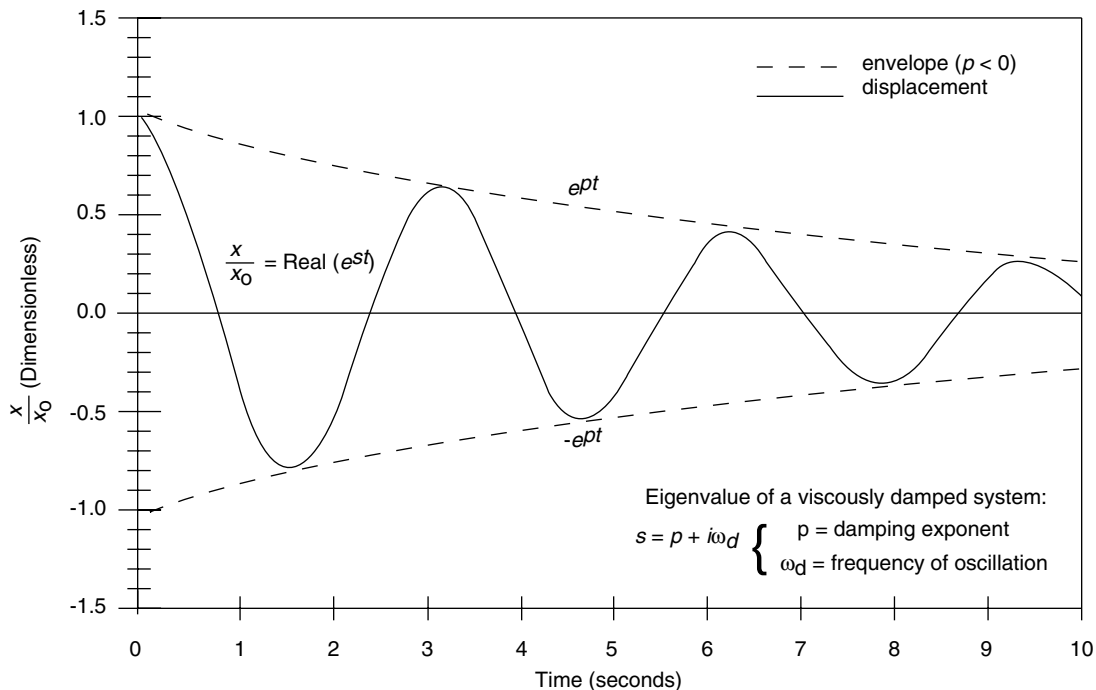


Figure 2-72—Motion of a Stable System Undergoing Free Oscillations

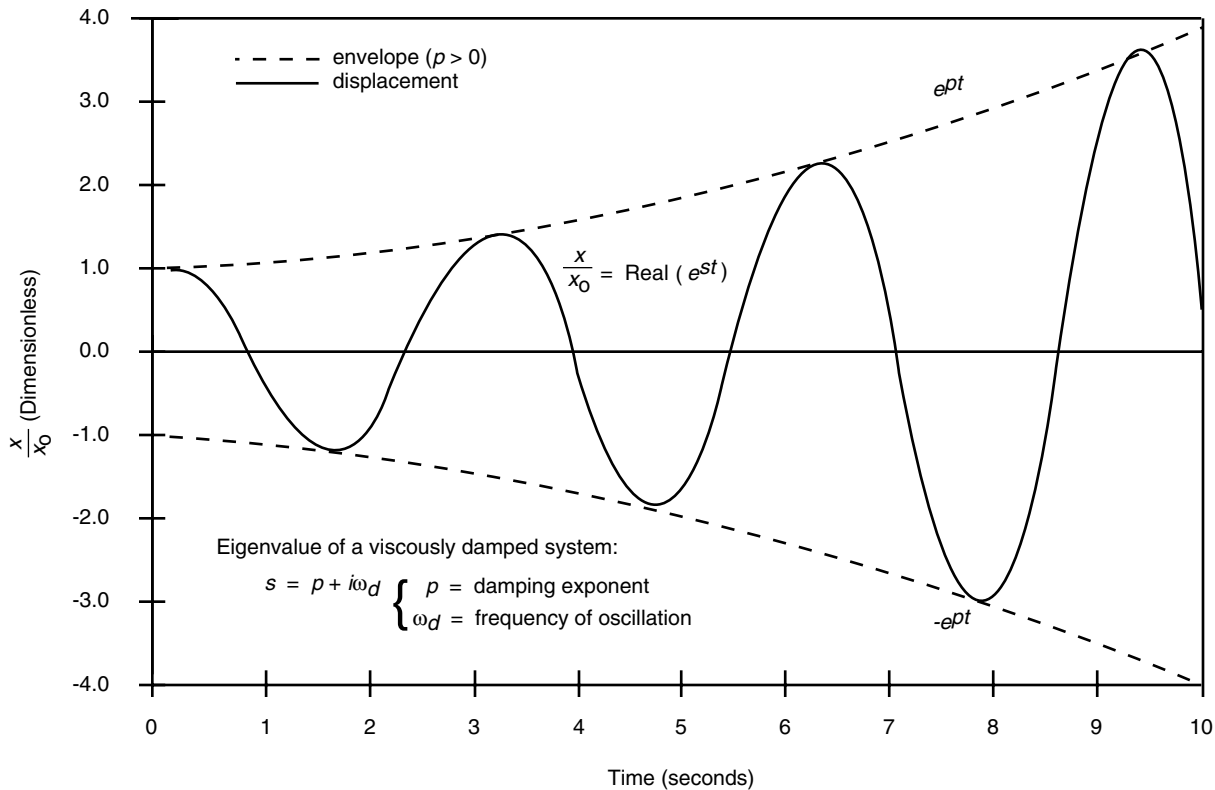


Figure 2-73—Motion of an Unstable System Undergoing Free Oscillations

5. Stodola, A., (1910) *Dampf und Gasturbinen*, Springer, Berlin, 1910.
6. Myklestad, N.O., (1944) "A New Method for Calculating Natural Modes of Uncoupled Bending Vibrations of Airplane Wings and Other Beams," *Journal of Aeronautical Sciences*, 11, pp. 153 – 162.
7. Prohl, M.A., (1945) "A General Method for Calculating Critical Speeds of Flexible Rotors," *Journal of Applied Mechanics*, Trans. ASME, 12(3), pp. A142 – A148.
8. Nelson, H.D., (1994) "Modeling, Analysis and Computation in Rotordynamics: A Historical Perspective," Proceedings of the IFToMM Fourth International Conference on Rotor Dynamics, Chicago, pp. 171 – 177.
9. Lund, J.W. and Orcutt, F.K. (1967) "Calculations and Experiments on the Unbalance Response of a Flexible Rotor," *ASME Journal of Engineering for Industry*, pp. 785 – 796.
10. Lund, J.W., (1974) "Stability and Damped Critical Speeds of a Flexible Rotor in Fluid-Film Bearings," *ASME Journal of Engineering for Industry*, 96(2), pp. 509 – 517.
11. Vance, J.M., Murphy, B.T., and Tripp, H.A. (1987) "Critical Speeds of Turbomachinery: Computer Predictions Vs. Experimental Measurements,—Part I: The Rotor Mass-Elastic Model," *ASME Journal of Vibration, Acoustics, Stress and Reliability in Design*, 109(1), pp. 1 – 7.
12. Vázquez, J.A. and Barrett, L.E. (1998) "Comparison Between the Calculated and Measured Free-Free Modes for a Flexible Rotor," ASME Paper 98-GT-51.
13. Barrett, L.E., Gunter, E.J., and Allaire, P.E. (1978) "Optimum Bearing and Support Damping for Unbalance Response and Stability of Rotating Machinery," *ASME Journal of Engineering for Power*, 100, pp. 89 – 94.
14. Nicholas, J.C. (1989) "Operating Turbomachinery On or Near the Second Critical Speed in Accordance with API Specifications," Proceedings of the Eighteenth Turbomachinery Symposium, Texas A&M University, pp. 47 – 54.

2.8 MACHINERY SPECIFIC CONSIDERATIONS

2.8.1 Steam Turbines

2.8.1.1 Introduction

Bearing support flexibility and partial admission forces are important in the rotordynamics analysis of steam turbines.

2.8.1.2 Bearing Supports

In a steam turbine the bearing support can be softer than that typically found in centrifugal compressors. This softer support is due to the flexibility needed on the steam end to allow for the large axial thermal expansion of the turbine casing, as is discussed in Edney and Lucas [1]. A typical outline

drawing of a steam turbine case is shown in Figure 2-74. The steam end bearing is housed in a bearing case that is supported by a flex plate to allow for axial thermal expansion. The exhaust end bearing case is supported within the exhaust casing that sits on two sets of thick horizontal plates with gussets for added stiffness. These plates along with the flex plate are attached to the baseplate. Support stiffness effects are discussed in 2.4. The support stiffness coefficients can be from measurements, as discussed in Nicholas, et. al. [2]. The support coefficients may also be estimated from a simple single degree of freedom spring mass model, based on experience from a given size of machine and design of bearing case and support [1].

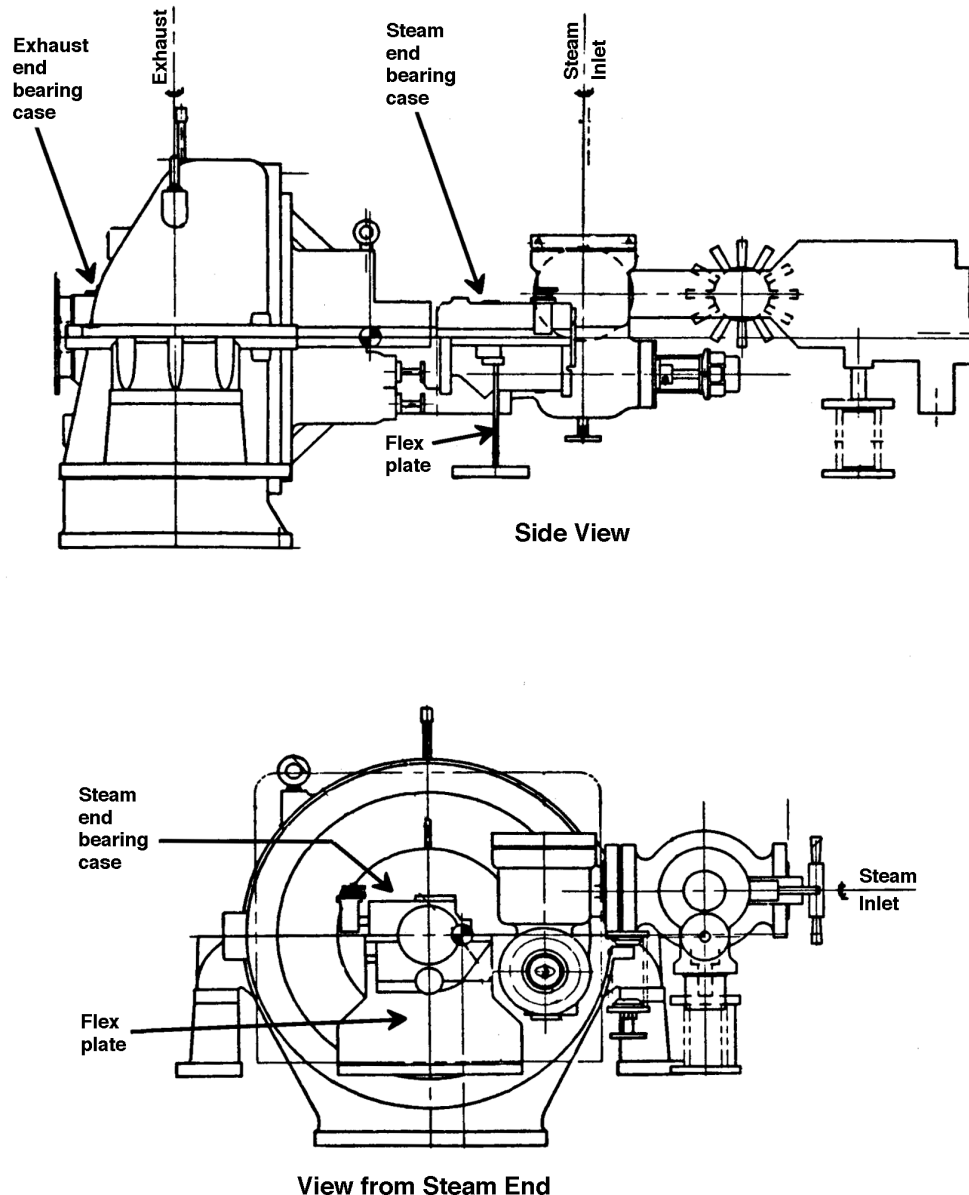


Figure 2-74—Steam Turbine Support Schematic

2.8.1.3 Partial Admission Forces

Partial admission forces are a factor since they affect rotor position and bearing loading causing changes in stiffness and damping characteristics. An analysis methodology and example is presented in [1].

It has long been recognized that the entire control valve opening sequence and the effect of partial admission diaphragm stages must be considered in a rotor response analysis. This is especially so in cases where partial admission forces are large relative to the rotor weight. The resultant effect can be one in which the rotor is loaded into a sector of the bearing where the dynamic characteristics are significantly different from what they would be due to gravity load alone, Figure 2-75. Consequently, changes in turbine load can yield significantly different operating vibration amplitudes as reported in Caruso, et al. [3]. There are two sources of partial admission force. The primary source is the inlet and extraction (if included) control stages which, depending on the operating point, can have a wide range of admission arcs and hence loading conditions. Another source is partial admission diaphragm stages that are occasionally used for flow-path efficiency considerations.

The resultant forces imposed on the rotor are of two types; a tangential component derived from the stage torque reaction, and an axial thrust from the pressure drop across the nozzles. The axial thrust is orientated at the centroid of the admission arc and can be resolved into radial force couples at the bearings. The axial thrust forces are usually small compared to the tangential torque reactions and are typically neglected. A possible situation where they might need to be accounted for, however, would be at the inlet control stage with only one or two valves open yielding a small admission arc. Since the pressure drop across the control stage is typically quite high, the axial thrust on the first row of blades would also be high and the location of the centroid at a large radius. As the admission arc increases, the radius to the centroid reduces, as does the resultant bearing loading. A typical force diagram illustrating how to resolve these forces into journal bearing reactions is shown in Figure 2-76. In this figure, stage torque reactions typical of an inlet and extraction control stage are represented, given by the subscripts 'i' and 'e' respectively.

2.8.1.4 Analysis Methodology

The analysis methodology and acceptance criteria for the damped response analysis are outlined in 6.8.1, 6.8.2, 6.8.3, and 6.8.4 of Appendix A. The following procedure is given for general guidance only. Appendix A should be reviewed for additional detail. The damped response analysis should be conducted including the effects of any external bearing loading such as from partial arc admission.

a. Create a mass-elastic model of the rotor. One consideration is what is the effective stiffness diameter at the wheel stages.

b. Calculate the stiffness and damping coefficients of the radial bearings. The bearing loading should include both the static rotor weight and any external loading such as from partial arc forces as appropriate.

c. For tilt pad bearings, combine the bearing coefficients in series with pad pivot stiffness [4].

d. Combine these coefficients in series with squeeze film dampers [5], if used, and with the support coefficients [1,2].

e. Create an undamped critical speed map with the combined support coefficients superimposed on this map and show the mode shape plots of the undamped critical speeds from zero to at least 125% of trip speed.

f. The damped response analysis should be conducted using an appropriate rotordynamics computer code. The analysis shall be run at both minimum and maximum extremes of component clearance and oil inlet temperature.

g. Use separate types of unbalance for the translatory (symmetric) modes and conical (asymmetric) modes. Typically, for a steam turbine for the translatory mode, a single unbalance at the midspan, for the maximum displacement of the first mode, would be used. For the conical mode, two unbalances 180 degrees out of phase at the maximum displacements of the second mode would be used (probably near the $1/4$ and $3/4$ span points.)

h. Amplitude vs. speed plots at the bearing radial probes from the damped response analysis for the two types of modes should be shown from zero to at least 125% of trip speed. 6.8.2.7 of the Standard Paragraph says that the total unbalance used should be four times U , where:

In SI units:

$$U = 6350 \frac{W}{N} (\text{g-mm}) \quad 2-17$$

In Customary units:

$$U = \frac{4W}{N} (\text{oz-in}) \quad 2-18$$

where:

W = Rotor weight, kg (lbm),

N = Maximum Continuous Speed, rpm.

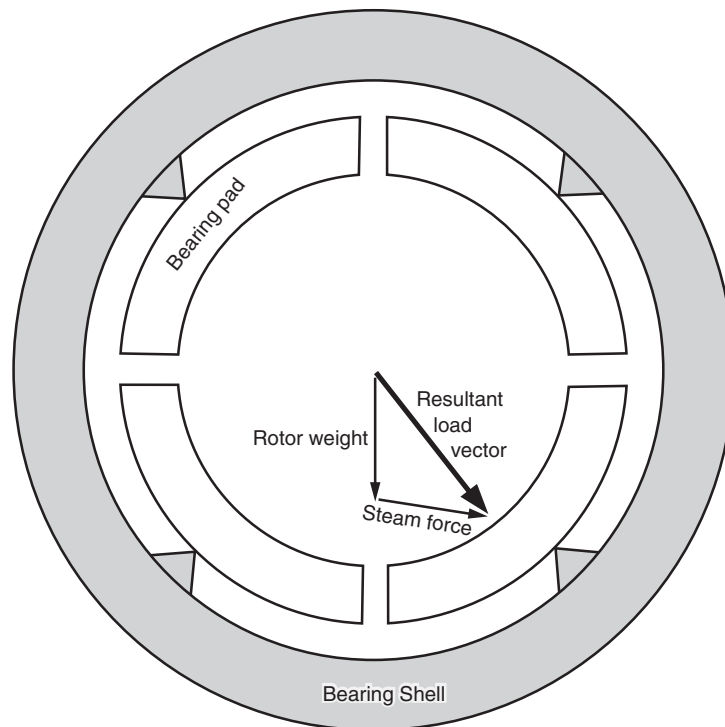


Figure 2-75—Typical Resultant Bearing Load Vector Including Partial Admission Steam Forces

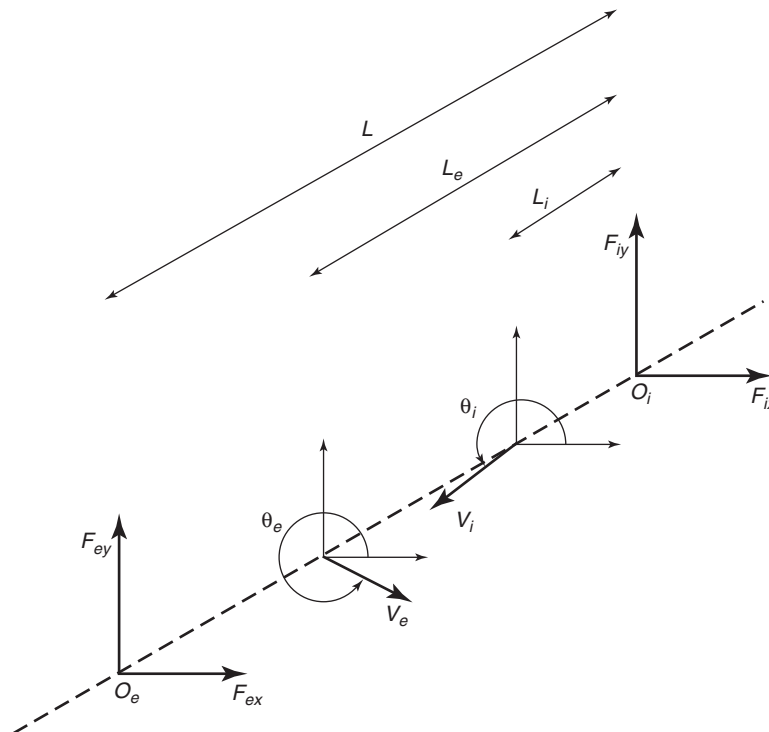


Figure 2-76—Resolution of Partial Admission Forces into Journal Bearing Reactions

i. Mode shape plots should be shown for each critical speed in the range zero to 125% of trip speed, as identified by the two types of unbalances above.

j. The calculated separation margins from the operating speed range and amplification factors of the critical speeds should be compared to the requirements of 6.8.2.10 of the SP.

k. A separate unbalance response run should be considered for the verification test. The amount of unbalance should be no more than 8 times U above, except if the unbalance is placed on the end of the shaft, probably at the coupling, then W in the equation above should be the overhung mass, i.e., mass of the rotor outboard of the bearing, including the half-coupling.

l. 6.8.2.12 of the SP requires that at any speed from zero to trip speed the calculated amount of amplitude at the seal locations (except floating seals) should not exceed 75% of the minimum design running clearances. If stainless steel toothed labyrinths are used this requirement would be very important in a steam turbine. The amount of unbalance used at a speed is not as above, but by 6.8.2.11 of the SP is the amount needed to raise the vibration at the radial probe location at that speed to the amount A_1 given by:

In SI units:

$$A_1 = 25.4 \sqrt{\frac{12,000}{N}} (\mu\text{m}) \quad 2-19$$

In Customary units:

$$A_1 = \sqrt{\frac{12,000}{N}} (\text{mil}) \quad 2-20$$

where

N = Maximum Continuous Speed, rpm.

- Thus for the mode shape plots at the critical speeds as required in 6.8.2.8 of the SP it would be appropriate to use the amount required by 6.8.2.11 of the SP, and not the amount given in 6.8.2.7 of the SP.

2.8.1.5 References

1. Edney, S. L. and Lucas, G. M., 2000, "Designing High Performance Steam Turbines with Rotordynamics as a Prime Consideration," Proceedings of the Twenty-Ninth Turbomachinery Symposium, Turbomachinery Laboratory, Texas A&M University, College Station, Texas, pp. 205 – 224.
2. Nicholas, J. C., Whalen, J. K. and Franklin, S. D., 1986, "Improving Critical Speed Calculations Using Flexible Bearing Support FRF Compliance Data," Proceedings of the Fifteenth Turbomachinery Symposium, Texas A&M University, College Station, Texas, pp. 69 – 78.
3. Caruso, W. J., Gans, B. E. and Catlow, W. G., 1982, "Application of Recent Rotor Dynamics Developments to Mechanical Drive Turbines," Proceedings of the Eleventh Turbomachinery Symposium, Turbomachinery Laboratory, Texas A&M University, College Station, Texas, pp. 1 – 17.
4. Nicholas, J. C. and Wygant, K. D., 1995, "Tilting Pad Journal Bearing Pivot Design for High Load Applications", Proceedings of the Twenty Fourth Turbomachinery Symposium, Turbomachinery Laboratory, Texas A&M University, College Station, Texas, pp. 33 – 47
5. Edney, S. L. and Nicholas, J. C., 1999, "Retrofitting A Large Steam Turbine with a Mechanically Centered Squeeze Film Damper", Proceedings of the Twenty Eighth Turbomachinery Symposium, Turbomachinery Laboratory, Texas A&M University, College Station, Texas, pp. 29 – 40.

Nomenclature

- F_{ex} = Exhaust end bearing partial admission force reaction X direction (lbf),
- F_{ey} = Exhaust end bearing partial admission force reaction Y direction (lbf),
- F_{ix} = Inlet end bearing partial admission force reaction X direction (lbf),
- F_{iy} = Inlet end bearing partial admission force reaction Y direction (lbf),
- L = Bearing span (in.),
- L_e = Length from inlet end bearing to extraction control stage (in.),
- L_i = Length from inlet end bearing to inlet control stage (in.),
- O_e = Origin extraction control stage,
- O_i = Origin inlet control stage,
- V_e = Extraction control stage partial admission force vector (lbf),
- V_i = Inlet control stage partial admission force vector (lbf),
- θ_e = Angle from X direction to extraction control stage force vector (deg),
- θ_i = Angle from X direction to inlet control stage force vector (deg).

2.8.2 Electric Motors and Generators

When developing the mass-elastic model for an electric motor or generator, the mass of the windings must be considered. However, the stiffness contribution of the windings is negligible and should not be considered. Since the rotor cross-section will usually be slotted for the windings, determining the equivalent stiffness diameter of the rotor center section can be challenging. One approximate method is to determine the equivalent mass diameter and use that as the stiffness diameter. Often, the motor or generator manufacturer can provide a total rotor weight. This is helpful in determining the equivalent mass diameter. Also, the exciter must be included in the model as well as the fan mass and inertia if appropriate. Finally, the motor box support stiffness must be included for accurate critical speed prediction (see 2.4).

2.8.3 Gearboxes

Gearboxes, Figure 2-77, have unique characteristics that must be considered when performing a rotordynamics study.

Torque is transmitted from one shaft to another through radial forces acting between the gear teeth. These tooth forces are directly proportional to the torque. The bearings supporting the shafts have a very significant change in load as a result of these tooth forces (as shown in Figure 2-78). As a result, the stiffness and damping of the bearings also have significant changes. Therefore, transmitted torque must be considered in rotordynamics studies of gearboxes. Usually, the analysis is performed at 10, 50, and 100% of full torque,

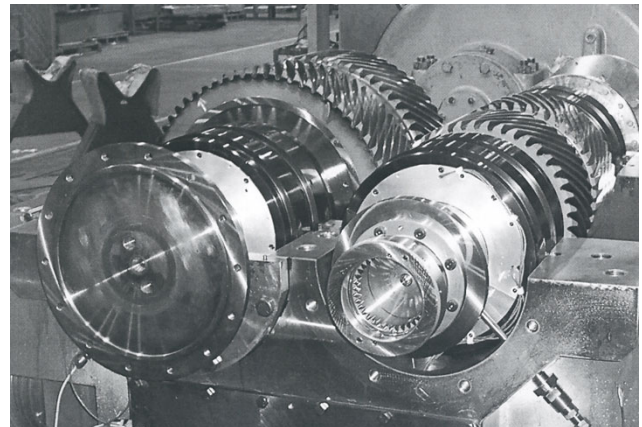


Figure 2-77—Gear Set

but it is common to also perform the calculations at the expected test stand torque.

The high radial loads on gearbox bearings reduce the tendency for bearing instability at normal operating conditions. However, it is important to select the shaft offset and shaft rotation to load the bearings in the most favorable way. The combination of the rotor weight and the direction of load from the gear teeth can increase or reduce the bearing loads.

Operating at reduced torque may cause the normally uploaded radial bearing to be loaded down (as shown in Figure 2-79). In general, for horizontal offset gearboxes, downloading the gear bearings and uploading the pinion bearings is preferable. When there is insufficient torque to prevent bearing instability, such as during start up or on a test stand, the use of a stability feature such as a pressure dam or tilt pad bearing is necessary.

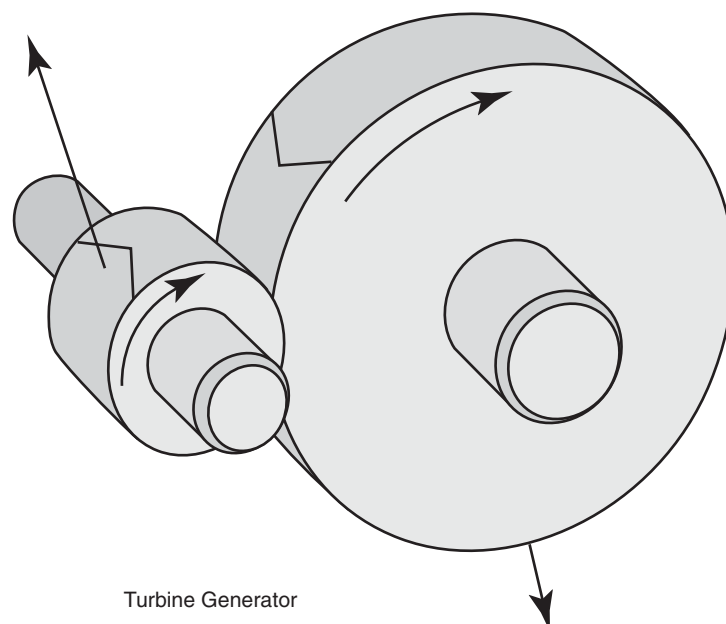


Figure 2-78—Gear Force Schematic

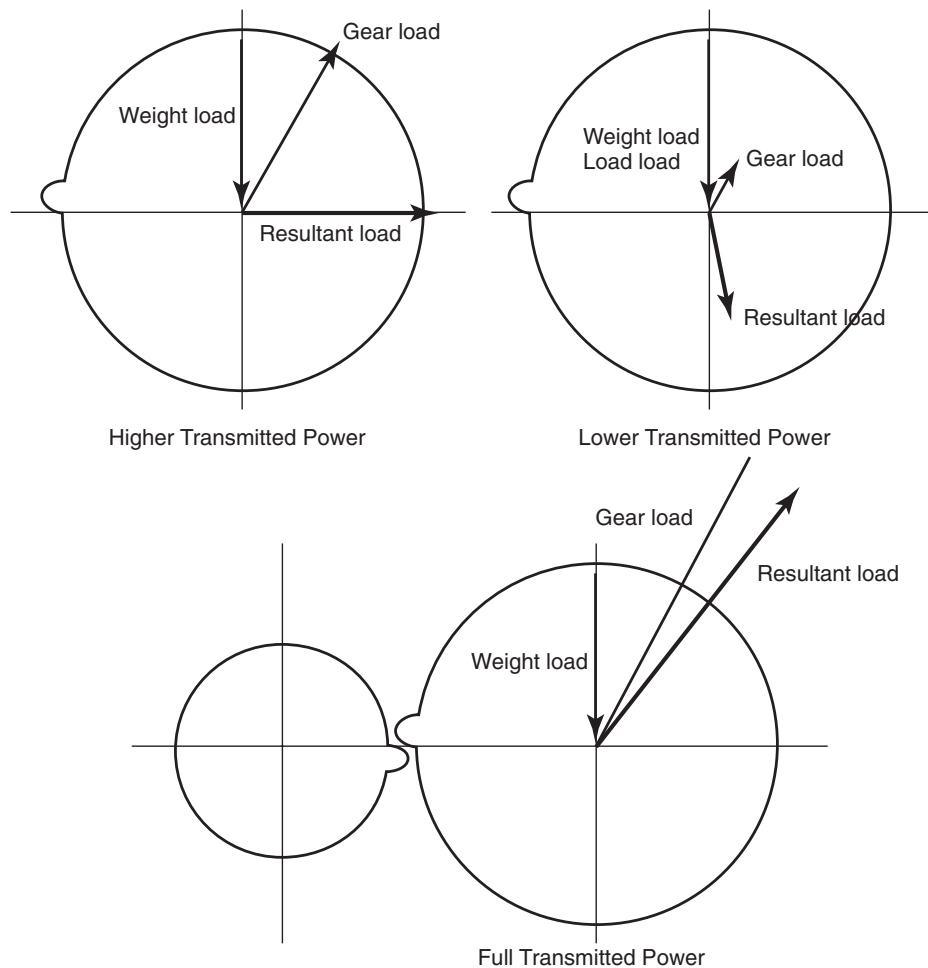


Figure 2-79—Gear Load Angles at Partial and Full Load

Unlike most machines, lateral vibrations and torsional vibrations are related in gearboxes. Torque variations result in radial load variations, therefore it is possible for torsional and radial vibrations to interact. If unexpected radial vibrations occur, consider the possibility of a torsional and radial vibration interaction.

Gearbox rotors are usually relatively stiff; therefore, support stiffness can have a significant impact on lateral rotordynamics. Most pinions are designed to operate below their first lateral critical speed with a mode shape that has the highest amplitude at the coupling. This can make gearboxes sensitive to coupling unbalance and misalignment. However, most gear rotors operate far enough below the first lateral critical speed to be considered stiff shafts, so special balancing procedures are seldom necessary.

It is important that careful evaluation be performed if the operating speed of a rotor coincides with the critical speed of a meshing pinion or gear; however, generally the effect is not noticed on the test stand. All gears and pinions have groups of teeth that are minutely closer together, then farther apart than desired due to manufacturing tolerances. The errors result in a

slight increase in rotational speed followed by a slight decrease at a first order frequency. This feature, known as “accumulated pitch error,” can result in a substantial excitation in addition to any unbalance forces. It is possible to have a second order frequency if the part is elliptical. Usually higher orders of accumulated pitch error are a result of wear caused by continued vibration. Figure 2-80 shows an accumulated pitch error chart from a gear tooth checker showing a wear pattern at the tenth order.

Most analysis is concerned with shaft speed or low order multiples of shaft speed. However, gearboxes are unique in that the gear teeth enter and leave engagement at a frequency equal to the rotor speed times the number of teeth. This frequency is called the “tooth mesh frequency.” For instance, a pinion with thirty teeth will have a thirtieth order meshing frequency. This frequency is higher than normally evaluated during a rotordynamics study. It is not purely sinusoidal and higher order harmonics of the tooth meshing frequency are common. Resonance in gear blanks or casings or support structures at tooth mesh frequency are rare but do occur and can occasionally cause problems.

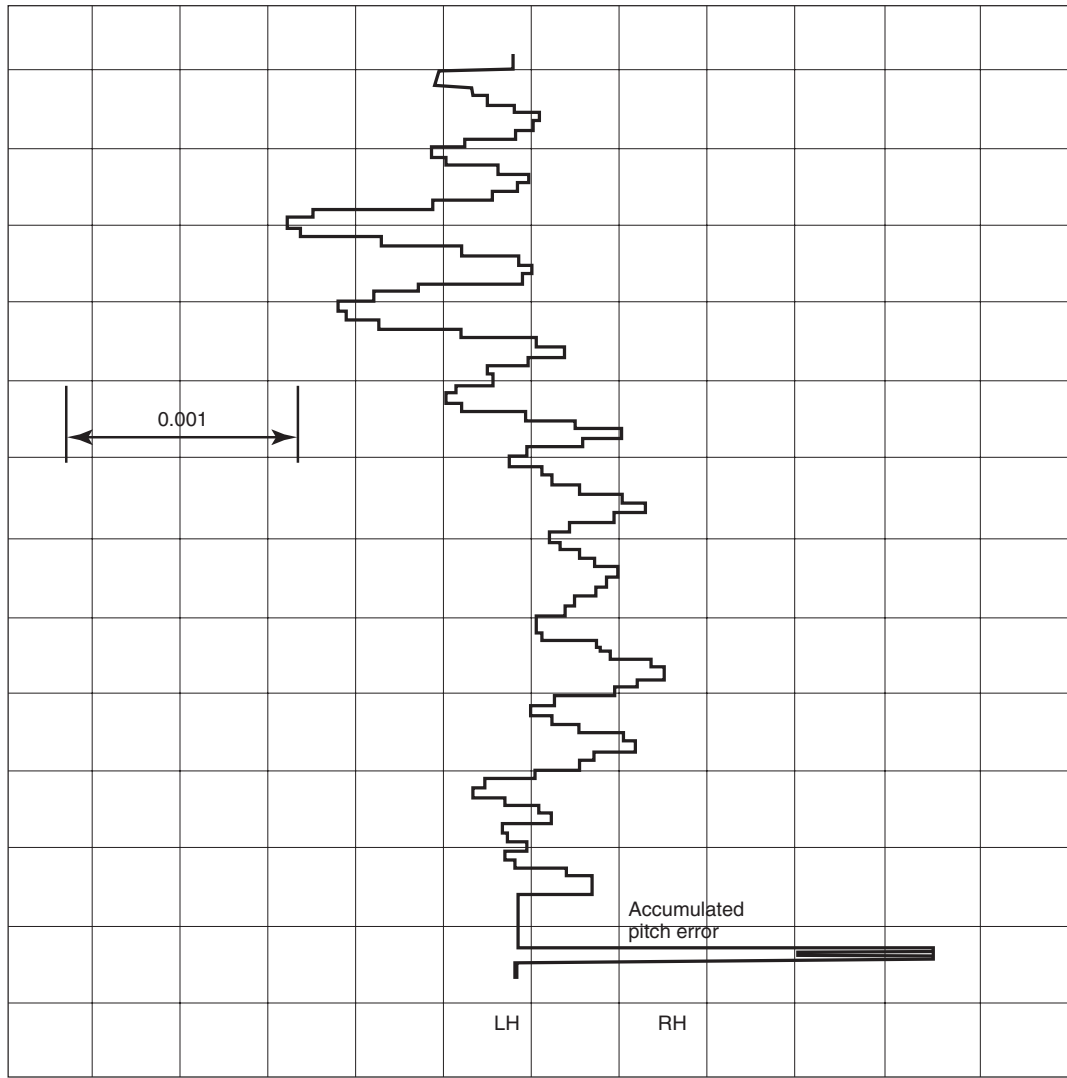


Figure 2-80—Accumulated Pitch Error Chart

It is possible to have an excitation because of the “assembly frequency.” The assembly frequency is the tooth mesh frequency divided by a common prime number. As an example, a gearset with 9 teeth in the pinion and 15 teeth in the gear have a common prime number of three. This would result in a third order excitation. If a gearset is ran and then reassembled with the teeth in a different combination, there is often substantial excitation at the assembly frequency. This example is taken from Winterton, [1]. A “hunting tooth design”, required by API, by definition does not have a common prime number so the assembly frequency is the same as the tooth passing frequency. A hunting tooth is usually supplied in a modern design.

Historically, analysts have not included the gear mesh stiffness in the model. The following formula is a common method used to calculate principal and cross couple stiffness’ from the gear mesh if desired.

$$K_{xx} = K' \cos^2(\gamma) \quad 2-21a$$

$$K_{xy} = K' \sin(\gamma) \cos(\gamma) \quad 2-21b$$

$$K_{yx} = K_{xy} \quad 2-21c$$

$$K_{yy} = K' \sin^2(\gamma) \quad 2-21d$$

$$K' = C(FW) \cos^2(\beta) 10^6 \quad 2-22$$

where

FW = Net facewidth of gear, mm (in.),

β = Helix angle, deg,

$\gamma = (A \times \alpha) + B,$

- α = Normal pressure angle, deg,
 A = 1 for downloaded rotors, or
 A = -1 for uploaded rotors,
 B = 90° for CW rotation looking into coupling end,
 or
 B = 270° for CCW rotation looking into coupling
 end,
 C = 12.057 (1.75),
 K = Stiffness, N/m (lbf/in.).

2.8.3.1 References

1. John G. Winterton, "Identification of Gear Generated Spectra," *Bentley Nevada Corporation Orbit Magazine*, 2nd Quarter (June 1991).

2.8.4 Power Turbines and FCC Power Recovery Expanders

The following discussion applies to overhung one or two stage power turbines and Fluid Catalytic Cracking (FCC) power recovery expanders. This equipment is subjected to adverse operating conditions: inlet temperatures exceed 1200°F and, in the case of FCC expanders, the working gas can be laced with solid particles or contain high levels of corrosive compounds. For the purpose of this discussion, it is assumed that fluid film journal bearings and not rolling element bearings support the rotating element.

Typically, this type of equipment appears to have an extremely stiff rotor, as the first undamped rigid bearing synchronous forward critical speed of the rotor is generally above the operating speed range. A typical undamped forward synchronous critical speed map for a FCC expander rotor is illustrated in Figure 2-81.

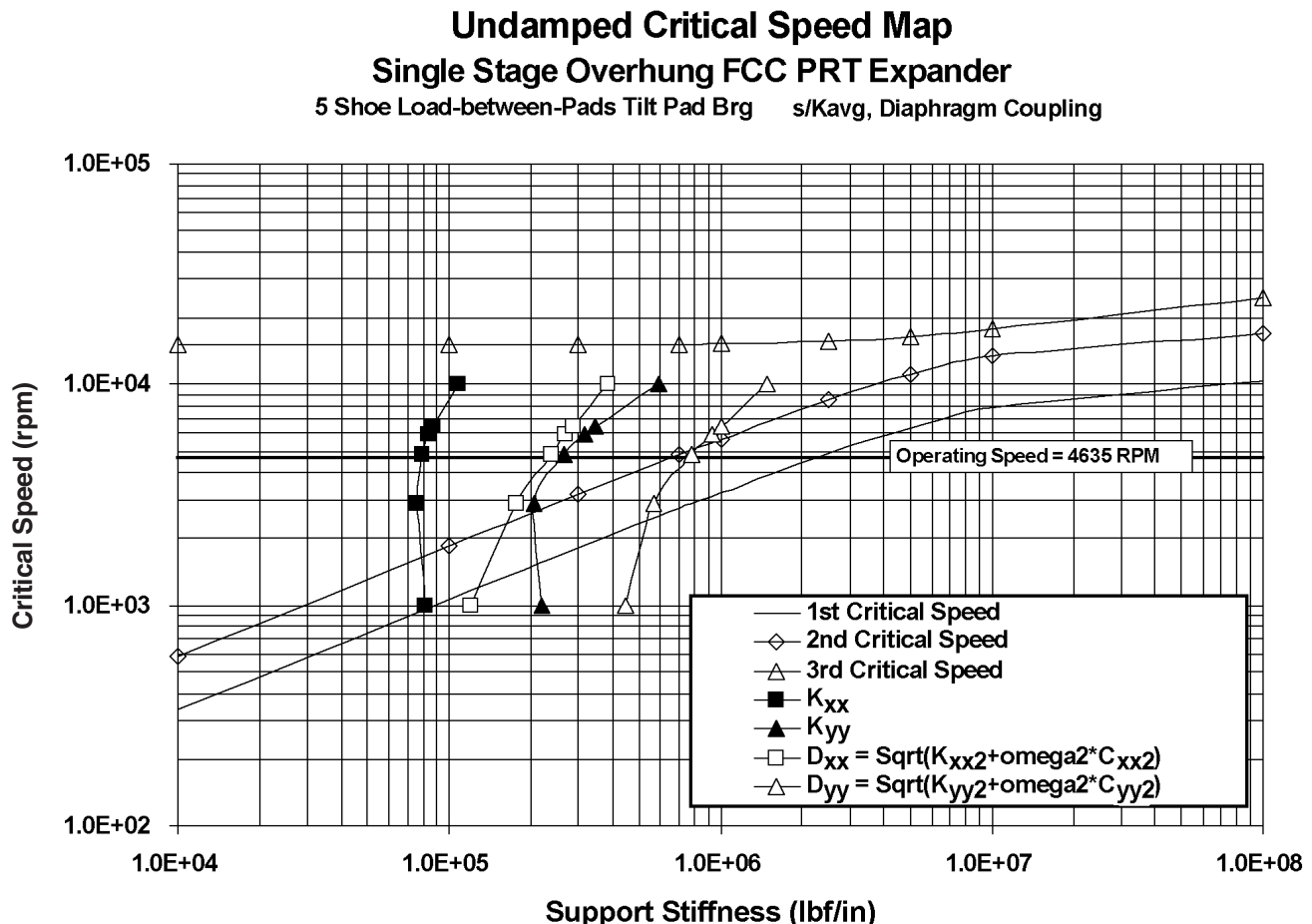


Figure 2-81—FCC Expander Critical Speed Map

The bearing support structure is flexible, with the stiffness typically less than 3.5 times the journal bearing stiffness. Thus the effect of the bearing support structure should be included in the rotordynamics model. Because of the flexible bearing support structure, the first critical speed of the rotor-bearing-support system could be both well below the first undamped rigid bearing critical speed of the rotor and below the operating speed range. This first critical speed is a system mode, principally determined by the mass of the rotor in series with the hot end journal bearing and the flexible bearing support.

Because of the large overhung mass and inertia, the first undamped free-free (third mode on soft supports) synchronous backward critical speed of the rotor can be considerably lower than the first undamped free-free (third mode on soft supports) forward critical speed of the rotor [1]. This mode is the first rotor mode. It is critical to complete a rotor response study to see if this mode will respond to unbalance, and, if it has an amplification factor greater than 2.5, that it has sufficient margin above the operating speed range. This also could be studied through a damped eigenvalue map of damped natural frequency vs. speed [2]. The location of this mode is influenced by the diameter of the rotor near the hot end, the journal bearing stiffness, and the stiffness of the bearing support.

Because of the large overhung mass on the hot end as compared to the mass of the coupling on the opposite end, the center-of-gravity will be somewhat close to the disc(s) end bearing. Designers try to keep the center-of-gravity of the entire rotating element as far from the disc(s) end bearing as possible (i.e., toward the coupling end bearing) in order to maintain load on the coupling end bearing. In fact, because the overhung mass of the turbine/expander discs is so high, the center-of-gravity can never be that far from the disc(s) end bearing. A downward load on the coupling end bearing (without the coupling installed) tends to prevent the rotor from tipping during assembly/disassembly, but caution must be maintained. Keeping a net downward load on the coupling end bearing in a two stage overhung unit may require a massive centerbody section (large shaft section between journal bearings).

A low resultant load on the coupling end bearing may make the coupling end rotor synchronous response sensitive to unbalance. Coupling end unbalance sensitivity may be reduced by decreasing coupling end bearing assembly clearance, increasing tilting pad bearing preload, or using offset tilt pads. If fixed geometry bearings are used, the lightly loaded coupling end bearing may be susceptible to oil whirl. A case history of a sleeve bearing induced instability for an overhung power turbine is summarized in 3.3.2.4.

Because of sleeve bearing induced instability problems, many manufacturers have installed or retro-fitted stabilizing bearing designs such as pressure dam or multi-pocket sleeve bearings [3], offset half bearings, or tilt pad bearings. This has been done on both the hot and the cold end. In general, such retrofits have eliminated subsynchronous vibrations but have not eliminated misalignment problems that are common to "hot" equipment. For this reason, the trend has been for new overhung units to be supported by tilting pad journal bearings whose tilting pads have some degree of axial misalignment capability. These bearings have been shown to virtually eliminate babbitt edge-loading problems.

In cases where rotor instability cannot be solved by bearing modifications, inadequate lubricant drainage may be the cause of the problem. Elimination of standing pools of lubricant in the bearing carrier by increasing drain size will generally cure this type of instability problem.

Unlike most "cold" units such as centrifugal compressors, the bearing support structure must be capable of accommodating the thermal growths associated with "hot" operation. This generally means the supporting structure is light and/or flexible relative to the rotating assembly. Figure 2-82 illustrates a cross-section of a FCC power recovery expander. Note that the coupling end bearing is well supported in the radial direction by a pedestal box-structure while the disk end bearing is only supported by a box-like structure that is cantilevered from the pedestal.

For the expander displayed in Figure 2-82, the static stiffness of the coupling end bearing support is greater than 3.0×10^6 lbf/in. while the static stiffness measured for the disk end bearing support is much less than 1.0×10^6 lbf/in. The low stiffness associated with the disk end bearing support reduces the effectiveness of the disk end journal bearing's damping capability [4]. This, in turn, reduces the ability of the disk end bearing to suppress rotor vibrations and to promote stable rotor operation. For this reason, among others, expander designers have increased the diameter of the disk end journal in an effort to reduce disk end journal bearing unit loading and thus, disk end journal bearing stiffness. Also the bearing diameter on the disc(s) end has been increased in power turbines in order to raise the first rotor mode above the operating speed range.

Any lateral model of an overhung power turbine or FCC expander must incorporate accurate descriptions of the bearing support's dynamic properties. Such properties may be calculated or measured, but should always be tempered by experience. Figure 2-83 contains a schematic of the resulting rotor-bearing-support model of this equipment. Inclusion of the flexible support data in lateral models can dramatically lower calculated critical speeds [4] and damped natural frequencies for these types of units (see 2.4 and 3.6).

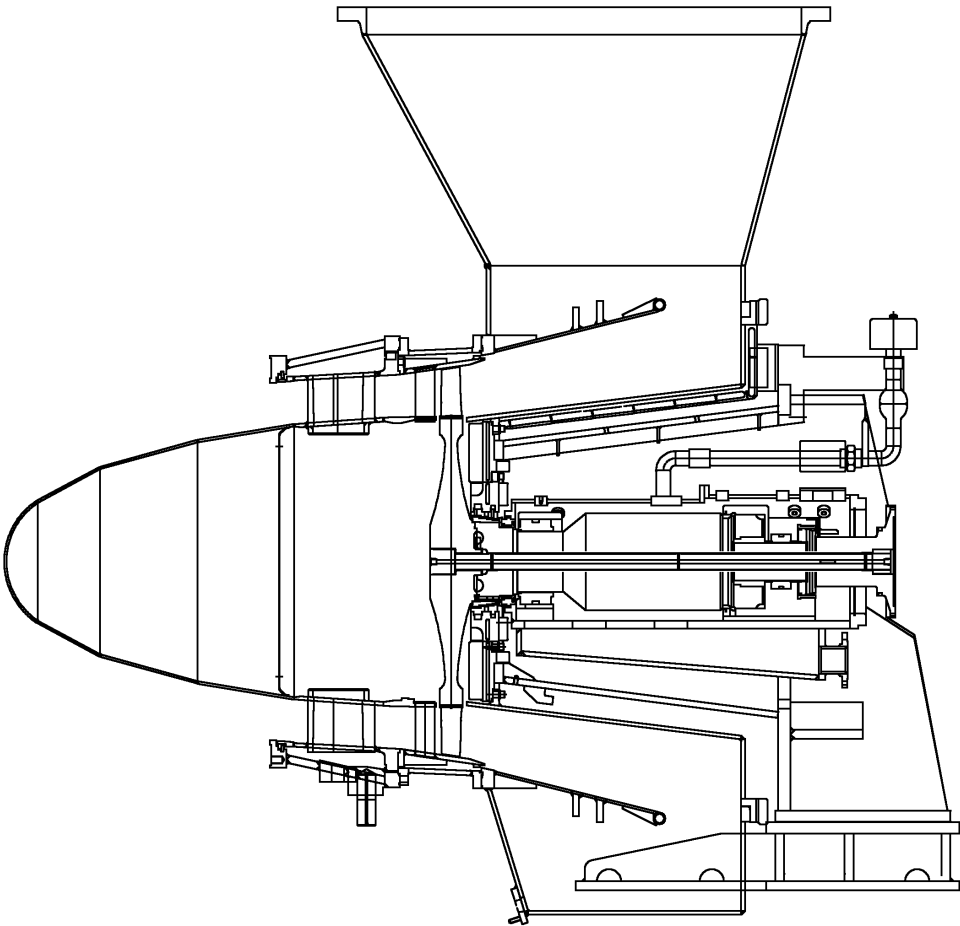


Figure 2-82—FCC Expander Cross-Section

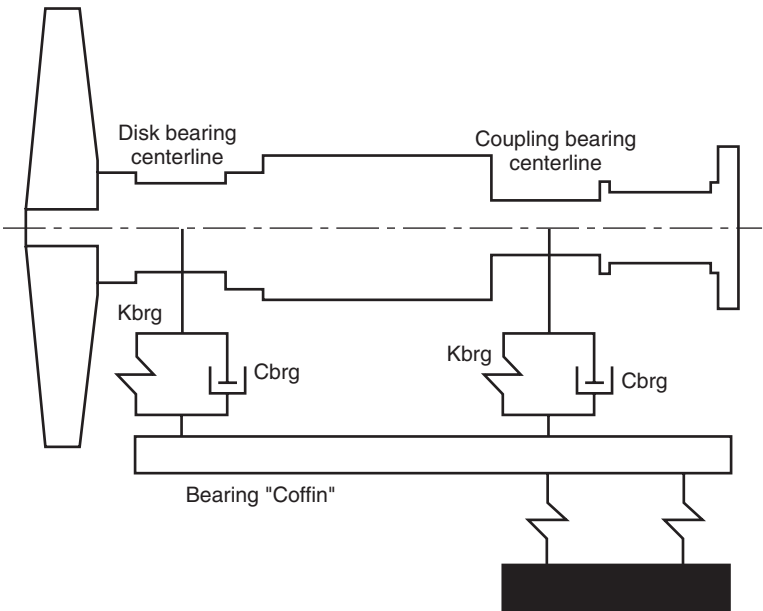


Figure 2-83—FCC Expander Rotor-Bearing-Support Model

It is not an easy matter to measure or calculate the dynamic stiffness and damping properties of the bearing supports for the following reasons:

1. Static deflection tests of the bearing pedestal appear to indicate that the exhaust casing may influence support properties.
2. Support properties may be influenced by temperature.

Given the unknowns in the support data, any lateral analysis of these overhung machines should incorporate previously accumulated experience. Specifically, the calculated critical speeds should be compared to those measured for similar units, if available.

Typical rotordynamics procedures are described.

A flexible support is included under each bearing. A percentage of critical damping is used, which is usually in the range of 2 to 10% of critical damping. The percentage used is based on the manufacturers experience with similar equipment. Critical damping is given by the formula $2 \times \text{square root of (stiffness} \times \text{mass)}$.

Unbalances are applied one at a time, one on the disc(s) end, and one at the coupling.

The disc(s) end bearing will run hotter than the coupling end bearing. When modeling this bearing, there may be a need to account for a loss of clearance (from the cold or assembly dimensions) and for heating up of the oil before it gets to the journals.

2.8.4.1 References

1. Green, R. B., 1948, "Gyroscopic Effects of the Critical Speeds of Flexible Rotors," *Journal of Applied Mechanics*, pp. 369 – 376, Dec.
2. Lund, J. W., 1974, "Spring and Damping Coefficients for the Tilting-Pad Journal Bearing," *ASLE Transactions*, Vol. 7, pp. 342 – 352
3. Nicholas, J. C., 1985, "Stability, Load Capacity, Stiffness and Damping Advantages of the Double Pocket Journal Bearing," *ASME Journal of Tribology*, 107 (1), pp. 53 – 58.
4. Nicholas, J. C., Whalen, J. K. and Franklin, S. D., 1986, "Improving Critical Speed Calculations Using Flexible Bearing Support FRF Compliance Data," Proceedings of the Fifteenth Turbomachinery Symposium, Turbomachinery Laboratory, Texas A&M University, College Station, Texas, pp. 69 – 78.

2.8.5 Axial Compressors

The rotordynamic characteristics of axial compressors normally do not present any particular rotordynamic problems. The rotor mass-elastic characteristics depend on the method of rotor construction and blade attachment. The four typical methods of rotor constructions are disc-on-shaft shrink fit (similar to most centrifugal compressors), stacked disk with through tie bolts, drum rotors with studs or tie bolts, and solid rotors. Four typical axial compressor rotor construction examples are illustrated in Figures 2-84 – 2-87.

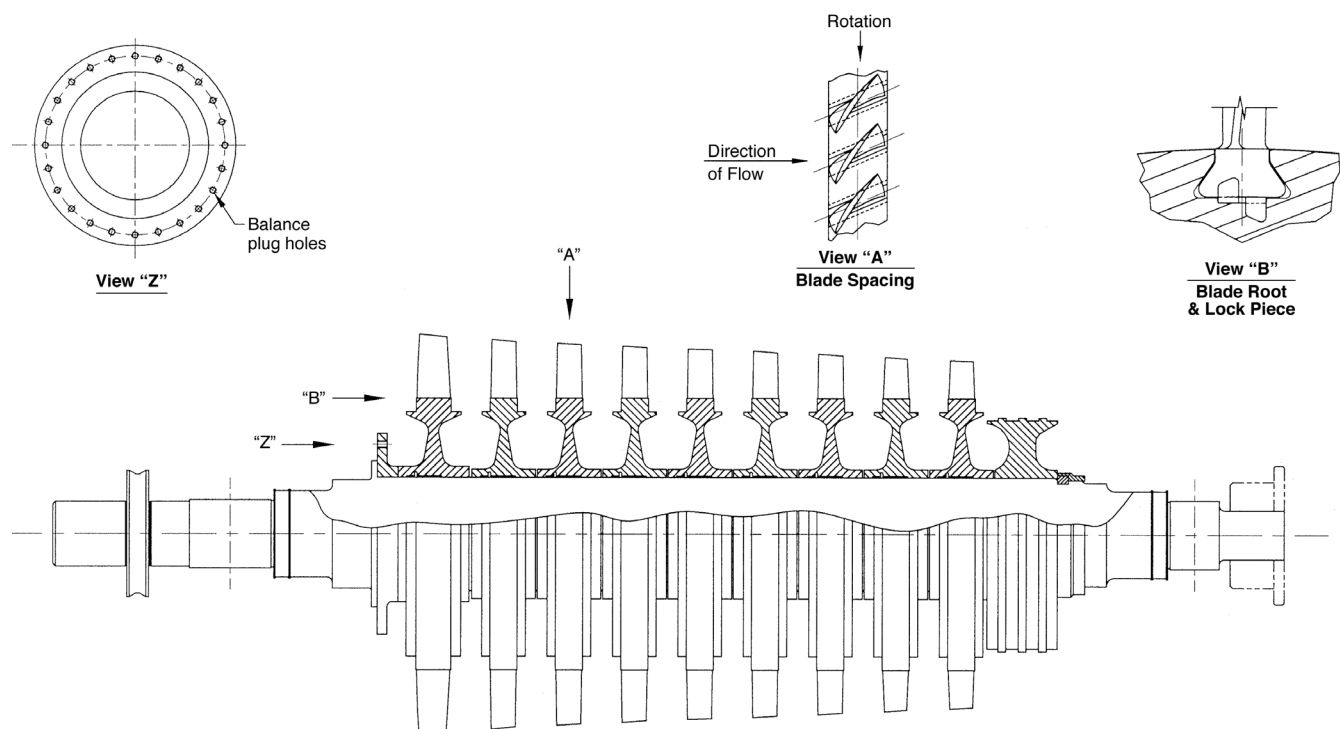


Figure 2-84—Axial Compressor Rotor Construction: Disc-on-shaft Shrink Fit

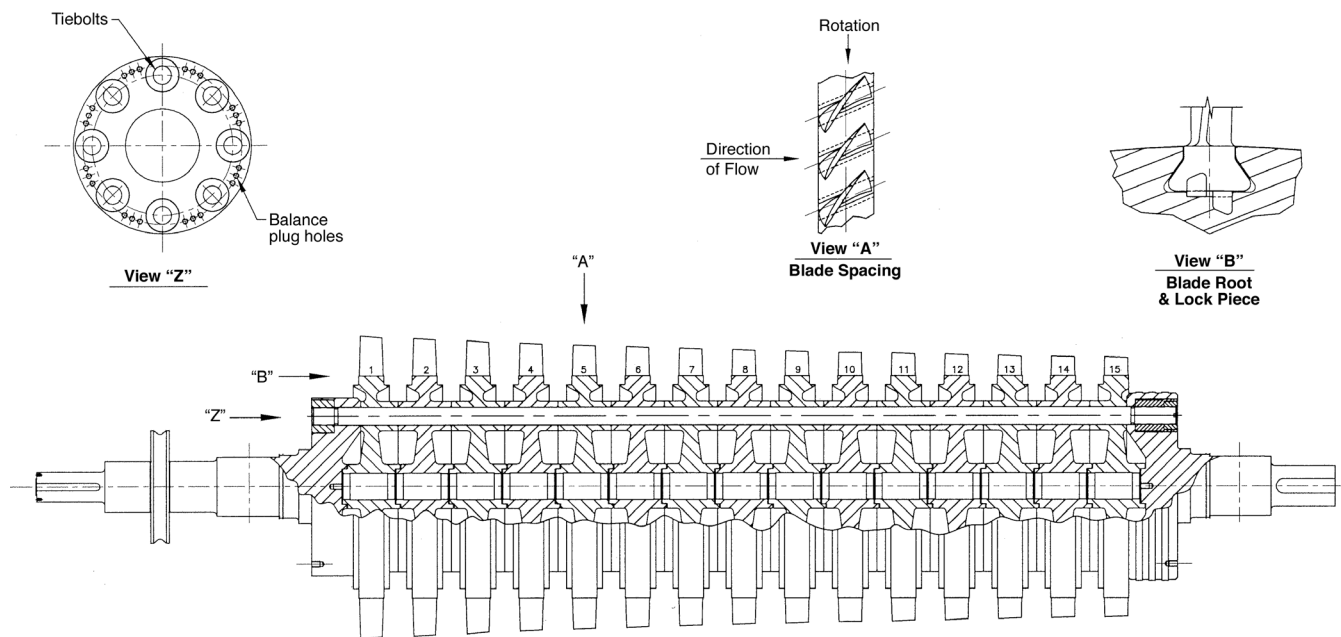


Figure 2-85—Axial Compressor Rotor Construction: Stacked Discs with Tie Bolts

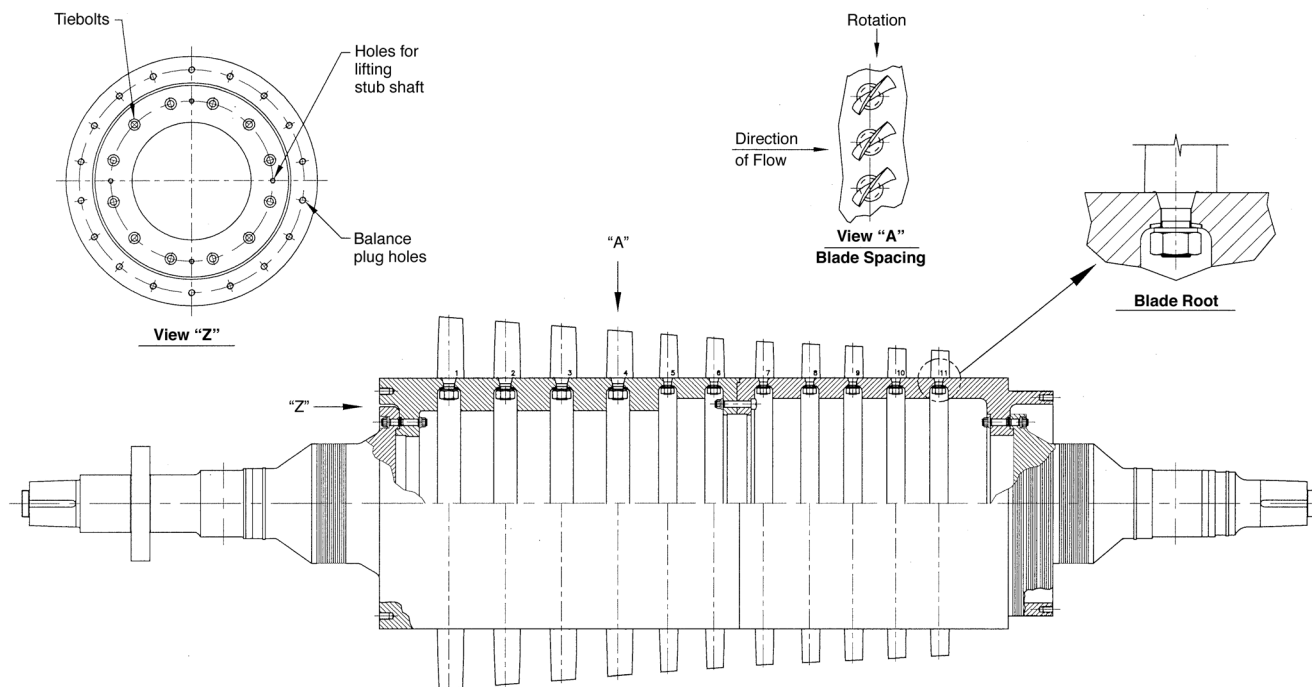


Figure 2-86—Axial Compressor Rotor Construction: Drum Rotor with Studs

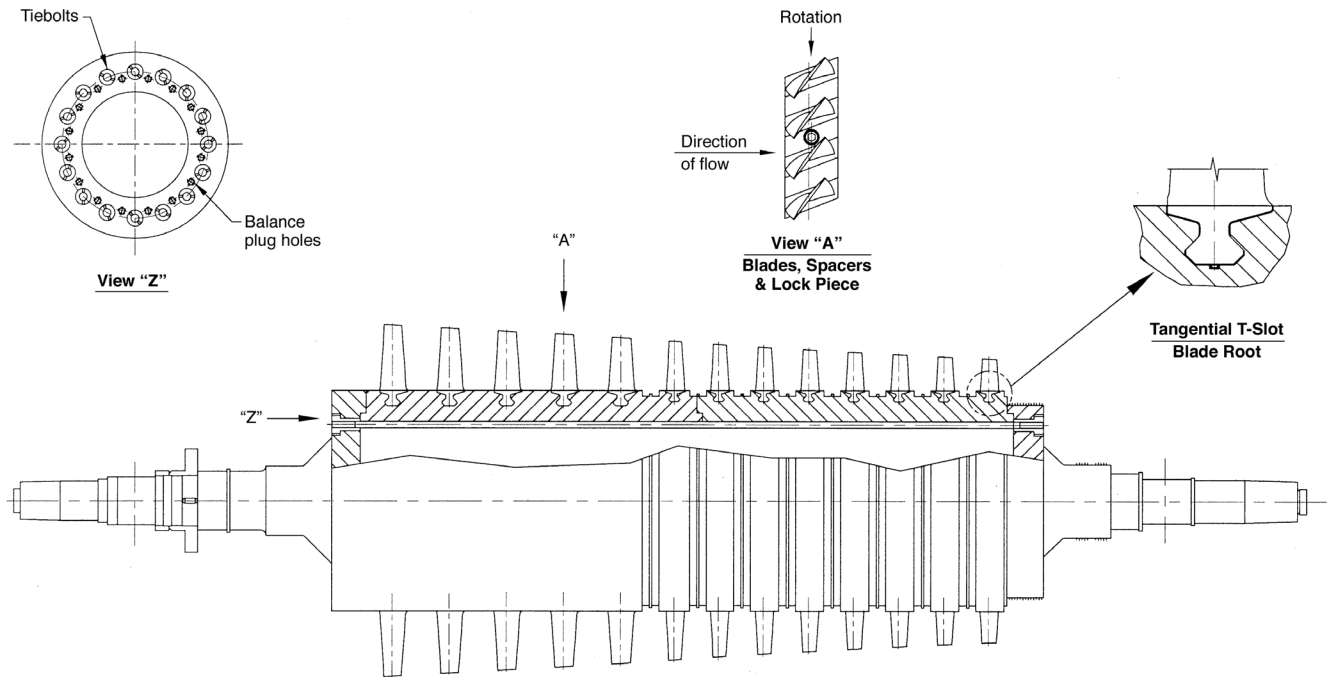


Figure 2-87—Axial Compressor Rotor Construction: Drum Rotor with Tie Bolts

Because of their complex construction features, the modeling of axial compressor rotors demands significant attention. Tie rod and stud torque levels along with stacked disk surface interactions greatly affect the stiffness properties of the rotor. In general, axial compressor rotors are more rigid than other process turbomachinery because of their large mid-span diameters and their hollow construction. For a solid cylinder and a hollow cylinder of equal cross-sectional area, the hollow cylinder will have higher lateral bending stiffness.

Furthermore, the support characteristics (pedestals) of axial compressors could be of the same order of magnitude as the fluid film characteristics of the journal bearings in which the rotor is supported. Hence this should be accounted for in the rotordynamic analysis as required, Nicholas and Kirk [1] (see 2.4 and 3.6).

The destabilizing aerodynamic cross coupling stiffness in an axial compressor stage can be estimated from Alford's equation which is discussed in detail and given as Equation 3-3 in 3.5.1.1. If deemed necessary, the stability characteristics of an axial compressor due to aerodynamic cross coupling forces can be evaluated using the cross coupling coefficients calculated from Alford's equation. Stability characteristics of axial compressor should also be evaluated if supported by fixed geometry bearings [1] as sleeve bearings can induce an excitation force that may drive the axial compressor rotor unstable (see 3.3.2). In general, stability is not a problem associated with axial compressors.

Table 2-4 provides a summary of the rotordynamic characteristics of several axial compressors of different frame sizes operating in the field with 5-pad tilting pad journal bearings. The data in Table 2-4 illustrates typical parameters associated with axial compressors that are in operation without any vibration problems. Note that the journal bearing unit loads all range between 125 and 255 psi.

2.8.5.1 References

1. Nicholas, J. C. and Kirk, R. G., 1982, "Four Pad Tilting Pad Bearing Design and Application for Multi-Stage Axial Compressors," *ASME Journal of Lubrication Technology*, 104 (4), pp. 523 – 532.

2.8.6 Centrifugal Compressors

2.8.6.1 Introduction

Centrifugal compressors present equipment designers with challenges not typically found in other rotating equipment. They arise from such factors as the aerodynamic characteristics of the centrifugal impeller and the containment of the process pressure within the case. These challenges impact the dynamic behavior of the rotor/bearing system by restricting the design flexibility. As an example, axial flow machinery (turbines and compressors) derives efficiency benefits from locating the aerodynamic components, blades and vanes, at larger diameters in the flow path. In contrast, efficiency gains with centrifugal impellers are obtained from using smaller

Table 2-4—Rotordynamic Characteristics of Axial Compressors

No.	Maximum Continuous Speed (rpm)	Minimum Continuous Speed (rpm)	Critical Speed Ratio (MCOS/Nc1)	Bearing Geometry and Diameter, D (in) x Length, L (in)	Average Bearing Unit Load, L_u^* (psi)
1	6240	6080	1.64	5-LBP 5x2.125	213.5
2	7046	6039	1.60	5-LBP 5x2.125	190.0
3	6225	6225	1.20	5-LBP 6x3	128.5
4	6090	4567	1.57	5-LBP 5x2.125	215.5
5	7065	6575	1.81	5-LBP 5x2.125	216.5
6	7046	6375	1.60	5-LBP 5x2.125	217.0
7	6199	5996	1.63	5-LBP 5x2.125	234.5
8	5775	5500	2.14	5-LBP 6x3	190.0
9	6245	6140	1.52	5-LBP 5x2.125	162.5
10	5890	4485	2.18	5-LBP 6x3	209.5
11	5180	4864	2.25	5-LBP 6x3	254.5
12	5890	4488	1.90	5-LBP 6x3	173.5
13	3780	3600	1.99	5-LBP 8x7	200.5
5-LBP = Five pad tilting pad journal bearing (load between pads). L_u = bearing load/($L \times D$) psi					

inlet eye diameters. The rotordynamics impact of this factor is that centrifugal compressors will tend to operate more in the flexible shaft region than axial flow machinery.

Another challenge involves containing the higher pressures levels developed within a centrifugal compressor in the case. These levels in combination with the high rotating speeds magnify the effects of sealing components. The seal dynamic behavior impacts both unbalance response and stability. This increases the complexity of both analyses. The development of the API lateral analysis specifications for centrifugal compressors in comparison to other rotating equipment mirrors this complexity. Weaver [1] presented an early attempt to define the critical dimensions governing the dynamic behavior of multi-stage and overhung compressors.

Special considerations of centrifugal compressors for the undamped critical speed and unbalance response analyses will be presented in the following sections. Section 3.8.6 discusses the factors/components that require careful examination to obtain accurate stability predictions.

2.8.6.2 Multi-stage Compressors

Modeling of multi-stage compressor rotors, Figure 2-88 does not normally require special consideration. Past construction trends have used solid shafts with impellers, thrust collars and couplings applied by interference fits. Basic FEA and lumped mass techniques have proven more than adequate in modeling these rotors. A few manufacturers use a tie-bolt or built-up construction technique more reminiscent of gas turbines or axial compressors. These require special attention

to the shaft diameter that is used to determine the shaft bending stiffness (see 2.3).

Additionally, support stiffness considerations beyond the bearing are not normally required. Due to the pressure containment requirements, the case construction is normally very stiff in relation to the bearings. With lower thermal growth than steam or gas turbines, soft and/or separate housing supports are also not usually required. This combination of a stiff case and bearing housings produces support stiffness in excess of 3.5 times the bearing stiffness and can be treated as infinite without a great loss of accuracy.

The unique characteristic of multi-stage compressors is the seals and their contribution to the dynamic behavior of the rotor/bearing system. These include the impeller eye, balance piston, section inlet and the casing end seals. While a significant portion of the attention has been paid to their impact on the rotor stability (see 3.4), the impact of liquid film seals on the synchronous behavior of compressors can be just as great (see 2.6.2). Accurate models of oil film seals are necessary to ensure reliable critical speed predictions.

Typical mode shapes of multi-stage compressors from an undamped analysis follow the classical examples. Figures 2-89 and 2-90 illustrate the soft and rigid support modes from a typical multi-stage compressor. The bounce and rocking rigid body mode shapes can be seen, as well as, the classic bending mode shapes one might expect from a beam with central weight addition. The shaft bending stiffness, between bearing weight and bearing properties, will determine the location and shape of the modes during operation.

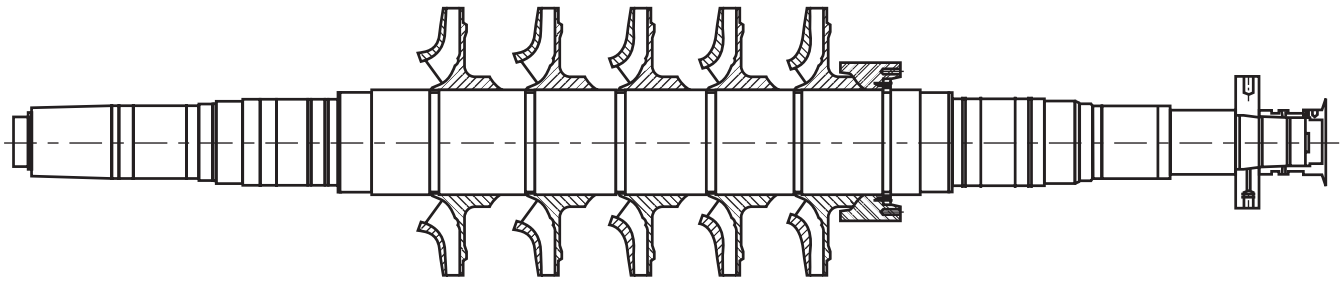


Figure 2-88—Typical Multi-stage Compressor

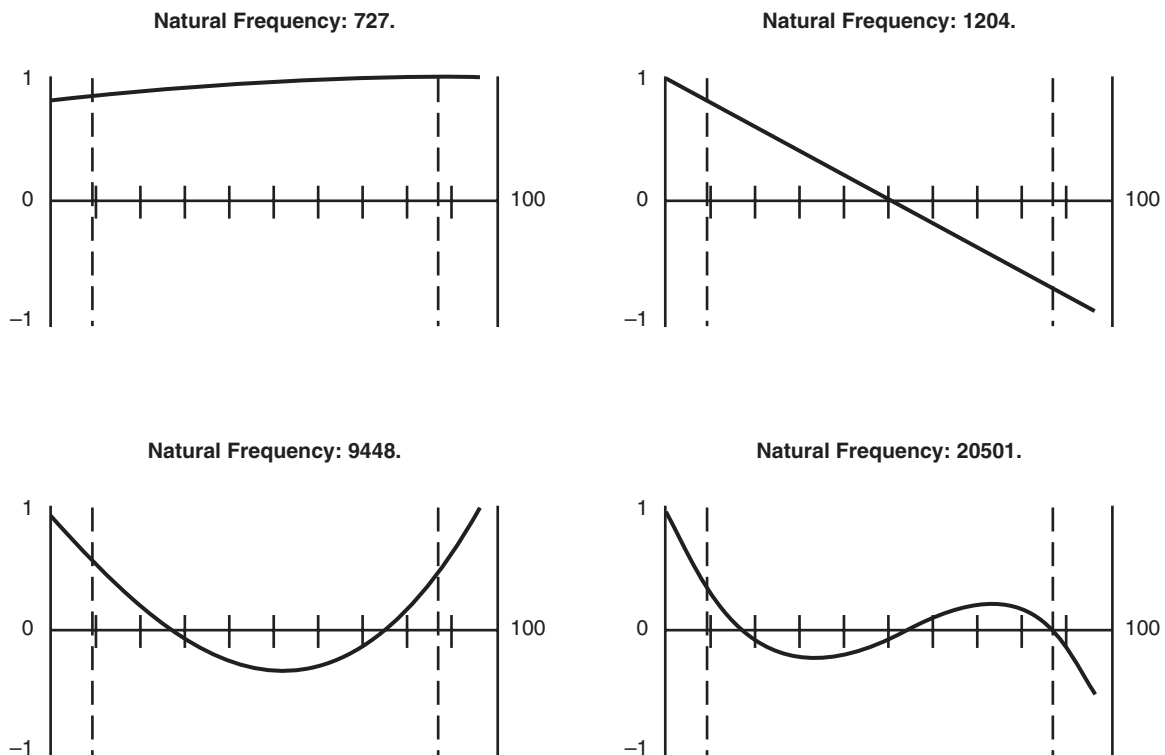


Figure 2-89—Soft Support Undamped Mode Shapes—Multi-stage Compressor

It is worth noting that for the last two modes pictured in both regions, the coupling weight determines which shaft end will possess the maximum displacement at the lower (3rd) mode. In this example, the coupling is on the right end of the shaft. Thus, this end of the shaft will have the maximum displacement at the lower mode. For drive-through compressors (couplings at both ends), the overhung moment of the shaft end will determine the maximum shaft end displacement at the lower mode.

Typical unbalance weight distributions used to excite the first four modes in the unbalance response are shown on Fig-

ure 2-91. The magnitudes of the weights are sized according to the rotor weight, journal reaction and overhung weight. While the primary mode of interest is listed under the unbalance distribution, it should be noted that excitation of higher modes using these distributions is possible.

For drive-through compressors, an additional unbalance may be used to excite the fourth mode. Higher modes may be excited by using a single unbalance weight at each end or by placing two unbalances in-phase and out-of-phase with each other. In the first case, dynamics of each end may be identified separately. In the second, a higher level of

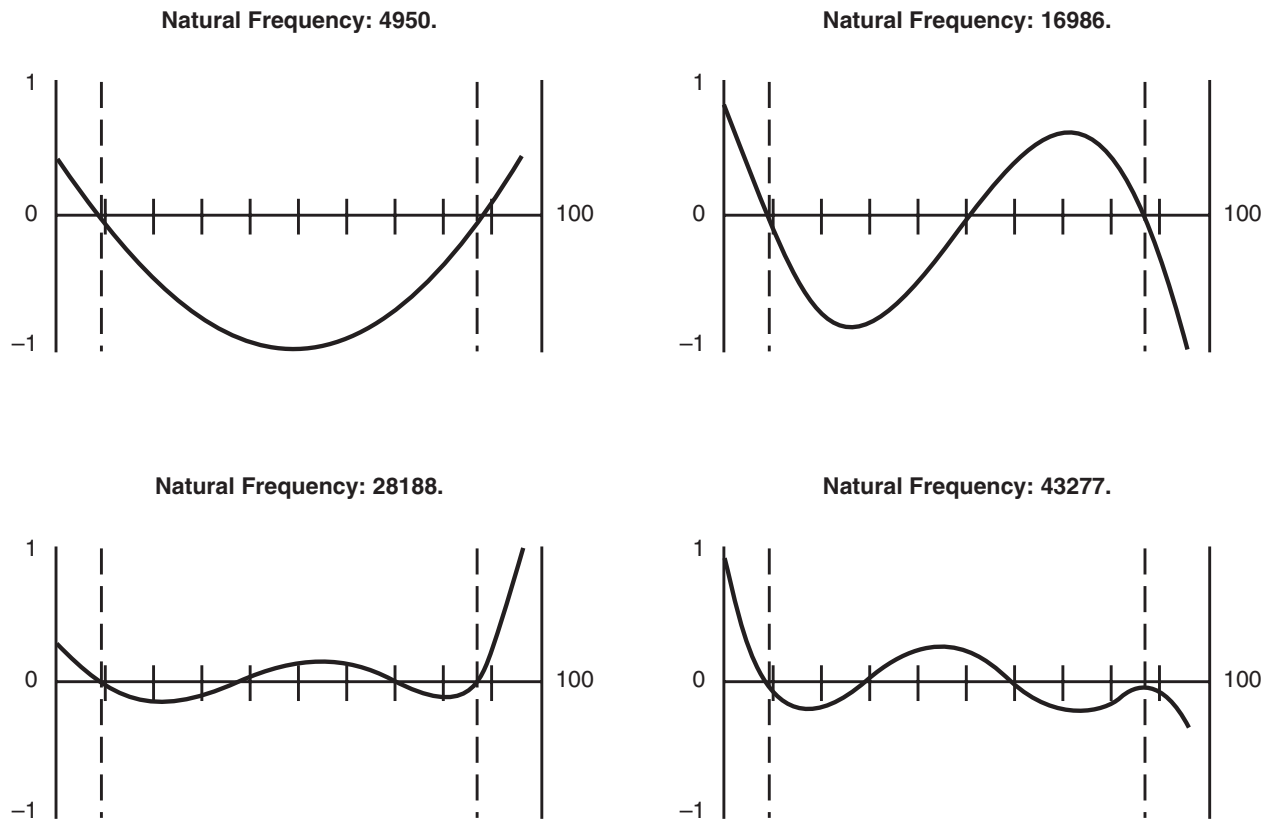


Figure 2-90—Stiff Support Undamped Mode Shapes—Multi-stage Compressor

response may be achieved for an insensitive system. The advantages of each need to be weighed to select the optimum unbalance configuration.

Due to trade-offs of aerodynamic efficiency versus rotordynamic behavior, the first mode in a multi-stage compressor will normally have significant bending and an amplification factor exceeding 2.5. However, the second mode may easily be more representative of a rigid body mode and heavily damped, $AF < 2.5$. Figures 2-92 through 2-95 plot the unbalance response and mode shape of the first two unbalance response peaks. The compressor operates between these modes.

2.8.6.3 Overhung Compressors

The overhung gyroscopic effects and weight of the single stage impeller and coupling govern the dynamics of the overhung compressor, Figure 2-96. In contrast to multi-stage compressors, overhung compressors have short bearing spans and relatively stiff shafts. As a result, the first two modes are characterized by rigid body motion. The frequency of the first mode is determined by the overhung mass moment of the impeller, impeller polar and transverse inertia and impeller bearing properties. The second mode is influenced by the same mass properties of the coupling and coupling end bearing.

The magnitude of the overhung moment also increases the likelihood of experiencing another dynamic phenomenon referred to as synchronous thermal instability. Synchronous thermal instability or “Morton’s Effect” (see 3.5.2.5) occurs when the overhung dynamics couples with asymmetric heating of the journal. Simply stated, synchronous vibration causes non-uniform heating of the shaft under the bearing. This will lead to a thermal bow of the shaft end, producing unbalance. If the overhung dynamics exist that magnify the journal response to that bow or unbalance, than an unstable system results. An excellent reference to this dynamic effect can be found at de Jongh [2]. “Morton’s Effect” has also be shown to afflict integrally geared and drive-through compressors and double-ended drive turbines. Note that there are no API analysis requirements for this behavior. However, API vibration limits may be exceeded during testing.

While the rotor support in multi-stage compressors is similar end-to-end, in overhung compressors they are very different. At the coupling end, journal loads can approach zero and in some cases actually be loaded upwards. The impeller end bearing may also be subjected to loads other than gravity loading of the shaft. Some researchers have reported volute loading at levels significant enough to affect the impeller end bearing dynamic characteristics. A commonly used equation

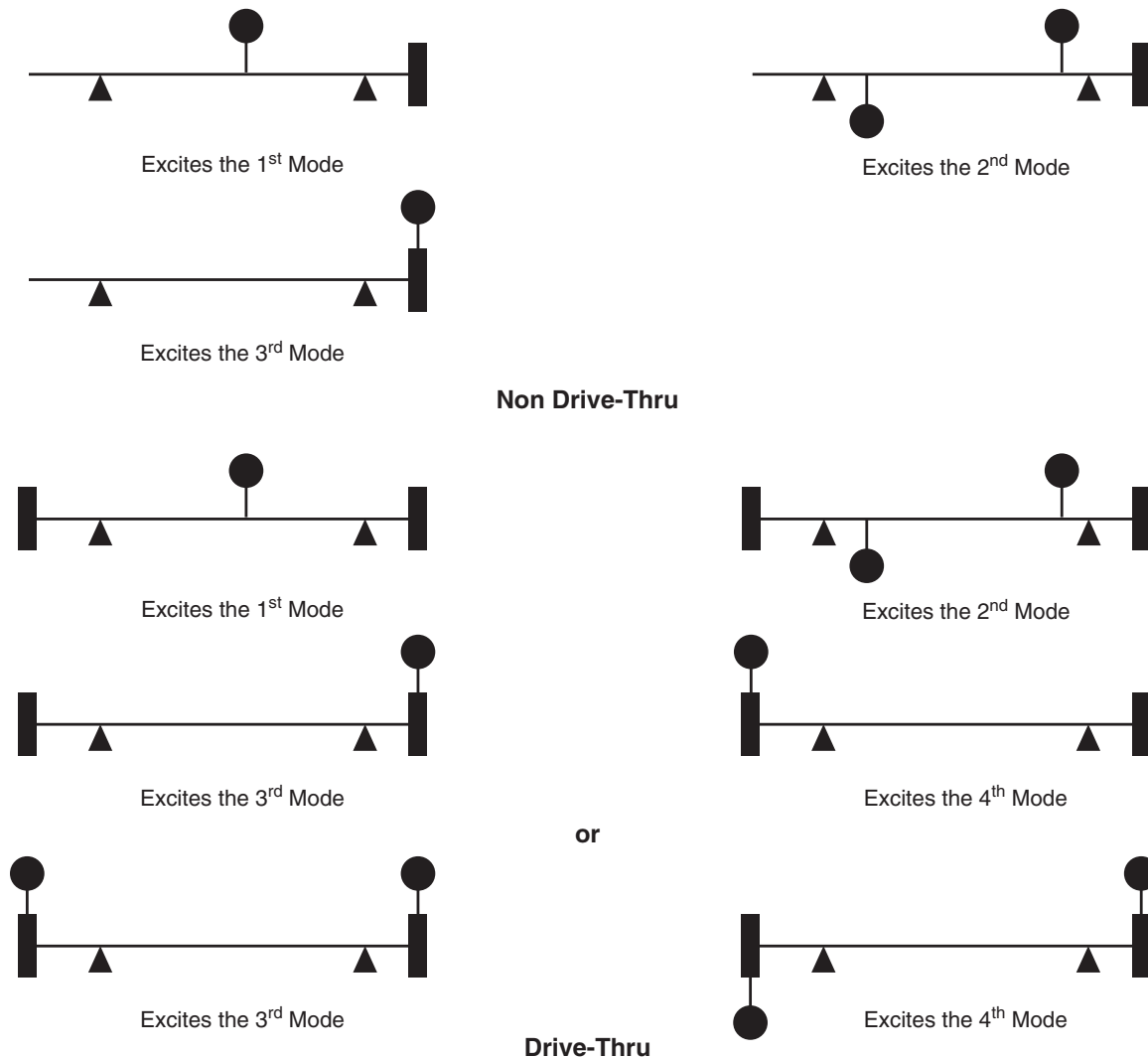


Figure 2-91—Typical Unbalance Distributions for Multi-stage Compressors

to compute the volute loading is the Stepanoff equation, Moore and Flathers [3]:

$$F_r = K_r P_2 D L \quad 2-23$$

where

- F_r = radial force, N (lbf),
- K_r = non-dimensional factor,
- P_2 = discharge pressure, Pa (psia),
- D = impeller outer diameter, m (in.)
- L = active impeller length, m (in.) (includes shroud surface and impeller exit).

The support structure behind the bearings also varies. A typical case is shown on Figure 2-97. A simple beam supports

the coupling end bearing while the impeller end bearing is nested within the case. The combination of the two produces support stiffness that can differ by a factor of three or greater.

Figure 2-98 illustrates the undamped modes associated with an overhung compressor, soft and stiff supported. As expected, the lower rigid and bending modes show maximum displacement at the impeller end of the shaft. These were generated with equal support stiffness at the bearing locations. Mode shapes representative of the actual system are not as easily generated. Several different approaches to incorporating the support stiffness into the analysis are possible. The more accurate is to use the actual support stiffness at the mode frequency. However, this would take an iterative process using the mode frequency and support stiffness.

For equipment with equivalent support stiffness characteristics, undamped maps are generated using the same stiffness

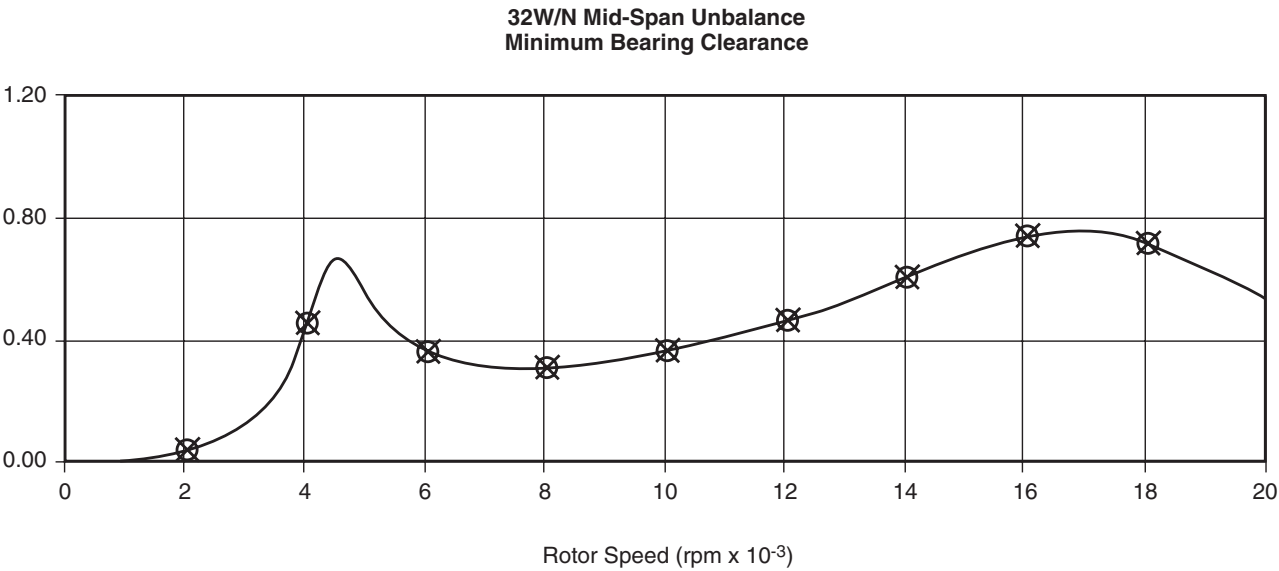


Figure 2-92—Unbalance Response of 1st and 3rd Critical Speeds

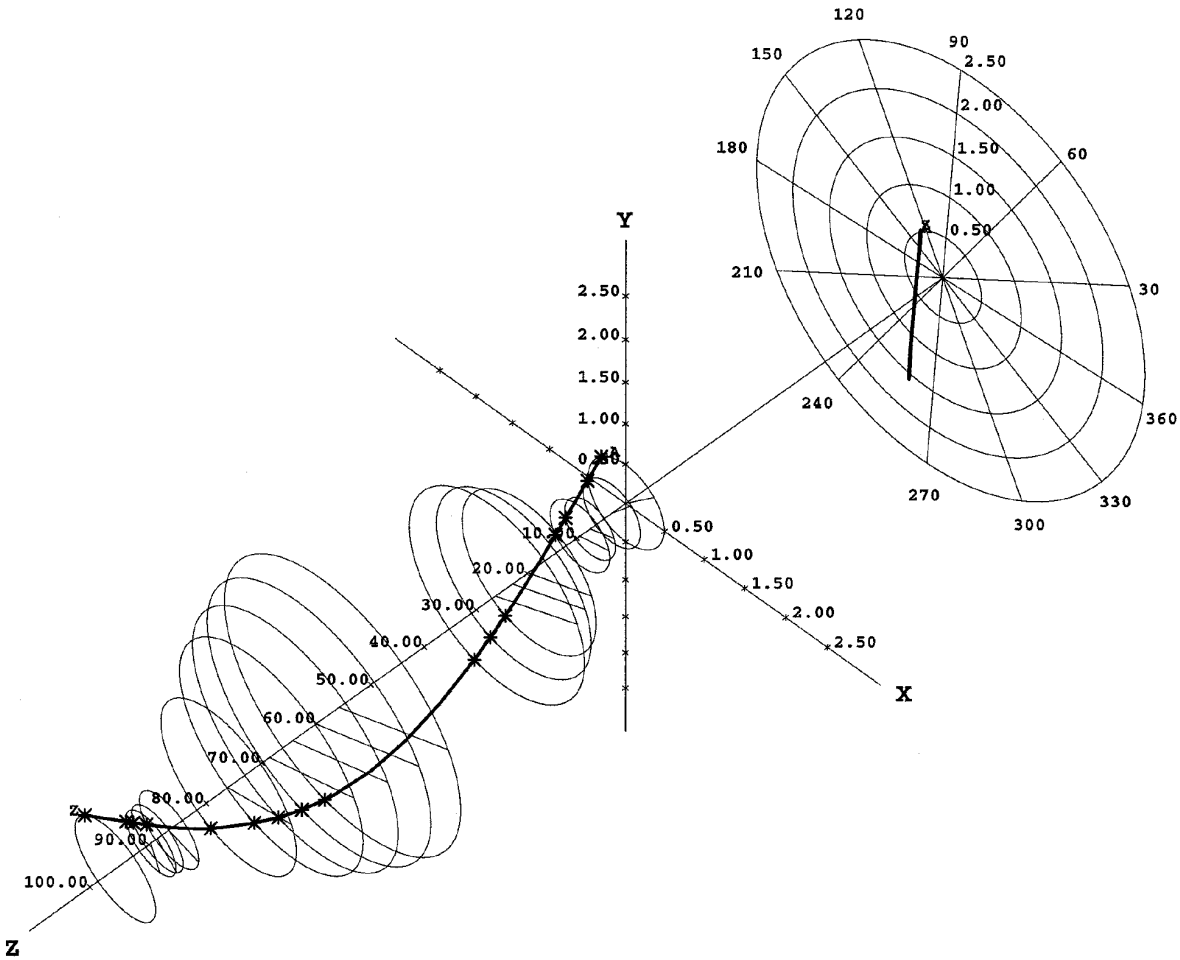


Figure 2-93—Rotor Response Shape @ 4500 rpm

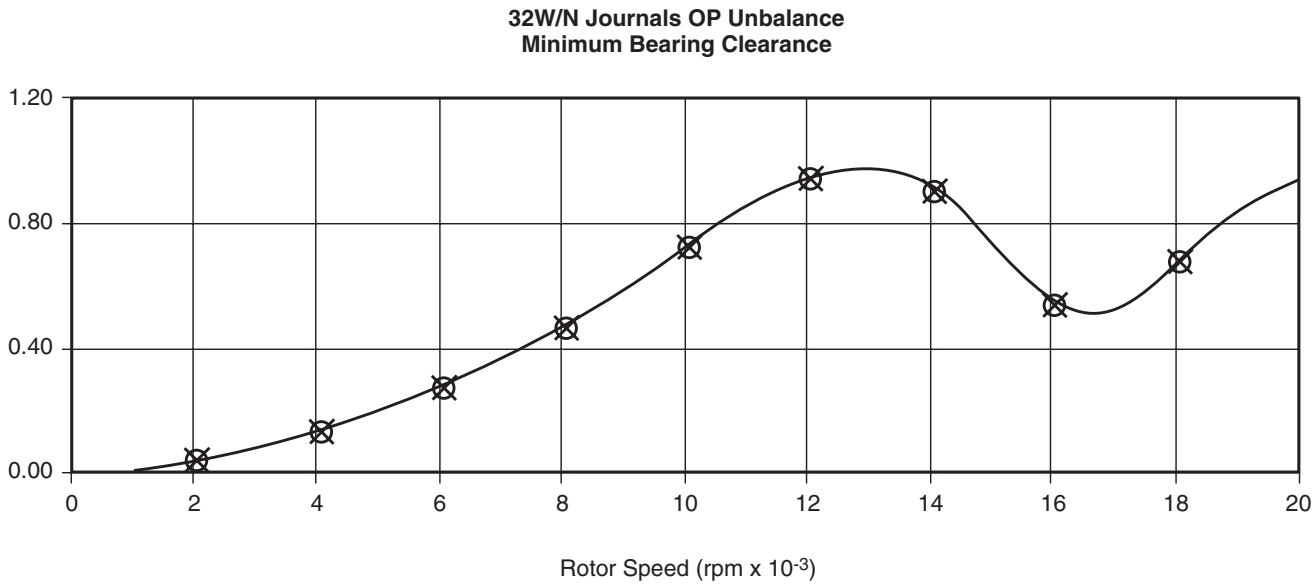


Figure 2-94—Unbalance Response of 2nd Critical Speed

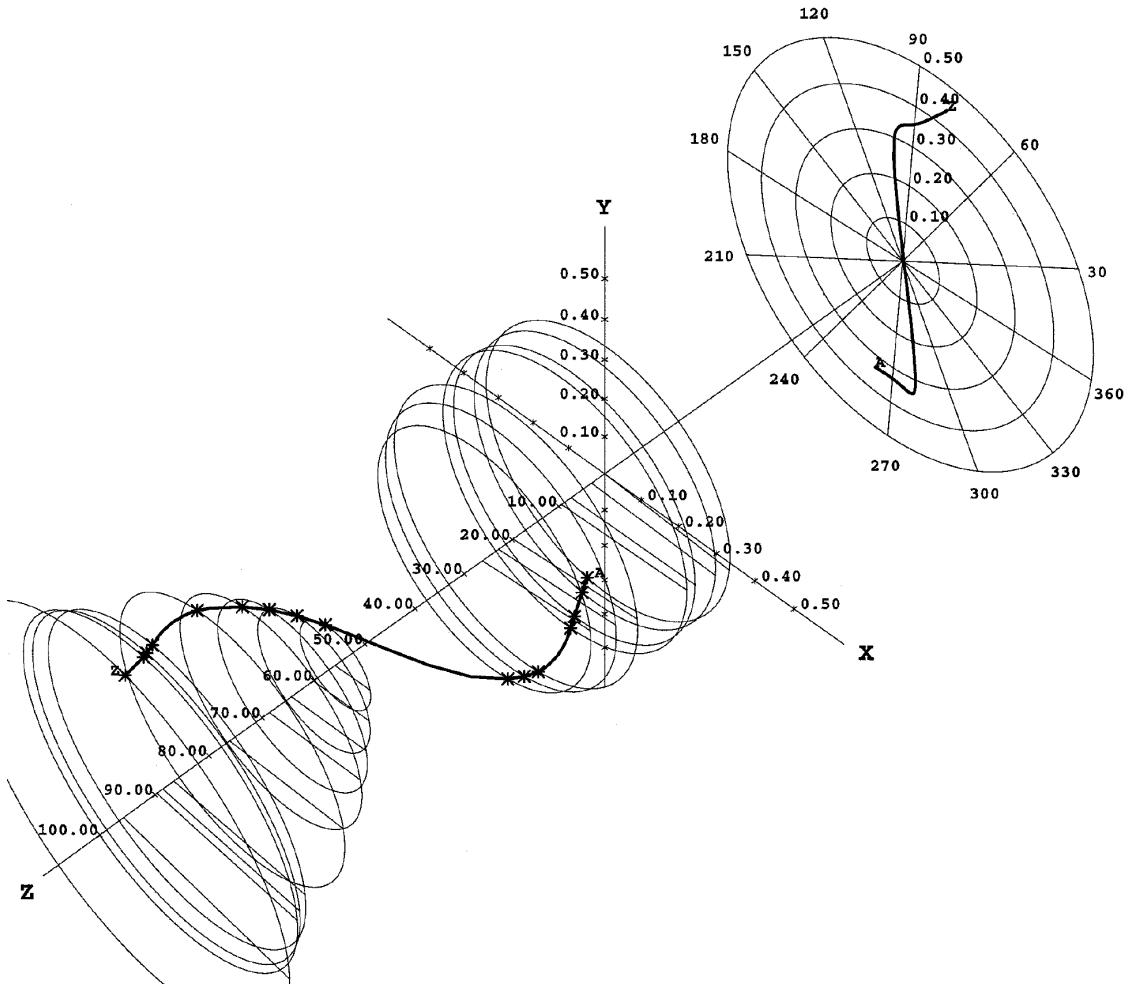


Figure 2-95—Rotor Response Shape @ 12,800 rpm

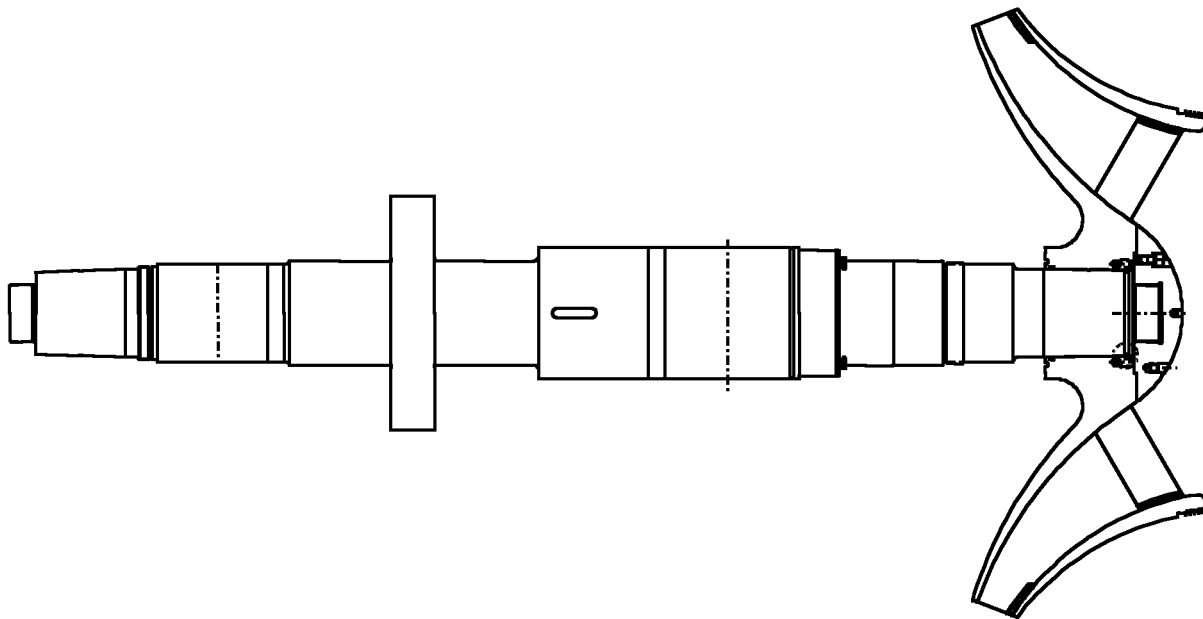


Figure 2-96—Typical Overhung Compressor

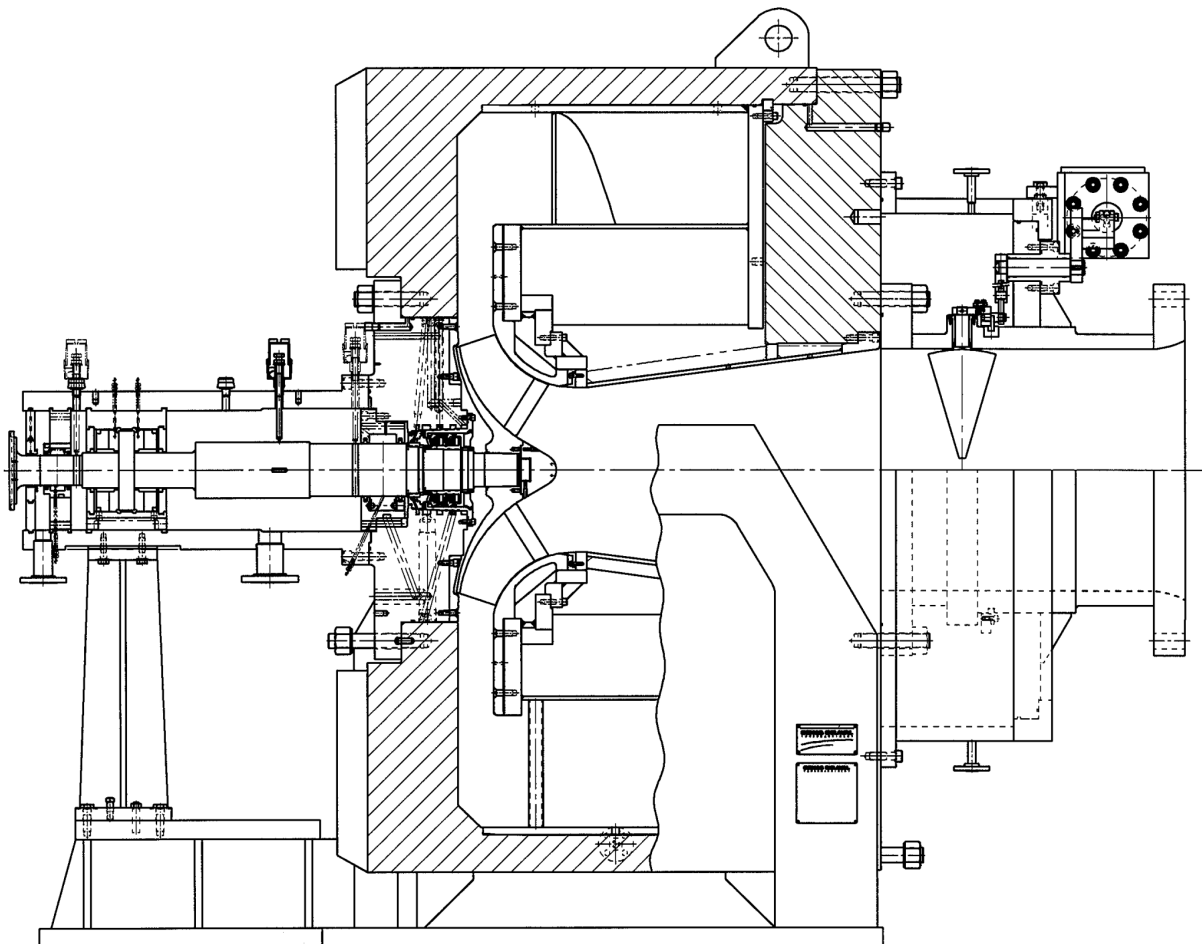


Figure 2-97—Overhung Compressor Assembly

magnitudes at each bearing location (see 2.7.2). Generating a map for overhung compressors requires special treatment of the support stiffness. One possible approach is to ratio the stiffness used at the journal locations to the stiffness calculated at some reference speed. For example, the undamped map plotted on Figure 2-99 was generated with a stiffness ratio of 2:1 for the impeller end bearing versus the coupling end bearing. This represents the approximate ratio of vertical stiffness near the operating speed. Obviously, the shortcoming of this approach is that the map is truly valid only in the region where the stiffness ratio applies. Given the diminished role that undamped critical speeds play in predictive analysis of centrifugal compressors, it is understandable that some analysts question the usefulness in generating an undamped map for overhung compressors.

A possible combination of unbalance weights is displayed on Figure 2-100. This combination is suggested to clearly

excite the expected mode shapes of the overhung compressor. Due to the stiffer nature of the shaft, a clear peak at the critical speed in an unbalance response may not occur. For the example shown, the rotor is expected to operate between the first and second modes. It would be sufficient to use excitation at the impeller and then the coupling to excite these modes. The alternate combination of placing two unbalance weights in-phase and then out-of-phase works well for modes that are either very rigid or very flexible as indicated in Figures 2-98a and 2-98b. For modes in between these extremes, the single unbalance weight applied at the impeller or coupling is a better choice. Notice that for the rigid body mode shapes, the first mode has the shaft ends out-of-phase. However, the first rigid support mode has ends that are in-phase. For support stiffness that model actual conditions, the two unbalance distribution may actually excite both modes and not produce a distinct peak at either.

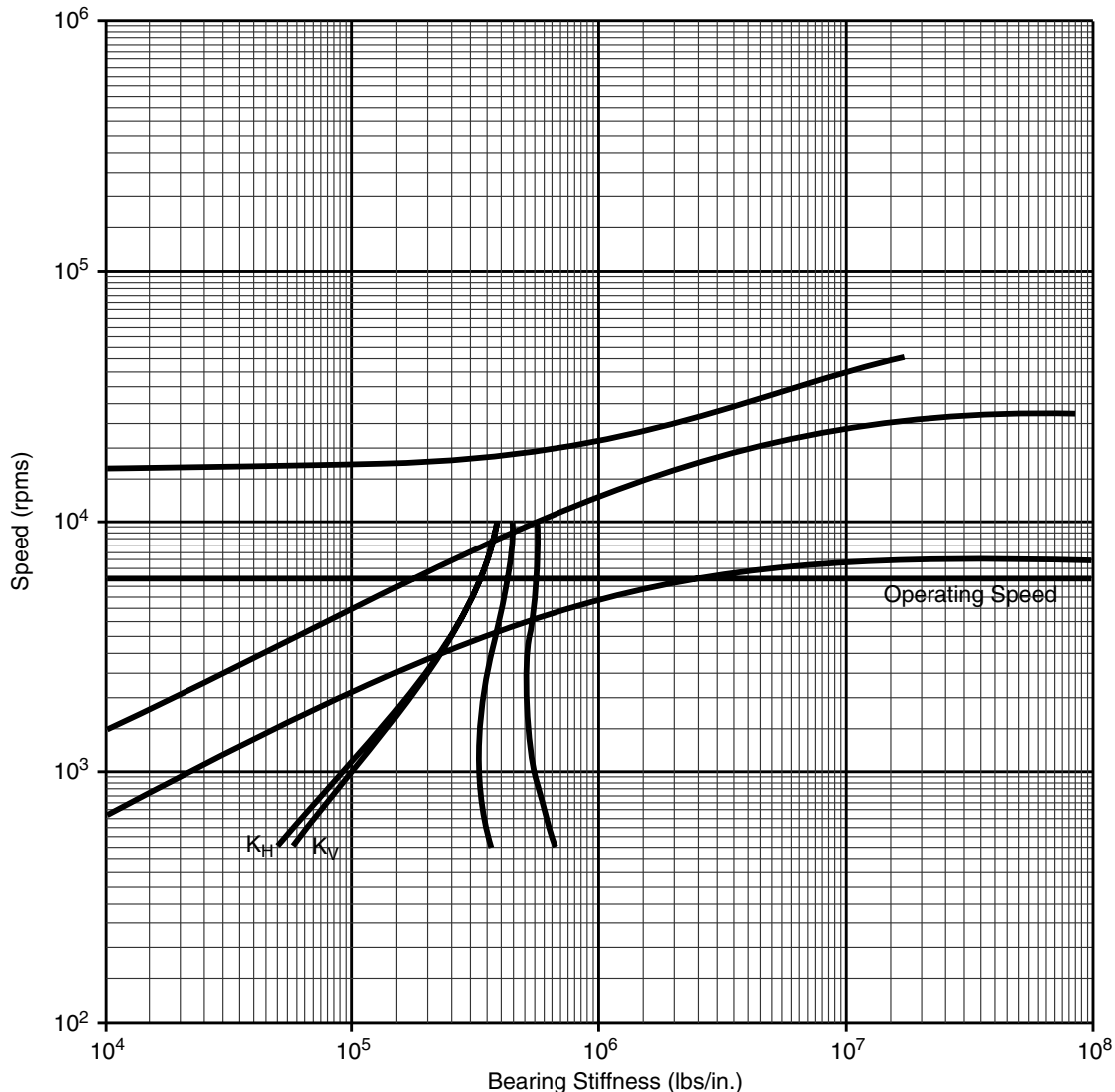


Figure 2-99—Undamped Critical Speed Map—Overhung Compressor

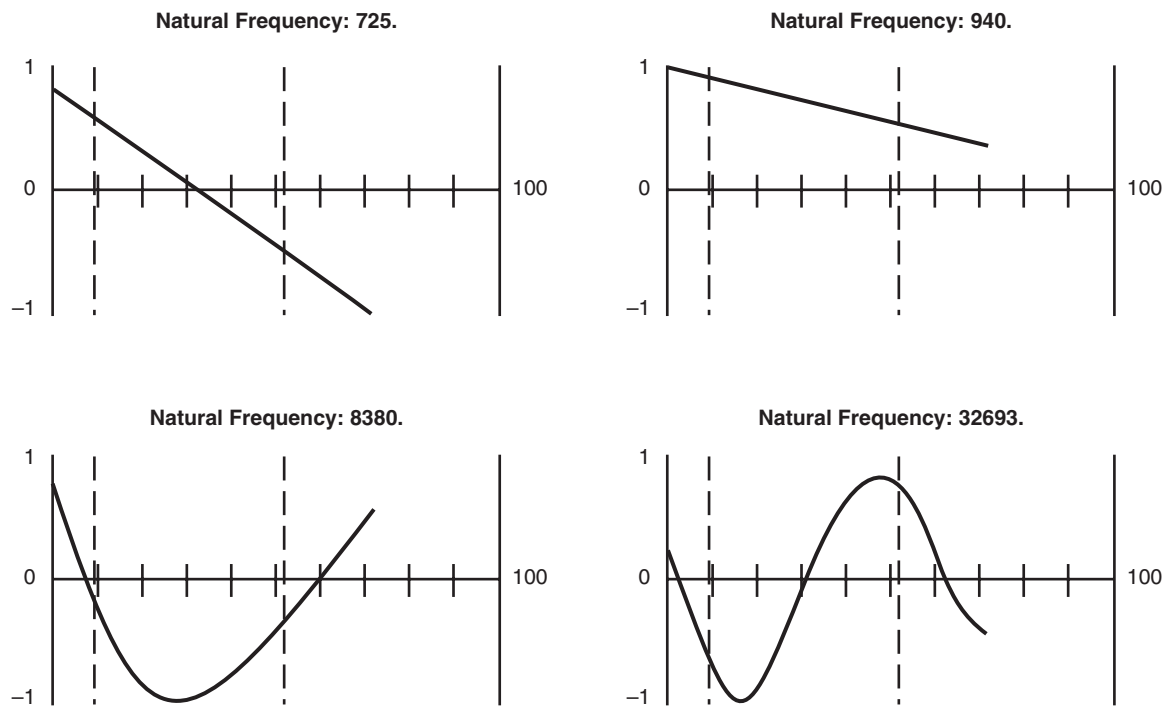


Figure 2-98a—Soft Support Undamped Mode Shapes—Overhung Compressor

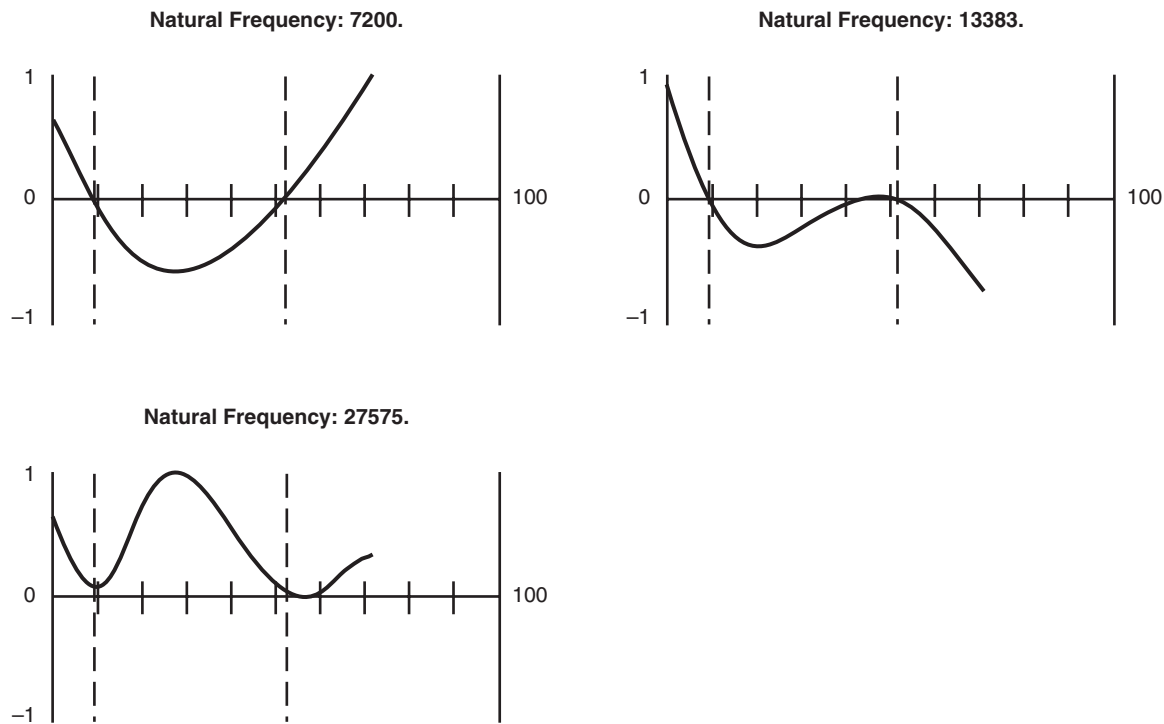


Figure 2-98b—Stiff Support Undamped Mode Shapes—Overhung Compressor

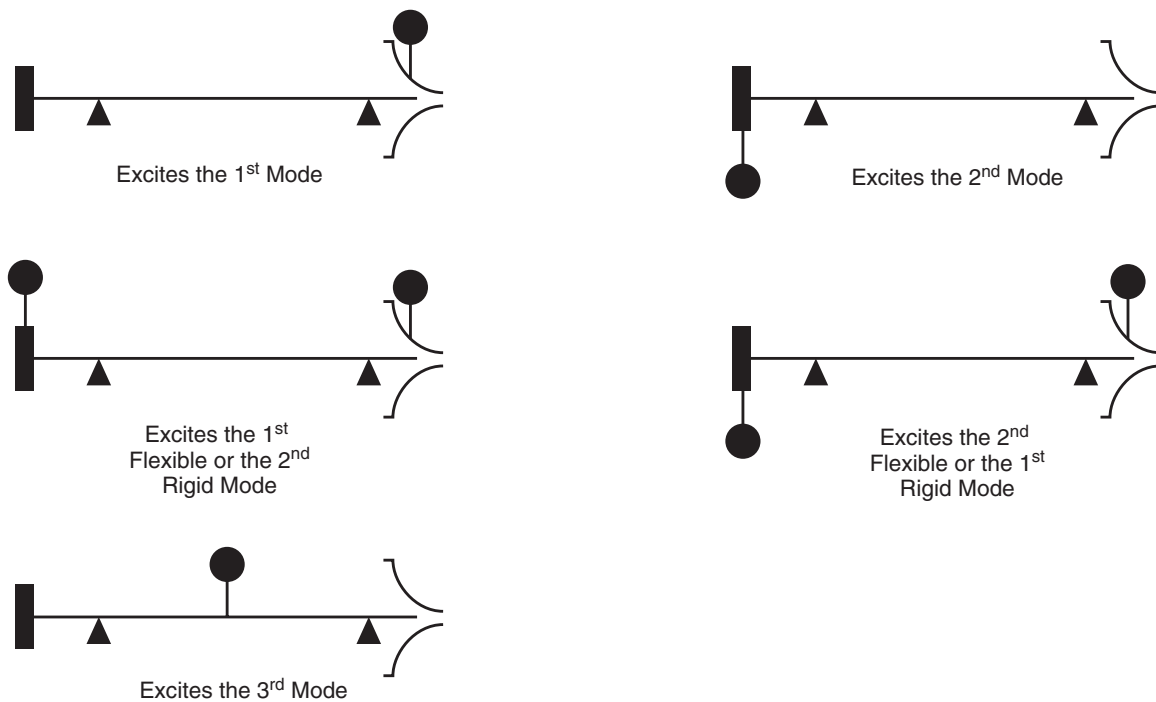


Figure 2-100—Typical Unbalance Distribution—Overhung Compressors

Figures 2-101 through 2-103 display the unbalance response and rotor shape for the first two cases. Notice that a peak response is not identified for the coupling excitation case. The second mode does occur above the analysis range.

As expected, the peak response of the first mode in Figure 2-101 is very broad with a low amplification factor. This is characteristic of an excitation of a rigid body mode. The response shape can be seen on Figure 2-102 and shows little bending over the length of the rotor. The coupling unbalance was unable to excite a peak in the response range as shown in Figure 2-103.

2.8.6.4 Integrally Geared Compressors

The integrally geared compressor is composed of two rotor types; the bull gear which can be treated in the same way as in typical gear sets and the pinion rotor. Dynamically, the pinion rotor behaves much the same as overhung compressors, i.e., the overhung mass controls the behavior. The differing feature of the pinion rotor is the gear loading at the shaft center. This is taken into account during the calculation of the bearing characteristics as an additional load.

With integrally geared compressors, the complication of unequal journal loading experienced in overhung compressors is not as significant for two reasons. First, identical bearings are normally used at both ends. Second, the gear loading at the rotor center is typically greater than the rotor weight. This evens the journal load distribution in pinions with two impellers of different weights or even just one impeller. Figures 2-104 and 2-105 present typical pinion rotors and a

model for an integrally geared compressor pinion rotor with two stages (impellers at both ends).

Typical undamped modes shapes are shown on Figure 2-106. An unbalance distribution to excite each mode is also shown. While the undamped map would look very similar to that of an overhung compressor, assumptions concerning the gear load are needed. The gear load is required to compute the bearing coefficients. The complications arise from the fact that the gear load does not behave in a similar fashion from one application to another. One assumption frequently made is that the torque (and thus the gear load) will vary as the square of the speed reaching full load at full speed. However, integrally geared compressors equipped with variable inlet guide vanes (VIGV) are able to unload the compressor during starting sequences.

Another complication arises at maximum continuous speed. The VIGV also enable the operating conditions to be changed independently of speed. Thus, whatever assumptions were applied to the load versus speed function may no longer be valid at MCS. Additionally, integrally geared compressors are frequently used with multiple process streams. Often the sequencing of those streams is critical for the plant process resulting in loading that may vary significantly (and not uniformly) with both speed and time. For these reasons, the validity and usefulness of undamped critical speed maps are questioned. (It should be noted that the same assumptions are required to perform the unbalance response analysis. As before, these assumptions define the regions where the analysis is valid.)

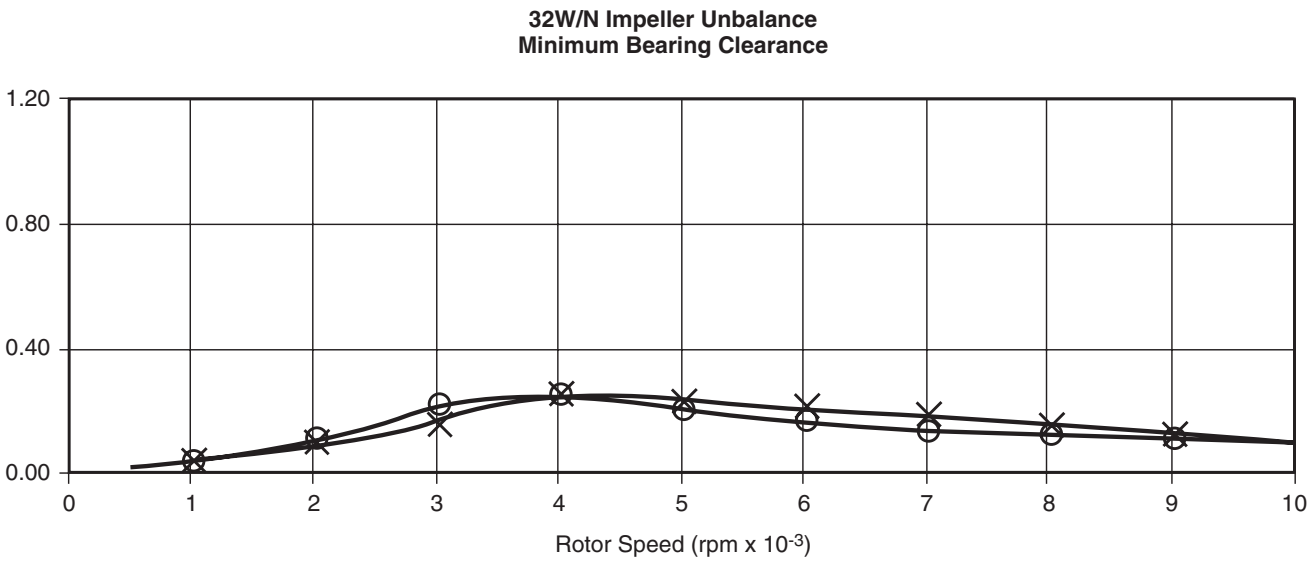


Figure 2-101—Impeller Unbalance Response—Overhung Compressor

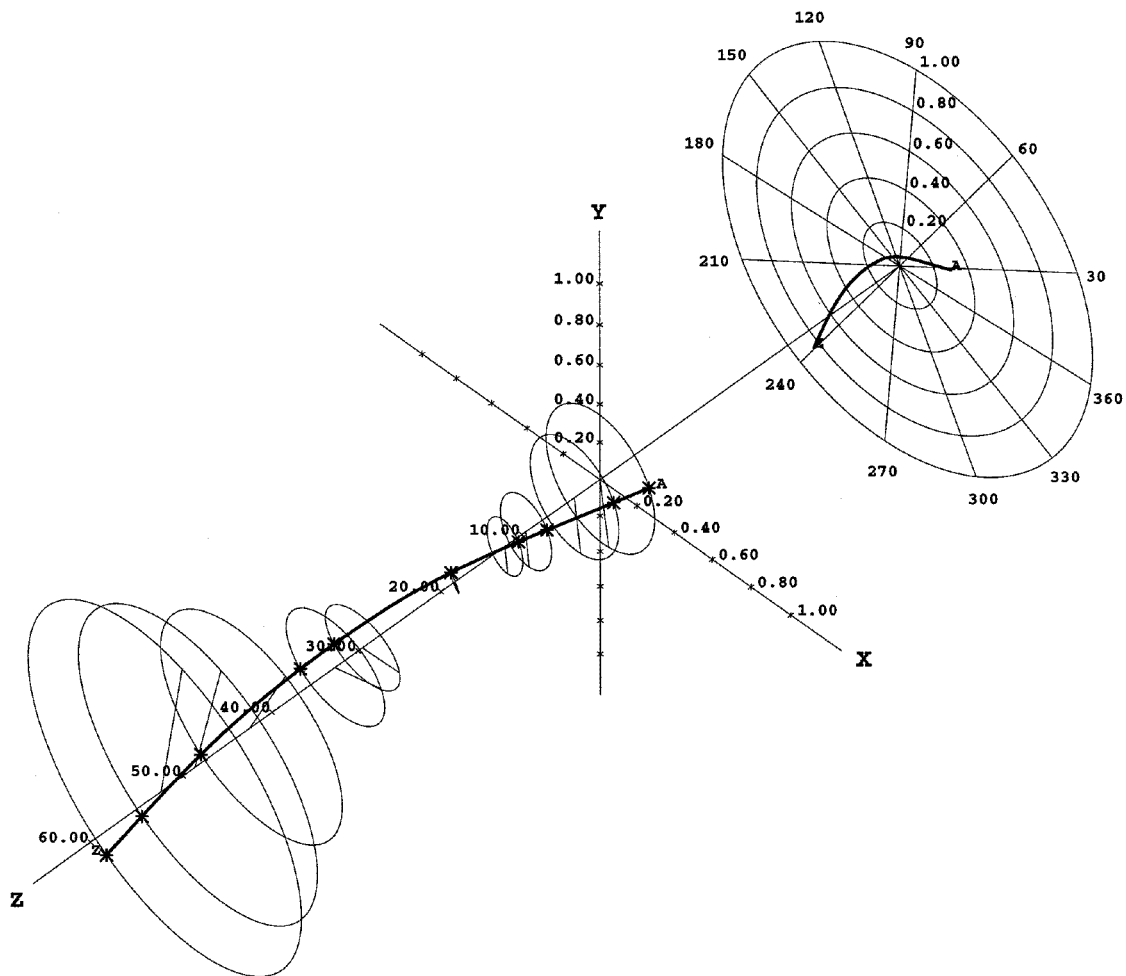


Figure 2-102—Rotor Response Shape at 4,300 rpm

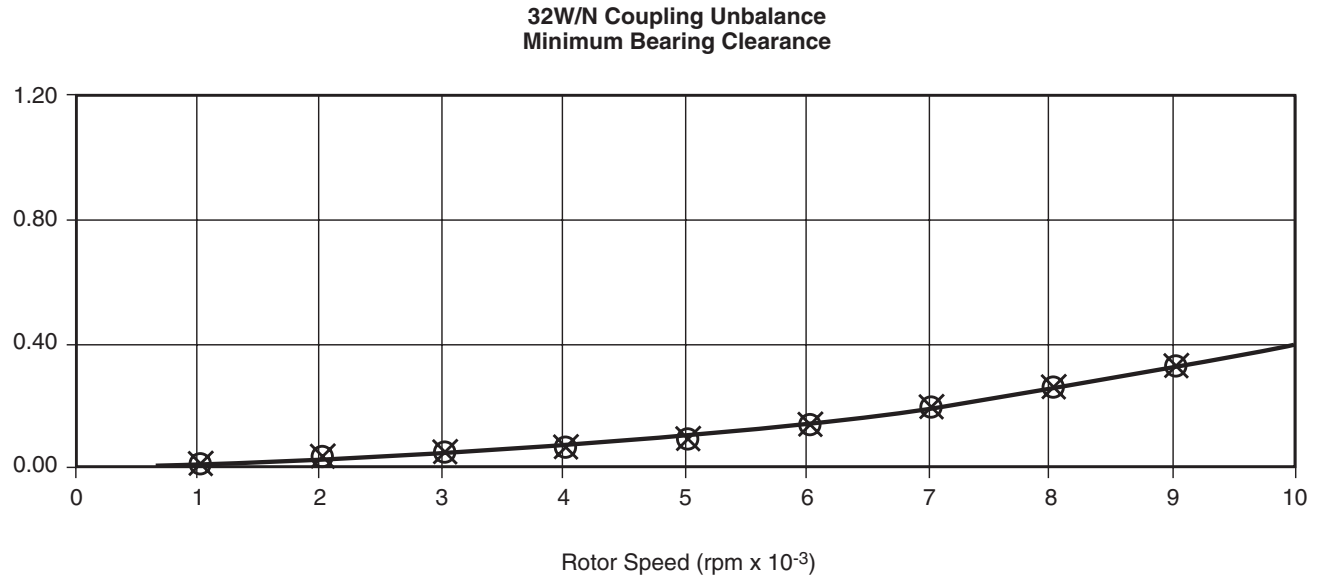


Figure 2-103—Coupling Unbalance Response—Overhung Compressors

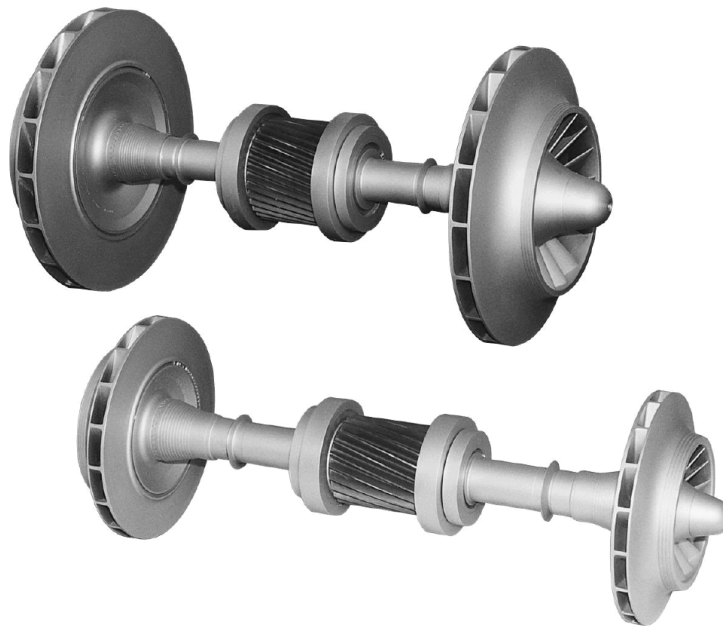


Figure 2-104—Typical Pinion Rotors from an Integrally Geared Compressor

2.8.6.5 References

1. Weaver, F. L., 1972, "Rotor Design and Vibration Response," Proceedings of the 1st Turbomachinery Symposium, Turbomachinery Laboratory, Texas A&M University, College Station, Texas, pp. 142 – 147.
2. de Jongh, F. M. and van der Hoeven, P., 1998, "Application of a Heat Barrier Sleeve to Prevent Synchronous Rotor Instability," Proceedings of the 27th Turbomachinery Symposium, Turbomachinery Laboratory, Texas A&M University, College Station, Texas, pp. 17 – 26.
3. Moore, J. J. and Flathers, M. B., 1998, "Aerodynamically Induced Radial Forces in a Centrifugal Gas Compressor: Part 1 Experimental Measurement," *Journal of Engineering for Gas Turbines and Power*, Vol. 120, April, pp. 383 – 390.

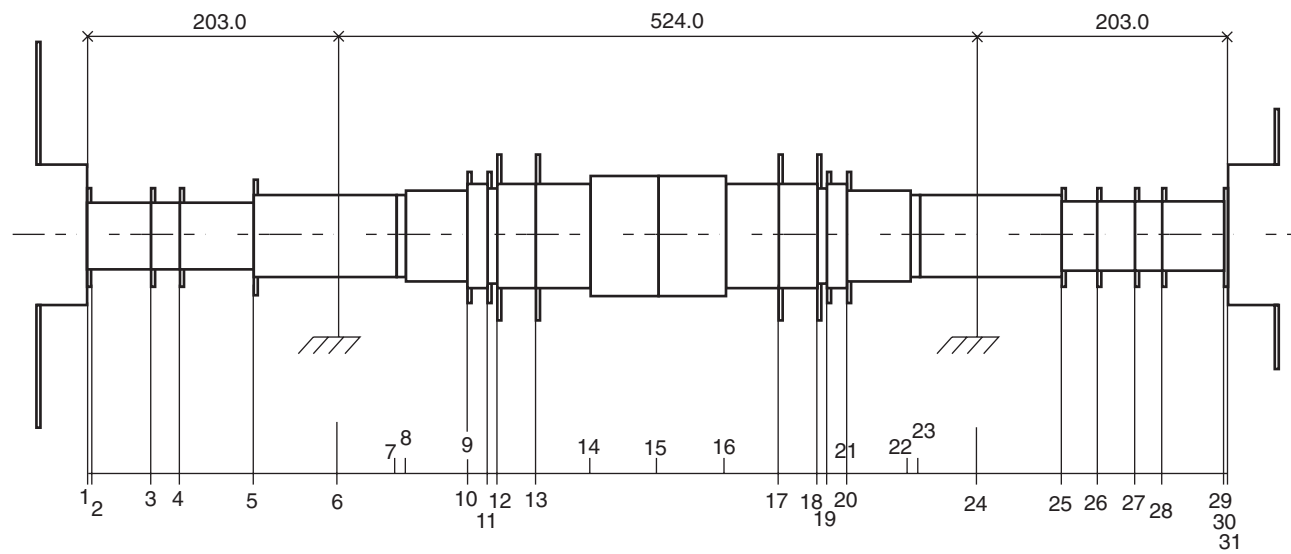


Figure 2-105—Pinion Rotor Model—Integrally Geared Compressor

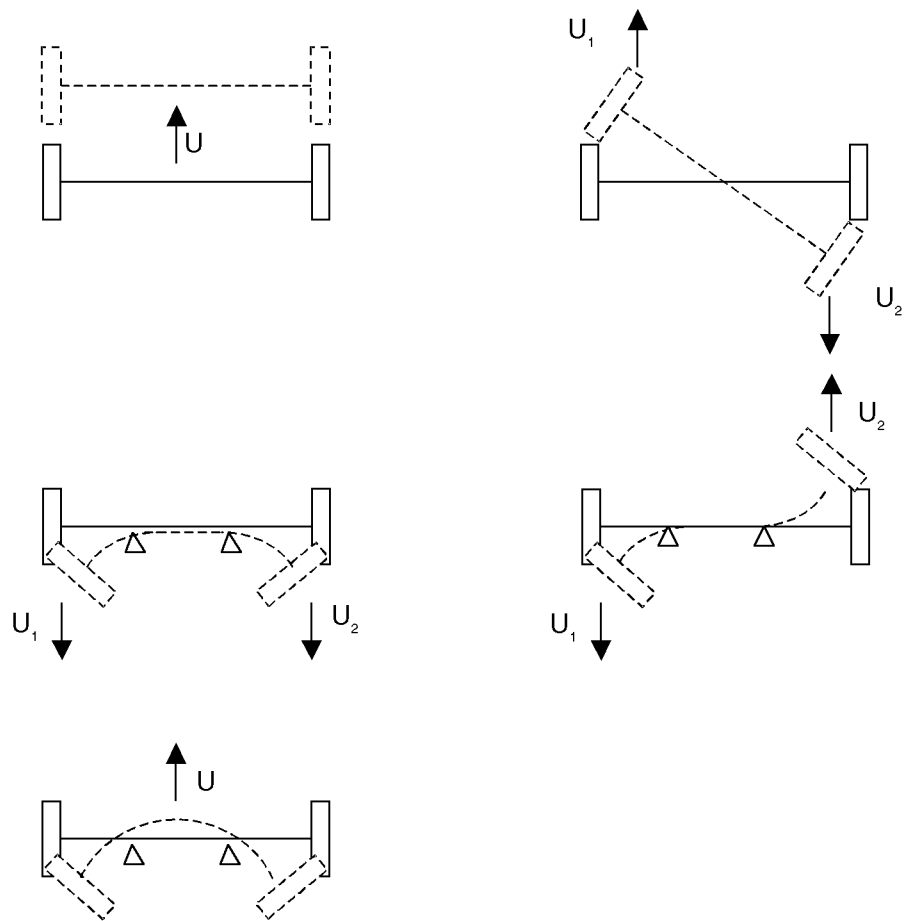


Figure 2-106—Typical Rigid and Flexible Body Mode Shapes & Unbalances Used to Excite Each

2.9 API TESTING AND RESULTS

2.9.1 Unbalance Verification Testing

The primary goal of API testing is to verify the unit design by observing the dynamic behavior. This applies to both performance testing and unbalance response verification tests. With the latter, the dynamic behavior of the rotor, bearings and support structure is measured against the rotordynamics predictions.

Ideally, a one-to-one comparison would be made, i.e., compare the predicted mid-span response at the first critical to an applied unbalance at mid-span. However, the freedom to completely examine the behavior of the rotor/bearing system that analytical methods possess is not available on the test stand. While certain parameters can be measured (journal response, bearing temperatures, etc.) others are impractical, if not, impossible.

The restrictions faced during verification testing are summarized below. The list is not intended to be all encompassing. Different machine types and test setups may present more possibilities and be less restrictive than others.

a. *Residual Unbalances & Forces Exist*—Unbalance response analysis predicts the rotor response to a known unbalance or distribution of unbalances. Unfortunately, real life rotors will possess a residual unbalance distribution and are subjected to varying levels of dynamic forces. While these factors are minimized by careful balancing, precise alignment, and reduced aerodynamic forces during testing, they do exist and can raise the vibrations levels to a significant percentage of the limit. Efforts are required to identify the response due solely to the applied unbalance trial weight.

b. *Few Choices Exist for the Applied Trial Weight Location*—In many instances, the possible locations in which a trial may be applied is limited to one, the coupling. (Some steam turbines, generators and motors have the potential for other locations if discussed during the design phase of the equipment.) A coupling applied trial weight has many advantages and disadvantages. It is a poor location to excite the first mode but may be better suited to excite higher order modes. However, isolation of the coupling response may prove difficult due to the decreased sensitivity of newer designs. Recent advances in rotordynamic analyses permit designers to fine-tune the rotor/bearing design and accurately predict the dynamic behavior.

c. *Applied Trial Weight is Normally Limited in Size*—Analytically, it is possible to apply unlimited amounts of unbalance to the rotor. This is not possible during testing due to safety concerns and physical limitations. In some cases, attempting to raise the vibration levels to the limit employing coupling trial weights may require an unbalance force application in excess of the rotor weight. Stress considerations and physical space may prove this impractical and unsafe. The verification

test and analytical prediction need to be coordinated to ensure a successful test.

d. *Risks Associated with Elevating Vibration Levels*—Previous testing methods relied on raising the vibration levels measured at the probe locations to the API limit. The rotordynamics analysis was then used to determine if internal clearances were exceeded. However, the verification of the analysis was the original point of the test. Any inaccuracies in the analysis could result in damage during the shop testing at elevated levels, leading to repairs, retesting and delayed shipments.

e. *Limited Measurement Capabilities*—Without Herculean efforts, vibrations levels at the probe locations (usually situated near the journals) are the only response measurements made of the rotor. Taking these measurements only at the critical speed of concern greatly limits the ability to compare the test results to the analytical predictions. It should be noted that some manufacturers are offering to perform verifications tests in a high speed balancing facility. This permits application of the unbalance weights at mid-span, quarter-span and other combinations not possible on the test stand in the case. Additionally, mid-span vibration readings are possible.

The verification test seeks to confirm the response prediction for one unbalance distribution. The response predictions share a common rotor/bearing model, which form the core of the analyses. The various response analyses apply different unbalance forces to this common model. Confirmation of the accuracy of one response prediction is a verification of the model, and thus, all other response predictions using that model.

2.9.2 Qualitative Aspects of the Verification Test

While the verification test is based on quantitative comparisons (the ability to isolate the effects of the unbalance weight), all qualitative aspects could not be removed. These arise due to several factors, multiple probe readings, instrumentation sampling differences, operation condition changes and plane reading choice, to name a few. A brief description of these factors is contained below.

a. *Multiple Probe Readings*—As anyone who has run a test can attest to, the vibration probes used to monitor the shaft vibrations will produce slightly different results. Some of the differences are expected due to bearing loading and geometry. Others cannot be easily explained. This is primarily the reason behind removing the calculated amplification factor as one of the comparison values.

b. *Instrumentation Sampling Differences*—To identify the effects of the unbalance weight, a baseline reading of the machine is necessary. This gives the effect of the residual unbalance and force in the machine. After adding the unbalance weight, the data (usually in the form of a Bode plot) is

taken again. The effect of the weight is obtained from a vector subtraction of the two data sets. However, slight differences in the data points in speed will produce small errors in the vector subtraction. For the most part, these are insignificant and do not affect the results. In the areas of critical speeds where larger phase changes occur over smaller speed ranges, the errors may result in changes to the “measured” values.

c. *Operation Condition Changes*—During a “normal” verification test, the final X-Y data for the Bode plot is taken following the 4-hour mechanical run. Following this, the machine is shutdown to add the unbalance weight and brought back up to speed to reach steady state. Some conditions may not return to levels reached at the end of the four-hour run. In those situations, the response at the critical speeds (the most sensitive area) will vary for reasons other than the addition of the unbalance weight. Since these cannot be isolated, they will be attributed to the unbalance weight during the vector subtraction.

d. *Multiple Plane Readings*—Most API equipment has probe reading at both journal locations. During verification tests using the coupling as the weight location, the probe readings at the opposite end of the shaft may see a relatively small influence. The small effect can be significantly influenced by other background noise and result in an erroneous unbalance weight vibration.

Differences between the predicted and measured influence of the trial weight should be discussed prior to proclaiming the test as a failure. These “qualitative” aspects of the test may alter the results but not affect the underlying integrity of the predictions.

2.9.3 Pre-testing Preparations

For an effective verification test, the rotordynamic analysis of the equipment should be examined at the design stage. Areas of concern would include critical speed locations, amplification factor, and unbalance sensitivity. Beyond configuration and design changes, the verification test can be used to satisfy these concerns by confirming the rotordynamic analysis.

A summary of how the verification test can be used is presented below:

a. *High amplification factors through the first critical speed*—This is usually accompanied by high ratios of mid-span to journal vibration. Careful balancing cannot hide high

amplification factors. A high amplification factor implies a more sensitive rotor and is a function of the damping and rotor stiffness (not the amount of unbalance present.) Normally, high amplification factors can be seen on the baseline data taken during the mechanical test. Verification testing performed in an at-speed bunker may permit more flexibility in weight placement and center span vibration readings but also include different rotor support properties. These trade-offs should be discussed to determine the feasibility of this option.

b. *High unbalance sensitivity of the equipment*—This is easily measured by the verification weight applied to the rotor. However, care in selecting the size of the weight should be exercised. Always applying (or asking to apply) the maximum weight may prove damaging to the rotor internals. High sensitivity implies that the influence of smaller weights can be properly identified and will satisfy API requirements.

c. *Critical speed locations of the lower mode*—Location of the first critical speed in most turbomachinery is easily identifiable during the mechanical test. The exception comes with stiff rotors whose first mode is heavily damped. In this case, it is unlikely that location of the first mode will be enhanced during a verification test without additional efforts. Of course, the location of heavily damped modes is also less important since they are heavily damped. Higher order modes infringing on the MCS may be excited by the verification test even with unbalance weights at the coupling. Should verification of the predictions not be possible with a coupling weight (due to the reasons in the previous section), alternate means of performing the test should be discussed.

2.9.4 Identifying the Unbalance Weight Influence

The cornerstone of the API verification test is the identification of the unbalance weight influence. This permits direct comparison of the predicted to the measured response without the residual influences. This process can be described both graphically and vectorially for a single speed and probe. The method can be easily expanded for a speed range and several probes.

To illustrate the method, a simple example is presented. During the baseline run (the X-Y Bode plot data), Rotor A has readings for a given probe and speed as shown on Figure 2-107. The vibration, V_1 , is a result of the residual unbalance, U_r , left in the rotor. (For the purpose of this explanation external or residual forces will be ignored.)

Expressed as a vector, the total vibration and unbalance are:

$$\vec{V}_1 = 1.2 \text{ mils @ } 40^\circ \quad 2-24$$

$$\vec{U}_1 = \vec{U}_r \quad 2-25$$

After adding the unbalance weight, U_t , to Rotor A, the vibration readings, V_2 , are taken at the same speed and location. Figure 2-108 presents the measurements before and after the addition of the unbalance weight.

Since the only change to Rotor A was the addition of the unbalance weight, U_t , the change in vibration from point 1 to point 2 must be the influence of the weight. The vibration influence, V_t , is shown on Figure 2-109.

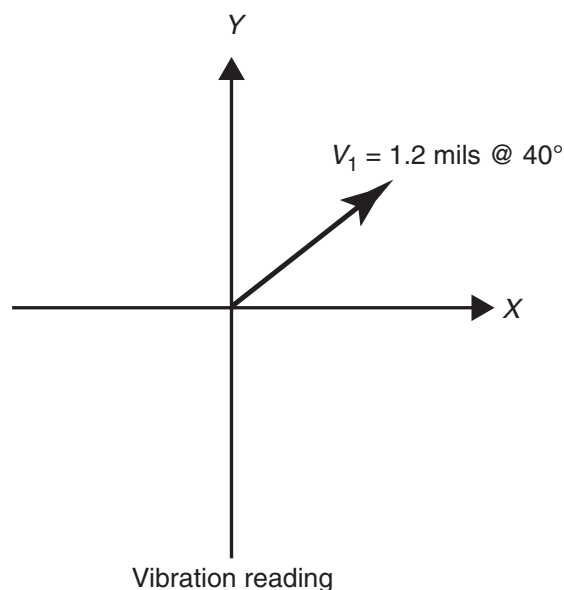


Figure 2-107—Baseline Vibration Reading (Graphically)

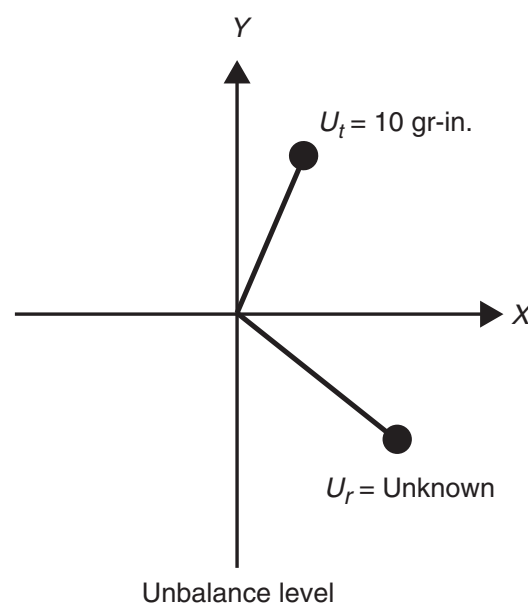
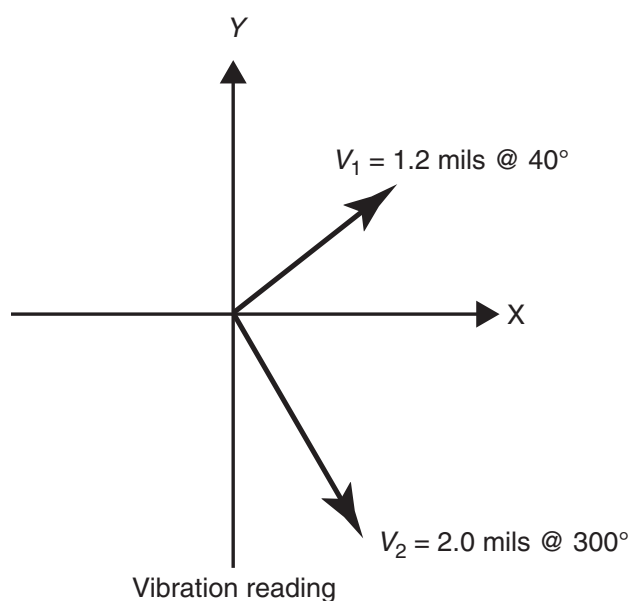
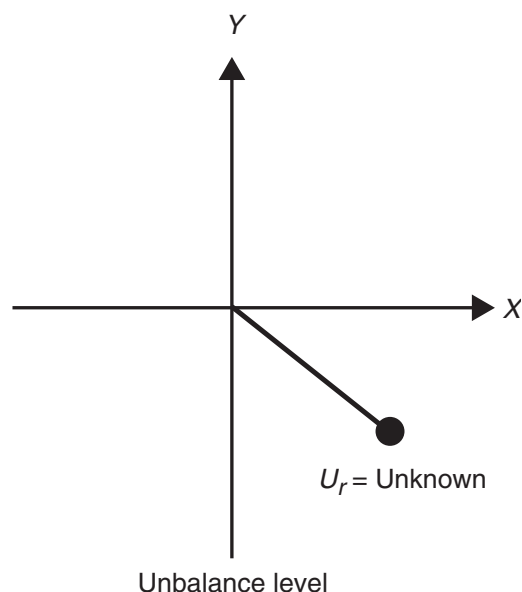


Figure 2-108—Readings After the Addition of the Unbalance Weight

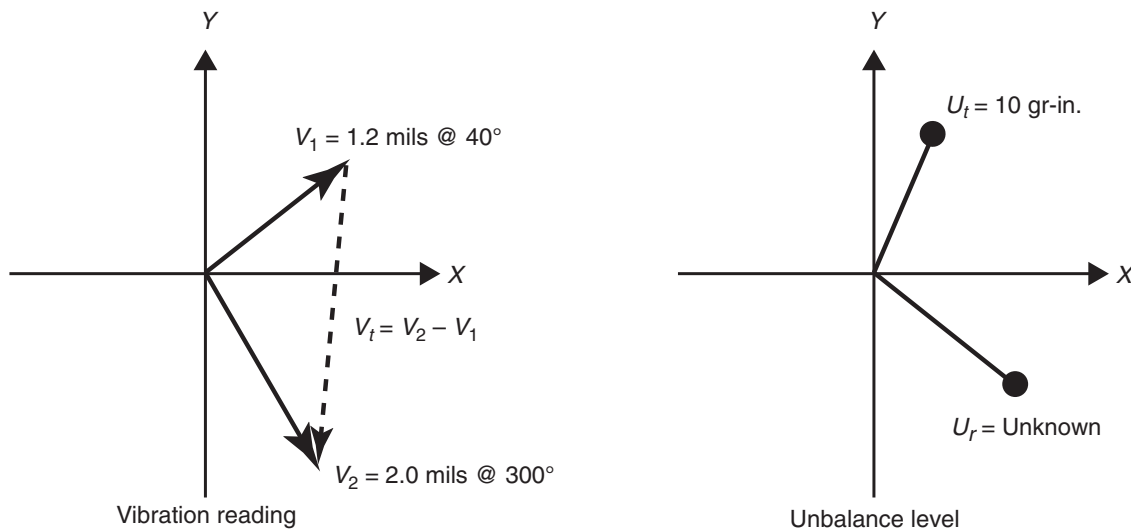


Figure 2-109—Influence of the Unbalance Weight

At point 2 following the addition of the weight, the total vibration and unbalance are:

$$\vec{V}_2 = \vec{V}_1 + \vec{V}_t \quad 2-26$$

$$\vec{U}_2 = \vec{U}_r + \vec{U}_t \quad 2-27$$

The vector math to compute the effect of the unbalance weight is simply:

$$\vec{U}_{2-1} = (\vec{U}_r + \vec{U}_t) - \vec{U}_r = \vec{U}_t \quad 2-28$$

$$\vec{V}_{2-1} = \vec{V}_2 - \vec{V}_1 = (\vec{V}_1 + \vec{V}_t) - \vec{V}_1 = \vec{V}_t \quad 2-29$$

or:

$$\vec{V}_t \approx 2.5 \text{ mils @ } 272 \text{ deg}$$

Notice that the residual unbalance magnitude and location does not need to be known to identify the influence of the unbalance weight. This method is automated by several commercially available software packages to perform the vector math for a data set encompassing the operating range.

2.9.5 Verification Test Examples

The identification method was presented in the previous section for a simple example of a single probe and speed. Three examples of actual verification tests are presented next. The first two examples contain vibration data from two

rotors representing flexible and rigid shaft designs. These examples are taken from Nicholas [1]. This reference also contains excellent examples of the process applied to steam turbines. The third illustrates the influences that force qualitative decisions on the accuracy of the test. (Note: While not discussed here, the analyses indicated that vibration levels would not exceed 75% of the internal clearances for all examples.)

The first rotor is an eight-stage compressor with a MCS to critical speed ratio of 3.1. Figure 2-110 plots the baseline vibration (solid) and results with the unbalance weight added to the rotor (dotted) at the coupling. (Vibration data is taken from the coupling end probe.) The first critical speed is clearly identified by the peak in both response curves. The shaded region represents the range of critical speed predicted by the analysis for minimum and maximum bearing clearances. As expected with flexible rotors, the first critical speed frequency is not sensitive to the change in bearing stiffness. (The bearing stiffness changes as a result of the clearance range specified for the journal bearings.)

Taking the two data sets obtained for the eight-stage compressor and performing the vector subtraction yields the solid curve on Figure 2-111. Overlaid upon the test data is the predicted response at minimum and maximum bearing clearance. For the most part, the test data lies within the predicted range. The response at MCS is within the range predicted by the analysis.

The verification test was also performed on a three-stage compressor operating at 13,500 rpm. As required, the vibration data was taken following the four hour run (baseline) and after the unbalance weight was added to the coupling. Figure 2-112 plots the vibration data taken from the coupling end probe. The first critical is clearly evident ($\approx 10,000$ rpm) even though it is well damped. Since the rotor has only

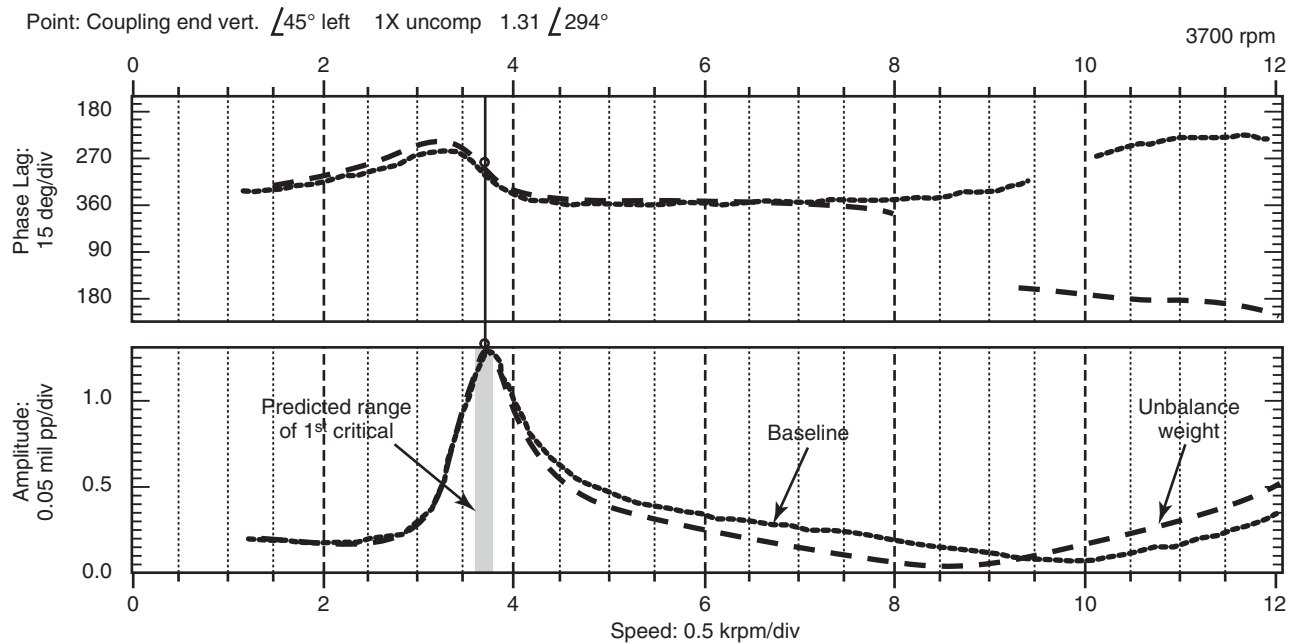


Figure 2-110—Bode Plot for Eight-Stage Compressor

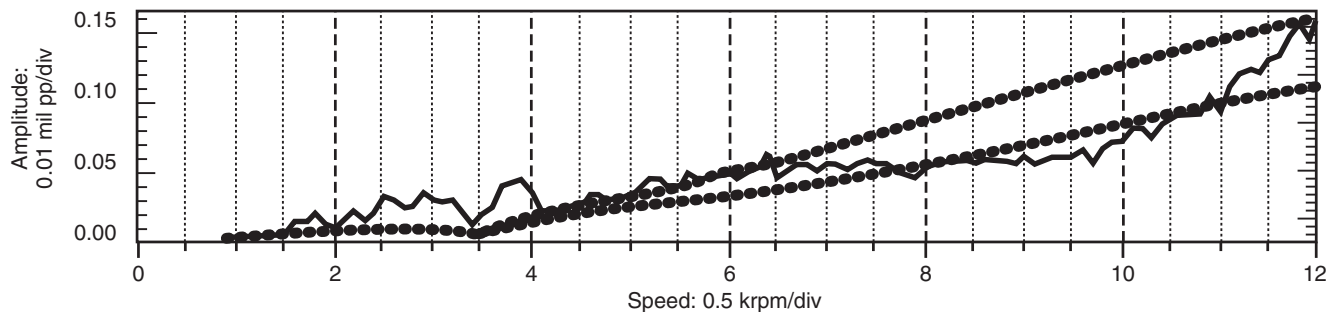


Figure 2-111—Unbalance Weight Influence (.... Predicted ____ Test)

three stages, the shaft bending to support stiffness ratio is significantly larger than with the eight-stage compressor. This rotor is characterized by modes more closely resembling rigid body motion. Rigid body modes are more sensitive in frequency to changes in the bearing/support stiffness. This can be seen by the larger shaded region predicted for the location of the first mode over the bearing clearance range.

Computing the influence of the unbalance weight and overlaying this data with the predicted response yields Figure 2-113. The measured response has the curve shape of the predicted response at minimum clearance. The rotor appears to be more sensitive than predicted with the measured response 20% greater than predicted at MCS and a curve shape that exaggerates the predicted plot. However, amplitude levels are more inline with the maximum clearance. The variations wit-

nessed are in the 0.05 mil range. Additionally, the predicted response is taken at the extremes of the bearing clearance range. Different combinations of pad curvature and pad placement, while still within the predicted range of response, may have a different curve shape depending on the stiffness and damping properties calculated.

The final example details some of the influences that complicate the process of verifying the rotordynamic analysis. The vibration response of a seven-stage compressor before and after application of the unbalance weight is shown on Figure 2-114. In this case, both the run up and rundown are included in the Bode plot. Differences between the two arise from changes in the steady state conditions that are reached at MCS (7150 rpm) before the speed sweeps begin. These may include bearing temperature differences, both oil and pad, among others.

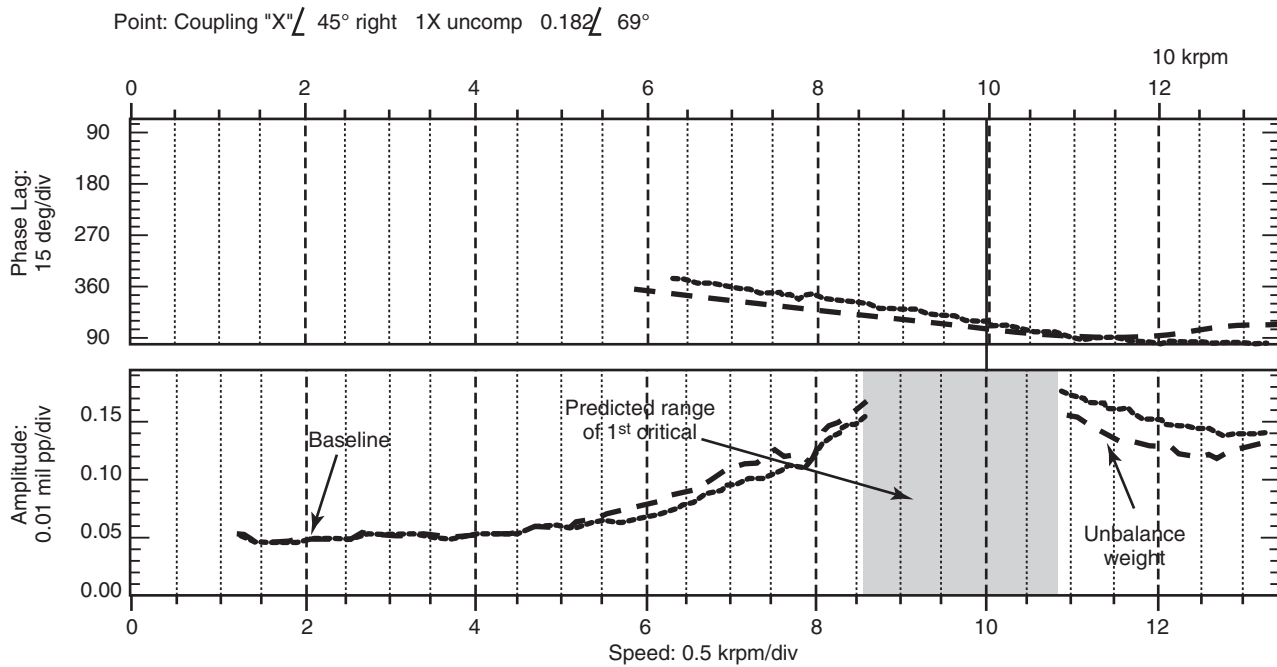


Figure 2-112—Bode Plot for Three-Stage Compressor

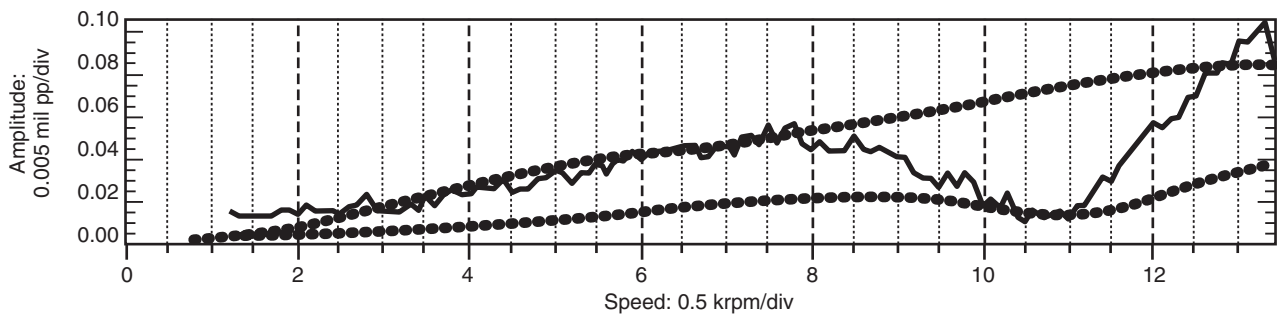


Figure 2-113—Unbalance Weight Influence (.... Predicted ____ Test)

Note that runout is not removed from the vibration data in this case. Ideally, slow roll readings would not change during the mechanical testing. Since the vector subtraction removes all constant aspects of the vibration data, the runout would therefore be eliminated in the process. Figure 2-115 plots the influence of the unbalance weight as determined from the data in Figure 2-114. At the lower speeds, the influence is nearly zero, as one would expect. This indicates that the runout was unchanged between runs and successfully removed.

Figure 2-115 identifies three areas in the plot that require further discussion. First is the region around the 1st critical speed, region 1. As noted earlier, the region surrounding the critical speeds is more sensitive to minor changes in the rotor/bearing system. Thus, any differences in support stiffness, rotor balance condition, etc., between runs are emphasized in this region. This can be seen on Figure 2-115. While the anal-

ysis predicts that the 1st critical is not excited by the weight, a peak nonetheless exists. This is due to the minor changes being emphasized by the 1st critical speed.

The differences in the run up and rundown were noted on Figure 2-114. Region 2 on Figure 2-115 indicates that these differences are not uniform from run to run. From the baseline run to the unbalance weight run, the system changes between the speed sweeps varied roughly 0.03 mils, not a significant amount but nearly 50% of the predicted response to the unbalance weight at the lower speeds. The mean of the two measured curves nearly equals the predicted response indicating the behavior is as predicted.

Finally, thermal changes as the system stabilizes at MCS can be seen at Region 3. While time dependent vibrations are not normally plotted on a Bode plot, they can influence the results depending on the rate of acceleration to MCS. For slower ramp rates, time dependency can creep into the

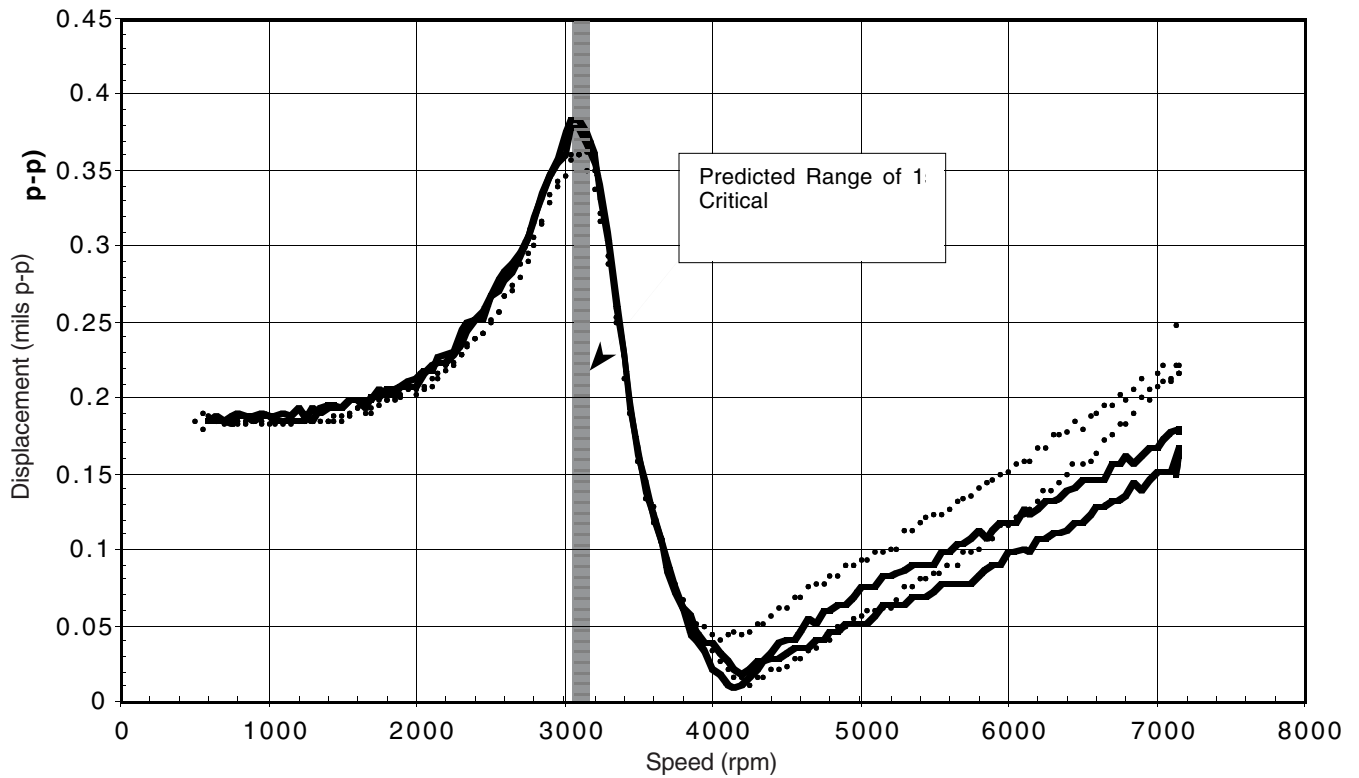


Figure 2-114—Bode Plot of Example #3

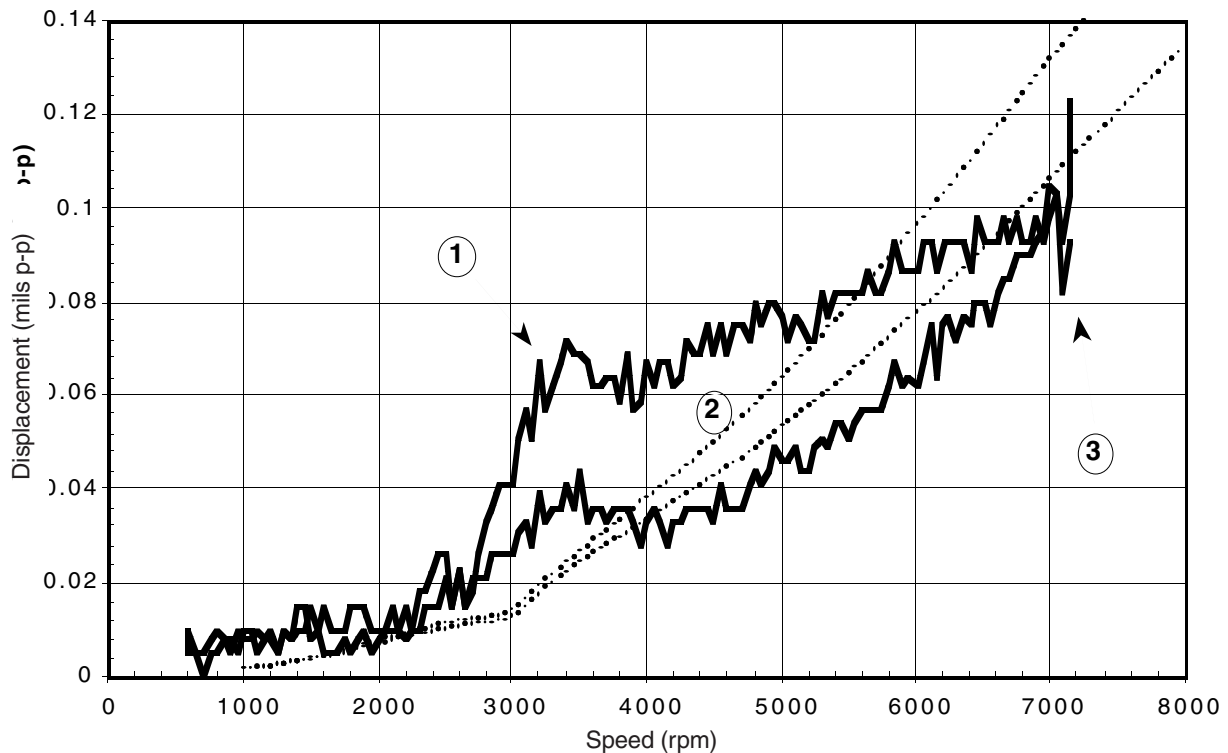


Figure 2-115—Unbalance Weight Influence (....Predicted ____ Test)

Table 2-5—Summary of the Results of the Tests

Example	8-stage Compressor	3-Stage Compressor	6-Stage Compressor
Predicted 1 st Critical Speed (rpm)	3,700 – 3,750	8,600 – 10,800	3,050 – 3,150
Measured 1 st Critical Speed (rpm)	3,700	10,000	3,050
Predicted Verification Response @ MCS (mils p-p)	0.11 – 0.16	0.04 – 0.085	0.11 – 0.135
Measured Verification Response @ MCS (mils p-p)	0.16	0.09 – 0.105	0.085 – 0.125
Discussions	API verification test requirements met. Good agreement between predictions and test results.	Most API verification test requirements met. Measured data may indicate a greater sensitivity to unbalance than predicted. However, short span rotor is already insensitive so indicated change has no influence. Additionally, response close to predicted levels.	API verification test requirements met. Influence response indicates excitation of 1 st critical, transient effects at MCS, and differences between run up and run-down plots. All of which is not attributable to the unbalance weight.

response levels. From the plotted results, it appears that the baseline run included some of these effects which translated in to the weight influence on Figure 2-115 at MCS. Since the speed changed only slightly, the rise is nearly vertical identifying it as a time dependent effect. In the worst case where the speed is varying slowly, this may appear as a rise to a response peak.

2.9.6 References

1. Nicholas, J. C., Edney, S. L., Kocur, J. A., and Hustak, J. F., 1997, "Subtracting Residual Unbalance for Improved Test Stand Vibration Correlation," Proceedings of the 26th Turbomachinery Symposium, Turbomachinery Laboratory, Texas A&M University, College Station, TX, pp. 7 – 18.

SP6.8.2.2 The location of all critical speeds below the trip speed shall be confirmed on the test stand during the mechan-

ical running test (see SP6.8.3.1). The accuracy of the analytical model shall be demonstrated (see SP6.8.3).

SP6.8.2.3 Before carrying out the damped unbalanced response analysis, the vendor shall conduct an undamped analysis to identify the undamped critical speeds and determine their mode shapes located in the range from 0% – 125% of trip speed. Unless otherwise specified, the results of the undamped analysis shall be furnished. The presentation of the results shall include:

- Mode shape plots (relative amplitude vs. axial position on the rotor).
- Critical speed-support stiffness map (frequency vs. support stiffness). Superimposed on this map shall be the calculated system support stiffness, horizontal (k_x), and vertical (k_y) (see Figure SP-2).

Note: For machinery with widely varying bearing loads and/or load direction such as overhung style machines, the vendor may propose to substitute mode shape plots for the undamped critical speed map and list the undamped critical speed for each of the identified modes.

SP6.8.2.4 The damped unbalanced response analysis shall include but shall not be limited to the following:

Note: The following is a list of items the analyst is to consider. It does not address the details and product of the analysis which is covered in SP6.8.2.7 and SP6.8.2.8.

- Rotor masses, including the mass moment of coupling halves, stiffness, and damping effects (for example, accumulated fit tolerances, fluid stiffening and damping).
- Bearing lubricant-film stiffness and damping values including changes due to speed, load, preload, range of oil temperatures, maximum to minimum clearances resulting from accumulated assembly tolerances, and the effect of asymmetrical loading which may be caused by gear forces, side streams, eccentric clearances, etc.
- For tilt-pad bearings, the pad pivot stiffness.
- Support stiffness, mass, and damping characteristics, including effects of frequency dependent variation. The term “support” includes the foundation or support structure, the base, the machine frame and the bearing housing as appropriate. For machines whose bearing support system stiffness values are less than or equal to 3.5 times the bearing oil film stiffness values, support stiffness values derived from modal testing or calculated frequency dependent support stiffness and damping values (impedances) shall be used. The vendor

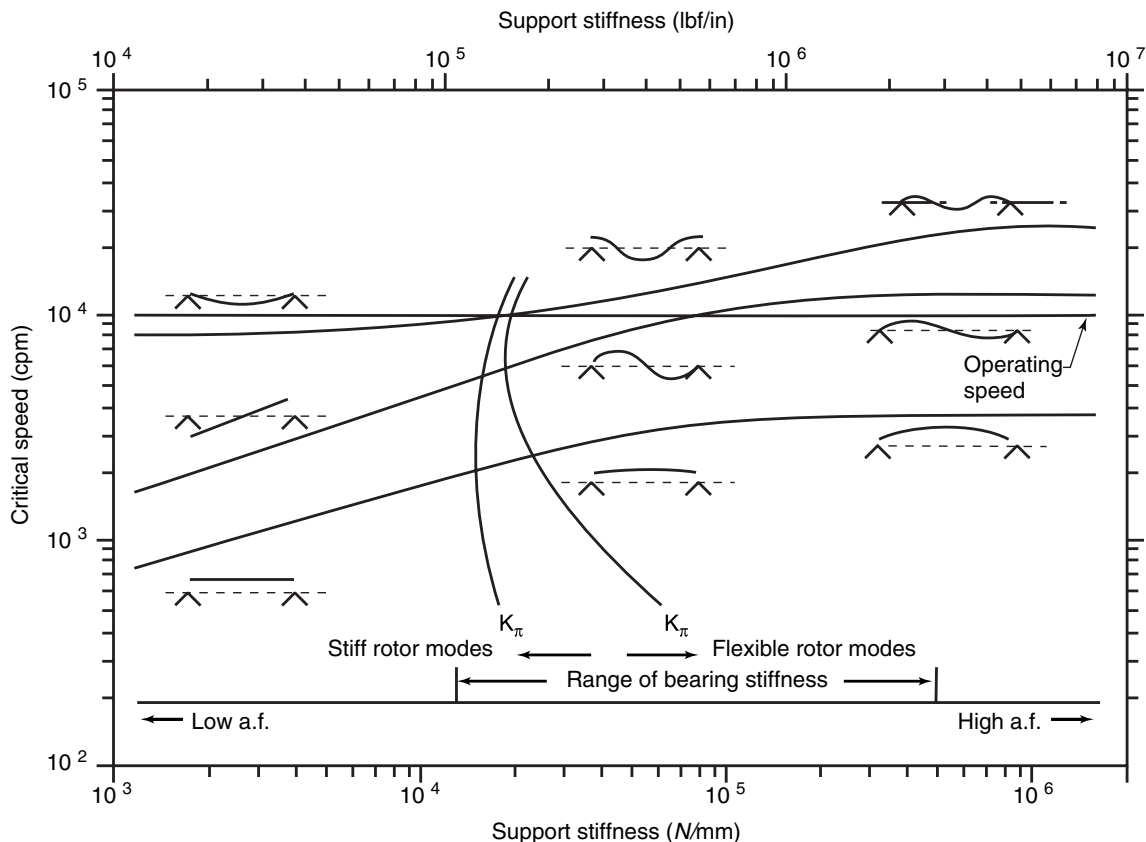


Figure SP-2—Undamped Critical Speed Map

shall state the support stiffness values used in the analysis and the basis for these values (for example, modal tests of similar rotor support systems, or calculated support stiffness values).

Note 1: The support stiffness should in most cases be no more than 8.75×10^6 N/mm (5×10^6 lb./in.).

Note 2: Guidelines are used to define whether or not bearing support stiffness should be considered. While modal testing of the actual bearing support system would be preferred, an analytical analysis (such as FEA) is permitted.

e. Rotational speed, including the various starting-speed detents, operating speed and load ranges (including agreed upon test conditions if different from those specified), trip speed, and coast-down conditions.

f. The influence, over the operating range, of the hydrodynamic stiffness and damping generated by the casing shaft end seals.

g. The location and orientation of the radial vibration probes which shall be the same in the analysis as in the machine.

h. Squeeze film dampers.

SP6.8.2.5 In addition to the damped unbalanced response analysis requirements of SP6.8.2.4, for machines equipped with rolling element bearings, the vendor shall state the bearing stiffness and damping values used for the analysis and either the basis for these values or the assumptions made in calculating the values.

- **SP6.8.2.6** When specified, the effects of other equipment in the train shall be included in the damped unbalanced response analysis (that is, a train lateral analysis shall be performed).

Note: In particular, this analysis should be considered for machinery trains with rigid couplings.

SP6.8.2.7 A separate damped unbalanced response analysis shall be conducted for each critical speed within the speed range of 0% – 125% of trip speed. Unbalance shall analytically be placed at the locations that have been determined by the undamped analysis to affect the particular mode most adversely. For the translatory (symmetric) modes, the unbalance shall be based on the sum of the journal static loads and shall be applied at the location of maximum displacement. For conical (asymmetric) modes, an unbalance shall be added at the location of maximum displacement nearest to each journal bearing. These unbalances shall be 180 degrees out of phase and of a magnitude based on the static load on the adjacent bearing. Figure SP-3 shows the typical mode shapes and indicates the location and definition of U for each of the shapes. The magnitude of the unbalances shall be 4 times the value of U as calculated by Equation 1.

In SI units:

$$U = 6350 (W/N) \quad (1)$$

or 254 μ m mass displacement, whichever is greater.

In U.S. Customary units:

$$U = 4 (W/N)$$

or 10 mil mass displacement, whichever is greater.

where

U = input unbalance for the rotordynamic response analysis in g-mm (oz-in.),

N = maximum continuous operating speed,

W = journal static load in kg (lb), or for bending modes where the maximum deflection occurs at the shaft ends, the overhung mass (that is the mass of the rotor outboard of the bearing) in kg (lb) (see Figure SP-3).

Note: The limits on mass displacement are in general agreement with the capabilities of conventional balance machines, and are necessary to invoke for small rotors running at high speeds.

SP6.8.2.7.1 For rotors where the impellers are cantilevered beyond the journal bearings, unbalance shall be added at the impellers and components such as locknuts, shaft end seals and the coupling for the case of the non-integrally geared rotors. Each mode that is less than 125% of trip speed shall be analyzed. The modes shall be calculated at minimum and maximum support stiffness and in the case of integrally geared rotors include the change in support stiffness resulting from minimum to maximum torque transmitted through the gearing. The unbalance shall be located at or close to the component center of gravity and phased to create maximum synchronous response amplitude.

SP6.8.2.7.2 For rotors which are between bearing designs, unbalance shall be added at the impellers and major rotor components such as balance drums and couplings. The unbalance shall be located at or close to the component center of gravity and phased to create maximum synchronous response amplitude.

SP6.8.2.8 As a minimum, the unbalanced response analysis shall produce the following:

The following is the list of analysis details and identifies the deliverables. The items to be considered in the analysis were identified in SP6.8.2.4.

- a. Identification of the frequency of each critical speed in the range from 0% – 125% of the trip speed.
- b. Frequency, phase and response amplitude data (Bode plots) at the vibration probe locations through the range of

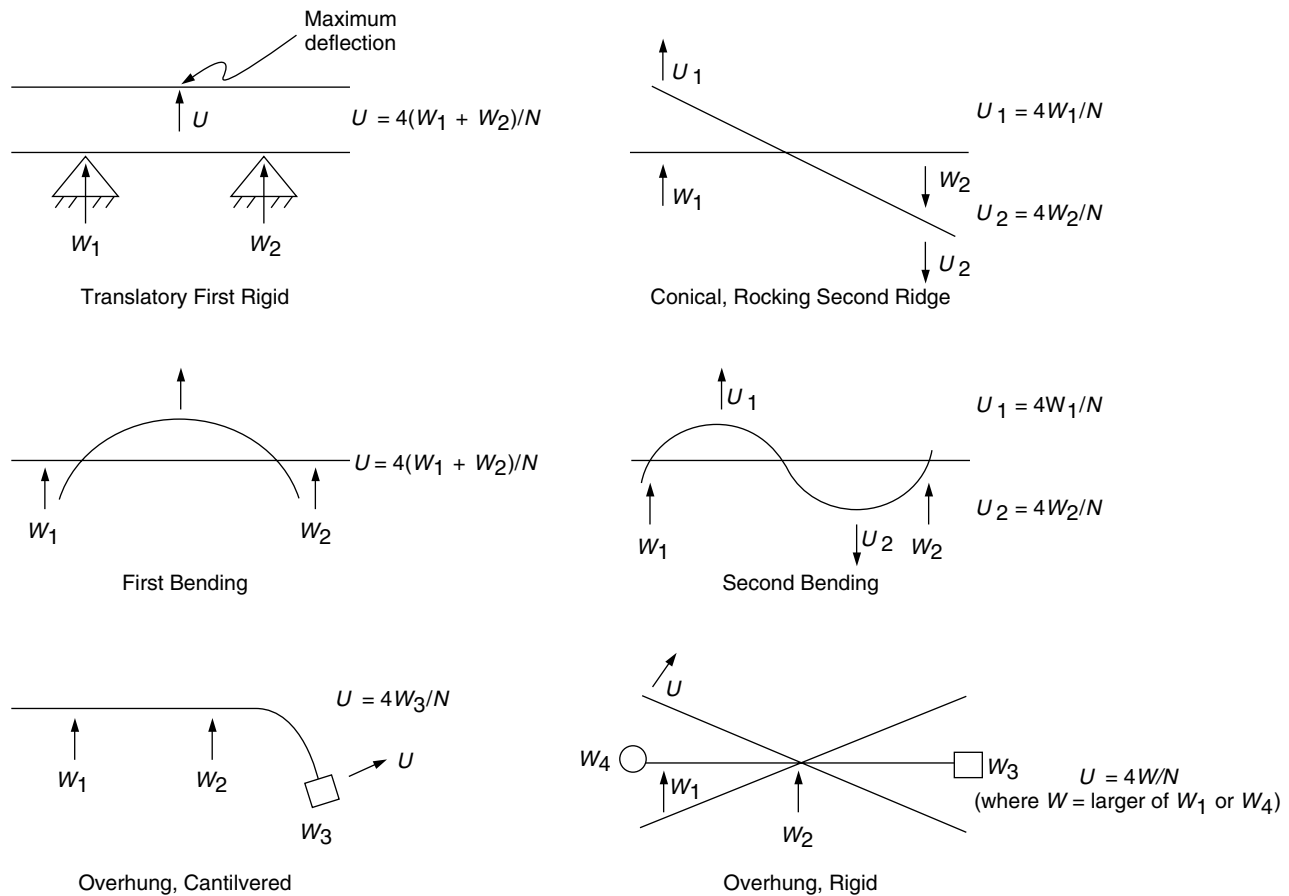


Figure SP-3—Typical Mode Shapes

each critical speed resulting from the unbalance specified in SP6.8.2.7.

c. The plot of deflected rotor shape for each critical speed resulting from the unbalances specified in SP6.8.2.7, showing the major-axis amplitude at each coupling plane of flexure, the centerlines of each bearing, the locations of each radial probe, and at each seal throughout the machine as appropriate. The minimum design diametral running clearance of the seals shall also be indicated.

d. Additional Bode plots that compare absolute shaft motion with shaft motion relative to the bearing housing for machines where the support stiffness is less than 3.5 times the oil-film stiffness.

SP6.8.2.9 Additional analyses shall be made for use with the verification test specified in SP6.8.3. The location of the unbalance shall be determined by the vendor. Any test stand parameters which influence the results of the analysis shall be included.

Note: For most machines, there will only be one plane readily accessible for the placement of an unbalance; for example, the coupling

flange on a single ended drive machine, or the impeller hub or disk on an integrally geared machine, or expander-compressors. However, there is the possibility that more planes are available such as axial compressor balance planes, or on through drive compressors. When this occurs, and there is the possibility of exciting other criticals, multiple runs may be required.

SP6.8.2.10 The damped unbalanced response analysis shall indicate that the machine will meet the following separation margins (see Figure SP-1):

a. If the amplification factor (AF) at a particular critical speed is less than 2.5, the response is considered critically damped and no separation margin is required.

b. If the amplification factor at a particular critical speed is 2.5 or greater and that critical speed is below the minimum speed, the separation margin (SM) (as a percentage of the minimum speed) shall not be less than the value from Equation 2 or the value 16, whichever is less.

$$SM = 17 \left(1 - \frac{1}{AF - 1.5} \right) \quad (2)$$

c. If the amplification factor at a particular critical speed is equal to 2.5 or greater and that critical speed is above the maximum continuous speed, the separation margin (as a percentage of the maximum continuous speed) shall not be less than the value from Equation 3 or the value of 26 which ever is less.

$$SM = 10 + 17 \left(1 - \frac{1}{AF - 1.5} \right) \quad (3)$$

SP6.8.2.11 The calculated unbalanced peak to peak amplitudes (see 6.8.2.8, Item b) shall be multiplied using the correction factor calculated from Equation 4. The correction factor shall have a value greater than 0.5.

$$CF = \frac{A_l}{A_{4X}} \quad (4)$$

where

CF = correction factor,

A_l = amplitude limit, calculated using Equation 5 in μm (mils) peak to peak,

A_{4X} = peak-to-peak amplitude at the probe location per requirements of SP6.8.2.8c in μm (mils) peak to peak.

In SI units, μm :

$$A_l = 25.4 \sqrt{\frac{12,000}{N}} \quad (5)$$

In U.S. Customary units, mils:

$$A_l = \sqrt{\frac{12,000}{N}}$$

where

N = maximum continuous speed, rpm.

SP6.8.2.12 The calculated major-axis, peak-to-peak, unbalanced rotor response amplitudes, corrected in accordance with SP6.8.2.11 at any speed from zero to trip speed shall not exceed 75% of the minimum design diametral running clearances throughout the machine (with the exception of floating-ring seal locations). For machines with abraidable seals, the response amplitude to the running clearance shall be mutually agreed.

Note: Running clearances may be different than the assembled clearances with the machine shutdown.

SP6.8.2.13 If the analysis indicates that the SMs still cannot be met or that a non-critically damped response peak falls within the operating speed range and the purchaser and vendor have agreed that all practical design efforts have been exhausted, then acceptable amplitudes shall be mutually agreed upon by the purchaser and the vendor, subject to the requirements of SP6.8.3.3.

• **SP6.8.2.14** When specified, in addition to the other requirements of SP6.8.2, the lateral analysis report shall include the following:

a. Dimensional data of the bearing design in sufficient detail to enable calculations of stiffness and damping coefficients.

b. Shaft geometry with sufficient detail to model the shaft including the location of bearing centerlines and mounted components.

c. The weight, polar and transverse moments of inertia and center of gravity of the impellers, balance piston, shaft end seals and coupling(s) with sufficient detail to conduct an independent analysis of the rotor.

d. The input model used for the vendors analysis.

e. The support stiffness used in the analysis and its basis.

SP6.8.3 Unbalanced Rotor Response Verification Test

SP6.8.3.1 An unbalanced rotor response test shall be performed as part of the mechanical running test (Note: See Section of the applicable chapter), and the results shall be used to verify the analytical model. The actual response of the rotor on the test stand to the same arrangement of unbalance and bearing loads as was used in the analysis specified in SP6.8.2.9 shall be the criterion for determining the validity of the damped unbalanced response analysis. To accomplish this, the requirements of SP6.8.3.1.1 through SP6.8.3.1.6 shall be followed.

SP6.8.3.1.1 During the mechanical running test (Note: See Section of the applicable chapter), the amplitudes and phase angle of the shaft vibration from zero to trip speed shall be recorded. The gain of any analog recording instruments used shall be preset before the test so that the highest response peak is within 60% – 100% of the recorder's full scale on the test unit coast-down (deceleration).

Note: This set of readings is normally taken during a coastdown, with convenient increments of speed such as 50 rpm. Since at this point the rotor is balanced, any vibration amplitude and phase detected should be the result of residual unbalance and mechanical and electrical runout.

SP6.8.3.1.2 The location of critical speeds below the trip speed shall be established.

SP6.8.3.1.3 The unbalance which was used in the analysis performed in SP6.8.2.9, shall be added to the rotor in the location used in the analysis. The unbalance shall not exceed 8 times the value from Equations 2a or 2b.

SP6.8.3.1.4 The machine shall then be brought up to the trip speed and the indicated vibration amplitudes and phase shall be recorded using the same procedure used for SP6.8.3.1.1.

SP6.8.3.1.5 The corresponding indicated vibration data taken in accordance with SP6.8.3.1.1 shall be vectorially subtracted from the results of this test.

Note: It is practical to store the residual unbalance vibration measurements recorded in the step at SP6.8.3.1.1 and by use of computer code perform the vectorial subtraction called for in this paragraph at each appropriate speed. This makes the comparison of the test results with the computer analysis of SP6.8.2.9 quite practical. It is necessary for probe orientation be the same for the analysis and the machine for the vectorial subtraction to be valid.

SP6.8.3.1.6 The results of the mechanical run including the unbalance response verification test shall be compared with those from the analytical model specified at SP6.8.2.9.

SP6.8.3.2 The vendor shall correct the model if it fails to meet either of the following criteria:

a. The actual critical speeds determined on test shall not deviate from the corresponding critical speeds predicted by analysis by more than 5%. Where the analysis predicts more than one critical speed in a particular mode (due, for example, to the bearing characteristics being significantly different horizontally and vertically or between the two ends of the machine), the test value shall not be lower than 5% below the lowest predicted value nor higher than 5% above the highest predicted value.

Note: It is possible, particularly on electric motors, that the vertical and horizontal stiffness are significantly different and the analysis will predict two differing critical speeds. Should the operating speed fall between these critical speeds, these two critical speeds should be treated separately, as if they resulted from separate modes.

b. The actual major axis amplitude of peak responses from test, including those critically damped, shall not exceed the predicted values. The predicted peak response amplitude range shall be determined from the computer model based on the four radial probe locations.

SP6.8.3.3 If the support stiffness is less than 2 times the bearing oil film stiffness, the absolute vibration of the bearing housing shall be measured and vectorially added to the relative shaft vibration, in both the balanced (see SP6.8.3.1.1) and in the unbalanced (see SP6.8.3.1.3) condition before proceeding with the step specified in SP6.8.3.1.6. In such a case, the measured response shall be compared with the predicted absolute shaft movement.

SP6.8.3.4 Unless otherwise specified, the verification test of the rotor unbalance shall be performed only on the first rotor tested, if multiple identical rotors are purchased.

SP6.8.3.5 The vibration amplitudes and phase from each pair of *x-y* vibration probes shall be vectorially summed at each vibration response peak after correcting the model, if required, to determine the maximum amplitude of vibration. The major-axis amplitudes of each response peak shall not exceed the limits specified in SP6.8.2.12.

SP6.8.4 Additional Testing

SP6.8.4.1 Additional testing is required (see SP6.8.4.2) if from the shop verification test data (see SP6.8.3) or from the damped, corrected unbalanced response analysis (see SP6.8.3.3), it appears that either of the following conditions exists:

- a. Any critical response which fails to meet the SM requirements (see SP6.8.2.10) or which falls within the operating speed range.
- b. The clearance requirements of SP6.8.2.12 have not been met.

Note: When the analysis or test data does not meet the requirements of the standard, additional more stringent testing is required. The purpose of this additional testing is to determine on the test stand that the machine will operate successfully.

SP6.8.4.2 Unbalance weights shall be placed as described in SP6.8.2.7; this may require disassembly of the machine. Unbalance magnitudes shall be achieved by adjusting the indicated unbalance that exists in the rotor from the initial run to raise the displacement of the rotor at the probe locations to the vibration limit defined by Equations 5a or 5b (see SP6.8.2.11) at the maximum continuous speed; however, the unbalance used shall be no less than twice or greater than 8 times the unbalance limit specified in SP6.8.2.7, Equations 2a or 2b. The measurements from this test, taken in accordance with SP6.8.3.1.1 and SP6.8.3.1.2, shall meet the following criteria:

- a. At no speed outside the operating speed range, including the SM, shall the shaft deflections exceed 90% of the minimum design running clearances.
- b. At no speed within the operating speed range, including the SM, shall the shaft deflections exceed 55% of the minimum design running clearances or 150% of the allowable vibration limit at the probes (see SP6.8.2.11).

SP6.8.4.3 The internal deflection limits specified in SP6.8.4.2 items a and b shall be based on the calculated displacement ratios between the probe locations and the areas of concern identified in SP6.8.2.12 based on a corrected model, if required. Actual internal displacements for these tests shall be calculated by multiplying these ratios by the peak readings

from the probes. Acceptance will be based on these calculated displacements or inspection of the seals if the machine is opened. Damage to any portion of the machine as a result of this testing shall constitute failure of the test. Minor internal seal rubs that do not cause clearance changes outside the vendor's new-part tolerance do not constitute damage.

SP6.8.8.8 During the shop test of the machine, assembled with the balanced rotor, operating at its maximum continuous speed or at any other speed within the specified operating speed range, the peak-to-peak amplitude of unfiltered vibration in any plane, measured on the shaft adjacent and relative to each radial bearing, shall not exceed the following value or 25 μm (1 mil), whichever is less:

In SI units, μm :

$$A_1 = 25.4 \sqrt{\frac{12,000}{N}} \quad (6)$$

In U.S. Customary units, mils:

$$A_1 = \sqrt{\frac{12,000}{N}}$$

where

A = amplitude of unfiltered vibration, μm (mil) true peak-to-peak,

N = maximum continuous speed, rpm.

At any speed greater than the maximum continuous speed, up to and including the trip speed of the driver, the vibration

level shall not increase more than 12.7 μm (0.5 mil) above the maximum value recorded at the maximum continuous speed.

Note: These limits are not to be confused with the limits specified in SP6.8.3 for shop verification of unbalanced response.

SP6.8.8.9 Electrical and mechanical runout shall be determined by rotating the rotor through the full 360 degrees supported in V blocks at the journal centers while continuously recording the combined runout with a non-contacting vibration probe and measuring the mechanical runout with a dial indicator at the centerline of each probe location and one probe-tip diameter to either side.

Note: The rotor runout determined above generally may not be reproduced when the rotor is installed in a machine with hydrodynamic bearings. This is due to pad orientation on tilt pad bearings and effect of lubrication in all journal bearings. The rotor will assume a unique position in the bearings based on the slow roll speed and rotor weight.

SP6.8.8.10 Accurate records of electrical and mechanical runout, for the full 360 degrees at each probe location, shall be included in the mechanical test report (see SP6.8.3.1.1).

SP6.8.8.11 If the vendor can demonstrate that electrical or mechanical runout is present, a maximum of 25% of the test level calculated from Equation 6 or 6.5 μm (0.25 mil), whichever is greater, may be vectorially subtracted from the vibration signal measured during the factory test. Where shaft treatment such as metallized aluminum bands have been applied to reduce electrical runout, surface variations (noise) may cause a high frequency noise component which does not have an applicable vector. The nature of the noise is always additive. In this case, the noise shall be mathematically subtracted.

SECTION 3—STABILITY ANALYSIS

3.1 INTRODUCTION

3.1.1 Historical Perspective

A stability analysis is also referred to as a damped natural frequency or damped eigenvalue analysis. For a rotor-bearing-seal system, a stability analysis leads to a multitude of solutions corresponding to each of the system's damped natural frequencies. The solutions to the equations of motion are complex with real (growth factor or stability indicator) and imaginary (damped natural frequency or instability frequency) parts called eigenvalues. The associated mode shapes are called eigenvectors.

Measuring the rate of decay of free oscillations (real part of the eigenvalue) is a convenient way to determine the amount of damping present in the system. Greater damping values produce faster rates of decay. For stability analysis of rotating equipment, the logarithmic decrement (log dec) is a common measure of damping present and thus, the stability. The log dec is defined as the natural logarithm of the ratio of any two successive amplitudes, Figure 3-1. The expression for the log dec is then:

$$\delta = \ln\left(\frac{X_1}{X_2}\right) \quad 3-1$$

For stable systems with a positive rate of decay, the log dec is positive. For unstable systems with a negative rate of decay

(growth rate), the log dec is negative (see 3.11). From a damping point of view, stable systems with positive log dec values contain sufficient damping to overcome the excitation, resulting in a negative decay rate. Conversely, unstable systems with negative log dec values do not contain sufficient damping to overcome the excitation, resulting in a positive decay rate.

The evaluation of dynamic stability has become an essential element for rotating machinery design analysis. The current capability to compute the damped eigenvalues of complex rotor-bearing-seal systems was motivated by major field problems in the 1960s and early 70s wherein the major vibration characteristic was self-excited sub-synchronous vibration. Two famous and classic centrifugal compressor instability cases from the early 1970s are referred to as Kaybob, Smith [1] and Ekofisk, Booth [2] (see Figure 3-50).

The ability to compute the eigenvalues of a six degree of freedom system (i.e., a six rotor station model) was considered a great design tool in the 1960s and early 70s. Attempts to find higher order system eigenvalues (i.e., rotor models with more than six stations) proved very difficult and time consuming. The first attempt at the development of a stability computer code was by Jorgen Lund [3] in 1965. This code, however, was not easy to use and it was said that only if you knew the approximate answer would it converge on the solution. Also of note from the mid 1960s are two classic publications by Gunter where basic stability methodology [4] and internal friction excitation [5] are discussed.

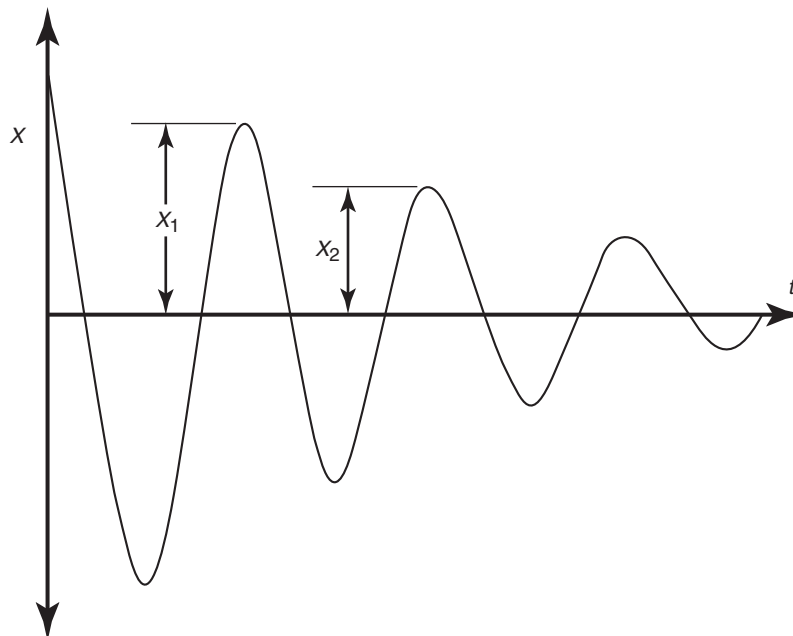


Figure 3-1—Definition of Log Dec Based on Rate of Decay

The work of Ruhl and Booker [6] published in 1972 presented both finite element and transfer matrix techniques for rotor systems employing a solver known as Muller's method. For lightly damped systems, their transfer matrix solution analysis worked fine but for more heavily damped structures, such as turbomachinery supported on fluid film bearings, the program's analysis methodology produced incorrect and false modes.

Jorgen Lund presented his landmark paper on rotor bearing stability in 1973. Lund's paper [7], published first in 1974 and again in 1987, not only gives a detailed transfer matrix solution procedure, but also describes how the results may be presented to study machine design parameters. The most basic result of a damped eigenvalue or damped natural frequency analysis is the stability prediction from the real part of the eigenvalues. It is usually the lowest mode, which corresponds to the rotor's first fundamental natural frequency, that is "re-excited" causing a subsynchronous vibration and rotor instability. Coincidentally, the beauty of the transfer matrix solution is that it is able to search for the first 6 – 10 modes very efficiently, finding the lowest frequency modes first.

Ruhl's transfer matrix analysis was updated to include flexible supports by Bansal and Kirk [8] in 1976, replacing Muller's solver with a Cauchy-Riemann condition finite difference algorithm plus a Newton-Raphson search solution specified by Kirk [9]. This was essentially the same solution as used by Lund [7] but with minor differences. Both procedures work but will occasionally skip modes. This problem is more likely to occur when asymmetric flexible supports are included at the bearing locations. Other transfer matrix computer programs have been developed based on Lund's original analysis such as Barrett and Gunter [10].

More recent computer codes are based on a finite element solution that is successful in extracting all of the correct modes. These finite element code authors include Nelson [11], Rouch [12], Chen [13], Edney [14], and Ramesh [15]. One disadvantage of the finite element analysis is that the problem size increases dramatically with the number of elements used to model the rotor. Consequently, the run times with the finite element analysis are longer than with the transfer matrix analysis depending on the solution technique employed. Generally, however, the numerical techniques used with the finite element analysis are quite robust and do not miss any roots. Some methods require that all of the roots are found extracting the highest eigenvalue (and hence natural frequency) first and ending with the lowest, which is usually the only mode of interest. The run times associated with these methods, therefore, are considerably longer than those used with the transfer matrix analysis. Another approach employs a substitution technique to reduce the second order set of equations to first order form in which the efficient QR algorithm can be used. Other methods used to reduce run times involve extracting the lowest eigenvalues

first, either by solving the inverse problem or using determinant search techniques.

3.1.2 Controversial Issues

There are two main areas of a rotor-bearing-seal stability analysis that remain controversial. The first is what should be used for the tilting pad journal bearing stiffness and damping coefficients, which are a function of the pad tilt frequency. The frequency in question is the synchronous or once per shaft revolution frequency versus the subsynchronous damped natural frequency or instability frequency. The use of both synchronous and subsynchronous characteristics has been commonly applied over the years and both methods have been successful in predicting and solving complicated turbomachinery stability problems. This issue is further discussed in 3.3.3.1.

The second area of controversy concerns the labyrinth seals and aerodynamic cross coupling. For years, it was believed that the major destabilizing driving force was an aerodynamic excitation produced by impeller or blade interaction with the stator. Empirical equations by Alford and Wachel were developed and used extensively to predict these destabilizing aerodynamic cross coupling forces. Recently, labyrinth seal code development has shown that the labyrinth seals produce a major destabilizing excitation. This has led to the belief by some rotordynamicists that the labyrinth seals and balance piston produce the major destabilizing excitation in centrifugal compressors. Others maintain that impeller aerodynamic excitation is a significant driving force for compressor instability. These topics are covered in detail in 3.4.2, 3.5.1, and 3.8.6.

3.1.3 Stability Specifications—Standard Paragraphs

The stability specification is segmented into two parts: a simplified Level 1 analysis and a detailed Level 2 analysis (see flow chart, Figure 3-2). The Level 1 analysis is meant to be a screening process in which a quick and simple analysis can be conducted to filter out machines that are well away from the instability threshold. Level 1, therefore, utilizes a modified Alford's equation to estimate the destabilizing forces. Level 2, however, requires that the dynamic properties of labyrinth seals be included implicitly through the use of an appropriate labyrinth seal code.

The stability specification has adopted the use of synchronous tilting pad bearing characteristics. Since experimental data addressing the use of subsynchronous characteristics is virtually nonexistent, tilting pad bearing synchronous properties are specified (see 3.3.3.1). Furthermore, different acceptance criteria apply when using synchronous or subsynchronous tilting pad bearing data, making it impossible to compare each method directly. Therefore, in order that analyses conducted by several different parties may be evalu-

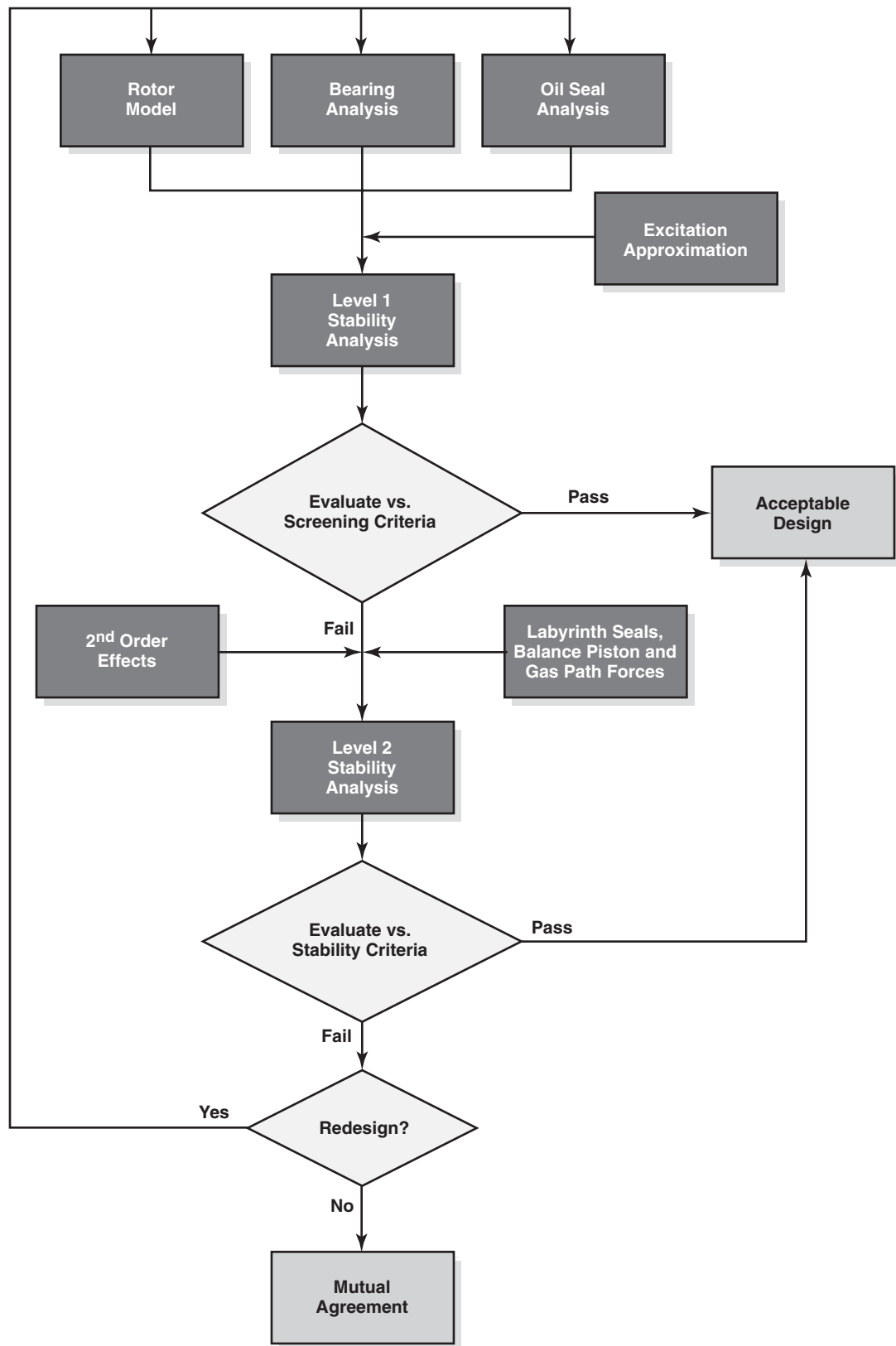


Figure 3-2—Stability Analysis Flow Chart

ated consistently, only one method has been adopted for analytical consistency.

Note: It is recognized that the stability specification is a work in progress and that revisions will be made as the state-of-the-art in rotor, bearing, and seal dynamics progresses.

The following tutorial sections basically outline the critical components of a stability analysis. These are grouped and presented in a flow chart of a typical process as depicted in Figure 3-2. The procedure follows the specification set forth in 6.8.5 and 6.8.6 of the SP R22. For analysis of rotors with field related problems, a Level 2 analysis should be used, as outlined in 6.8.6, even if the rotor passes the Level 1 analysis, as described in 6.8.5.

3.1.4 References

1. Smith, K. J., 1975, "An Operational History of Fractional Frequency Whirl," *Proceedings of the Fourth Turbomachinery Symposium*, Turbomachinery Laboratory, Texas A&M University, College Station, Texas, pp. 115 – 125.
2. Booth, D., 1975, "Phillips' Landmark Injection Project," *Petroleum Engineering*, pp.105 – 109.
3. Lund, J. W., 1965, "Rotor Bearing Dynamics Design Technology, Part V," AFAPL-TR-65-45, Aero Propulsion Laboratory, Wright-Patterson Air Force Base, Dayton, Ohio.
4. Gunter, E. J., 1966, *Dynamic Stability of Rotor-Bearing Systems*, NASA SP-113.
5. Gunter, E. J., 1967, "The Influence of Internal Friction on the Stability of High Speed Rotors," *ASME Journal of Engineering for Industry, Series B*, 89 (4), pp. 683-688.
6. Ruhl, R. L. and Booker, J. F., 1972, "A Finite Element Model for Distributed Parameter Turborotor Systems," *ASME Journal of Engineering for Industry, Series B*, 94 (1), pp. 126-132.
7. Lund, J. W., 1974, "Stability and Damped Critical Speeds of a Flexible Rotor in Fluid Film Bearings," *ASME Journal of Engineering for Industry*, 96 (2), pp. 509-517.
8. Bansal, P. N. and R. G. Kirk, 1975, "Stability and Damped Critical Speeds of Rotor-Bearing Systems," *ASME Journal of Engineering for Industry, Series B*, 97 (4), pp. 1325-1332.
9. Kirk, R. G., 1980, "Stability and Damped Critical Speeds: How to Calculate and Interpret the Results," *CAGI Technical Digest*, 12 (2).
10. Barrett, L. E., Gunter, E. J. and Allaire, P. E., 1976, "The Stability of Rotor-Bearing Systems Using Linear Transfer Functions – A Manual for Computer Program ROTSTB," Report No. UVA/643092/MAE81/124, School of Engineering and Applied Science, University of Virginia, Charlottesville, Virginia.
11. Nelson, H. D. and McVaugh, J. M., 1975, "The Dynamics of Rotor-Bearing Systems using Finite Elements," *ASME Journal of Engineering for Industry*, 98 (2), pp. 593 – 600.
12. Rouch, K. E. and Kao, J. S., 1979, "A Tapered Beam Finite Element for Rotor Dynamics Analysis," *ASME Journal of Sound and Vibration*, 66, pp. 119 – 140.
13. Chen, W. J., 1996, "Instability Threshold and Stability Boundaries of Rotor-Bearing Systems," *ASME Journal of Engineering for Gas Turbines and Power*, 118, pp.115 – 121.
14. Edney, S. L., Fox, C. H. J. and Williams, E. J., 1990, "Tapered Timoshenko Finite Elements for Rotor Dynamics Analysis," *Journal of Sound and Vibration*, 137 (3).
15. Ramesh, K. and Kirk, R. G., 1993, "Stability and Response of Rotors Supported on Active Magnetic Bearings," *Proceedings of the 14th ASME Vibrations and Noise Conference*, DE- 60, *Vibration of Rotating Systems*, pp. 289 – 296.

3.2 ROTOR MODELING

3.2.1 Baseline Stability

Baseline stability refers to a stability analysis performed with only the affects of the rotor's support system included in the stability model. The support system includes the journal bearings (see 2.5 and 3.3), the oil seals (see 3.4.1, if applicable), the squeeze film dampers (see 3.3.4, if applicable) and the support or casing flexibility (see 2.4 and 3.6). The mechanical rotor model is identical to that of an undamped critical speed analysis or a synchronous response analysis without defined unbalance.

Fixed geometry bearings are modeled with eight coefficients. Four coefficients represent the direct axis stiffness and damping while the remaining four represent the cross coupled stiffness and damping. Tilting pad bearings will have additional frequency dependant coefficients as described in 3.3.3.1. The tilting pad bearing may be modeled in either of three methods. The bearing may be represented by $5N+4$ stiffness and $5N+4$ damping coefficients referred to as "full" or "pad dynamic" coefficients where N = number of tilting pads. For simplicity, the bearing is often modeled using the standard four stiffness and four damping coefficients that have been "reduced" from the full pad dynamic coefficients using the synchronous frequency (synchronously reduced coefficients) or reduced using the instability or damped natural frequency (frequency dependent coefficients). For a more detailed explanation, refer to 3.3.3.1.

It should be recognized that the method chosen to represent tilt pad bearings may affect the results of the stability analysis. In some cases, the difference between an analysis with frequency dependent coefficients and synchronously

reduced coefficients may be quite large (see 3.3.3.1). Any resulting stability specification must consider which tilting pad journal bearing modeling method is employed and the “pass/fail” criteria adjusted accordingly. In either case, the bearing coefficients should be calculated at the extremes of the manufacturing tolerances that result in minimum and maximum values of clearance and the minimum and maximum values of preload for fixed lobe or tilting pad bearings. Stability calculations should be made at such extremes.

Another important modeling consideration is the pedestal or support stiffness and damping properties. These support characteristics, acting in series with the bearing’s oil film stiffness and damping coefficients, can have a profound effect on the resulting rotor system stability parameters. The support flexibility includes everything past the bearing’s oil film: the bearing case, the bearing pedestal, the machine casing, the base plate, the supporting columns and the foundation. When tilting pad journal bearings are used, the flexibility of the tilting pads and the pad pivots must also be modeled. In general, the support flexibility is dynamic. That is, the support stiffness and damping properties are a function of the applied vibration frequency. Refer to 3.6 for a more detailed discussion.

Any external forces, such as gear reaction components, shall be included when the bearing coefficients are calculated. In the event that several operating conditions are specified for the machinery, these also must be evaluated to insure that the extremes in the stability analysis have been accounted for. Any factor that is a variable in the specified operating condition that influences the bearing Sommerfeld Number should be considered to insure that the minimum and maximum log decrement of the rotor has been determined. The Sommerfeld Number, S , is defined below:

$$S = \frac{\mu N L D}{60 W} \left(\frac{D}{C_d} \right)^2 \quad 3-2$$

where

μ = average fluid viscosity, Pa · s (lb · s/in.²),

N = rotor speed, rpm,

L = bearing length, m (in.),

D = bearing diameter, m (in.),

W = bearing load, N (lbf),

C_d = bearing diametral clearance, m (in.).

3.2.2 Analysis with Additional Cross Coupling

The baseline model shall be modified to include one or more additional bearing locations to represent the destabilizing effects of components such as internal close clearance seals, for example labyrinth seals, or other identified areas within the machinery that will destabilize the rotor. The

model may represent the combination of the destabilizing forces at one rotor location, such as mid span for a conventional centrifugal compressor or steam turbine, or the center of gravity of an impeller on an overhung design.

The combined destabilizing effects will be represented by a “bearing” with equivalent cross coupled stiffness. For an axial turbine or axial compressor the combined equivalent cross coupled stiffness is represented by the Alford equation (see 3.5.1.1). For a centrifugal compressor the combined equivalent cross coupled stiffness is represented by the modified Wachel—Alford equation (see 3.5.1.2). The model can also use these equations on a stage by stage basis and locate the excitation at specific locations along the rotor.

In cases where the destabilizing effects are quantified more directly, using the results of specialized codes to analyze seals, the destabilizing effects may be located at each component that has been analyzed. In such cases, the destabilizing effects may be represented with the eight coefficients obtained from the component analysis or with an equivalent cross coupled stiffness. Regardless of which method is used to determine the destabilizing mechanism, the excitation must be evaluated at the conditions that will result in the maximum and minimum log decrement of the rotor.

3.3 JOURNAL BEARINGS

3.3.1 General

The stability of a turbomachine or any dynamic system is significantly influenced by the amount of damping present. Since the bearings provide the majority of damping in the rotor system, their design is crucial for maintaining adequate stability.

The following subsections describe some of the special aspects of fixed geometry bearings, tilting pad bearings and squeeze film dampers with regards to stability. Identified early as a major influence on rotor stability, Newkirk [1], bearing characteristics can now be predicted fairly accurately in order to avoid such phenomena as oil whirl and shaft whip.

While stability improvements can be obtained by reducing the destabilizing forces of particular components (seals, bearings, etc.), the bearings along with the rotor govern the machine’s ability to withstand and dissipate such forces, i.e., the machine’s stability robustness. The key to such stability robustness is the optimization of the bearing characteristics relative to the shaft stiffness. The degree of asymmetry between the bearing’s horizontal and vertical characteristics can also greatly impact the system’s stability [2–4]. Since there are many design variables available which determine a bearing’s stiffness and damping properties, proper design is often attainable, Nicholas, et al. [3]. In some cases, however, the bearing characteristics cannot be optimized adequately, making squeeze film dampers an attractive option.

3.3.1.1 References

1. Newkirk, B. L. and Taylor, H. D., 1925, "Shaft Whipping Due to Oil Action in Journal Bearing," *General Electric Review*, 28, pp. 559 – 568.
2. Gunter, E. J., 1966, "Dynamic Stability of Rotor-Bearing Systems," NASA SP-113, pp. 153 – 157.
3. Nicholas, J. C., Gunter, E. J. and Barrett, L. E., 1978, "The Influence of Tilting Pad Bearing Characteristics on the Stability of High-Speed Rotor Bearing Systems," Report No. UVA/643092/MAE81/141, School of Engineering and Applied Science, University of Virginia, Charlottesville, Virginia, pp. 30-32. Also in *Topics in Fluid Film Bearing and Rotor Bearing System Design and Optimization*, an ASME publication, April 1978, pp. 55 – 78.
4. Wohlrab, R., 1976, "Einflub der Lagerung auf die Laufstabilitat einfacher Rotoren mit Spalterregung," *Konstruktion*, 28, pp. 473 – 478.

3.3.2 Fixed Geometry Journal Bearing Stability

3.3.2.1 Unstable Journal Bearings

Fixed geometry or sleeve bearings have the annoying property of creating an excitation force that can drive the rotor unstable by creating a subsynchronous vibration. This phenomena usually occurs at relatively high rotor speeds and/or

light bearing loads, or, more generally, at high Sommerfeld Numbers (see 3.2.1). The problem is that sleeve bearings (i.e., all journal bearings excluding tilting pad bearings) support a resultant load with a displacement that is not directly in line with the resultant load vector but at some angle with rotation from the load vector. This angle can approach 90° for light loads and high speed. The specific case of a vertically downward gravity load is illustrated in Figure 3-3 for a two axial groove bearing. Now, the sleeve bearing supports this vertically downward load with a displacement that is not directly downward but at some angle with rotation from bottom dead center. This angle is defined as the attitude angle, Ψ as shown in Figure 3-3.

Figure 3-4 illustrates the hydrodynamic pressure distribution for a high speed, lightly loaded, unstable journal bearing, Nicholas [1]. Note that the bearing eccentricity ratio, $\mathcal{E} = e/c$ (Figure 3-3), is very small and the attitude angle, Ψ , approaches 90° . In this manner, a light $-Y$ direction load is supported by a $+X$ displacement. This occurs since the load is so light, the resulting pressure profile becomes very small with very little change from the maximum film to the minimum film locations. For equilibrium, the summation of all vertical components of the hydrodynamic forces times the area must be equal and opposite to the external load, W . Likewise, the sum of all horizontal forces must be zero. This can only occur for attitude angles that approach 90° .

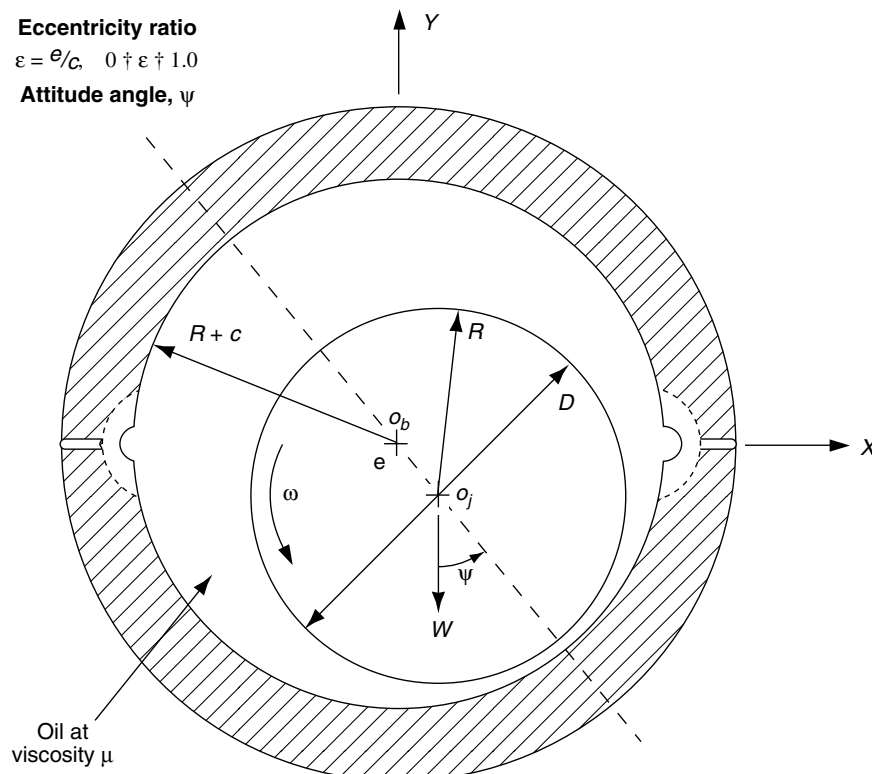


Figure 3-3—Fixed Geometry Bearing Schematic

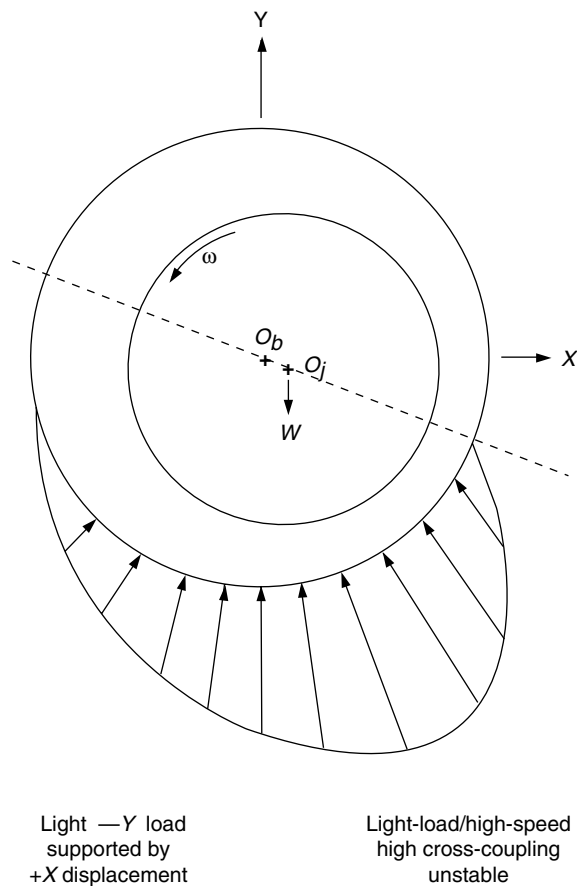


Figure 3-4—High-Speed, Lightly-Loaded, Unstable Bearing

Since a downward load is supported by a horizontal displacement, any downward force perturbation will result in a horizontal displacement which will result in a horizontal force which in turn produces a vertical displacement, etc. Thus, the bearing generates unstable cross coupling forces that actually drive the rotor and cause it to vibrate at a frequency that is normally in the range of 40% – 50% of running speed.

3.3.2.2 Stable Journal Bearings

Figure 3-5 [1] illustrates a relatively low speed, heavily loaded (i.e., low Sommerfeld Number, Section 3.2.1), stable journal bearing. Note that the bearing eccentricity ratio, ϵ , is very large and the attitude angle, Ψ , approaches 0° . In this manner, a heavy $-Y$ direction load is supported by a $-Y$ displacement. This occurs since the load is so heavy, the resulting pressure profile becomes very large with very large gradients from the maximum film to the minimum film locations. From a force summation, $\Sigma F_x = 0$ and $\Sigma F_y = W$. This can only occur for attitude angles that approach 0° . Since a downward load is now supported by a vertical displacement, cross coupling forces are at a minimum and the bearing is stable.

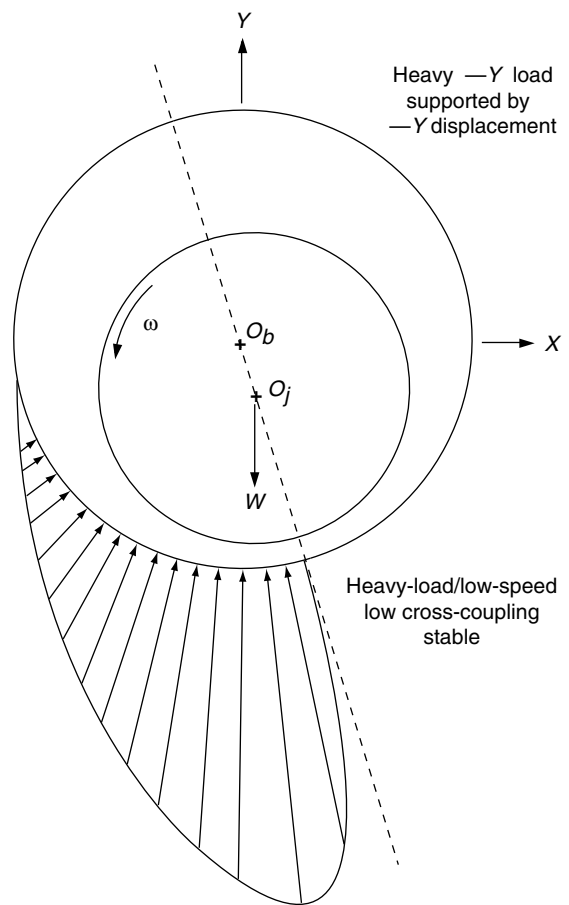


Figure 3-5—Low-Speed, Heavily-Loaded, Stable Bearing

3.3.2.3 Oil Whirl and Shaft Whip

Sleeve journal bearing induced oil whirl and shaft whip are illustrated in Figure 3-6 [1]. The 1x or synchronous vibration line is clearly indicated on the plot. Oil whirl, caused by the destabilizing cross coupling forces produced by high speed, lightly loaded sleeve bearings (i.e., high Sommerfeld Number, Section 3.2.1), manifests itself as approximately a 50% of running speed frequency (shaft vibrates approximately once per every two shaft revolutions). This can be seen in Figure 3-6 at speeds below about 7,500 rpm (below twice the rotor's first critical).

Above 7,500 rpm, the instability frequency locks onto the rotor's first fundamental natural frequency, which is at about 3,800 cpm. This re-excitation of the rotor's first natural frequency is sleeve bearing induced shaft whip which shows up as a vibration component that is below 50% of running speed and occurs at speeds that are above twice the rotor's first critical.

Usually, sleeve bearings are designed not to go unstable until the rotor speed exceeds twice the rotor's first critical

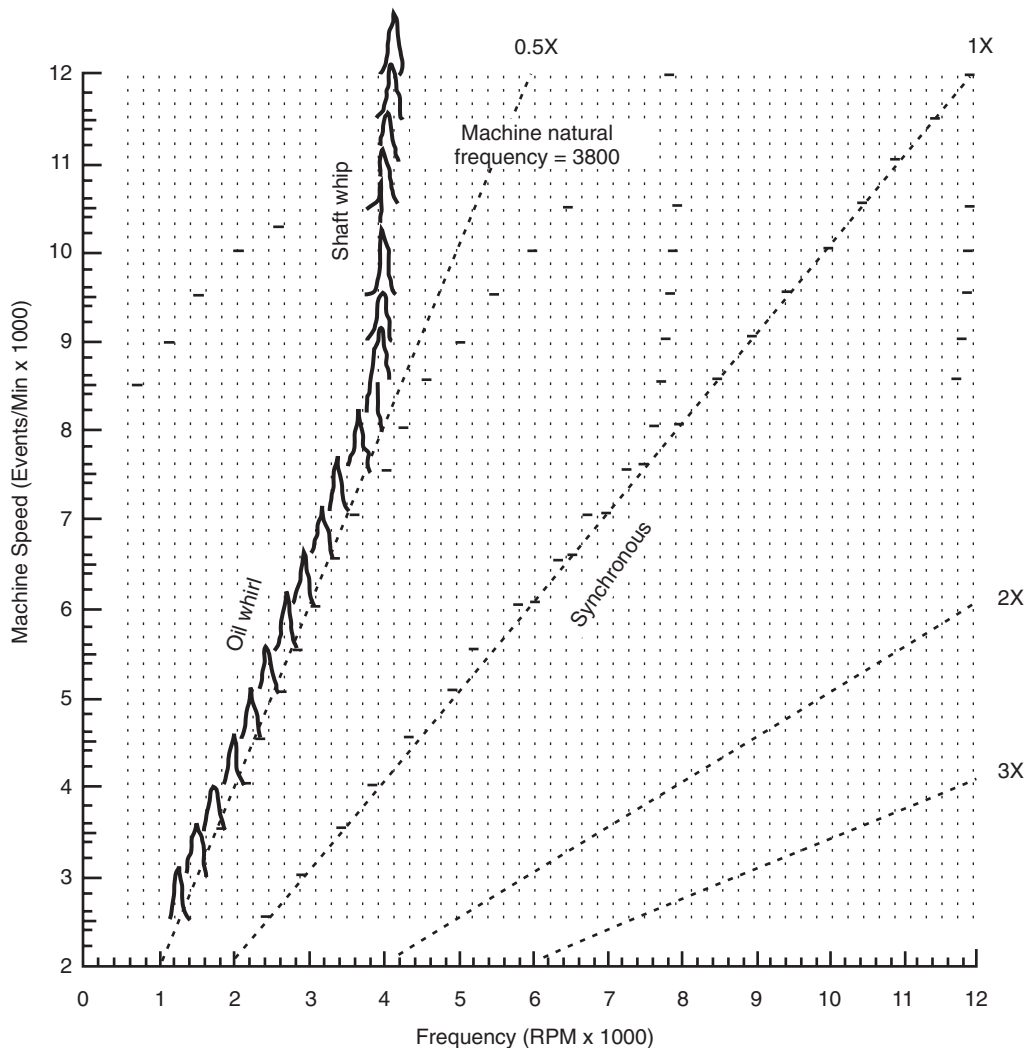


Figure 3-6—Bearing-Induced Shaft Whirl and Oil Whirl

speed. Thus, an approximate 0.5x is a rare occurrence and bearing induced instabilities usually show up as shaft whirl at frequencies less than 50% of synchronous speed.

Axial groove bearings have a cylindrical bore with typically 2- to 4-axial oil feed grooves. These bearings are very popular in relatively low speed equipment. For a given bearing load magnitude and orientation, the stability characteristics of axial groove bearings are primarily controlled by the bearing clearance. Tight clearances produce higher instability thresholds but tight clearance bearings present other problems that make them undesirable. For example, as clearance decreases, the bearing's operating oil temperature increases. Furthermore, babbitt wear during repeated start-ups will increase the bearing's clearance thereby degrading stability. In fact, many bearing induced instabilities in the field are caused by bearing clearances that have increased due to wear from oil contamination, repeated starts or slow-rolling with boundary lubrication.

Because of these limitations, other fixed-bore bearing designs have evolved to counteract some of the poor stability characteristics of axial groove bearings. Some anti-whirl sleeve bearing examples include pressure dam bearings [2,3], offset half bearings, Mehta and Singh [4] and multi-lobe bearings, Lanes and Flack [5]. These bearing designs have been successful in increasing the instability threshold speed compared to axial groove bearings [1–5].

3.3.2.4 Double Pocket Bearing Gas Turbine Application

A frequency spectrum is shown in Figure 3-7, Nicholas [1, 6] for a large overhung power turbine operating on test with 3 axial groove bearings. A large subsynchronous component is evident at 40 Hz (0.033 mm, 1.3 mils peak-to-peak at 5,000 rpm) predominately in the horizontal direction. The amplitude of the 40 Hz component exceeded 6.0 mils soon after

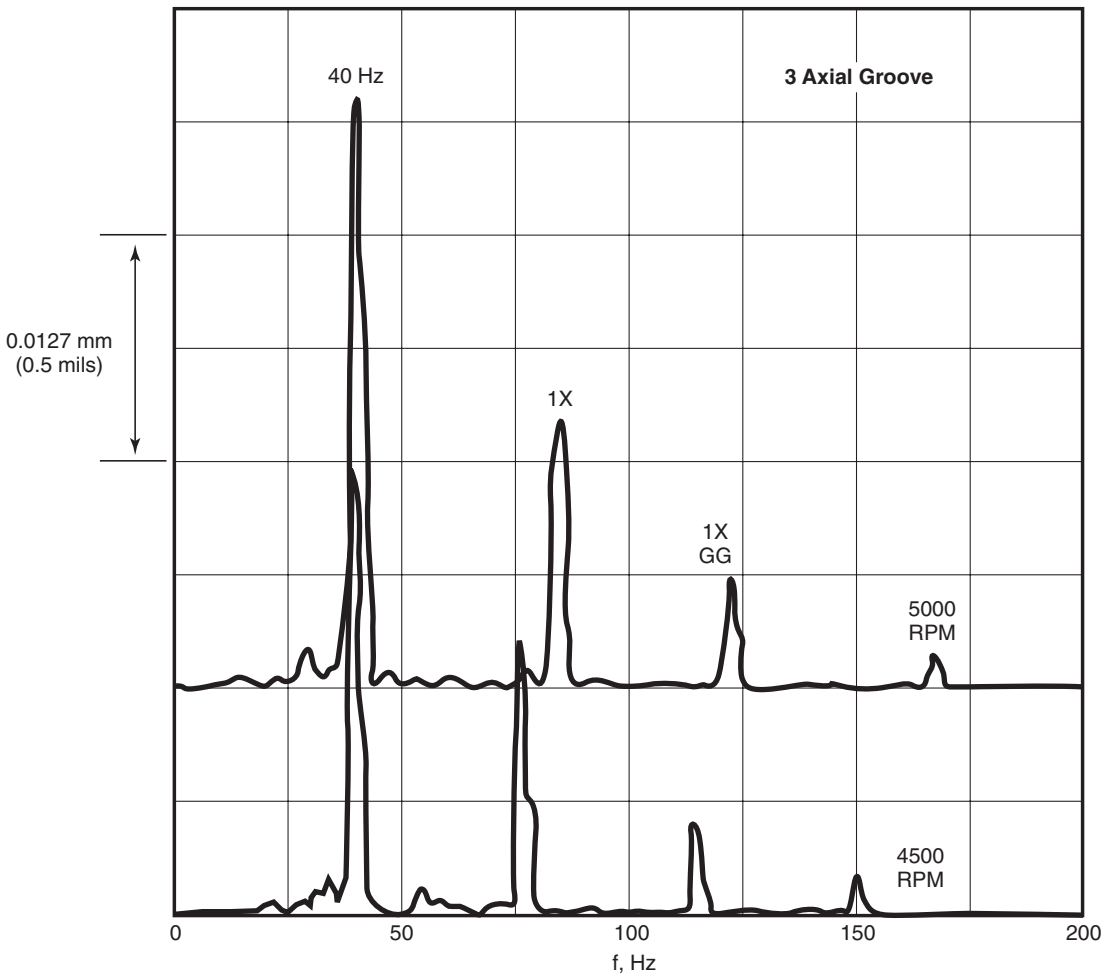


Figure 3-7—Frequency Spectrum, Power Turbine Test, 3-axial Groove Bearings

this signature was recorded. Also indicated on Figure 3-7 are the synchronous power turbine component labeled “1X” and the synchronous gas generator component labeled “1X GG.”

The 40 Hz instability is 48% of synchronous speed at 5,000 rpm and is thought to be caused by a combination of oil whirl and aerodynamic excitations from the turbine blades. In an attempt to improve the turbine’s stability characteristics, a double pocket bearing is considered, [1,6]

Results from a full rotor-bearing system stability analysis are presented in Figure 3-8. From Figure 3-8, the logarithmic decrement is plotted against aerodynamic cross coupling, Q , a destabilizing excitation placed at the turbine disk location. The original design 3-axial groove bearings place the rotor in the unstable region of the map with a log decrement value of -0.25 for low cross coupling levels. The damped natural frequency is 2,389 cpm (39.8 Hz) at a cross coupling level of 1.0×10^4 lb/in. This corresponds to the 40 Hz instability illustrated in Figure 3-7. The double pocket bearing designs, however, are well into the stable area with log decrement values above 0.75.

Figure 3-9 shows the turbine’s frequency spectrum operating on the modified double pocket bearings. The 40 Hz sub-synchronous component is suppressed to an amplitude of 0.25 mils at 5,000 rpm. This level is bounded and well within customer specifications.

3.3.2.5 References

1. Nicholas, J. C., 1996, “Hydrodynamic Journal Bearings - Types, Characteristics and Applications,” Mini Course Notes, 20th Annual Meeting, The Vibration Institute, Willowbrook, Illinois, pp. 79 – 100.
2. Nicholas, J. C. and Allaire, P. E., 1980, “Analysis of Step Journal Bearings—Finite Length, Stability,” ASLE Transactions, 23 (2), pp. 197 – 207.
3. Nicholas, J. C., 1986, “Stabilizing Turbomachinery with Pressure Dam Bearings,” *Encyclopedia of Fluid Mechanics*, 2, Gulf Publishing Co.

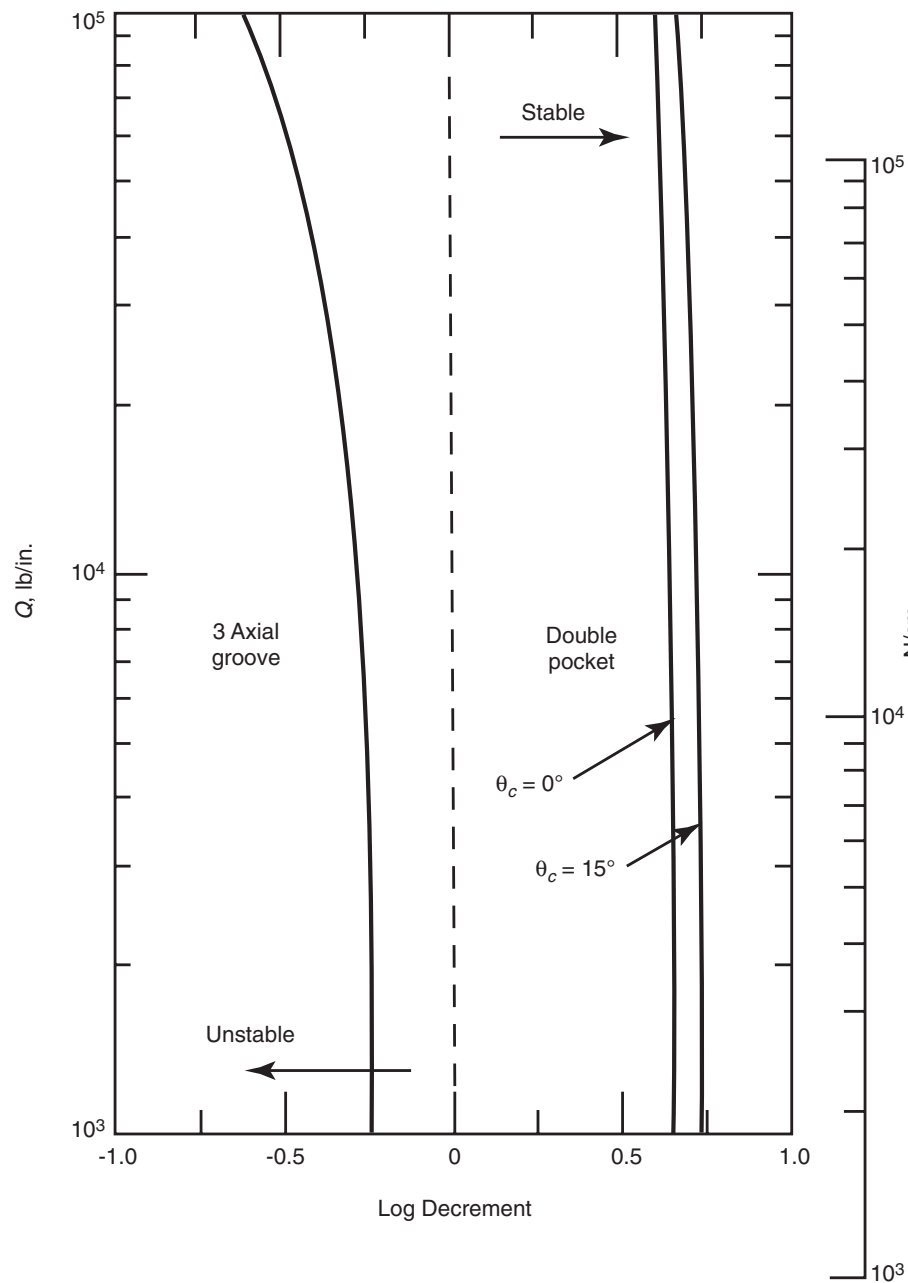


Figure 3-8—Rotor Bearing System Stability, Power Turbine $N = 5,000$ rpm

4. Mehta, N. P. and Singh, A., 1986, "Stability Analysis of Finite Offset-Halves Pressure Dam Bearings", *ASME Journal of Tribology*, 108 (2), pp. 270 – 274.
5. Lanes, R. F. and Flack, R. D., 1982, "Effects of Three-Lobe Bearing Geometries on Flexible Rotor Stability", *ASLE Transactions*, 25 (3), pp. 377 – 385.
6. Nicholas, J. C., 1985, "Stability, Load Capacity, Stiffness and Damping Advantages of the Double Pocket Journal Bearing," *ASME Journal of Tribology*, 107 (1), pp. 53 – 58.

3.3.3 Tilting Pad Journal Bearings

Even though they are costlier than fixed geometry bearings, tilting pad bearings have gained popularity because of their superior stability performance. Unlike fixed geometry bearings, tilt pad bearings generate very little destabilizing cross coupled stiffness regardless of geometry, speed, load or operating eccentricity. However, rotors supported on tilting pad bearings are still susceptible to instabilities due to other components within the machine such as labyrinth seals, impellers, etc. which can generate destabilizing forces.

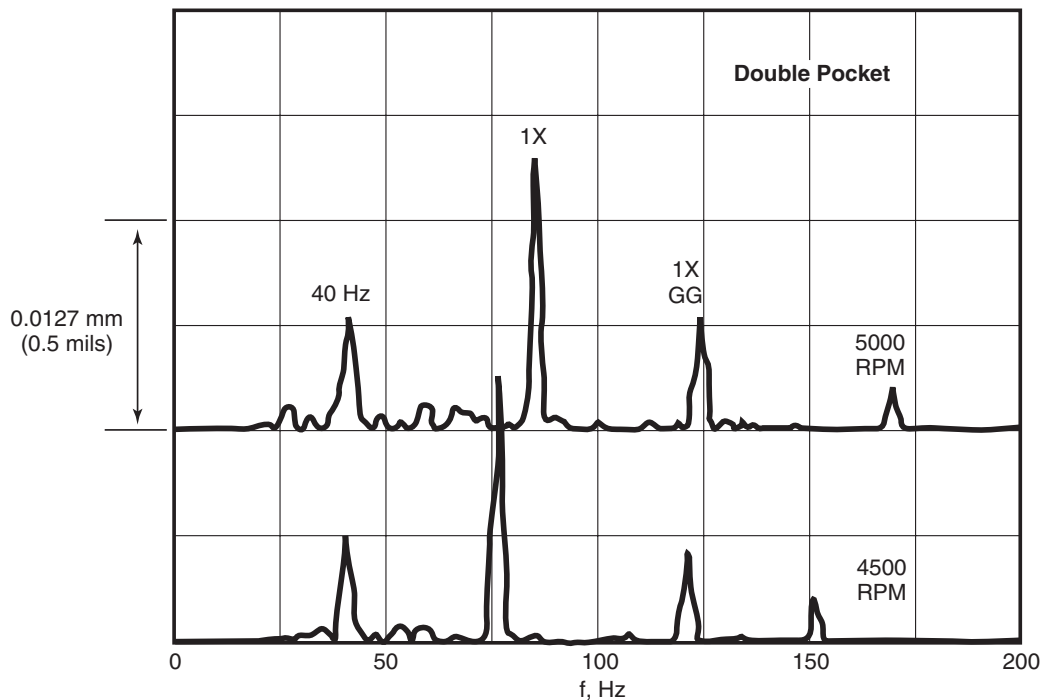


Figure 3-9—Frequency Spectrum, Power Turbine Test, Double Pocket Bearings

3.3.3.1 Tilting Pad Bearing Frequency Dependency

The low destabilizing nature of tilting pad bearings is a direct result of the pad's ability to rotate or pivot, Lund [1]. These pad rotations also result in the bearing's stiffness and damping characteristics becoming frequency dependent, in addition to their dependence on geometry, load, speed, etc. [2, 3]. This additional dependence on vibrational frequency is important with respect to stability because instabilities almost invariably occur at vibrational frequencies other than shaft speed, particularly, at subsynchronous frequencies, as discussed for fixed geometry bearings in 3.3.2.

FIXED GEOMETRY JOURNAL BEARING:

$K \text{ \& } C = f(\text{geometry, oil, materials, load, shaft speed})$

TILTING PAD JOURNAL BEARING:

$K \text{ \& } C = f(\text{geometry, oil, materials, load, shaft speed, vibrational frequency})$

Because only 2 degrees of freedom (shaft lateral motion) are predominant, fixed geometry bearing's dynamic characteristics can be represented by 4 stiffness and 4 damping coefficients as described in 2.5.2. However, a tilting pad bearing, with N pads has $N+2$ degrees of freedom, and requires $5N+4$ stiffness and $5N+4$ damping coefficients, called "full" or "pad dynamic" coefficients, to define its dynamic properties. For a 5 pad bearing, this means 29 stiffness and 29 damping coefficients determine its dynamic characteristics [2,4].

This large number of coefficients introduces increased mathematical and computational complexity into the rotordynamic analyses. Furthermore, it is difficult to physically interpret their meaning, and their impact on the rotor system. To alleviate these problems, a method can be used to reduce these coefficients into the more common 8 stiffness and damping coefficients. This reduction requires a vibrational frequency to be assigned to the pads, thus, establishing a frequency dependence upon the 8 dynamic coefficients. When the vibrational frequency is set at the shaft rotational speed, these 8 reduced coefficients for the tilting pad bearing are designated "synchronously reduced" bearing coefficients [1–5].

Figure 3-10 illustrates the importance of vibrational frequency on the reduced stiffness and damping characteristics of tilting pad bearings. The whirl ratio represents the ratio of shaft (and pad) vibrational frequency to shaft rotational frequency. Synchronously reduced coefficients are associated with a whirl ratio of 1.0. Figure 3-10 shows that when the shaft is vibrating subsynchronously (for instance, near its first natural frequency, whirl ratio of about 0.4), the predicted stiffness, K , and damping, C , properties that the bearing imposes on the rotor are altered. Typical of a turbomachine's bearing design, this particular bearing increases the equivalent stiffness and decreases the equivalent damping available as the shaft vibrates subsynchronously (whirl ratio < 1). Generally, such stiffness and damping trends degrade a machine's stability characteristics.

As with the characteristics of many common turbomachinery components, very little experimental work has been con-

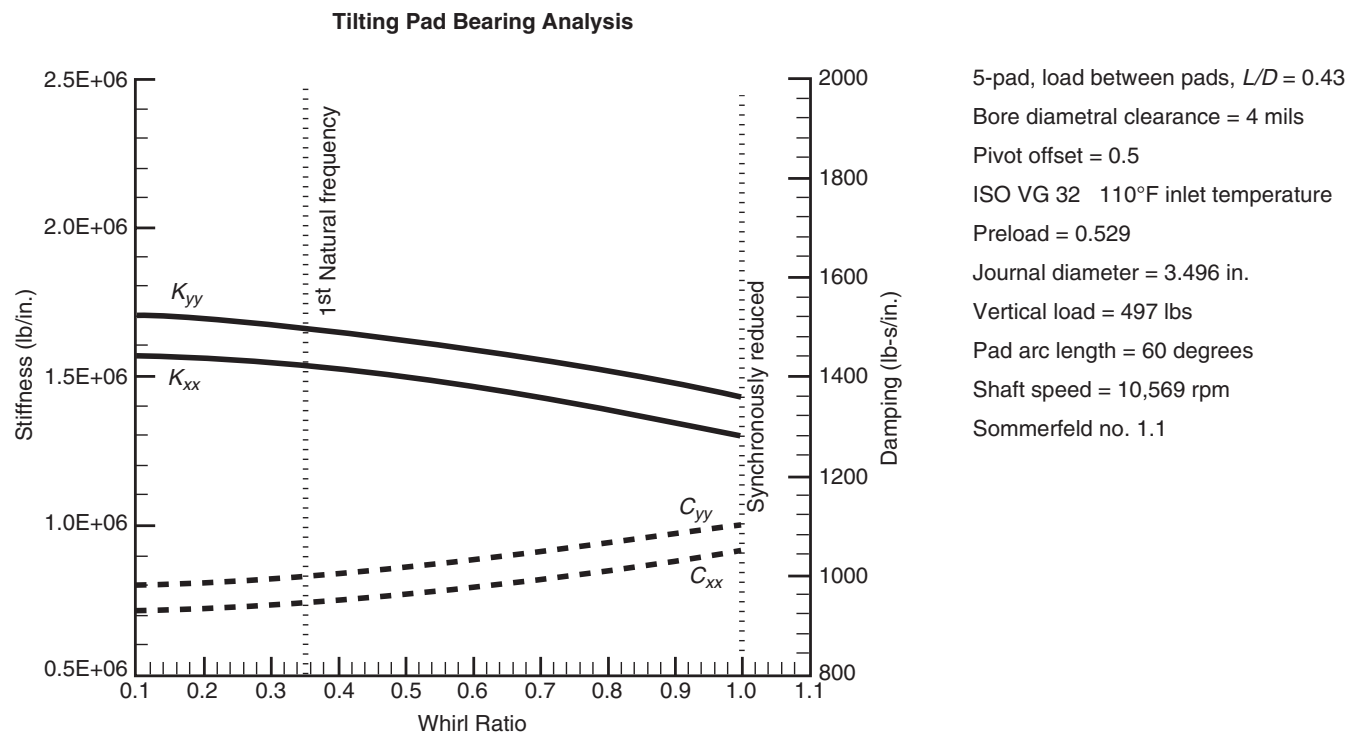


Figure 3-10—Frequency Dependent Stiffness and Damping

ducted to verify this frequency dependent nature of tilting pad bearing's stiffness and damping properties. Published experiments to date have correlated with predictions when additional influences such as pivot design and dynamic loading magnitude are considered [5,6]. Further research is being conducted in this area.

The extent of the frequency dependence is a function of several parameters; preload, pivot offset and Sommerfeld Number (see 3.2.1). Increasing preload and pivot offset decreases the amount of frequency dependence, i.e., reduces the difference between the synchronously reduced and the nonsynchronously reduced coefficients. Frequency effects also decrease as the Sommerfeld Number diminishes due to higher loading or lower speed [2–4].

Current trends in petrochemical machinery design are leading toward bearing designs running at higher Sommerfeld Numbers. In addition, low preload bearings ($m < 0.3$) are also a popular design trend because of their improved unbalance response and/or stability performance. For both trends (lower preloads and higher Sommerfeld Numbers), the frequency dependency is increased, leading toward bearings which provide higher equivalent stiffness and lower equivalent damping at subsynchronous frequencies. These effects translate into a reduction in predicted stability levels compared to those predicted using synchronously reduced coefficients.

Figure 3-11 reveals these prediction differences for a particular industrial compressor. At the bearing's maximum preload, the compressor exhibits its worst stability characteristics. Furthermore, one can see how influential the bearing's frequency dependence can be in decreasing the predicted base log decrement (i.e., log decrement for $K_{xy} = 0$). For the maximum preload in the tolerance range, $m = 0.367$, the predicted log decrement is 0.28 using synchronous coefficients and 0.17 using full coefficients. For the minimum preload in the tolerance range, $m = 0.178$, the predicted log decrement is 0.38 using synchronous coefficients and 0.23 using full coefficients.

Because of limited computational resources, early stability analysis techniques did not incorporate the $5N + 4$ full stiffness and $5N + 4$ full damping coefficients of tilting pad bearings.

Stability levels were determined using the 8 synchronously reduced coefficients. As shown in Figure 3-11, such an approach can yield stability predictions, which can be significantly different from an analysis incorporating the full set of non-reduced coefficients [7,8].

However, many manufacturers still incorporate synchronously reduced coefficients for their tilting pad bearing properties. In fact, most of the confidence factors surrounding destabilizing force models (such as Wachel's equation) and historically acceptable stability levels (i.e., $\delta \geq 0.1$ for stable

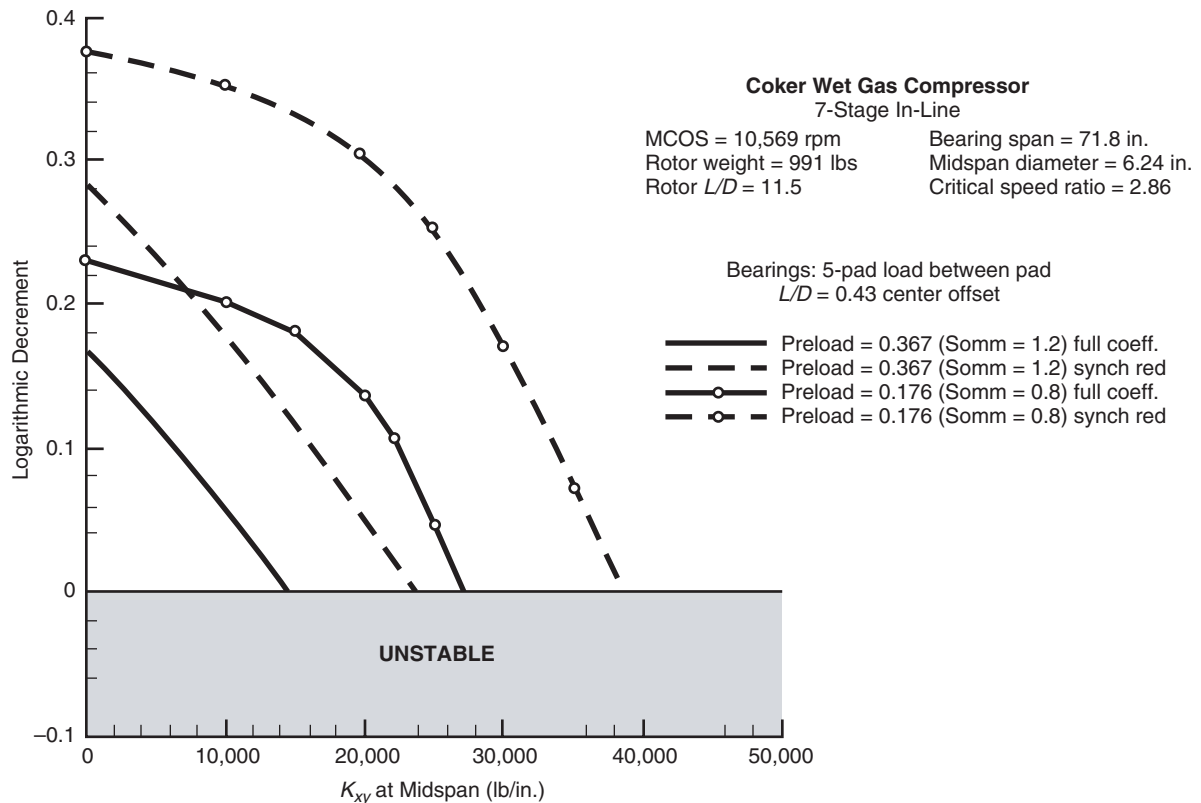


Figure 3-11—Full Coefficient vs. Synchronous Reduced Tilting Pad Bearing Stability Sensitivity

operation) are based on many years of design experience using synchronously reduced tilting pad bearing characteristics for stability calculations.

Furthermore, using synchronous tilting pad bearing characteristics in stability predictions may be physically justified since, prior to an instability, the shaft (and pads) vibrate synchronously ($1\times$) as illustrated in Figure 3-12, Gunter, et al. [9]. Thus, the destabilizing forces that increase with speed and finally produce a subsynchronous component at about 10,500 rpm, are counteracted by a rotor-bearing system that is vibrating synchronously. Even at speeds above 12,500 rpm where a strong subsynchronous vibration component is evident, a equally strong synchronous component is also present causing the tilting pads to vibrate both synchronously and subsynchronously.

Given these factors, combined with the lack of experimental data surrounding tilting pad bearings frequency characteristics, the stability specification has adopted the use of synchronous tilting pad bearing characteristics. The corresponding acceptance criteria in both the Level 1 and the Level 2 analyses was developed specifically for the use of synchronous coefficients. Clearly, further experimental research in this area is necessary before a final judgment can be made concerning the correctness of one method compared to the other.

3.3.3.1.1 References

1. Lund, J. W., 1964, "Spring and Damping Coefficients for the Tilting-Pad Journal Bearing," *ASLE Transactions*, 7, pp. 342 – 352.
2. Parsell, J. K., Allaire, P. E. and Barrett, L. E., 1983, "Frequency Effects in Tilting-Pad Journal Bearing Dynamic Coefficients," *ASLE Transactions*, 26, pp. 222 – 227.
3. White, M. F. and Chan, S. H., 1992, "The Subsynchronous Dynamic Behavior of Tilting-Pad Journal Bearings," *ASME Journal of Tribology*, 114, pp. 167 – 173.
4. Barrett, L. E., Allaire, P. E. and Wilson, B. W., 1988, "The Eigenvalue Dependence of Reduced Tilting Pad Bearing Stiffness and Damping Coefficients," *ASLE Transactions*, 31, pp. 411 – 419.
5. Ha, H. C., and Yang, S. H., 1999, "Excitation Frequency Effects on the Stiffness and Damping Coefficients of a Five-Pad Tilting Pad Journal Bearing," *ASME Journal of Tribology*, 121 (3), pp. 517 – 522.
6. Wygant, K. D., 2001, "The Influence of Negative Preload and Nonsynchronous Excitation on the Performance of Tilting Pad Journal Bearings," Ph.D. Dissertation, University of Virginia, Charlottesville, Virginia.

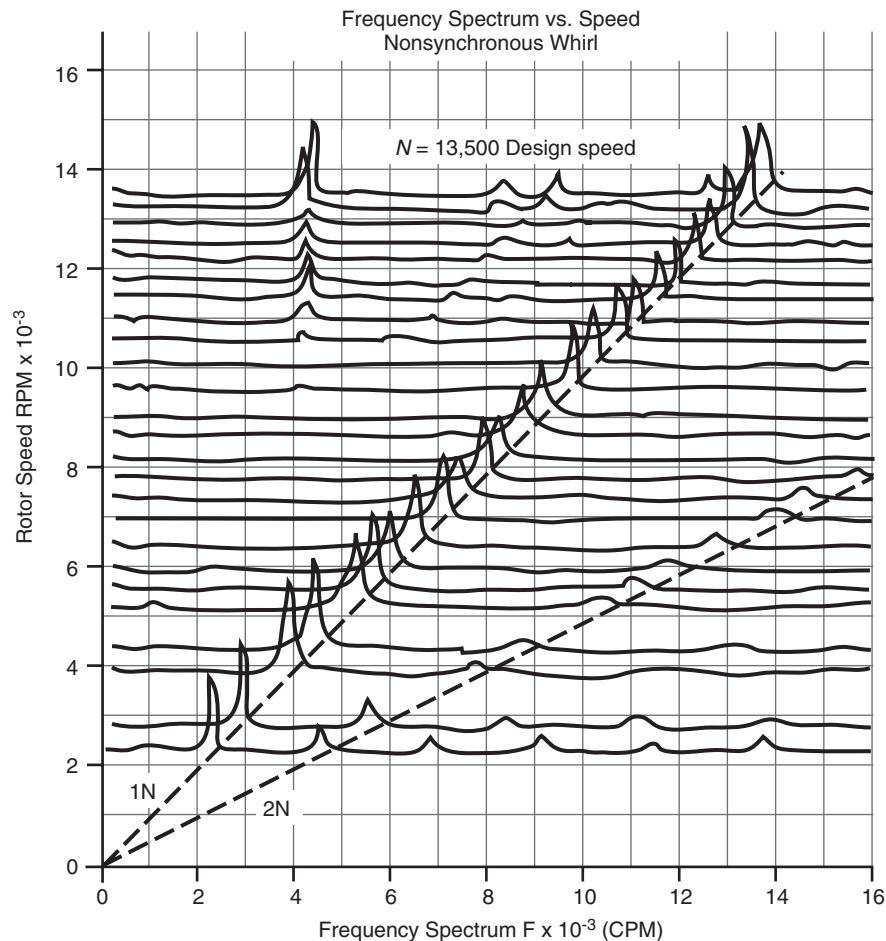


Figure 3-12—Waterfall Showing Self-Excited Instability

7. Brockett, T. S. and Barrett, L. E., 1993, "Exact Dynamic Reduction of Tilting-Pad Bearing Models for Stability Analyses," *STLE Tribology Transactions*, 36, pp. 581 – 588.
8. Chan, D. S. H. and White, M. F., 1996, "Stability Thresholds of Rotor Systems Supported on Tilting-Pad Journal Bearings," *I.Mech.E.*, pp. 235 – 257.
9. Gunter, E. J., Barrett, L. E. and Allaire, P. E., 1975, "Design and Application of Squeeze Film Dampers for Turbomachinery Stabilization," Proceedings of the Fourth Turbomachinery Symposium, Turbomachinery Laboratory, Texas A&M University, College Station, Texas, pp. 127 – 141.

3.3.3.2 Lubrication Starved Tilting Pad Bearings

In 1991, Tanaka [1] introduced the concept of removing the end seals from tilting pad journal bearings. He found that evacuating the bearing housing cavity produced significantly lower pad operating temperatures compared to the conventional flooded housing designs. This concept has been developed further by Nicholas [2] with the introduc-

tion of spray bars and wide open housing drains as illustrated in Figure 3-13.

While the Figure 3-13 design has been successful in reducing pad operating temperatures from 10% – 15% [2], care must be taken when implementing the design. The wide open end seals and housing drains result in low housing cavity pressures, often below 1.0 psig. Conversely, conventional flooded housing designs have typical housing pressures that range from 5 psig – 15 psig for a 20 psig oil inlet. These low housing pressures can lead to oil starvation and subsynchronous vibration if improperly applied.

Figure 3-13 illustrates one misapplication example. Open end seals and open housing drains will not work in a high speed balance vacuum. Even though the inlet oil is introduced to the housing through a spray bar at around 20 psig, the housing cannot maintain a positive pressure and the oil immediately atomizes, resulting in oil starvation. This manifests itself as a subsynchronous rotor vibration.

The solution is to use dummy end seals with a reasonable clearance and to temporally block the open housing drains. Dummy end seal clearances of around twice the bearing

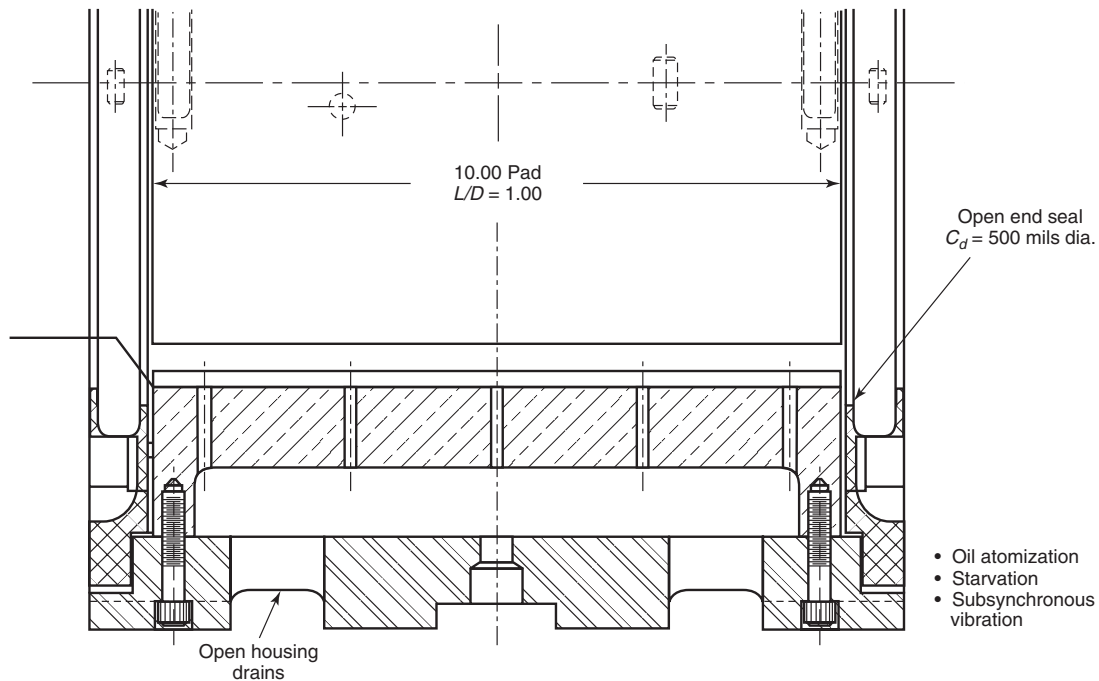


Figure 3-13—High Speed Balance Vacuum Pit Oil Atomization Resulting in Subsynchronous Vibration

clearance will produce a reasonable housing pressure of around 10 psig. In this case, the inlet oil exiting the spray bars will not atomize even in a high speed balance vacuum bunker.

Another example of the misapplication of the evacuated housing design is shown in Figure 3-14. In this case, the oil is introduced with a single housing hole between each set of tilting pads at the pad's axial centerline. The pad length to diameter ratio is 1.0 resulting in a relatively long pad. The designer, desiring lower pad operating temperatures, used open end seals that resulted in a relatively low housing pressure of 1.3 psig. This low housing pressure coupled with the long pad caused oil starvation and a subsynchronous rotor vibration. The spray bar design shown in Figure 3-16 distributes the oil along the full axial length of the pad and was successful in eliminating the subsynchronous rotor vibration.

A final example of the misapplication of the evacuated housing design is shown in Figure 3-15. In this case, the oil is introduced with a mushroom orifice spray between each set of tilting pads at the pad's axial centerline. Again, the pad length to diameter ratio is 1.0 resulting in a relatively long pad. As before, lower pad operating temperatures were desired prompting the designer to use open end seals. Clearly from Figure 3-15, no oil is directly sprayed toward the pad's axial ends resulting in a 1.9-in. "oil free" zone at both pad ends. This again caused oil starvation and a subsynchronous rotor vibration. A spray bar similar to the one illustrated in Figure 3-16 again solved the problem.

While it may appear that these tilting pad bearings caused a rotor instability, it was the misapplication of the evacuated

housing design that caused the subsynchronous vibration. This phenomena cannot be predicted or prevented by performing a rotor bearing stability analysis.

3.3.3.3 References

1. Tanaka, M., 1991, "Thermohydrodynamic Performance of a Tilting Pad Journal Bearing with Spot Lubrication," *ASME Journal of Tribology*, 113 (3), pp. 615 – 619.
2. Nicholas, J. C., 1994, "Tilting Pad Bearing Design," Proceedings of the Twenty-Third Turbomachinery Symposium, Turbomachinery Laboratory, Texas A&M University, College Station, Texas, pp. 179 – 194.

3.3.4 Squeeze Film Dampers

It is widely known from early investigations on rotordynamic instability that the use of flexible damped supports can eliminate or at least alter the speed at which instability occurs. Installing a squeeze film damper in series with the radial bearings is the easiest and perhaps most common method of adding a flexible damped support. In addition to enhancing stability, they are also used to reduce critical speed peak response amplitudes of highly flexible rotors. In the past, squeeze film dampers were often inappropriately regarded as a last resort solution applied to problem machinery. In more recent years, however, they have gained acceptance not only as a credible fix in problem machinery but also as a design tool routinely used in new equipment.

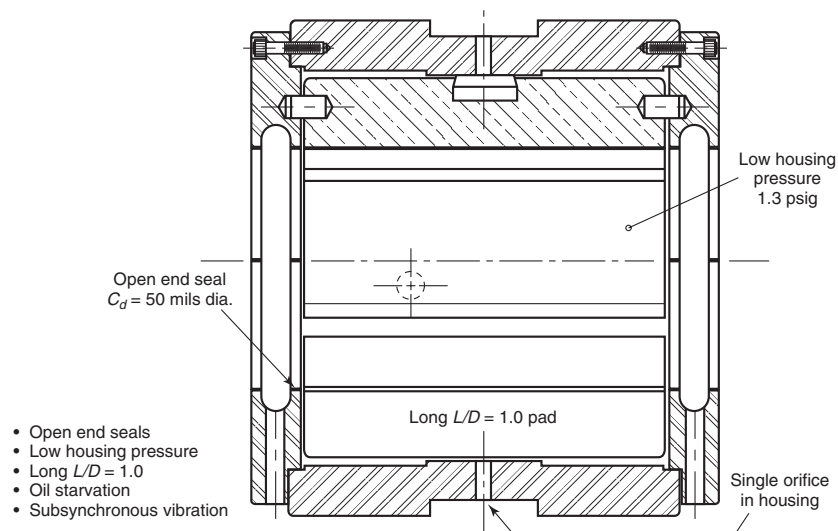


Figure 3-14—Single Housing Orifice Design Resulting in Subsynchronous Vibration

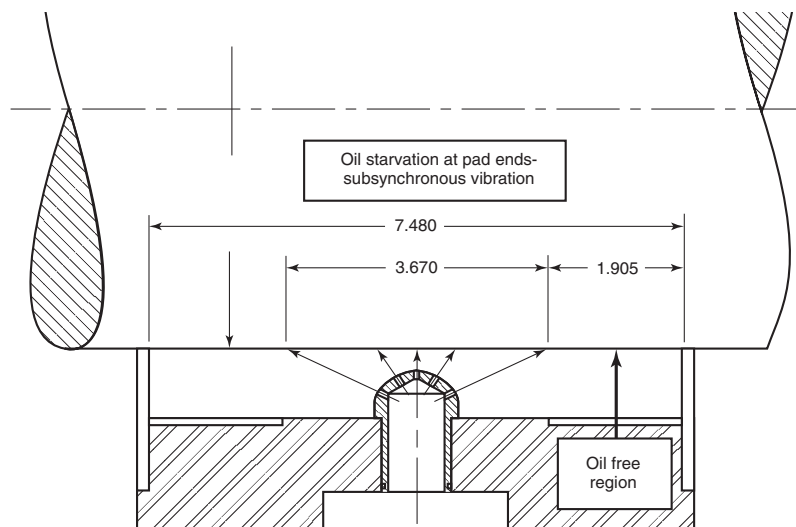


Figure 3-15—Button Spray Design Resulting in Subsynchronous Vibration

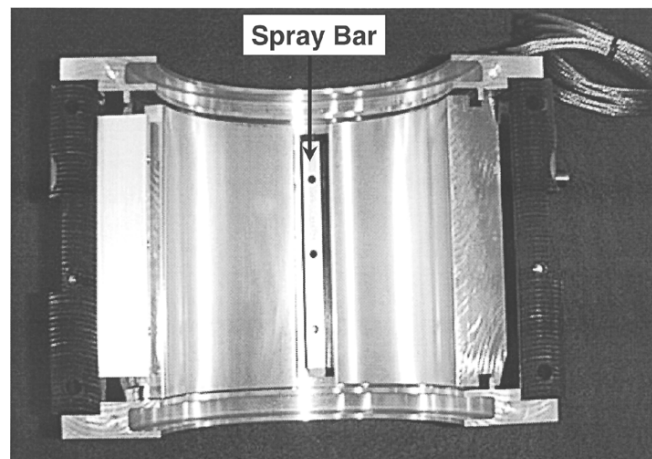


Figure 3-16—Spray Bar Evacuated Housing Design

Squeeze film dampers are widely applied in aircraft jet engines to supplement the otherwise negligible damping inherent in the rolling element bearings used in this type of machinery. Although their main purpose is to reduce rotor response amplitudes, they provide some improvement in the stability of the rotor system. Squeeze film dampers are also used in a variety of land-based machinery operating on oil film bearings. Of these applications, they are more frequently used in high-pressure centrifugal compressors to eliminate instability problems, although they are also used to reduce the critical speed response characteristics of machines with highly flexible rotors. A brief history of the development and early applications of squeeze film dampers along with a general discussion on theoretical models and design considerations is given in Zeidan, et al. [1].

Although tilting pad bearings are routinely used to avoid oil whirl instability problems, machines with flexible rotors supported on tilting pad journal bearings may be prone to instability if there exists an external destabilizing force of magnitude that exceeds the restoring damping of the bearing. This instability may be avoided by either eliminating the destabilizing mechanism, raising the rotor's first damped natural frequency, or by adding sufficient external damping to raise the stability threshold. In cases where it is not possible to eliminate the instability mechanism or raise the natural frequency, the only practical solution is to add external damping. Since damping is also a dynamic stiffness, adding external damping to a rotor supported on relatively stiff

bearings in most cases will not work. Consequently, the support stiffness also must be lowered to allow rotor motion at the bearings in order to make the available damping more effective. One of the key features in the successful design of a squeeze film damper, therefore, is the introduction of flexibility as well as damping at the bearing support structure. By allowing the bearing to move increases its ability to remove vibration energy in the form of heat. Other benefits include lower transmitted forces and increased bearing life, particularly in the case of machinery operating above the first critical speed.

3.3.4.1 Design Considerations

A schematic of a typical squeeze film damper bearing is given in Figure 3-17. The inner bearing element is a conventional hydrodynamic tilting pad journal bearing that is supported and centered in a fixed housing. A small radial clearance is required between the housing and inner element to provide a cavity for an oil film. Unlike with a conventional journal bearing, the inner element is free to float within this cavity and not rotate. In most designs, oil is supplied to this cavity and the inner bearing via a central annular groove machined into either the housing or the bearing shell. End seals are typically used to enclose this cavity to minimize axial through flow and increase damping. The most common end seal arrangement incorporates a circumferential elastomeric o-ring as illustrated in Figure 3-18.

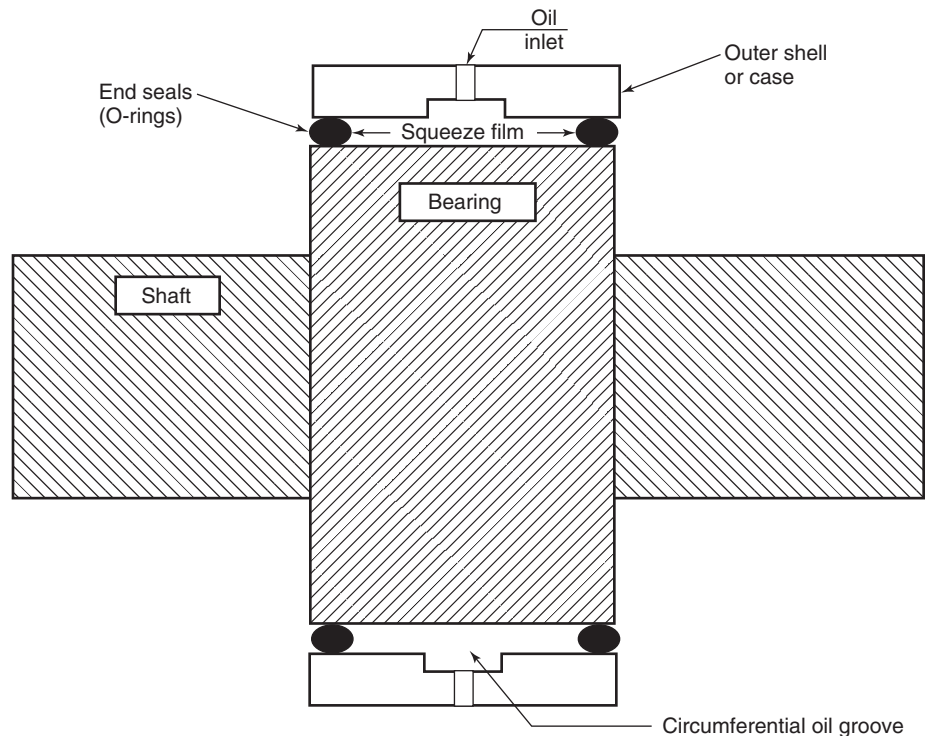


Figure 3-17—Squeeze Film Damper Schematic

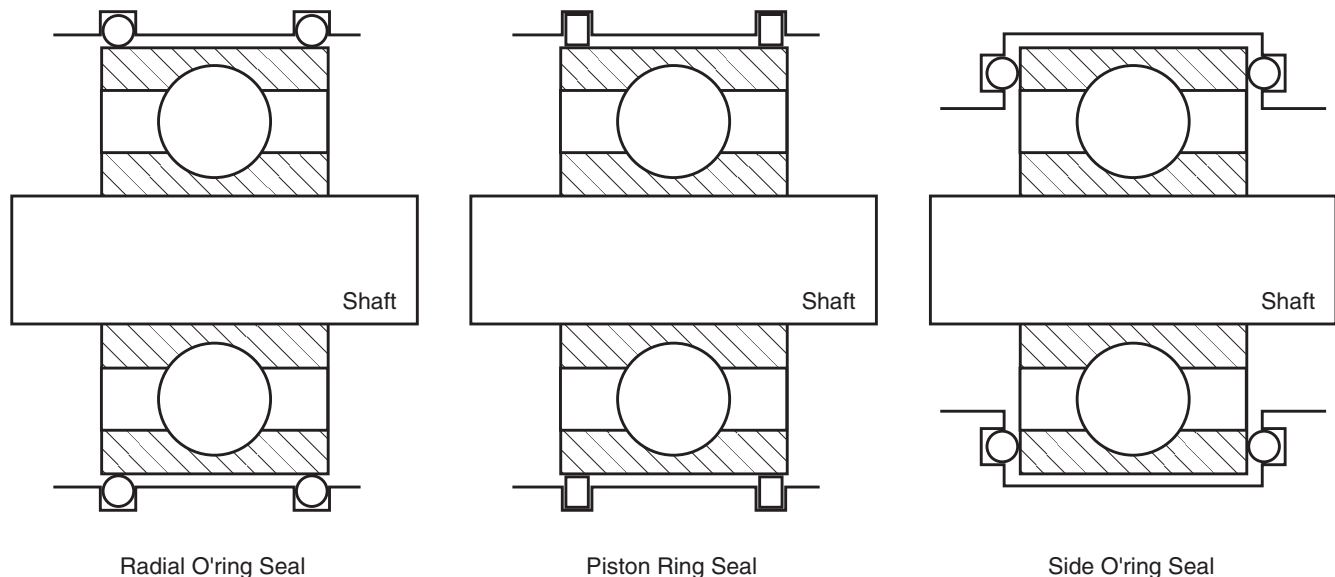


Figure 3-18—Typical End Seal Arrangements

Other designs more typically used with rolling element bearings include circumferential piston rings or side mounted o-rings, also depicted in Figure 3-18. The outside diameter of the inner element forms the damper journal, which is prevented from spinning by a loose anti-rotation pin. This feature allows the inner element (or damper journal) to whirl but not spin in a precession motion, thus squeezing the oil in the clearance cavity that in turn generates an oil film pressure and hence a damping force. Since the inner element cannot rotate, there is no net fluid rotation in the cavity to develop a destabilizing cross coupled stiffness, only direct coefficients as a result of the orbital motion of the inner element. For optimum damping, a centering device of the inner element is often incorporated into the design to keep the damper centered within the cavity. On machines with lightweight rotors, the o-ring end seals provide enough support to center the inner bearing, Leader, et al. [2]. Machines with heavy rotors, however, present a unique challenge requiring a mechanical spring element that can support a large weight and yet retain some inherent flexibility, Edney and Nicholas [3].

3.3.4.2 Stiffness and Damping Coefficients

Gunter, et al. [4] originally proposed the theory on which many squeeze film damper analyses are based. A squeeze film damper is essentially a plain journal bearing in which radial motion only is allowed. As with conventional bearings, the stiffness and damping coefficients may be derived from a solution of the incompressible fluid Reynolds' equation, but for a non-rotating journal assuming laminar flow, and a circular whirl orbit. Typical axial pressure profiles of four different

combinations of damper end seal and oil feed are illustrated in Figure 3-19. Cases 3 and 4 are more traditional arrangements with a center feed groove. Without end seals, Case 3, the damper is equivalent to a plain journal bearing with two lands of equal length $L/2$. The film pressure reduces to atmosphere at the oil groove and damper ends creating two separate pressure profiles equivalent to two parallel dampers of length $L/2$. Consequently the maximum pressure in each side of the damper is reduced by a factor of four and the force on each side by a factor of eight. The net effect is a reduction in hydrodynamic force, and hence both bearing coefficients, by a factor of four. With end seals, Case 4, the pressure profile is equivalent to that of a plain land without an oil groove and without end seals of overall length L . The values for total force, stiffness and damping, therefore, are also the same. Most practical dampers are designed with some type of end seal to reduce the axial through flow and increase damping. Axial pressure profiles for a damper with a central feed hole, Cases 1 and 2, are other options although much less popular.

For unrestricted end flow (Cases 2, 3 and 4) Reynolds' equation is solved using boundary conditions appropriate to the short or Ocvirk bearing theory. Without end flow (Case 1) the boundary conditions are those referred to as the long or Sommerfeld bearing theory.

Another factor in the determination of the stiffness and damping coefficients is whether the oil film is cavitated or not. By virtue of their design, squeeze film dampers may be prone to two types of cavitation: vapor and gaseous. The damper may be susceptible to cavitation if the oil inlet pressure is in the 15 to 30 psig range and the damper operates

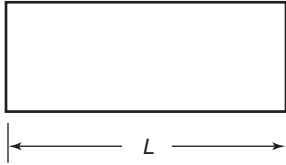
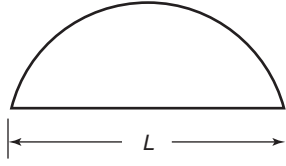
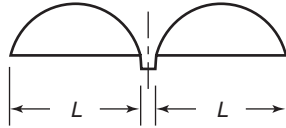
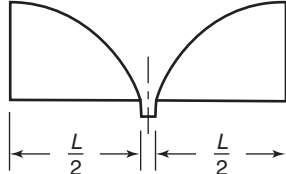
Case No.	Sealing and Feeding Configuration	Pressure Profile	Spring and Damping Constants
1	Closed ends center hole feed		Long journal bearing theory
2	Open ends center hole feed		Short journal bearing theory
3	Open ends center groove feed		Short journal bearing theory
4	Closed ends center groove feed		Short journal bearing theory Equivalent to Case 2

Figure 3-19—Axial Pressure Profiles of Various Damper Arrangements [Ehrich, 10]

highly eccentric in the damper housing resulting in high peak pressures. The damper will be less susceptible to cavitation if the oil inlet pressure is high and the damper operates nearly centered in the damper housing resulting in low peak pressures. In the solution of Reynolds' equation, cavitation is represented as a pi-film model, which in the case of vapor cavitation is a reasonable assumption. With gaseous cavitation, however, a compressible fluid model assuming properties of a mixture of oil and air would be more appropriate, although the random nature of the air entrapment may not yield any significant improvement in the results. Diaz and San Andres [5] provide a more detailed discussion on this topic, along with a review of the many conceptual approaches that have been considered. These authors also conclude that air ingestion leading to a bubbly mixture can substantially affect the dynamic performance of a squeeze film damper [6].

Despite the concern expressed in the preceding section, most squeeze film damper analyses employ the stiffness and damping coefficients derived from Reynolds' equation. Expressions for the direct stiffness and damping based on the

work of Gunter, et al. [4] are given in Table 3-1 for a damper precessing in steady state circular motion. Formulae are given for both the short and long bearing theory solutions, and for both a cavitated (pi-film) and uncavitated (full film) model are given.

Practical experience has shown that damper bearings with small L/D ratios (< 0.5) which can be more reasonably modeled using the short bearing theory yield predictions that correlate well with actual damper performance.

For the short bearing model with cavitation, the stiffness and damping coefficients expressed in dimensionless form are plotted against eccentricity ratio in Figure 3-20. Both coefficients clearly increase sharply at values of eccentricity ratio above 0.4 tending to infinity at a ratio of 1.0. Since a damper's effectiveness degrades significantly with eccentricity, it is important for optimum performance that the damper is positioned and remains well centered in the clearance cavity. Similar trends are observed with the coefficients of the long bearing model.

Table 3-1—Formula for Squeeze Film Damper Stiffness and Damping Coefficients

Film Model	Short Bearing Theory		Long Bearing Theory	
	Stiffness: K_d	Damping: C_d	Stiffness: K_d	Damping: C_d
Cavitated: pi-film	$\frac{2 \mu R L^3 \epsilon \omega}{c_r^3 (1 - \epsilon^2)^2}$	$\frac{\pi \mu R L^3}{2 c_r^3 (1 - \epsilon^2)^{3/2}}$	$\frac{24 \mu R^3 L \epsilon \omega}{c_r^3 (2 + \epsilon^2)(1 - \epsilon^2)}$	$\frac{12 \pi \mu R^3 L}{c_r^3 (2 + \epsilon^2)(1 - \epsilon^2)^{1/2}}$
Uncavitated: full film	0	$\frac{\pi \mu R L^3}{c_r^3 (1 - \epsilon^2)^{3/2}}$	0	$\frac{24 \pi \mu R^3 L}{c_r^3 (2 + \epsilon^2)(1 - \epsilon^2)^{1/2}}$

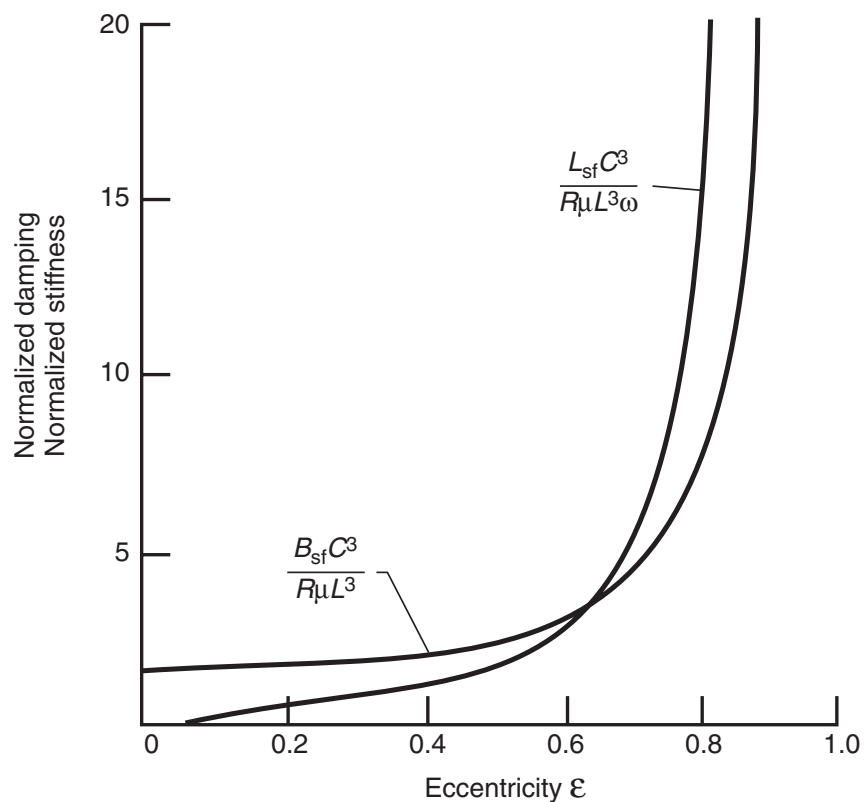


Figure 3-20—Squeeze Film Damper Coefficients vs. Eccentricity Ratio: Short Bearing Theory (Cavitated) [Ehrich, 10]

3.3.4.3 Support Model Representation

In the support model, the squeeze film damper is included in series with the bearing oil film and support characteristics as idealized in Figure 3-21. K_d and C_d are the direct stiffness and damping coefficients of the squeeze film damper and K_{ds} the stiffness of the centering device, which is included in parallel with the damper coefficients. In the vertical direction, K_{ds} is equal to either the o-ring or mechanical spring vertical stiffness. In the horizontal direction, practical experience has shown that with mechanically centered dampers, a value equal to one half of the vertical stiffness usually works well.

With o-ring centered dampers, the horizontal stiffness is nearly equal to the vertical stiffness. A method for calculating equivalent support values is outlined in Nicholas, et al. [7]. A good rule of thumb is that the dynamic stiffness of the damper should be at least one half but preferably one order of magnitude smaller than that of the oil film in order for the damper to be effective.

3.3.4.4 Centering Devices

The importance of statically centering a squeeze film damper is described in Kuzdzal and Hustak [8]. The authors

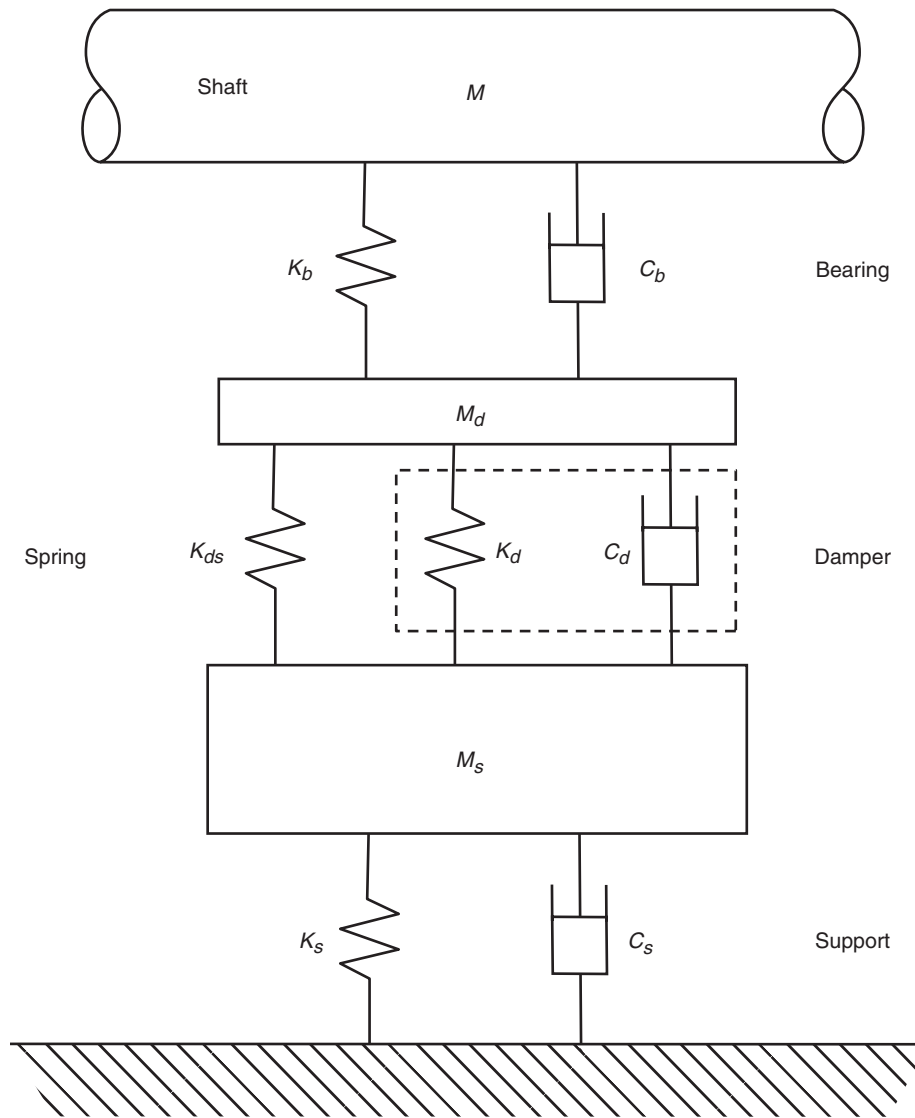


Figure 3-21—Idealization of Bearing-damper-support Characteristics

present results for a bottom resting damper vs. o-ring supported and mechanical spring supported dampers at various damper eccentricities. Regardless of the centering device employed, it's stiffness value must be carefully determined. Theoretical calculations are often approximate and should be used with caution. Leader, et al. [2] presents a method for measuring the stiffness of an o-ring and shows how to use the Nicholas, et al. [7] formulas. He also describes a method for installing the o-rings eccentrically to keep the inner element centered under the static weight of the rotor. A mechanical centering device [3,8] and a method for measuring stiffness is presented in [3]. With mechanical elements, hooks, bolted joints or other means of fixing the centering device in the housing often introduce some additional flexibility thus reducing the overall stiffness. This resultant value should be

used in the analysis. Test fixtures for measuring stiffness must insure that all such effects are properly accounted for. This is best accomplished by testing the centering device in its housing. A schematic showing a typical o-ring centered damper is illustrated in Figure 3-22 while a mechanical arc spring centered damper is shown in Figure 3-23, [9]. Similar photos may also be found in [8].

Particularly in the case of mechanical centering devices used to support heavy rotors, a fatigue calculation should be performed. The mean stress is the maximum stress with the centering device statically loaded. For the alternating stress, a worst case value should be assumed equal to the load that would deflect the centering device beyond the statically loaded condition an amount equal to the damper radial clearance.

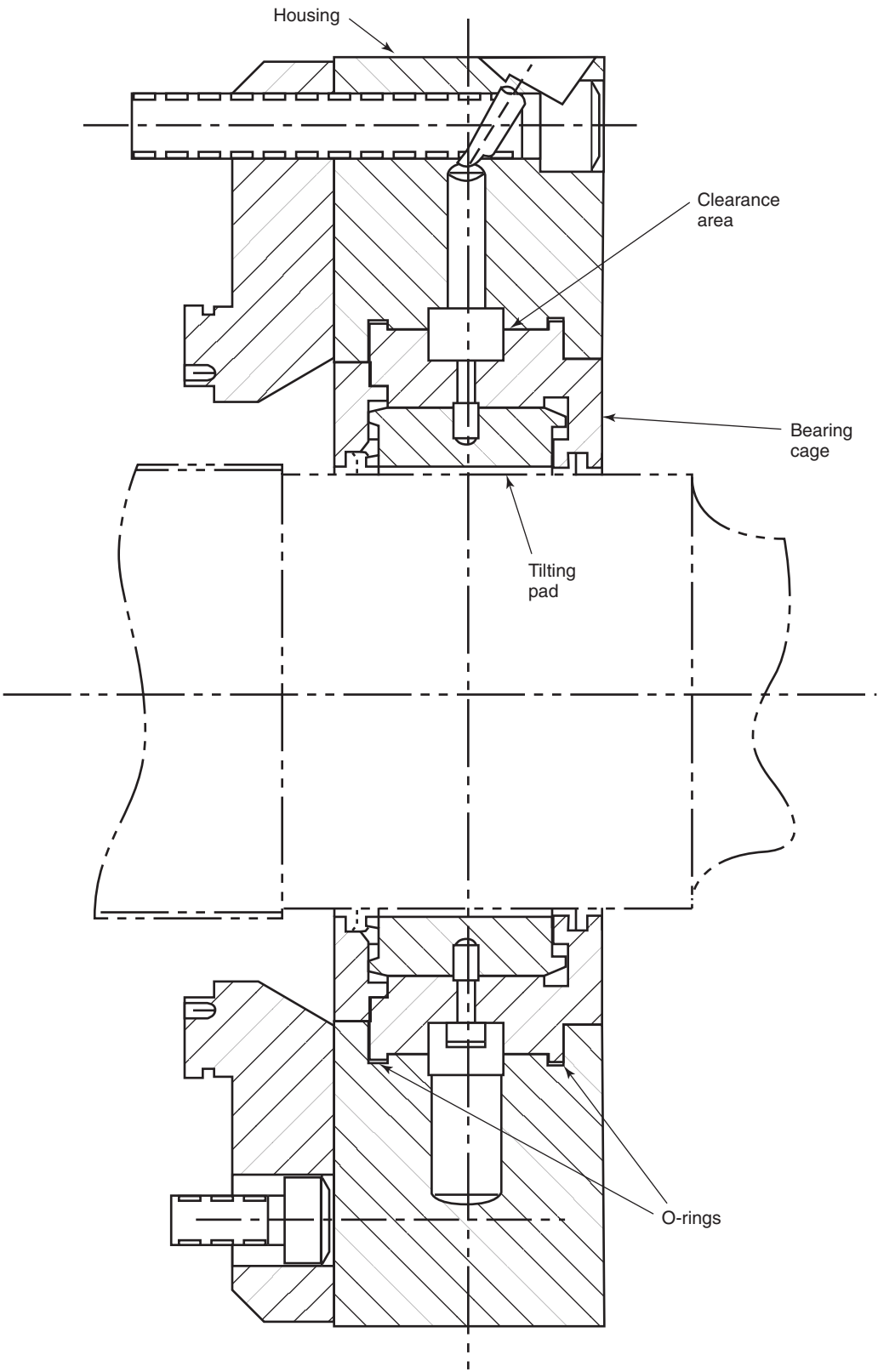


Figure 3-22—O-ring Supported Squeeze Film Damper Schematic

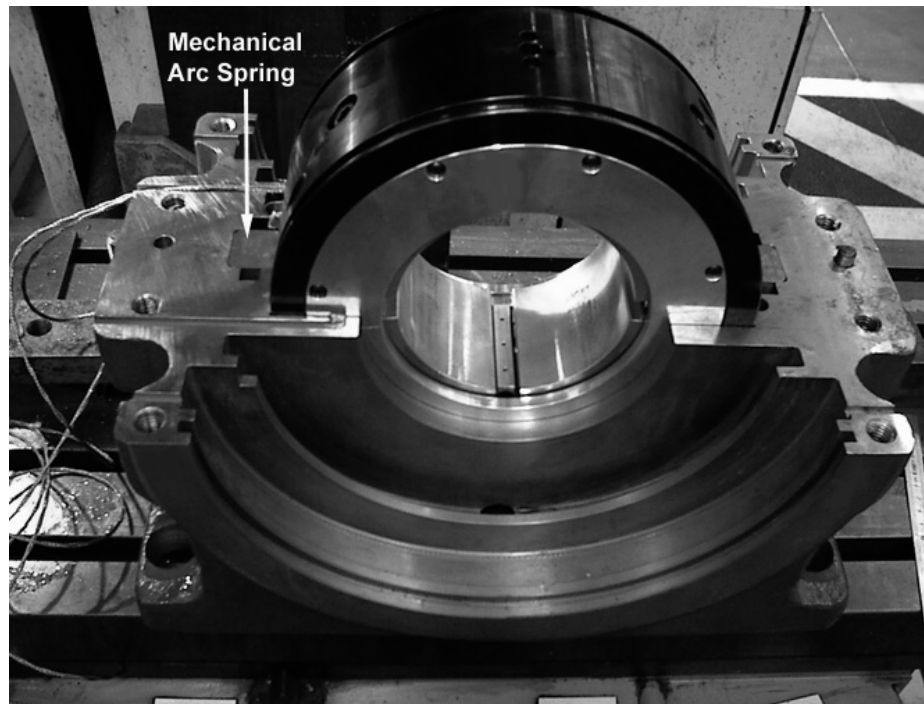


Figure 3-23—Mechanical Arc Spring Supported Squeeze Damper

3.3.4.5 Design Procedure

There is no single procedure that would adequately cover the design of a squeeze film damper for every application. Most designs and analysis procedures have evolved through the practical experience of the individual or manufacturer applying them. As a practical guide, however, the following general procedure is suggested:

- Identify the purpose of the squeeze film damper: eliminate subsynchronous instability or reduced critical speed synchronous response.
- Perform rotordynamic simulations to determine the optimum damping required to suppress the selected phenomena. If used to enhance stability, include all known destabilizing forces.
- Choose the damper design considering the available space and configuration of the machine. Determine centering device, end seal preference, and lubricant supply arrangement.
- Calculate the squeeze film damper stiffness and damping coefficients using the appropriate equations from Table 1 or, if available, a computer code. An eccentricity ratio of 0.4 should be used to calculate the damper coefficients.
- Add the squeeze film damper coefficients with the stiffness of the centering device. These coefficients are in parallel.
- Combine the resultant coefficients from the above step with the bearing oil film coefficients. Include the support values as appropriate. These coefficients are in series.

g. Input the resultant coefficients into an appropriate rotordynamics computer program to predict stability or synchronous response.

A useful design tool for optimizing damper stability performance is a stability map as shown in Figure 3-24 [4]. In this example, damper or support damping is plotted as a function log decrement for several damper stiffness values. Clearly, a near optimum squeeze film damper stiffness and damping range can be extracted from the map. For this case, a stiffness range of 50,000 – 100,000 lb/in. and a damping range of 500 – 1,000 lb-sec/in. would be near optimum. Design efforts to obtain these values can then be attempted by varying damper clearance and axial length.

3.3.4.6 General Comments

A squeeze film damper is an excellent design tool that can be used to improve the vibration characteristics of rotors by adding damping to either stabilize otherwise unstable machinery or reduce synchronous vibration amplitudes while passing through critical speeds. Research is continuing into the development of more advanced squeeze film models in an attempt to include the more detailed effects of fluid dynamic cavitation, two phase flows, and end seals on damper performance. Nevertheless, provided oil film cavitation is not excessive and the L/D ratio small (< 0.5), squeeze film dampers can be adequately modeled and successfully applied using the incompressible fluid Reynolds' equation based on the short bearing model.

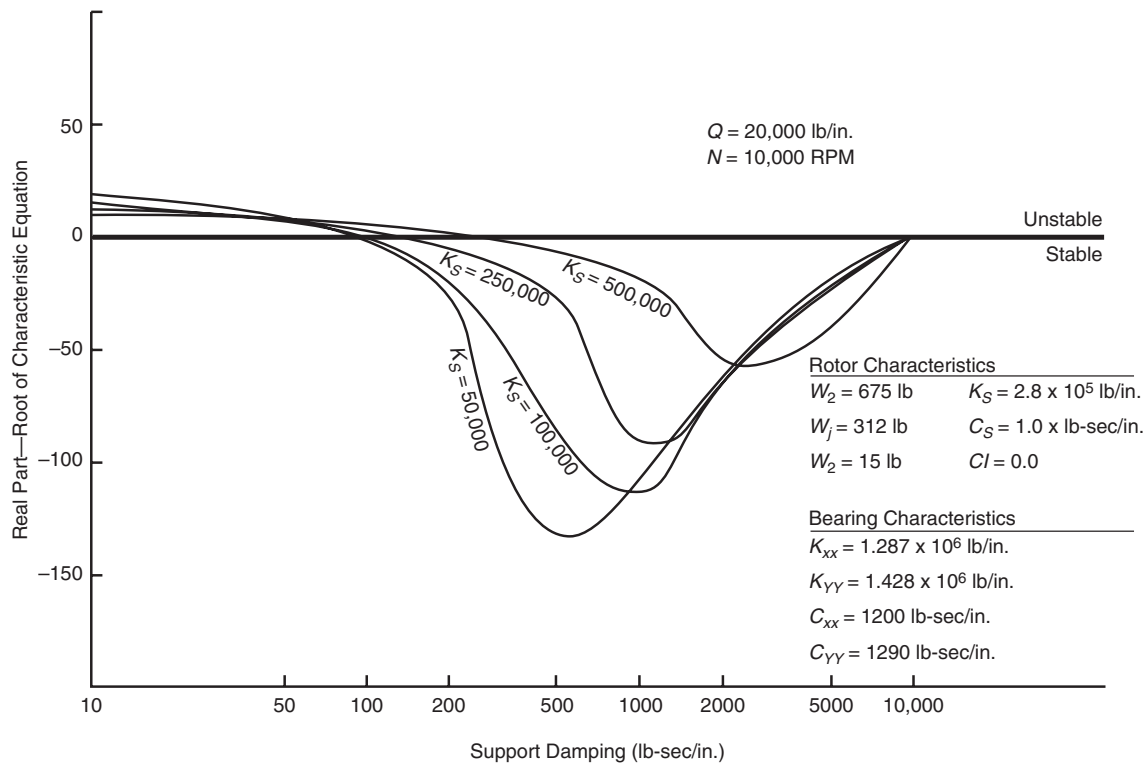


Figure 3-24—Squeeze Film Damper Stability Map

It must be recognized that with a damper the resultant damping will always be less than the tilting pad bearing damping. The overall stiffness, therefore, must also be lowered to allow rotor motion at the bearings in order to make the available damping more effective. Even so, the stiffness of the centering device and the clearance of the damper cavity must be chosen carefully to insure that the supports are not under or over-damped. Over damped supports may lockup and significantly reduce the effectiveness of the damping. This condition can be avoided by not specifying too small a clearance cavity and by insuring that the damper is well centered within the cavity. The latter is of particular concern since the stiffness and damping coefficients are highly nonlinear functions of eccentricity, sharply increasing at values of eccentricity ratio above 0.4.

3.3.4.7 References

1. Zeidan, F. Y., San Andres, L. and Vance, J. M., 1996, "Design and Application of Squeeze Film Dampers in Rotating Machinery," Proceedings of the Twenty-Fifth Turbomachinery Symposium, Turbomachinery Laboratory, Texas A&M University, College Station, Texas, pp. 169 – 188.
2. Leader, M. E., Whalen, J. K., Hess, T. D. and Grey, G. G., 1995, "The Design and Application of a Squeeze Film Damper Bearing to a Flexible Steam Turbine Rotor," Proceedings of the Twenty-Fourth Turbomachinery Symposium, Turbomachinery Laboratory, Texas A&M University, College Station, Texas, pp. 49 – 57.
3. Edney, S. L. and Nicholas, J. C., 1999, "Retrofitting a Large Steam Turbine with a Mechanically Centered Squeeze Film Damper Bearing," Proceedings of the Twenty-Eighth Turbomachinery Symposium, Turbomachinery Laboratory, Texas A&M University, College Station, Texas, pp. 29 – 40.
4. Gunter, E. J., Barrett, L. E. and Allaire, P. E., 1975, "Design and Application of Squeeze Film Dampers for Turbomachinery Stabilization," Proceedings of the Fourth Turbomachinery Symposium, Turbomachinery Laboratory, Texas A&M University, College Station, Texas, pp. 127 – 141.
5. Diaz, S. E. and San Andres, L. A., 1997, "Forced Response of SFDs Operating with a Bubbly (Air/Oil) Mixture," Texas A&M University Turbomachinery Research Consortium Progress Report, TRC-SFD-1-97.
6. Diaz, S. E. and San Andres, L. A., 1999, "Reduction of the Dynamic Load Capacity in a Squeeze Film Damper Operating with a Bubbly Lubricant," *ASME Journal of Gas Turbines and Power*, 121, pp. 703 – 709.
7. Nicholas, J. C., Whalen, J. K. and Franklin, S. D., 1986, "Improving Critical Speed Calculations Using Flexible Bearing Support FRF Compliance Data," Proceedings of the Fifteenth Turbomachinery Symposium, Turbomachinery

Laboratory, Texas A&M University, College Station, Texas, pp. 69 – 78.

8. Kuzdzal, M. J. and Hustak, J. F., 1996, “Squeeze Film Damper Bearing Experimental vs. Analytical Results for Various Damper Configurations,” Proceedings of the Twenty-Fifth Turbomachinery Symposium, Turbomachinery Laboratory, Texas A&M University, College Station, Texas, pp. 57 – 70.

9. Nicholas, J. C., Edney, S. L., Matthews, T. and Varela, F. J. M., 2001, “Eliminating a Rub Induced Start-Up Vibration Problem in an Ethylene Drive Steam Turbine,” Proceedings of the Thirtieth Turbomachinery Symposium, Turbomachinery Laboratory, Texas A&M University, College Station, Texas, pp. 65 – 78.

Nomenclature

c_r = Damper radial clearance, m (in.),

C_b = Bearing direct damping, N-s/m (lbf-s/in.),

C_d = Squeeze film direct damping, N-s/m (lbf-s/in.),

C_s = Support direct damping, N-s/m (lbf-s/in.),

D = Damper diameter, m (in.),

K_b = Bearing direct stiffness, N/m (lbf/in.),

K_d = Squeeze film direct stiffness, N/m (lbf/in.),

K_{ds} = Damper centering device spring stiffness, N/m (lbf/in.),

K_s = Support direct stiffness, N/m (lbf/in.),

L = Damper axial length, m (in.),

M = Journal mass, kg (lbm),

M_d = Damper mass, kg (lbm),

M_s = Support mass, kg (lbm),

R = Damper radius, m (in.),

ε = Damper eccentricity ratio, dim,

μ = Oil viscosity, Pa-s (lbf-s/in.²),

ω = Whirl frequency, rad/s.

3.4 SEALS

3.4.1 Oil Seals

The analysis to determine the influence of oil seals on the dynamic stability of the compressor rotor is essential for modern centrifugal compressors. The influence on forced

response was discussed in 2.6.2. The cross-section of a common oil bushing seal is shown in Figure 2-48. The outer seal ring is of major concern due to the high axial force that can lock the otherwise floating outer ring to the compressor casing. A typical pressure distribution for an outer ring is shown in Figure 2-49. Figures for other common oil seal designs are given in Figures 2-51 through 2-53.

Early oil seal analyses [1,2] used a constant operating oil film temperature obtained by an approximate temperature flow balance. An improved linear axial temperature distribution was used in the later analyses [3,4]. More recent publications [5,6] included the solution of the energy equation for a better estimation of the temperature distribution in an oil seal ring where the finite element technique was used to perform the thermo-hydrodynamic analysis. The influence of the circumferential grooves, tapered bore and axial grooves on the seal characteristics and the dynamic stability of the compressor rotor can also be estimated by the finite element method discussed in these more recent publications.

The two dimensional pressure and temperature distributions in the seal can be determined by solving the Reynolds and the energy equations respectively. The domain is made up of a thin fluid film between the rotor and the seal. This problem is not axi-symmetric because the fluid film around the rotor is not of constant thickness. Consequently, the governing equations must be solved over the whole domain.

These governing equations, Reynolds equation for pressure and the energy equations for temperature, are coupled and non-linear as the viscosity depends on both pressure and temperature while the density and specific heat depend on temperature. The Reynolds and the energy equations can be solved using a finite element iterative technique to obtain the pressure and temperature distributions in a seal ring. A detailed explanation of the finite element iterative technique is given in Baheti [7]. The hydrodynamic forces are obtained by integrating the pressure distribution axially and circumferentially. The stiffness and damping coefficients of the seal are determined using a perturbation technique.

The majority of centrifugal compressor design evaluation for oil seals is currently conducted using a simplified analysis as outlined in Kirk [2]. Multiple rings and circumferential grooving is found in modern high-pressure compressor end seals. The eight stiffness and damping coefficients for estimated design point operating eccentricity ratio are used in standard damped critical speed stability analysis evaluation. The computed average film temperature is used for the calculation at each speed point.

It is important to note that the influence of high-pressure oil seal should not be evaluated using 180 degree cavitated bearing coefficients. Important considerations for stability include the diameter and length of the seal land region, the operating clearance and the location and width of the casing sealing lip contact area. More extensive design guidelines are given in [2].

An example of frequency content for locked oil ring instability is shown in Figure 3-25 where the rotor is showing a strong sub-synchronous excitation of its first critical speed. Solutions to this type instability are dedicated to reducing the cross coupling and focus on either reducing this directly (larger clearances, circumferential grooves) or by improving the bushing's centering capability (soft starts, pressure balancing the bushing, tapering, reducing bushing weight). This is the type of oil seal induced rotor instability that can be predicted and prevented with a damped critical speed stability analysis that includes the oil seals.

The other major type of instability produced by oil seals is a low order tracking instability shown in Figures 3-26 and 3-27. Here the ring is not properly seated to the case and is driving the rotor at a frequency proportional to rotational speed and not at a system critical speed frequency. The solution to this could be a better surface finish on the sealing lip or reduced distortion of the casing end wall or an increased pressure drop across the sealing lip to prevent the ring from freely moving. This type of oil seal ring instability cannot be predicted or prevented with a damped natural frequency stability analysis.

One of the few papers documenting ring seal monitoring during compressor mechanical shop testing is discussed in Emerick [8] for one particular type of seal design. It is very difficult to get probes into the high-pressure cartridge. Tests conducted in a static seal test rig to evaluate effective fric-

tion factors are discussed in Kirk and Browne [9]. Overall, there exist very little experimental results to correlate with predictions.

3.4.1.1 References

1. Kirk, R. G. and Miller, W. H., 1979, "The Influence of High Pressure Oil Seals on Turbo-Rotor Stability," *ASLE Transactions*, 22 (1), pp. 14 – 24.
2. Kirk, R. G., 1986, "Oil Seal Dynamics: Considerations for Analysis of Centrifugal Compressors," Proceedings of the Fifteenth Turbomachinery Symposium, Turbomachinery Laboratory, Texas A&M University, College Station, Texas, pp. 25 – 34.
3. Reedy, S. W. and R. G. Kirk, 1992, "Advanced Analysis of Multi-Ring Liquid Seals," *ASME Journal of Vibration and Acoustics*, 114 (1), pp. 42 – 46.
4. Kirk, R. G. and S. W. Reedy, 1990, "Analysis of Thermal Gradient Effects in Oil Ring Seals," *STLE Tribology Transactions*, 33 (3), pp. 425 – 435.
5. Baheti, S. K. and Kirk, R. G., 1994, "Thermo-Hydrodynamic Solution of Floating Ring Seals for High Pressure Compressors Using Finite-Element Method," *STLE Tribology Transactions*, 37 (2), pp. 336 – 346.

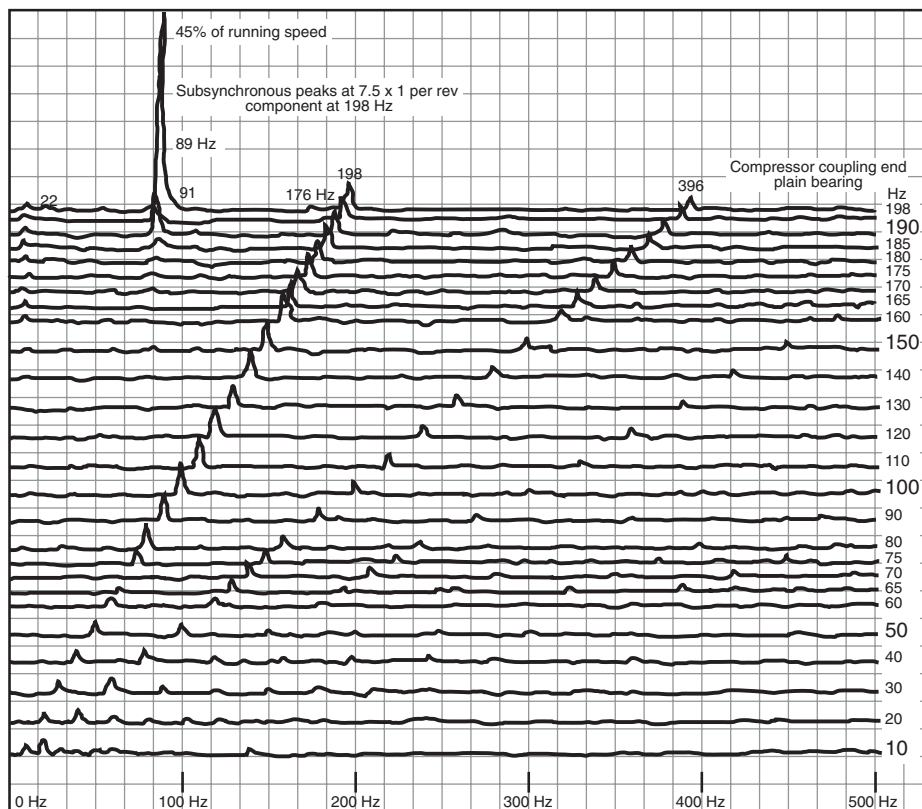


Figure 3-25—Re-excitation of Rotor First Critical from Oil Seal Excitation

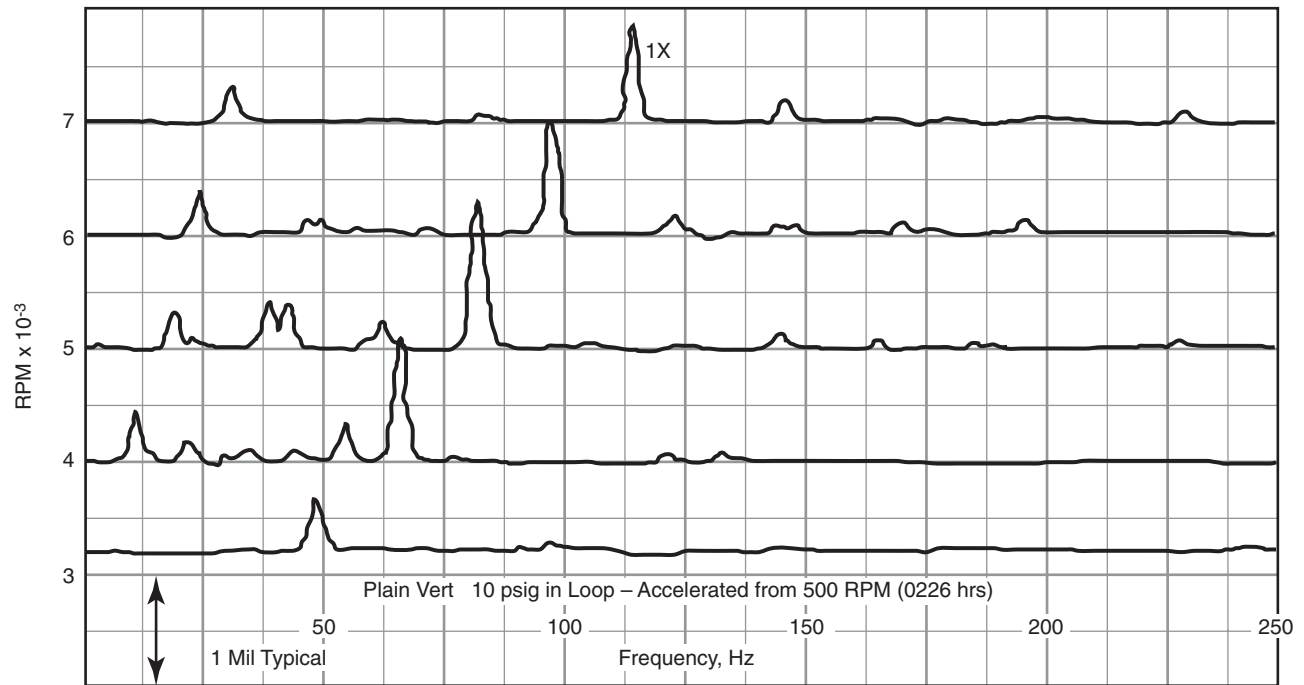


Figure 3-26—Rotor Tracking Instability from Low-pressure Oil Seal Test

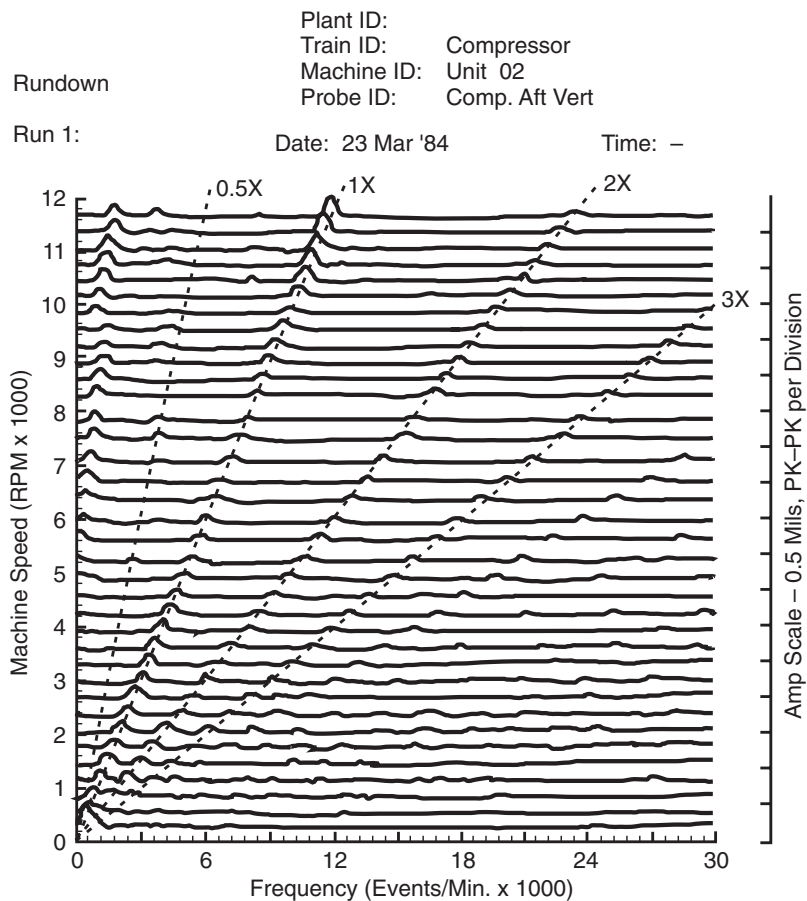


Figure 3-27—Rotor Tracking Instability from Distorted Oil Seal Lip Contact Area

6. Baheti, S. K. and Kirk, R. G., 1995, "Finite Element Thermo-Hydrodynamic Analysis of a Circumferentially Grooved Floating Oil Ring Seal," *STLE Tribology Transactions*, 38 (1), pp. 86 – 96.
7. Baheti, S. K., 1995, "Non-linear Finite Element Thermo-Hydrodynamic Analysis of Oil Ring Seals Used in High Pressure Centrifugal Compressors," Ph.D. Dissertation, Virginia Polytechnic Institute and State University, Blacksburg, Virginia.
8. Emerick, M., F., 1982, "Vibration and Destabilizing Effects of Floating Ring Seals in Compressors," NASA CP-2250, pp. 187 – 204.
9. Kirk, R. G. and D. B. Browne, 1990, "Experimental Evaluation of Holding Forces in Floating Ring Seals," *Proceedings of the IFTOMM International Conference*, Lyon, France, pp. 319 – 323.

3.4.2 Labyrinth Seals

One major goal for turbomachinery designers is to reduce seal leakage flow resulting in increased overall machine efficiency. This results in a desire for reduced clearances at all internal labyrinth seal locations. For a back-to-back centrifugal compressor configuration, there is a large labyrinth seal at mid-span called a balance piston which balances and reduces the thrust load, thereby reducing the size of the thrust bearing. The large pressure drop across the balance piston and the interaction of the gas flow in the small seal clearance spaces produce considerable destabilizing excitation forces that can potentially drive the rotor unstable. Since these forces are produced at or near rotor mid-span, which coincides with the point of maximum rotor deflection, their effect on rotor stability is maximized.

For series flow compressors, the balance piston is located closer to a bearing centerline. Hence, it is often considered to have less of an influence on rotor stability compared to a mid-span located balance piston. However, for series flow compressors with shaft end seals, the balance piston is located near the rotor's quarter-span region. At this location and with a typical rotor first bending mode shape, the balance piston will have significant modal influence on rotor stability.

In addition to the balance piston, a compressor with covered impeller stages also has seals at each of the impellers, located at the impeller eye (impeller eye seals) and on the shaft between adjacent impellers (inter stage shaft seals).

In the late 1960s and early 70s, an analytical calculation method to predict compressor shaft seal influence on dynamic stability did not exist. A method for computing multi-mass flexible rotor system stability was also unavailable. In the early to mid 1970s, computer analyses capable of predicting damped eigenvalues, and hence stability, were developed using both transfer matrix and finite element methods (see 3.1.1). By the late 1970s and 80s, a large percentage of

analytical rotordynamic research concerned oil and labyrinth seals. The analysis of floating oil ring seals (see 3.4.1), turbulent pump seals and gas labyrinth seals [1–6] were the key areas of development. Computer codes are now readily available to most turbomachinery designers to predict labyrinth seal stiffness and damping effects.

Figure 3-28 shows a typical configuration for the last stage of a centrifugal compressor depicting an impeller eye seal, an inter stage shaft seal and a typical balance piston seal configuration, Kirk [6]. The balance piston leakage flows down the backside of the impeller and across the balance piston labyrinth seal. The flow path between the impeller and the adjacent diaphragm of this particular example shows a converging section. Typically, the swirl velocity associated with the gas exit angle from the impeller blades is approximately 60% of impeller tip speed. This velocity will vary with the impeller's blade exit angle and with the amount of volume passing through the impeller. For the configuration shown, the entry swirl ratio for the balance piston will increase to 80% or more. When the flow passes through this balance piston seal, there is potentially a large cross coupling force generated, which may drive the rotor system unstable. A similar effect results from the impeller eye seal leakage that flows between the cover disc of the impeller and the adjacent diaphragm. The swirling gas flow along the impeller cover enters the labyrinth eye seal at a swirl rate of typically 50% – 70% of the surface speed of the impeller cover section at which the eye seal is located.

A flow is also created across the inter stage shaft seal due to the differential pressure across the diaphragm between stages. The pressure differential is created by the conversion of velocity head from the preceding impeller into static pressure through the diaphragm. Inter stage shaft seal leakage flows from the region upstream of an impeller entry through the inter stage shaft seal up through the passage formed by the previous impeller's hub disc and adjacent diaphragm. This flow mixes with the previous impeller's discharge flow. Thus, the entry swirl for an inter stage shaft seal can be from 20% – 50% of the impeller entry surface velocity.

All labyrinth seals have a forward driving mechanism for entry swirls in the range of 20% and higher. Although unlikely, lower entry swirl ratios or negative entry swirl can drive the system in backward whirl instability. The labyrinth seals are a likely source of forward driving sub-synchronous excitation for rotating machinery [4,5].

One solution to labyrinth excitation is larger clearances, but this lowers efficiency. A larger chamber size or tooth volume is also a design factor to reduce the cross coupled stiffness. Tooth spacing can be increased to reduce jet effect leakage, but longer spacing produces a larger net force on the rotor for a given pressure field. Therefore, of all the options to reduce a labyrinth seal's destabilizing nature, the most attractive becomes controlling the entry swirl. Often, this may not be enough to suppress an instability and other seal types may

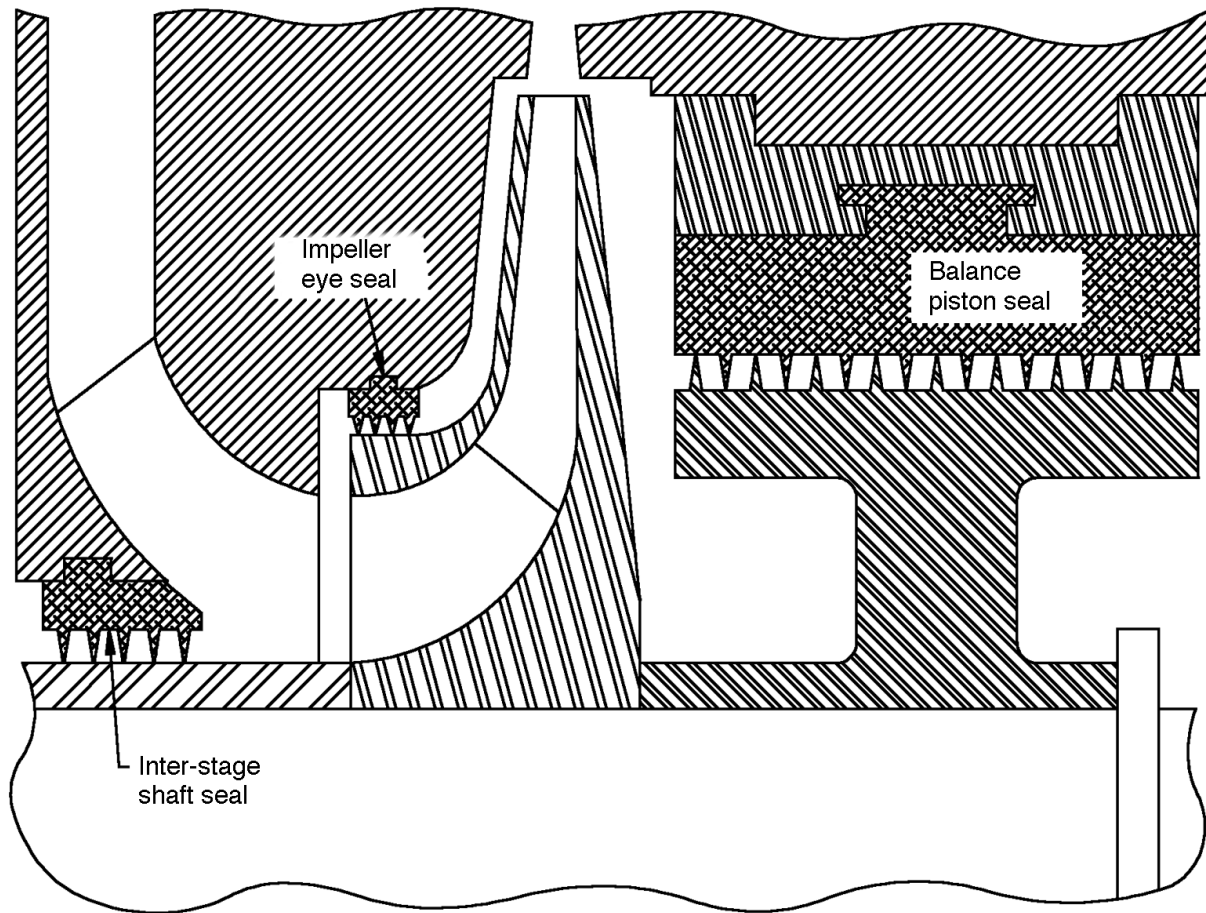


Figure 3-28—Typical Configuration for the Last Stage of a Series Flow Compressor Showing the Impeller Eye Seal, the Inter Stage Seal and a Typical Balance Piston Seal

be required such as a honeycomb or a hole pattern seal (see 3.4.3).

To reduce entry swirl velocity, most compressor manufacturers have used shunt lines, internal to the diaphragm, to reduce the volume of gas entering the balance piston seal or to produce a slight reverse blocking flow at the balance piston entrance, Kanki, et al. [7] (Figure 3-29). Unfortunately, when the compressor operates at volumes beyond the last stage impeller design point, the shunt differential pressure decreases thereby decreasing the effectiveness of the shunt line to block or reduce entry swirl. Other methods of providing aerodynamic or mechanical flow turning, commonly referred to as swirl brakes, have also been utilized with a great deal of success to force near zero swirl at the seal entrance, Childs and Ramsey [8], Moore, et al. [9] (Figure 3-30).

Figure 3-31 shows a compressor spectrum plot for (a) inert gas and (b) process gas during full load test runs. The increased molecular weight of the process gas results in a labyrinth seal induced compressor instability. The instability in (b), caused by the balance piston labyrinth seal, produces a

forward driving force that excites the rotor's first critical speed. This type of instability can be predicted and prevented with a damped critical speed stability analysis that carefully includes the labyrinth seals.

With the importance of labyrinth seal behavior on rotor stability known and demonstrated, testing efforts ran concurrently with the analytical development. Benckert [1,10,11] was the first published results of the stiffness coefficients of labyrinth gas seals. Teeth-on-stator seals were tested for interlocking, smooth, and stepped rotor configurations. Much of the data was for non-rotating seals at low pressures. Damping coefficients were not obtained since only static pressure measurements of the individual chambers were made. Kwanka, et al. [12] as well as Thieleke and Stetter [13] have also carried out similar efforts.

Wright [14] tested various configurations of a single cavity seal. While limited in its application, the results did provide insight into the effects of pressure drop, clearance divergence or convergence and forward or backward whirl of a seal. Leong and Brown [15] investigated various teeth-on-stator configurations for variations of pressure, rotor speed, geome-

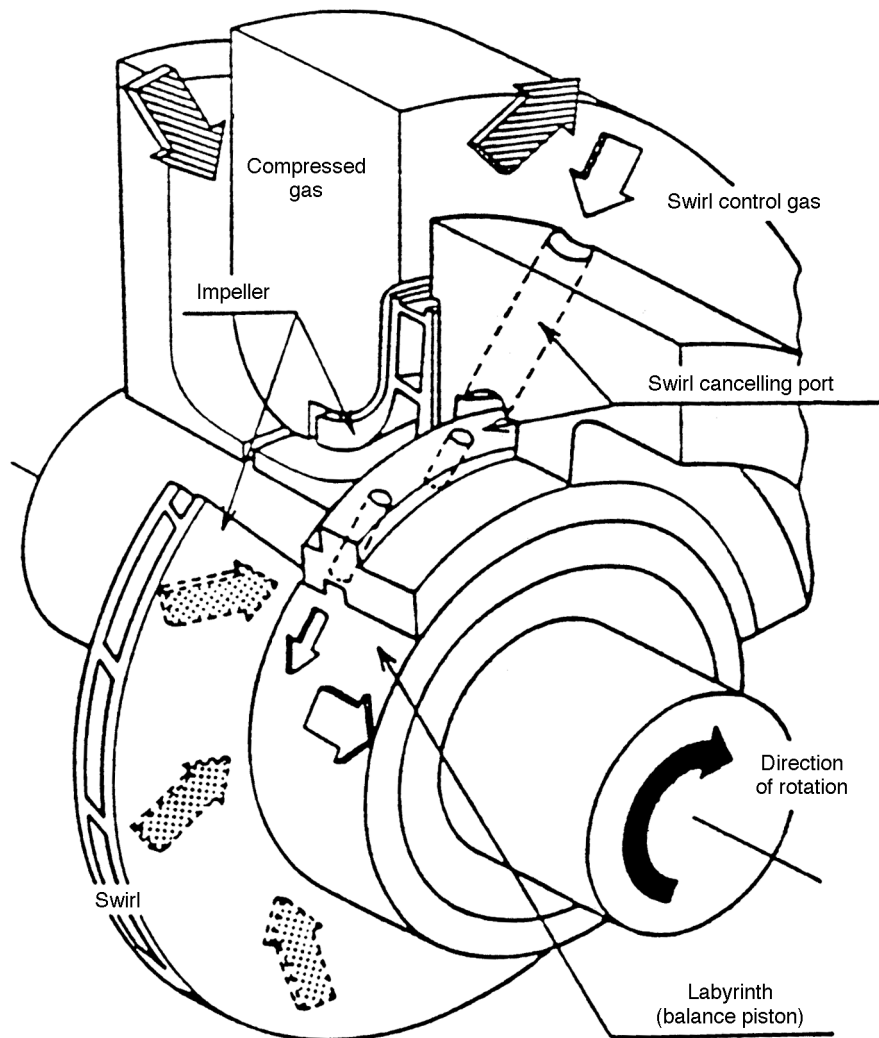


Figure 3-29—Typical Shunt Line Schematic to Reduce Entry Swirl

try and inlet tangential velocity. Again, damping was not considered.

On the basis of the results from Benckert [11] and recalculations made for various stable compressors, it was determined that stiffness-only measurements were incomplete. Damping needed to be considered to accurately determine the dynamic behavior of labyrinth gas seals.

The research summarized in Childs [16] provided the first measurements of the stiffness and damping coefficients. While the results gave the first comprehensive basis for comparison against predictions, [8] revealed the importance of testing at or near the application conditions. The test rig was extended toward this goal by Childs and Scharer [17] and then again by Elrod, et al. [18]. Teeth-on-stator, teeth-on-rotor, and interlocking configurations were tested.

Wagner and Steff [19] developed a test rig supported by magnetic bearings. The intent of the rig was to further expand the existing knowledge database to geometries and gas conditions matching industrial applications, namely, pressure differential, size and speed. The magnetic bearings made it possible to set the eccentricity and superimpose circulatory movement independent of speed. The rig permitted the inlet pressure and the backpressure to be set independently of one another. Pressures of 70 bar were possible at surface speeds up to 157 m/s.

3.4.2.1 References

1. Benckert, H. and Wachter, J., 1980, "Flow Induced Spring Coefficients of Labyrinth Seals for Application to Rotordynamics," NASA CP-2133, pp. 189 – 212.

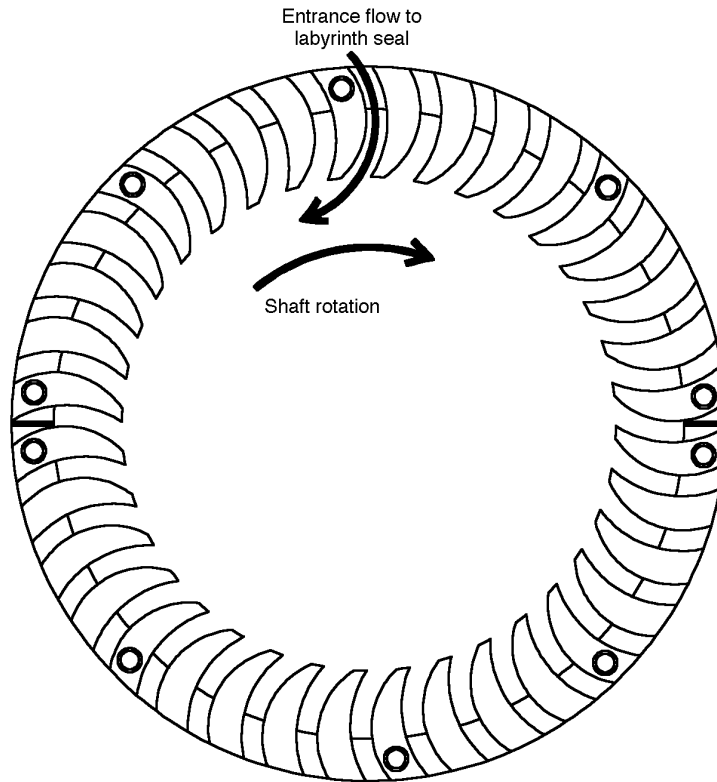


Figure 3-30—Typical Swirl Brake Schematic to Reduce Entry Swirl

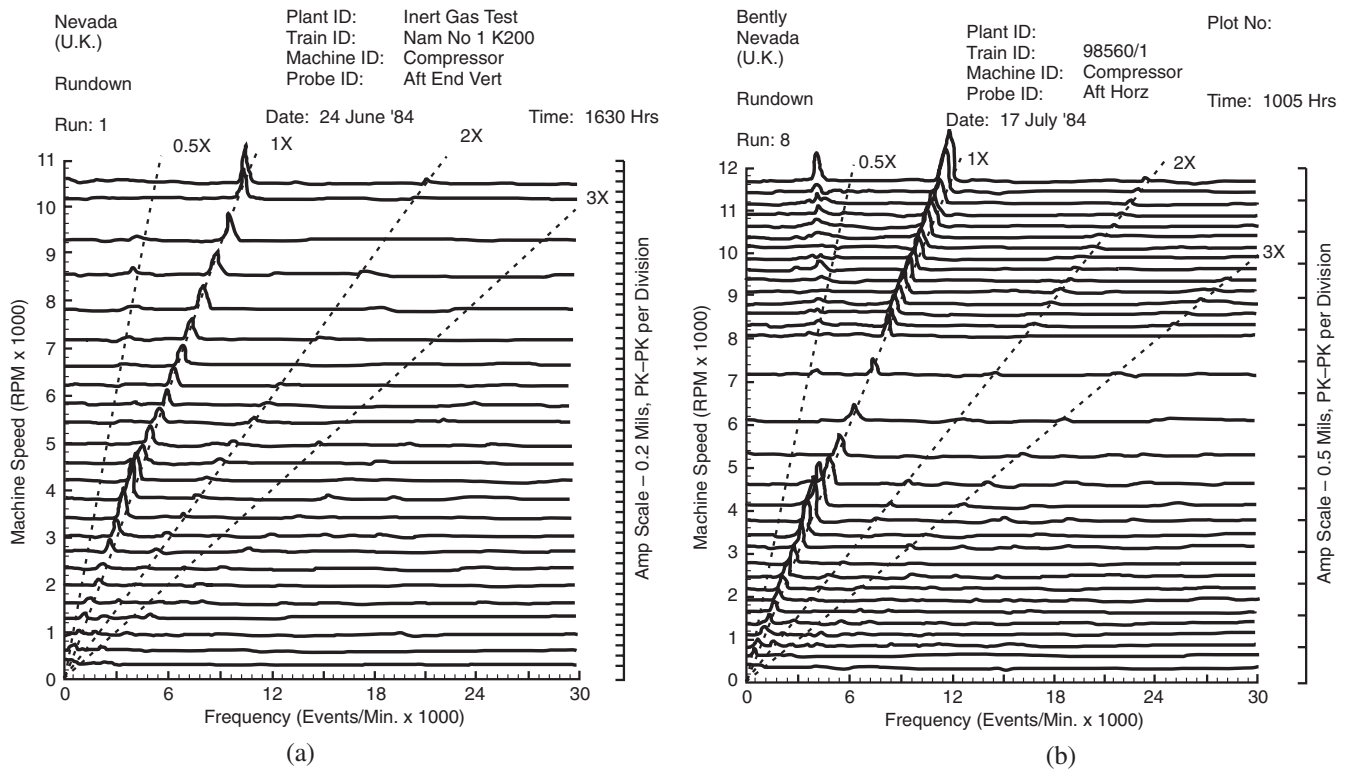


Figure 3-31—Compressor on Full Load Test: With Inert Gas Showing no Instability at Rotor First Critical Frequency, [20], with Process Gas Showing Instability from Balance Piston Excitation, [5, 20]

2. Iwatsubo, T., Matooka, N. and Kawai, R., 1982, "Spring and Damping Coefficients of the Labyrinth Seal," NASA CP-2250, pp. 205 – 222.
3. Childs, D. W. and Scharrer, J. K., 1986, "An Iwatsubo-Based Solution for Labyrinth Seals: Comparison to Experimental Results," *ASME Journal of Engineering for Gas Turbines and Power*, 108 (2), pp. 325 – 331.
4. Kirk, R. G., 1988, "Evaluation of Aerodynamic Instability Mechanisms for Centrifugal Compressors - Part I: Current Theory," *ASME Journal of Vibration, Acoustics, Stress, and Reliability in Design*, 110 (2), pp. 201 – 206.
5. Kirk, R. G., 1988, "Evaluation of Aerodynamic Instability Mechanisms for Centrifugal Compressors - Part II: Advanced Analysis," *ASME Journal of Vibration, Acoustics, Stress, and Reliability in Design*, 110 (2), pp. 207 – 212.
6. Kirk, R. G., 1990, "A Method for Calculating Labyrinth Seal Inlet Swirl Velocity," *ASME Journal of Vibration and Acoustics*, 112 (3), pp. 380 – 383.
7. Kanki, H., Katayama, K., Morii, S., Mouri, Y., Umemura, S., Ozawa, U. and Oda, T., 1988, "High Stability Design for New Centrifugal Compressor," *Rotordynamic Instability Problems in High-Performance Turbomachinery*, NASA CP-3026, pp. 445 – 459.
8. Childs, D. W., and Ramsey, C., 1991, "Seal Rotordynamic-Coefficient Test Results for a Model SSME ATD-HPFTP Turbine Interstage Seal With and Without a Swirl Brake," *ASME Journal of Tribology*, 113, pp. 113 – 203.
9. Moore, J. J., and Hill, D. L., 2000, "Design of Swirl Brakes for High Pressure Centrifugal Compressors Using CFD Techniques," Proceedings of the Eighth International Symposium of Transport Phenomena and Dynamics of Rotating Machinery (ISROMAC-8), March 26-30, Honolulu, Hawaii, pp. 1124 – 1132.
10. Benckert, H. and Wachter, J., 1979, "Investigations on the Mass Flow and the Flow Induced Forces in Contactless Seals of Turbomachines," Proceedings of the Sixth Conference on Fluid Machinery, Scientific Society of Mechanical Engineers, Akad miaki Kikado, Budapest, pp. 57 – 66.
11. Benckert, H., 1980, "Strömungsbedingte Federkennwerte in Labyrinthdichtungen," Doctoral Dissertation, Universität Stuttgart.
12. Kwanka, K., Ortinger, W. and Steckel, J., 1993, "Calculation and Measurement of the Influence of Flow Parameters on Rotordynamic Coefficients in Labyrinth Seals," *Rotordynamic Instability Problems in High-Performance Turbomachinery*, NASA CP-3239, pp. 209 – 218.
13. Thieleke, G. and Stetter, H., 1990, "Experimental Investigations of Exciting Forces Caused by Flow in Labyrinth Seals," *Rotordynamic Instability Problems in High-Performance Turbomachinery*, NASA CP-3122, pp. 109 – 134.
14. Wright, D. V., 1983, "Labyrinth Seal Forces on Whirling Rotor," Rotordynamical Instability, Proceedings of the ASME Applied Mechanics, Bioengineering, and Fluids Engineering Conference, June 20-22, Houston, Texas, pp. 19 – 31.
15. Leong, Y. and Brown, D., 1984, "Experimental Investigation of Lateral Forces Induced by Flow Through Model Labyrinth Seals," *Rotordynamic Instability Problems in High-Performance Turbomachinery*, NASA CP-2388, pp. 187 – 210.
16. Childs, D. W., 1993, *Turbomachinery Rotordynamics: Phenomena, Modeling, and Analysis*, John Wiley & Sons, Inc., New York.
17. Childs, D. W. and Scharrer, J. K., 1986, "Experimental Rotordynamic Coefficient Results for Teeth-on-Rotor and Teeth-on-Stator Labyrinth Gas Seals," ASME 86-GT-12.
18. Elrod, D. A., Pelletti, J. M. and Childs, D. W., 1995, "Theory Versus Experiment for the Rotordynamic Coefficients of an Interlocking Labyrinth Gas Seal," ASME paper 95-GT-432, presented at the International Gas Turbine and Aeroengine Congress and Exposition, Houston, Texas, June 5 – 8.
19. Wagner, N. G. and Steff, K., 1996, "Dynamic Labyrinth Coefficients From a High-Pressure Full-Scale Test Rig Using Magnetic Bearings," *Rotordynamic Instability Problems in High-Performance Turbomachinery*, NASA CP-3344, pp. 95 – 111.
20. Kirk, R. G. and Simpson, M., 1985, "Full Load Shop Testing of 18,000 HP Gas Turbine Driven Centrifugal Compressor for Offshore Platform Service: Evaluation of Rotordynamics Performance," *Instability in Rotating Machinery*, NASA CP-2409, pp. 1 – 13.

3.4.3 Honeycomb and Other Seals

Historically, as operating conditions across annular compressor shaft seals have become more extreme (higher pressure differential, higher gas density, and increased speed), a corresponding decrease in rotor stability has been manifested. Oil and labyrinth seals have been the mainstay of the industry for many years and have been discussed above. Oil seals have been largely replaced by dry gas seals due in part to stability and environmental concerns. In some cases an alternative to labyrinth seals is required to obtain stable operation. However, industry has been slower to embrace alternatives to ordinary toothed labyrinth seals and today does so on a case-by-case basis as dictated by stability calculations or existing unstable operation. A delicate balance between the economics of cost and the technical benefit usually controls seal selection.

Theoretical analyses have shown that toothed annular seals can develop relatively high cross coupled stiffness and low direct damping values which in turn give rise to excessive

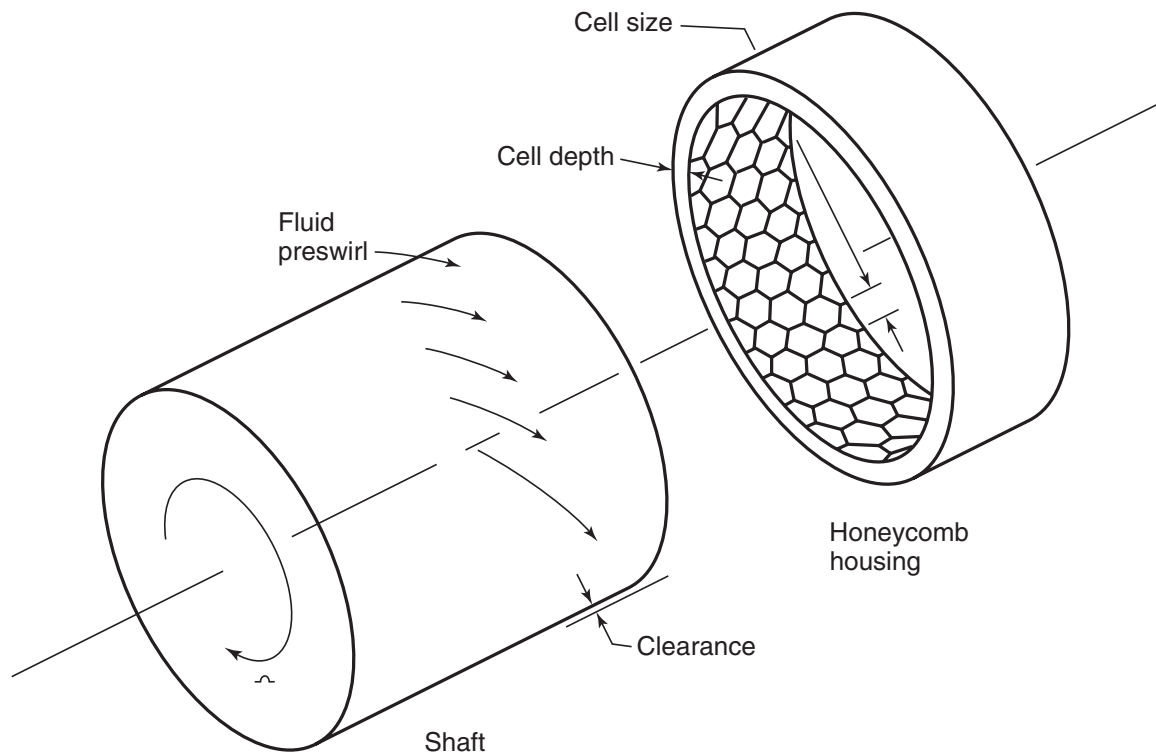


Figure 3-32—Honeycomb Seal Arrangement

destabilizing forces exerted on the rotor (see 3.4.2). These are the same bad actors that have driven tremendous development advances in bearing design. While not all seal rotordynamic coefficient analyses have been verified with test rigs operating at or near field conditions, enough work has been done to obtain a general qualitative understanding and provide direction for an experienced designer in applying solutions to achieve increased stability margins.

In simple terms, investigations have shown the originating phenomena for destabilizing forces in annular seals to be at least partially due to the circumferential swirling velocity component of an axial leakage flow in close clearance spaces between rotor and stator. This occurs at seals associated with balance pistons, impeller eyes, and interstage division walls. While the leakage flow cannot be avoided, its characteristics and interactions with the rotor and stator have been successfully controlled to provide a reduced detrimental effect on stability and in some cases to reportedly improve rotor stability.

Two common approaches of controlling the destabilizing influences arising in compressor seals are entry swirl reduction and cavity isolation. The former reduces or eliminates the circumferential velocity component of the flow before the fluid actually enters the seal. This can be accomplished with what are commonly called swirl brakes that redirect the flow into a more axial direction (and possibly into an anti-rotation direction) and/or by shunt injection (see 3.4.2).

The second approach relies on various cavity isolation techniques to reduce swirl and increase direct damping, thereby reducing the seal's destabilizing effects. When properly applied, alternative annular seals can prevent destabilizing forces from building to unacceptable levels. Some examples of cavity isolation are honeycomb, hole pattern, and pocketed labyrinth seals, which can be referred to generically as damper seals. All three typically consist of a smooth rotor and a "roughened" stator. While the roughened stator is effective in reducing the circumferential velocity component of the leakage flow (i.e., reducing swirl), swirl brakes are often used in conjunction with these seals.

Honeycomb seals usually replace the tooth on stator labyrinth design with a metallic material insert with individual cells shaped in a honeycomb pattern. This is illustrated in Figure 3-32 from Childs [1]. Cell size and depth along with overall seal length and clearance are parameters that can be varied to optimize the dynamic characteristics of the honeycomb seal. Research indicates that these dynamic characteristics may be strongly frequency dependent due to the acoustic frequencies of the cells, Kleynhans, and Childs [2].

Typically the honeycomb material cannot support the high axial forces by itself and is thus contained as an insert in a carrier. Only very limited contact with the rotor can be tolerated before the honeycomb is damaged. If enough cells are damaged, the effectiveness of the seal may be diminished. Additionally, some believe that the honeycomb cells

are small enough to be susceptible to fouling (i.e., filling in of the honeycomb cells). However, to date, there is no published supporting evidence to say that damaged cells or fouling contributes to the reduction in the damping effectiveness of the seal.

Figure 3-33 from Yu and Childs [3] shows a honeycomb seal compared to a hole pattern seal that use a smooth rotor running against a stator surface filled with radial holes or dimples. Hole diameter, depth, spacing, clearance and seal length are optimization parameters. This seal can be manu-

factured from a solid piece and thus be more robust, being able to withstand some contact with the rotor without a significant decay of damping properties. Figure 3-34, [3], shows a relative comparison of surface area for 3 different hole pattern geometries and a honeycomb pattern.

Pocketed design seals implement cavity isolation by incorporating multiple radial blades or baffles within a conventional tooth on stator labyrinth design as shown in Figure 3-35, Richards, Vance et, al. [4].

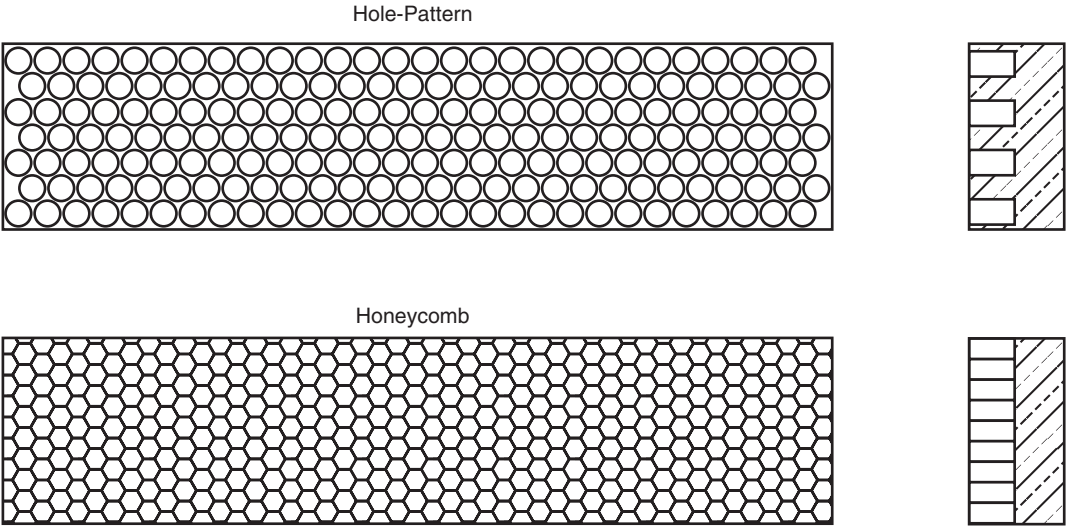


Figure 3-33—Comparison of Honeycomb and Hole Pattern Seals

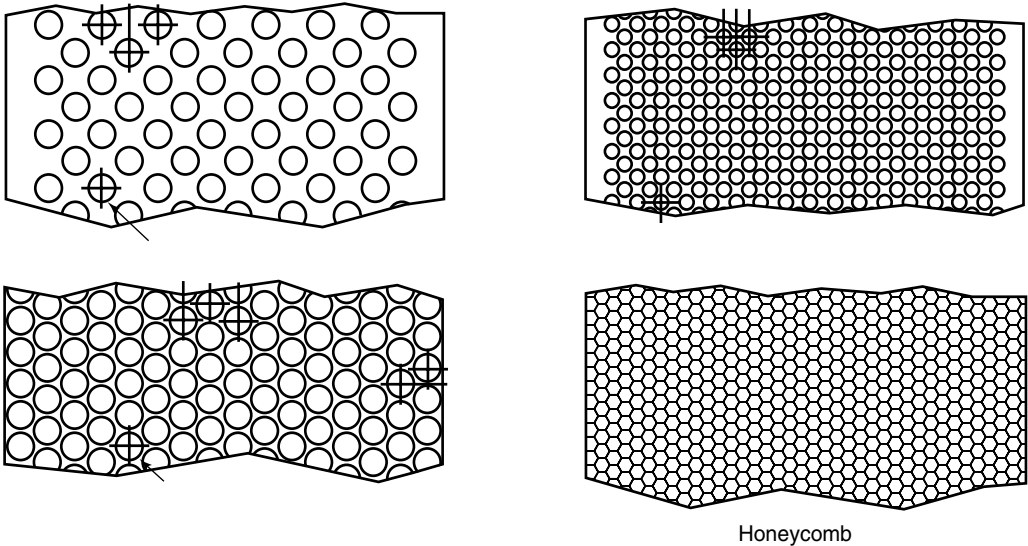


Figure 3-34—Various Hole Pattern Surface Areas Relative to Honeycomb



Figure 3-35—Pocket Seal Arrangement

This seal is closer to the traditional labyrinth design than to the honeycomb or hole pattern design. It is less susceptible to fouling than the honeycomb or hole pattern design, but cannot withstand rubbing contact as well as the hole pattern or toothed labyrinth seal.

Test programs have been carried out to lend validation to rotordynamic property prediction codes for the honeycomb and hole pattern designs. At least two sources of dynamic property prediction programs are available that have some degree of validation for honeycomb seals. Additional work on the hole pattern and pocketed designs is in progress and preliminary results are impressive. As with the application of any damping device, careful consideration must be given to the installed geometry and operating conditions. Off design operation must be evaluated, especially at increased clearance.

Implementing any of these damper seals into a rotordynamic analysis and into a hardware design is not a trivial task, Memmott [5], and should only be attempted with a degree of caution by experienced design and rotordynamic experts. Recent experiences have shown that large dynamic coefficients are possible with these seals. Principle stiffness, both positive and negative, can be created depending on the selection of the clearance profile. This can and will have an impact on the rotor's behavior and may produce unwanted results.

3.4.3.1 References

1. Childs, D. W., 1993, *Turbomachinery Rotordynamics Phenomena, Modeling, and Analysis*, John Wiley & Sons, Inc., New York.
2. Kleynhans, G., and Childs, D. W., 1997, "Acoustic Influence of Cell Depth on the Rotordynamic Characteristics of Smooth-Rotor/Honeycomb-Stator Annular Gas Seals," NASA CP-3344, pp. 49 – 76.
3. Yu, Z., Childs, D. W., 1998, "Comparison of Experimental Rotordynamic Coefficients and Leakage Characteristics Between Hole-Pattern Gas Damper Seals and a Honeycomb Seal," *ASME Journal of Engineering for Gas Turbines and Power*, 120 (4), pp. 778 – 783.
4. Richards, R. L., Vance, J. M., Paquette, D. J. and Zeidan, F. Y., 1995, "Using a Damper Seal to Eliminate Subsynchronous Vibrations in Three Back-to-Back Compressors," Proceedings of the Twenty-Fourth Turbomachinery Symposium, Turbomachinery Laboratory, Texas A&M University, College Station, Texas, pp. 59 – 71.
5. Memmott, E. A., 1999, "Stability Analysis and Testing of a Train of Centrifugal Compressors for High Pressure Gas Injection," *ASME Journal of Engineering for Gas Turbines and Power*, 121 (3), pp. 509 – 514.

3.4.4 Dry Gas Seals

One of the attractions to using dry gas seals in compression applications is the neutral dynamic behavior of the seal. While oil seals have been shown to possess large magnitudes of damping and cross coupled stiffness, Section 3.4.1, dry gas seals values are several orders of magnitude less. In fact, it is common practice to only include the added mass of the dry gas seal to the stability rotor model. Since they are treated as “neutral”, dry gas seal retrofits can either correct existing stability problems, Atkins & Perez, [1], or create problems, Kocur, et. al., [2], depending on the behavior of the seals they are replacing.

3.4.4.1 References

1. Atkins, K. E. and Perez, R. X., 1988, “Influence of Gas Seals on Rotor Stability of a High Speed Hydrogen Recycle Compressor,” Proceedings of the Seventeenth Turbomachinery Symposium, Turbomachinery Laboratory, Texas A&M University, College Station, Texas, pp. 9– 18.
2. Kocur, Jr., J. A., Platt, Jr., J. P. and Shabi, L. G., 1987, “Retrofit of Gas Lubricated Face Seals in a Centrifugal Compressor,” Proceedings of the Sixteenth Turbomachinery Symposium, Turbomachinery Laboratory, Texas A&M University, College Station, Texas, pp. 75 – 83.

3.5 EXCITATION SOURCES

3.5.1 Aerodynamic Cross Coupling

The stability analysis of turbomachinery requires the examination of many forces arising from fluid/structure interactions. Labyrinth seals are an excellent example of this interaction, which can produce significant destabilizing cross coupling forces. Numerous research papers on the instability of labyrinth seals have been published. A less understood phenomenon is “aerodynamic cross coupling.” This term has been used to refer to all fluid/structure interactions including impeller and/or blade seals. This practice was mainly followed prior to the development of analytical tools for labyrinth seals. Aerodynamic cross coupling, as defined in this context, refers to the rotor/stator interaction forces. These forces may arise from such phenomena as tip leakage flows, secondary flow in an impeller, and shroud/stator cavity flows [1]. Due to the complex geometry involved, the transient nature of the interaction, and the difficulty in developing test apparatus, adequate design tools describing these forces are relatively unavailable. While significant work continues on this subject, the end result is most often a CFD (computational fluid dynamics) model of these rotor/stator interaction forces that requires specialized knowledge of the software package and/or significant computational and personnel resources.

3.5.1.1 Axial Stages

One of the earliest attempts to quantify the fluid/structure interactions as a design tool was performed by Alford [2]. Alford established a theory and mathematical model to describe the aerodynamic cross coupling produced in axial flow stages due to eccentric operation. As described by Alford, forces are produced normal to the shaft deflection due to the circumferential variation in the blade tip clearance. The normal direction of the force to deflection is the nature of cross coupled terms, i.e. a displacement in the $\pm x$ -direction produces a force in the $\pm y$ -direction. (The converse is also true.)

Figure 3-36 presents the forces found in an axial stage from either a turbine or compressor. The torque force produced by an eccentric turbine stage is unbalanced due to the increased efficiency of blades with decreased tip clearance (solid arrows.) Thus, a turbine stage with rotation and deflection shown in Figure 3-36 will produce a net vertical force in response to the horizontal displacement. In axial compressors, the inlet face has a uniform pressure. Additionally, the stage will discharge into a region of equal static pressure. Therefore, the pressure rise for every blade must be the same in any given stage. For eccentric operation, the increased tip clearance will lower the efficiency of blades in that region. These blades will require more work in the form of larger input forces to generate the same pressure rise (dashed arrows.) As in the turbine, a net vertical force is produced. In both cases, the resultant force is normal to the displacement and tends to cause the rotor to whirl in the direction of rotation.

Alford accordingly developed a simple equation for the cross-coupled stiffness as a function of the stage torque (T), blade length (H_t), pitch diameter (D_t) and change in efficiency coefficient (B_t).

$$q_i = \frac{TB_t}{D_t H_t} = \frac{(HP)B_t C}{D_t H_t N} \quad 3-3$$

The equation provided designers with a simple relation to determine the expected aerodynamic cross coupling for axial flow stages. Alford’s equation has remained one of the few mathematical design tools available to calculate the destabilizing forces in turbomachinery. Vance and Laudadio [3] attempted to provide some experimental background for Alford’s equation. While they were able to confirm the existence of the force, qualitative conclusions were mainly reached.

3.5.1.2 Centrifugal Stages

Numerous attempts to develop a similar tool for centrifugal impellers have been made. While CFD approaches have yielded some success, none have provided the necessary ease

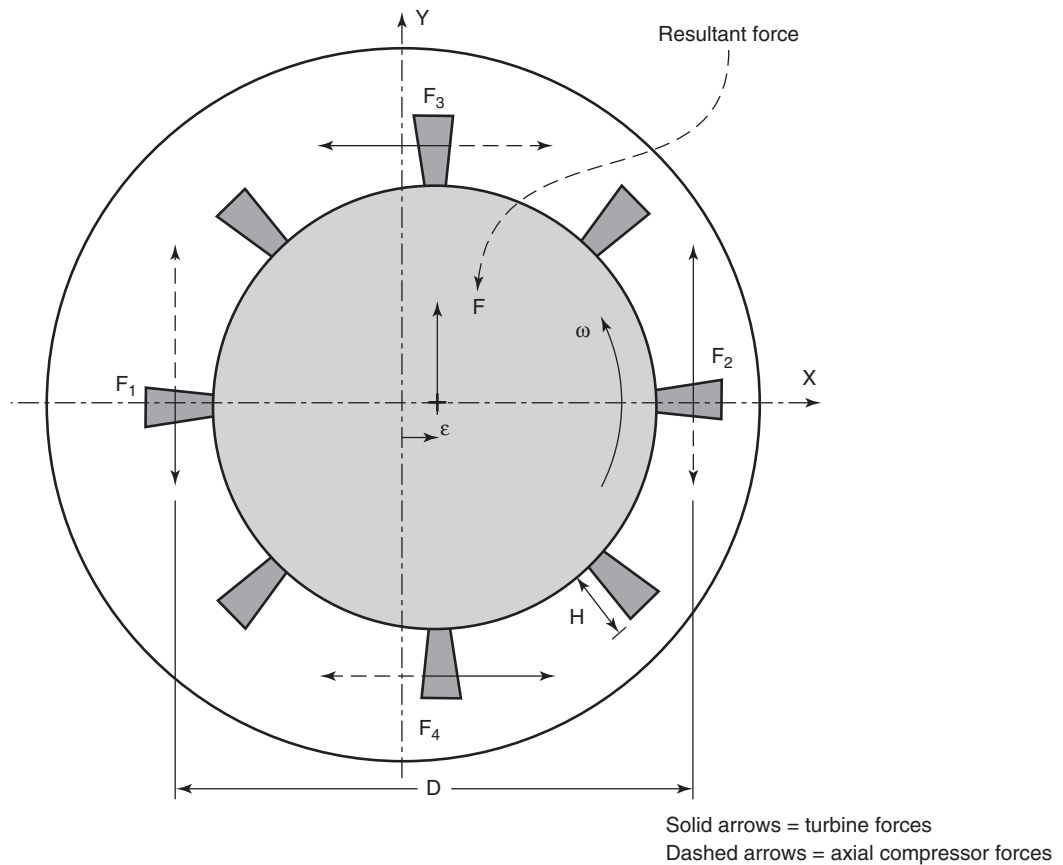


Figure 3-36—Blade Forces Due To Centerline Displacement

of use that rotordynamicists need at the design stage. To date, most design tools for centrifugal turbomachinery represent all destabilizing forces found between the casing end seals. Specifically, aerodynamic cross coupling, impeller eye and hub seals and case labyrinth seals are treated as one “global” destabilizing mechanism.

One popular tool was developed empirically by Wachel [4] while at Southwest Research Institute. The relation was developed using Alford’s equation as starting point and applying it to compressor case histories where the stability (or instability) was known. It was found that several additional parameters (density ratio and molecular weight) were needed to adequately estimate this “global” destabilizing force. However, as designers gained experience applying Wachel’s relationship to a larger database, the equation was thought to erroneously predict the destabilizing force for molecular weight gases much different than a molecular weight of 30. To remedy this, the “modified Alford’s” equation was developed, Memmott [5]. As with Wachel’s equation, the density ratio is added but the molecular weight is removed. As defined, the “modified Alford’s” equation takes the form:

$$q_i = \frac{(HP)B_cC}{D_cH_cN} \times \left(\frac{\rho_d}{\rho_s} \right) \quad 3-4$$

Comparing the “modified Alford’s” equation to Wachel’s, we find that the two equations agree for gases with a molecular weight of 30. For lighter molecular weights, the “modified Alford’s” force predicts a stronger destabilizing force. For heavier molecular weights, a smaller destabilizing force is predicted. These differences were based on experience with a larger database of compressors, [5].

Benckert [6] has also developed a relationship that has been applied to approximate this “global” destabilizing force. Used with more regularity in Europe, the equation was developed explicitly for labyrinth seals forces. However, it has been shown to sufficiently represent all destabilizing terms within centrifugal compressor applications.

Kirk [7,8] compared theory against the actual operating experience of the compressor stability for several applications. Alford’s and Benckert’s equations were used to approximate the “global” destabilizing effects in the compressors. These were measured against two analytical methods developed solely to predict the labyrinth seal dynamic behavior, [7,8] and Childs [9]. While a more in-depth discussion on the destabilizing effect of labyrinth seals is included in 3.4.2, the major findings in [7,8] are emphasized here.

In comparing the estimated equations to the actual operating experience, Kirk [7,8] concluded that Alford’s equation

provided a reliable predictor of the actual operating stability. Benckert's equation over-predicted the destabilizing forces by two to three times. More importantly was that either Kirk's or Childs' labyrinth seal coefficient prediction nearly equaled the destabilizing force predicted by Alford's equation. The conclusion that was drawn then and holds true now is that the labyrinth seals play a dominant role in the instability of centrifugal compressors and may actually reflect the true source of the "global" destabilizing effects predicted by either Alford's or Benckert's equations. Stated another way, the aerodynamic forces within centrifugal impellers may be insignificant in comparison to the labyrinth seal forces. However, not everyone agrees with this conclusion. Some in the industry agree that the aerodynamic forces may not be significant in comparison to the labyrinth seal forces with respect to the destabilizing cross coupling in centrifugal compressor applications. Others have concluded that the aerodynamic forces represented by the modified Wachel - Alford equation for centrifugal compressors are the same order of magnitude and independent from the labyrinth seal forces with respect to the destabilizing cross coupling in centrifugal compressor applications, Memmott [5,10].

3.5.1.3 References

1. Ehrich, F. F. and Childs, D. W., 1984, "Self-Excited Vibration in High-Performance Turbomachinery," *Mechanical Engineering*, May, pp. 66 – 79.
2. Alford, J. S., 1965, "Protecting Turbomachinery from Self-Excited Rotor Whirl," *ASME Journal of Engineering for Power*, 87 (4), pp. 333 – 344.
3. Vance, J. M. and Laudadio, F. J., 1984, "Experimental Measurement of Alford's Force in Axial Flow Turbomachinery," *ASME Journal of Engineering for Gas Turbines and Power*, 106 (3), pp. 585-590.
4. Wachel, J. C. and von Nimitz, W. W., 1981, "Ensuring the Reliability of Offshore Gas Compression Systems," *Journal of Petroleum Technology*, pp. 2252 – 2260.
5. Memmott, E. A., 2000, "Empirical Estimation of a Load Related Cross-Coupled Stiffness and The Lateral Stability Of Centrifugal Compressors," CMVA, Proceedings of the Eighteenth Machinery Dynamics Seminar, Halifax, April 26-28, 2000, pp. 9 – 20.
6. Benckert, H. and Wachter, J., 1980, "Flow Induced Spring Coefficients of Labyrinth Seals for Application in Rotordynamics," NASA CP-2123.
7. Kirk, R. G., 1988, "Evaluation of Aerodynamic Instability Mechanisms for Centrifugal Compressors—Part I: Current Theory," *ASME Journal of Vibration, Acoustics, Stress, and Reliability in Design*, 110 (2), pp. 201 – 206.
8. Kirk, R. G., 1988, "Evaluation of Aerodynamic Instability Mechanisms for Centrifugal Compressors—Part II: Advanced Analysis," *ASME Journal of Vibration, Acoustics, Stress, and Reliability in Design*, 110 (2), pp. 207 – 212.
9. Childs, D. W. and Scharrer, J. K., 1986, "An Iwatsubo-Based Solution for Labyrinth Seals: Comparison to Experimental Results," *ASME Journal of Engineering for Gas Turbines and Power*, 108 (2), pp. 325 – 331.
10. Memmott, E. A., 2000, "The Lateral Stability Analysis of a Large Centrifugal Compressor in Propane Service at an LNG Plant," IMechE, Proceedings of the 7th International Conference on Vibrations in Rotating Machinery, Nottingham, England, pp. 187 – 198.

Nomenclature

B_c = Impeller efficiency change per displacement, 3,

B_t = Stage efficiency change per displacement, 1.5,

C = Units conversion constant, 9.55 (63),

D_c = Impeller diameter, m (in.),

D_t = Blade pitch diameter, m (in.),

H_c = Minimum diffuser width per impeller, m (in.),

H_t = Effective blade height, m (in.),

HP = Rated power per stage/impeller, W (HP),

N = Operating speed, rpm,

q_i = Cross coupling per stage/impeller, kN/m (klbf/in.),

ρ_d = Discharge gas density per impeller, kg/m³ (lbm/in.³),

ρ_s = Suction gas density per impeller, kg/m³ (lbm/in.³).

3.5.2 Other Excitation Sources

3.5.2.1 Internal Friction, Shrink Fits and Shaft Material Hysteresis

The internal friction generated by rotor component shrink fits or in the rotor material itself can generate a destabilizing force that may drive the rotor unstable at subsynchronous frequencies that are generally greater than 50% of synchronous rotor speed, Ehrich [1]. This instability, often referred to as hysteretic whirl, was the first self-excited rotor instability phenomena identified, Newkirk [2] and Kimball [3]. The internal friction that is generated internally in the rotor material is sometimes referred to as material hysteresis or internal damping.

Referring to Figure 3-37 [1], as the rotor deflects, the rotor's neutral strain axis is normal or perpendicular to the

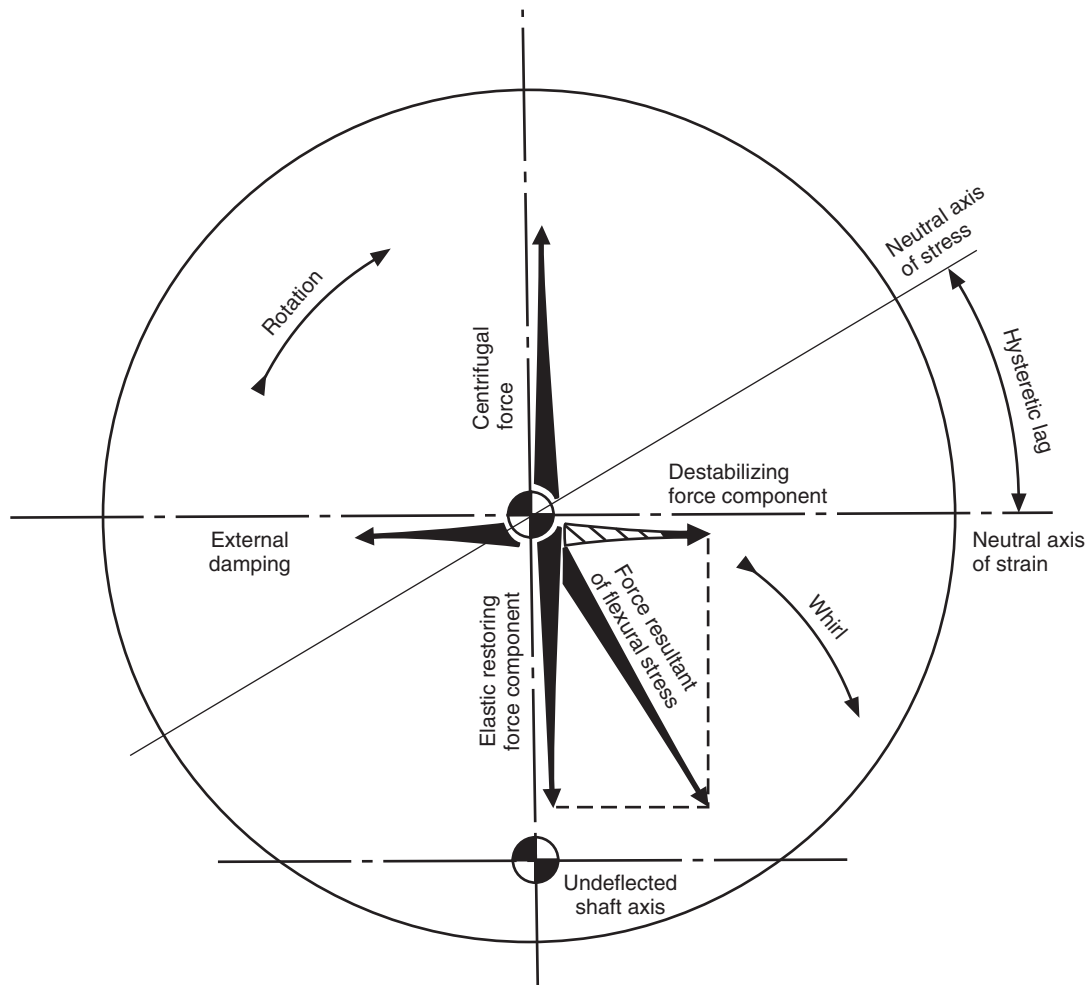


Figure 3-37—Shrink Fit Internal Friction and Shaft Material Hysteresis Destabilizing Force

deflected direction. Usually, the neutral stress axis would be coincident with the neutral strain axis resulting in an elastic restoring force that is parallel and opposite to the rotor displacement. However, material hysteresis or internal friction in a rotating shaft causes a phase shift in the neutral stress axis. This leads to a hysteretic lag angle where the neutral stress axis “lags” the neutral strain axis by some angle against rotation. Now, the restoring force is not parallel and opposite to the rotor displacement. In fact, the neutral stress axis phase lag results in a component of the restoring force that is perpendicular to the rotor displacement (and hence destabilizing) and in the direction of rotation. If this force is large enough, forward whirl will be induced, resulting in a subsynchronous rotor vibration. Unfortunately, a method of analytically quantifying this internal friction induced destabilizing force is not readily available.

Gunter [4], Ehrich [5] and Vance and Ying [6] have shown that internal friction from rotor component shrink fits can cause substantial destabilizing forces. Wheel, sleeve or other shaft component shrink fit axial lengths should not exceed the

shaft diameter. Additionally, sleeve fits should be relieved allowing for contact at the axial ends only.

3.5.2.2 Dry Friction Rubs

A dry friction rub is experienced when a rotating surface contacts a stationary surface without lubrication. Examples include lubrication-starved journal bearing rubs (see 3.3.3.2), labyrinth seal rubs and impeller-to-stator rubs.

Figure 3-38 illustrates a rub phenomena [1]. As the rotating part hits the stationary part, a tangential friction force results that is in a direction opposite of shaft rotation. This results in a backward whirl where the rotor whirls or precesses in the opposite direction of shaft rotation. Rubs often produce a rotor vibration that is exactly 50% of synchronous rotor speed, Goggin [7]. Depending on the location of the rotor’s critical speeds, rubs can also produce rotor vibration frequencies at $1/n$ of synchronous rotor speed with $n = 2, 3, 4, 5, 6$, etc., Lee and Allaire [8].

In terms of a damped natural frequency analysis, a rub induced subsynchronous vibration is not technically an “insta-

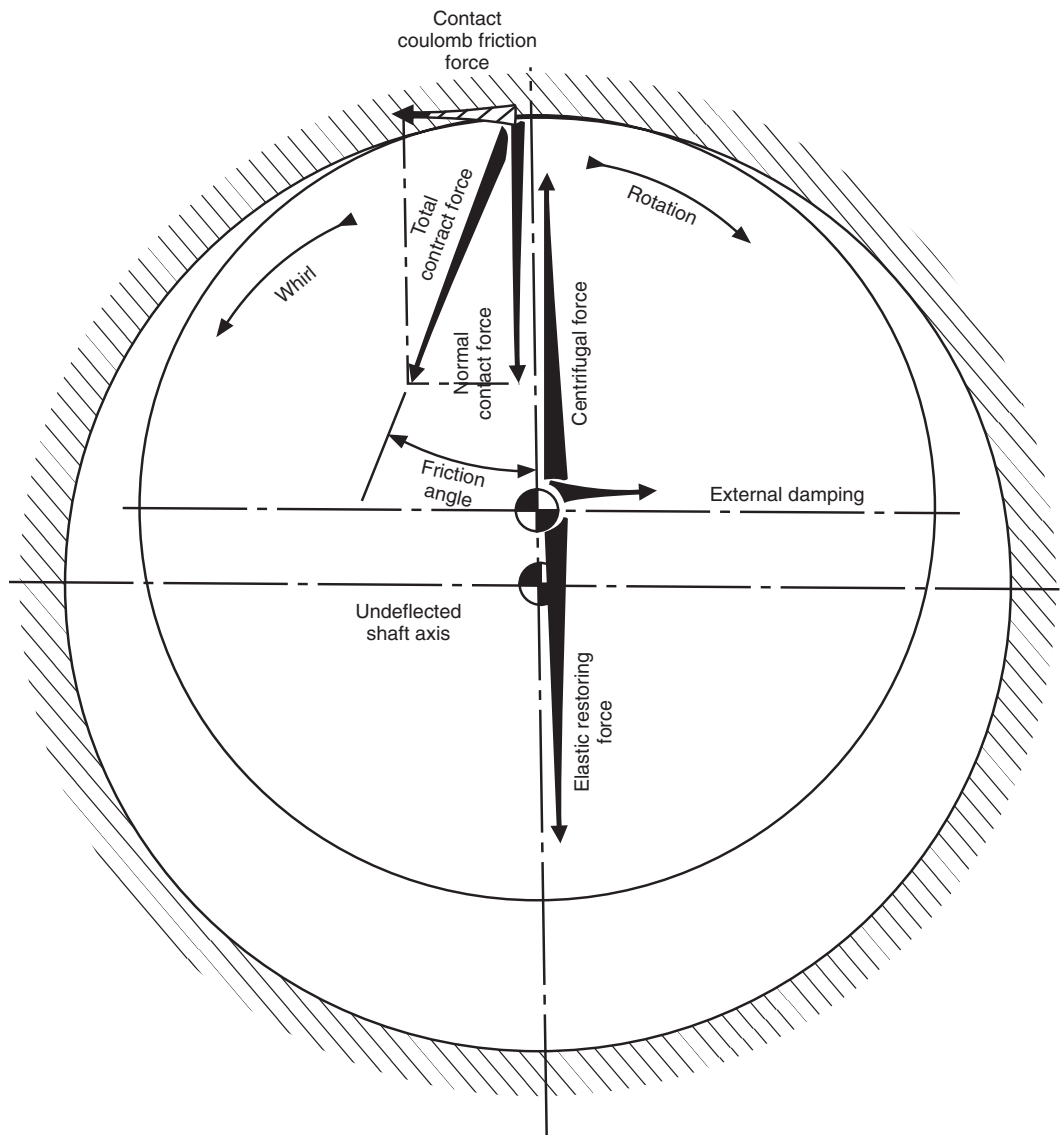


Figure 3-38—Dry Friction Rub Backward Whirl Excitation

bility". Since the vibration can be subsynchronous and appear suddenly with rapid growth, it has been labeled by researchers as a "rub induced instability." However, rubs cannot be predicted or prevented by performing a rotor damped natural frequency stability analysis. Rubs are more appropriately classified and analyzed as a transient response problem [8].

3.5.2.3 Entrapped Fluids

Entrapped fluids in hollow rotors or coupling spacer tubes, Kirk, et al. [9], Wolf [10] and Saito, et al. [11], can also induce a subsynchronous rotor vibration. This phenomenon is illustrated in Figure 3-39 and described in detail in [1]. At some rotor deflection, the entrapped fluid is flung out radially in the direction of shaft deflection. The rotating surface of the

cavity drags the fluid in the direction of rotation. This results in a phase "lead" angle for the fluid's centrifugal force. The entrapped fluid force has a component that is perpendicular to shaft displacement, in the direction of shaft rotation. Thus, forward whirl may result at frequencies that range from roughly 80% – 95% of synchronous speed [9].

Entrapped fluid induced subsynchronous vibration should not be treated as instability of the rotor-bearing system. The vibration, while subsynchronous, will not grow unbounded. It cannot be predicted or prevented by performing a rotor damped natural frequency stability analysis. It is more appropriately classified as a subsynchronous forced response problem where the forcing function, the entrapped fluid, excites the rotor at a frequency that is less than once per shaft revolution.

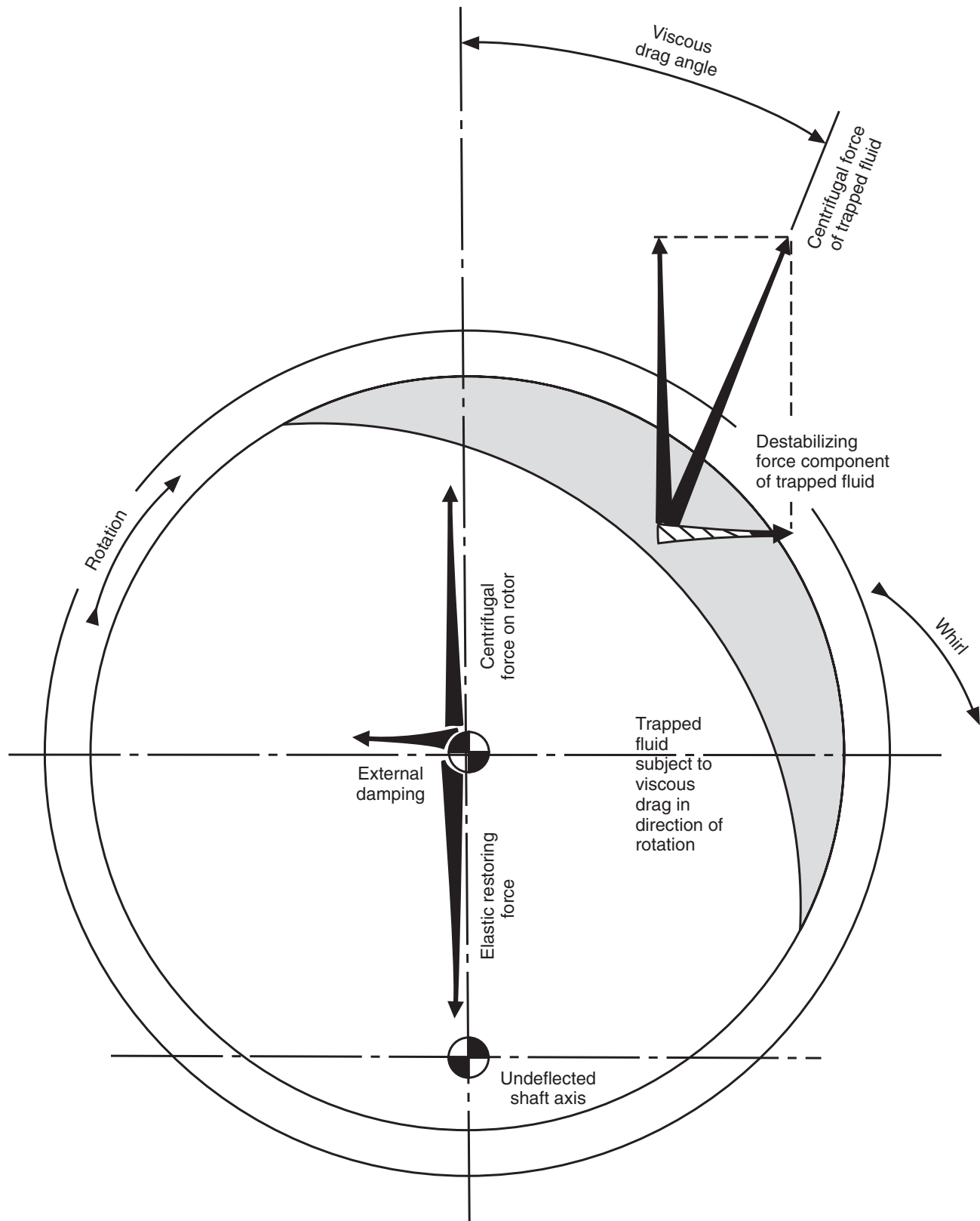


Figure 3-39—Entrapped Fluid Cross-coupled Force

3.5.2.4 Rotating Stall

Rotating stall is an aerodynamic phenomenon that occurs in vaneless diffusers of centrifugal compressors. The periodic unsteady flow pattern consists of low and high pressure regions that rotate in the direction of the impeller rotation at speeds, typically, of 5% – 20% of the shaft speed. Rotating stall is usually encountered near the surge line of a compressor. However, poor diffuser design practices can place stall well within the operating range.

Stall normally forms at low flows. Basically, stall occurs when the radial velocity component at the impeller discharge is insufficient to allow the gas to escape the diffuser. In this instance, pockets of recirculating gas form and proceed to rotate within the diffuser. The pockets actually reduce the diffuser area permitting gas to escape. Further reduction of the radial component would lead the compressor into surge or a total collapse of the flow attempting to leave the diffuser.

Stall has an adverse effect on performance witnessed as drops in the efficiency and head curves usually near surge. Additionally, the rotating pressure regions can be a source of mechanical excitation of the impeller blades and shaft. The shaft vibration will be seen as a subsynchronous vibration at

5% – 20% of rotational speed. Some have erroneously classified this as rotor instability since the vibration is subsynchronous and associated with a flow instability. Rotating stall is a forced response phenomenon with the forcing function being the rotating cells of gas. Design guidelines to avoid stall in centrifugal compressors can be found in [12].

3.5.2.5 Synchronous Thermal Instability “Morton’s Effect”

Research has shown that rotors supported in fluid film bearings will exhibit a nonuniform temperature distribution around the bearing journals circumference under synchronous vibration. The thermal effect arises from the viscous shearing of the oil film during synchronous vibratory motion. The phenomenon occurs only at 1x vibration since the shaft under synchronous motion does not undergo alternating stresses. Stated in simpler terms, one specific point on the will always be on the outside of the orbit (the high spot) and will therefore be closer to the bearing wall, Figure 3-40. This surface will have a smaller film thickness averaged over the period of one orbit than the opposite side of the shaft.

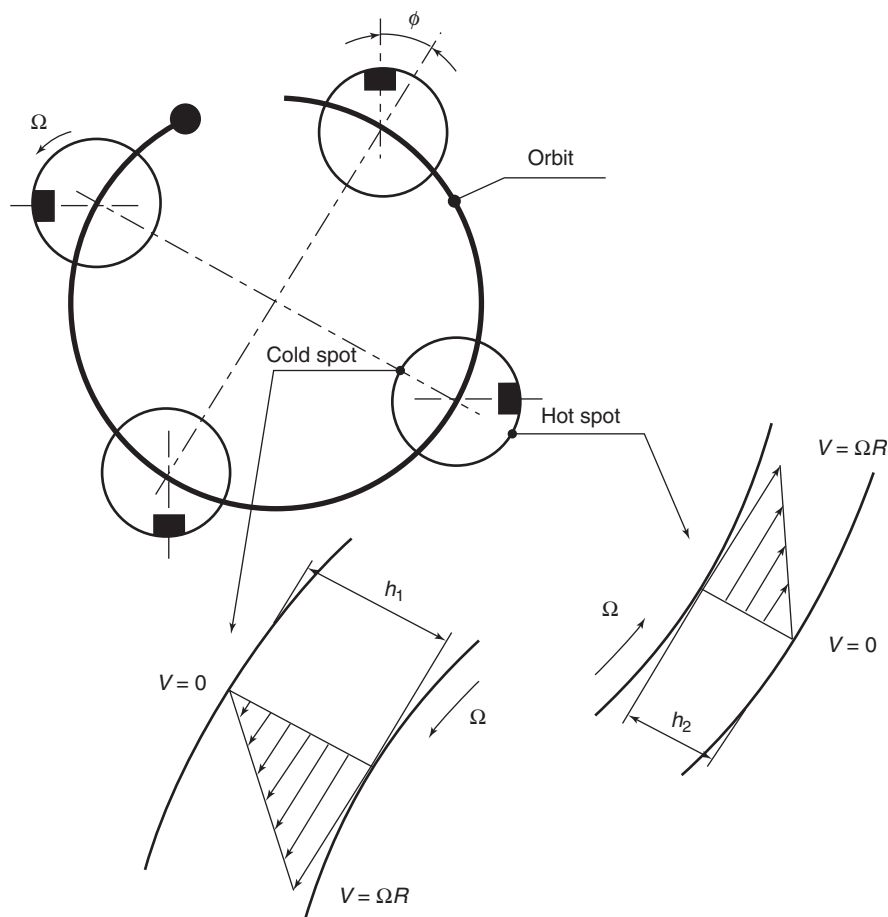


Figure 3-40—Differential Heating at Bearing Journal for Synchronous Forward Whirl

At the journal locations, the oil film's viscous shear will perform more work at the minimum clearance location. The difference in work over the circumference of the shaft produces a hot and cold spot on the journal. The temperature difference has been shown in test conditions to exceed 7°C over the circumference, [13], thereby producing a thermal bend in the shaft end nearest the journal location. Larger shaft orbits produce greater temperatures differences and, thus, greater shaft bending.

The excitation source of this phenomenon is the shaft unbalance that is produced by the thermally induced shaft bending. If the rotor system is sensitive to shaft end unbalance, the thermal bend will result in an increased vibration level (and larger orbit). The larger orbit produces a greater thermal differential, which results in a greater bend or bow. In this case, the system is unstable and the synchronous vibrations will grow unbounded until the system becomes non-linear or a failure occurs in one of the components.

While synchronous thermal instability fits the classical definition of an unstable system, rotor stability codes are currently not used to predict its existence. As outlined in [13], a combination of an unbalance response code and empirically derived data is used to test for the stability condition of the rotor/bearing system. Additionally, this phenomenon occurs only at synchronous frequencies.

3.5.2.6 References

1. Ehrich, F. F., 1992, *Handbook of Rotordynamics*, McGraw Hill.
2. Newkirk, B. L., 1924, "Shaft Whipping," *General Electric Review*, 27 (3), pp. 169 – 178.
3. Kimball, A. L., 1924, "Internal Friction Theory of Shaft Whirling," *General Electric Review*, 27 (4), pp. 244 – 251.
4. Gunter, E. J., 1967, "The Influence of Internal Friction on the Stability of High Speed Rotors," *ASME Journal of Engineering for Industry*, Series B, 89 (4), pp. 683 – 688.
5. Ehrich, F. F., 1964, "Shaft Whirl Induced by Rotor Internal Damping," *Journal of Applied Mechanics*, 23 (1), pp. 109 – 115.
6. Vance, J. M. and Ying, D., 2001, "Effect of Interference Fits on Threshold Speeds of Rotordynamic Instability," *International Symposium on Stability Control of Rotating Machinery*, August 20-24, 2001, South Lake Tahoe, California.
7. Goggin, D. G., 1982, "Field Experiences with Rub Induced Instabilities in Turbomachinery," *Rotordynamic Instability Problems in High-Performance Turbomachinery*, NASA CP-2250, pp. 20 – 32.

8. Lee, C. C. and Allaire, P. E., 1999, "Nonlinear Transient Analysis of Point Rub Effects in a Flexible Rotor," *Journal of Applied Mechanics and Engineering*, 4.

9. Kirk, R. G., Mondy, R. E. and Murphy, R. C., 1984, "Theory and Guidelines to Proper Coupling Design for Rotor Dynamic Considerations," *ASME Journal of Vibration, Acoustics, Stress, and Reliability in Design*, 106 (1), pp. 129 – 138.

10. Wolf, J. A., 1968, "Whirl Dynamics of a Rotor Partially Filled with Liquid," *ASME Journal of Applied Mechanics*, 4, pp. 676 – 682.

11. Saito, S. and Someya, T., 1979, "Self-Excited Vibration of a Rotating Hollow Shaft Partially Filled with Liquid," *ASME Paper No. 79-DET-62*.

12. Aungier, R. H., 2000, *Centrifugal Compressors, A Strategy for Aerodynamic Design and Analysis*, ASME Press, New York.

13. de Jongh, F. M. and van der Hoeven, P., 1998, "Application of a Heat Barrier Sleeve to Prevent Synchronous Rotor Instability," *Proceedings of the Twenty-Seventh Turbomachinery Symposium*, Turbomachinery Laboratory, Texas A&M University, College Station, Texas, pp. 17 – 26.

3.6 SUPPORT STIFFNESS EFFECTS

Requirements to accurately predict rotor critical speed locations, rotor critical speed amplification factors and rotor stability necessitate the accurate prediction of the effective bearing stiffness and damping coefficients acting upon the rotor. An important consideration in predicting these effective coefficients is the influence of the pedestal support stiffness and damping characteristics. These support characteristics act in series with the bearing oil film characteristics and the combined effective characteristics may be quite different from either of these. For fixed geometry hydrodynamic journal bearings that have cross coupling between horizontal and vertical motion of the rotor within the bearing, the overall effective bearing-support characteristics will also be cross coupled. In some instances, the flexibility of the bearing support structure may include significant cross talk between bearings through the machine case and foundation, further complicating the prediction of the critical speeds, amplification factors and stability.

The bearing support flexibility includes everything past the bearing's oil film all the way to ground. This includes the bearing case, the bearing pedestal, the machine casing, the base plate, the supporting columns and the foundation. With tilting pad journal bearings, the flexibility of the tilting pads and the pad pivots must also be considered. In general, the support flexibility is dynamic. That is, the support stiffness and damping properties are a function of the applied vibration

frequency. For most cases, the support damping is small and can often be neglected or small values are assumed as in Nicholas, et al. [1]. The frequency dependent support stiffness is often referred to as the dynamic support stiffness. The inverse of dynamic stiffness is dynamic compliance. Thus, the support compliance is frequency dependent and the inverse of dynamic support stiffness.

In general, support compliance produces effective damping coefficients that are lower than the bearing damping coefficients alone resulting in larger amplification factors than would occur if the supports were rigid. The effective stiffness coefficients are also generally lower than those for the bearing alone resulting in lower critical speeds than would occur if the supports were rigid.

This reduction in effective damping coefficients generally reduces the stability of rotors where the instability mechanism is due to seals, balance pistons or impeller flows. It may, however, increase the instability onset speed when the bearings are the primary source of instability (i.e., fixed geometry bearing induced rotor instability discussed in 3.3.2). In either case, including appropriate models for the bearing supports can drastically alter the prediction of stability levels and instability onset speeds for rotors.

Predicting the bearing stiffness and damping characteristics is fairly easy and reasonably accurate using currently available software. Predicting the support stiffness and damping characteristics is not always straightforward. Although it is possible to make reasonable assumptions of the support characteristics for some support configurations, most situations require the characteristics to be predicted from finite element analyses of the support structure or to be determined from test data. Further complicating the situation is the fact that the support characteristics may vary with the vibration frequency of the rotor.

One support model that is frequently used is shown in Figure 3-41 and is reasonably accurate for rotors supported in tilting pad bearings. The simplest form of this single mass model uses the static (low frequency) support stiffness, which

can be determined from a static deflection test. This model may also be employed at any frequency utilizing the dynamic stiffness at a particular frequency of concern (i.e., at a critical speed frequency, for example). Equations for the equivalent bearing and support stiffness and damping coefficients for the single mass model are given in [1] and Barrett et al. [2]. Reference [1] also contains experimental test stand rotor vibration data for a steam turbine showing the effects of bearing support flexibility. Several levels of support stiffness single mass models of increasing complexity are also presented along with the dynamic compliance data for the turbine support (see 2.4).

The more complex support compliance models described previously that include vibration frequency effects may be obtained by measuring or calculating the frequency response functions or transfer functions of machine supports, [1]. Measurements may be obtained using an arrangement like that shown in Figure 3-42. An impact hammer is used to excite the bearing supports. A load cell in the hammer registers the impact force. The support motion is measured, usually with accelerometers. Using a frequency analyzer, the ratio of output motion to input force is obtained on a frequency-by-frequency basis, which forms the frequency response function (FRF). If the output is displacement, the FRF is called a compliance function. The inverse of the compliance function is the dynamic stiffness. These data are complex values and therefore contain both amplitude and phase information. A typical compliance function magnitude plot is shown in Figure 3-43. These data were obtained from a flexible rotor test rig with flexible supports shown in Figure 3-44. A complete description of this test rig can be found in Vázquez, et al. [3].

If $G(\omega)$ represents the complex value of the FRF at frequency ω , from Ewins, [4], the dynamic stiffness at that frequency is

$$K_{dyn}(\omega) = \frac{1}{G(\omega)} \quad 3-5$$

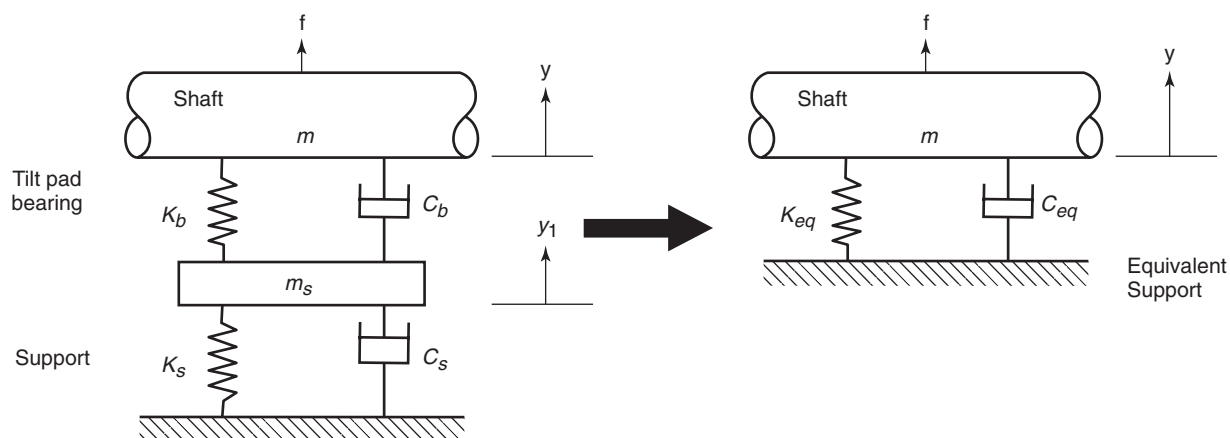


Figure 3-41—Simple Bearing—Support Model

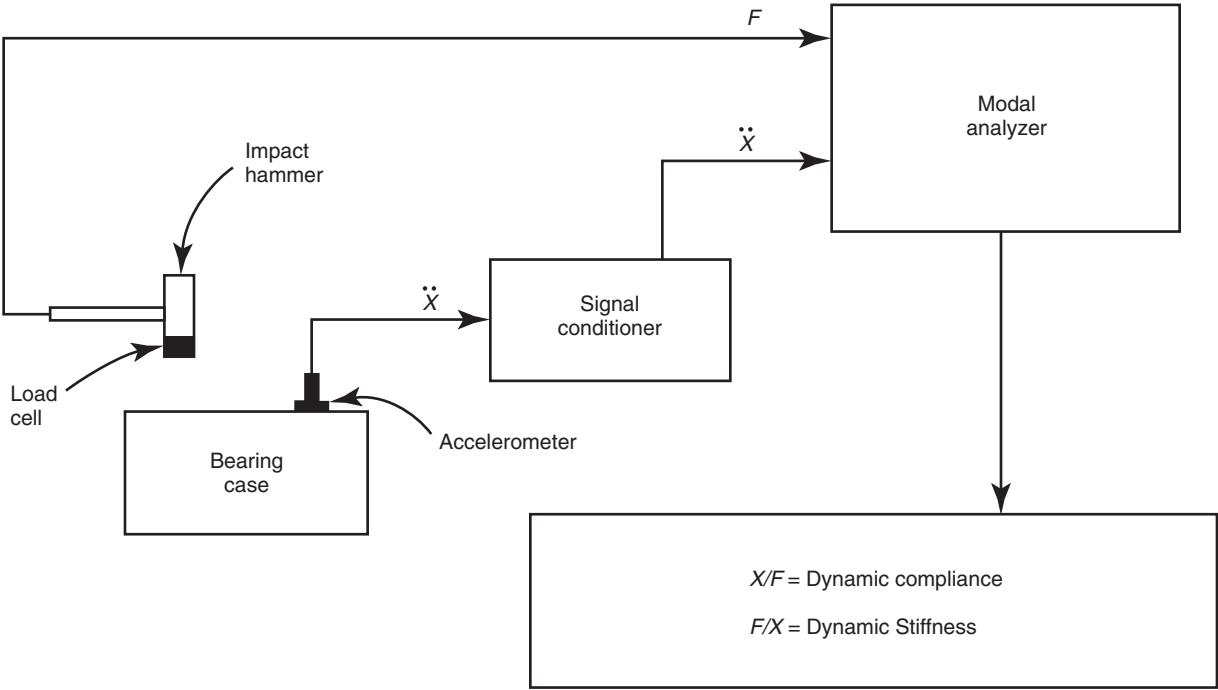


Figure 3-42—System for Measuring Support Compliance

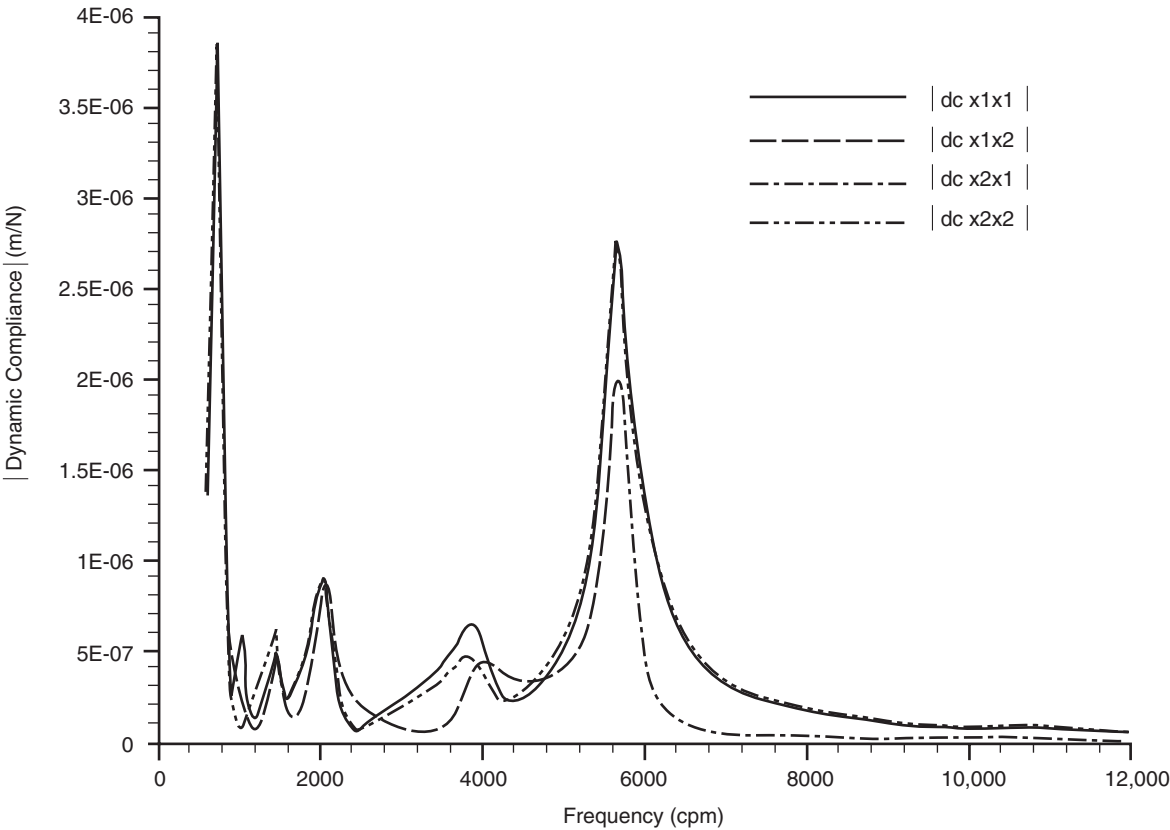


Figure 3-43—Horizontal Dynamic Compliance of the Bearing Supports

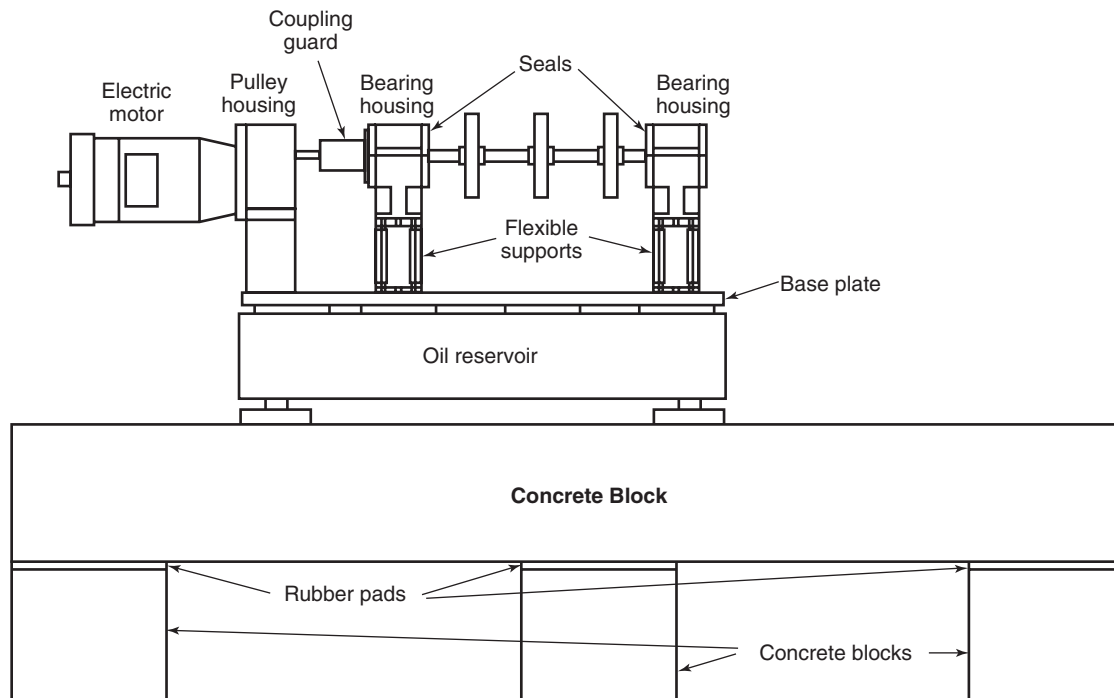


Figure 3-44—Experimental Flexible Rotor with Flexible Supports

Equivalent support stiffness and damping coefficients can then be found from

$$k_s(\omega) = \operatorname{Re}(K_{dyn}(\omega)) \quad 3-6$$

$$c_s(\omega) = \frac{\operatorname{Im}(K_{dyn}(\omega))}{\omega} \quad 3-7$$

These calculations can be utilized to determine the support characteristics at each vibration frequency being analyzed and combined with the bearing coefficients at each frequency in order to perform rotordynamic calculations [1,2 and 5].

Typical effects of including or not including support compliance are shown in Figures 3-45 and 3-46 [5]. These results are for the rotor test set-up illustrated in Figure 3-44. The predominant support flexibility is in the horizontal (x) direction. It is seen that the response (particularly at the rotor center, Figure 3-45) at the first critical speed of approximately 3,000 rpm, is under-predicted by neglecting the bearing support characteristics. This is directly a result of the reduction in effective damping when support flexibility is accounted for. Also when the bearing supports are considered rigid, the second critical speed is above the 7,500 – 8,000 rpm speed range analyzed. However, when support flexibility is included, the second critical speed has been lowered to approximately 7,400 rpm as seen in the response at the bearings shown in Figure 3-46. The response peak in the 5,800 – 6,200 rpm range is due to a resonance in the support in the horizontal

direction. This resonance is seen in the compliance data shown in Figure 3-43.

Figure 3-47 shows the predicted and measured instability onset speeds for the rotor test set-up illustrated in Figure 3-44. The bearings are fixed geometry multi-lobe bearings and are the source of instability in this rotor. The rotor is predicted to be unstable above 5,200 rpm if the bearing supports are considered rigid. A simple single mass flexible bearing support model over-predicts the instability onset speed by a considerable margin. However, the predicted instability onset speed using a more complex transfer function support model, [5], closely predicts the measured instability onset speed of the rotor.

3.6.1 References

1. Nicholas, J. C., Whalen, J. K. and Franklin, S. D., 1986, "Improving Critical Speed Calculations Using Flexible Bearing Support FRF Compliance Data", Proceedings of the Fifteenth Turbomachinery Symposium, Turbomachinery Laboratory, Department of Mechanical Engineering, Texas A&M University, College Station, Texas, pp. 69 – 78.
2. Barrett, L. E., Nicholas, J. C. and Dhar, D., 1986, "The Dynamic Analysis of Rotor-Bearing Systems Using Experimental Bearing Support Compliance Data," Proceedings of the Fourth International Modal Analysis Conference, Union College, Schenectady, New York, pp. 1531 – 1535.

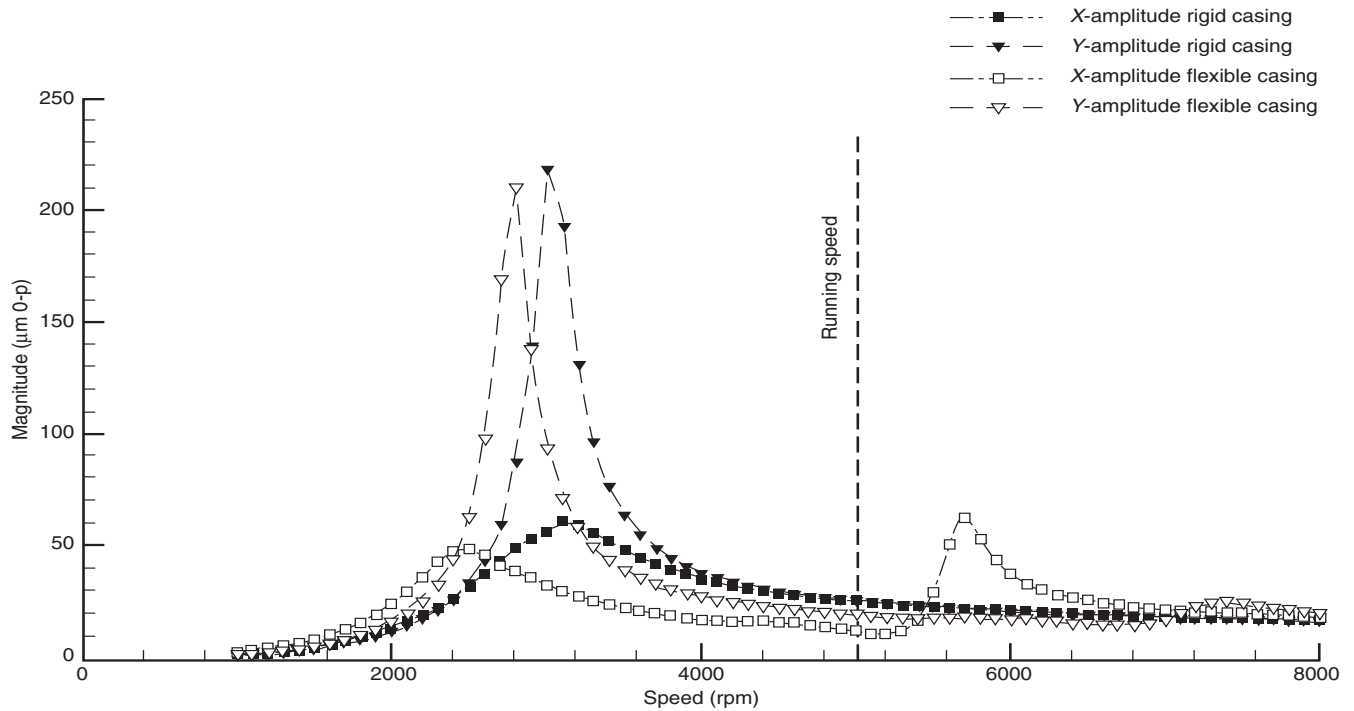


Figure 3-45—Predicted Response at the Rotor Center with and without Bearing Support

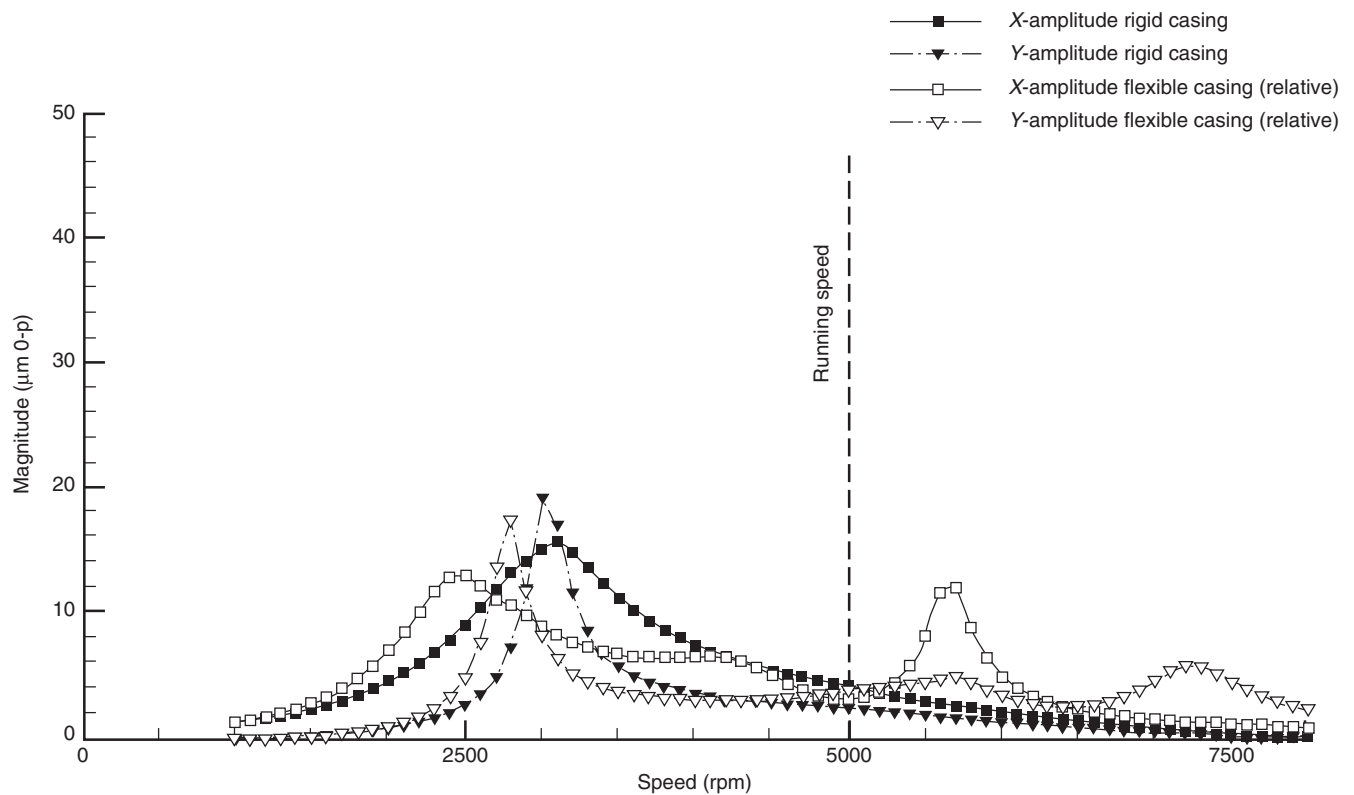


Figure 3-46—Predicted Response at the Bearings with and without Bearing Support Models

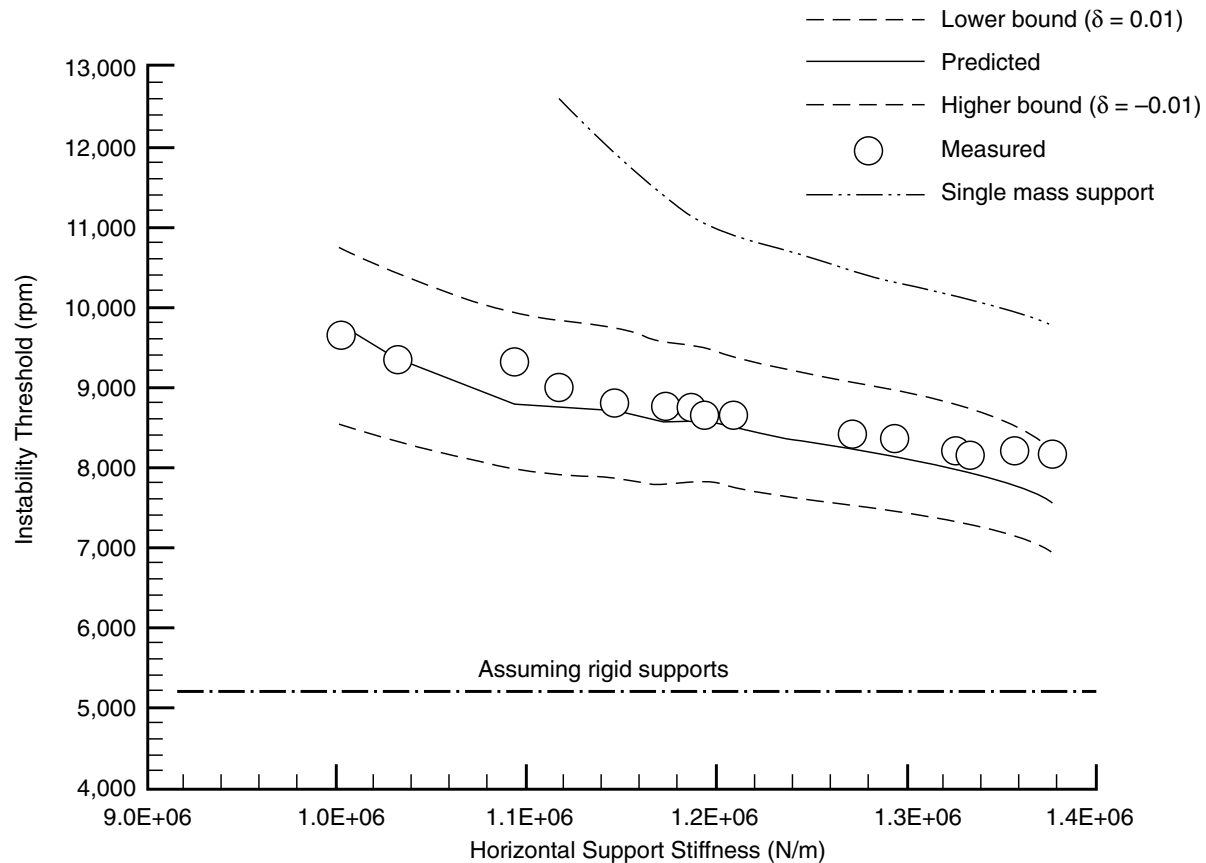


Figure 3-47—Predicted and Measured Stability Threshold with and without Bearing Support Models

3. Vázquez, J. A., Barrett, L. E. and Flack, R. D., 2000, "Including the Effects of Flexible Bearing Supports in Rotating Machinery," Eighth International Symposium on Transport Phenomena and Dynamics of Rotating Machinery, March 26 – 30, Honolulu, Hawaii.

4. Ewins, D. J., 1984, *Modal Testing: Theory and Practice*, Research Studies Press, Taunton, Somerset, England.

5. Vázquez, J. A. and Barrett, L. E., 1999, "Transfer Function Representation of Flexible Supports and Casings of Rotating Machinery," Proceedings of the Seventeenth International Modal Analysis Conference, February 8 – 11, Kissimmee, Florida, pp.1328 – 1334.

3.7 EXPERIENCE PLOTS

From the earliest designs of turbomachinery, manufacturers had the ability to design and build rotating equipment beyond what could be analyzed or predicted. This arose in part to competitive pressures to build higher pressure, higher horsepower equipment in a single case and to the inability to foresee all possible outcomes of every design change or component implementation. Rotor stability is an excellent example of this.

In the 60s and early 70s, the need for high pressure gas reinjection machines was created by the natural gas production techniques in use. This represented an extension of the design capabilities and operating experience of rotating equipment manufacturers. For the most part, mechanical and aerodynamic knowledge existed to permit the construction of these higher pressure compressors. What was lacking was the ability to accurately predict the dynamic behavior of these rotors. This led to several highly published failures resulting from self-excited subsynchronous vibrations, i.e., instability.

As discussed in the introduction, analytical methods were soon developed to calculate the damped eigenvalues and eigenvectors of rotating equipment. Basic stability calculations became possible coupled with the development of the computer. However, the impact on rotor stability of several key components still lagged behind, namely, oil seals, labyrinth (gas) seals and impellers. It soon became apparent to many users and manufacturers that a good understanding of the destabilizing effects of these components would be years in the development. Additionally, initial attempts were often complicated requiring extensive computational resources.

Experience plots were created to fill the void and to provide an initial screening criteria in the design or acceptance process. The plots were based on existing experience that

each author had concerning both operating machinery and analytical capabilities. The plots involved a mix of calculated factors like the critical speed ratio and process variables like the gas density. These plots were intended to alert designers and users to rotors that may be susceptible to instability.

Sood [1] presented an experience plot in 1979 that was in use as a general design criteria for the rotor stability evaluation of high pressure compressors, Figure 3-48. His curve plotted the rotor flexibility ratio versus the average gas density. Rotor flexibility ratio was defined as the ratio of maximum continuous speed to the first critical speed on rigid supports. A low flexibility ratio indicates a more rigid rotor. His experience had shown that compressors with a low flexibility ratio are less susceptible to subsynchronous vibration in high-density applications. It was also noted that compressors in lower pressure applications (lower average gas density) could be operated with higher flexibility ratios. Due to proprietary constraints, no numbers were included with the plot.

Fulton [2], incorporating his company's compressor experience and published data from unstable rotors, attempted to put some numerical values to Sood's curve. Plotting three known cases with instability, he drew a "Typical Threshold Line," Figure 3-49. A "Worst Case Threshold Line" was developed using the least stable case that was known at the time by Fulton for Sood's coordinates. Fulton suggested the following strategy for use of the curves: "We recommend that proposals for compressors on the unstable side of the worst case line be required to include prices for an optional full speed, full gas density test with rated differential pressure across the compressor. The final decision to test could then be made later when the information from complete analytic studies is available."

Kirk [3] proposed an empirical curve based on the pressure parameter defined as discharge pressure multiplied by the differential pressure across the compressor, Figure 3-50. The pressure parameter was used to represent the work being done by the compressor (differential pressure) and the discharge pressure both thought to be important parameters in determining the rotor stability. The slope and relative placement of the lines forming the boundaries were located using the Ekofisk and Kaybob compressors (see 3.1.1). Operating to the left of the "acceptable" line was achieved through use of standard design features. Advanced features such as stabilized oil seal designs and labyrinth seal and balance piston designs (i.e. swirl brakes) were needed for operation to the right of the "acceptable" line. A gray zone between the "acceptable" and "unacceptable" lines indicated the zone where advanced features may be needed.

The differences in experience with stability problems are noted in a paper presented by Shemeld [4]. In this reference, the Sood/Fulton curve is used as a basis to plot this manufacturer's compressor experience from 1969 to 1985, Figure 3-51. As noted by Shemeld, only a few of the units lying above the "Worst Case Threshold" line, for those with average gas density below 160 kg/m³, were ever full load tested. But, for those with average gas density above 160 kg/m³, about half of them were full load tested. The rest received only the API 617 mechanical tests. The analytical process developed by Shemeld's company, incorporating continual data feedback, component development and aerodynamic concepts, was believed to be effective in addressing solutions to rotordynamic/stability concerns without resorting to full load testing and/or major geometry changes to the rotor.

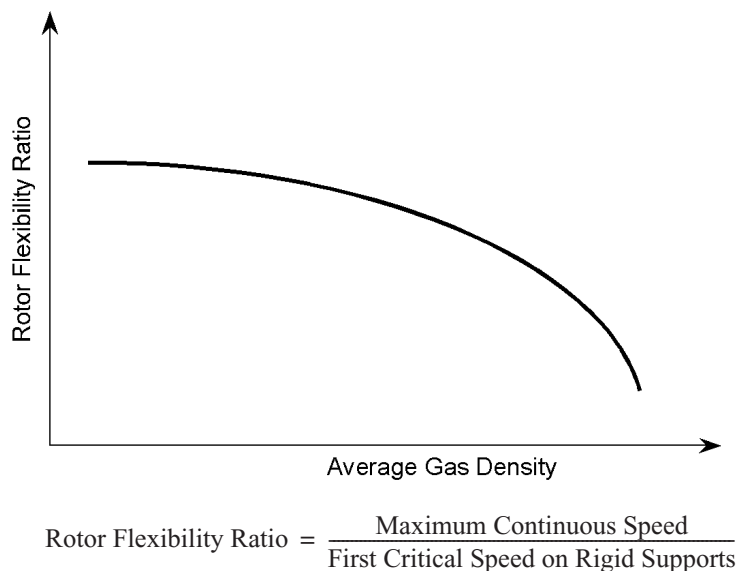


Figure 3-48—Sood's General Rotor Stability Criteria

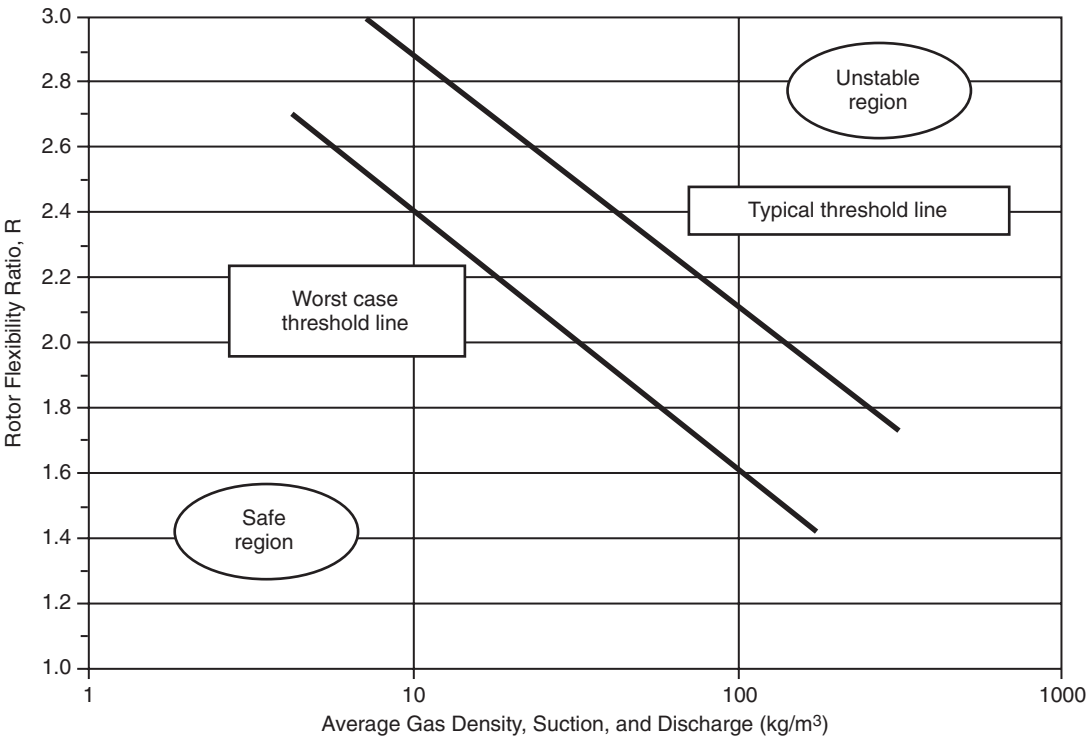


Figure 3-49—Sood/Fulton Empirical Stability Criteria

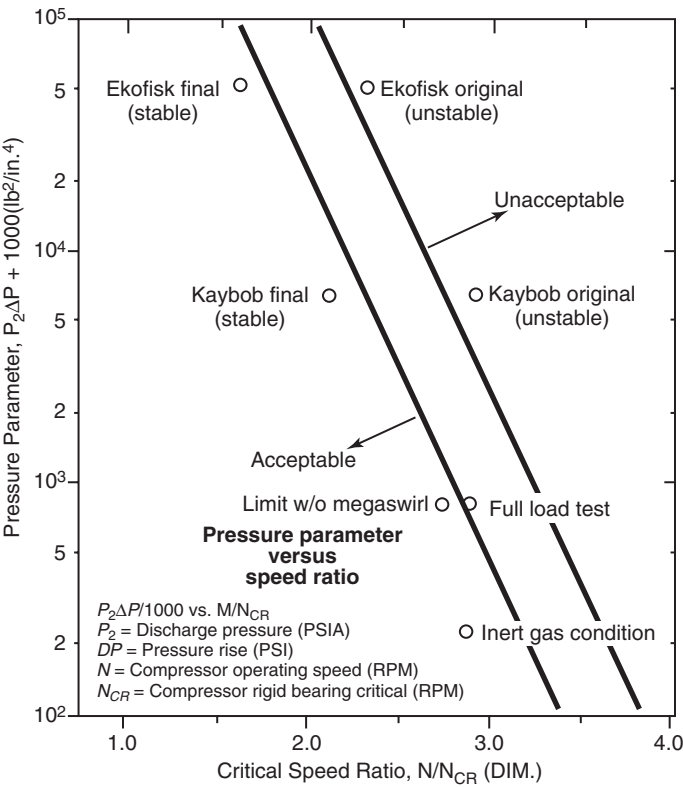


Figure 3-50—Kirk's Compressor Design Map

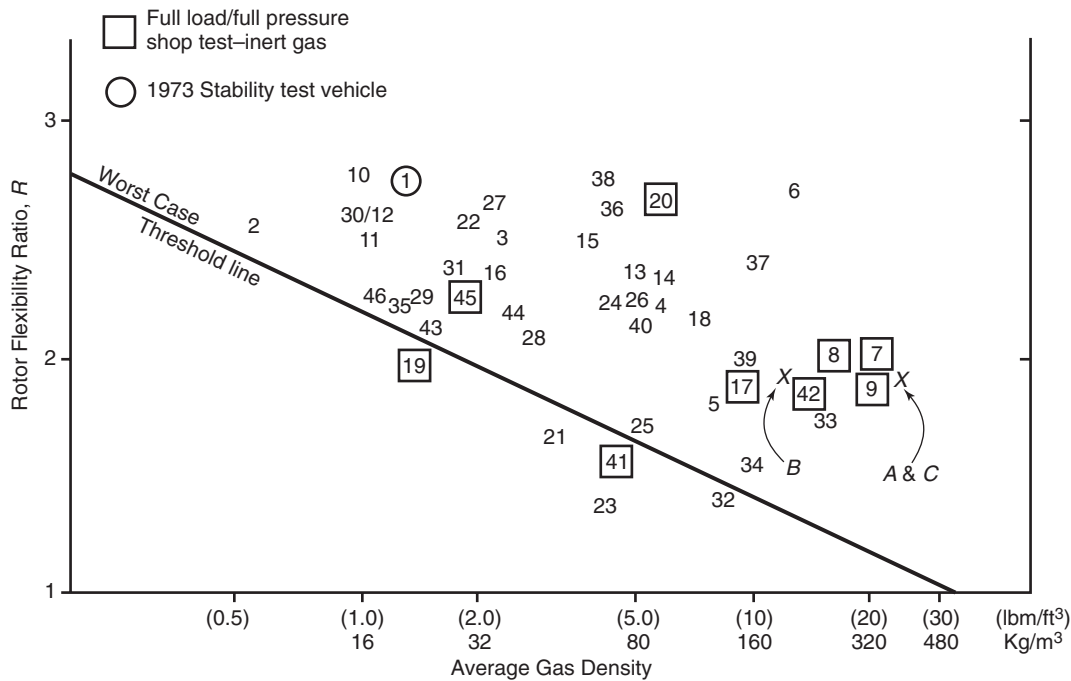


Figure 3-51—Shemeld's Compressor Experience Using Fulton's Criteria

3.7.1 References

1. Sood, V. K., 1979, "Design and Full Load Testing of a High Pressure Centrifugal Natural Gas Injection Compressor," Proceedings of the Eighth Turbomachinery Symposium, Turbomachinery Laboratory, Texas A&M University, College Station, Texas, pp. 35 – 42.
2. Fulton, J. W., 1984, "Full Load Testing in the Platform Module Prior to Two-Out: A Case History of Subsynchronous Instability," *Rotordynamic Instability Problems in High-Performance Turbomachinery*, NASA CP-2338y, pp. 1 – 16.
3. Kirk, R. G. and Simpson, M., 1985, "Full Load Shop Testing of 18,000 HP Gas Turbine Driven Centrifugal Compressor for Offshore Platform Service: Evaluation of Rotor Dynamics Performance," *Instability in Rotating Machinery*, NASA CP-2409, pp. 1 – 13.
4. Shemeld, D. E., 1986, "A History of Development in Rotordynamics – A Manufacturer's Perspective," *Rotordynamic Instability Problems in High-Performance Turbomachinery*, NASA CP-2443, pp. 1 – 18.

3.8 MACHINERY SPECIFIC CONSIDERATIONS

3.8.1 Steam Turbines

Early observations of instability problems in steam turbines reported a load dependent phenomenon. Pollman and Termeuhlen [1] described several cases in which they classified the instability as "steam whirl." Some of these cases, however, turned out to be oil whirl caused by the unloading of

fixed arc hydrodynamic bearings due to partial admission forces. Other cases clearly were not caused by unloading of the bearings but were a genuine instability. Greathead and Bostow [2] described a load dependent instability in which the unit could be satisfactorily operated at 90% power, but would whirl subsynchronously at its first natural frequency at higher powers. In steam turbines, these observations led to the characterization of an "onset power level" of instability in deference to the more widely known "onset speed" of instability associated with fixed arc hydrodynamic bearings.

Steam turbines, in general, are much less prone to instability compared to other classes of turbomachinery such as high-pressure centrifugal compressors. Those turbines that might be susceptible to instability typically operate at high rotational speeds with high inlet steam pressures, and/or develop very high stage horsepower. The destabilizing forces that drive these instabilities are caused by steam leakage through eccentric peripheral clearances, as illustrated in Figure 3-52, Greathead and Bostow [2]. These forces are often referred to as aerodynamic since they are the result of fluid forces acting on the rotor. In steam turbines, the two sources of concern are labyrinth shaft seals and blade tip clearance leakage. Partial admission forces are a factor also since they affect rotor position and bearing loading causing changes in stiffness and damping characteristics. An instability problem and solution on a 3600 rpm generator drive steam turbine operating on tilting pad bearings is presented in Armstrong and Perricone [3]. An analysis methodology and example is presented in Edney and Lucas [4].

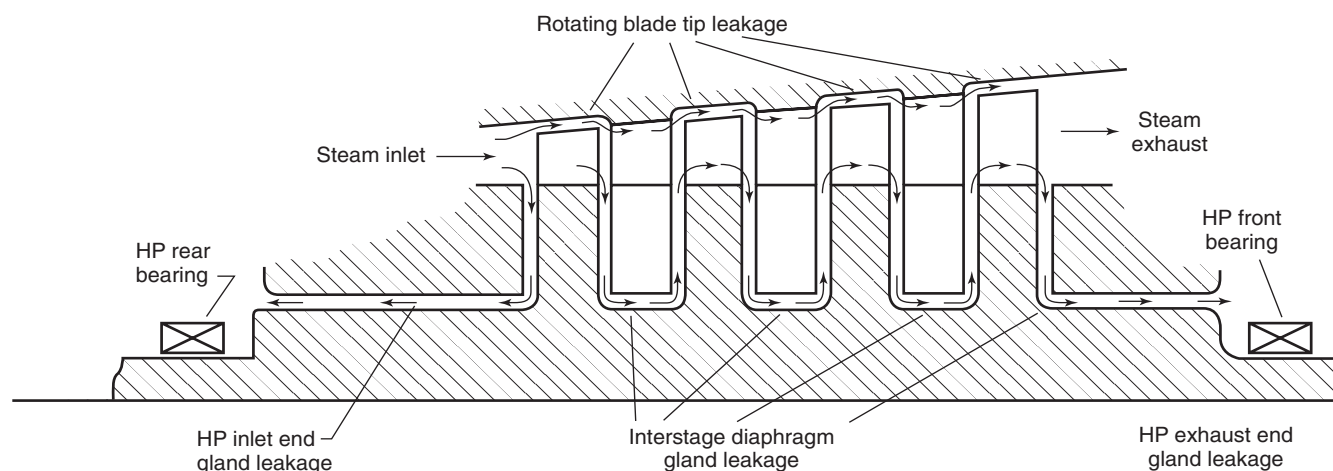


Figure 3-52—Steam Turbine Leakage Path

3.8.1.1 Labyrinth Shaft Seals

In steam turbines, labyrinth shaft seals are the primary destabilizing source. The magnitude of the destabilizing force, and hence the likelihood of unstable operation, increases with pressure, speed, and rotor-seal eccentricity. Due to the large pressure drop and number of seals used, the labyrinths located in the high-pressure end gland of the machine typically generate the highest destabilizing forces. On the other hand, the seals located near the center of the rotor can have a greater destabilizing influence due to the increased potential for rotor-seal eccentricity due to rotor sag (particularly on long flexible rotors) and/or higher rotor response amplitudes.

The destabilizing forces are a resultant combination of the axial flow associated with the pressure drop across the seal plus the accompanying fluid circumferential velocity due to shaft rotation. The axial component can be more easily explained by considering a stationary rotor. As the eccentricity increases, a larger average pressure develops on the side of the seal with the smaller local clearance and vice versa. The resultant pressure differential produces a restoring force that opposes the rotor displacement and acts to restore the rotor to the center of the seal, which can be represented as a direct stiffness. When the rotor starts to spin, the fluid forces acting on it become more complicated as illustrated in Figure 3-53 for clockwise rotation. As the rotor eccentricity increases the clearance cavity becomes more offset. Similar to a sleeve bearing, the hydrodynamic effects in the highly offset clearance cavity cause an increase in pressure in the converging region and a reduction in pressure in the diverging region. This pressure differential yields a net force F_t , tangential to the rotor's displacement or, as illustrated for the case in Figure 3-53, to the right in a clockwise (or forward whirl) direc-

tion around the center of the seal. The radial force component $F_r = (K + c\omega)e$, is negligible for labyrinth seals. The tangential force component $F_t = (k - C\omega)e$, will either destabilize ($F_t > 0$) or stabilize ($F_t < 0$) a rotor in forward whirl. Refer to 3.4.2 for additional information.

3.8.1.2 Blade Tip Clearance Leakage

A secondary aerodynamic source is from tip clearance leakage of the rotating blades in eccentric operation. This excitation arises due to the variation in blade efficiency associated with a change in tip clearance, which was first postulated by Thomas [5] in connection with instability problems on steam turbines. Alford [6] later identified the same mechanism associated with instability problems on aircraft gas turbines. In steam turbines these forces are sometimes neglected due to their relatively small magnitude compared to labyrinth seal forces. The cross coupled stiffness is approximated from Alford's equation, which is given in 3.5.1.1 as Equation 3-3. For steam turbines, the B_T in equation 3-3 is an empirical adjustment factor, usually in the range from 1.0 to 3.

The clearance excitation force is purely destabilizing without any direct stiffness or damping. For further information, the experimental work of Urlichs [7] on un-shrouded, and Leie and Thomas [8] on shrouded tip leakage effects are suggested. Although these researchers have measured values for B_T of up to 5, experience has shown that for practical purposes a value of 1.5 yields more appropriate results.

3.8.1.3 Partial Admission Forces

It has long been recognized that the entire control valve opening sequence and the effect of partial admission diaphragm stages must be considered in a rotor response analy-

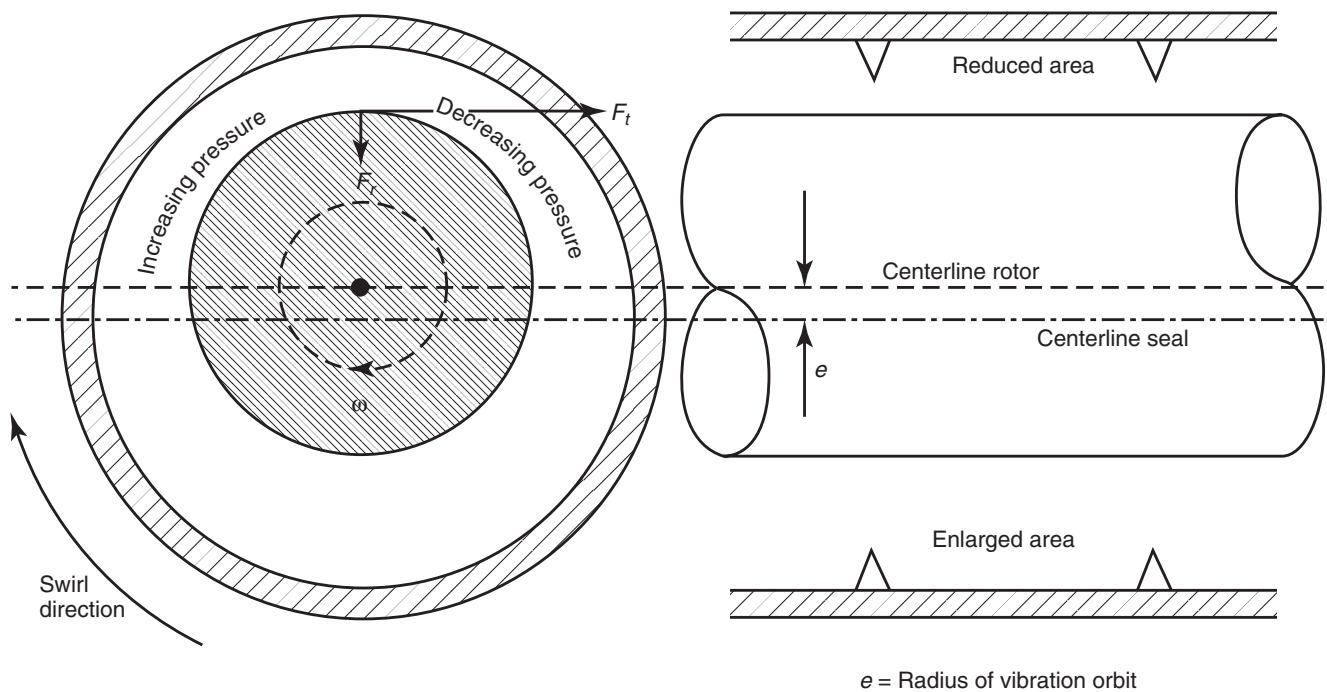


Figure 3-53—Aerodynamic Labyrinth Seal Forces

sis. This is especially so in cases where partial admission forces are large relative to the rotor weight. The resultant effect can be one in which the rotor is loaded into a sector of the bearing where the dynamic characteristics are significantly different from what they would be due to gravity load alone in Figure 3-54. Consequently, changes in turbine load can yield significantly different operating vibration amplitudes as reported in Caruso, et al. [9]. Similarly, the stability of the rotor system can be affected. In the case of a machine with small stability margin, the change in bearing loading associated with a change in admission arc could alter the oil film stiffness and damping characteristics sufficiently to cause the machine to go unstable. There are two sources of partial admission force. The primary source is the inlet and extraction (if included) control stages which, depending on the operating point, can have a wide range of admission arcs and hence loading conditions. Another source is partial admission diaphragm stages that are occasionally used for flow-path efficiency considerations.

The resultant forces imposed on the rotor are of two types; a tangential component derived from the stage torque reaction, and an axial thrust from the pressure drop across the nozzles. The axial thrust is orientated at the centroid of the

admission arc and can be resolved into radial force couples at the bearings. The axial thrust forces are usually small compared to the tangential torque reactions and are typically neglected. A possible situation where they might need to be accounted for, however, would be at the inlet control stage with only one or two valves open yielding a small admission arc. Since the pressure drop across the control stage is typically quite high, the axial thrust on the first row of blades would also be high and the location of the centroid at a large radius. As the admission arc increases, the radius to the centroid reduces, as does the resultant bearing loading. A typical force diagram illustrating how to resolve these forces into journal bearing reactions is shown in Figure 3-55. In this figure, stage torque reactions typical of an inlet and extraction control stage are represented, given by the subscripts 'i' and 'e' respectively.

3.8.1.4 Analysis Methodology

The analysis methodology and acceptance criteria that should be followed are outlined in 3.12. The following procedure is given for general guidance only. The Stability Standard Paragraphs should be reviewed for additional

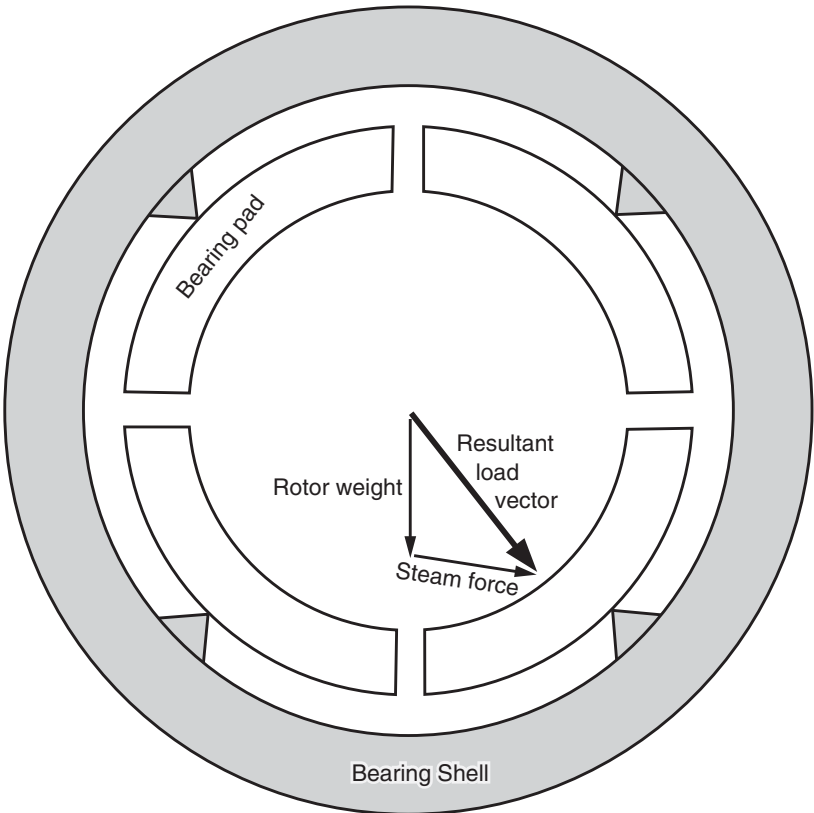


Figure 3-54—Typical Resultant Bearing Load Vector Including Partial Admission Steam Forces

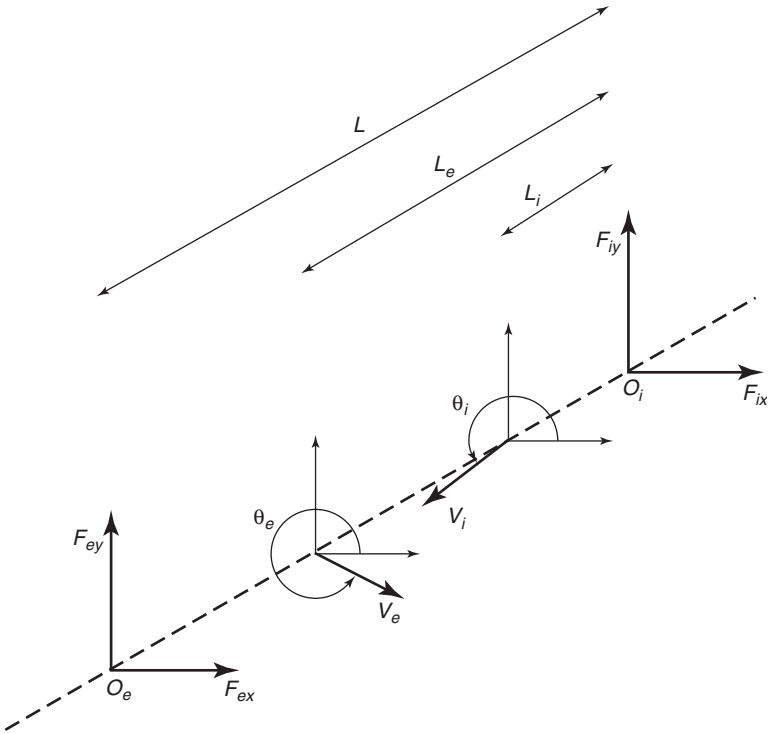


Figure 3-55—Resolution of Partial Admission Forces into Journal Bearing Reactions

detail. The stability analysis should be conducted including the effects of any external bearing loading such as from partial arc admission.

- a. Create a mass-elastic model of the rotor.
- b. Calculate the stiffness and damping coefficients of the radial bearings. The bearing loading should include both the static rotor weight and any external loading such as from partial arc forces as appropriate.
- c. Combine the bearing coefficients in series with the support coefficients, and squeeze film dampers where used.
- d. Apply cross coupling as detailed below.
- e. In a Level I stability analysis, the applied cross coupling, Q_a , should be the sum of the stage cross coupling as given by Alford's equation (as defined in SP6.8.5.6.b in 3.12.2) and placed at the rotor's mid-span. The cross coupling should be calculated at the rated condition of the machine as specified in SP6.8.5.1 in 3.12.2, or as mutually agreed by purchaser and vendor. This analysis provides an initial screening that is intended to eliminate only those rotors that do not require a more detailed study.
- f. The stability analysis should be conducted using an appropriate rotordynamics computer code. The analysis shall be run at the mean value of oil inlet temperature for both minimum and maximum extremes of component clearance. A stability plot corresponding to the first forward mode should then be developed containing a minimum of five calculated points for each clearance analyzed (see SP6.8.5.9 in 3.12.2).
- g. If the logarithmic decrement with the applied cross coupling as above is greater than 0.1, stability is acceptable and no further analysis is required. If the logarithmic decrement is less than 0.1, then a Level II analysis is required.
- h. If a Level II stability analysis is required, the labyrinth cross coupling and stage cross coupling should be applied explicitly at the appropriate seal and wheel locations. Alford's equation should be used for the stage cross coupling and an appropriate seal code for the labyrinth cross coupling. The cross coupling should be calculated at the rated conditions of the machine extrapolated to the maximum continuous operating speed.
- i. The final stability analysis shall be run at the extreme values of oil inlet temperature for both minimum and maximum of component clearance. The following conditions should be analyzed. The first is a baseline of the rotor and support system only. The second is with the addition of each group of destabilizing effects (e.g., seal forces, blade loading, etc.), and the third with all the destabilizing forces included.
- j. With all destabilizing forces included, stability is acceptable and no further analysis required if the logarithmic decrement at the maximum operating speed is greater than 0.1.

3.8.1.5 References

1. Pollman, E. and Termuehlen, H., 1975, "Turbine Rotor Vibrations Excited by Steam Forces," ASME Paper 75-WA/Pwr-11.
2. Greathead, S. and Bostow, P., 1976, "Investigations into Load Dependent Vibrations of the High Pressure Rotor on Large Turbo-Generators," Proceedings of the Institution of Mechanical Engineers Conference on Vibrations in Rotating Machinery, Cambridge, England, pp. 279 – 286.
3. Armstrong, J. and Perricone, F., 1996, "Turbine Instability Solution – Honeycomb Seals," Proceedings of the Twenty-Fifth Turbomachinery Symposium, Turbomachinery Laboratory, Texas A&M University, College Station, Texas, pp. 47 – 56.
4. Edney, S. L. and Lucas, G. M., 2000, "Designing High Performance Steam Turbines with Rotordynamics as a Prime Consideration," Proceedings of the Twenty-Ninth Turbomachinery Symposium, Turbomachinery Laboratory, Texas A&M University, College Station, Texas, pp. 205 – 224.
5. Thomas, H., 1958, "Instabile Eigenschwingungen von Turbinenlaufern, Angefacht durch die Spaltströmungen Stopfbuchsen und Beschaufelungen," *Bull de L'AIM*, 71.
6. Alford, J. S., 1965, "Protecting Turbomachinery from Self-Excited Rotor Whirl," *ASME Journal of Engineering for Power*, 87 (4), pp. 333 – 344.
7. Urlichs, K., 1976, "Die Spaltströmung bei Thermischen Turbo-Maschinen als Ursache für die Entstehung Schwingungsanfacher Querkraft," *Ingenieur-Archiv*, 45.
8. Leie, B. and Thomas, H., 1980, "Self-Excited Rotor Whirl due to Tip-Seal Leakage Forces," NASA CP-2133.
9. Caruso, W. J., Gans, B. E. and Catlow, W. G., 1982, "Application of Recent Rotor Dynamics Developments to Mechanical Drive Turbines," Proceedings of the Eleventh Turbomachinery Symposium, Turbomachinery Laboratory, Texas A&M University, College Station, Texas, pp. 1 – 17.

Nomenclature

- B_t = Empirical adjustment factor = 1.5,
- c = Labyrinth seal cross coupled damping, N-s/m (lbf-s/in.),
- C = Labyrinth seal direct damping, N-s/m (lbf-s/in.),
- e = Synchronous precession orbit, m (in.),
- F_{ex} = Exhaust end bearing partial admission force reaction X direction, N (lbf),
- F_{ey} = Exhaust end bearing partial admission force reaction Y direction, N (lbf),

- F_{ix} = Inlet end bearing partial admission force reaction X direction, N (lbf),
 F_{iy} = Inlet end bearing partial admission force reaction Y direction, N (lbf),
 F_r = Radial force component, N (lbf),
 F_t = Tangential force component, N (lbf),
 H_t = Effective blade height, m (in.),
 k = Labyrinth seal cross coupled stiffness coefficient, N/m (lbf/in.),
 K = Labyrinth seal direct stiffness coefficient, N/m (lbf/in.),
 L = Bearing span, m (in.),
 L_e = Length from inlet end bearing to extraction control stage, m (in.),
 L_i = Length from inlet end bearing to inlet control stage, m (in.),
 O_e = Origin extraction control stage,
 O_i = Origin inlet control stage,
 q_A = Clearance excitation cross coupled stiffness, N/m (lbf/in.),
 V_e = Extraction control stage partial admission force vector, N (lbf),
 V_I = Inlet control stage partial admission force vector, N (lbf),
 θ_e = Angle from X direction to extraction control stage force vector, rad (deg),
 θ_I = Angle from X direction to inlet control stage force vector, rad (deg),
 ω = Whirl frequency, rad/s.

3.8.2 Electric Motors and Generators

Electric motors and generators are inherently stable, as their rotor-stator systems do not contain any cross coupling force generating mechanisms such as oil seals or labyrinth seals. However, if they operate on fixed geometry bearings, a bearing stability analysis should be conducted as sleeve bearings can produce cross coupling forces that may be strong enough to drive the motor and/or generator rotor unstable (see 3.3.2).

3.8.3 Power Turbines and FCC Power Recovery Expanders

The following discussion applies to overhung one or two stage power turbines and Fluid Catalytic Cracking (FCC)

power recovery expanders. This equipment is subjected to adverse operating conditions: inlet temperatures exceed 1200°F and, in the case of FCC expanders, the working gas can be laced with solid particles or contain high levels of corrosive compounds. Typically, this type of equipment possesses an extremely stiff rotor as the first undamped rigid bearing critical speed is generally above operating speed. A typical undamped critical speed map for an FCC expander rotor is illustrated in Figure 3-56. Since the rotating element is much stiffer than most ordinary compressors or steam turbines, the journal bearings and bearing support structures largely determine the critical speed and stability characteristics of these types of units. For the purpose of this discussion, it is assumed that the rotating element is supported by fluid film journal bearings and not rolling element bearings.

Assuming that the rotating element is “stiff” relative to the journal bearings and bearing support stiffnesses, the lateral behavior of overhung power turbines or FCC expanders is governed by the mass distribution of the rotating element and the frequency dependent stiffness and damping characteristics of the bearings and bearing supports. The mass distribution of the rotating element is important because of its influence on the applied bearing loads. In particular, designers try to keep the center-of-gravity of the entire rotating element as far from the disk end bearing as possible (i.e., toward the coupling end bearing) in order to maintain load on the coupling end bearing. A downward load on the coupling end bearing prevents the rotor from tipping during disassembly. Keeping a net downward load on the coupling end bearing in a two stage overhung unit may require a massive centerbody section (large shaft section between journal bearings) resulting in a relatively stiff rotor compared to the journal bearings.

A low resultant load on the coupling end bearing may make the coupling end rotor synchronous response sensitive to unbalance. Coupling end unbalance sensitivity may be reduced by decreasing coupling end bearing assembly clearance and increasing tilting pad bearing preload. If fixed geometry bearings are used, the lightly loaded coupling end bearing may be susceptible to oil whirl. A case history of a sleeve bearing induced instability for an overhung power turbine is summarized in 3.3.2.4.

Because of sleeve bearing induced instability problems, many manufacturers have installed or retro-fitted stabilizing bearing designs such as pressure dam or multi-pocket sleeve bearings in favor of two or three axial groove sleeve bearings, Nicholas [1]. In general, such retrofits have eliminated sub-synchronous vibrations but have not eliminated misalignment problems that are common to “hot” equipment. For this reason, the trend has been for new overhung units to be supported by tilting pad journal bearings whose tilting pads have some degree of axial misalignment capability. These bearings have been shown to virtually eliminate babbitt edge-loading problems.

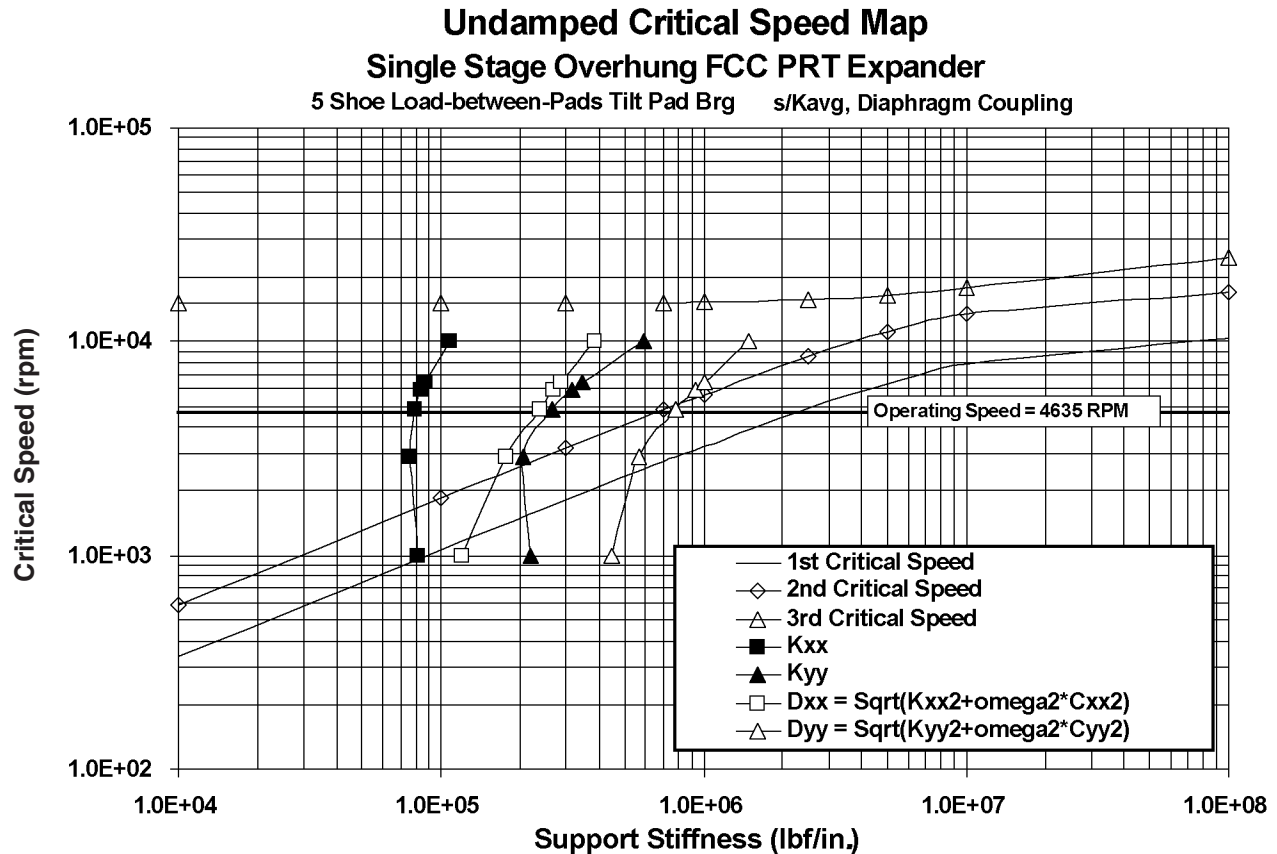


Figure 3-56—FCC Expander Critical Speed Map

In cases where rotor instability cannot be solved by bearing modifications, inadequate lubricant drainage may be the cause of the problem. Elimination of standing pools of lubricant in the bearing carrier by increasing drain size will generally cure this type of instability problem.

Unlike most “cold” units such as centrifugal compressors, the bearing support structure must be capable of accommodating the thermal growths associated with “hot” operation. This generally means the supporting structure is light and/or flexible relative to the rotating assembly. Figure 3-57 illustrates a cross-section of an FCC power recovery expander. Note that the coupling end bearing is well supported in the radial direction by a pedestal box-structure while the disk end bearing is only supported by a box-like structure that is cantilevered from the pedestal.

For the expander displayed in Figure 3-57, the static stiffness of the coupling end bearing support is greater than 3.0×10^6 lbf/in. while the static stiffness measured for the disk end bearing support is much less than 1.0×10^6 lbf/in. The low stiffness associated with the disk end bearing support reduces the effectiveness of the disk end journal bearing’s damping capability [2]. This, in turn, reduces the ability of the disk end bearing to suppress rotor vibrations and to promote stable rotor operation. For this reason, among others, expander

designers have increased the diameter of the disk end journal in an effort to reduce disk end journal bearing unit loading and thus, disk end journal bearing stiffness.

It is not an easy matter to measure or calculate the dynamic stiffness and damping properties of the bearing supports for the following reasons:

1. Static deflection tests of the bearing pedestal appear to indicate that the exhaust casing may influence support properties.
2. Support properties may be influenced by temperature.

Given the unknowns in the support data, any lateral analysis of these overhung machines should incorporate previously accumulated experience. Specifically, the calculated first critical speed should always be compared to those measured for similar units.

In summary, any lateral model of an overhung power turbine or FCC expander must incorporate accurate descriptions of the bearing support’s dynamic properties. Such properties may be calculated or measured but should always be tempered by experience. Figure 3-58 contains a schematic of the resulting rotor-bearing-support model of this equipment. Inclusion of the flexible support data in lateral models can dramatically lower calculated critical speeds [2] and damped

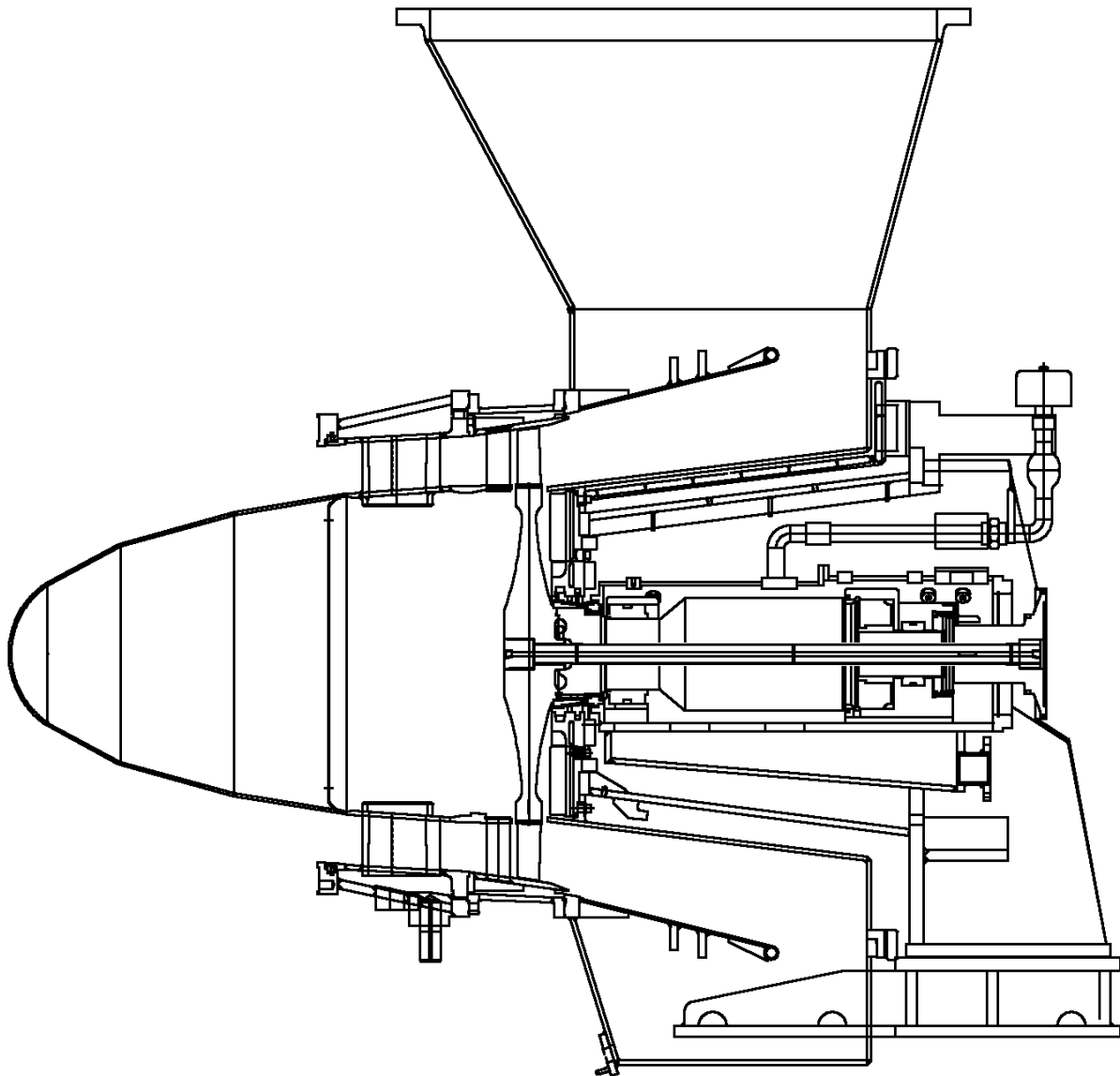


Figure 3-57—FCC Expander Cross-section

natural frequencies for these types of units (see 3.6). Unfortunately, since these units are so dependent upon bearing and bearing support dynamic properties, it is difficult to accurately predict critical speed and stability log decrement values without accurate bearing and support models. Manufacturer's experience with similar equipment will also help in providing an accurate measure of lateral critical speed and stability performance.

3.8.3.1 References

1. Nicholas, J. C., 1985, "Stability, Load Capacity, Stiffness and Damping Advantages of the Double Pocket Journal Bearing," *ASME Journal of Tribology*, 107 (1), pp. 53 – 58.

2. Nicholas, J. C., Whalen, J. K. and Franklin, S. D., 1986, "Improving Critical Speed Calculations Using Flexible Bearing Support FRF Compliance Data," Proceedings of the Fifteenth Turbomachinery Symposium, Turbomachinery Laboratory, Texas A&M University, College Station, Texas, pp. 69 – 78.

3.8.4 Axial Compressors

The rotordynamic characteristics of axial compressors normally do not present any particular rotordynamic problems. The rotor mass-elastic characteristics depend on the method of rotor construction and blade attachment. The four typical methods of rotor constructions are disc-on-shaft shrink fit

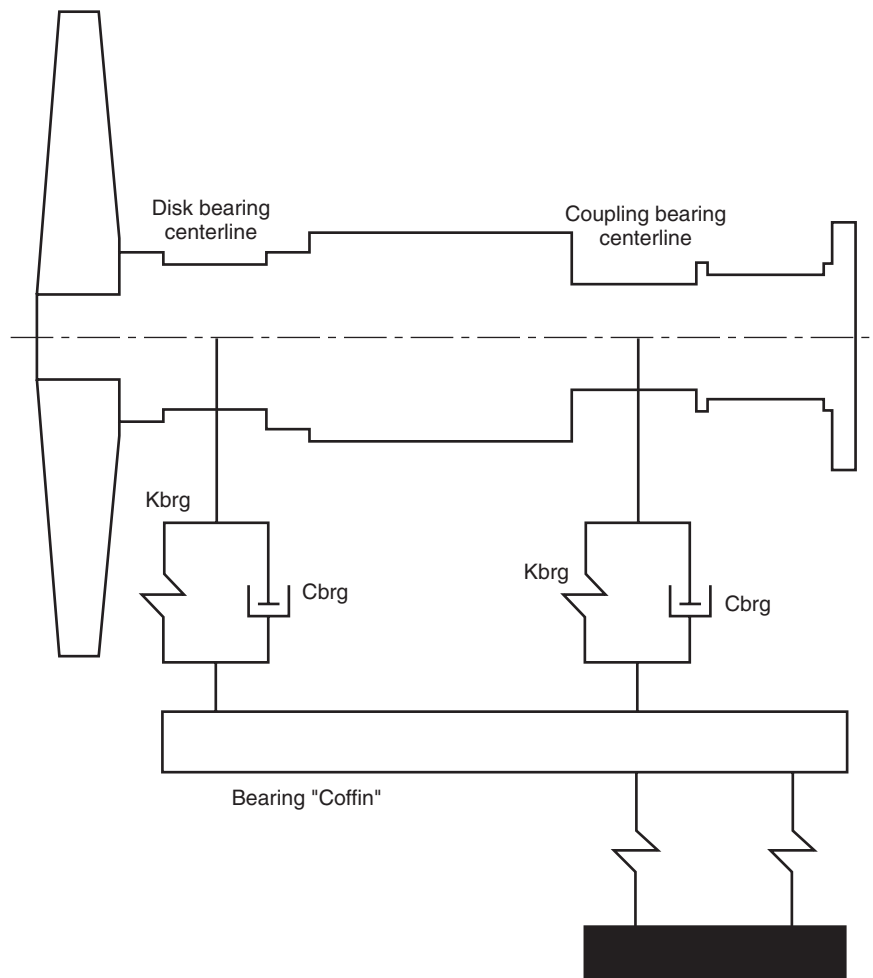


Figure 3-58—FCC Expander Rotor-bearing-support Model

(similar to most centrifugal compressors), stacked disk with through tie bolts, drum rotors with studs or tie bolts, and solid rotors. Four typical axial compressor rotor construction examples are illustrated in Figures 3-59 through 3-62.

Because of their complex construction features, the modeling of axial compressor rotors demands significant attention. Tie rod and stud torque levels along with stacked disk surface interactions greatly affect the stiffness properties of the rotor. In general, axial compressor rotors are more rigid than other process turbomachinery because of their large mid-span diameters and their hollow construction. For a solid cylinder and a hollow cylinder of equal cross-sectional area, the hollow cylinder will have higher lateral bending stiffness.

Furthermore, the support characteristics (pedestals) of axial compressors could be of the same order of magnitude as the fluid film characteristics of the journal bearings in which the rotor is supported. Hence this should be accounted for in the rotordynamic analysis as required, Nicholas and Kirk [1] (see 3.6).

The destabilizing aerodynamic cross coupling stiffness in an axial compressor stage can be estimated from Alford's equation which is discussed in detail and given as Equation 3-3 in 3.5.1.1. If deemed necessary, the stability characteristics of an axial compressor due to aerodynamic cross coupling forces can be evaluated using the cross coupling coefficients calculated from Alford's equation. Stability characteristics of axial compressor should also be evaluated if supported by fixed geometry bearings [1] as sleeve bearings can induce an excitation force that may drive the axial compressor rotor unstable (see 3.3.2). In general, stability is not a problem associated with axial compressors.

Table 3-2 provides a summary of the rotordynamic characteristics of several axial compressors of different frame sizes operating in the field with 5-pad tilting pad journal bearings. The data in Table 3-2 illustrates typical parameters associated with axial compressors that are in operation without any vibration problems. Note that the journal bearing unit loads all range between 125 and 255 psi.

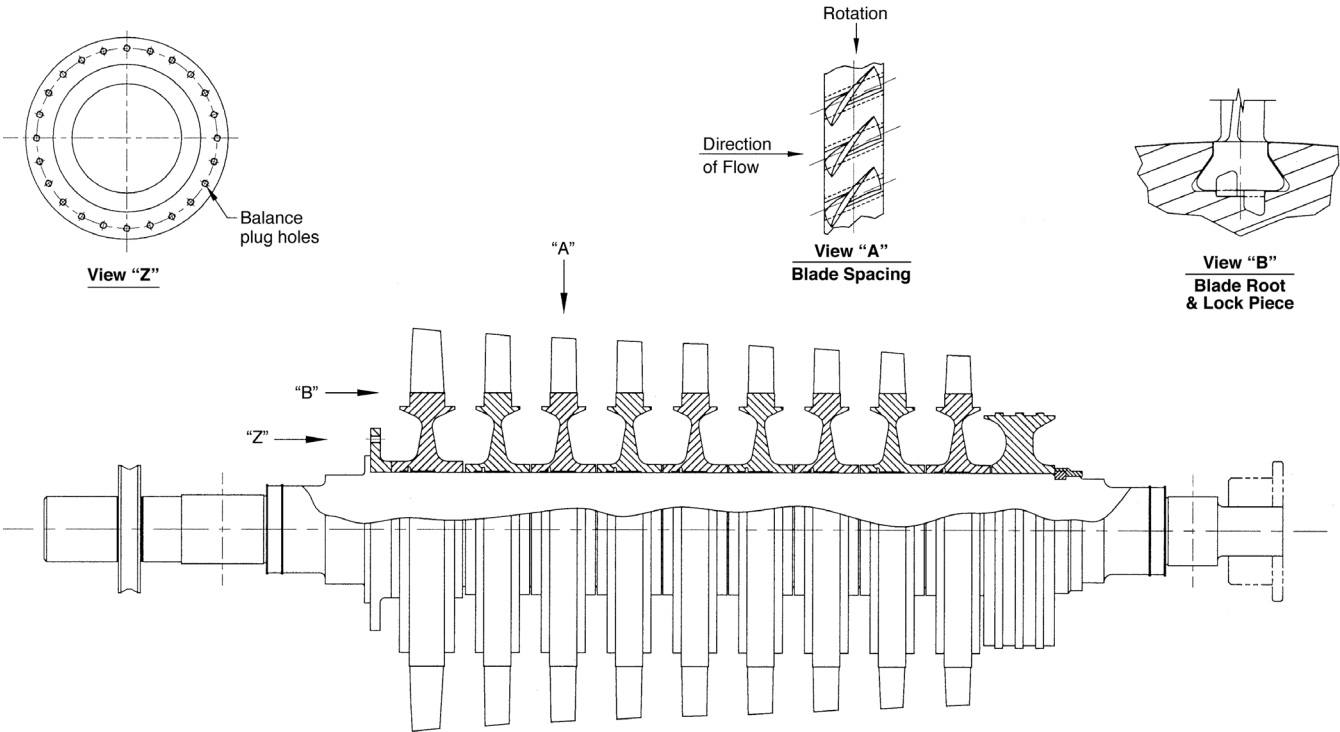


Figure 3-59—Axial Compressor Rotor Construction: Disk-on-shaft Shrink Fit

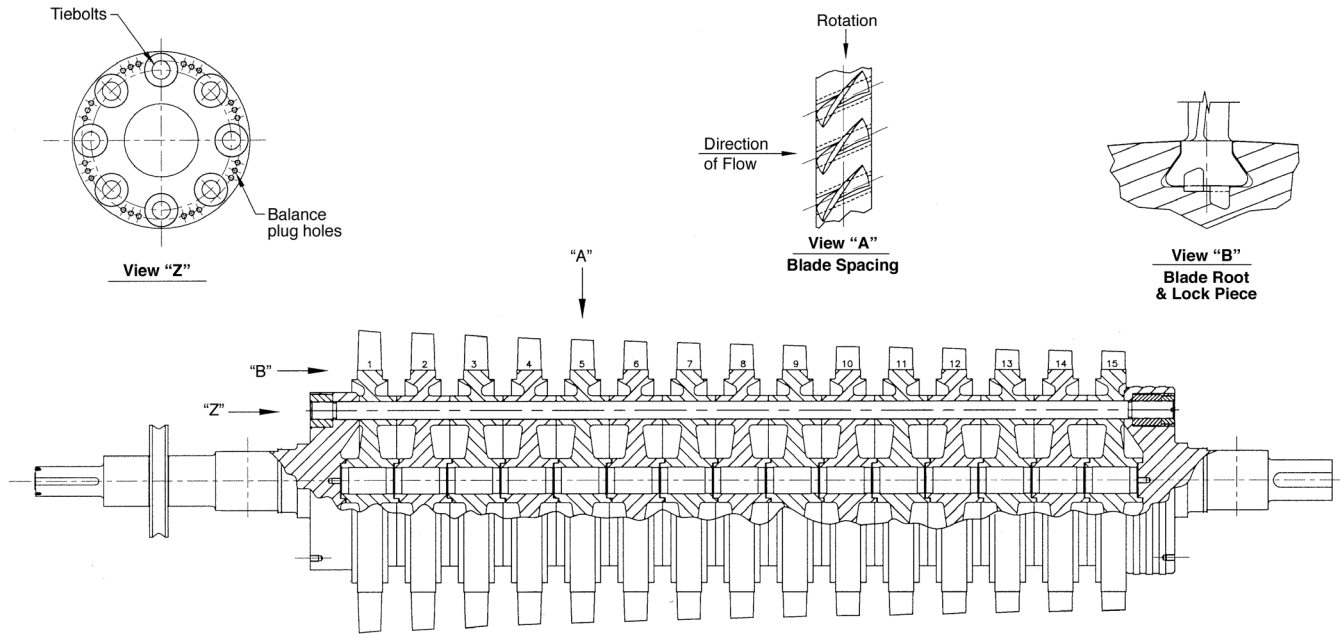


Figure 3-60—Axial Compressor Rotor Construction: Stacked Disks with Tie Bolts

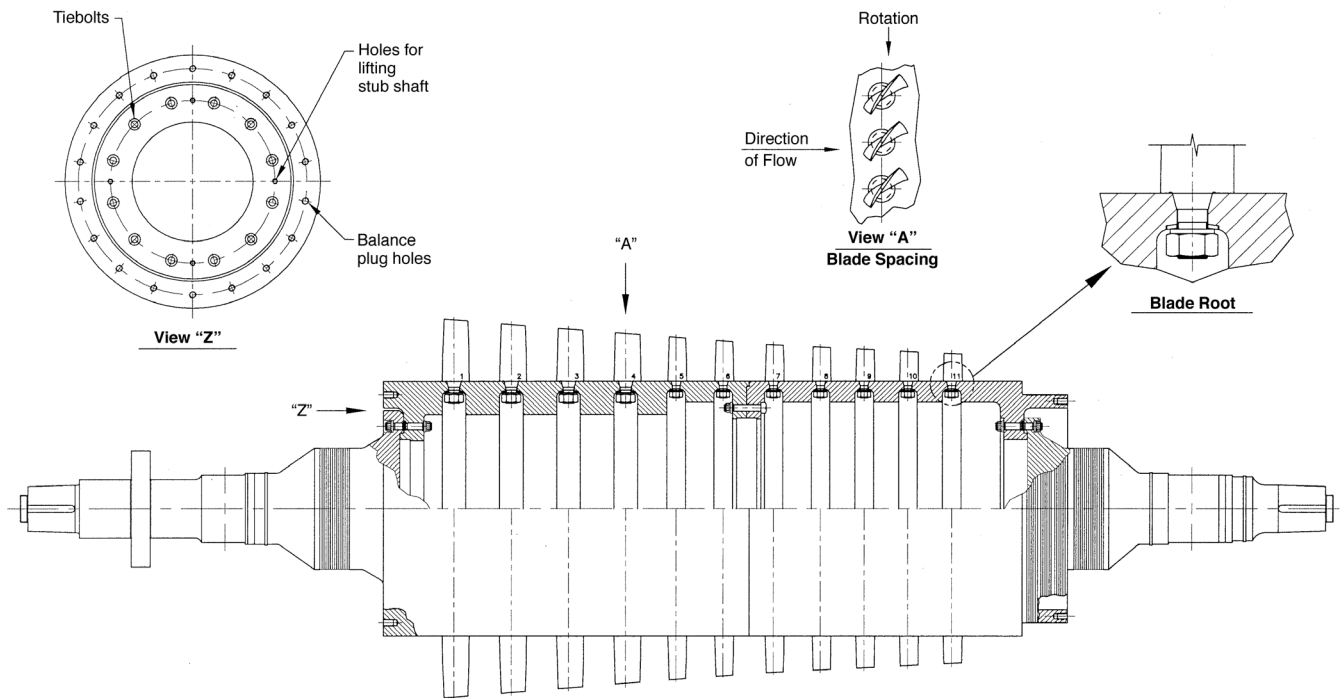


Figure 3-61—Axial Compressor Rotor Construction: Drum Rotor with Studs

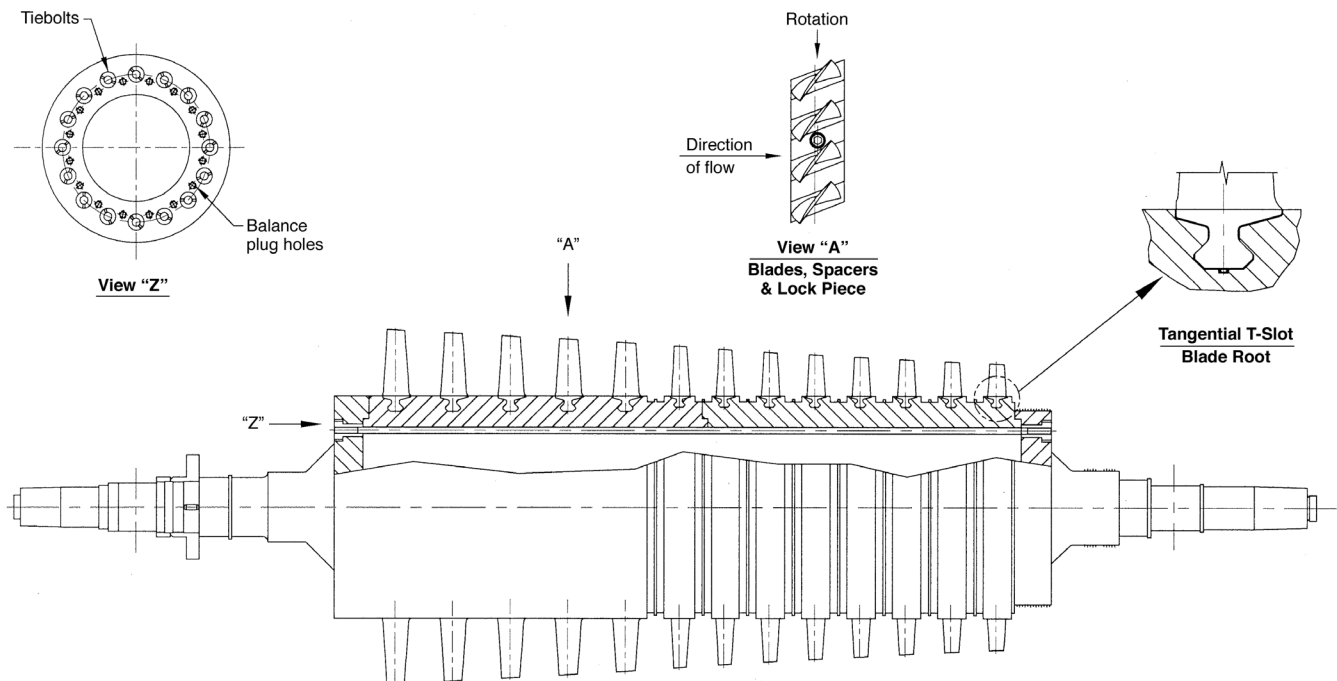


Figure 3-62—Axial Compressor Rotor Construction: Drum Rotor with Tie Bolts

Table 3-2—Rotordynamic Characteristics of Axial Compressors

No.	Maximum Continuous Speed (rpm)	Minimum Continuous Speed (rpm)	Critical Speed Ratio (MCOS/Nc1)	Bearing Geometry and Diameter, D (in) x Length, L (in)	Average Bearing Unit Load, L_u^* (psi)
1	6240	6080	1.64	5-LBP 5 x 2.125	213.5
2	7046	6039	1.60	5-LBP 5 x 2.125	190.0
3	6225	6225	1.20	5-LBP 6 x 3	128.5
4	6090	4567	1.57	5-LBP 5 x 2.125	215.5
5	7065	6575	1.81	5-LBP 5 x 2.125	216.5
6	7046	6375	1.60	5-LBP 5 x 2.125	217.0
7	6199	5996	1.63	5-LBP 5 x 2.125	234.5
8	5775	5500	2.14	5-LBP 6 x 3	190.0
9	6245	6140	1.52	5-LBP 5 x 2.125	162.5
10	5890	4485	2.18	5-LBP 6 x 3	209.5
11	5180	4864	2.25	5-LBP 6 x 3	254.5
12	5890	4488	1.90	5-LBP 6 x 3	173.5
13	3780	3600	1.99	5-LBP 8 x 7	200.5
<p>5-LBP = Five pad tilting pad journal bearing (load between pads). L_u = bearing load/($L \cdot D$) (psi)</p>					

3.8.4.1 References

1. Nicholas, J. C. and Kirk, R. G., 1982, "Four Pad Tilting Pad Bearing Design and Application for Multi-Stage Axial Compressors," *ASME Journal of Lubrication Technology*, 104 (4), pp. 523 – 532.

3.8.5 Gearboxes

Gearbox instability problems usually occur at partial gear loads with sleeve bearings. Often, during start-up or shut-down, the gear mesh is unloaded or only partially loaded. The bull gear and pinion bearings must be sized to handle the full gear load. Thus, they are oversized for the partial load condition. As described in 3.3.2, lightly loaded sleeve bearings are susceptible to oil whirl instability. This usually occurs on the pinion, as the bull gear is normally heavy enough to maintain a reasonable gravity load on the bull gear bearings.

For this reason, a full stability analysis should be conducted on the pinion and bull gear at light or partial load conditions to insure stable operation. A stabilized sleeve bearing design, such as a pressure dam bearing, Nicholas and Allaire [1], is often utilized to help overcome lightly loaded sleeve bearing induced oil whirl instabilities.

An example of pressure dam bearings designed for gearbox application is shown in Figures 3-63 and 3-64, Nicholas [2]. Figure 3-63 shows a pressure dam bearing design for the high-speed pinion. Since the resultant external gear force,

W_g , is directed downward, the pressure dam is placed in the upper half. This insures that the bearing's load capacity is at a maximum for 100% load. Note that for the 100% load case the load vector as well as the minimum film thickness are located in the lower half, but for the 25% load case, although the load vector is located in the lower half, the minimum film thickness is located at the horizontal split. The pressure dam helps to load the bearing at partial gear load conditions, thereby improving the sleeve bearing's stability performance.

Figure 3-64 shows the pressure dam bearing design for the bull gear. Now, the gear force is directed upward and the pressure dam is placed in the lower half. This insures that the bearing's load capacity is at a maximum for 100% load. Note that the 25% and 100% load vectors as well as the minimum film thickness for both cases are all located in the upper half.

The above example is for a "down mesh" configuration where the bull gear "drives" the pinion downward due to the tangential gear force. The pinion is also pushed away from the bull gear due to the gear separating force. This results in the resultant load shown in Figure 3-63 at 18° (25% load condition) and 19° (100% load condition) with rotation from bottom dead center, which is approximately the gear pressure angle.

Gearboxes may also be found with "up mesh" gear sets where the bull gear drives the pinion upward. The choice of down or up mesh is at the discretion of the gear manufacturer as there are advantages of both. With down mesh sets, the

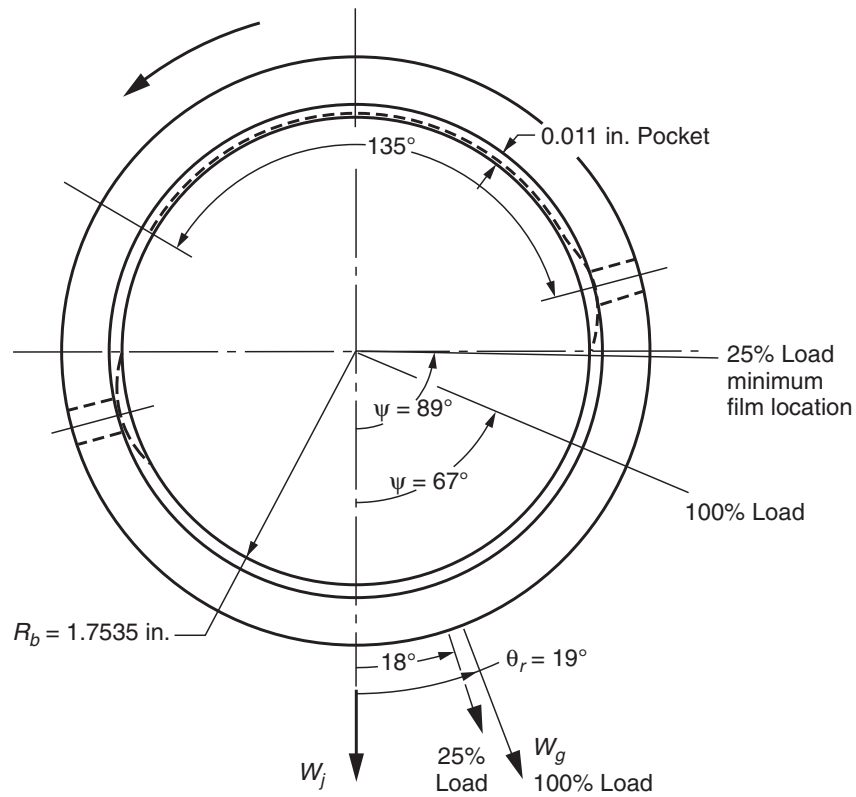


Figure 3-63—High-speed Gearbox Pressure Dam Pinion Bearing

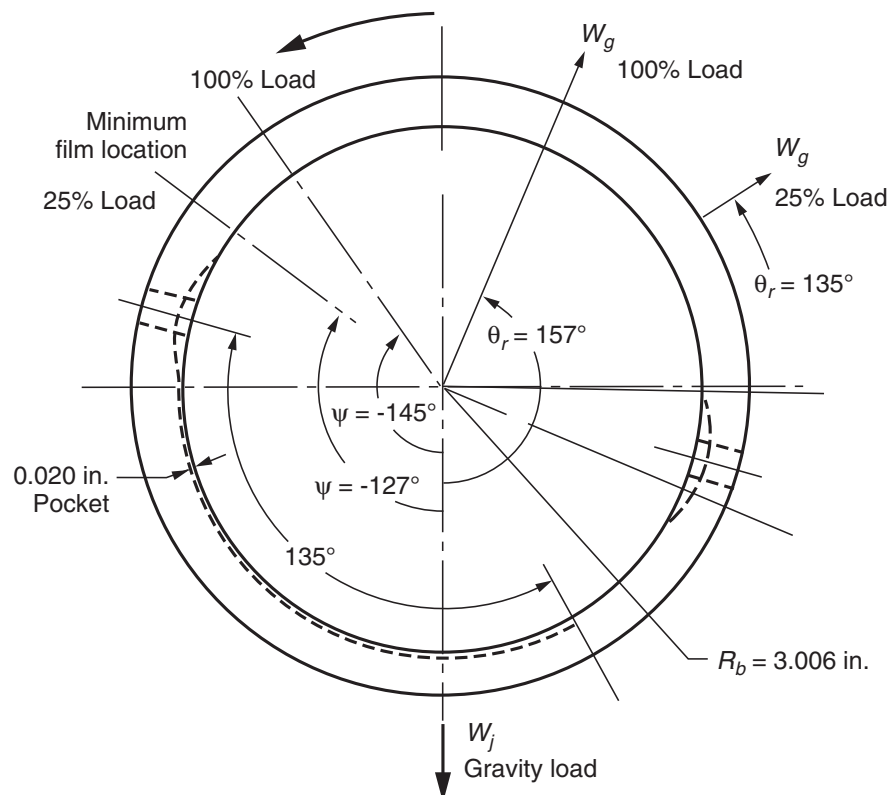


Figure 3-64—High-speed Gearbox Pressure Dam Bull Gear Bearing

pinion is always loaded downward from zero load to full load. However, the bull gear lifts up at full load. With up mesh sets, the bull gear bearings are always loaded downward from zero load to full load while the pinion bearings transition from down loads to up loads. There are sleeve bearing stability concerns in both cases during the transition from down to up bearing loads.

High-speed pinions with tilting pad bearings will not go unstable, as there are no destabilizing mechanisms. The only exception is if the tilting pad bearing's oil inlet and discharge flow geometries are designed poorly thereby starving the bearing. Oil starvation can result in a subsynchronous rotor vibration. This phenomenon is described in detail in 3.3.3.2 and Figures 3-14, 3-15 and 3-16, from 3.3.3.2 all which are concerned high-speed gearbox pinion bearings.

3.8.5.1 References

1. Nicholas, J. C. and Allaire, P. E., 1980, "Analysis of Step Journal Bearings—Finite Length, Stability," ASLE Transactions, 23 (2), pp. 197 – 207.
2. Nicholas, J. C., 1996, "Hydrodynamic Journal Bearings - Types, Characteristics and Applications," Mini Course Notes, 20th Annual Meeting, The Vibration Institute, Willowbrook, Illinois, pp. 79 – 100.

3.8.6 Centrifugal Compressors

In previous sections, factors/components that require careful examination to obtain accurate stability predictions have been discussed. What remains is the incorporation of these factors/components into an analysis procedure applicable to centrifugal compressors. Ideally, the process illustrated in the stability analysis flow chart Figure 3-2 is universal in its application (see 3.1). However, the criticality of some aspects of the analysis does change with the rotor application. Special considerations for various configurations of centrifugal compressors are handled in the following subsections.

In general, the procedure for performing a stability analysis on centrifugal compressors can be outlined as below:

- a. Develop rotor model—Includes shaft model, added mass of impellers, coupling(s), thrust collar, and sleeves (see 3.2).
- b. Analyze bearing dynamic behavior—Account for assembly and machining tolerances of clearance and lube oil supply temperature range on the dynamic behavior (see 3.3).
- c. Analyze oil seals (if used)—Following the rotor and bearings, the most influential item on the rotor stability condition (see 3.4.1).
- d. Approximate the level of destabilizing forces remaining—The modified Alford's equation approximates the "internal" cross coupling anticipated for the specified compressor parameters (see 3.5.1).

e. Level I stability analysis—Intended for newly designed or revamped compressors. Investigations into field related problems would be more likely to skip steps d and e.

f. Labyrinth seals and balance piston—Proceeding to a Level II analysis requires that a detailed analysis of the "internal" cross coupling sources be made. This should start with an accounting of the labyrinth seals in the compressor (see 3.4.2).

g. Aerodynamic cross coupling—Add appropriate terms due to flow path excitation (see 3.5.1).

h. Second order effects—Consider minor destabilizing forces (material hysteresis, shrink fits, torque whirl, etc.). These can play an important role if the rotor stability appears marginal (see 3.5.2).

i. Level II stability analysis—This should reflect the state-of-the-art predictive capability on the stability condition of the compressor.

j. Redesign or mutual agreement—Failure of the Level II specifications would require a rotor redesign or mutual agreement on acceptance.

3.8.6.1 Multi-Stage Compressors

The multi-stage configuration covers perhaps the largest variety of compression equipment, from large rotors in cracked gas service to high compression equipment in re-injection service, Figure 3-65. This equipment category also contains the highest risk in terms of instability. Paradoxically (or consequently), applying the stability analysis process to multi-stage compressors is the most straightforward.

The factors affecting stability in multi-stage compressors are numerous. A list of some of those is included below:

- a. The ratio of bearing span to shaft diameter (slenderness ratio)—This is used extensively to approximate the degree of bending of the first critical speed.
- b. Power requirement of the compressor—There is a correlation between the magnitude of the instability mechanisms and the gas power requirements, Wachel [1].
- c. Pressure rise across the compressor and final discharge pressure—Large pressure differentials and high discharge pressures increase the dynamic coefficients of labyrinth seals, Elrod [2], Wyssmann [3] and Kirk [12].
- d. Suction pressure of the compressor—Determines the sealing pressure of the compressor. Higher suction pressures equate to higher differentials across the main seals.
- e. Shaft speed—Taken on its own, higher shaft speed will increase the ratio of operating speed to the first critical speed and, thus, the likelihood of instability, Wachel [4].
- f. Bearing configuration—More of a concern on older designs with fixed pad bearings. The application of tilt pad

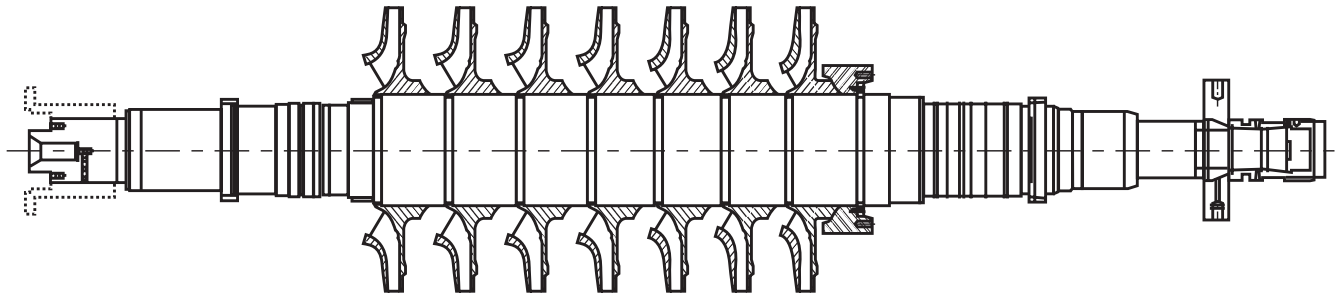


Figure 3-65—Typical Multi-stage High-pressure Centrifugal Compressor Rotor

bearings has eliminated the bearing as a major source of cross coupling and possible whirl (see 3.3).

g. Casing end seal type—As with tilt pad bearings, the dry gas seal, as a substitute for oil seals, has greatly reduced the instability drivers in newer designs. While oil seals have been shown to be a possible source of destabilizing cross coupling, dry gas seals are considered dynamically neutral, Atkins [5] (see 3.4.4). Note that oil seals may also be designed to drastically lower their associated cross coupled stiffness, Memmott [13].

h. Compressor configuration (back-to-back vs. straight through)—The compressor configuration is usually dictated by the performance requirements (e.g., inter-stage cooling). There may be some advantage in terms of rotor stability of one configuration over the other, Kirk [6, 7], but it also has been shown that either configuration can have instability problems, [13].

i. Gas molecular weight—Another parameter that experience has shown is directly related to the level of destabilizing forces present in a centrifugal compressor. Heavier molecular

weight gases tend to increase the possibility of instability, Kirk [8].

j. Gas density—Related to the discharge pressure and molecular weight, it is not surprising that higher gas densities are associated with an increased likelihood of instability, Wagner [9]. This factor is also found as the abscissa on numerous stability experience charts, Shemeld [10], Sood [11], Fulton [14] and Memmott [13,15].

3.8.6.2 Overhung Compressors

Stability is not normally a concern with this type of centrifugal compressor, Figure 3-66, due to the relatively high bending stiffness of the shaft. There are, however, high speed and power applications where stability should be examined. In these instances, the anticipated cross coupling should be applied at the overhung impeller center-of-gravity (CG). In the case of multiple overhung impellers, the placement should coincide with the combined CG of the impellers.

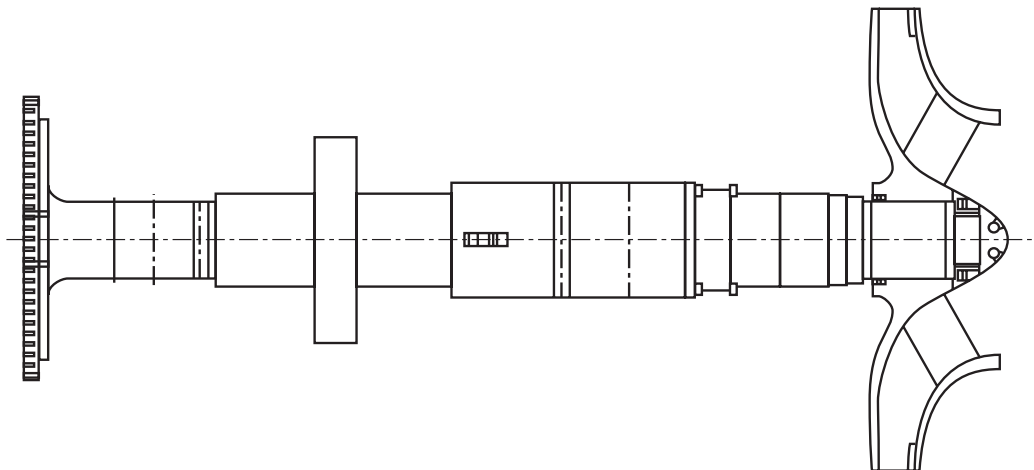


Figure 3-66—Overhung Compressor Rotor

An accurate rotor model is vital for any type of lateral analysis. However, certain factors have different effects on the prediction accuracy for given configurations. One example is the mass properties of centrifugal impellers: inertia and CG location. For multi-stage (or beam type) compressors, minor deviations in the magnitude from the “true” value will not vary the critical speed predictions significantly. In overhung compressors, the relevancy of the critical speed prediction is absolutely determined by the accuracy of the impeller inertia and CG location. Minor errors in these properties are magnified when dealing with overhung dynamics.

3.8.6.3 Integrally Geared Compressors

Integrally geared compressors differ from overhung compressors in two important aspects. First is the existence of the gear mesh at the center of the shaft (or pinion). The second difference is the possibility of having overhung impellers at both ends of the shaft. These distinguishing features can be seen on Figure 3-67. The gear mesh is unique for centrifugal compressors in that a significant radial load is produced which needs to be accounted for in the stability analysis. The radial load is treated as a vector addition to the rotor weight at the bearings. Variable inlet guide vanes make it possible to change the gas load at a constant speed. The varying loads may change the dynamic behavior of the radial bearing, thus, influencing the rotor stability. (The extent of the influence is greatly dependent on many factors of which the bearing type is one.) The range in gear loads in these cases should be considered when performing the stability analysis.

The possibility of having impellers at both ends of the shaft does add one small complication to the Level 1 analysis. Each impeller should be treated as a separate compressor. The implication here is that an anticipated cross coupling will be calculated and applied to each impeller for the Level 1 analysis. This is the only instance where more than one anticipated cross coupling is applied in a Level 1 analysis for centrifugal compressors. In the case of having a blind end pinion (one impeller only), the anticipated cross coupling is calculated and applied at the location of the individual impeller.

3.8.6.4 References

1. Wachel, J. C. and von Nimitz, W. W., 1981, “Ensuring the Reliability of Offshore Gas Compression Systems,” *Journal of Petroleum Technology*, pp. 2252 – 2260.
2. Elrod, D. A., Pelletti, J. M. and Childs, D. W., 1995, “Theory Versus Experiment for the Rotordynamic Coefficients of an Interlocking Labyrinth Gas Seal,” ASME paper 95-GT-432, presented at the International Gas Turbine and Aeroengine Congress and Exposition, Houston, Texas, June 5 – 8.
3. Wyssman, H. R., Pham, T. C. and Jenny, R. J., 1984, “Prediction of Stiffness and Damping Coefficients for Centrifugal Compressor Labyrinth Seals,” *ASME Journal of Engineering for Gas Turbines and Power*, 106, pp. 920 – 926.
4. Wachel, J. C., 1982, “Rotordynamic Instability Field Problems,” *Rotordynamic Instability Problems in High-Performance Turbomachinery*, NASA CP-2250, pp. 1 – 19.

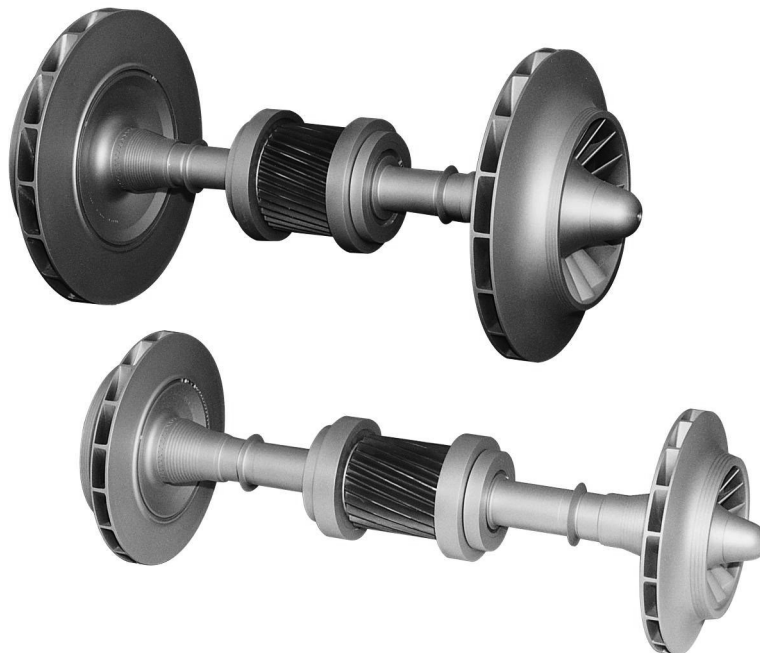


Figure 3-67—Pinion Rotors from an Integrally Geared Compressor

5. Atkins, K. E. and Perez, R. X., 1988, "Influence of Gas Seals on Rotor Stability of a High Speed Hydrogen Recycle Compressor," *Proceedings of the Seventeenth Turbomachinery Symposium*, Turbomachinery Laboratory, Texas A&M University, College Station, Texas, pp. 9 – 18.
6. Kirk, R. G., 1988, "Evaluation of Aerodynamic Instability Mechanisms for Centrifugal Compressors -- Part I: Current Theory," *ASME Journal of Vibration, Acoustics, Stress, and Reliability in Design*, 110 (2), pp. 201 – 206.
7. Kirk, R. G., 1988, "Evaluation of Aerodynamic Instability Mechanisms for Centrifugal Compressors--Part II: Advanced Analysis," *ASME Journal of Vibration, Acoustics, Stress, and Reliability in Design*, 110 (2), pp. 207 – 212.
8. Kirk, R. G. and Simpson, M., 1985, "Full Load Shop Testing of 18,000 HP Gas Turbine Driven Centrifugal Compressor for Offshore Platform Service: Evaluation of Rotordynamics Performance," *Instability in Rotating Machinery*, NASA CP-2409, pp. 1 – 13.
9. Wagner, N. G. and Steff, K., 1996, "Dynamic Labyrinth Coefficients From a High-Pressure Full-Scale Test Rig Using Magnetic Bearings," *Rotordynamic Instability Problems in High-Performance Turbomachinery*, NASA CP-3344, pp. 95 – 111.
10. Shemeld, D. E., 1986, "A History of Development in Rotordynamics – A Manufacturer's Perspective," *Rotordynamic Instability Problems in High-Performance Turbomachinery*, NASA CP-2443, pp. 1 – 18.
11. Sood, V. K., 1979, "Design and Full Load Testing of a High Pressure Centrifugal Natural Gas Injection Compressor," *Proceedings of the Eighth Turbomachinery Symposium*, Turbomachinery Laboratory, Texas A&M University, College Station, Texas, pp. 35 – 42.
12. Kirk, R. G. and Donald, G. H., 1983, "Design Criteria for Improved Stability of Centrifugal Compressors," *AMD Vol. 55*, ASME, pp. 59 – 71.
13. Memmott, E. A., 1992, "Stability of Centrifugal Compressors by Applications of Tilt Pad Seals, Damper Bearings, and Shunt Holes," *IMEchE, 5th International Conference on Vibrations in Rotating Machinery*, Bath, pp. 99 – 106.
14. Fulton, J. W., 1984, "Full Load Testing in the Platform Module Prior to Tow-Out: A Case History of Subsynchronous Instability," *Rotordynamic Instability Problems in High-Performance Turbomachinery*, NASA CP-2338y, pp. 1 – 16.
15. Memmott, E. A., 1999, "Stability Analysis and Testing of a Train of Centrifugal Compressors for High Pressure Gas Injection," *ASME Journal of Engineering for Gas Turbines and Power*, 121 (3), pp. 509 – 514.

3.9 SOLVING STABILITY PROBLEMS

Rotordynamic instability is perhaps the most damaging and disruptive vibration problem experienced in the field. While less frequent than other sources of vibration¹, the potential for machine damage and extended downtime is much greater. This is due in large part to the nature of an instability problem. The onset of the subsynchronous vibration is sudden and virtually unbounded. Furthermore, rotor instability is normally a re-excitation of the rotor's 1st critical speed with a peak deflection near the mid-span for multi-stage rotors. This is coupled with a tangential force that encourages whirling. This is not the case with unbalance excitation of the 2nd critical, the 1st critical or, in fact, any critical speed. With large peak internal deflections and little control of the vibratory motion, the likelihood of rotor damage due to instability is greatly increased.

The lengthy disruption to operations caused by rotordynamic instability stems from three sources: the consequential rotor damage, an inability to operate in conjunction with the instability, and the complexity of the solution. As previously mentioned, instability has a high probability of causing internal flow path damage and loss of performance. Repairs may involve extended shutdowns to remove the aero bundle for replacement of parts not normally spared.

Most sources of vibration permit continued operation under all but extreme situations. Unfortunately, it is rare that instability vibration levels will not be damaging to the rotor. Most cases involve immediate shutdown and protracted outtings, Doyle [1].

Finally, solutions to instability problems tend to be more complicated involving reconfiguration of the rotor-bearing system to some extent. These can range from bearing parametric changes to shaft modifications. The solution will almost always entail the replacement of some part (i.e. new bearings, modified labyrinth seals) and may include redesigning and/or re-machining of the internal configuration (i.e., bearing span reduction, shrink fit modification, etc.). This is very costly and time consuming in contrast to field balancing, realignment, or tightening of mechanical fits that can be performed immediately to remedy other types of vibration problems.

These solutions can be grouped into one of two categories: decreasing or eliminating the excitation force and increasing the effective damping. If the instability problem is modeled as a sum of the tangential forces inducing whirl at any particular natural frequency (see Figure 3-68 for a graphical description of these forces), then the rationale behind this grouping becomes obvious. Describing the tangential force as:

¹ The low occurrence of instability is due in large part to the seriousness of the problem and cost of the solution. Given a poor design or predictive capability, instability can occur just as easily as other vibration problems.

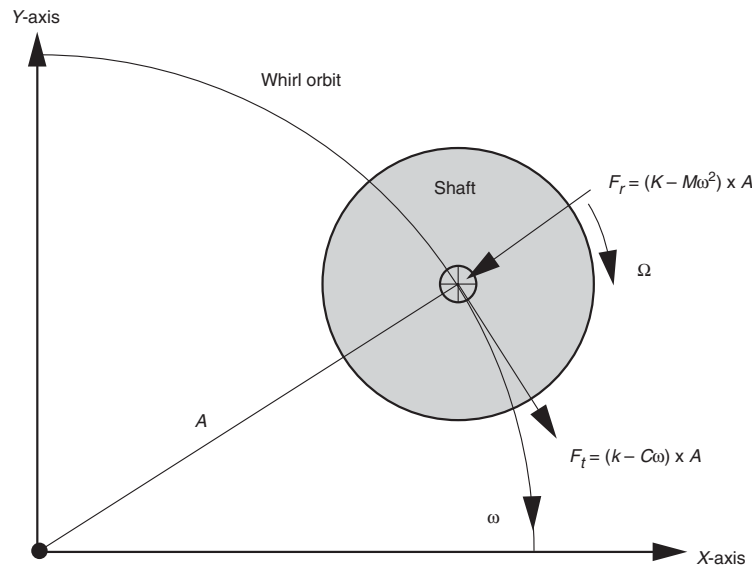


Figure 3-68—Forces Exerted on a Whirling Shaft

$$\frac{F_t}{A} = \sum (k - \omega C) \quad 3-8$$

In this expression, the destabilizing forces contained in the rotor-bearing system are represented by the modal sum of k . The second term, ωC , represents the effective damping at frequency, ω , that is available to counteract the tendency to whirl. Viewed in this sense, the tangential whirling force, F_t , may be reduced by decreasing k and/or by increasing ωC .

Before proceeding, a brief definition of the effective bearing damping is presented as used in the context of this section. Effective damping is defined as the percentage of damping provided by the rotor supports available to control the particular critical speed in question. For beam compressors, this mode is usually the first and control of the mid-span is critical. For a mode behaving as a rigid body, ($K_{\text{shaft}} \gg K_{\text{support}}$), the percentage of damping available to control the motion is nearly 100% (top mode shape in Figure 3-69). Inversely, for modes behaving as a flexible body, ($K_{\text{shaft}} \ll K_{\text{support}}$), the bearings become nodal and the percentage of damping available to control the vibratory motion is nearly 0% (bottom mode shape in Figure 3-69). Keep in mind that motion at the bearings is needed for the bearing damping terms to generate a suppressing force. In the case of stiff bearings, no motion exists at the bearing location and therefore, no bearing damping force is created. Thus, the options to increase the effective damping are to stiffen the shaft, soften the supports or increase the overall damping present.

Section 3.9.1 and 3.9.2 give some guidelines for performing either task of eliminating the excitation or increasing the

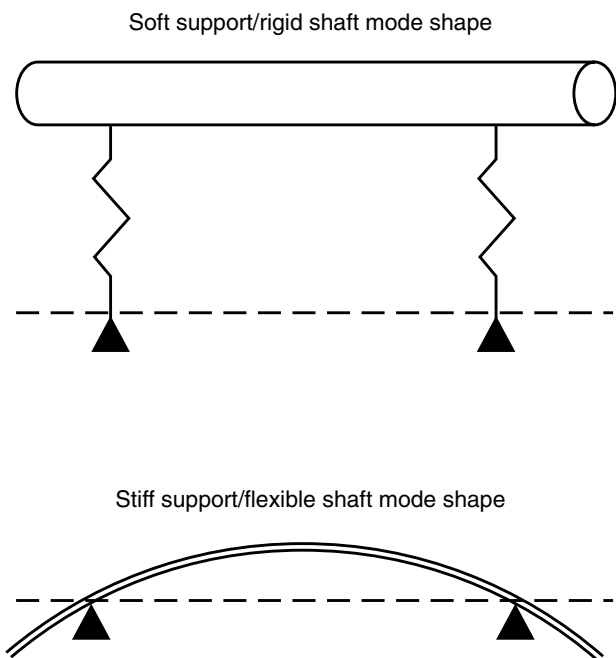


Figure 3-69—Mode Shapes for Various Support/Rotor Stiffnesses

effective damping. However, instability mechanisms and predictor tools are complicated and greatly intertwined with other dynamic effects within the turbomachine. These guidelines are not intended as a substitute for thorough field investigation or a detailed stability analysis. The most common practices are shown in **bold**.

3.9.1 Decreasing or Eliminating Excitation Forces

Component	Modifications	Benefits	Drawbacks	References
Oil Seals (see 3.4.1)	Increase Clearance	Dynamic properties decrease with increasing clearance. $Crosscoupling = f\left(\frac{1}{clearance^3}\right)$	Increases oil leakage, decreases principle stiffness. Reduces the force that keeps oil rings floating.	Emerick [2]
	Circumferential Grooves	Grooving separates the seals into individual units. $Crosscoupling = f(length^3)$	Reduces the force that keeps oil rings floating. Decreases principle stiffness. Increases oil leakage.	Allaire [3]
	Pressure Balance Seal	Reduces the force that locks up floating seal ring eccentrically.	May require extensive seal modifications, i.e. face lip change (reduce axial force) or seal face coating (reduce friction force).	Allaire [3]
	Reduced Suction Pressure Start	Enables floating seal rings to center during start transients.	May require piping or process control modifications.	
	Gas Seal Retrofit	Replaces oil seals with a dynamically neutral component.	Cost and machining. Removal of the oil seals may also increase the response of critical speeds to synchronous and non-synchronous forces.	Kocur [4]
Labyrinth Seals (see 3.4.2)	Clearance Changes	Unfortunately, there is no clear trend on how clearance affects the stability.	Leakage is directly proportional to clearance.	Childs [5] & Kirk [6]
	Number of teeth	No clear trends. All dynamic coefficients increase with greater number of teeth (and thus length).	Leakage is inversely proportional to number of teeth.	Iwatsubo [7] & Scharrer [8]
	Increase Tooth Height	Reduces all dynamic coefficients.	Increased height will reduce tooth strength and rub durability.	Wyssmann [9]
	Decrease swirl	Reduces tangential force (can change sign for smaller values or against rotation pre-swirl.) Normally achieved with swirl brakes, shunt injection or roughened stator surface.	Increased machining complexity and space requirements. May influence performance if labyrinth seal is shortened or if number of teeth is reduced.	Wagner [10]
Journal Bearings (see 3.3)	Fixed to Tilting Pad	Tilting pad bearings have been shown to have little or no destabilizing effect. Removal of fixed pad configurations eliminates a large source of cross coupling and potential bearing whirl.	Fixed pad bearings may have more damping for control of synchronous vibrations. Care needs to be taken to avoid creating an unbalance response problem.	

	Configuration or clearance modifications.	There are considerable differences in the stability characteristics of the various fixed pad bearings, more so than in varying tilting pad bearing characteristics.	As before, bearing changes will also affect the synchronous behavior of the rotor-bearing system.	Nicholas [12]
Shrink Fits (see 3.5.2.1)	Reduce (remove material from the fit axial center or reduce fit length) or eliminate (integral wheels) fits.	Eliminate sources of internal friction that has been shown to cause rotordynamic instabilities.	Keyways may be needed to offset the loss in fit contact area. Machining cost and balance complexities are added.	Doyle [1]
Aero Forces (see 3.5.1)	None	Minimal positive benefits.	Due to the large impact on efficiency, stage changes (tip clearance, etc.) are avoided at all costs. Solutions usually involve increasing the effective damping.	
Partial Arc Admission (see 3.8.1.3)	Reschedule the valve opening sequence.	Partial arc emission will alter the bearing loading. Inappropriate sequencing can unload bearings causing whirl or instability (especially in the case of fixed pad designs).	May require modifications to valve system.	Caruso [13]

3.9.2 Increasing Effective Damping

Component	Modifications	Benefits	Drawbacks	References
Squeeze Film Dampers (see 3.3.4)	Incorporate into bearing design.	Squeeze film dampers are intentionally designed to be soft supported. This increases the effective damping of the rotor-bearing system.	Increased bearing complexity. Soft supports also affect the synchronous behavior of the system.	Gunter [14] & Kuzdzal [15]
Damper Seals (see 3.4.3)	Honeycomb, hole pattern or pocket seal retrofit.	Provides high levels of damping to produce a stabilizing tangential force.	Reconfiguration of existing design. Rub intolerance and pocket fouling with honeycomb seals. Possible complexities due to large dynamic behavior.	Li [11], Sorokes [17] & Zeidan [18]
Rotor	Decrease bearing span.	Increases the bending stiffness of the shaft and, thus, the effective damping provided by the bearings.	Major redesign of the turbomachine. Manufacturers usually reduce bearing span for cost and dynamic considerations to practical limits.	
	Increase shaft diameter between bearings.	Increases shaft bending stiffness.	Aerodynamic efficiency normally suffers as shaft diameter is increased.	
	Changing components from interference fits to integral.	Increases shaft bending stiffness.	Assembly may become complicated. Increased cost of shaft forging.	

Tilting Pad Geometry	Bearing optimization studies: <ul style="list-style-type: none"> • L/D (+) • Clearance (+) • Preload (-) • # of pads 	Intent is to optimize stability through geometry changes in the tilting pad bearing. The parameter changes that lead to higher stability levels are: (+) Increasing (-) Decreasing NOTE: These are general trends only. They are not absolute!!!	Limited ability to change stability levels through pad changes. Space, design practice and synchronous response considerations may limit possibilities.	Nicholas [16]
-----------------------------	--	---	--	----------------------

3.9.3 References

- Doyle, H. E., 1980, "Field Experience with Rotordynamic Instability in High-Performance Turbomachinery," *Rotordynamic Instability Problems in High-Performance Turbomachinery*, NASA CP-2133, pp. 3 – 13.
- Emerick, M. F., 1982, "Vibration and Destabilizing Effects of Floating Ring Seals in Compressors," *Rotordynamic Instability Problems in High-Performance Turbomachinery*, NASA CP-2250, pp. 187 – 204.
- Allaire, P. E. and Kocur, J. A., 1985, "Oil Seal Effects and Subsynchronous Vibrations in High-Speed Compressors," *Rotordynamic Instability Problems in High-Performance Turbomachinery*, NASA CP-2409, pp. 205 – 223.
- Kocur, J. A., Platt, J. P. and Shabi, L. G., 1987, "A Retrofit of Gas Lubricated Face Seals in a Centrifugal Compressor," Proceedings of the Sixteenth Turbomachinery Symposium, Turbomachinery Laboratory, Texas A&M University, College Station, Texas, pp. 65 – 74.
- Childs, D. W. and Scharrer, J. K., 1987, "Theory Versus Experiment for the Rotordynamic Coefficients of Labyrinth Gas Seals: Part II – A Comparison to Experiment," *Rotating Machinery Dynamics*, presented at the 1987 ASME Design Technology Conferences – Eleventh Biennial Conference on Mechanical Vibration and Noise, Boston, Massachusetts, September, 2, pp. 427 – 434.
- Kirk, R. G., 1986, "Labyrinth Seal Analysis for Centrifugal Compressor Design Theory and Practice," Proceedings of the International Conference on Rotordynamics, Tokyo, September 14 – 17.
- Iwatsubo, T., Fukumoto, K. and Mochida, H., 1993, "An Experimental Study of Dynamic Characteristics of Labyrinth Seal," *Rotordynamic Instability Problems in High-Performance Turbomachinery*, NASA CP-3239, pp. 219 – 237.
- Scharrer, J. K., 1988, "Rotordynamic Coefficients for Stepped Labyrinth Gas Seals," *Rotordynamic Instability Problems in High-Performance Turbomachinery*, NASA CP-3026, pp. 177 – 195.
- Wyssmann, H. R., Pham, T. C. and Jenny, R. J., 1984, "Prediction of Stiffness and Damping Coefficients for Centrifugal Compressor Labyrinth Seals," *Journal of Engineering for Gas Turbines and Power*, Transactions of the ASME, 106, pp. 920 – 926.
- Wagner, N. G., 1999, "Reliable Rotor dynamic Design of High-Pressure Compressors Based on Test Rig Data," ASME International Gas Turbine and Aeroengine Congress and Exhibition, Indianapolis, Indiana, ASME 99-GT-150.
- Li, J., Kushner, F. and DeChoudhury, P., 2000, "Gas Damper Seal Test Results, Theoretical Correlation and Applications in Design of High-Pressure Compressors," Proceedings of the Twenty-Ninth Turbomachinery Symposium, Turbomachinery Laboratory, Texas A&M University, College Station, Texas, pp. 55 – 64.
- Nicholas, J. C., 1996, "Hydrodynamic Journal Bearings—Types, Characteristics and Applications," Mini Course Notes, 20th Annual Meeting, The Vibration Institute, Willowbrook, Illinois, pp. 79 – 100.
- Caruso, W. J., Gans, B. E. and Catlow, W. G., 1982, "Application of Recent Rotor Dynamics Developments to Mechanical Drive Turbines," Proceedings of the Eleventh Turbomachinery Symposium, Turbomachinery Laboratory, Texas A&M University, College Station, Texas, pp. 1 – 17.
- Gunter, E. J., Allaire, P. E. and Barrett, L. E., 1975, "Design and Application of Squeeze Film Dampers for Turbomachinery Stabilization," Proceedings of the Fourth Turbomachinery Symposium, Turbomachinery Laboratory, Texas A&M University, College Station, Texas, pp. 127 – 142.
- Kuzdzal, M. J. and Hustak, J. F., 1996, "Squeeze Film Damper Bearing Experimental Versus Analytical Results for Various Damper Configurations," Proceedings of the Twenty-Fifth Turbomachinery Symposium, Turbomachinery Laboratory, Texas A&M University, College Station, Texas, pp. 57 – 70.
- Nicholas, J. C. and Kirk, R. G., 1979, "Selection and Design of Tilting Pad and Fixed Lobe Journal Bearings for Optimum Turborotor Dynamics," *Proceedings of the Eighth Turbomachinery Symposium*, Turbomachinery Laboratory, Texas A&M University, College Station, Texas, pp. 43 – 58.
- Sorokes, J. M., Kuzdzal, M. J., Sandberg, M. R. and Colby, G. M., 1994, "Recent Experiences in Full Load Pressure Shop Testing of a High Pressure Gas Injection Centrifugal Compressor," Proceedings of the Twenty-Third

Turbomachinery Symposium, Turbomachinery Laboratory, Texas A&M University, College Station, Texas, pp. 3 – 18.

18. Zeidan, F., Perez, R. and Stephenson, E. M., 1993, “The Use of Honeycomb Seals in Stabilizing Two Centrifugal Compressors,” Proceedings of the Twenty Second Turbomachinery Symposium, Turbomachinery Laboratory, Texas A&M University, College Station, Texas pp. 3 – 15.

Nomenclature

- C = Labyrinth seal direct damping, N-s/m (lbf-s/in.),
 A = Precession orbit, m (in.),
 F_r = Radial force component, N (lbf),
 F_t = Tangential force component, N (lbf),
 k = Cross-coupled stiffness coefficient, N/m (lbf/in.),
 K = Direct stiffness coefficient, N/m (lbf/in.),
 M = Direct mass coefficient, N/m (lbf/in.),
 ω = Whirl frequency, rad/s,
 Ω = Shaft speed, rad/s (rpm).

3.10 IDENTIFYING FLUID INDUCED INSTABILITIES

If a fluid induced instability is suspected to be present on a rotating machine, the data must be properly reviewed to confirm its presence. The pieces of data to be reviewed are:

- Frequency of vibration,
- Form of the vibration, i.e., orbit,
- Direction of the orbit precession,

- Time-base waveform,
- Eccentricity ratio,
- Shaft attitude angle.

Vibration frequency alone is insufficient confirmation of an instability. Fluid induced instabilities will have a subsynchronous vibration frequency typically in the range of 0.3x to 0.5x (30% – 50% of synchronous speed). However, there are a number of other malfunctions that can occur with a subsynchronous vibration in the same frequency range. For example, certain types of rubs can produce subsynchronous vibrations at 0.333x or 0.50x. Frequency alone cannot quantify the root cause of the vibration. Consider the following example of a half spectrum plot as shown in Figure 3-70. The half spectrum clearly indicates a subsynchronous vibration at 0.5x.

The required information that is necessary to confirm that the Figure 3-70 subsynchronous vibration is due to an instability is the orbit form, the precession, and the eccentricity ratio. The orbit shape must be nearly circular, the precession must be “forward” and the eccentricity ratio must be low. If the orbit precession is “reverse”, the source of the subsynchronous vibration cannot be due to an instability.

Oil whirl and whip are self-excited limit cycle rotor vibrations caused by interaction between the fluid and the rotor. The fluid forces are circumferential in nature and act in the same circumferential direction as the rotor rotates. These forces cause the rotor to operate in a nearly circular orbit path at a frequency equal to the fluid circumferential average velocity. Instability occurs after a threshold of stability is exceeded. The fluid-induced vibrations are conven-

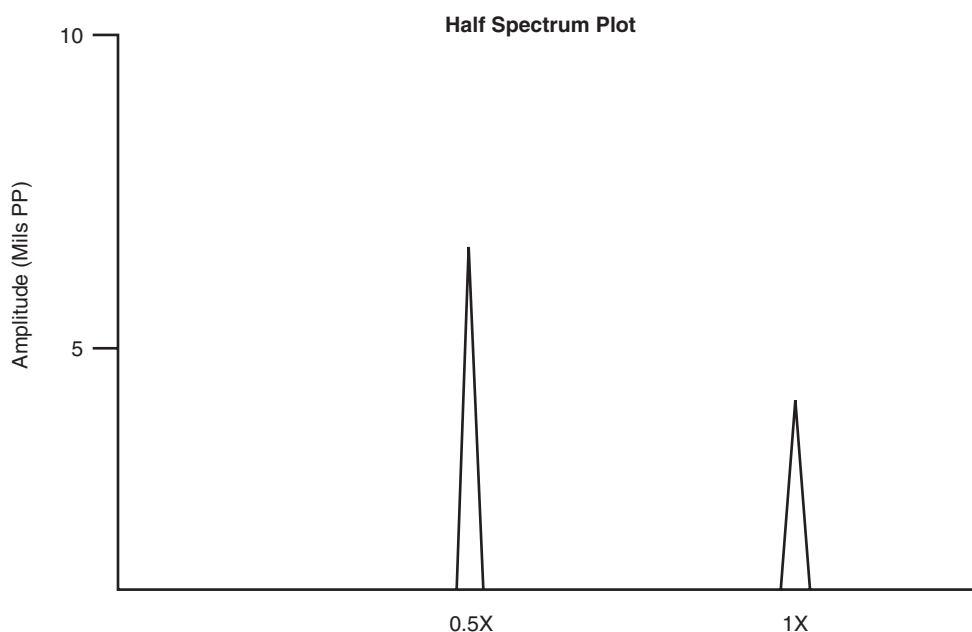


Figure 3-70—Half Spectrum Plot

tionally separated into two regimes called whirl and whip. Whirl has a frequency proportional to shaft rotational speed, with the coefficient of proportionality close to the fluid circumferential average velocity ratio in the bearing, seal or rotor periphery. Typically, whirl for bearings occurs at a frequency of approximately one-half of shaft rotational speed (see 3.3.2).

With an increase in rotational speed, whirl transforms into whip as the instability frequency approaches the first natural frequency of the rotor system (at higher rotational speeds, fluid whirl and whip of the higher modes may also occur). The vibration frequency of oil whip will remain essentially at a constant frequency, usually in the range of $0.3x - 0.49x$, even with an increase in rotor speed.

Fluid instability, characterized by a forward, almost circular, vibration orbit, is a property of the rotor/bearing/seal system. Thus, the mechanism is not limited to oil lubricated bearings. It can occur when any fluid (e.g., oil, steam, process gas, etc.) is enclosed within a small clearance area, between two body surfaces forming a cylinder within a cylinder, one of which is rotating and dragging the enclosed fluid into circumferential rotation.

Figures 3-71 and 3-72 represent confirming evidence of an instability; i.e., the orbit is circular and the shaft centerline location is nearly coincident with the geometric center of the bearing (low eccentricity ratio). The circle in Figure 3-72 represents the available diametral clearance of the bearing. The plotted points and curve define the shaft centerline position within the bearing as a function of time. This could also be plotted as a function of rotational speed during a startup or shutdown. For this example the shaft rotation is counterclockwise (ccw). The shaft can be seen to rise in the bearing to its operating position near the bearing geometric center under steady state conditions; i.e., a very low eccentricity ratio. This represents the lowest margin of stability to any form of perturbation forces. The bearing stiffness properties of a hydrodynamic bearing are very low at the geometric center. As the rotor operates at higher eccentricity ratios, the hydrodynamic oil wedge contributes to increased bearing stiffness.

Figure 3-73 is a typical orbit for a subsynchronous vibration due to a rub. The complex unfiltered orbit indicates both a forward and a reverse precession component. Observing the orbit filtered to $0.5X$, the precession is reverse (opposite to the direction of rotation). This example reinforces the need to view the data in the correct formats to determine if an instability is the root cause of a subsynchronous vibration.

The terms “forward” and “reverse” precession refer to the direction of the shaft centerline motion (orbits) that are (cw or ccw) relative to the direction of shaft rotation. If the orbit precession is in the same direction as the shaft rotation, it is referred to as a “forward” precession orbit. Conversely, if the orbit precession is opposite to the direction of the shaft rotation, it is referred to as “reverse” precession. This is an impor-

tant diagnostic consideration in determining which malfunction may be present on a machine.

There are several ways to determine shaft precession. The two most common techniques are the time-base presentation of the vibration waveforms or the use of a full spectrum plot. Figures 3-74 and 3-75 are typical time base presentations that can be used to differentiate forward or reverse precession. Figure 3-74 indicates a forward precession orbit. The individual time-base waveforms are evaluated based on their peak amplitude occurrence relative to real time. For the example shown in Figure 3-74, the shaft rotation is ccw. Based upon the probe orientation, the horizontal probe will see the peak vibration first (t_0) followed by the vertical probe at time t_{0+1} . Figure 3-75 indicates reverse precession vibration. The vertical probe detects the peak vibration at t_0 followed by the horizontal transducer at time t_{0+1} .

A diagnostic technique referred to as a “full spectrum” can also be utilized to determine the precession of an orbit. An example of reverse precession shaft centerline motion is shown in Figure 3-76. The full spectrum plot presents the vibration components in the frequency domain. It identifies the forward and reverse components on the same plot. If the magnitude (amplitude) of a reverse frequency component is larger than the amplitude of the forward component at the same frequency, the shaft centerline motion at that frequency is a reverse precession.

3.11 STABILITY TESTING OF MACHINERY

For the purposes of practical testing, rotor stability is the susceptibility of a rotor-bearing system to experience subsynchronous vibrations associated with self-excitation of the first rotor natural frequency. While other types of instabilities do occur, re-excitation of the rotor’s first natural frequency is by far the most common.

The most popular means of assessing a machine’s actual stability is through shop testing at full pressure, load, and speed such as an ASME PTC Type I compressor test (Power Test Code 10, Type 1, a full density test). However, such testing can only identify the presence or absence of instabilities without verifying the machine’s actual stability level. In order to determine the stability level of an operating rotor (i.e., to measure a machine’s log decrement), it is necessary to excite the rotor’s first fundamental natural frequency by applying a sufficient amount of non-synchronous energy to the rotor. While enough energy must be applied to register meaningful results, a great deal of caution must be exercised in order to avoid applying too strong of an excitation force that might result in rotor damage. Since each machine is different, the required magnitude of the excitation force will be different for each case. Ideally, for accurate stability level measurement, the excitation force would be fully characterized. Shaft relative displacement data is the most useful response information since seismic vibration information may be altered by the structure dynamic response.

Some of the mechanisms that can produce the type of non-synchronous excitation required are mechanical impact [1,2], seismic shaker with white noise, swept sine [3,4] or specific frequency inputs, and some type of aerodynamic or process flow variations [5,6]. Direct excitation of the shaft has been accomplished using magnetic actuators, Baumann [7] as well as other devices, Bently and Muszynska [8]. Moore, et al. [9] used a magnetic bearing attached to the free end of a 7-stage centrifugal compressor to determine the logarithmic decrement during a full load, full pressure shop test. The device, used as a dynamic exciter, injected an asynchronous force on the compressor exciting its first forward whirling mode.

Mechanical impact to an operating rotor is not recommended and is usually not practical due to space and safety limitations. Seismic shaker energy must be applied to a stationary object like a bearing housing and a fairly large force is sometimes required to impart sufficient energy to the rotor. Aerodynamic excitation of the rotor may be possible on some machinery. An example of this is shown in Figure 3-77 for a 5,500 HP axial air compressor, Jackson and Leader [6]. This trace was derived from a shaft-relative proximity probe. The data was captured on an FM tape recorder and reproduced on a digital signal analyzer.

Using data from such an excitation test, the stability is determined by estimating the damping available to the first rotor natural frequency. This measurement can be accomplished using either frequency domain or time domain data. In the frequency domain, the most common damping estimation method is amplification factor. In the time domain, the

most common damping estimate is log decrement, which is defined below for values of n greater than 1.

$$\delta = \left(\frac{1}{n-1} \right) \ln \left(\frac{A_1}{A_n} \right) \quad 3-9$$

In Figure 3-77, the maximum amplitude is used as the A_1 value. Since the subsynchronous amplitude decayed rapidly in this case, the next cycle, A_2 , was used to determine that the logarithmic decrement was approximately 0.35 with $n = 2$ in the above equation. It was determined that the frequency of this transient vibration was significantly less than the compressor's operating speed vibration and equal to the first critical speed or first fundamental natural frequency of the compressor.

The amplification factor of the first critical speed, as measured on a Bode plot during a machine's startup or shutdown, should not be used as a measurement of stability level. The damping of interest for stability is that available at operating speed, which can be significantly different (and typically lower) than the damping present when running at lower speeds or when passing through a critical speed.

The environmental conditions of the machine should be considered when attempting to determine the logarithmic decrement. As described in the previous sections, the mechanical tolerance variations and condition of the machine parts, especially bearings and seals, are very important in determining the machine's stability level. Synchronous vibration excitations like excessive unbalance and misalignment

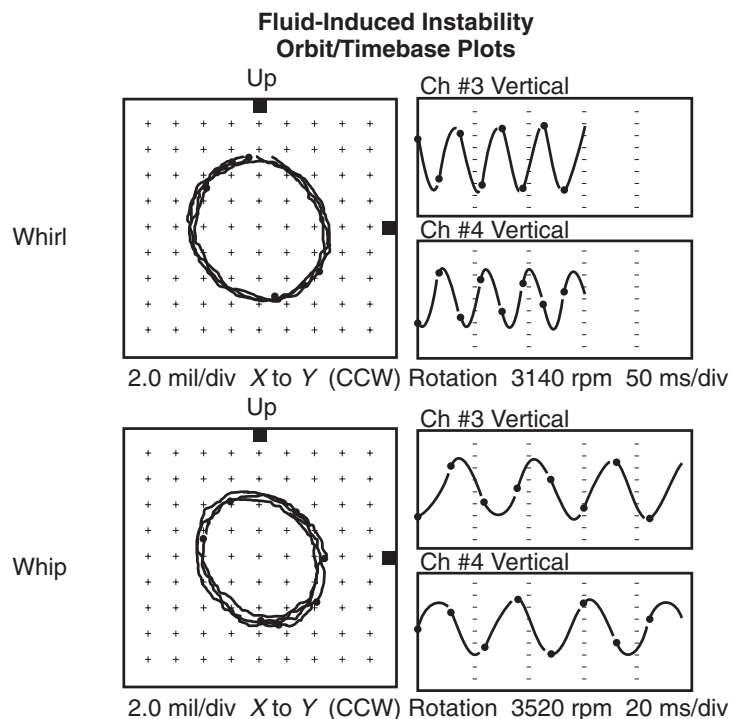


Figure 3-71—Fluid Induced Instability Orbit Plots

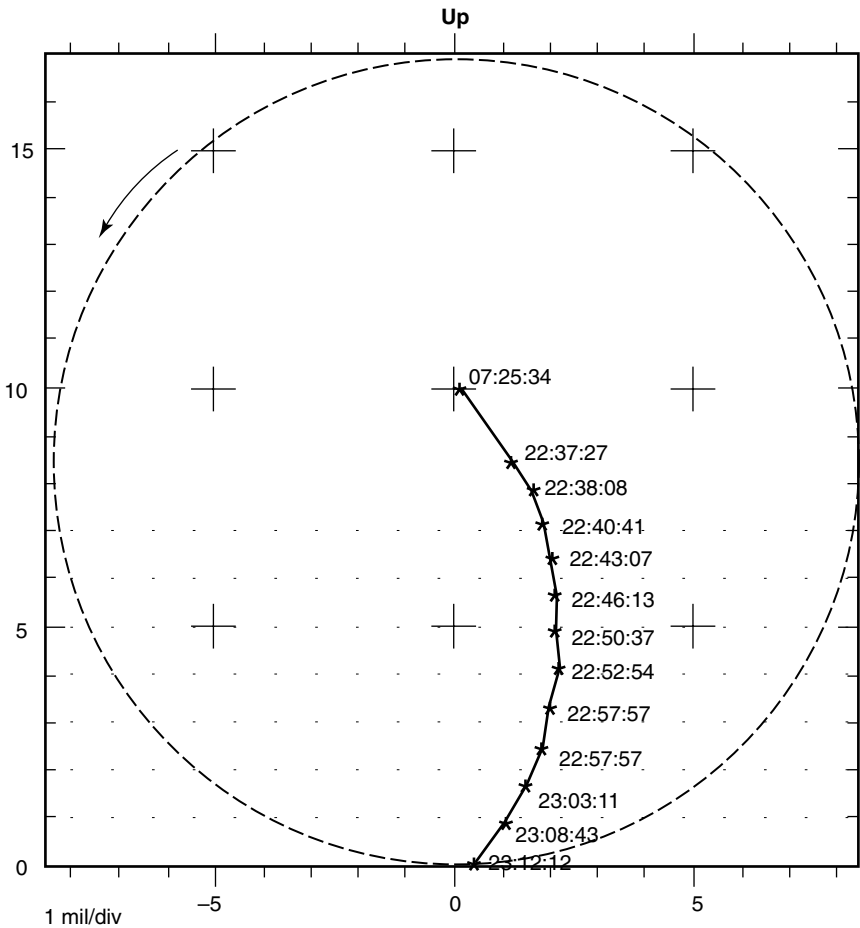


Figure 3-72—Shaft Centerline Plot

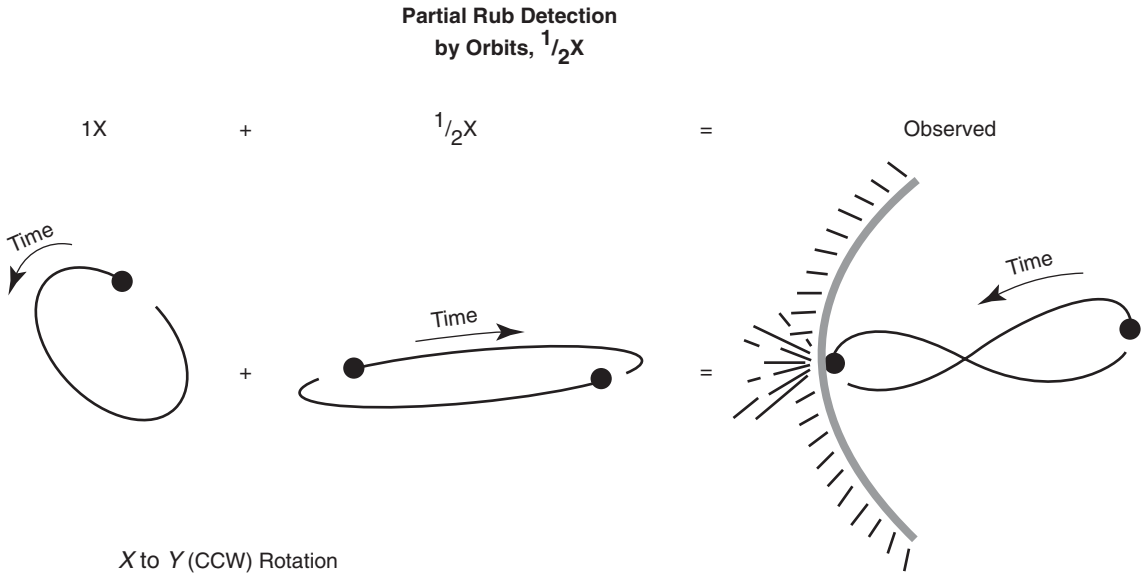


Figure 3-73—Typical Subsynchronous Rub Orbits

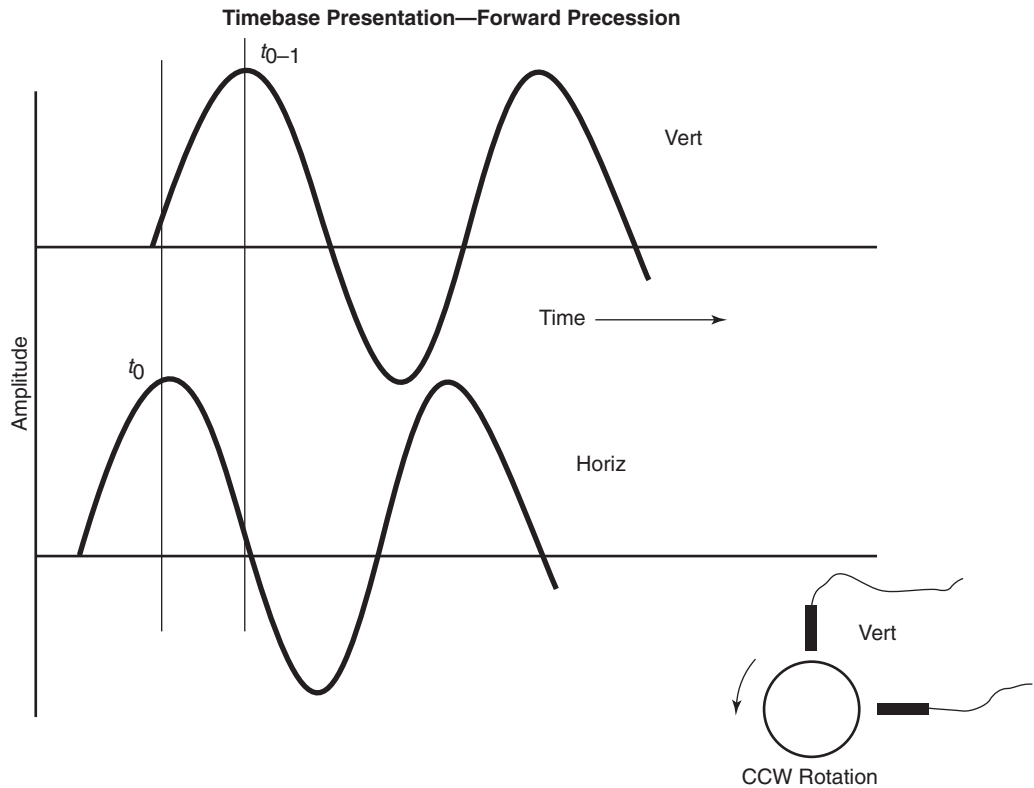


Figure 3-74—Forward Precession Vibration

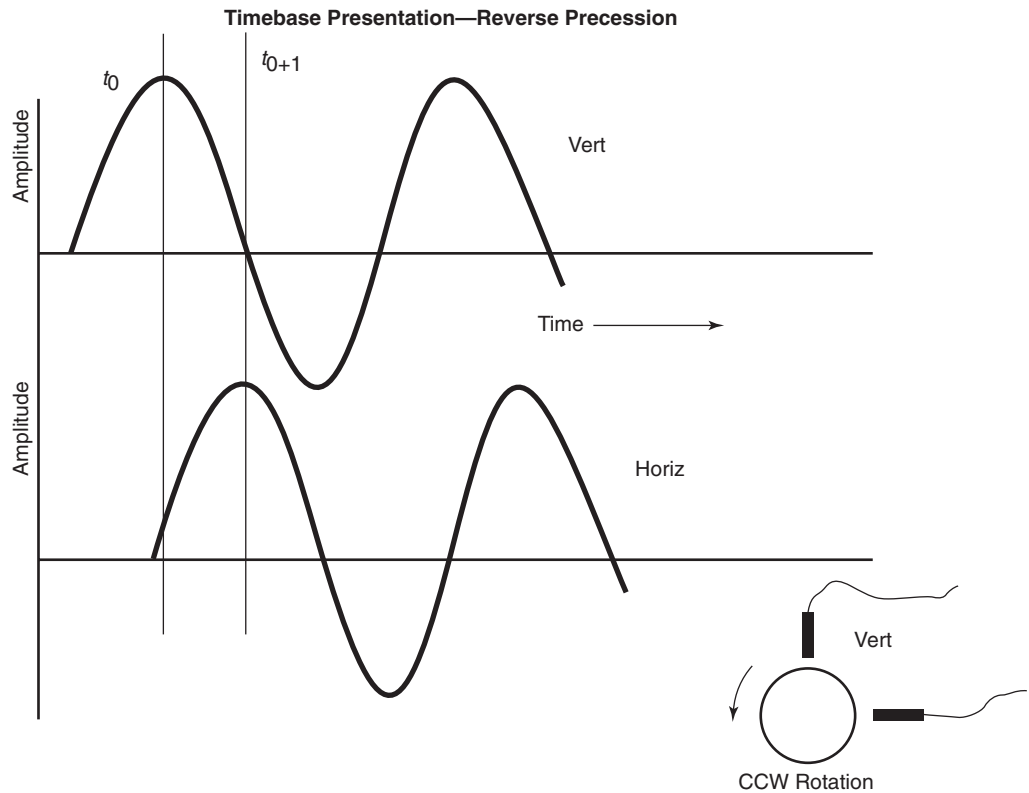


Figure 3-75—Reverse Precession Vibration

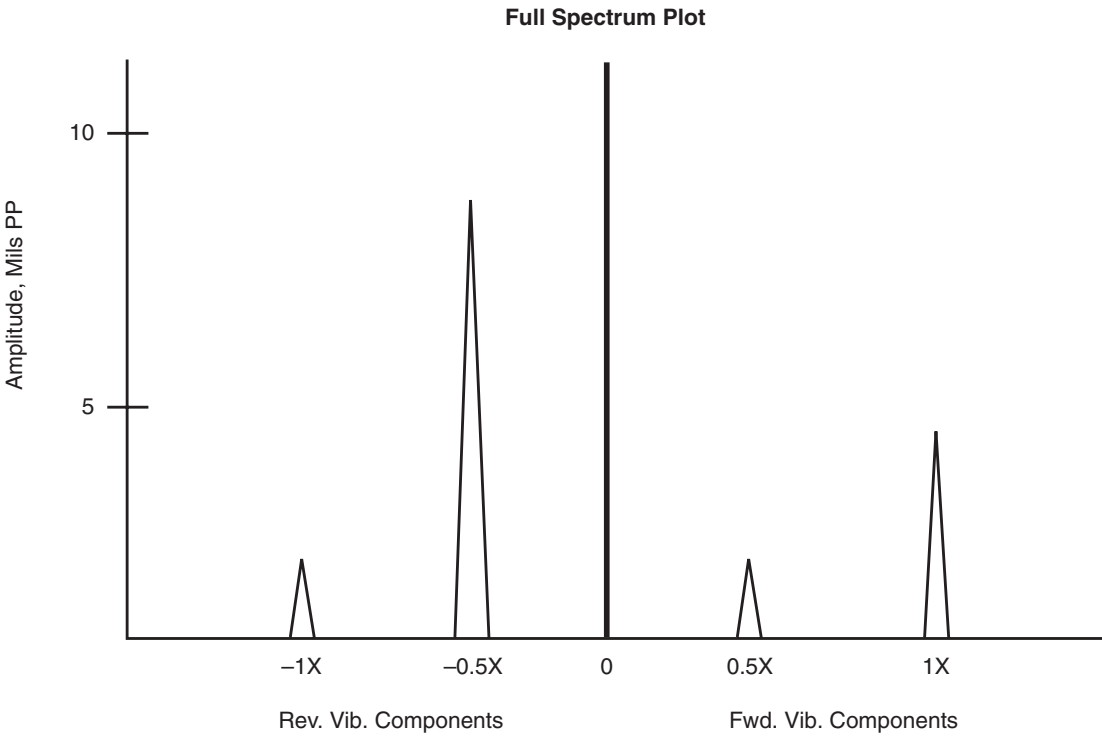


Figure 3-76—Full Spectrum—Reverse Precession of 0.5X

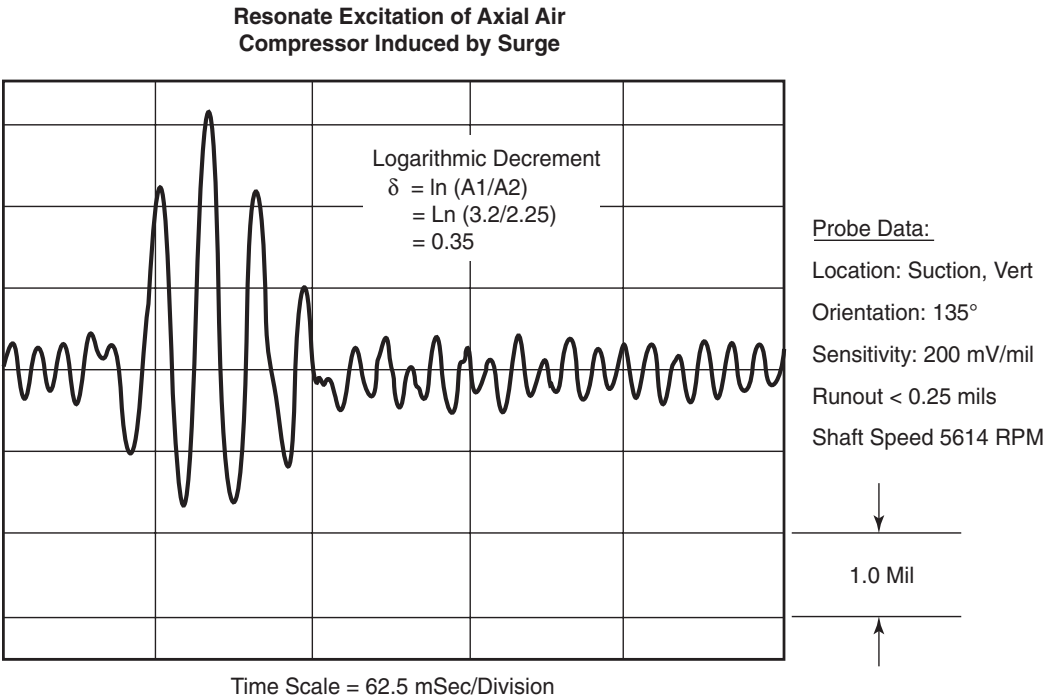


Figure 3-77—Calculating Logarithmic Decrement from Test Data

may affect the test results substantially. Process variables such as gas density, molecular weight, temperatures, pressures and mass flow must be carefully noted and controlled and the machine should be thermally stable during testing. Finally, results from a test stand may differ significantly from the installed field results due to differences in foundation and piping configurations as well as process conditions.

3.11.1 References

1. Nordmann, R., 1984, "Identification of Modal Parameters of an Elastic Rotor With Oil Film Bearings," *ASME Journal of Vibration, Acoustics, Stress, and Reliability in Design*, 106, pp. 107 – 112.
2. Wohlrab, R., 1975, "Experimentelle Ermittlung spaltstromungsbedingter Krafte an Turbinenstufen und deren Einfluss auf die Laufstabilitat einfacher Rotoren," Ph. D. Dissertation, Technical University of Munich, Germany.
3. Kanki, H., Fujii, H., Hizume, A., Ichimura, T. and Yamamoto, T., 1986, "Solving Non-Synchronous Vibration Problems of Large Rotating Machineries By Exciting Test in Actual Operating Condition," Proceedings of the IFTOMM International Conference on Rotordynamics, pp. 221 – 225.
4. Atkins, K. E. and Perez, R. X., 1992, "Assessing Rotor Stability Using Practical Test Procedures," Proceedings of the Twenty-First Turbomachinery Symposium, Turbomachinery Laboratory, Texas A&M University, College Station, Texas, pp. 151 – 159.
5. Jackson, C., 1981, "Four Compressor Trains of a Large Ethylene Plant – Design Audit, Testing and Commissioning," Proceedings of the Tenth Turbomachinery Symposium, Turbomachinery Laboratory, Texas A&M University, College Station, Texas, pp. 4 – 19.
6. Jackson, C. and Leader, M. E., 1983, "Design, Testing and Commissioning of a Synchronous Motor-Gear-Axial Compressor," Proceedings of the Twelfth Turbomachinery Symposium, Turbomachinery Laboratory, Texas A&M University, College Station, Texas, pp. 97 – 111.
7. Baumann, U., 1999, "Rotordynamic Stability Tests on High-Pressure Radial Compressors, Proceedings of the Twenty-Eighth Turbomachinery Symposium, Turbomachinery Laboratory, Texas A&M University, College Station, Texas, pp. 115 – 122.
8. Bently, D. E. and Muszynska, A., 1982, "Stability Evaluation of Rotor/Bearing System by Perturbation Tests," NASA CP-2250, pp. 307 – 322.
9. Moore, J. J., Walker, S. T. and Kuzdzal, M. J., 2002, "Rotordynamic Stability Measurement During Full-Load, Full-Pressure Testing of a 6000 psi Re-Injection Centrifugal Compressor," Proceedings of the Thirty-First Turbomachin-

ery Symposium, Turbomachinery Laboratory, Texas A&M University, College Station, Texas.

Nomenclature

A_1 = Amplitude of the first cycle before decay begins (in.),

A_n = Amplitude of the n^{th} cycle (in.),

\ln = Natural logarithm,

$n-1$ = Number of decay cycles,

δ = Logarithmic decrement.

3.12 STANDARD PARAGRAPH SECTIONS FOR STABILITY ANALYSIS SP6.8.5 – SP6.8.6

The philosophy and detailed explanation of the stability paragraphs are presented in this appendix. Application of the paragraphs to two types of centrifugal compressors is included as an example following these sections.

3.12.1 Philosophy

The task of creating specifications for stability was undertaken to reflect the general philosophy behind the standard rotordynamic paragraphs. In a manner similar to the unbalance response calculations, a procedure was formulated which explicitly outlines the method, tools and equations, while at the same time, serving as a simplified screening tool. The screening tool employs a simplified but conservative approach to efficiently serve as a first stage filter and provide the structure and commonality to permit database construction. To reflect the state-of-the-art that exists, along with the experience that has developed at the different vendors, a more involved analysis is employed to predict the actual operating conditions of the rotor. This analysis is expected to more closely follow the vendor's development of tools through innovation and experience. From this desire, a two-tiered procedure was created. This is represented by the Level I and Level II analyses.

3.12.1.1 Level I

The Level I analysis was created with two specific purposes in mind. First, a common methodology was defined. Second, a simplified but conservative screening criterion was created to identify individual rotors and classes of applications that require a more involved analysis.

With the lack of an existing standard approach to rotor stability, a uniform methodology is needed. As described in 3.1, uncertainty remains in several key areas of rotor/bearing stability due to the complexity of the problem. Over the years, experience and development efforts have created predictor tools that vary from vendor to vendor to address these

unknowns. The tools are closely guarded and reflect the different design philosophies, construction techniques, and application experiences of each vendor. These differences also influence the stability analysis by varying the type of excitations to include, which tools to employ and what stability level is acceptable. In response, the Level I analysis was developed.

The Level I analysis was intended to create a common basis for comparison. Similar to the unbalance response analysis, a procedure was developed that specifies what is to be included, how to include it and how to measure the results. Thus, purchasers could compare new equipment proposals from different vendors on a common basis. Additionally, this methodology could be used to generate a database for existing equipment of both the purchaser and vendor with minimized effort.

The second purpose that the Level I analysis serves is that of a screening tool. The tool, as defined, is conservative and straightforward. The intent is not to accurately represent the stability condition of the rotor/bearing system but to provide a step that can efficiently and effectively identify rotors or groups of applications that require a more detailed analysis. This is an attempt to balance the desire (by the purchaser) to have a stability analysis performed for every turbomachine and the contention (by the vendor) that some machines never need a stability analysis let alone a detailed study. As an example, high-pressure gas re-injection compressors will always undergo a stability analysis by the thorough vendor whether required or not. That same vendor would, as common practice, not perform a stability analysis for rotors that operate below their first natural frequency. Thus, a screening tool was developed that is simply applied, straightforward and conservative.

An initial analysis is done on all rotors operating above the first mode that identifies those that require a more in-depth study of the dynamic behavior. Some applications that are characterized by high discharge gas densities are always flagged for additional analysis. Rotors that operate well above the first mode are also flagged for the Level II analysis. In between the extremes, a method that drew from the experiences of several vendors and purchasers was formulated. While acknowledged as not completely representative of the dynamic behavior, it is nonetheless capable of identifying those rotors requiring a Level II analysis.

3.12.1.2 Level II

For those rotors identified in the Level I analysis as requiring a more in-depth investigation, the Level II analysis was created. The Level II analysis more accurately represents the dynamic behavior of the rotor at the maximum operating conditions. As previously mentioned, many unknowns remain pertaining to the instability drivers within turbomachines. The various vendors have addressed these unknowns in different

manners. Rather than select an “optimum” approach, especially considering the lack of experimental data, it was left to the individual vendor to determine the best method to analyze the rotor. This takes advantage of the vendor’s experience with both the analytical tools and operating experience of their own equipment.

The Level II analysis describes the operating conditions, bearing coefficients and instability mechanisms that should be included in the analysis and the final acceptable stability level. Proper consideration of these factors, given the uncertainties involved, will require levels of effort not justifiable for all rotors. By specifying the mechanisms and not the tools, the Level II analysis is open-ended permitting future developments to be applied without changes to the specification.

3.12.2 Stability Standard Paragraph Discussion

A detailed discussion of the individual *API Standard Paragraphs* (SP) relating to rotordynamic stability will be presented. The following format is employed for this discussion: each of the paragraphs are individually reproduced in sequence, followed by commentary designed to illustrate or clarify the material presented in the paragraph. The stability paragraphs are displayed in **bold** type with the numbering scheme intact. Comments immediately follow in each paragraph in normal type.

SP6.8.5 Level I Stability Analysis

SP6.8.5.1 A stability analysis shall be performed on all centrifugal compressors, steam turbines and axial and/or radial flow rotors except those rotors whose maximum continuous speed is below the first critical speed in accordance with SP6.8.2.3 as calculated on rigid supports. For this analysis, the machine inlet and discharge conditions shall be at the rated condition unless the vendor and purchaser mutually agree upon another operating point.

Note: Level I analysis was developed to fulfill two purposes: First, it provides an initial screening to identify rotors that do not require a more detailed study. The approach as developed is conservative and not intended as an indication of an unstable rotor. Second, the Level I analysis specifies a standardized procedure applied to all vendors similar to that found in SP6.8.2. (Refer to API 684 Section 3 for a detailed explanation.)

To avoid confusion, the first critical speed is defined using the undamped critical speed analysis of SP6.8.2.3. This is consistent with most empirical stability criteria that use the undamped critical speed on rigid supports as one measurement. The rated condition was selected for the Level I analysis since this operating condition is specifically defined in 3.42 & 3.43. The reference to a specific point facilitates the creation of a standardized procedure.

Historical data and experience has indicated that instability in sub-critical machinery (operating below the first undamped critical speed on rigid supports) is non-existent in centrifugal

compressor, steam turbine and axial and/or radial flow rotors. For this reason, it was felt safe to exclude this class of machinery from the stability analysis requirements.

It bears emphasizing again that the Level I analysis is a screening tool. It is fully expected that some rotors, regardless of their design, will not satisfy the screening criteria and require a Level II analysis. This should not be viewed as a deficiency in the design. Additionally, it is possible to have a more conservative design requiring a Level II analysis than one needing only a Level I analysis for the same application. The intent of the Level I analysis is to identify rotors that have the possibility of being more sensitive to destabilizing forces (i.e., high Critical Speed Ratio [CSR]) or having greater destabilizing force levels (i.e., high gas density).

SP6.8.5.2 The model used in the Level I analysis shall include the items listed in SP6.8.2.4 together with the effects of squeeze film dampers and oil seals when used.

To maintain consistency with the damped unbalance response, the analysis shall include the same items required for that analysis. Due to their potential impact on stability, oil seals and squeeze film dampers (SFD) are emphasized for inclusion.

SP6.8.5.3 All components shall be analyzed using the mean value of oil inlet temperature and the extremes of the operating limits for clearance.

The range of bearing clearance has a first order impact on the rotor stability and is included in the Level I analysis. By examining the entire range of clearance, additional conservatism is built into the analysis. In contrast, the oil inlet temperature has a second order impact on stability and can be effectively represented with a mean value in the analysis.

SP6.8.5.4 When tilt pad journal bearings are used, the analysis shall be performed with synchronous tilt pad coefficients.

The committee recognizes that there is a question as to which bearing coefficients to use for tilt pad bearings for a stability analysis: synchronous or frequency dependent (see 3.3.3.1). Pending future experimental validation, synchronous coefficients were selected.

SP6.8.5.5 For rotors that have quantifiable external radial loading (e.g., integrally geared compressors, partial arc emission steam turbines), the stability analysis shall also include the external loads associated with the operating conditions defined in SP6.8.5.1. For some rotors, the unloaded (or minimum load) condition may represent the worst stability case and should be considered.

Recognizing that external loading effects the dynamic behavior of the journal bearings, and thus the stability, they were included in the Level I analysis. In some instances, (e.g., the pinion shaft in a gearbox) the unloaded case may repre-

sent the worst stability case (see 3.8.5). This should be discussed between the purchaser and vendor. For the Level II analysis, the loads at the rated condition are extrapolated to the maximum continuous speed as necessary.

SP6.8.5.6 The anticipated cross coupling, Q_A , present in the rotor is defined by the following procedures:

a. For centrifugal compressors

The parameters in Equation 7 shall be determined based on the specified operating condition in SP6.8.5.1.

$$q_A = \frac{(HP)B_c C}{D_c H_c N} \left(\frac{\rho_d}{\rho_s} \right) \quad (7)$$

Equation 7 is calculated for each impeller of the rotor. Q_A is equal to the sum of q_A for all impellers.

b. For steam turbines and axial flow rotors

$$q_A = \frac{(HP)B_t C}{D_t H_t N} \quad (8)$$

Equation 8 is calculated for each stage of the rotor. Q_A is equal to the sum of q_A for all stages.

The anticipated cross coupling is derived from Alford's force for steam turbines and axial flow rotors, Equation (8), and a modified form of the same equation for centrifugal compressors, Equation (7). Section 3.5 describes the development of each equation. These equations are calculated for each individual stage. In steam turbines and axial flow rotors, this is consistent with the development of Alford's force. For centrifugal compressors, this was determined to yield the most representative application of the equation across a wide range of configurations.

SP6.8.5.7 An analysis shall be performed with a varying amount of cross coupling introduced at the rotor mid-span for between bearing rotors or at the center of gravity of the stage or impeller for single overhung rotors. For double overhung rotors, the cross coupling shall be placed at each stage or impeller concurrently and should reflect the ratio of the anticipated cross coupling, q_A , calculated for each impeller or stage.

This is part of the conservatism built into the Level I analysis. The location that most adversely affects the stability was selected. This location should normally coincide with the peak modal displacement. For between bearing rotors with the typical first bending mode, this corresponds to the mid-span. For overhung rotors, the first mode is driven by the overhung weight displaced from the centerline.

By varying the amount of cross-coupling applied, a sensitivity study is created. The study contains two important pieces of information. First, at zero applied cross-coupling, the log decrement of the rotor/support system is identified.

This usually represents the most stable condition of the turbo-machine. Second, the amount of cross coupling needed to zero the log decrement (produce an unstable rotor) is calculated. This is used in comparison to the anticipated cross coupling to determine the rotor's sensitivity.

While a single amount of cross coupling is applied for between bearing and single overhung rotors, two values are used for double overhung rotors. The values used should reflect the ratio of anticipated cross coupling. For example, a double overhung compressor rotor is calculated to have an anticipated cross coupling of 10,000 lbf/in. for the first impeller and 15,000 lbf/in. for the second impeller. Therefore, in applying the two cross couplings to the rotor for this analysis, the amounts will be varied according to the ratio of q_A (i.e., If 1,000 lbf/in. is applied to impeller #1, 1,500 lbf/in. should be applied concurrently to the second impeller. For 20,000 lbf/in. applied to the first impeller, 30,000 lbf/in. should be applied to the second impeller, etc.)

SP6.8.5.8 The applied cross coupling shall extend from zero to the minimum of:

- a. A level equal to ten times the anticipated cross coupling, Q_A .
- b. The amount of the applied cross coupling required to produce a zero log decrement, Q_0 . This value can be reached by extrapolation or linear interpolation between two adjacent points on the curve.

This dictates that the sensitivity study either shows the point that the log decrement reaches zero or that it applies at least ten times the anticipated cross coupling. While the first objective is obvious, the second is used to indicate that the rotor is basically insensitive to cross coupling for its given application. Stated another way, the analysis would state that the rotor is still stable even after applying ten times the amount of cross coupling that is expected to occur for the application. In this case, the rotor is considered to be insensitive to the levels of anticipated cross coupling.

SP6.8.5.9 A plot of the calculated log decrement, d , for the first forward mode shall be prepared for the minimum and maximum component clearances. Each curve shall contain a minimum of five (5) calculated stability points. The ordinate (y-axis) shall be the log decrement. The abscissa (x-axis) shall be the applied cross coupling with the range defined in 6.8.5.8. For double overhung rotors, the applied cross coupling will be the sum of the cross coupling applied to each impeller or stage.

A typical plot is presented in Figure SP-4. Q_0 and d_A are identified as the minimum values from either component clearance curves.

The graphical presentation of the results of the sensitivity study is outlined in this section. The plot shows the anticipated cross coupling, Q_A , corresponding log decrement, δ_A ,

and the cross coupling needed to destabilize the rotor, Q_0 (if less than ten times Q_A). These values are taken as the minimum δ_A at the anticipated cross coupling, Q_A and the minimum Q_0 derived from the minimum or maximum bearing clearance. (Note: δ_A and Q_0 may be taken from different clearance conditions, i.e., one from minimum and the other from maximum bearing clearance.)

Several pieces of information are contained in the graph. Two of which are discussed here. First, the slope of the curve is an indication of the sensitivity of the rotor to destabilizing forces. For example, the benefit of having $\delta_A = 0.5$ if Q_0 is only 10% greater than Q_A is questionable. In this case, minor deviations in the destabilizing forces, whether from changes in the operating conditions or uncertainties in the analysis, would be sufficient to cause the rotor to become unstable. Second, the stability of the rotor/support system is shown at the left-hand side of the plot with no excitation present. In most situations, this will be the highest level of stability achieved. (The situation where this may not be true is with the incorporation of honeycomb, hole pattern or pocket balance pistons and seals. See 3.4.3 for further information.)

SP6.8.5.10 Level I screening criteria

a. For centrifugal compressors

If any of the following criteria apply, a Level II stability analysis shall be performed:

- i. $Q_0/Q_A < 2.0$.

A Level II analysis is necessary if the cross coupling needed to destabilize the compressor is less than two times the anticipated amount. It was felt that an adequate safety margin (expressed as the ratio Q_0/Q_A) did not exist to cover uncertainties in the estimation equation and analytical predictions. For safety margins less than two, a reduction in these uncertainties is provided by a more accurate prediction of the instability mechanisms in the Level II analysis.

- ii. $\delta_A < 0.1$.

For similar reasons as with a), a log decrement of less than 0.1 requires a Level II analysis. Once again, an inadequate separation margin from the unstable region exists that requires a more accurate prediction of the instabilities. Additionally, the destabilizing effects of projecting the operating condition to maximum continuous speed needs to be examined.

- iii. $2.0 < Q_0/Q_A < 10$ and CSR is contained in Region B of Figure SP-5.

For ratios between 2 and 10, a further examination of the rotor susceptibility and application sensitivity is required. The rotor susceptibility to unstable operation is represented by the

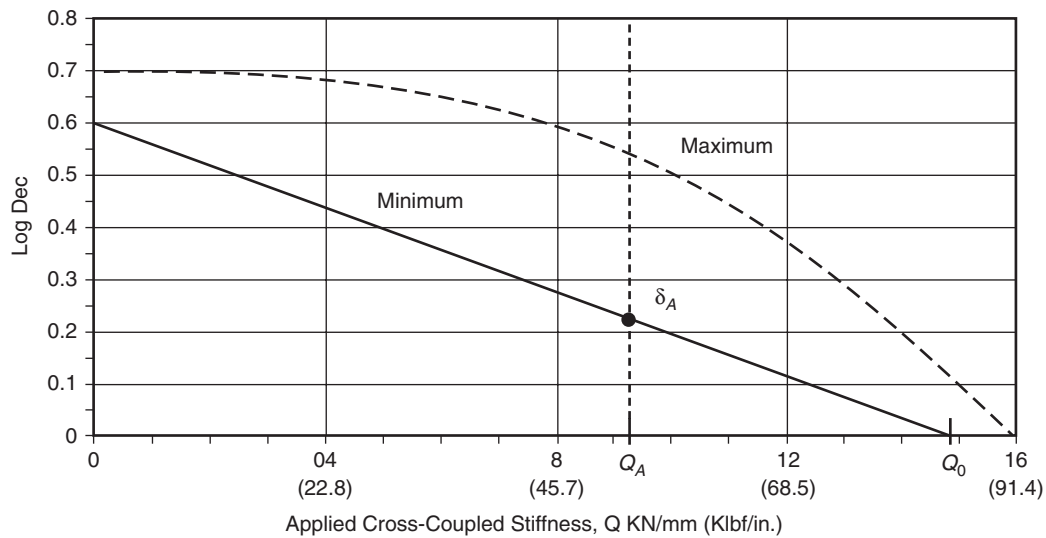


Figure SP-4—Typical Plot of Applied Cross-Coupled Stiffness vs. Log Decrement

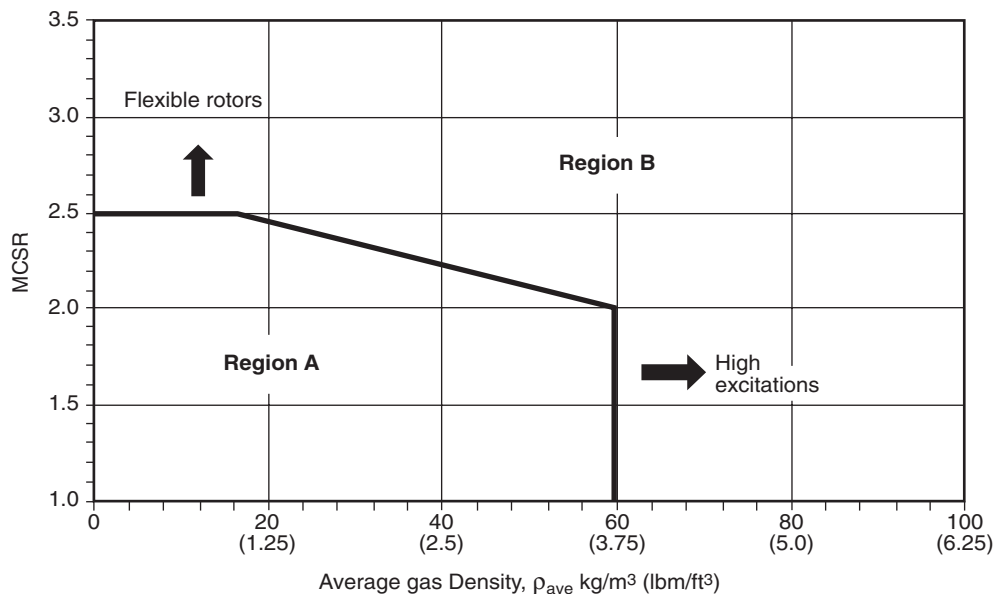


Figure SP-5—CSR Plot to Determine Analysis Level

CSR (see Symbols section at the end of SP6.8.6 for CSR definition).

The average gas density measures the application sensitivity. In Region B, it was determined that the compressor is susceptible to destabilizing forces (flexible rotor), or the excitation forces themselves will be large (high gas densities) (see 3.8.6), and, thus, the analytical stability screening criteria are more comprehensive. In Region A, the combination of flexibility and excitation is low enough so that the analytical stability screening criteria are not as comprehensive. Figure

SP-5 was derived from the experience plots described in 3.7. Gas density was selected as the independent variable since it was felt to more represent the excitation levels in the compressor.

Otherwise, the stability is acceptable and no further analyses are required.

Essentially, this includes only compressors that have a $\delta_A \geq 0.1$ and $Q_0/Q_A \geq 10$ in Region B or ≥ 2 in Region A of Figure SP-5. This defines a rotor that is insensitive to the anticipated levels of destabilizing forces and has a log dec-

rement sufficient to overcome any analytical prediction uncertainties.

b. For steam turbines and axial flow rotors

If $\delta_A < 0.1$, a Level II stability analysis shall be performed. Otherwise, the stability is acceptable and no further analyses are required.

For turbines and axial flow rotors, Alford's force lumped at the center span (or stage center of gravity for overhung rotors) is sufficient to conservatively represent the destabilizing forces present. In this case, a log decrement at the anticipated level of cross coupling of less than 0.1 warrants a Level II analysis for the rotor.

SP6.8.6 Level II Stability Analysis

SP6.8.6.1 A Level II analysis, which reflects the actual operating behavior of the rotor, shall be performed as required by SP6.8.5.10.

The Level II analysis is a more in-depth and time-consuming analysis. For those rotors deemed susceptible to or exposed to large levels of cross coupling, an analysis shall be performed that takes advantage of the vendor's experience and analytical developments.

6.8.6.2 The Level II analysis shall include the dynamic effects from all sources that contribute to the overall stability of the rotating assembly as appropriate. These dynamic effects shall replace the anticipated cross coupling, Q_A . These sources may include, but are not limited to, the following:

- a. Labyrinth seals**
- b. Balance piston**
- c. Impeller/blade flow**
- d. Shrink fits**
- e. Shaft material hysteresis**

It is recognized that methods may not be available at present to accurately model the destabilizing effects from all sources listed above. The vendor shall state how the sources are handled in the analysis.

The anticipated cross coupling calculated by Equation (7) or (8) is replaced with a more detailed analysis of the possible sources of instability. A list of sources is presented. (Damper bearings and oil seals are already included in the analysis.) The list is not intended to be all-inclusive. Other sources are to be discussed as necessary by the vendor.

In contrast to the Level I analysis, the vendor shall determine the most appropriate procedure to use to predict the dynamic effects of the instability drivers in their rotor. This should be based on their experience, current research and applicability. In many instances, this will differ between the various vendors reflecting the continued uncertainties in the knowledge base. The purchaser and user should also be aware

that adequate research or knowledge currently might not exist to accurately predict or confirm the behavior of some of these effects. While their impact on the overall rotor stability can be shown in individual cases or experiments, a predictor tool does not exist that can be applied across a wide range of applications (maybe even a narrow range in some cases.) This includes aerodynamic cross coupling produced by centrifugal impellers, shrink fits and shaft hysteresis, to name a few. For these instances, reliance upon the combined and shared knowledge of the vendor and purchaser is required.

SP6.8.6.3 The Level II analysis shall be calculated for the operating conditions defined in SP6.8.5.1 extrapolated to maximum continuous speed. The modeling requirements of SP6.8.5.2, SP6.8.5.4 and SP6.8.5.5 shall also apply. The component dynamic characteristics shall be calculated at the extremes of the allowable operating limits of clearance and oil inlet temperature to produce the minimum log decrement.

The Level II analysis is intended to represent the worst possible case for rotor stability. With this in mind, the maximum continuous operating speed (MCS) is selected since stability normally degrades with increasing rotor speed. Operating conditions used in the Level II analysis shall be extrapolated to the MCS. Additionally, the bearing (including SFD) and seal dynamic coefficients shall be calculated with the combination of clearance and oil inlet temperature that produce the minimum stability condition.

SP6.8.6.4 The frequency and log decrement of the first forward damped mode shall be calculated for the following conditions (except for double overhung machines where the first two forward modes must be considered):

The first forward mode is the mode of concern for rotor stability. Double overhung rotors will have modes associated with each impeller that can be excited and possibly driven unstable. Thus, the first two modes must be considered in the analysis.

a. Rotor and support system only. (Basic log decrement, δ_b).

b. For the addition of each group of destabilizing effects utilized in the analysis.

c. Complete model including all destabilizing forces. (Final log decrement, δ_f).

The Level II analysis should identify the relative impact of adding each destabilizing item to the system. By separating the effects, the critical component affecting the rotor stability is identified. This will permit effective troubleshooting of problems and behavior impact assessment of damage, operation changes or geometry variations. Should instability problems occur, it might be more advantageous to address or modify the

component that is causing the greatest destabilizing force. This analysis should help identify that component or effect.

SP6.8.6.5 Acceptance criteria

The Level II stability analysis shall indicate that the machine, as calculated in 6.8.6.1 through 6.8.6.3, shall have a final log decrement, δ_f , greater than 0.1.

The minimum acceptable level of the stability in this worst-case scenario is a log decrement > 0.1 . At this log decrement and given the conservative approach of the worst-case scenario, sufficient margin remains to guarantee stability during operation.

SP6.8.6.6 If after all practical design efforts have been exhausted to achieve the requirements of 6.8.6.5, acceptable levels of the log decrement, δ_f , shall be mutually agreed upon by the purchaser and vendor.

If the final log decrement > 0.1 cannot be reached, the vendor and purchaser shall mutually agree to an acceptable level based on historical data, operating experience and analysis methods of the vendor.

Note: This stability analysis section represents the first uniform methodology specified for centrifugal compressors, steam turbines and axial and/or radial flow rotors. The analysis method and the acceptance criteria specified are unique in that no vendor has used these exact methods to evaluate the susceptibility of their equipment to subsynchronous instability. When these requirements are included within a specification, all vendors are expected to analyze their rotors accordingly. However, it should be recognized that other analysis methods and continuously updated acceptance criteria have been used successfully since the mid-1970's to evaluate rotordynamic stability. The historical data accumulated by machinery vendors for successfully operated machines may conflict with the acceptance criteria of this specification. If such a conflict exists and a vendor can demonstrate that his stability analysis methods and acceptance criteria predict a stable rotor, then the vendor's criteria should be the guiding principle in the determination of acceptability.

This note highlights the fact that this is the first attempt to develop stability specifications and methodology for API equipment. As noted earlier, that even in the absence of specifications, vendors have applied their own design rules to achieve stable rotors for 25 years. This specification is a combination of their experience mixed with purchaser's desires and does not represent a single existing method. Conflicts may exist between this specification and the vendor's experience as to what is deemed acceptable. If sufficient proof is presented to the purchaser's satisfaction, this experience can be used as the determining factor to measure the rotor stability.

3.12.3 Analysis Examples

To illustrate the analysis procedure, two compressors were selected. One is typical of process compressors. It has six

stages, 3.23 MW and a rated speed of 13,600 rpm. The other compressor represents a gas injection rotor. This compressor has seven stages, 4.7 MW, a rated speed of 13,751 rpm and an average density of 107 kg/m³. Both compressors were designed to maximize rotor stability and meet API 617 specifications.

3.12.3.1 Compressor Cross-Sections

A cross-section of the process compressor rotor is shown on Figure 3-78. Future design conditions necessitated the increased impeller spacing. To avoid lateral critical speed and stability problems, the shaft diameter was increased wherever practical. Similar efforts were made during the design process of the injection compressor, Figure 3-79. Stability concerns over the high discharge pressure (275 bar) and gas density led to design efforts to stiffen the shaft. The larger shaft is reflected in the ratio between the impeller OD and the shaft OD.

Before proceeding with the stability analysis requirements of the standard paragraphs, some relevant points need to be addressed concerning the Level I analysis. As discussed, efforts were made during the design phase of both compressors to maximize the rotor stability. Both compressors are operating without evidence of instability. A full load, full pressure test was performed on the injection compressor also looking for signs of instability. The compressor was tested from surge to carry out at maximum continuous speed with no subsynchronous vibrations present. These points are emphasized because this compressor will be required to undergo a Level II analysis. This reflects the intention of the Level I analysis to require most high-density applications to undergo a Level II analysis. It does not imply that there is a deficiency in the injection compressor rotor design. To emphasize the purpose of the Level I analysis again, it is to identify those rotors or class of applications that require a more intensive analysis. It is not intended as a judgment of the design merits of the rotors undergoing the analysis.

3.12.3.2 Level I Analysis

Both rotors were modeled according to SP6.8.2.4. Neither contained damper bearings or oil seals, so the support system was comprised entirely of tilt pad bearings. Housing stiffness in both cases was an order of magnitude higher than the bearing stiffness and was disregarded without having an impact on the dynamic predictions. Minimum and maximum values were used for the bearing clearance and mean values for the oil inlet temperature. Synchronous coefficients were used to model the tilt pad bearings.

To facilitate the calculation of Equation (7), a spreadsheet was used. For the process compressor, the design values used

Per SP6.8.5.9, a plot of the log decrement versus mid-span cross-coupled stiffness was created for both compressors at the bearing conditions stated above. Since the Q_0 value was reached before ten times the anticipated cross coupling (per Worksheets 3-1 and 3-2) for either compressor, the x -axis of the plot was extended to include Q_0 only. The graphs are shown on Figures 3-80 and 3-81.

For reference, the values in Table 3-3 were obtained for each compressor.

The 1st critical speed was taken from the undamped critical speed analysis on rigid supports and determined in accordance with SP6.8.2.3. Details of the lateral analysis were omitted for space considerations.

3.12.3.3 Level I Screening Criteria

- Neither compressor has a Q_0/Q_A ratio of less than two. This criterion does not then call for a Level II analysis.
- The log decrement at the anticipated cross coupling for the process compressor is 0.44. For the gas injection compressor, the log decrement is 0.55. Thus, this criterion does not require that a Level II analysis be performed.
- The Q_0/Q_A ratio for both compressors is between 2 and 10. Thus, the average gas density to CSR ratio needs to be examined. For the process compressor with an CSR of 2.38

and an average gas density of 12.3 kg/m^3 (shown as point Process Compressor, Figure 3-82), it lies within Region A and $Q_0/Q_A \geq 2$. Thus, no further analysis is required. The combination of shaft stiffness and excitation levels is such that the predictions based on the Level I analysis are sufficient to ensure a stable rotor.

The gas injection compressor has an average gas density of 107 kg/m^3 . At this density, a Level II analysis is required regardless of the CSR because $Q_0/Q_A < 10$, point Injection Compressor (relative shaft stiffness measurement.) High gas density applications have the potential for creating large destabilizing forces (see 3.5.1). Under these conditions (average gas density exceeding 60 kg/m^3 and $Q_0/Q_A < 10$), a Level II analysis is used to more accurately model these destabilizing forces.

3.12.3.4 Level II Analysis

A Level II analysis of the gas injection compressor is required due to the high gas density and the Q_0/Q_A ratio of the application. Per SP6.8.6.2 and SP6.8.6.3, the stability analysis is now performed at MCS of the compressor. For components sensitive to pressure differential, operating conditions near surge (representing the maximum differential attainable) should be examined. Additionally, the clearance

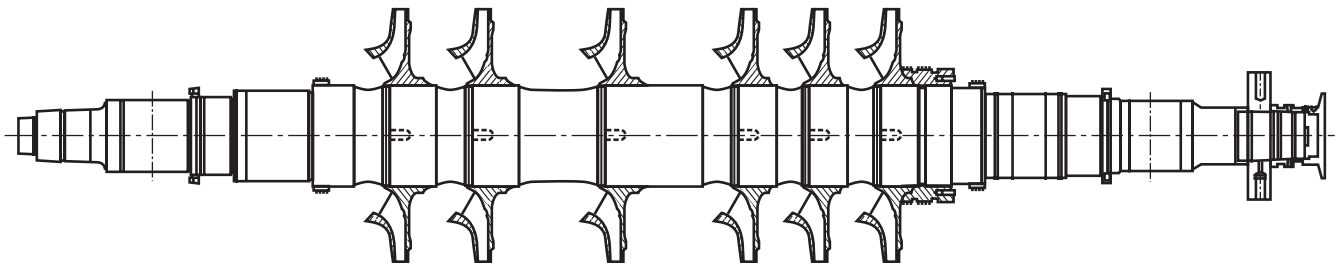


Figure 3-78—Process Compressor Cross-section

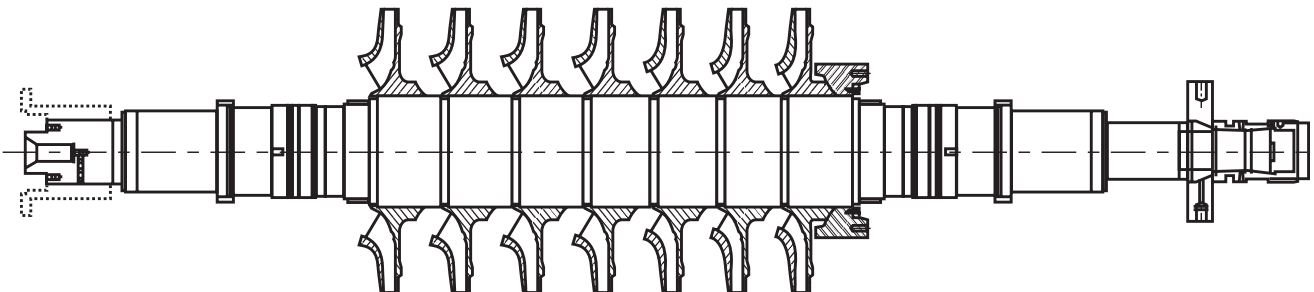


Figure 3-79—Gas Injection Compressor Cross-section

Job Title:

Process Compressor**Modified Alford's Method**

(Compressors)

HP = Horsepower

 $B = 3$ (Standard) D = Impeller OD (in) H = Minimum of Diffuser or Impeller Discharge Width per Impeller (in) N = Speed (rpm) $C = 63,000$

$$K_{xy} = \frac{B * HP * C}{D * H * N} * \frac{\rho_d}{\rho_s}$$

Compressor Stage Data for Highest HP Case

Speed = 13,600 rpm

Stage Data P_{in} (psia) T_{in} (deg R) Z_{in} P_{out} T_{out} Z_{out}

Density Ratio

HP

 D (in) H (in)

Used: 1=Yes 0=No

Stage									
1	2	3	4	5	6	7	8	9	10
219	266	317	361	451	554				
609	641	672	550	586	622				
0.9817	0.9821	0.9828	0.9565	0.9578	0.96				
266	317	376	451	554	671				
641	672	703	586	622	657				
0.9821	0.9828	0.9836	0.9578	0.96	0.9631				
1.15	1.14	1.13	1.17	1.15	1.14				
712	692	697	738	747	751				
13.65	13.65	13.65	13.65	13.65	13.65				
0.615	0.502	0.449	0.386	0.339	0.295				
1	1	1	1	1	1				

K_{xy}	1,360	1,594	1,790	2,279	2,590	2,962	0	0	0	0
----------	-------	-------	-------	-------	-------	-------	---	---	---	---

Total K_{xy} (lbf/in) 12,576**Worksheet 3-1—Modified Alford's Force—Process Compressor**

and oil inlet temperature are varied within the operating tolerances to produce the worst stability condition.

The anticipated cross coupling was replaced with the following excitation sources:

- Impeller eye labyrinths—Impeller eye seals are exposed to the pressure rise developed in the impeller. Depending on the number and compressor configuration, their collective effect may be similar in magnitude to the balance piston. For this example, the impeller hub seals were ignored due to the small differential across each.
- Balance piston—Large destabilizing forces were created by the balance piston. In its original configuration, the com-

pressor was predicted to be unstable. Swirl brakes were required to reduce the destabilizing forces in the balance piston (see 3.4.2).

c. Aerodynamic cross coupling—Introducing cross coupling as predicted by one the empirical equations duplicates the destabilizing forces already in the model from the labyrinth seal analysis (see 3.5.1). Since experimental evidence indicates these forces may be small in centrifugal impellers, the aerodynamic cross coupling was assumed to be zero for the example.

d. All remaining terms were assumed to be second order in magnitude and neglected for the example.

Job Title:

HP Gas Injection Compressor**Modified Alford's Method**

(Compressors)

HP = Horsepower

B = 3 (Standard)

D = Impeller OD (in)

H = Minimum of Diffuser or Impeller Discharge Width per Impeller (

N = Speed (rpm)

C = 63,000

$$K_{xy} = \frac{B * HP * C}{D * H * N} * \frac{\rho_d}{\rho_s}$$

Compressor Stage Data for Highest HP Case

Speed = 13,751 rpm

Stage Data

	Stage									
	1	2	3	4	5	6	7	8	9	10
Pin (psia)	1375	1663	1982	2330	2709	3113	3542			
Tin (deg R)	567	599	629	659	687	715	741			
Zin	0.833	0.8563	0.8829	0.9125	0.9444	0.9782	1.0131			
Pout	1663	1982	2330	2709	3113	3542	4000			
Tout	599	629	659	687	715	741	767			
Zout	0.8563	0.8829	0.9125	0.9444	0.9782	1.0131	1.0567			
Density Ratio	1.11	1.10	1.09	1.08	1.07	1.06	1.05			
HP	842	856	872	890	903	913	928			
D (in)	13.032	13.032	13.032	13.032	13.032	13.032	13.032			
H (in)	0.177	0.161	0.15	0.142	0.134	0.126	0.122			
Used: 1=Yes 0=No	1	1	1	1	1	1	1			

Kxy	5,583	6,173	6,656	7,123	7,576	8,10	8,39	0	0	0
-----	-------	-------	-------	-------	-------	------	------	---	---	---

Total Kxy (lbf/in) 49,609

Worksheet 3-2—Modified Alford's Force—Gas Injection Compressor

Per **SP6.8.6.4**, a table of the log decrement is developed for each stage of the analysis of the gas injection compressor (see Table 3-4).

The minimum log decrement at the initial step is produced by the combination of bearing clearance and oil inlet temperature within the operating range. This combination is held throughout the remainder of the analysis.

Displaying the results in this fashion highlights the balance piston as the major influence on stability. With no pre-swirl control, the balance piston degrades the log decrement by 0.65. Thus, it is clear which component should be redesigned to address the deficiency in rotor stability. Adding swirl

brakes to the balance piston increases the final log decrement to an acceptable level of 0.32. This may be further improved with swirl brakes on the eye labys.

3.12.3.5 Level II Acceptance Criteria

The gas injection compressor was predicted to have an acceptable level of stability with swirl brakes added to the balance piston (0.322 vs. the required 0.1.) This configuration is what was assembled and successfully tested. The unit has been commissioned and is operating.

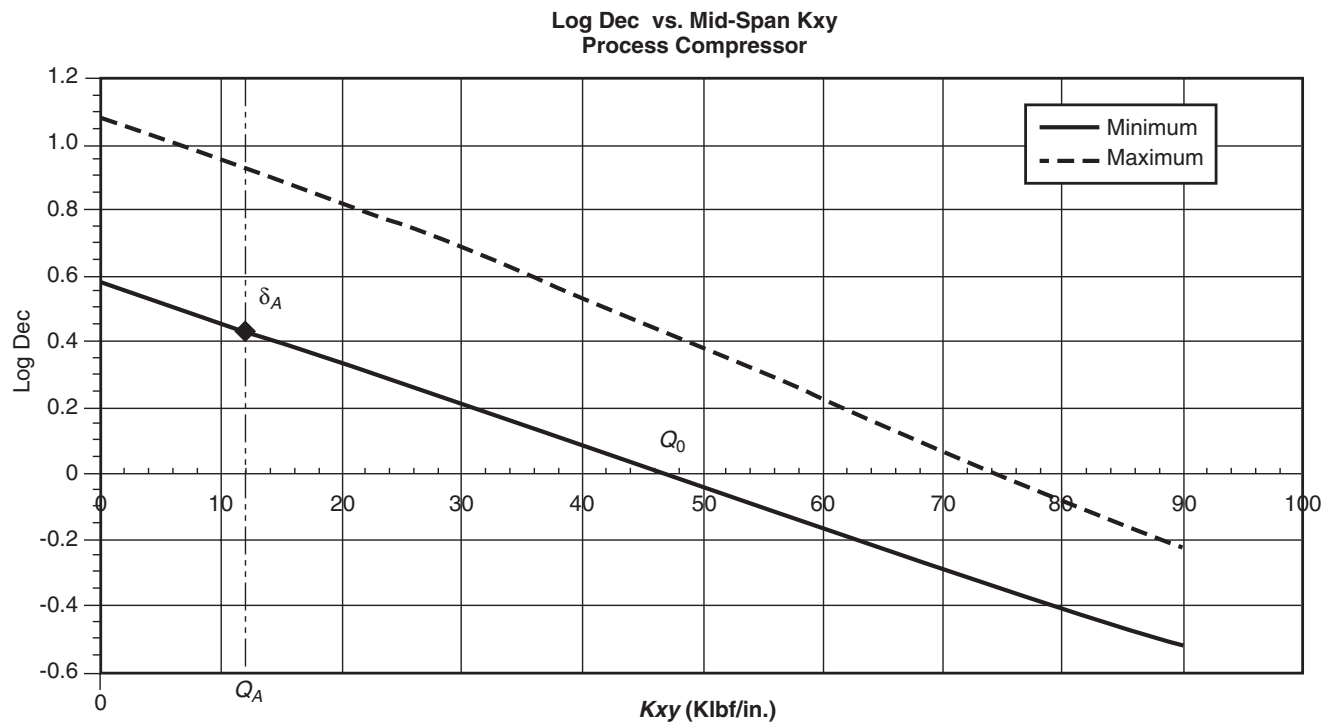


Figure 3-80—Process Compressor Stability Plot

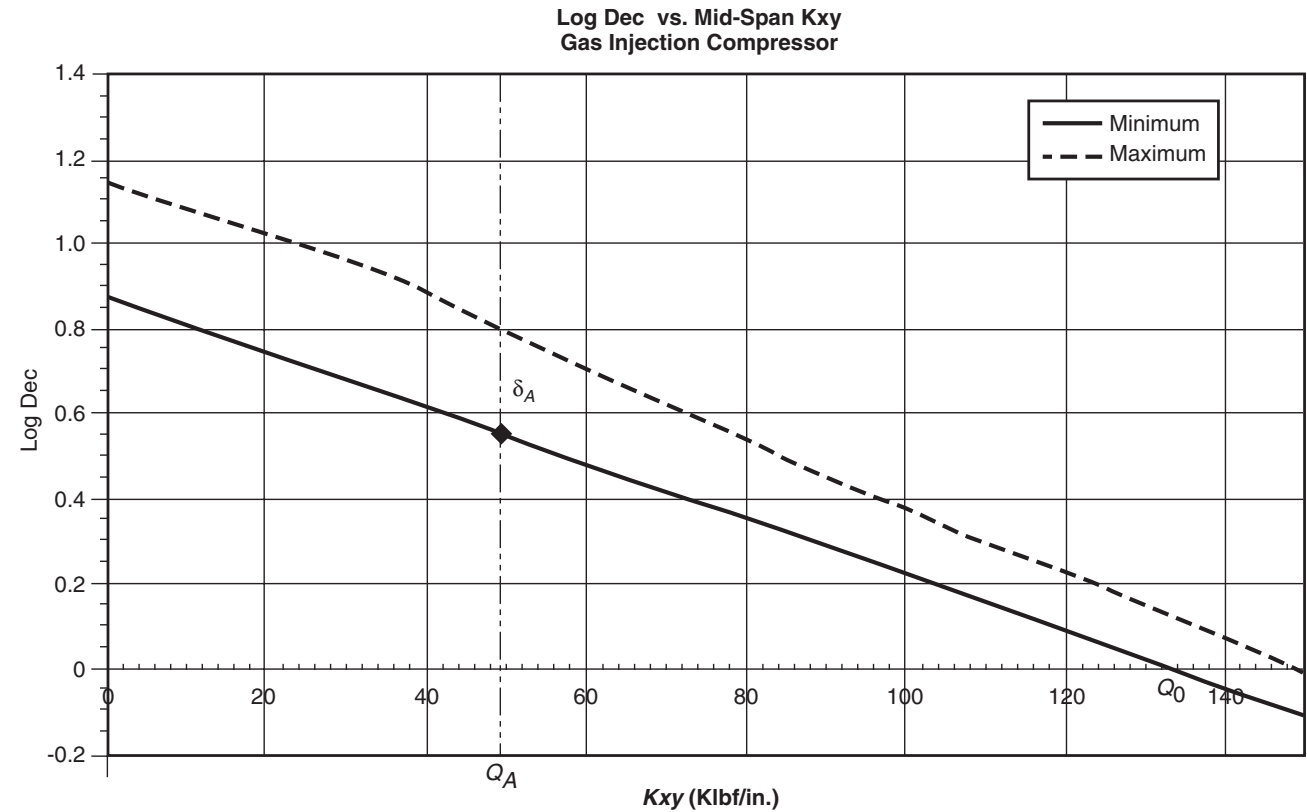


Figure 3-81—Gas Injection Compressor Stability Plot

Table 3-3—Level I Stability results for Process and Gas Injection Compressor

	Process Compressor	Gas Injection Compressor
Q_0 (lbf/in)	46,700	133,300
Q_A (lbf/in)	12,576	49,609
δ_A	0.44	0.55
Q_0/Q_A	3.71	2.69
1 st Critical Speed (rpm)	5,994	8,677
MCS	14,280	14,440
CSR	2.38	1.66
Gas Density (kg/m ³)	12.3	107

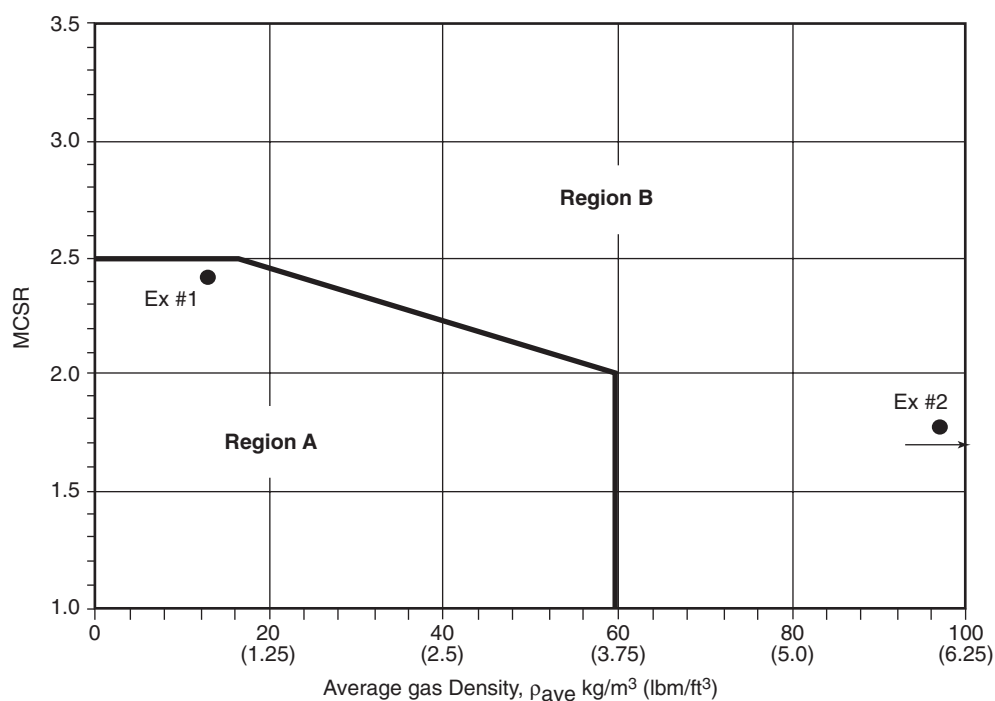


Figure 3-82—Process and Gas Injection Compressors on Experience Plot

Table 3-4—Minimum Log Decrement for Gas Injection Compressor

Configuration	Minimum Log Decrement
Rotor & Bearings (Basic Log Decrement)	0.871
Rotor & Bearings + Impeller Eye Labys	0.492
Rotor & Bearings + Impeller Eye Labys +Balance Piston	– 0.159
Rotor & Bearings + Impeller Eye Labys +Balance Piston w/ Swirl Brake (Final Log Decrement)	0.322

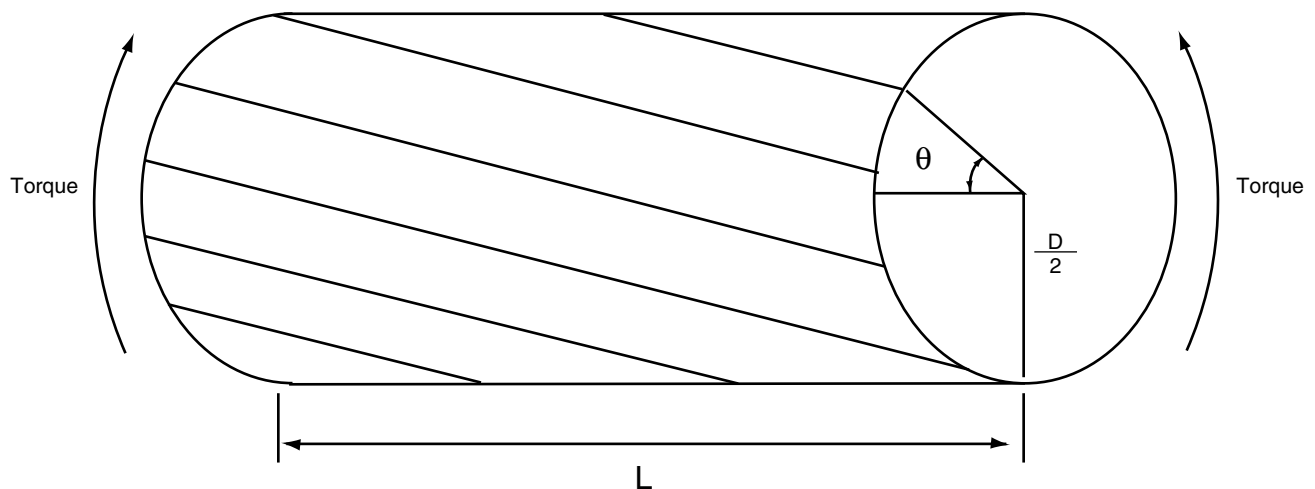
SECTION 4—TORSIONAL ANALYSIS

4.0 INTRODUCTION AND SCOPE

Ensuring mechanical reliability in rotating machinery trains begins in the design phase of each train component. The vendor of each individual train component is called on to perform sufficient analysis of the proposed unit design such that, when finally constructed, the train component will perform reliably throughout its intended service life. When these components are combined into an equipment train, problems may arise that are different in nature from those the vendor must address during component design. Specifically, the torsional vibration behavior of the complete train is of importance in assuring that the individual units will reliably operate when coupled. Any new design or significant design modification in a machine's rotating system, including its impellers, couplings, gears, and drivers, typically requires a train torsional natural frequency analysis. Information required to model a system can be found in 4.1. This analysis is necessary to determine the location of the torsional natural frequencies relative to potential excitation, such as those identified in

4.5, and determine whether this meets with acceptance criteria set forth by API. Torsional vibrations refer to oscillatory torsional deformations encountered by the shafts in the subject train during all phases of operation, including start-up. A diagram of a circular beam (shaft) undergoing a torsional deformation is presented in Figure 4-1. Reciprocating machinery is addressed in 4.3.

The typical approach to designing an equipment train from a torsional dynamics standpoint is to calculate the train's undamped torsional natural frequencies and attempt to locate them away from frequencies of potential excitation such as those identified in 4.5. Section 4.4 identifies elements of a torsional analysis. By placing a train's torsional natural frequencies outside of the excitation frequency range, the torsional natural frequencies will not cause operating problems such as a coupling or shaft end torsional failure. If, during the initial design phase, a torsional natural frequency interferes with an excitation the designer usually eliminates the interference by a modification to one or more



For a solid isotropic cylinder,

$$\theta = \frac{TL}{GJ}$$

θ = Angle of twist

T = Applied torque

L = Cylinder length

G = Shear modulus

J = Second moment of area of cross section
about the axis of twist

$$= \frac{\pi D^4}{32} \text{ (Circular cross-section)}$$

Figure 4-1—Diagram of a Shaft Undergoing Torsional Elastic Deflection

couplings. Occasionally, however, interference may occur where the natural frequency of an individual unit cannot be moved by a coupling stiffness change. When this happens, consideration must be given to the potential sources of the excitation and whether these excitations are at a location that will create a torsional response in the system. If these excitations can cause the system to respond, that is create a torsional response which produce high stresses, further modifications to the system must be made. If this is not practical, a high cycle fatigue analysis as outlined in 4.6.1, shall be conducted to verify that the system is reliable.

In addition to the conventional analysis to identify system torsional natural frequencies, there may be a requirement to perform transient analysis if the system will be exposed to transient torsional excitation, as identified in 4.5.2. A low cycle fatigue analysis, as identified in 4.6.2, will insure that the equipment is not damaged during transient excitation.

A report of the results of the torsional analysis shall be submitted to the purchaser. Typical contents of a report for a torsional analysis are discussed in 4.7.

Section 4.8 identifies methods to accomplish testing of a coupled system.

Section 4.9 identifies the occasional condition when lateral vibration may be caused by significant torsional vibration.

Section 4.10 identifies standard paragraphs related to torsional vibration and specific paragraphs on torsional vibration found in API documents.

References [1] and [2] contain an excellent overview of the aspects of torsional vibration analysis. Reference [2] is particularly noteworthy for the comprehensive tabulation of references regarding the subject of torsional vibration.

References

1. J. C. Wachel and Fred R. Szenasi, "Analysis of Torsional Vibrations in Rotating Machinery," 22nd Turbomachinery Symposium Proceedings, 1993, Pages 127 – 151.
2. Mark A. Corbo and Stanley B. Malanoski, "Practical Design against Torsional Vibrations," 25th Turbomachinery Symposium Proceedings, 1996 Pages 189 – 223.

4.1 MODELING

4.1.1 Mass Elastic System Modeling Considerations

4.1.1.1 Introduction

Care must be exercised in the detailed modeling of a torsional system in order to ensure the required accuracy. A consistent set of engineering units must be used throughout the analysis in order to avoid potential errors. This is especially true of torsional analysis work where several sets of vendor prints and/or data sets, which may contain a different system of units, may be used.

Train modeling begins by dividing the component shafts into discrete sections or finite elements. Locations on the rotor that contain significant inertia, such as compressor impellers, turbine discs, bull gears, etc. are identified and lumped inertia is concentrated at these locations. Connection between rotors, such as couplings, are identified as lumped inertia connected by an equivalent stiffness to complete the mechanical model. The model contains information regarding speed ratios between rotors so that all the system inertia and stiffness are properly referenced to one speed. The final data required for the model is the identification of the material properties of the connected system.

Prior to analyzing a system, the analyst must have accurate drawings to model the rotors and couplings used in the system. These may consist of actual manufacturing drawings or an accurate summary of the rotor construction, also known as a mass elastic drawing. The mass elastic drawing should include the following information:

- a. Materials used for the rotor and how the properties will change with operating temperature, if appropriate.
- b. Shaft section lengths and diameters and any non circular cross-section details.
- c. Details of rotor attachments such as shrunk on or bolted on components including lumped inertia.

The analyst should not rely on a single sketch of a rotor which tabulates inertia and stiffness. Unless the shaft stiffness is properly calculated between major lumped inertias and coupling stiffness, a serious misrepresentation may be made of the torsional system model. Such modeling errors can result in significant errors of the torsional natural frequencies of a system.

Coupling drawings are required to accurately model the system. Correct modeling of the coupling is crucial as these components have a major impact on the first mode of a directly coupled system and the first two modes of motor/gear/compressor system. Systems with multiple bodies may have the first three or four modes influenced by couplings between components. Coupling drawings usually contain the inertia of the drive and driven halves as well as the torsional stiffness of the coupling assembly including the torsional stiffness of the shaft section protruding into the coupling hub. It is important to identify how the shaft penetration into the coupling has been treated when calculating the complete coupling stiffness. For metallic couplings, the coupling stiffness is a single value, however for elastomeric couplings the stiffness is a function of the applied torque. The data for an elastomeric coupling should include a curve of the torsional stiffness versus the applied torque.

If train units are accurately modeled, the undamped torsional natural frequency analysis usually predicts actual train natural frequencies within a small margin of error because

most equipment trains generally possess low levels of system torsional damping.

Figures 4-2 through 4-7 present, in sequence, the general approach to torsional modeling for a typical motor-gear-compressor train and a turbine-compressor train. Side view drawings of the two trains are presented in Figures 4-2 and

4-5. Cross-sectional views of the rotating elements for these two trains are displayed in Figures 4-3 and 4-6. Finally, using geometric and inertia properties of the rotating elements, computer models of the trains can be assembled. Schematics of the train computer models are presented in Figures 4-4 and 4-7.

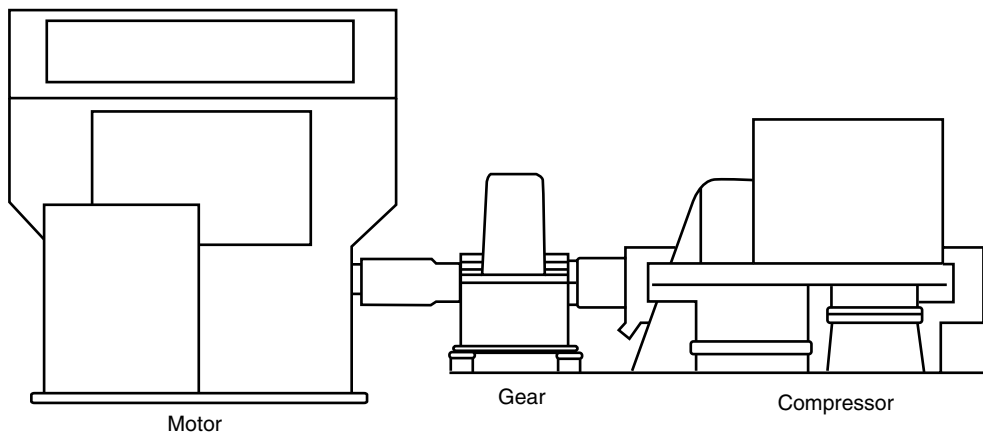
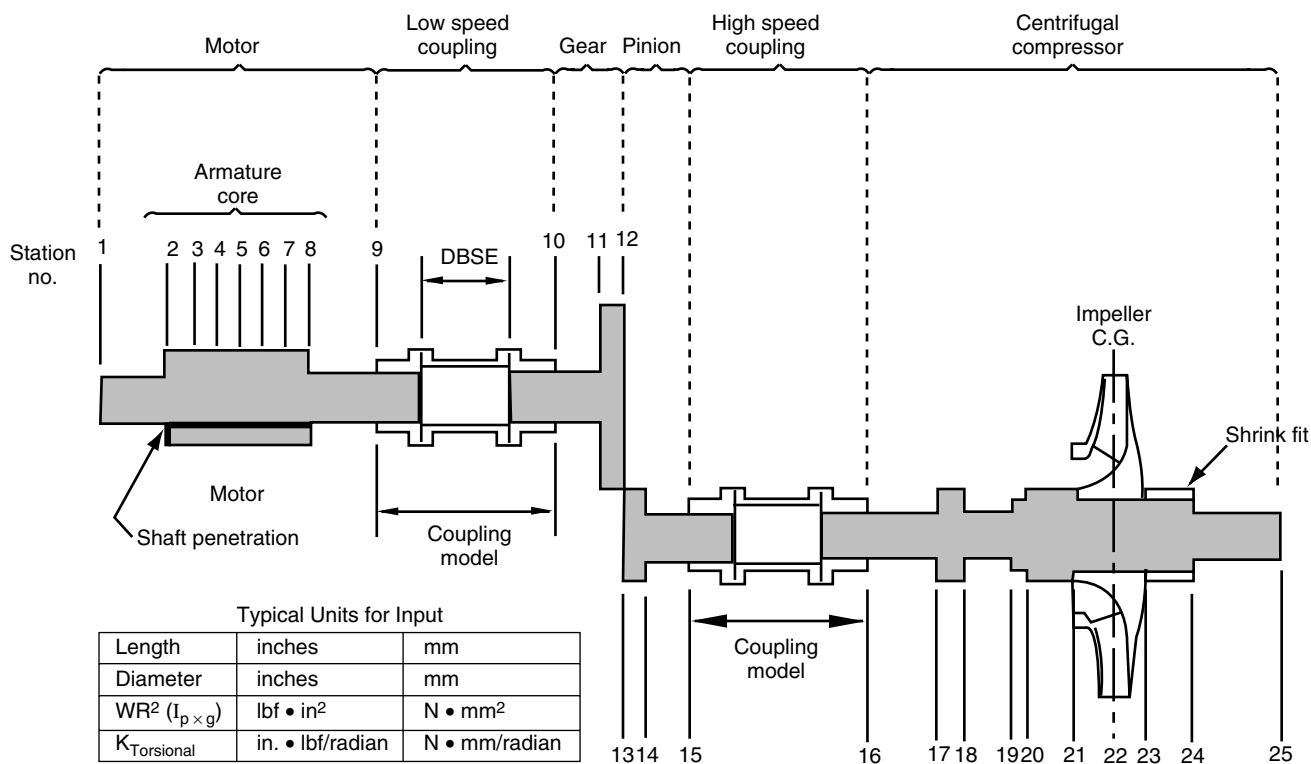
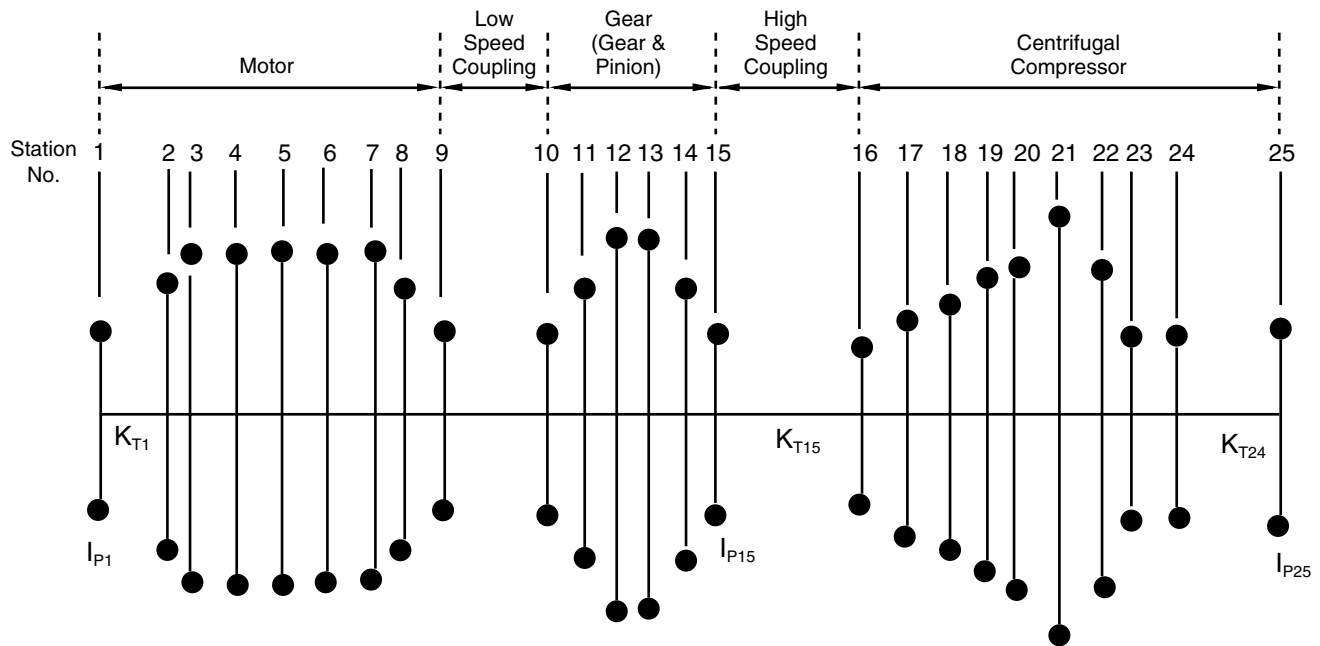


Figure 4-2—Side View of a Typical Motor/Gear/Compressor Train



Note: Coupling vendors typically provide WR^2 and $K_{Torsional}$ for each coupling. The WR^2 value does not include the WR^2 of the coupling journal (shaft inside the coupling HUB). The $K_{Torsional}$ value typically assumes $1/3$ shaft penetration into the coupling HUB.

Figure 4-3—Modeling a Typical Motor/Gear/Compressor Train



Notes:

1. I_{Pi} = i th station lumped polar moment of inertia.
 K_{Ti} = i th shaft section torsional stiffness.
2. All WR^2 values have been converted into polar mass moments of inertia (I_p) at each station.
3. All I_p and K_T values have been referenced to a single shaft rotation speed.

Figure 4-4—Schematic Lumped Parameter Model for the Motor/Gear/Compressor Train

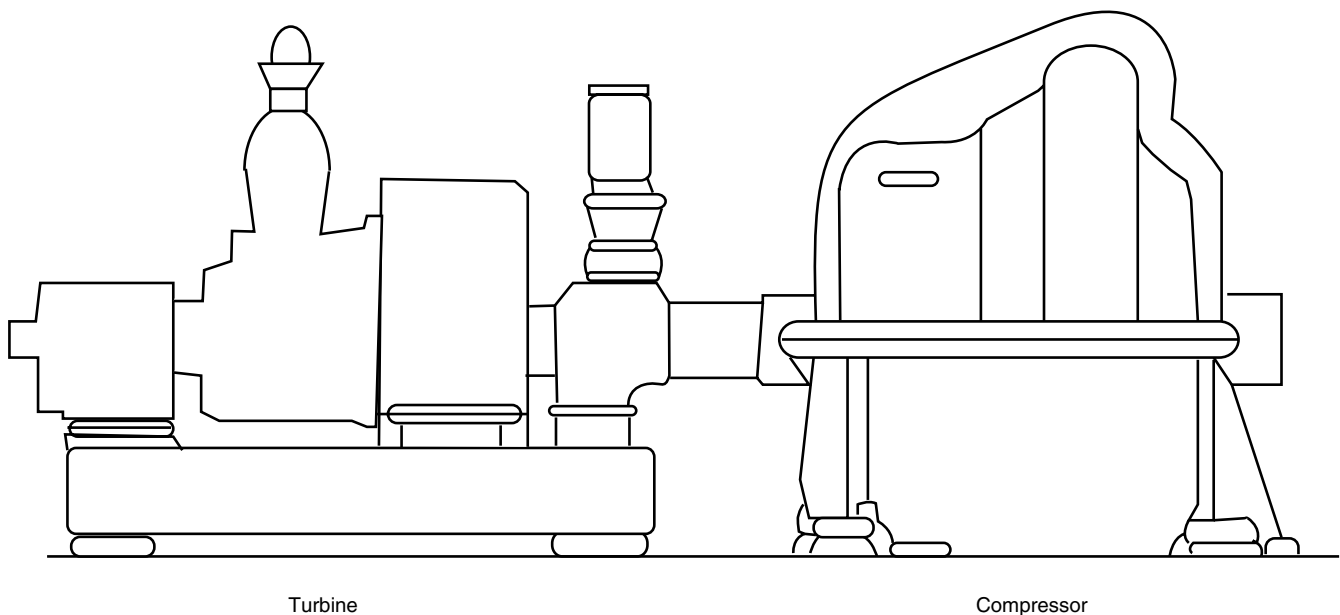
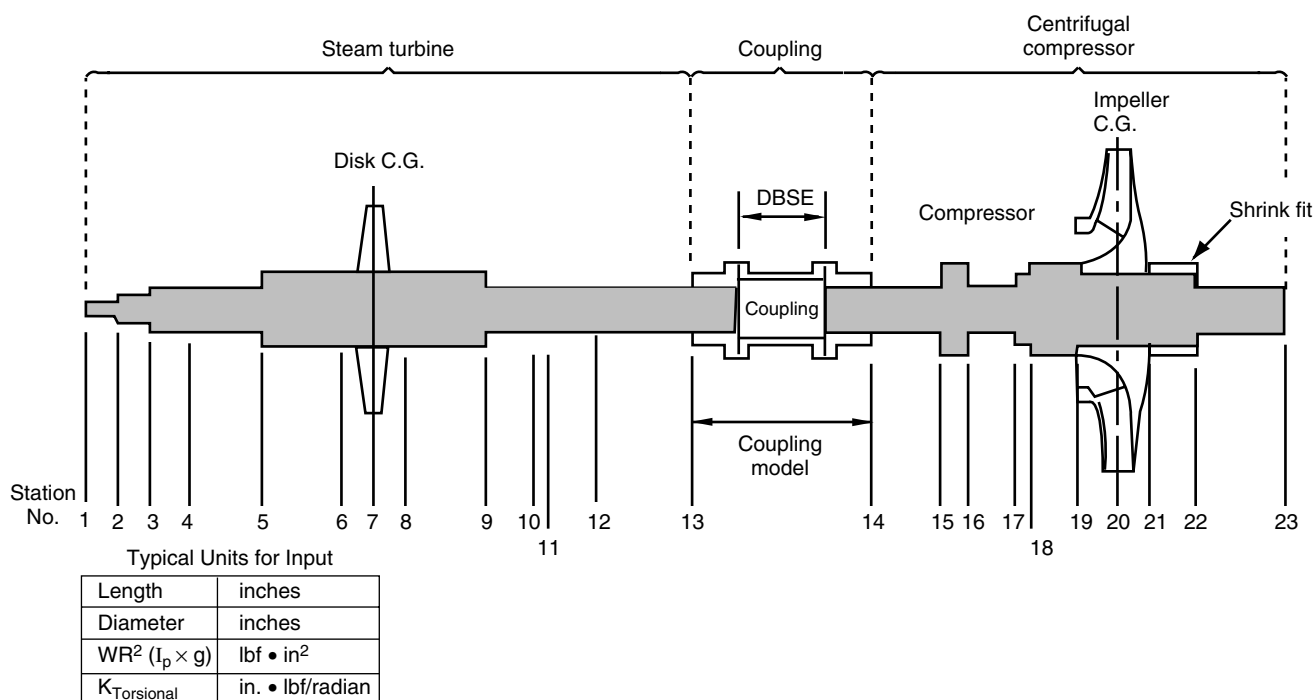
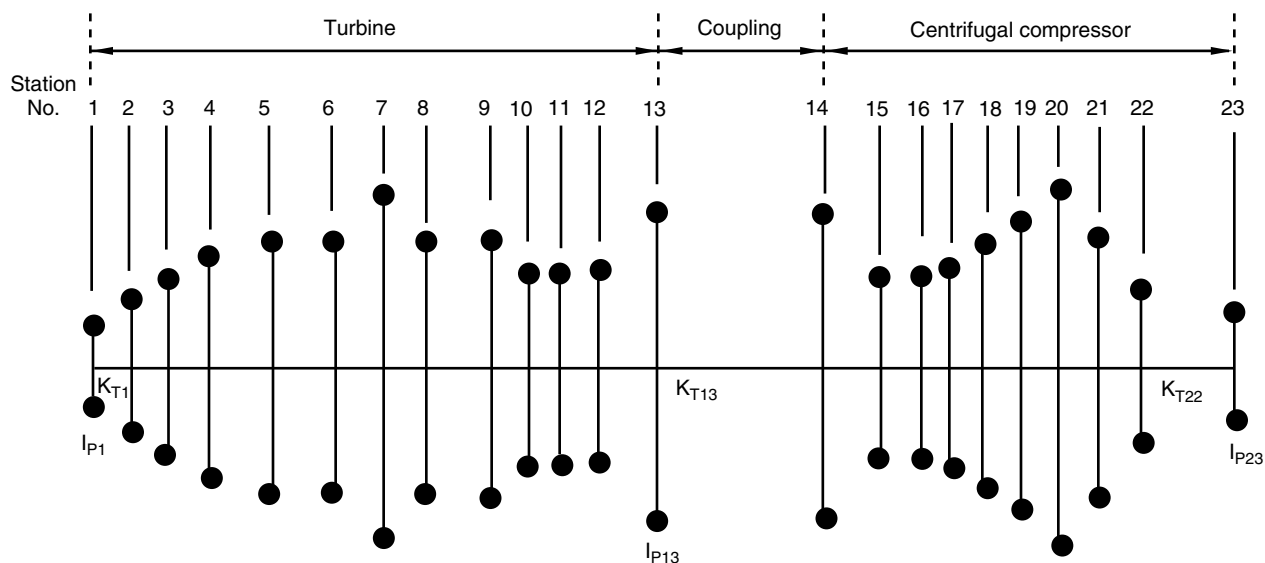


Figure 4-5—Side View of a Typical Steam Turbine Driven Compressor Train



Note: Coupling vendors typically provide WR^2 and $K_{Torsional}$ for each coupling. The WR^2 value does not include the WR^2 of the coupling journal (shaft inside the coupling HUB). The $K_{Torsional}$ value typically assumes $1/3$ shaft penetration into the coupling HUB.

Figure 4-6—Modeling a Typical Steam Turbine Drive Compressor Train



Notes:

1. I_{p_i} = i th station lumped polar moment of inertia.
 K_{T_i} = i th shaft section torsional stiffness.
2. All WR^2 values have been converted into polar mass moments of inertia (I_p) at each station.
3. All I_p and K_T values do not require speed referencing since train elements all spin at the same speed.

Figure 4-7—Schematic Lumped Parameter Model for the Steam Turbine Driven Compressor Train

Typical items which can easily be modeled by concentrated mass-elastic data exclusively are couplings, gears, impellers, turbine stages, and motor rotor attachments. Experience has shown that metallic flexible couplings are most appropriately modeled as a single torsional spring (vendor supplied torsional stiffness) with the respective half-coupling inertias at each end. Elastomeric couplings are more complex to model as the torsional stiffness is nonlinear. The torsional stiffness of an elastomeric coupling is a function of the transmitted torque. A typical elastomeric coupling torsional stiffness versus torque curve is shown in Figure 4-8. It can be

seen from Figure 4-8 that the coupling stiffness is dependant upon the elastomer used in the coupling. The coupling manufacturer can provide the stiffness at a given torque or provide an explanation of how to calculate the stiffness from the non-linear torque deflection plot. In addition, for transient conditions, the coupling vendor can recommend appropriate stiffness and damping to be used for a transient analysis. Also, if the torque supplied by the driver has a significant variation then the system may have to be analyzed with the minimum and maximum torque conditions to define a range of frequencies for a given mode.

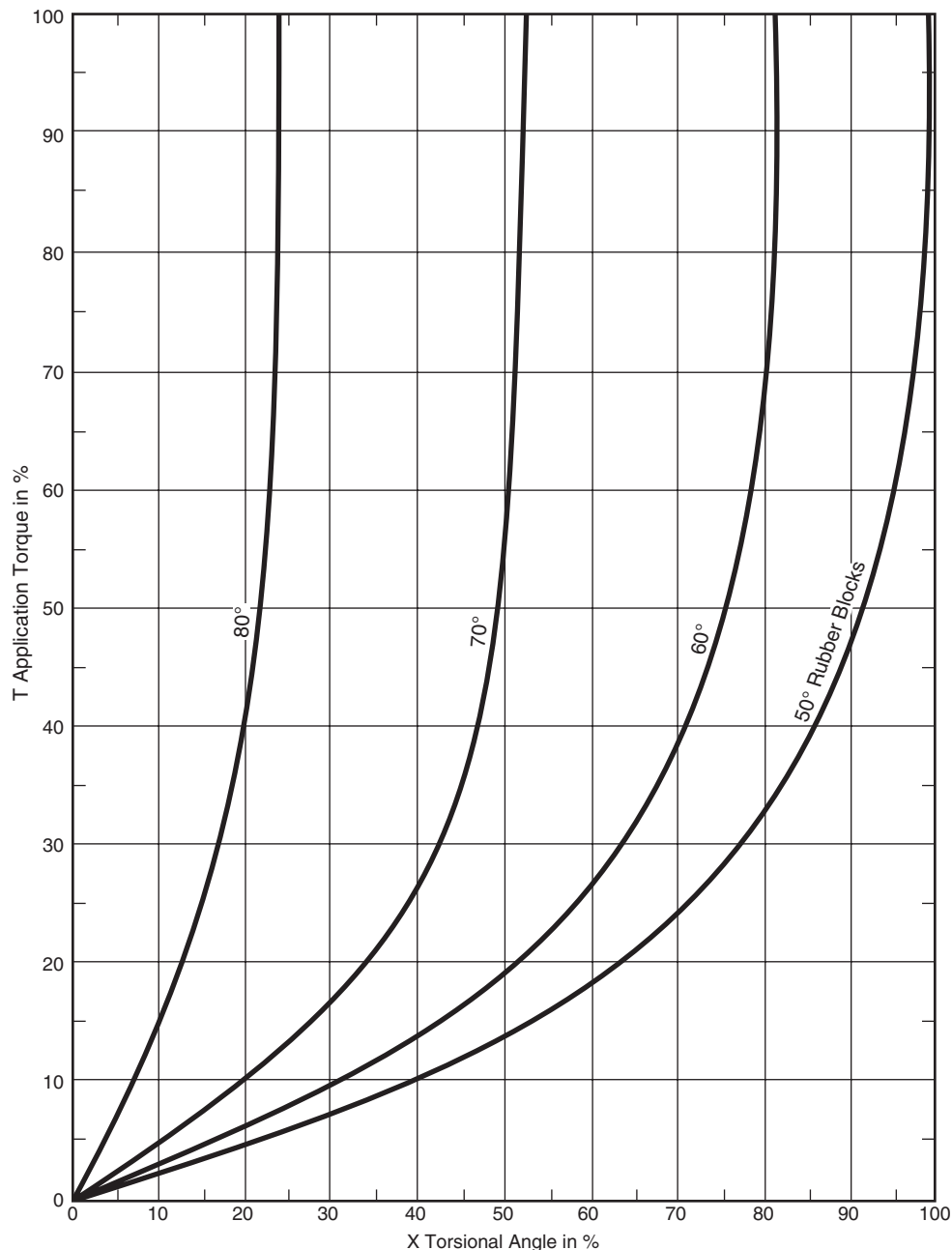


Figure 4-8—Typical Non-linear Stiffness vs. Torque for an Elastomeric Coupling

Gears lend themselves to lumped mass modeling since the bulk of their inertia is in the gear wheels, and the shafts closely approximate low inertia torsional springs. Impellers and turbine stages can usually be modeled as discrete lumped inertias since they typically do not contribute to the torsional stiffness of their respective shafts. Motor rotor attachments such as rotor cores and brushless exciters are not easily modeled because they are typically shrunk onto the shaft over an extended length. It is not obvious how the attachment's inertias and stiffnesses affect the motor shaft inertias and stiffnesses. Caution must be exercised with approaches that lump the inertia and stiffness of a whole unit because inaccuracies may result if the shaft ends are sufficiently torsionally flexible relative to couplings.

This section presents some of the more important modeling problems and concerns typically encountered in torsional vibration analysis:

- Speed referencing inertia (I_p) and stiffness (K_t).
- Step shafting.
- Shrink fits.
- Integral disks or hubs.
- Couplings.

4.1.1.2 Speed Referencing Inertia and Stiffness

A computer code for calculating undamped train torsional natural frequencies should have the capability to analyze a train of coupled rotors that operate at different rotational speeds (for example, an equipment train with multiple speed-changing gears). An equivalent single shaft model for a geared train is required before calculating the undamped torsional natural frequencies and mode shapes of the system. An equivalent single shaft model requires all inertia and stiffness to be referenced to a common speed. The relationship between inertia and stiffness of units that operate at a different speed from a selected reference speed is written as follows:

$$I_{pr} = I_{pa} \left(\frac{N_a}{N_r} \right)^2 \quad (4-1)$$

$$K_{tr} = K_{ta} \left(\frac{N_a}{N_r} \right)^2 \quad (4-2)$$

where

Quantity	Typical SI Units	Typical US Customary Units
I_p = polar mass moment of inertia	kg-m ²	lbm-in. ²
K_t = torsional stiffness	N-m/rad	in.-lbf/rad
N = rotation speed	rpm	rpm

Note:

Subscript a denotes actual.

Subscript r denotes reference.

If the software used to calculate the undamped torsional natural frequencies does not have the capability to analyze a train whose elements are operating at different speeds, then the analyst must manually perform speed referencing using the above relationships.

Simple gear reductions (single or multiple) represent single-branch systems, and combined with possible simple branches (single inertia, one-degree of freedom) can be analyzed with the basic Transfer Matrix (Holzer) computer code. Multiple-branch systems of greater complexity require a more sophisticated computer analysis, typically, a finite element formulation. A side view drawing of a train with a single reduction gear is displayed in Figure 4-2. An example of a multiple branch system, a multi-stage integrally geared plant air compressor, is displayed in Figure 4-9. This unit has four overhung compressor stages driven through a single bull gear. Note that the two pinions operate at different speeds.

4.1.1.3 Shaft Stepping

When the shaft geometry length (L) and diameter (D), are used as input, the computer code should consider the effective penetration of smaller diameter shaft sections into adjacent larger diameter sections. The smaller shaft, in effect, penetrates the larger by the distance defined as the penetration factor (PF). As a result, the length of the smaller diameter shaft is effectively increased by the amount PF and the length of the larger diameter shaft is reduced by the same amount. Figure 4-10 displays the effective length increase of the smaller diameter section as a function of the step geometry. Allowance for penetration effects enables one to more accurately approximate the actual flexibility of the physical system than by simply summing the calculated flexibility of the individual shaft sections. For this type of discontinuity, the effective length of a shaft which joins another of larger diameter is greater than the actual length due to local deformation at the juncture. As shown in Figure 4-10 this penetration factor (PF) depends on the ratio of shaft diameters and can be determined by the following Equation (4-3).

$$L_e = \left(\frac{L_1 + PF}{D_1^4} + \frac{L_2 - PF}{D_2^4} \right) D_e^4 \quad (4-3)$$

where

Quantity	Typical SI Units	Typical US Customary Units
L_e = effective length	mm	in.
D_e = effective diameter	mm	in.
PF = penetration factor	dim	dim
D_1 = smaller diameter	mm	in. (see Figure 4-10)
D_2 = smaller diameter	mm	in. (see Figure 4-10)

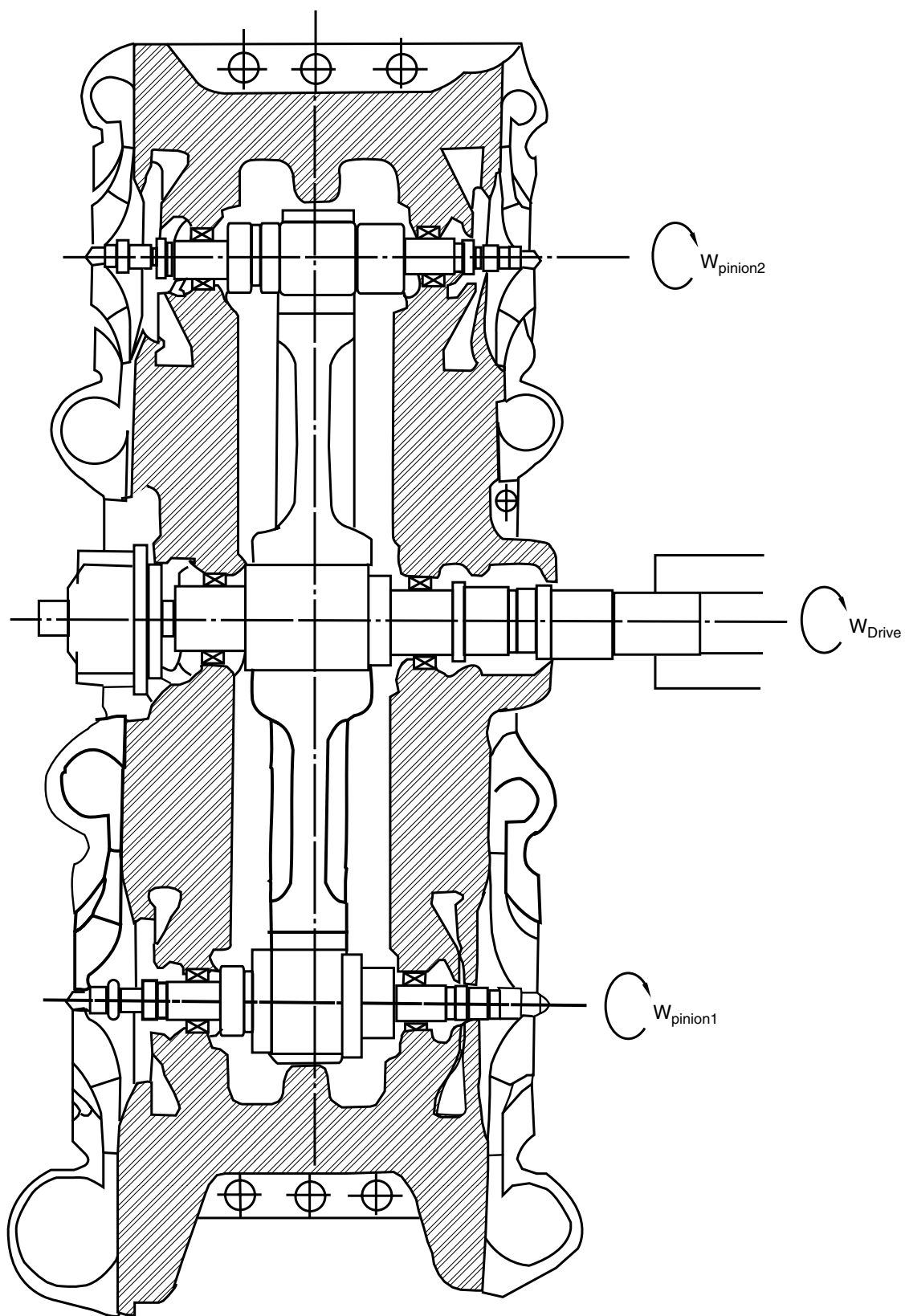
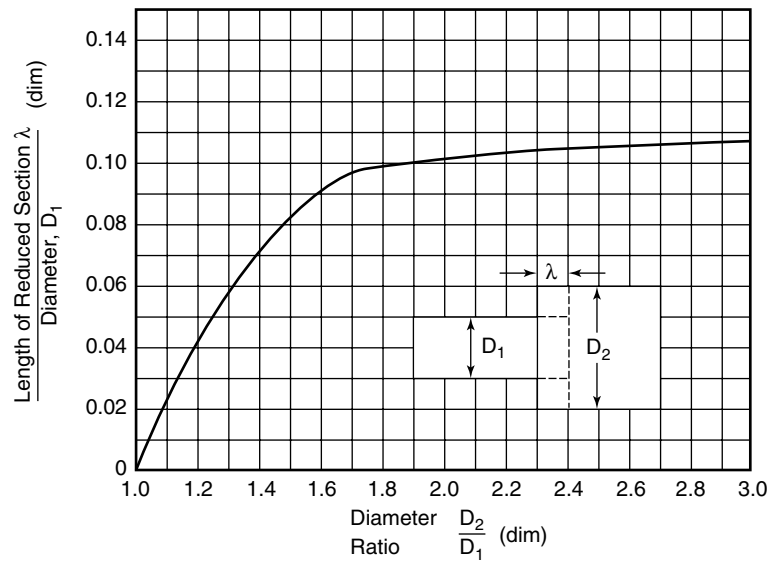


Figure 4-9—A Typical Twin-pinion Integrally-geared Centrifugal Compressor That Should be Modeled as a Branched System



Note: Lambda λ represents a length added to the smaller diameter which will yield the actual torsional stiffness of a stepped shaft section.

Figure 4-10—Effective Penetration of a Smaller Diameter Shaft Section into a Larger Diameter Shaft Section

Table 4-1 gives some characteristic results.

Table 4-1—Penetration Factors for Selected Shaft Step Ratios

D_2/D_1	PF/D_1
1.00	0
1.25	0.055
1.50	0.085
2.00	0.100
3.00	0.107
∞	0.125

Note: Refer to Figure 4-10 for definition of parameters. Lambda (λ) in Figure 4-10 represents a length added to the smaller diameter which will yield the actual torsional stiffness of a stepped shaft section. Penetration factor (PF) equals lambda.

4.1.1.4 Shrink Fits

Most rotating assemblies used in machinery trains have non-integral collars, sleeves, and so on, that are shrunk onto the shaft to create a rotor assembly. These shrunk-on components may or may not contribute to the torsional stiffness of the shaft, depending on the degree of the interference fit, the length of the shrink fit and the size of the shrunk-on component. Precise guidelines regarding inclusion or exclusion of the effect of the shrunk-on member on the shaft torsional stiffness are difficult to quantify; however, the following general principles apply:

a. If the fit of the shrunk-on component is relieved over most of its length, then the torsional stiffening effect is negligible.

A fit is relieved when some portion of the designed interference has been removed. Schematics of shaft sleeves with and without typical relieved fits are displayed in Figure 4-11. Sleeves and impellers often possess relieved fits to aide the rotor assembly process and to minimize internal friction forces that contribute to rotor system instability. The stiffening effect of shaft sleeves and impellers with a high degree of relief (small fit length) is often neglected.

b. If the fit of a shrunk-on component is (1) not relieved over a significant part of its length, (2) made of the same material as the shaft, and (3) manufactured with a shrink fit equal to or greater than 1 mil/in. of shaft diameter, then the effective stiffness diameter of the shaft should be assumed equal to the actual diameter under the sleeve plus the thickness of the sleeve.

c. If the shrunk-on component has a large rotational inertia, then centrifugal force due to rotation may diminish the degree of the shrink fit and the attendant torsional stiffening effects of the component over the rotor operating speed range.

d. If a shrunk on component has a nominal fit length with an L/D greater than or equal to 1, the shaft is assumed to be free to twist torsionally by the hub over an axial length equal to one-third of the total length of shrunk surface. This $1/3$ penetration is typically used by coupling vendors when specifying coupling torsional stiffness of an assembled coupling.

4.1.1.5 Integral hubs or discs

The effect of integral thrust collars or disks forged on the shaft can be determined by the method used for stepped shafts (see 4.1.1.3). For short collars, with an axial length less

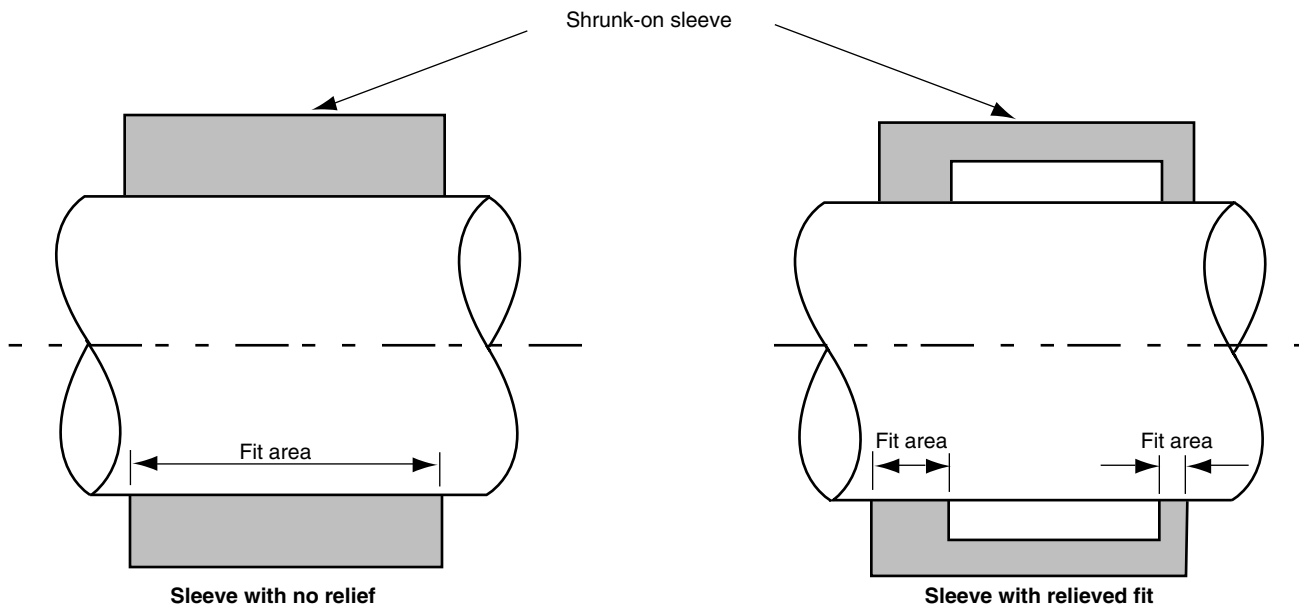


Figure 4-11—Examples of Shrunk on Sleeves With and Without Relieved Fits

than $1/4$ of the shaft diameter, the effect is negligible and the axial length of the collar may be assumed to have an effective torsional stiffness diameter equal to the diameter of the shaft.

4.1.1.6 Couplings

The two types of couplings that normally connect train components are lubricated gear couplings and flexible element dry couplings. The flexible element dry couplings are usually the disc or diaphragm type. Sample cross-sectional drawings of these types of couplings are displayed in Figures 4-12, 4-13, and 4-14.

Normally, a vendor-supplied torsional stiffness value is input for the total coupling and includes the stiffness of the hub to shaft connection(s) and/or the bolted integral flange connection(s). With a hub/shaft connection, the total coupling stiffness value should include the portion of the shaft inside the mounted coupling hub. Therefore, the stiffness of this part of the shaft should not be duplicated in the overall analysis model. With a flange connection, the stiffness value will include the coupling flange and the bolted connection, but will not include the stiffness of the flange to which the coupling is bolted.

The coupling can be thought of as an assembly of torsional springs in series. For example, the reduced moment gear coupling of Figure 4-12 can be modeled with:

- K_{a1}, K_{a2} = Hub-to-shaft connection stiffness (for each hub includes the portion of the shaft inside the mounted hub and the hub body),
- K_{b1}, K_{b2} = Gear mesh stiffness,
- K_{c1}, K_{c2} = Sleeve stiffness (for each sleeve includes the sleeve tube and sleeve flange),

d. K_{d1}, K_{d2} = Bolted connection stiffness,

e. K_e = Spacer stiffness (includes spacer flanges and the spacer tubular section).

The total coupling stiffness, K_t , would be then be found from the equation:

$$\frac{1}{K_t} = \frac{1}{K_{a1}} + \frac{1}{K_{a2}} + \frac{1}{K_{b1}} + \frac{1}{K_{b2}} + \frac{1}{K_{c1}} + \frac{1}{K_{c2}} + \frac{1}{K_{d1}} + \frac{1}{K_{d2}} + \frac{1}{K_e} \quad (4-4)$$

Where typical SI units for K_t are N-m/rad, and typical US Customary Units are in.-lbf/rad.

For a reduced moment flexible element dry coupling as shown in 4-14, the method of calculation is the same, except that instead of the gear mesh stiffness, the flexible element stiffness and any flange connection stiffness are used.

The formulas for calculating the stiffness are relatively simple, but the assumptions used to define certain variables make the analysis more complex. As an example, the length to use in the formula for the tubular section of a spacer is not the overall length of the spacer, but is the overall length of the spacer minus half the thickness of each flange.

The spacer flanges are considered to be disk sections, which are circular sections through which the torque is transmitted between the outside diameter and the inside diameter of the section. When the torque transmitting path changes from a tube section to a disk section, as in a coupling spacer, the tubular length is taken from the center of the disk section. Moreover, the outside diameter used in the disk (flange) section is not the extreme outer diameter, but the bolt circle diameter. All this is shown in Figure 4-15. For detailed equations and calculation examples, refer to Reference [1].

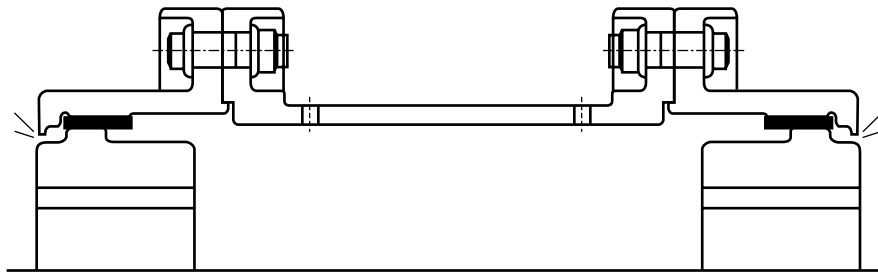


Figure 4-12—A Reduced Moment Gear Coupling

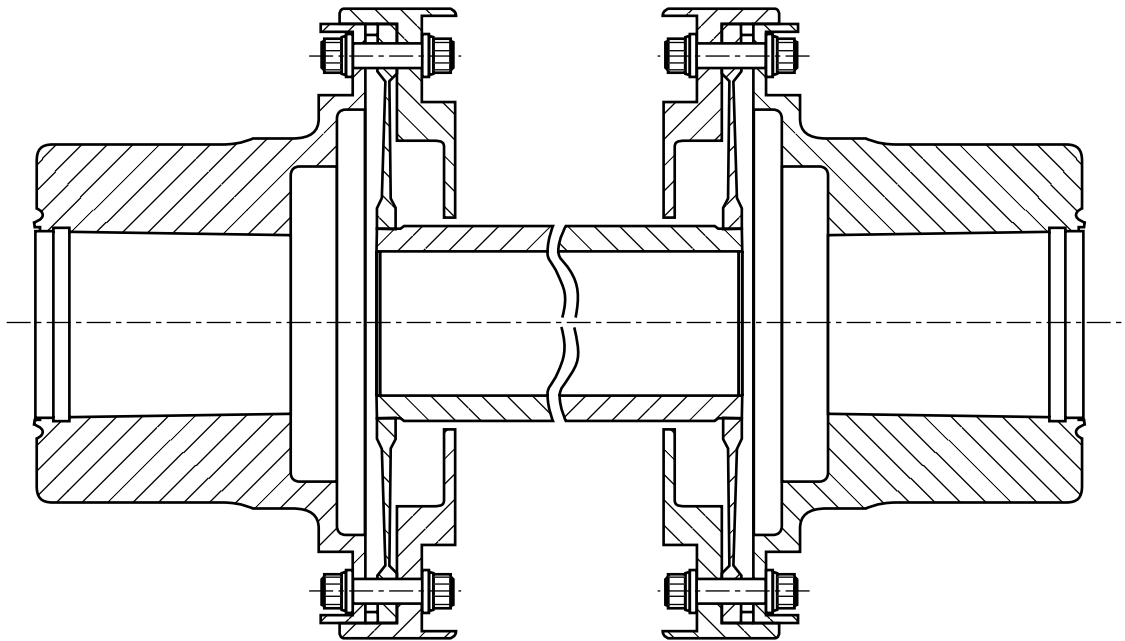


Figure 4-13—A Marine-style Diaphragm Coupling

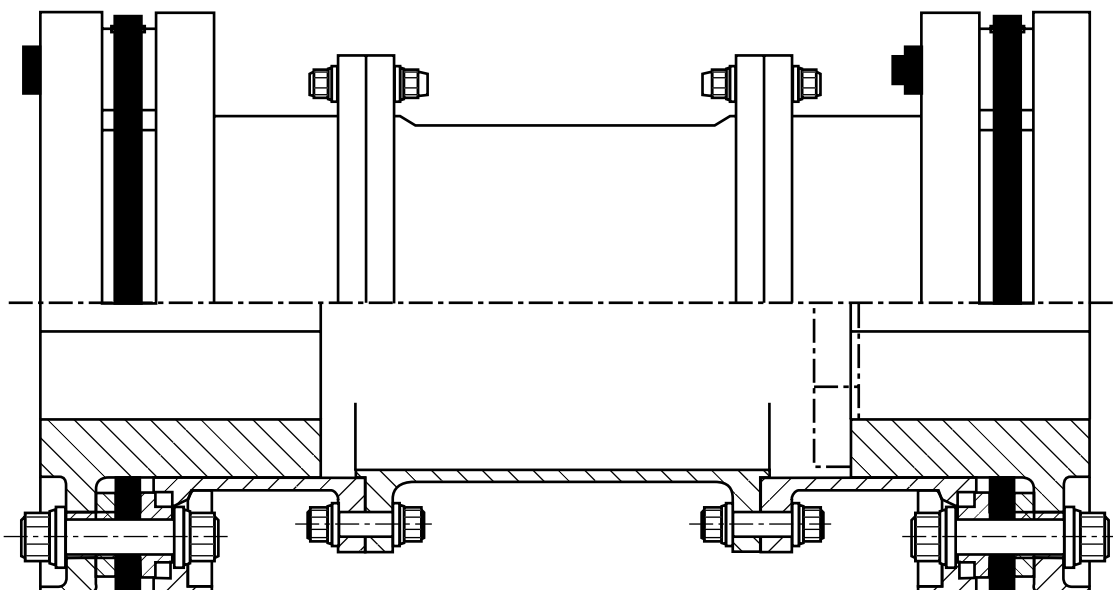


Figure 4-14—A Reduced Moment Disc Coupling

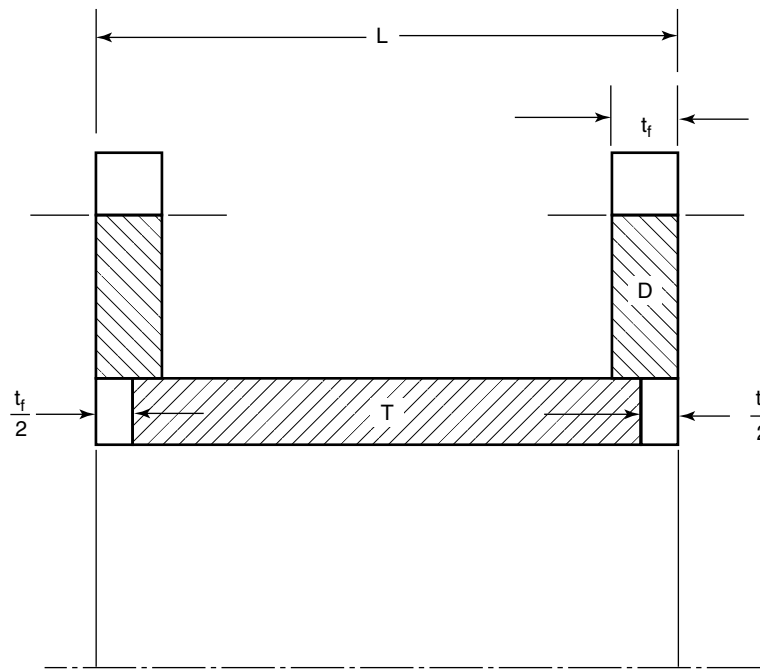


Figure 4-15—Coupling Spacer Torsional Stiffness Model

Even more complex is the hub-to-shaft connection stiffness analysis. Refer to Reference [1] 4.4.1.3 Hub/shaft connection which reads, “Some of the parameters that affect torsional stiffness of a hub/shaft connection include: the type of fit (clearance, interference, keyed or non-keyed), magnitude of torque, speed, and hub flange location.

A simplified method commonly known as “ $1/3$ shaft penetration” was introduced in Reference [2]. When applicable, the $1/3$ shaft penetration should be included in the coupling stiffness. Other methods such as found in Reference [3] or the vendor’s standard can also be used upon mutual agreement.

Further, “The $1/3$ shaft penetration method assumes, through experience, that the shaft is regarded as unrestrained for one third the length of the hub. The torque travels through only the shaft for the first one-third of the hub shaft engagement, and through only the hub...for the remaining two-thirds.” [2]

Of course, the actual penetration varies with hub connection design. For typical applications of flexible element dry couplings, the $1/3$ penetration model is a very good assumption, since the torsional stiffness of the flexible elements will generally be much less than the hub/shaft connection stiffness. In gear couplings, the situation is different, because the gear mesh stiffness is much higher than the flexible element stiffness. In that case, the hub/shaft stiffness plays more of a role. Unless the gear coupling has a short shaft separation (or an otherwise very stiff spacer) the $1/3$ penetration assumption is still reasonable, since longer shaft separations have a much lower spacer tube stiffness which reduce the overall coupling stiffness.

Elastomeric couplings are sometimes used to add torsional damping to equipment trains, especially ones with high steady state or transient vibratory torques, such as those containing variable speed or synchronous motors. This damping, which varies with the different elastomeric materials, reduces the amplification factor of a resonant frequency, typically by absorbing the torsional vibration energy. This energy is converted to heat inside the elastomer.

From Reference [4] for a two-mass system with shaft damping (Figure 4-16), the vibratory torque at resonance can be calculated by:

$$T_{VIB} = T_{EX} \times \left(\frac{J_2}{J_1 + J_2} \right) M \quad (4-5)$$

where

T_{VIB} = vibratory torque at resonance, \pm N-m (lbf-in.),

T_{EX} = motor excitation torque, \pm N-m (lbf-in.),

J_1 = motor polar mass moment of inertia (mass subjected to the excitation torque) kg-m^2 (lbf-in. 2),

J_2 = driven machinery polar mass moment of inertia, kg-m^2 (lbf-in. 2),

M = basic dynamic magnifier, dim.

$$M = \frac{K}{\omega C} \quad (4-6)$$

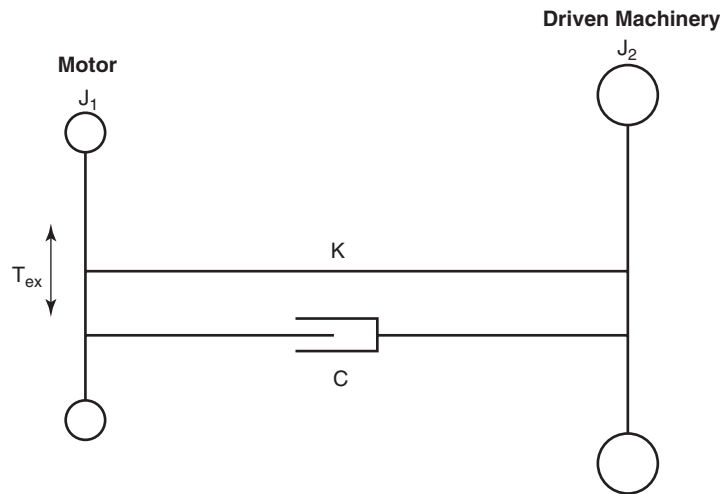


Figure 4-16—Two Mass Torsional System with Damping

where

K = torsional stiffness, N-m (lbf-in./rad),

ω = torsional natural frequency, rad/s,

C = specific damping (torque), N-m-s/rad (lbf-in.-s/rad).

The elastomeric coupling vendor can provide information necessary to define the torsional stiffness and damping as addressed previously.

Note that rotor systems with elastomeric damper couplings are not quite so simply formulated, especially when considering a third mass; a gearbox, for example. Reference [4] gives more detailed analysis. There are some other considerations which limit the use of elastomeric couplings. An elastomeric coupling will weigh much more than a corresponding flexible element dry or gear type coupling. This will affect balance and lateral rotor dynamics. Note that a hybrid coupling, where an elastomeric coupling is mated with a more conventional style (see Figure 4-17) can alleviate this situation, by having the heavier elastomeric portion on the shaft more able to handle the weight.

Moreover, although elastomeric couplings are considered dry non-lubricated couplings, they are more maintenance intensive than flexible element dry couplings. The elastomeric material torsional (and other) properties are not stable over long periods of time and are affected by exposure to light, chemical exposure (e.g., ozone), degradation due to heat from operating ambient temperature, heat from torsional vibration energy dissipation, and even time. The elastomeric materials age harden, and have a shelf life of typically 5 years or less, where the durometer can increase more than 10%. These changes will affect the stiffness and damping properties. The material needs to be inspected at least once a year, or more frequently if there have been operational problems and frequent start-ups. Where a synchronous motor is involved

which does not have soft start technology, the start-up vibration magnitudes are high, and heating of the elastomeric material occurs each start-up. If the start-ups are severe enough, and a sufficient time has not elapsed from one to another, the material can begin to melt and lose its damping properties, or worse, fail.

With all the potential drawbacks though, in many cases these type couplings will solve a torsional problem, and operate successfully for years at a time. Care should be taken to account for the long term effects of material property changes.

4.1.1.7 Material Properties Consideration

The torsional modulus, G , of the shaft material(s) varies with temperature. Figure 4-18 displays the effect of temperature on the shear modulus. The temperature dependence of the shear modulus should be considered in torsional analysis when large temperature changes in the shafting occurs between start-up and steady state operation. Temperature dependant shear modulus occurs in machinery such as steam and gas turbines and hot gas expanders. Experience indicates that temperature effects can result in a several percent difference in calculated undamped torsional natural frequencies. Reference [5] is one source for the temperature dependant modulus of metals.

4.1.1.8 Built up Rotors

Accurate modeling of the following shaft geometry and mechanical fits (often associated with built-up shafts) is important for accurate torsional natural frequency calculation:

- Tapered (solid or hollow) shaft sections.
- Splined fits.
- Curvics or serrated couplings.

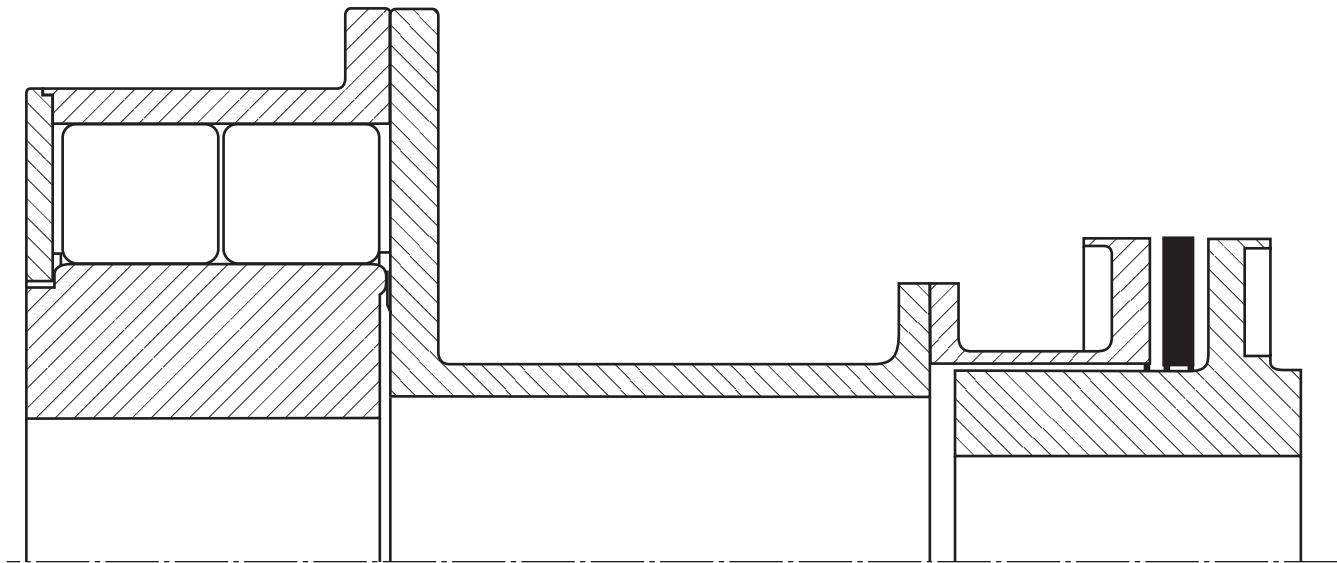


Figure 4-17—An Elastomeric Hybrid Coupling (w/Disc Type)

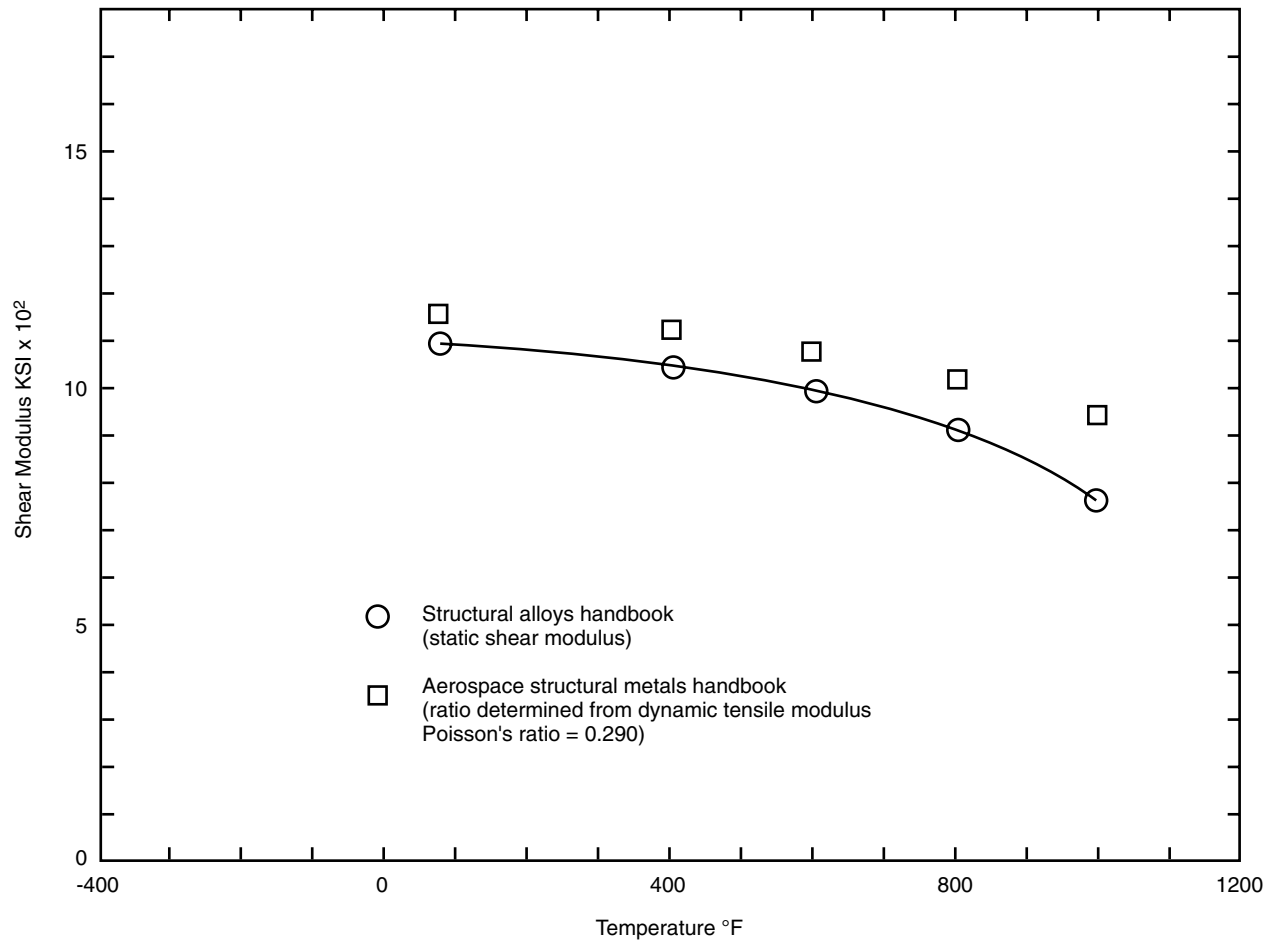


Figure 4-18—Temperature Dependent Shear Modulus Curve

4.1.1.9 References

1. ANSI/AGMA 9004-A99, *Flexible Couplings-Mass Elastic Properties and Other Characteristics*.
2. Wilson, W.K., *Practical Solution of Torsional Vibration Problems*, Volume 1, Frequency Calculation, New York, New York, John Wiley & Sons Inc. 1956.
3. ASME 72-PTG-37, *Torsional Stiffness of Interference Fit Connections*.
4. ASME 75-DE-15, *A Practical Solution to Torsional Vibration in Synchronous Motor Drive Systems*.
5. *ASME Unfired Pressure Vessel Code Section II*.

4.2 MACHINERY SPECIFIC MODELING CONSIDERATIONS

4.2.1 Introduction

There may be features of particular types of machinery that may not lend themselves to an easily defined system consisting of shape segments defined by length, diameter and constant material properties and locations of lumped inertia. The material in this section will identify methods used to model unique types of machinery.

4.2.2 Gearing

Simple gear reductions (single or double) represent single-branch systems that can be analyzed using the basic Transfer Matrix (Holzer) torsional method. As displayed in Equations 4-1 and 4-2, formulation of an equivalent single shaft model requires that all inertia and stiffness be referenced to the reference speed by the square of the gear ratio. In modeling the shaft stiffness characteristics of gears (both integral and shrink-fit gear construction), it is necessary to consider penetration of the shaft into the gear mesh. The rotational inertia of the gear and pinion are normally given on the drawings supplied by the manufacturer and are typically referenced to their own respective speeds. The torsional model of the gear will include stiffness and inertia of the bull gear from the input coupling to the centerline of the gear; then the model will include the pinion's stiffness and inertia from the centerline to the coupling end of the pinion. The inertia of the shaft sections opposite the coupling extensions for the bull gear and the pinion are lumped at the centerline of the gear (see Figures 4-19 and 4-20). These two inertias are coupled in the gearbox through the torsional stiffness generated by the gear mesh. The gear mesh torsional stiffness is calculated using Equation 4-7 if the reference speed equals the pinion rotation speed, or Equation 4-8 if the reference speed equals the gear rotation speed:

$$K_{tMESH} = (0.013625) W_f E (PD_P)^2 \cos^2 \chi \quad (4-7)$$

$$K_{tMESH} = (0.013625) W_f E (PD_G)^2 \cos^2 \chi \quad (4-8)$$

where

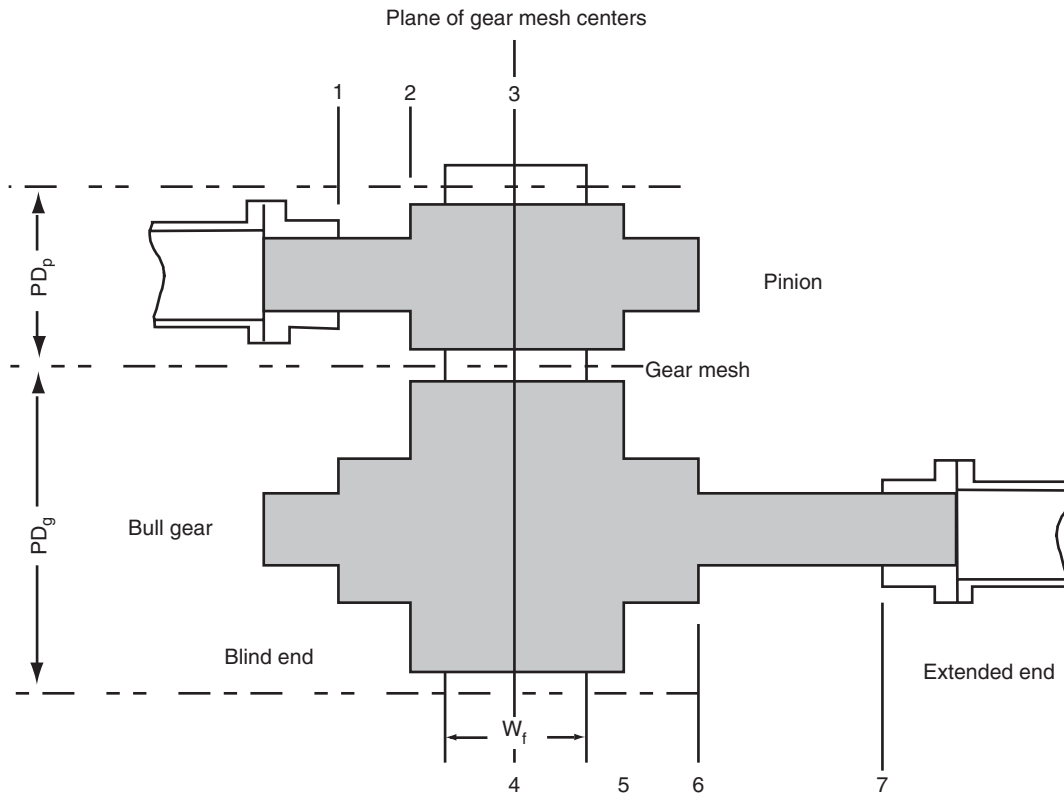
Quantity	Typical SI Units	Typical US Customary Units
K_{tMESH} = mesh torsional stiffness	N-m/rad	lbf-in./rad
W_f = face width of mating gears	m	in
PD_P = pitch diameter of pinion	m	in
PD_G = pitch diameter of bull gear	m	in
χ = helix angle of gear set	rad	deg
E = Young's modulus	N/m ²	lbf/in. ²

Since the design of high speed gearing usually results in numerous teeth with the base being relatively wide relative to the depth of the tooth, the resulting stiffness of the teeth is usually much stiffer than the torsional stiffness associated with the shafting or couplings used in the power transmission lineup. As a result, the calculated natural frequencies are usually not influenced when the stiffness of gear teeth is introduced into the torsional model.

4.2.3 Electric Motors

Precise, detailed torsional models of electric motors must be developed for inclusion in the train model to accurately calculate the train torsional natural frequencies. Some of the torsional natural frequencies of a system may actually represent the torsional natural frequency of a segment of the complete system model. For example, in motor-gear-compressor trains, the third torsional mode is almost exclusively governed by the stiffness and inertia characteristics of the motor core. This can be verified by modeling only the motor segment of the entire system. It will be found that the component first natural frequency is almost exactly the same as a higher order mode of the system. A comparison of the mode shapes for the segment and the higher order mode of the system will appear nearly identical when comparing only the motor sections of each model. Rotating motor exciters can also add an additional independent frequency to the torsional system. Accurate predictions of this mode or higher modes is greatly dependent on the number of torsional stations used in modeling the rotor.

For the purpose of torsional modeling, motors can be divided into two groups: those with spiders or webs attached to the base shaft to support the motor core and those that do not possess such construction. For the purpose of this document, electric machinery designed without the spider or web arms is said to possess laminated construction. Despite their simple appearance, motors with laminated construction are difficult to accurately model because the contribution of the shrunk-on core to the motor's midspan shaft stiffness is diffi-



Notes:

1. PD_p = pinion pitch diameter; PD_g = gear pitch diameter; W_f = face width of mating gears.
(All dimensions in mm, SI units, or inches, US Customary units.)
2. Modeling a parallel single reduction gear (see Figure 2-12 for model schematic):
 - Bull gear model extends from coupling hub to center of gear mesh.
 - Pinion model extends from center of gear mesh to coupling hub.
 - Lump rotor inertia outboard of plane of gear contact at the center of gear mesh.
 - Account for bull gear mesh penetration and stiffening.

Figure 4-19—Cross-sectional View of a Parallel Shaft Speed Increaser

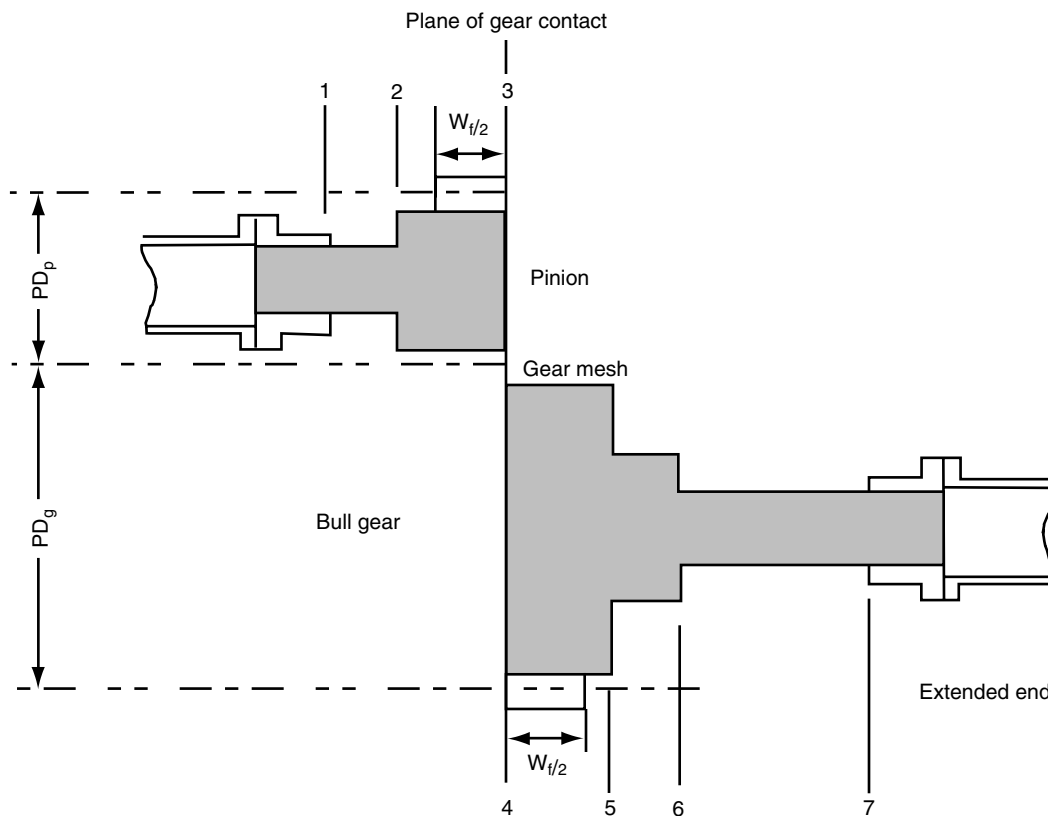
cult to analytically predict. The torsional/shear stress paths in the area of the motor core are complex and highly dependent on the exact magnitude of the interference fits. Tolerances in these fits may alter the depth of the effective base shaft penetration into the motor core and may substantially change the torsional stiffness characteristics of the motor.

Accurate modeling of webbed motors requires the following:

- a. The inertia of the rotating armature or poles must be distributed along the axial length of the core. Both the inertia of the rotating armature and the base shaft should be incorporated into the model.
- b. The stiffening effect of the web arms must be added to the base shaft.

Calculation of the torsional stiffness of non-circular cross-sections such as the webbed midspan area of an electric motor is a complicated problem. A schematic of a typical webbed motor cross-section is presented in Figure 4-21. Although numerous analytical approaches have been used to date, including detailed finite element techniques, the following approximate method has been used successfully (yielding good agreement upon correlation with test results). Non-circular section torsional rigidity can be satisfactorily approximated from Equation 4-9.

$$K_a = \pi^2 I_p \left[\frac{A^4}{4} \right] \quad (4-9)$$



Notes:

1. PD_p = pinion pitch diameter; PD_g = gear pitch diameter; W_t = face width of mating gears.
2. The polar mass moments of inertia from removed sections are lumped at the intersection of gear shaft centerlines and the plane of gear mesh centers.

Figure 4-20—Torsional Model of a Parallel Shaft Speed Increaser

where

Quantity	Typical SI Units	Typical US Customary Units
A = cross-sectional area of the shaft including ribs	This is an empirical equation suitable for use with US Customary Units only	in.^2
I_p = polar moment of inertia		lbm-in.^2
K_a = approximate torsional stiffness of the non-circular cross-section		lb-in./rad

Checks on several shapes that have known exact solutions show that this equation is fairly accurate. Refer to Table 4-2.

In general, the preceding equation gives torsional stiffness values slightly above the exact value. This formulation can be applied to motors with various geometric cross-sections. For example, the torsional stiffness of a six-ribbed rotor whose cross-section is displayed in Figure 4-21 can be accurately estimated using the following equation:

Table 4-2—Comparison of Exact and Approximate Results for Torsional Rigidity (Simple Geometric Cross-sectional Shapes)

Geometric Shape	$K_d/\text{exact torsional stiffness}$
Circular Area	1.000
Square Area	1.081
Equilateral Triangle	1.140
Rectangle	1.040

$$\frac{K_a}{K_b} = \frac{\lambda \left[1 + \frac{24TL}{\pi D_b^2} \right]}{1 + \frac{16TL^3}{\pi D_b^4} \left[1 + \left(\frac{T}{L} \right)^2 + 3 \left(1 + \frac{D_b}{L} \right)^2 \right]} \quad (4-10)$$

Note that

$\lambda = 1$ for integral construction.

$\lambda < 1$ for welded construction (typically 0.9).

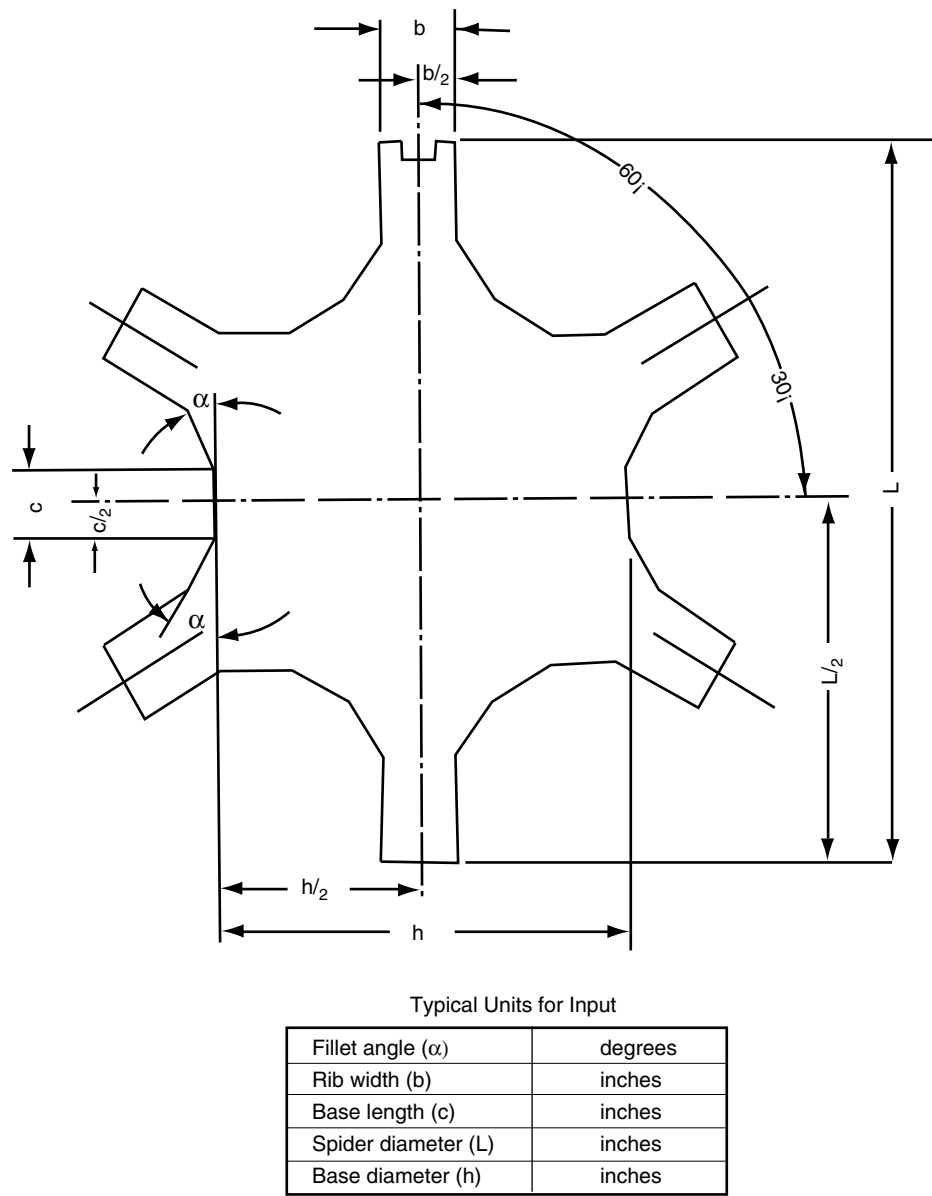


Figure 4-21—Cross-section of the Shaft Under the Windings of a Typical Induction Motor

where

Quantity	Typical SI Units	Typical US Customary Units
D_b = diameter of base shaft	m	in.
L = arm radial length above base shaft	m	in.
T = thickness of arm	m	in.
K_a = equivalent stiffness of non-circular cross-section	N-m/rad	lbf-in./rad
K_b = stiffness of base shaft	N-m/rad	lbf-in./rad
λ = web construction parameter	dim	dim

The torsional stiffness of a solid circular cylinder is written as follows:

$$K_t = \left(\frac{G}{L}\right)\left(\frac{\pi D^4}{32}\right) \tag{4-11}$$

where

Quantity	Typical SI Units	Typical US Customary Units
K_t = torsional stiffness	N-m/rad	lbf-in./rad
G = torsional modulus	N/m ²	lbf/in. ²
L = cylinder axial length	m	in.
D = cylinder diameter	m	in.

From Equation 4-12, the effective diameter of a cylinder that is equal in length and torsional stiffness to the non-circular shaft section, can be calculated as follows:

$$D_{eff} = \left[\frac{32LK}{\pi G} \right]^{0.25} \quad (4-12)$$

where

Quantity	Typical SI Units	Typical US Customary Units
$D_{effective}$ = effective diameter	m	in.
G = torsional modulus	N/m ²	lbf/in. ²
L = cylinder axial length	m	in.
K = torsional stiffness	N-m/rad	lbf-in./rad

$D_{effective}$ is the diameter of a cylinder that generates the torsional stiffness of the non-circular shaft section. The ratio of the effective cylinder diameter, $D_{effective}$, and the base shaft diameter, D_b , is written as follows:

$$\frac{D_{eff}}{D_b} = \left[\frac{K_a}{K_b} \right]^{0.25} \quad (4-13)$$

where

Quantity	Typical SI Units	Typical US Customary Units
$D_{effective}$ = effective diameter	m	in.
D_b = diameter of base shaft	m	in.
K_a = Equivalent stiffness of non-circular cross-section	N-m/rad	lbf-in./rad
K_b = stiffness of base shaft	N-m/rad	lbf-in./rad

The effective diameter of the equivalent cylindrical shaft section can be calculated using Equation 4-13. Typical values of $D_{effective}$ range from 12% – 25% above the base shaft diameter, D_b , for some of the more common types of construction of multi-pole synchronous and induction machines. For further discussion see Reference [1].

4.2.4 Pumps

When formulating a torsional rotor model for a centrifugal pump with an incompressible working fluid, it becomes necessary to distinguish between dry impeller inertia and wet impeller inertia. This difference is important because a liquid pump also exhibits increased rotational inertia due to the fluid within the rotating passages of the pump impeller. The magnitude of this fluid inertia is proportional to the specific gravity of the fluid being pumped. This data is normally available from the pump manufacturer and is typically used to calculate

a frequency range for the corresponding wet and dry torsional natural frequencies. The liquid pump provides a finite level of system damping due to viscosity effects of the fluid shearing between the surfaces of the impeller blades and discs.

4.2.5 Hydraulic Variable Speed Drives

The fluid drive influences two factors simultaneously, namely the torsional stiffness through the fluid drive and the speed relationship of the pinion, which operates at a fixed speed and the variable speed of the fluid coupled compressor rotor. The system natural frequencies become a function of the torsional stiffness of the fluid drive and the referred inertia between the compressor and the remainder of the system, which is a speed squared relationship. There remains some debate as to whether the fluid coupling behaves in a manner similar to a linear or non-linear elastomeric material. Therefore the system can be analyzed in two different ways.

4.2.5.1 Modeling Method 1

The first analysis method evaluates the input speed shaft system normally consisting of a motor, low speed coupling, gear, pinion and primary wheel of the fluid drive, as a separate system. The output shaft system, consisting of the secondary wheel of the fluid drive and the drive output shaft, high speed coupling and the connected machinery (compressor), is also analyzed as a separate system.

4.2.5.2 Modeling Method 2

The second analysis evaluates the equipment with the entire system including the stiffness of the fluid drive. The stiffness of the fluid drive is a variable that depends upon the transmitted power, the output speed of the fluid drive and the frequency of vibration in the torsional system. Depending upon the number of defined operating conditions there may be a number of fluid drive stiffness that have to be evaluated.

These stiffness values can be obtained from the manufacturer of the fluid drive. Some fluid drive manufacturers have stated that to obtain a proper solution for the torsional frequency analysis, the stiffness to be used must be chosen for the unique conditions of transmitted power, secondary wheel speed and the calculated torsional natural frequency of the system for a specific mode. The fluid drive is then modeled as a gear having a ratio through the fluid drive appropriate to the pinion speed and the secondary wheel output speed of the fluid drive.

Initially this seems like an enormous task as there could be three or four natural frequencies for typical compressor system operating below 300 Hz, and several defined cases of customer operating conditions. Fortunately the actual analysis is not as difficult as imagined.

Further it is interesting to compare the results for a typical compressor system where the two methods were used. The

1st mode of the coupled system became a new mode with a frequency lower than either of the separate system analysis. The 2nd mode of the coupled system appears identical to the 1st mode of the input system used in method one. The 3rd mode of the coupled system appears identical to the 1st mode of the output system used in method one. Thus it appears that the coupled system introduces a much lower frequency mode than either of the separate input or output system models alone. The higher order modes of the coupled system then become individual modes of the input and output systems that were analyzed.

4.2.6 Screw Compressors

The principle of compression in a rotary screw compressor requires that the male and female rotor lobes mesh in very close proximity to one another but not physically touch each other. Refer to Figure 4-22 for a typical screw compressor rotor set. There are two basic designs of rotary screw compressors. One type is referred to as a dry rotary screw compressor because no lubricant is used within the gas stream. This style of compressor utilizes a set of timing gears mounted on the rotor stub ends to position the male rotor relative to the female rotor to prevent rotor to rotor contact. These gears provide a speed ratio the same as the lobe ratio between the male and female rotor. The other style of compressor is referred to as a flooded screw compressor. This design intentionally introduces a lubricant into the inlet of the compressor. The flooded screw compressor does not use timing gears. The male and female rotors are timed relative to one another by utilizing the lobes as pseudo gear elements with the lubricant within the compressed gas preventing metal to metal contact of the male and female rotors. The lubricant is extracted from the discharge gas stream and recirculated back to the inlet for continuous lubrication. Some additional lubricant has to be added from time to time depending upon the efficiency of the lubricant extraction in the discharge flow stream.

4.2.7 Rotor Body Modeling

The male and female rotors are constructed with multiple helical flutes cut into a cylindrical rotor. The resulting surface is a series of protruding lobes about a base cylinder for the male rotor and valley shaped recesses on the base cylinder surface of the female rotor. The final rotor model must account for the torsional stiffness and inertia of the base cylinder plus the influence of the rotor lobes that increase the overall rotor torsional stiffness and inertia. The section of the lobed male and female rotors are usually represented by a pseudo diameter that represents the effective torsional stiffness of the lobed center section. Since the pseudo diameter may not truly represent the correct polar moment of inertia of the rotor additional lumped inertia will have to be distributed along the length of the lobed center body. Some computer

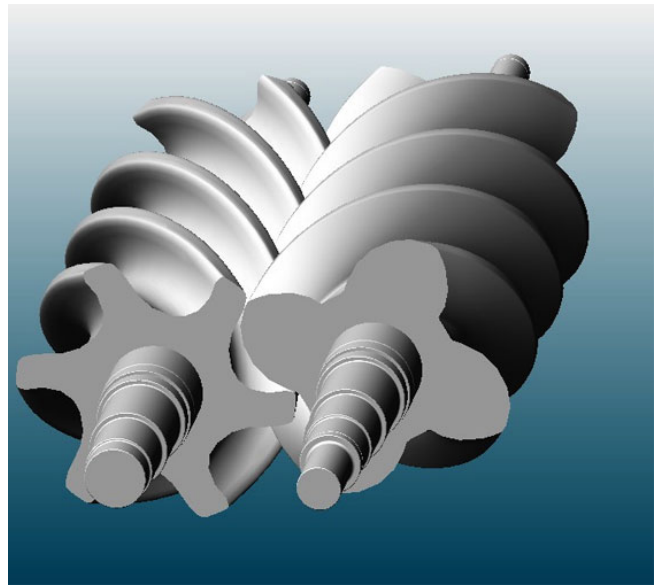


Figure 4-22—View of Typical Screw Compressor Rotor Pair

programs enable the user to identify two diameters, one that reflects the torsional stiffness and another which represents the polar moment of inertia.

The connection of the male and female rotors of a dry screw compressor which utilizes timing gears can be modeled similar to a geared connection between low and high speed shafts. Refer to Figure 4-23 for a typical system model of a dry screw compressor train.

The connection of the male and female rotors for a flooded screw compressor is more unique since no timing gears are used. In most cases, the damping associated with a flooded screw compressor precludes the need for a torsional analysis. If a flooded screw compressor system is analyzed, the coupled screw compressor rotor is modeled as a conventional screw compressor rotor. However, since the lobes of the coupled rotor act as the gears for the driven rotor, the speed referred inertia of the driven rotor must be distributed along the coupled rotor as discs uniformly distributed along the length of the coupled rotor. Refer to Figure 4-24 for a typical system model of a flooded screw compressor train.

4.2.8 References

1. E. J. Nestorides, *A Handbook on Torsional Vibration*, B.I.C.E.R.A Research Library.

4.3 RECIPROCATING MACHINERY

4.3.1 Scope

This section departs from the general format of the entire document pertaining to torsional vibration in that it does not separate the different aspects of modeling a reciprocating

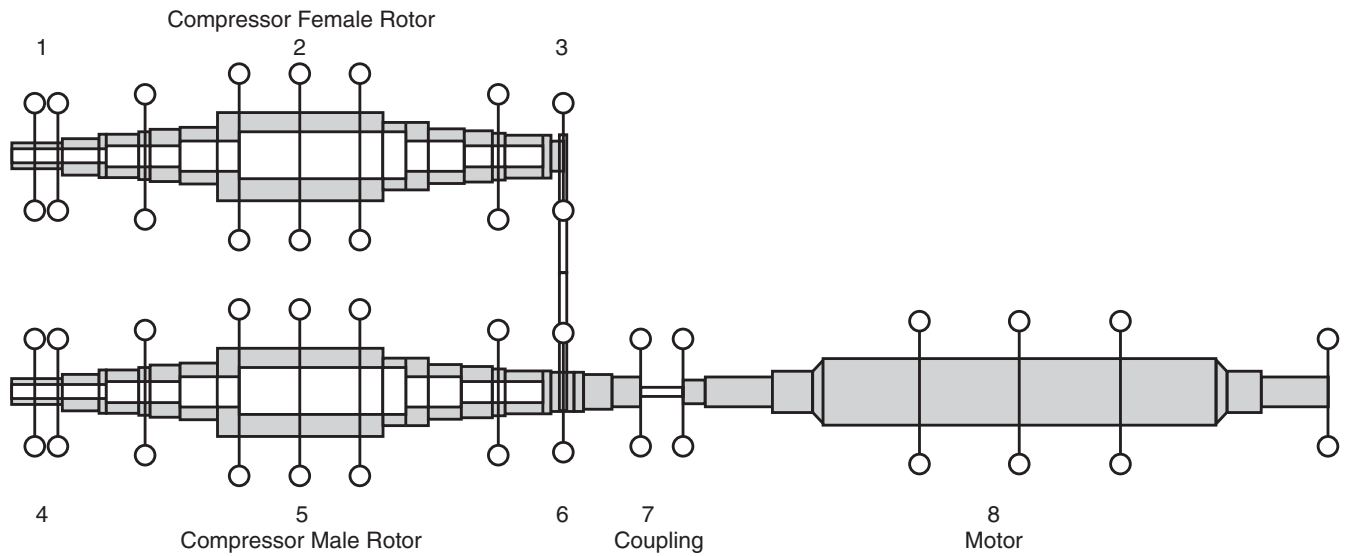


Figure 4-23—Typical System Model of a Dry Screw Compressor Train

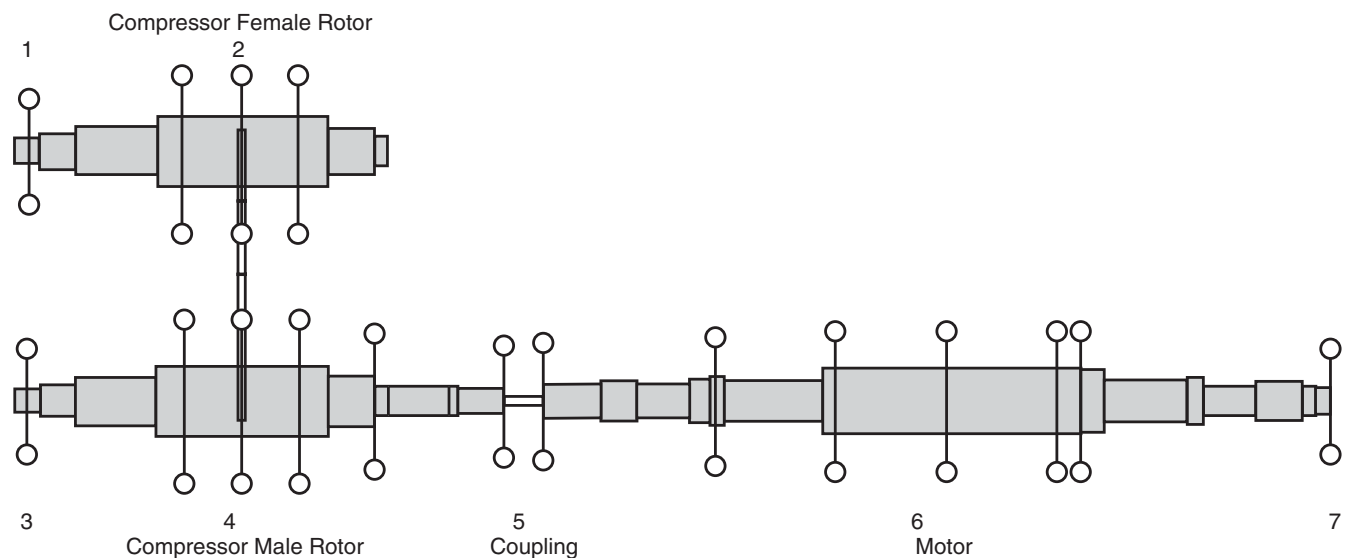


Figure 4-24—Typical System Model of a Flooded Compressor Train

machine and excitation from reciprocating machinery into different sections. The task force was of the opinion that the subject of torsional vibrations of reciprocating machinery would be better presented as a separate subject complete onto itself. However even though reciprocating machinery creates torsional excitation and the modeling of reciprocating machinery is unique to itself there can be other torsional aspects which are presented in the rest of the document such as transient vibration of synchronous motor driven reciprocating compressors or electric variable frequency drives (VFD) or torsional excitation associated with motor fault

conditions that must also be considered in addition to the potential non uniform torque associated with reciprocating machinery. The material in this section is a partial summary of Reference [1].

4.3.2 Modeling of Reciprocating Machinery

For more complicated geometries such as crankshafts, the following procedure can be used if the mass-elastic model is not provided by the manufacturer. A crankshaft can be simplified into several main components: the stub shaft that connects to a coupling or flywheel, journals where the main

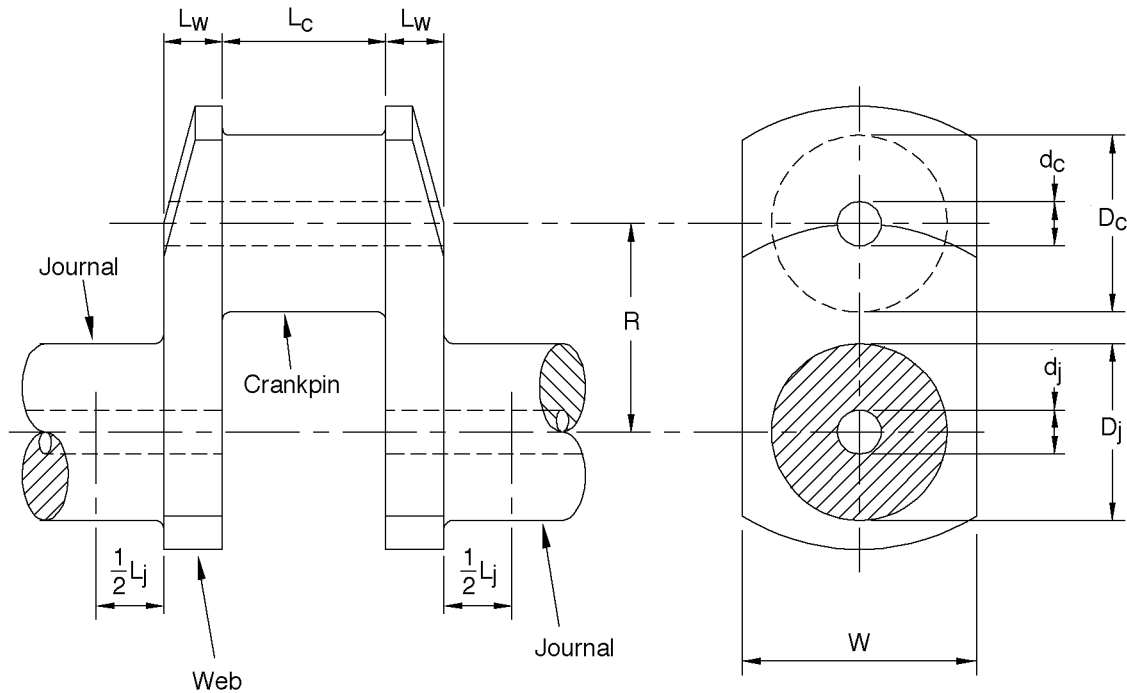


Figure 4-25—Portion of a Typical Crankshaft Throw

bearings are located, webs, and crankpins. A mass-elastic model of the crankshaft is typically created by lumping the inertia at each throw and calculating the equivalent torsional stiffness between throws. Additional mass stations are created for the flywheel, oil pump, etc., as necessary.

Figure 4-25 shows a basic crankshaft throw. A throw consists of two webs and a crankpin. Depending on the type of crankshaft, there may be one or two throws between journals. The crankpin usually drives a connecting rod, crosshead (for compressors) and a piston and piston rod. Engines with power cylinders in a “V” arrangement may have two connecting rods at each crankpin, or use an articulated rod design. Integral engine/compressor units can have two power cylinders articulated off the main connecting rod for the compressor cylinder for a total of three connecting rods per throw.

4.3.3 Modeling the torsional stiffness

Equations are given in Ker Wilson [2] and BICERA [3] for calculating the torsional stiffness of a crankshaft. The basic dimensions of the journals, webs, and crankpins are needed, as well as the shear modulus of the shaft material. BICERA also developed curves based on test data for various types of crankshafts. These can be more accurate, but also more complex and are not discussed here.

Carter’s Formula

$$K_t = \frac{\pi G}{32 \left[\frac{L_j + 0.8L_w}{D_j^4 - d_j^4} + \frac{0.75L_c}{D_c^4 - d_c^4} + \frac{1.5R}{L_w W^3} \right]} \quad (4-14)$$

Ker Wilson’s Formula

$$K_t = \frac{\pi G}{32 \left[\frac{L_j + 0.4D_j}{D_j^4 - d_j^4} + \frac{L_c + 0.4D_c}{D_c^4 - d_c^4} + \frac{R - 0.2(D_j + D_c)}{L_w W^3} \right]} \quad (4-15)$$

where

- d_c = crankpin inside diameter, m (in.),
- D_c = crankpin outside diameter, m (in.),
- d_j = journal inside diameter, m (in.),
- D_j = journal outside diameter, m (in.),
- G = shear modulus, N/m² (lbf-in.²),
- K_t = torsional stiffness, N-m/rad (lbf-in./rad),
- L_c = crankpin length, m (in.),
- L_j = crankshaft journal length, m (in.),
- L_w = web thickness, m (in.),
- R = throw radius, m (in.),
- W = web width, m (in.).

Carter's formula is applicable to crankshafts with flexible webs and stiff journals and crankpins, while Ker Wilson's formula is better for stiff webs with flexible journals and crankpins. When conducting a torsional analysis, Ker Wilson has suggested using the average of his and Carter's formulas to determine the stiffness between throws. To calculate the torsional stiffness of the stub shaft to the centerline of the first throw, the torsional stiffness of the straight shaft section can be combined in series with twice the torsional stiffness between throws. For coupling hubs or flywheels with an interference fit, the $1/3$ rule should also be applied.

Equations 4-14 and 4-15 were developed before finite element analysis (FEA) was readily available. A finite element program can be used to determine the torsional stiffness for a crankshaft section. The simple models shown in Figure 4-26 were developed from the basic dimensions and do not include fillet radii and oil holes. These models are from journal centers, which is the same as the distance between throw centers. One end was rigidly fixed and a moment was uniformly applied across the other end. The calculated torsional stiffness is equal to the moment divided by the angle of twist at the free end. It is interesting to note that for both cases, the calculated torsional stiffness using FEA fell between the values from the Carter and Ker Wilson formulas.

4.3.4 Polar Mass Moment of Inertia

The polar mass moment of inertia (commonly referred to as WR^2) at each throw depends on the rotating inertia and the

Carter's Formula	=	69.7 x 10 ⁶ N-m/rad (617 x 10 ⁶ lbf-in./rad)
Ker Wilson's Formula	=	61.46 x 10 ⁶ N-m/rad (544 x 10 ⁶ lbf-in./rad)
ANSYS Results	=	63.72 x 10 ⁶ N-m/rad (564 x 10 ⁶ lbf-in./rad)

reciprocating mass. The rotating inertia is constant, but the effective inertia of the reciprocating parts actually varies during each crankshaft rotation. This effect is considered to be negligible for most engines except in the case of large low-speed marine applications [4] when calculating the torsional natural frequencies. The reciprocating masses also produce dynamic torque that must be included in the applied torque-effort for forced response calculations.

The equivalent inertia, I_{eq} , at each throw can be approximated by adding the rotating inertia of the crankshaft section, I_{rot} , to half of the reciprocating mass, M_{recip} , times the throw radius, R , squared

$$I_{eqv} \approx I_{rot} + 1/2 M_{recip} R^2 \quad (4-16)$$

where

$$I_{eqv} = \text{equivalent inertia, kg-m}^2 \text{ (lbm-in.}^2\text{),}$$

$$I_{rot} = \text{rotational inertia of crankshaft throw, kg-m}^2 \text{ (lbm-in}^2\text{),}$$

$$M_{recip} = \text{reciprocating mass, kg (lbm),}$$

R = throw radius, m (in.).

The rotational inertia of the journal and crankpin can be calculated using the equation for a cylinder. Since the crankpin rotates at the throw radius and not about its center, the parallel axis theorem must also be used. The inertia of the webs can be estimated with an equation for a rectangular

Carter's Formula	=	154.68 x 10 ⁶ N-m/rad (1,369 x 10 ⁶ lbf-in./rad)
Ker Wilson's Formula	=	121.35 x 10 ⁶ N-m/rad (1,074 x 10 ⁶ lbf-in./rad)
ANSYS Results	=	124.96 x 10 ⁶ N-m/rad (1,106 x 10 ⁶ lbf-in./rad)

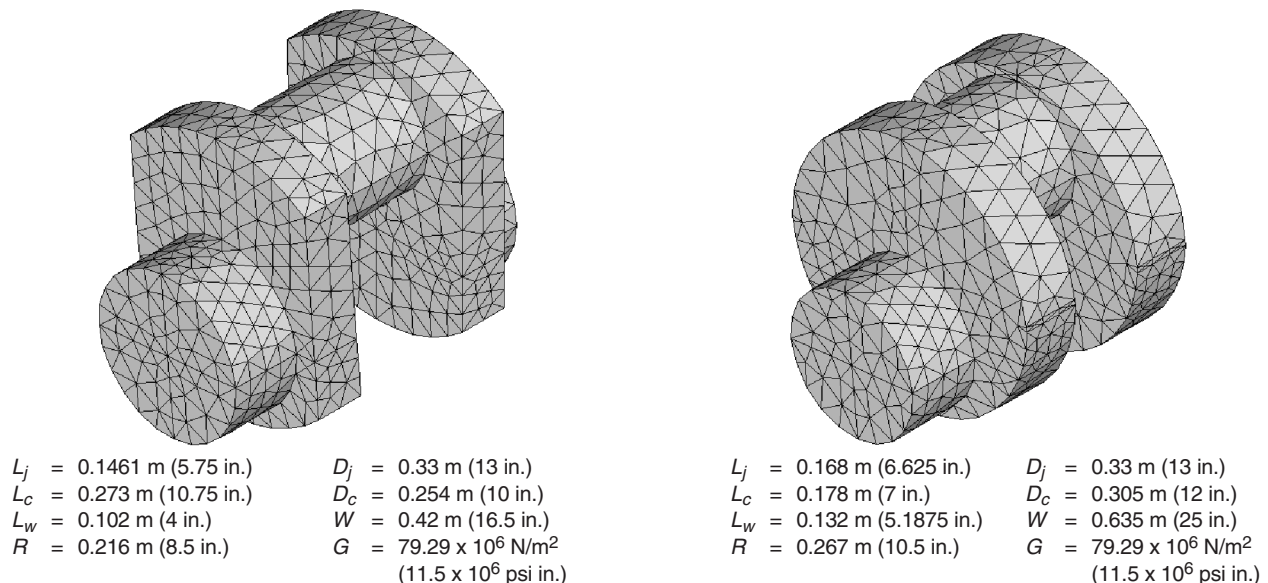


Figure 4-26—Finite Element Models Used to Calculate Torsional Stiffness of Crankshaft Sections

prism. Any rotating counter-weights that may be bolted to a web should also be included. There are solid model 3D CAD packages that can perform this calculation.

The connecting rod is generally heavier at the crankpin end and lighter at the reciprocating end. If the weight distribution of the connecting rod is unknown, a typical assumption is to use two-thirds of the weight as rotating and one-third as reciprocating weight. The rotating mass of the connecting rod is multiplied by the throw radius squared and added to the crankshaft rotating inertia to obtain the total rotational inertia, I_{rot} . The total reciprocating mass includes the small end of the connecting rod, cross-head (for compressors), nut, piston and piston rod.

4.3.5 Stress Concentration Factors

Stress concentration factors (SCFs) are used to account for stress risers caused by geometric discontinuities such as shaft steps, keyways, welds, shrink fits, etc. A good reference for determining theoretical stress concentration factors is Peterson [5]. Note that the SCF is different for shear and bending stress, so care should be taken to use the proper value.

For stepped shafts and keyways, the fillet radius and shaft diameter must be known to determine the SCF. The worst-case SCF occurs with a square cut and would be approximately 5 for a keyed shaft and 2 for a stepped shaft. If a keyway is required, use a fillet radius of at least 2% of the shaft diameter as described in USAS B17.1 – Keys and Keyseats [6]. This will limit the SCF at the base of the keyway to 3.

When possible, keyways should be avoided, particularly at coupling hubs, since the shaft diameter in this area is often reduced. Instead, an interference fit (heat shrink or hydraulic) should be considered. However, the shrink must be sufficient to prevent slippage and galling of the shaft.

Specific SCF details for reciprocating equipment can be found in Ker Wilson [2], Nestorides [3], and Lloyd's Registry [7]. The typical SCF for a crankshaft ranges from 1.5 to 2 in torsion (excluding any keyways). Therefore, using a stress concentration factor of 2 is reasonable for crankshafts when the fillet radii are unavailable and no keyways are present.

When performing a torsional analysis the fatigue SCF, K_f , should be used to calculate the alternating shear stress in a shaft section. The fatigue SCF is usually less than the theoretical SCF, especially for very small radii, and depends on the notch sensitivity, q , which is a function of the material and notch radius. Charts are available for determining the notch sensitivity factor, but were created using test data with considerable scatter. Therefore, it is conservative to use K_f = theoretical SCF if the notch sensitivity is unknown [8].

4.3.6 Viscous Dampers

Viscous dampers (Houdaille type) are often used in reciprocating engines to help limit torsional vibration and crankshaft stresses [9,10,11]. These dampers are normally intended

to protect the engine crankshaft and not necessarily the driven machinery. To be effective, dampers need to be located at a point with high angular velocity, i.e., near the anti-node of the crankshaft mode.

4.3.7 Equivalent Damping and Inertia

A viscous damper consists of a flywheel that rotates inside the housing, which contains a viscous fluid such as silicon oil (Figure 4-27). An untuned damper does not contain an internal torsional spring.

The shearing motion of the fluid between the flywheel and housing surfaces dissipates vibration energy as heat. The damping characteristics can be adjusted by changing the internal clearances between the housing and flywheel, h_1 and h_2 , and/or the fluid viscosity, μ . From the Shock and Vibration Handbook [11], the damping constant is

$$c = 2\pi\mu \left[\frac{r_2^3 b}{h_2} + \frac{r_2^4 - r_1^4}{2h_1} \right] \quad (4-17)$$

where

μ = viscosity, Pa-s (lbf-s/in.²),

b = width of damper flywheel, m (in.)

c = damping constant, N-m-s/rad (in.-lbf-s/rad),

r_1 = inside radius of damper flywheel, m (in.),

r_2 = outside radius of damper flywheel, m (in.),

h_1, h_2 = damper internal clearances, m (in.).

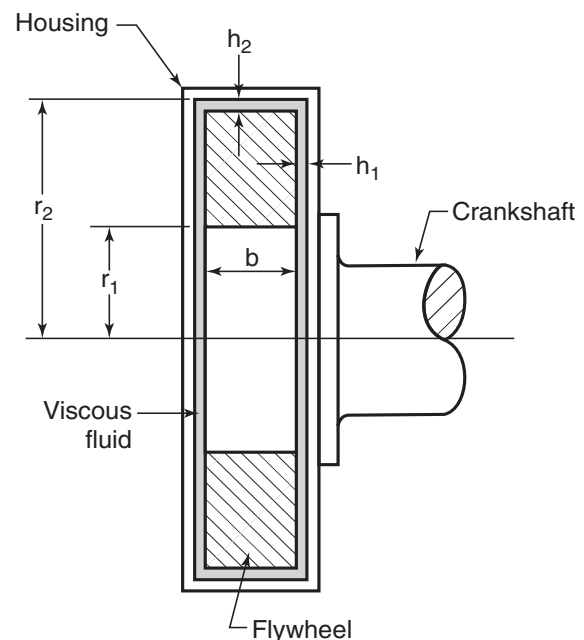


Figure 4-27—Untuned Damper

According to Den Hartog [12], the equivalent damper inertia is equal to half of the flywheel inertia plus the housing inertia at optimum damping.

$$I_{eqv} \approx 1/2 I_d + I_h \quad (4-18)$$

where

I_d = damper flywheel inertia, kg-m² (lbm-in.²),

I_{eqv} = equivalent inertia, kg-m² (lbm-in.²),

I_h = damper housing inertia, kg-m² (lbm-in.²).

If the lumped inertia is used for the damper, the system natural frequency calculations will be satisfactory, but will not predict the internal flywheel resonance, which is usually well damped and not of concern. The preferred method is to model a damper using separate inertias for the internal flywheel and housing. These two inertias are connected by equivalent damping and stiffness properties.

Viscous dampers have a limited service life and require periodic checks and maintenance. The heat build-up inside the damper should be calculated and compared to the allowable value provided by the manufacturer. In some situations, it may be beneficial to use two dampers to provide additional damping.

4.3.8 Considerations for Auxiliary Equipment with Reciprocating Machinery

4.3.8.1 Considerations for Low Stiffness or Resilient Couplings

There are several instances where using soft couplings could be beneficial in controlling torsional vibration such as: isolation of excitation between components [13], detuning a torsional natural frequency, or add damping to the system. A coupling is termed torsionally “soft” because it has a lower torsional stiffness than the steel shafts that it is connecting. Several types of soft couplings are: rubber-in-compression, rubber-in-shear, helical-spring, leaf-spring, and magnetic. Although not technically a coupling, a long torque shaft also has a low torsional stiffness.

Several factors must be considered when choosing a soft coupling. For rubber couplings, the trade-off is usually increased maintenance, since the rubber degrades over time due to heat and environmental factors. Various geometries (shear element, round and wedge blocks), materials (natural rubber, styrene-butadiene, neoprene, and nitrile), and durometers (50, 60, 70, and 80) are available. Special silicon blocks may be required for high temperature applications. The proper selection must be made to optimize the torsional stiffness and damping properties needed for the system. The

actual coupling stiffness can vary from catalog values and should be considered in the torsional analysis.

The torsional stiffness of a rubber-in-compression coupling is non-linear and varies with transmitted torque and temperature. This nonlinearity can make it difficult to tune natural frequencies between engine or compressor orders. Special analysis techniques are required to handle the nonlinearity during transient events such as synchronous motor start-ups [14]. The torsional natural frequencies of a system could be different for cold starts and hot restarts.

Running at or near a resonant condition for just a few minutes could elevate the temperature beyond the melting point of the rubber elements or blocks and damage the coupling. Therefore, the vibratory torque and heat dissipation (for damped couplings) must be calculated and should also be reviewed by the coupling manufacturer for acceptability. In systems with an electric motor the heat dissipation is a function of the vibratory torque and frequency and is normally specified in terms of power loss (Watts).

When applicable, the torsional analysis should consider all reciprocating compressor load steps, possible valve failure, and engine misfire. These off-design conditions could produce significant torque excitation at frequencies not considered for normal operation, which could be potentially damaging to the soft coupling. In systems with an electric motor variable frequency drive (VFD), the torque harmonics should be evaluated and the ramp rate at which the VFD controls the speed should not be coincident with a torsional natural frequency.

4.3.8.2 Considerations for Speed Increaser or Reducers

Special consideration should be given to gearboxes used with reciprocating equipment. Several gearbox manufacturers recommend limiting the dynamic torque at the gear mesh to 30% of the rated torque during steady-state operation. To prevent backlash at low load conditions, the dynamic torque should not exceed the transmitted torque.

Transient events such as startups and emergency loaded shutdowns (ESDs) can also cause high dynamic torque at the gear mesh. Depending on the speed ramp rate during startup, engines and synchronous motors can cause peak torques at the gear mesh that are much higher than recommended for continuous operation. If the peak torque exceeds the catalog rating of the gearbox, then the manufacturer should be contacted to discuss potential gear tooth damage from repeated starts.

Care should be taken for gears that are uploaded. The tangential and separating forces acting on the gears should be calculated for various loads and vectorially summed with the weight to compute the resultant. At full load, the uploaded gear will be lifted into the upper portion of the bearings. However, large torque modulation from a reciprocating compressor or engine could reduce the tangential force acting in

the upward direction to less than the shaft weight. In this case, the gear could be lifted then dropped once per revolution causing high shaft vibration. This lateral vibration could cause significant dynamic misalignment of the gear teeth and result in tooth overloading and rapid gear wear.

4.3.8.3 Considerations for Connected Auxiliary Equipment and Electric Motor Drivers

Oil pumps driven from the auxiliary end of a reciprocating compressor can fail due to high torsional vibration. Some compressor manufacturers have published allowable limits versus frequency. In general, overall torsional oscillation exceeding one degree peak-to-peak should be closely evaluated.

When electric motors are used to power reciprocating compressors consideration should be given to the non uniform torque demands of the reciprocating compressor that may affect the motor current. Torsional oscillation can cause current pulsation in the electrical system. Reference [15] makes a recommendation that when the driven load, such as that of reciprocating type pumps, compressors, etc., requires a variable torque during each revolution, it is recommended that the combined installation have sufficient inertia in its rotating parts to limit the variations in motor stator current to a value not exceeding 66% of full-load current.

4.3.9 Torsional Excitation Sources from Reciprocating Machinery

Reciprocating compressors and engines produce unsteady torque. This torque variation can be much higher than in rotating equipment and flywheels are often used to smooth the torque. The amplitudes and frequencies of the torque excitation should be considered to avoid coincidence with torsional natural frequencies, which could potentially cause problems.

4.3.9.1 Torque Variation Due to Inertial and Gas Forces

From a torsional standpoint, there are two types of forces that cause torque variation at each throw: inertial and gas load. The total force times the distance between the crankshaft centerline and throw centerline is equal to the moment imposed on the crankshaft. At top dead center (TDC) and bottom dead center (BDC), the throw is inline with the connecting rod and piston so that no moment can be imposed on the crankshaft. At 90 degrees from BDC and TDC, the moment arm is at the maximum length (full crank radius).

The rotating inertia of the crankshaft must be considered in the mass-elastic model, but does not cause any torque variation. The inertial forces are caused by the reciprocating mass of the connecting rod, cross-head and piston, which are dependent on the crank angular position and cannot be eliminated by balancing. The unbalance forces have components

which vary once per revolution (primary forces) and twice per revolution (secondary forces). These inertia forces will vary with the speed squared. Mehta, Farr, and DeWitt [16] give equations of motion for a slider-crank mechanism in terms of displacement, velocity, and acceleration. By multiplying the mass and acceleration of the reciprocating parts, the inertial forces at the crankpin can be determined.

The gas force is equal to the differential pressure across the piston times the cross-sectional area of the bore. The stroke, or travel of the piston, is equal to twice the crank throw radius. The swept volume for each cylinder is the bore area times the stroke. Next, the pressure versus crank angle must be determined for each cylinder over 360 degrees for compressor or two-stroke engine and 720 degrees for a four-stroke engine. The torque can then be determined versus crank angle. Any distortion in the pressure waveform will affect the dynamic torque and torsional response. A third type of curve that is often seen is called tangential effort (or tangential pressure), which is the torque normalized for unity crank radius and piston area.

Once the inertia and gas forces have been determined, they must be correctly added together for each cylinder. The torque at each throw must then be properly phased for the entire machine. A Fourier analysis can then be performed on these curves to represent the complex wave as a series of sinusoidal curves at various harmonics. At each harmonic, the amplitude and phase can be calculated, or the values can be presented as coefficients of sine and cosine functions. Compressors and two-stroke engines will have integer harmonics of running speed while four-stroke engines produce both integer and half orders. Depending on the cylinder phasing, certain orders may cancel out while others become dominant when examining the overall torque output from the machine.

Compressor and engine manufacturers will often provide this information in various forms with the performance calculations. To use their data in a torsional analysis, it is very important to understand the sign convention and if the values are only for gas forces or if the effect of reciprocating mass has also been included. Computer programs are used to calculate the torsional excitation for compressors and engines.

4.3.9.2 Compressors

Ideal pressure cards are often used for analysis since they can be computed from the compressor and gas properties. However, ideal cards do not include valve/manifold losses and gas pulsation, which can affect the resulting torque harmonics. Situations where the harmonic content is changed and the torsional excitation by the compressor could be increased are: valve failure, gas pulsation due to an acoustic resonance, and various load steps.

Single-acting (SA) compressors use only one side of the piston while double-acting (DA) cylinder use both the crank and head ends. A compressor valve failure can be analyzed by

unloading one end of a cylinder. All load steps must be considered in the analysis, such as unloaders, pockets, etc., as these load steps can significantly affect the harmonic content and influence the torsional responses. The maximum horsepower case will not necessarily correspond to the maximum torsional excitation at all harmonics. The full range of operating conditions (pressures, flows, gas mole weights, etc.) should also be considered.

4.3.9.3 Engines

For a two-stroke engine, intake, compression, expansion, and exhaust occur during one revolution of the crankshaft. However, with four-stroke engines, these cycles occur over two revolutions, which causes half-order excitations. Some engines have a choice of firing orders, which can change the strong harmonics. In critical systems, the best firing order could be chosen to reduce the torsional response.

Poorly maintained engines will tend to operate at non-ideal conditions that can cause high torsional vibration such as: engine misfire, pressure imbalance, ignition problems, and leaks. A misfire condition should be analyzed by assuming at least one cylinder does not fire. Misfire is common when the fuel is inconsistent, such as biogas from waste treatment or landfills.

4.3.10 References

1. Feese, T., and Hill, C., "Guidelines for Preventing Torsional Vibration Problems in Reciprocating Machinery," Gas Machinery Conference, Nashville, Tennessee, October 7, 2002.
2. Wilson, W. K., Practical Solution of Torsional Vibration Problems, 1, New York, New York: John Wiley & Sons Inc., 1956.
3. Nestorides, E. J., *A Handbook on Torsional Vibration*, British Internal Combustion Engine Research Association, pp. 84 – 88, 1958.
4. Pasricha, M. S., and Carnegie, W. D., "Torsional Vibrations in Reciprocating Engines," *Journal of Ship Research*, Vol. 20, No. 1, pp. 32 – 39, March 1976.
5. Peterson, R. E., Stress Concentration Factors, New York, New York: John Wiley & Sons, 1974.
6. USAS B17.1—1967 (1973), "Keys and Keyseats," American Society of Mechanical Engineers.
7. Lloyd's Register of Shipping, "Main & Auxiliary Machinery," Rules & Regulations for the Classification of Ships, Part 5, London, 2000.
8. Shigley, J. E., and Mischke, C. R., *Mechanical Engineering Design*, New York, New York: McGraw-Hill, Inc., 1989.

9. Brenner, Jr., R. C., "A Practical Treatise on Engine Crankshaft Torsional Vibration Control," Society of Automotive Engineers, Inc., West Coast Int'l Meeting, Portland, Oregon, 1979.

10. Lily, L. R. C., *Diesel Engine Reference Book*, London: Butterworth & Co. Publishers Ltd., 1984.

11. Harris, C. M., *Shock & Vibration Handbook*, 4th Ed., New York, New York: McGraw-Hill Companies, Inc., 1996.

12. Den Hartog, J.P., *Mechanical Vibrations*, New York, New York: Dover Publications, Inc., 1985.

13. Feese, T., "Torsional Vibration Linked to Water Pumping System Failure," *Pumps and System Magazine*, pp. 44 – 45, September 1997.

14. Feese, T., "Transient Torsional Vibration of a Synchronous Motor Train with a Nonlinear Stiffness Coupling," Thesis, University of Texas at San Antonio, December 1996.

15. NEMA Standard MG 1-1998, *Motors and Generators*.

16. Mehta, L. C., Farr, M. K., and DeWitt, R. L., "Computer Simulation and Verification of I.C. Engine Vibration Characteristics," ASME Paper 78-DGP-24, Energy Technology Conference & Exhibition, Houston, Texas, November 5 – 9, 1978.

4.4 TORSIONAL ANALYSIS CALCULATIONS

4.4.1 Undamped Torsional Natural Frequency Analysis

Several types of computer programs are available for calculating undamped torsional natural frequencies. Such software will calculate the undamped torsional modes using the Finite Element Method or the Transfer Matrix (Holzer) Method. Such codes should be properly validated and be sufficiently robust to analyze all systems of interest to the user. For convenience to the reader, some computational aspects of the Transfer Matrix (Holzer) Method are detailed in 4.4.5 as well as its limitations in predicting undamped torsional modes.

The primary results of the undamped torsional natural frequency analysis are the following:

- a. Undamped train torsional natural frequencies.
- b. Corresponding train torsional mode shapes.

A conventional presentation of the torsional natural frequencies is made using a Campbell Natural Frequency Interference Diagram, as shown in Figure 4-28 for a typical motor-gear-compressor train and Figure 4-29 for a typical steam turbine/compressor train. Campbell diagrams provide a graphical display of a rotor system's torsional natural frequencies versus the frequencies of potential excitation mechanisms. The reference operating speed or speed range is also displayed. The potential excitation frequency may be con-

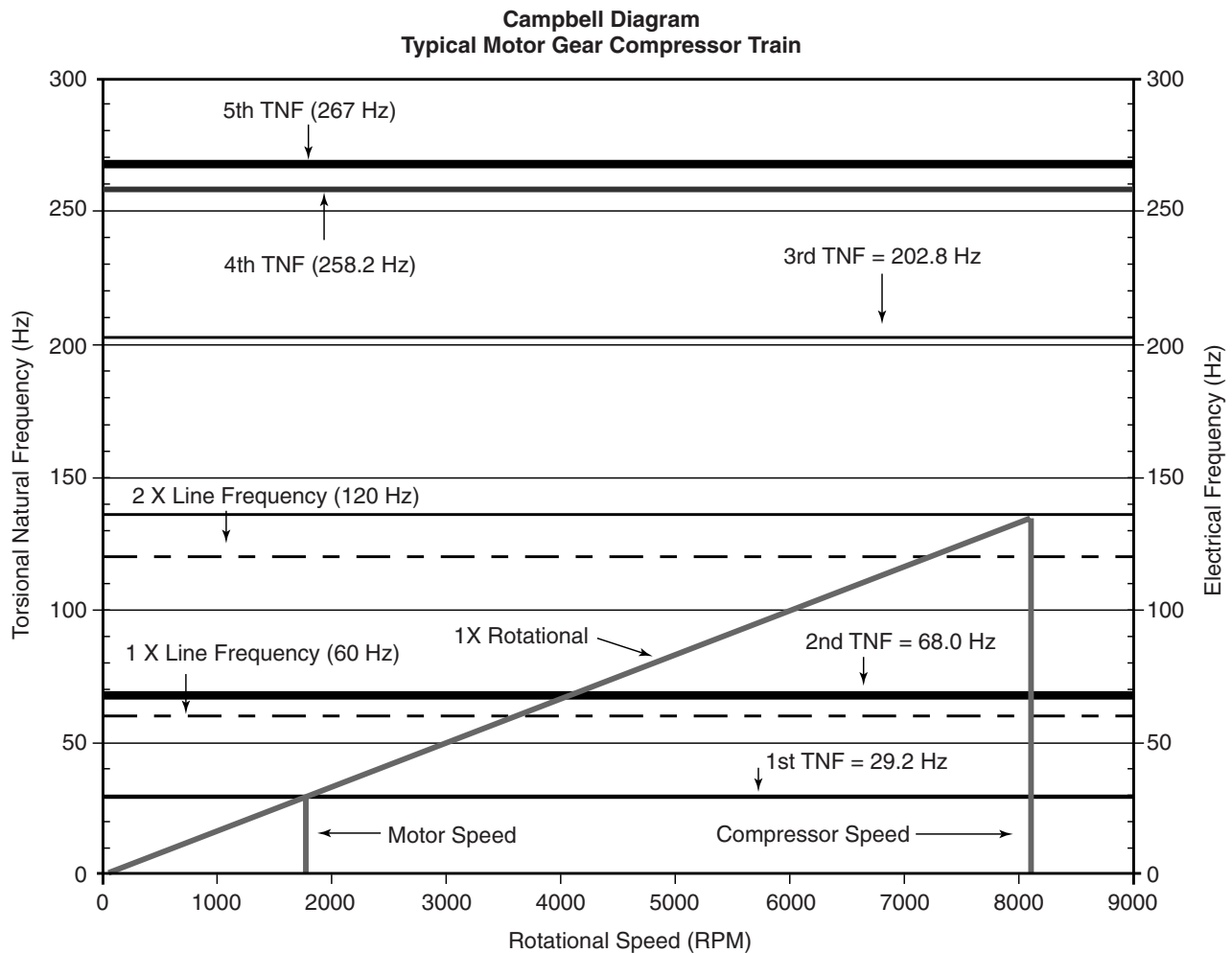


Figure 4-28—Campbell Diagram for a Motor-gear-Compressor System

stant, such as electrical line frequency and twice electrical line frequency or they may be variable in nature. Variable frequency excitations may be associated with rotational frequency or multiples of rotating frequency or may be associated with electrical excitation such as that associated with the harmonics of a variable frequency electric drives or asynchronous starting of a synchronous motor. The excitation may be of a steady nature or may be transient in nature such as the torsional excitation of a train driven by a synchronous motor. Constant frequency excitation appears as a horizontal line on a Campbell diagram. Variable frequency excitation appear as a sloped line. The coincidence of any torsional natural frequency with any steady state excitation frequency along the reference operating speed range must meet the API separation margin of $\pm 10\%$ or it must be shown that the torsional natural frequency is non responsive. Transient torsional

excitations may be impossible to detune, in which case the system should be evaluated for transient response.

The system rotor mode shape for each natural frequency is a plot of relative angular deflection versus axial distance along the coupled rotors. These plots are typically normalized to unity based on the location of maximum angular deflection. Figures 4-30 and 4-31 display several train torsional mode shapes calculated for a motor-gear-compressor train.

Mode shape information is important for the proper interpretation of the results. Should a torsional interference exist, a study of the train mode shape in question can yield information on nodal point locations and anti-nodal point locations along the deflected rotor train. This information allows the designer to understand where the system is sensitive to flexibility and where it is sensitive to inertia, respectively. The strain energy and kinetic energy, discussed in 4.4.1.1 and

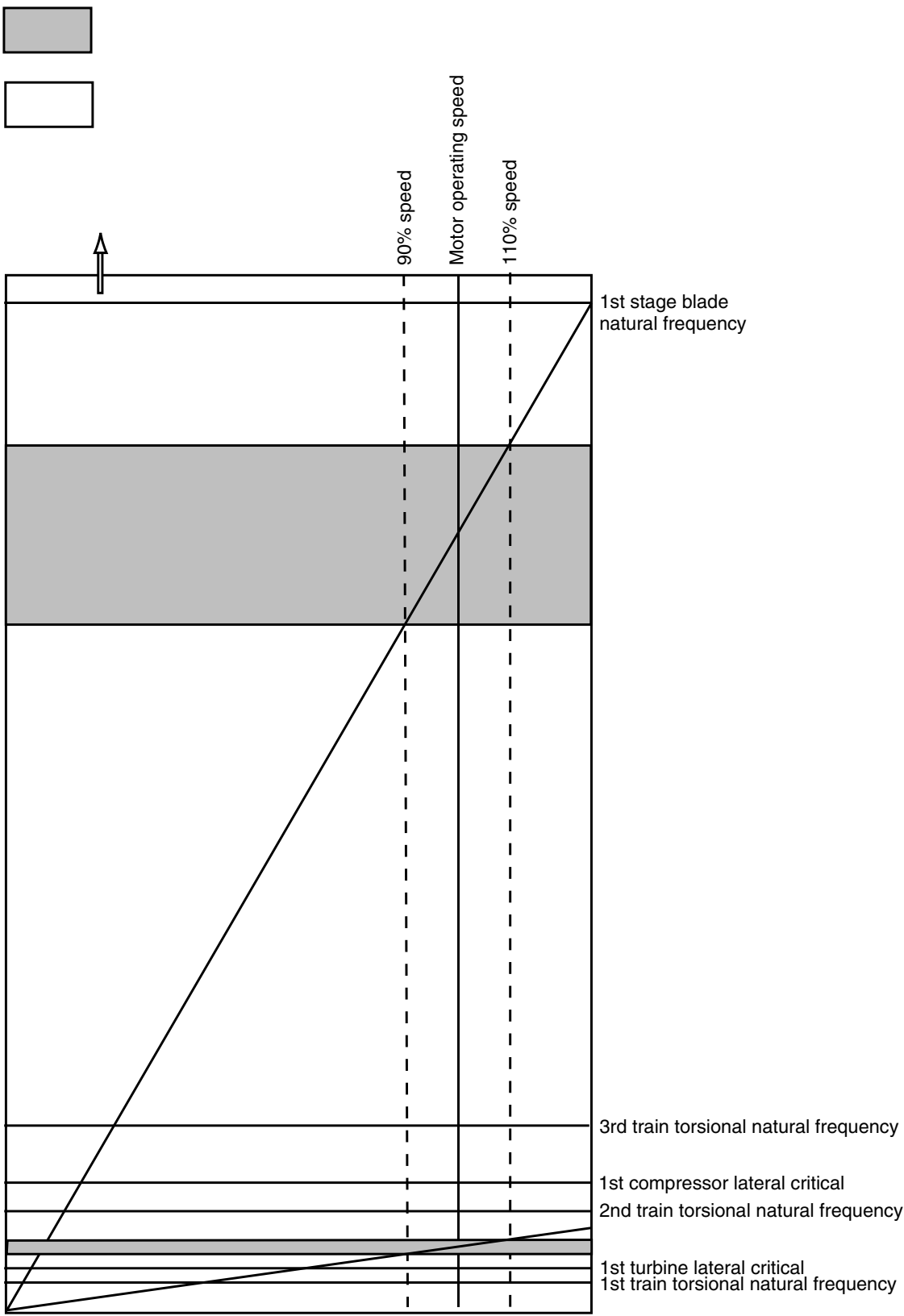


Figure 4-29—Campbell Diagram for a Steam Turbine Driven Compressor System

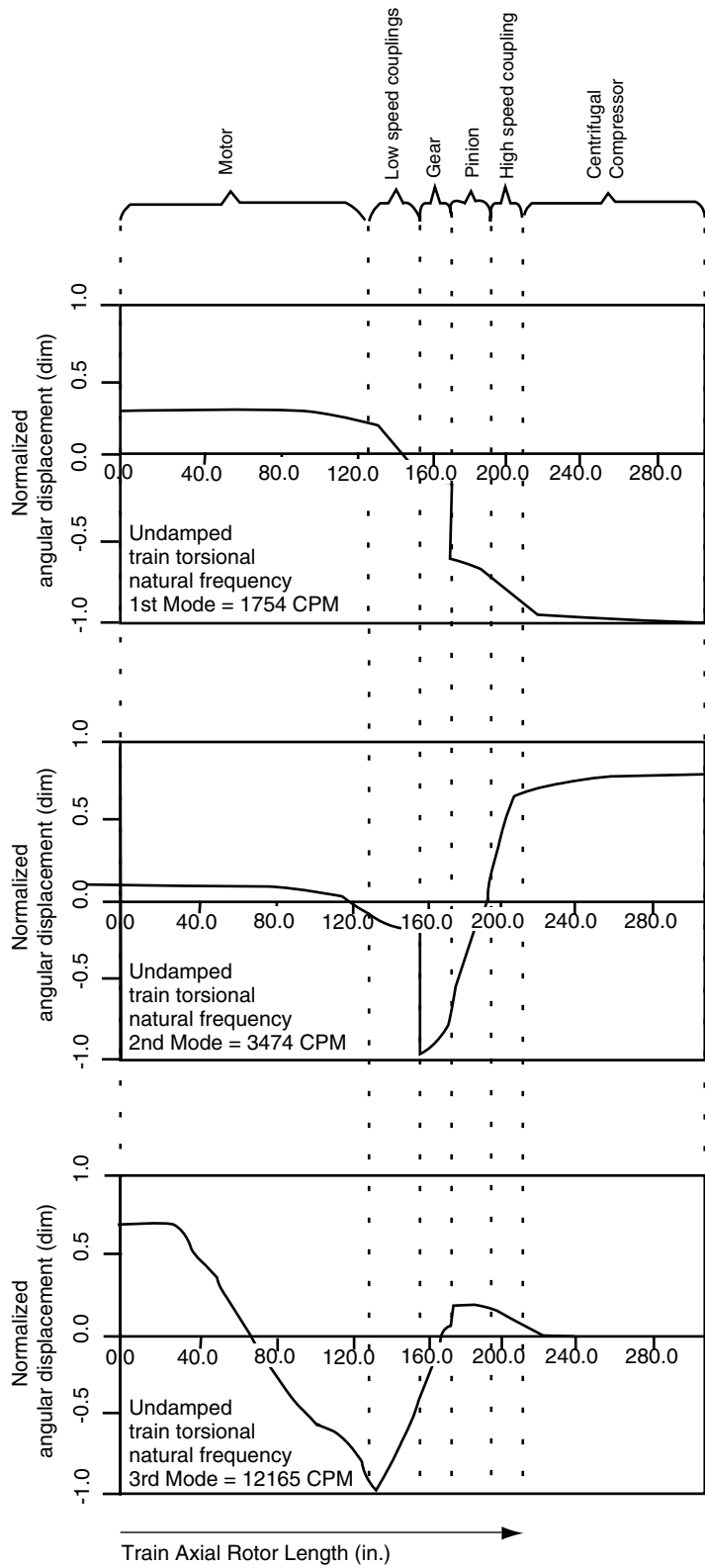


Figure 4-30—Torsional Mode Shapes for a Typical Motor-gear-compressor Train

4.4.1.2, also assist the analyst in identifying of the system best suited to tune a given mode and which locations are most important when regarding the response of a given mode. This knowledge allows the analyst to determine which changes in the system are most appropriate if modification of the system is required.

4.4.1.1 Strain Energy

The concepts of strain and kinetic energy are described in Reference [1]. Strain Energy is determined on an element-by-element basis for each calculated mode of the system being analyzed. Strain Energy is calculated by Equation (4-19)

$$U = \frac{K}{2} \theta^2 \quad (4-19)$$

where

U = Strain energy, N-m (lbf-in.),

K = Element spring constant, N-m/rad (in.-lbf./rad),

θ = Torsional deflection across the element, rad.

The calculated percent strain energy for a given element relative to the total strain energy of the system enables the analyst to determine the system segments that most significantly effect the natural frequency for a given mode. These element percent strain energies will vary from mode to mode. The following equations will enable one to estimate how a given change in an element will affect the natural frequency of a given mode (Reference [1]) A change can be made to an element stiffness and or mass, however the most common modification is to alter a system natural frequency by changing an element stiffness. The general form of the equation is found in Equation 4-20.

$$\omega' = \omega \left[\frac{100 + SE\% \left(\frac{\Delta K}{K} \right)}{100 + KE\% \left(\frac{\Delta I}{I} \right)} \right]^{\frac{1}{2}} \quad (4-20)$$

where

ω' = Modified system frequency, rad/s,

ω = Initial system frequency, rad/s,

$SE\%$ = The percent strain energy of the element being modified,

$KE\%$ = The percent kinetic energy of the element being modified,

ΔK = The change in stiffness of the element being modified, N-m/rad (lbf-in./rad),

K = The original stiffness of the element being modified, N-m/rad (lbf-in./rad),

ΔI = The change in inertia of the element being modified, kg-m² (lbm-in.²),

I = The original inertia of the element being modified.

For the case where only stiffness is modified, Equation 4-20 simplifies to

$$\omega' = \omega \left[\frac{100 + SE\% \left(\frac{\Delta K}{K} \right)}{100} \right]^{\frac{1}{2}} \quad (4-21)$$

Equation 4-21 can be rearranged to solve for the desired stiffness change

$$\Delta K = K \left[\frac{100 \left(\frac{\omega'}{\omega} \right)^2 - 100}{SE\%} \right] \quad (4-22)$$

Note: The accuracy of Equation 4-22 is subject to the magnitude of the calculated stiffness change. One may find that the actual frequency shift identified in 4-22 does not agree exactly with ω' . This is due to the fact that as the stiffness of the element changes so does the strain energy in that element. For stiffness changes of approximately 20%, the calculated frequency with the predicted stiffness will be reasonably accurate. For larger changes, a second iteration may be required after the torsional calculations are performed with the revised frequency.

If the desired change is a reduction of a system frequency, the section stiffness must be reduced thus increasing the torsional stress in the section. One must consider normal and transient conditions so that yielding of the section does not occur.

The concept of strain energy is a tool to assist the analyst to understand which segments are most influential in modifying the natural frequency of a given mode and how the degree of modeling accuracy may influence the results of the analysis. If the percent strain energy of a given element is significant to the total system strain energy, then this element will significantly affect the natural frequency of the mode that it is associated with. Accuracy of the model in this location will significantly impact the accuracy of the calculation. Conversely, a low strain energy level indicates that this element will not significantly impact the accuracy of the results for this mode. One should be aware that a given element may have significant impact on one mode and yet not impact another mode. In the event of uncertainties regarding the accuracy of modeling, a review of the strain energy at an ele-

ment in question can assist the analyst to determine if further refinement of an element geometry in question is warranted.

4.4.1.2 Kinetic Energy

Kinetic energy is determined on an element by element basis and for each disc represented as a lumped inertia. Equation 4-23 defines the kinetic energy in a system element or disc.

$$V = \frac{J}{2g_c}(\dot{\theta})^2 \quad (4-23)$$

where

V = Kinetic energy, N-m (lbf-in.),

J = Polar moment of inertia, kg-m² (lbf-in.²),

$\dot{\theta}$ = Torsional deflection across the element, rad/s

g_c = Gravitational constant, 1.0 kg-m/N-s² (386 lbf-in./lbf-s²).

The kinetic energy is calculated for each mode of the system being analyzed. When the kinetic energy of an element or disc is divided by the total system kinetic energy, the percent kinetic energy of the section can be identified. It is much more difficult to tune a torsional frequency by altering the inertia of an element or disc rather than altering the torsional stiffness of an element. The identification of the location of significant percentage kinetic energy of a disc or element can assist to identify locations that are influential in the response of a given torsional mode. If a potential excitation exists at a location of significant kinetic energy and that excitation can occur at the torsional frequency in question, then there is a strong probability that the mode can be excited.

There are several potential sources of torsional excitation from rotating machinery. Fortunately, most of these are small in magnitude generating minimal torsional excitation. Tables of potential excitations with associated frequencies and magnitudes can be found in Table 5 of Reference [2] and Tables 1 and 4 of Reference [3]. Details of these excitations are elaborated in the references and the material in 4.5.

4.4.1.3 Tuning a Mass Elastic System

Once the system has been analyzed, the system may have to be tuned if adequate separation margin does not exist between a torsional natural frequency and a potential excitation. This is normally effective for fixed speed drives with excitation that has a constant frequency. Usually, adjusting the torsional stiffness of the couplings is suitable to tune a system. One should use caution when reducing the torsional stiffness of a coupling to ensure that peak stress incurred during startup, or other specified off design conditions, does not

exceed the material yield strength. In the case of variable frequency excitation or variable speed drives (VFD) it may not be possible to tune a system. In such a case, the analyst must evaluate the excitation mechanism to determine if torsional response of the system is possible and, if so, will create cyclic torsional stresses that would be a concern with respect to either high cycle or low cycle fatigue. If the excitation is possible, a synchronous or transient analysis may be required. Refer to 4.4.2 for synchronous response calculations.

4.4.1.4 Examples

4.4.1.4.1 Compressor-Gear-Motor

Figure 4-3 presents the general layout of a typical motor driven compressor train. For this example, a motor running at 1788 rpm, drives a speed increasing gear which powers an 8100 rpm compressor. This train is modeled using data supplied by vendors of the various components (motor, gear, compressor, and couplings) to support a torsional natural frequency analysis. The Campbell diagram in Figure 4-28 cross-plots the frequencies of the modes with the shaft running speed. Figure 4-30 and Figure 4-31 presents the first five mode shapes. The Campbell diagram indicates a potential interference, within 10%, between the fundamental torsional mode and one times operating speed. The plot also indicates that no interference exists between the one and two times electrical line frequency and any undamped torsional natural frequency. Examination of the corresponding torsional mode shape indicates that shaft twisting of the three individual units is minimal; torsional twisting is principally confined to the couplings for this mode. This implies that the torsional stiffness of the couplings is significantly lower than the torsional stiffness of the surrounding shafts. Hence, the frequency of this mode is governed by the torsional stiffness of the couplings. Couplings are the torsionally soft elements in the train, therefore, their torsional stiffness will govern the locations of the fundamental two modes. In general, machinery trains will have the same number of coupling controlled modes as couplings. These modes are torsionally significant and require de-tuning if they interfere with potential excitation frequencies. Altering the torsional stiffness of one or both couplings will allow the design engineer to shift the frequency of the potentially problematic mode. Figure 4-32 displays the result of tuning the coupling torsional stiffness where the potentially problematic mode has been tuned away from the operating speed of the unit. Although motor drive trains typically possess more sources of torsional excitation than a turbine driven train, they are also usually limited to a single operating speed so torsional detuning is often not difficult to accomplish. Most coupling vendors will readily adjust the torsional stiffness of a coupling within a range of at least $\pm 25\%$. Note, however, that tuning the coupling stiffness may adversely impact the service factor of the coupling.

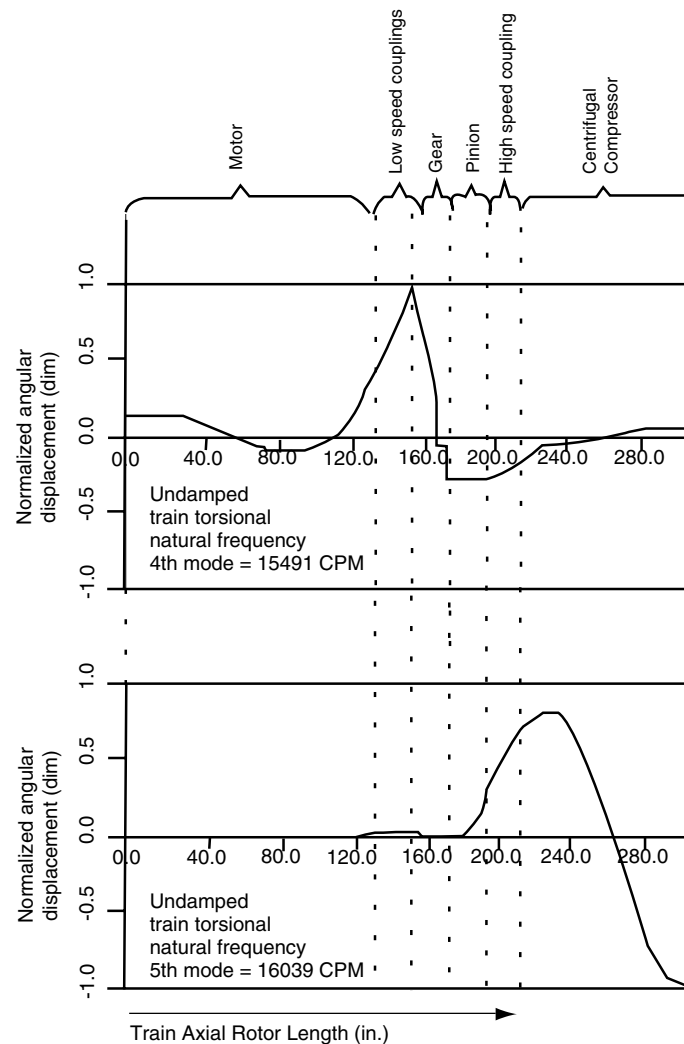


Figure 4-31—Torsional Mode Shapes for a Typical Motor-gear-compressor Train (Continued)

The third mode calculated for this example is typical of motor controlled modes where calculated angular deflections are predominantly found in the low-speed shafting with the largest change in angular deflection occurring through the motor. Note that the node point of the motion is located nearly at motor midspan so that the two ends of the core vibrate out of phase. This motion is analogous to the out-of-phase free vibration observed in a system composed of two masses connected by a single spring. Higher order modes contain single unit out-of-phase motions similar to the motor controlled mode. Figure 4-31, displays the fifth mode as a compressor controlled torsional mode.

4.4.1.4.2 Compressor/Turbine

This example considers a steam turbine direct connected to a centrifugal compressor as depicted in Figure 4-6. A torsional analysis is usually not required for this train because the torque characteristics of the turbine provides a smooth driver with low

amplitude torque pulsations in the frequency range likely to excite a lower torsional natural frequency. Without a major excitation mechanism, torsional natural frequencies will not be significantly amplified. Even in this case, however, a conservative design approach will ensure that there is no interference with the one times operating speed range, particularly with the fundamental (first) torsional natural frequency.

Figures 4-29 and 4-33 present the train Campbell diagram and first three mode shapes for the turbine-compressor train. The Campbell diagram shows no interference between the undamped torsional natural frequencies and the one times operating speed lines, indicating an acceptable design for this train. Note that the coupling stiffness controlled mode lies well below the operating speed range, while the resonant modes corresponding to the particular machines lie above the operating speed range. This is characteristic of most turbine-compressor trains and results in the typically acceptable torsional characteristics for these trains.

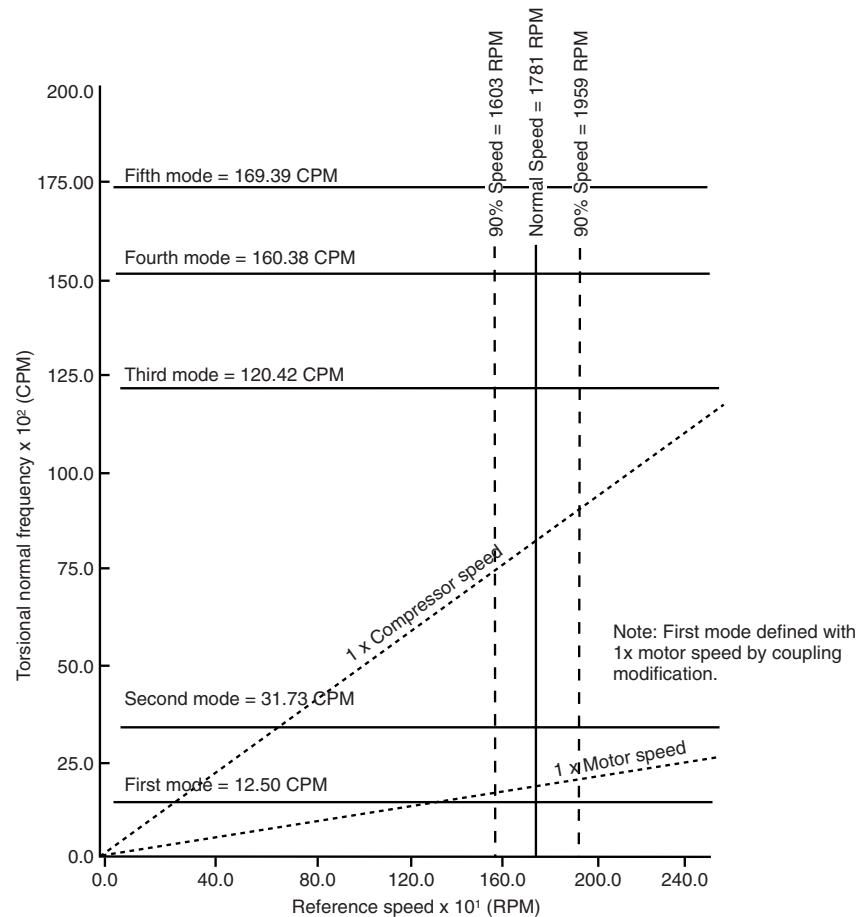


Figure 4-32—Campbell Diagram for a Motor-gear-compressor Train after Tuning

4.4.2 Synchronous Forced Response Calculations

In most fixed speed machinery trains, torsional natural frequencies can usually be tuned to avoid system torsional frequencies. However, it may not be possible to tune a system for a variable speed machinery train. This is especially true if the train contains potential excitation sources that are related to rotational speed, harmonics of rotational speed, variable electrical frequencies and their harmonics supplied to a motor or excitations that are related to “slip” frequencies in systems with variable frequency drives or synchronous motors.

If, after the torsional natural frequencies are determined for a system, there is a defined interference between an excitation and/or operating speed, a synchronous response analysis may have to be performed.

The following evaluation should be performed to determine if a system can be excited and, if the system can be excited, will the system be suitably designed to avoid high cycle fatigue failure:

The first step is to evaluate the torsional natural frequency of concern and its associated mode shape along with kinetic energy distribution. If from this observation it is apparent that

the mode can only be excited by an excitation at a location in a system without a defined source of excitation, then this condition need not be examined further.

An example of a torsional mode that is unique to one component in the system is shown in Figure 4-34. Figure 4-34 is a mode shape plot of a compressor system similar to that shown in Figure 4-3. Figure 4-34 identifies the 3rd mode torsional natural frequency as 279.2 Hz. It can be seen from the figure that all of the deflection in the system is associated with the sections, which represent the motor. There are no changes that can be made in the system that would alter this mode significantly. In order to prove this, a second calculation was performed where only the motor rotor was modeled. The remainder of the system was deleted. Figure 4-35 identifies the 1st mode torsional frequency of the motor at a frequency of 278.6 Hz. In addition to the frequency, the mode shape of the motor only model has the same modal distribution as that of the complete system. In order to excite a 3rd mode torsional natural frequency of the system this motor would have to have an excitation which has a frequency of 278.6 Hz and would require an out of phase excitation as shown by the mode shape plot.

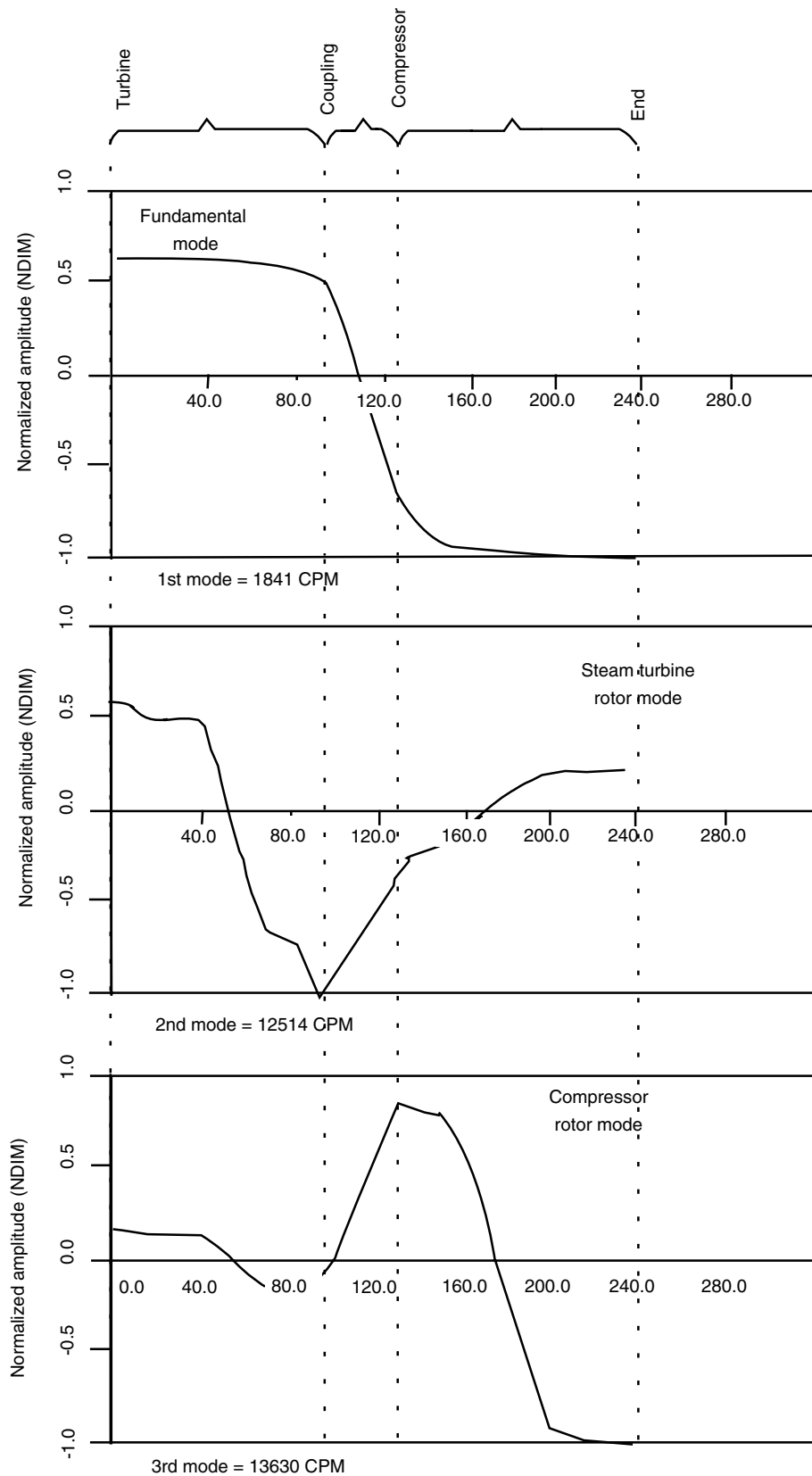


Figure 4-33—Torsional Mode Shapes for a Typical Steam Turbine Driven Compressor Train

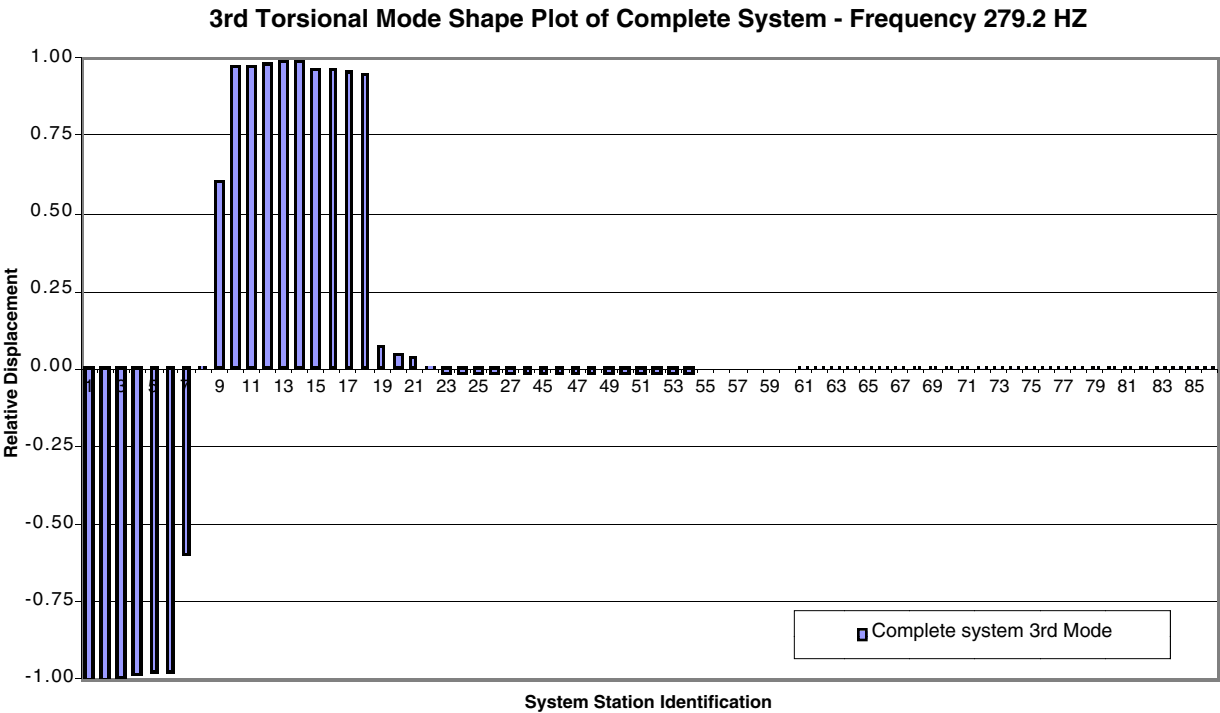


Figure 4-34—3rd Torsional Natural Frequency of a Motor-gear-compressor System

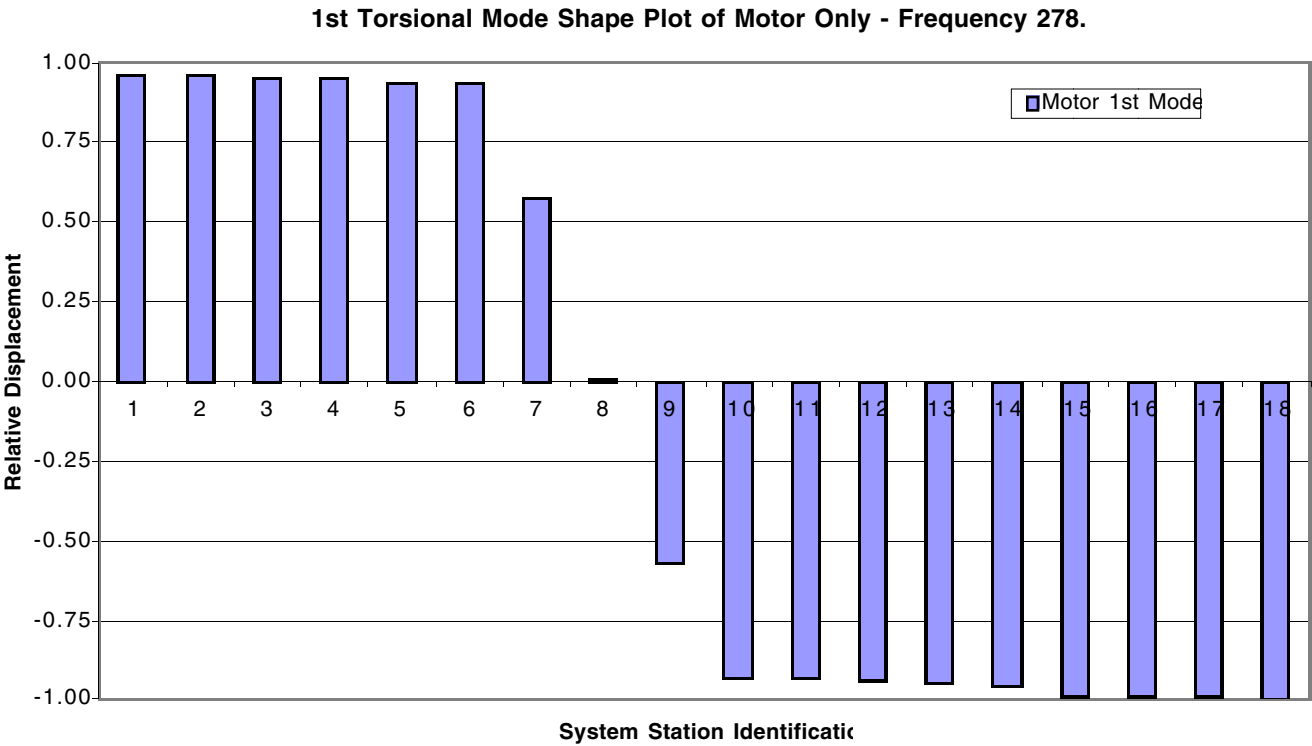


Figure 4-35—1st Torsional Natural Frequency of a Motor

Occasionally, a motor driven compressor system will have a third mode natural frequency that coincides with the operating speed of the compressor or twice the operating speed of the compressor. Since the system frequency is solely dependant on the motor design no tuning of components, such as couplings, would affect the frequency of this mode. The motor manufacturer would be contacted and provided with the results of the torsional analysis and would be requested to identify any source of torsional excitation at this frequency. If none exists then this mode would be deemed non responsive since no excitation source can be defined.

Similarly, if the excitation is of such a very high frequency, such as the tooth mode frequency of a gear which may be over 100 times the rotation speed of a gear or 30 or more times the pinion speed, the higher order torsional modes will be local to a single component of the system. It is for this reason that harmonics above two times rotational speed are usually disregarded in the evaluation of a system.

If the review of the mode shapes and potential excitation mechanisms do identify a potential excitation that can exist at a component with high modal displacement or a high percentage of the kinetic energy of a mode, then a synchronous forced response analysis should be performed.

If it has been determined that there is an excitation that can modally excite the system then the magnitude of this excitation must be quantified. Section 4.5 will identify potential torsional excitation from various types of rotating machinery. Section 4.3.6 identifies torsional excitation from reciprocating machinery. After the excitation frequency and magnitude are defined then damping in the system must be quantified. Many of these damping mechanisms are frequency and/or torque magnitude dependant. Examples of damping within a system are hysteric damping of elastomeric couplings, shaft material and fluid/disc interaction. An extensive discussion of these damping sources and magnitudes can be found in Reference [3].

After the synchronous response analysis is completed, the mean and dynamic stress must be computed from the steady state torque at the operating conditions consistent with the resonance being evaluated and the dynamic stress determined from the alternating torque magnitudes determined from the response analysis. Appropriate stress concentrations should be included in determining the highest stress occurring at the location in question. Finally, the mean and alternating stress should be super imposed on a Goodman diagram to determine if the design is acceptable. Discussion of the stress calculations can be found in References [2] and [3] and is discussed further in 4.6. Figure 4-36 is a plot of the magnification factor of all the model stations in a torsional system. The magnification factor is defined as the magnitude of the maximum torsional response divided by the magnitude of the response used as the excitation in the analysis. The magnification factor can be used to determine the torque in a tor-

sional system after the synchronous forced response analysis is completed.

4.4.3 Transient Torsional Response

Excitations that are transient in nature such as the starting of a system driven by a synchronous motor, the acceleration of a variable frequency drive motor, a restart of an induction motor after a power interruption or an electrical fault in a motor or generator all have the potential to introduce electrical excitation, which is converted to torque in the motor, any of which may excite torsional natural frequencies. Some of these events are not possible to avoid such as the start of a synchronous motor. Events such as premature breaker reclosure are preventable with proper time delay relays in the motor switch gear. Other potential problems are possible to avoid by fault detection relays in the switch gear. As a result, the only transient analysis normally performed is that of asynchronous startup of a synchronous motor or a ground fault condition for a generator. Classic references for torsional vibration problems with a synchronous motor start are identified in References [4] through [9].

The nature of transient torsional vibration is somewhat unique in rotating machinery. Some transient torsional vibration excitations may be caused by one event, such as the breaker reclosure of an electric motor or the short circuit of a motor or generator. Other transient torsional vibration may be caused by a rather limited number of events, such as the starting of a synchronous motor. Still others may occur more frequently, such as the start and variable speed operation of a variable frequency drive.

A failure of a power transmission component may occur in a single transient torsional vibration event. A transient torsional vibration may go undetected until a certain number of events occur after which a low cycle fatigue failure could occur. This potential failure can occur years after the initial startup of the machinery. In some cases, there are warning signs such as the "clatter" of gear teeth revealing complete torque reversals or there may be lateral vibration in a geared system created by torsional vibration (see 4.9). Usually transient torsional events in direct connected machinery have no outward warning signs.

The design of rotating machinery to avoid low cycle failure is somewhat unique. Often special couplings or torque limiting devices that interrupt torque transmission or fail intentionally are added to the power transmission components. Such devices are often used on generators where shorts or improper synchronization to existing grids are seen as potential problems. Often the stress may be rather high, in the case of synchronous motors certain stresses may exceed the yield strength of the material in shear. If the potential number of transient torsional events can be reliably estimated, then it is acceptable practice to design for a limited number of starts to avoid exceptionally large shafts and couplings. As an exam-

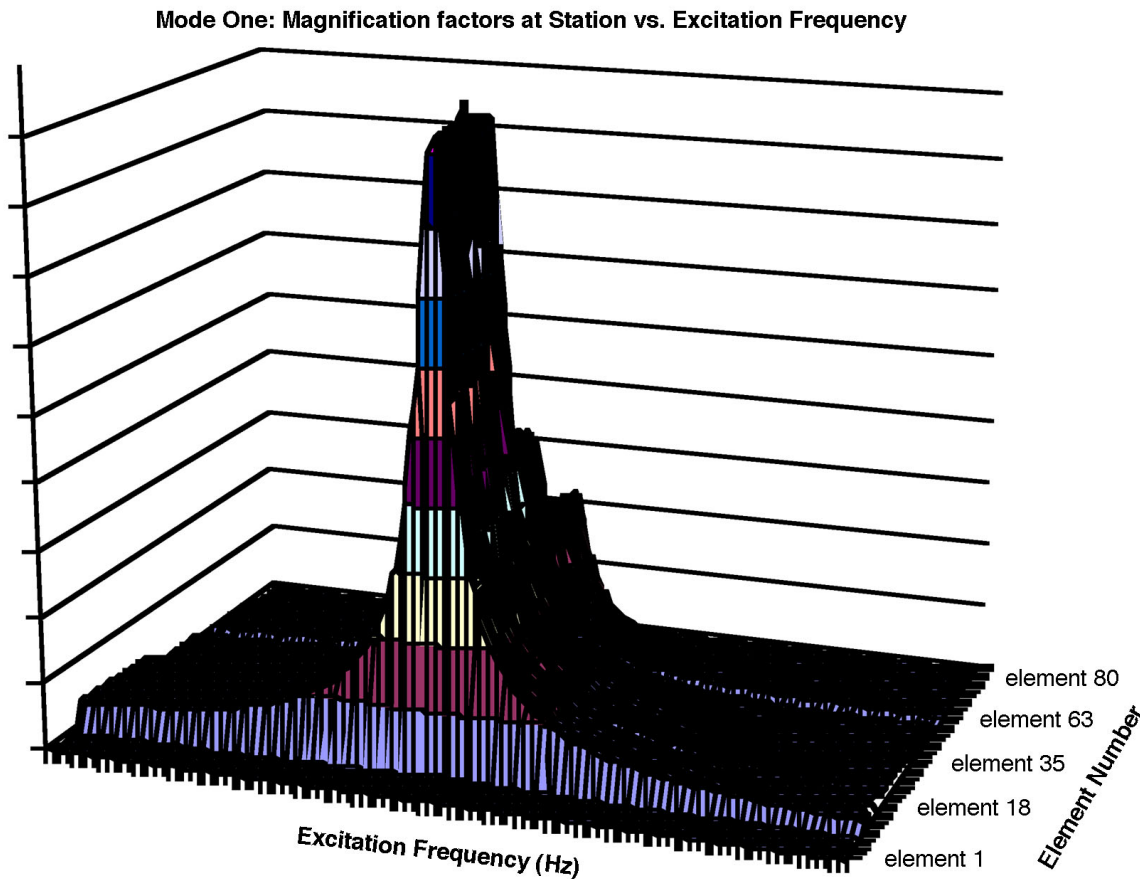


Figure 4-36—A Typical Magnification Factor Plot of a Torsional Synchronous Response Analysis

ple, starting of large synchronous motors is done infrequently. Even starting a motor once a week for 20 years would only result in 1040 starts. This philosophy is recognized and accepted in API standards.

Figure 4-37 is a typical output of a transient analysis of fault condition, namely a short between two phases of a motor.

4.4.3.1 Transient Analysis of a Synchronous Motor Driven System

In order to analyze the transient response of an equipment train driven by a synchronous motor, one needs a model of the equipment train, data to determine the mean and alternating torque developed by the synchronous motor, data on any torsional damping added to the system, speed torque requirements of the driven equipment, physical dimensions of the segments of the equipment train and material properties of the train segments.

The torsional excitation created by the motor is normally modeled in two manners:

A plot of mean and alternating torque or a plot of the direct and quadrature axis torque. The direct axis torque is that torque produced by the motor when the stator poles and the motor rotor poles are directly aligned. The quadrature axis torque is that produced when the motor rotor poles are located midway between the stator poles. The mean torque at a given speed is the average of the direct and quadrature torque. The alternating torque is the difference of the direct and quadrature axis torque. These plots are normally based on an assumed voltage. Figure 4-38 is a typical plot for the torque versus speed characteristics of a synchronous motor. Another method to determine the mean and alternating torque is to create a slip frequency dependant electrical circuit model of the motor and an electrical circuit of the electrical supply system from the grid bus to the terminal connections of the motor [9]. A model such as this combined with the load speed torque curve and a torsional model will develop the instantaneous torque which will account for the precise motor terminal voltage and the position of the motor rotor relative to the stator. Since the motor torque is proportional to the motor terminal voltage squared, this model eliminates the assump-

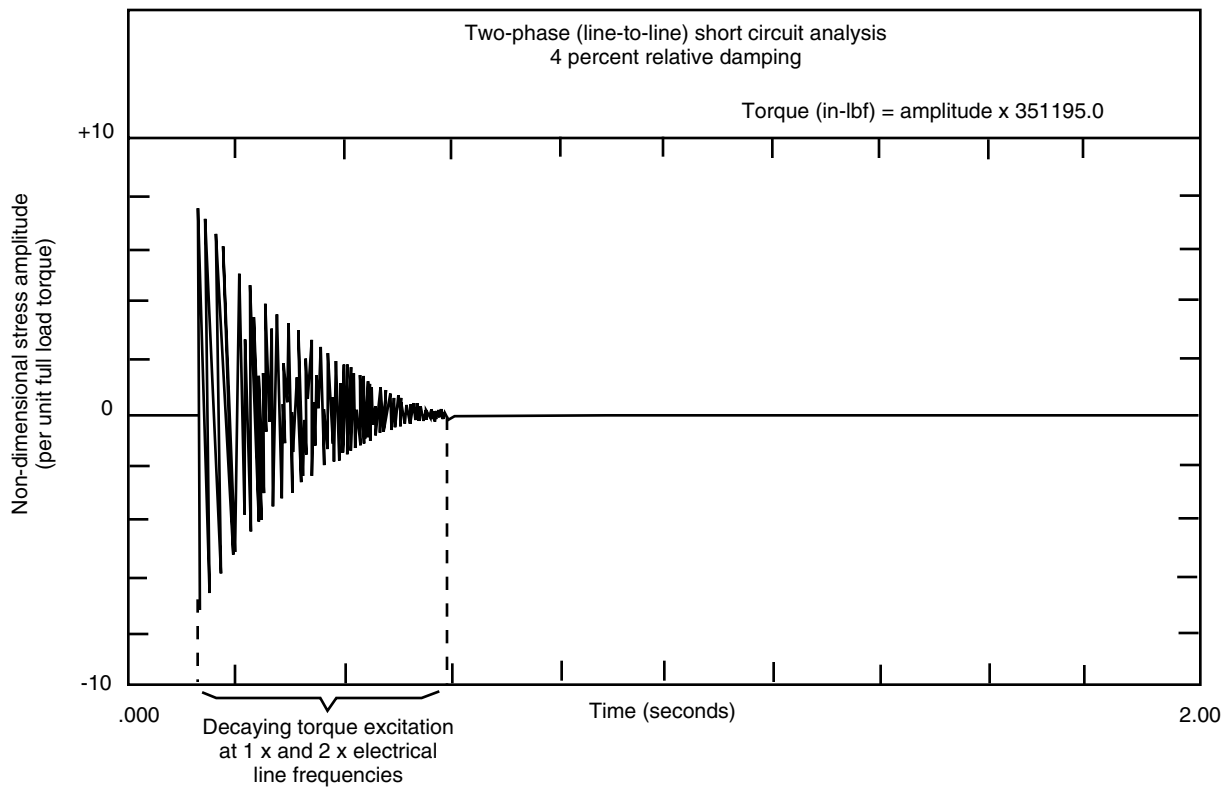
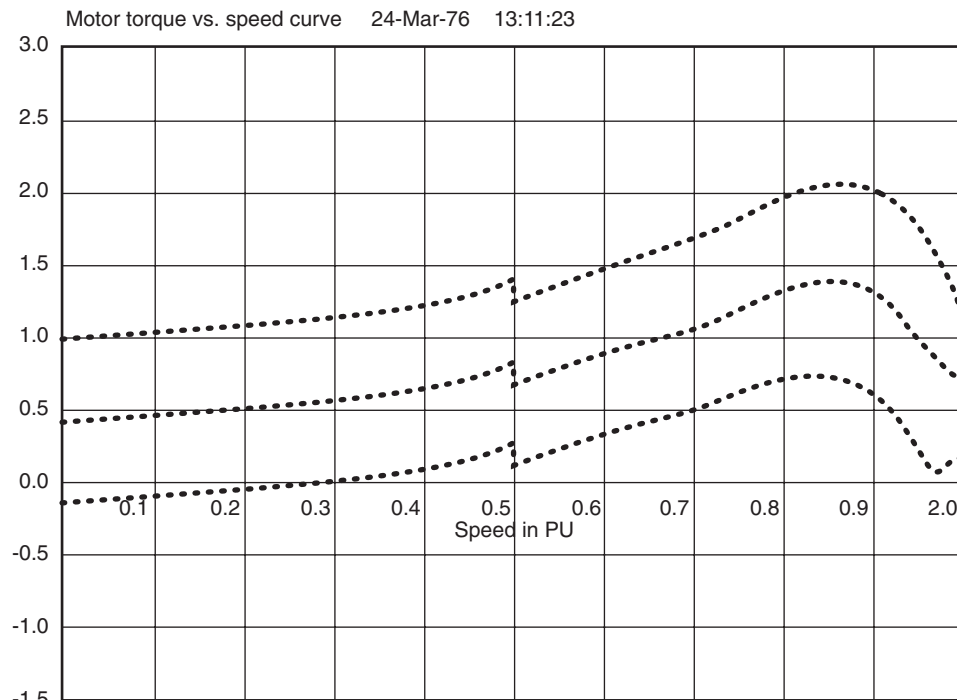


Figure 4-37—Transient Torsional Motor Fault Analysis Plot



The upper curve is the Direct Axis Torque.
The center curve is the Average Torque.
The lower curve is the Quadrature Axis Torque.

Figure 4-38—Speed Torque Curve for a Synchronous Motor

tion of constant voltage throughout the motor speed range. A coupling that is introduced into the system to add damping must be accurately modeled. Many of the couplings introduced to add damping have elastomeric elements, which have non linear stiffness and damping. The variable properties of the coupling must be properly represented as the torque varies during the starting sequence including resonance. Section 4.1.1.6 has addressed this topic. If the torques are of a magnitude that would create stresses in the power transmission components that would not have infinite life, then a low cycle fatigue analysis which includes plastic strain, must be performed. To accomplish this analysis, the power transmission component dimensions and material properties must be known. Further details of this analysis are discussed in 4.6.

Once the system properties and mean and excitation torque are defined, a transient torsional response analysis can be conducted to determine the system response. Figure 4-39-1 is a plot of the excitation torque of a synchronous motor during a startup and the response of the system as the compressor train passes through torsional resonance. Section 4.6 discusses the analysis of the system when the stresses exceed the infinite fatigue life of the material.

4.4.4 References

1. Simmons, H. R., "Vibration Energy: A Quick Approach to Rotor dynamic Optimization," ASME Paper Number 76-PET-60, 1976.
2. J. C. Wachel and Fred R. Szenasi, "Analysis of Torsional Vibrations in Rotating Machinery," 22nd Turbomachinery Symposium Proceedings, 1993, pp. 127 – 151.
3. Mark A. Corbo and Stanley B. Malanoski, "Practical Design against Torsional Vibrations", 25th Turbomachinery Symposium Proceedings, 1996, pp. 189 – 223.
4. Brown, R.N., "A Torsional Vibration Problem As Associated With Synchronous Motor Driven Machines," *Journal of Engineering for Power*, July 1960, Paper No. 59-A-141, pp. 215 – 220.
5. Pollard, E.I., "Torsional Response of Systems," Paper No. 66-WA/Pwr-5, Dec. 1966.
6. Godwin, G.L. and Merrill, E.F., "Oscillatory Torques During Synchronous Motor Starting," IEEE Transactions on Industry and General Applications, May/June 1970, Paper No. 70 TP 16-IGA, pp. 258 – 265.

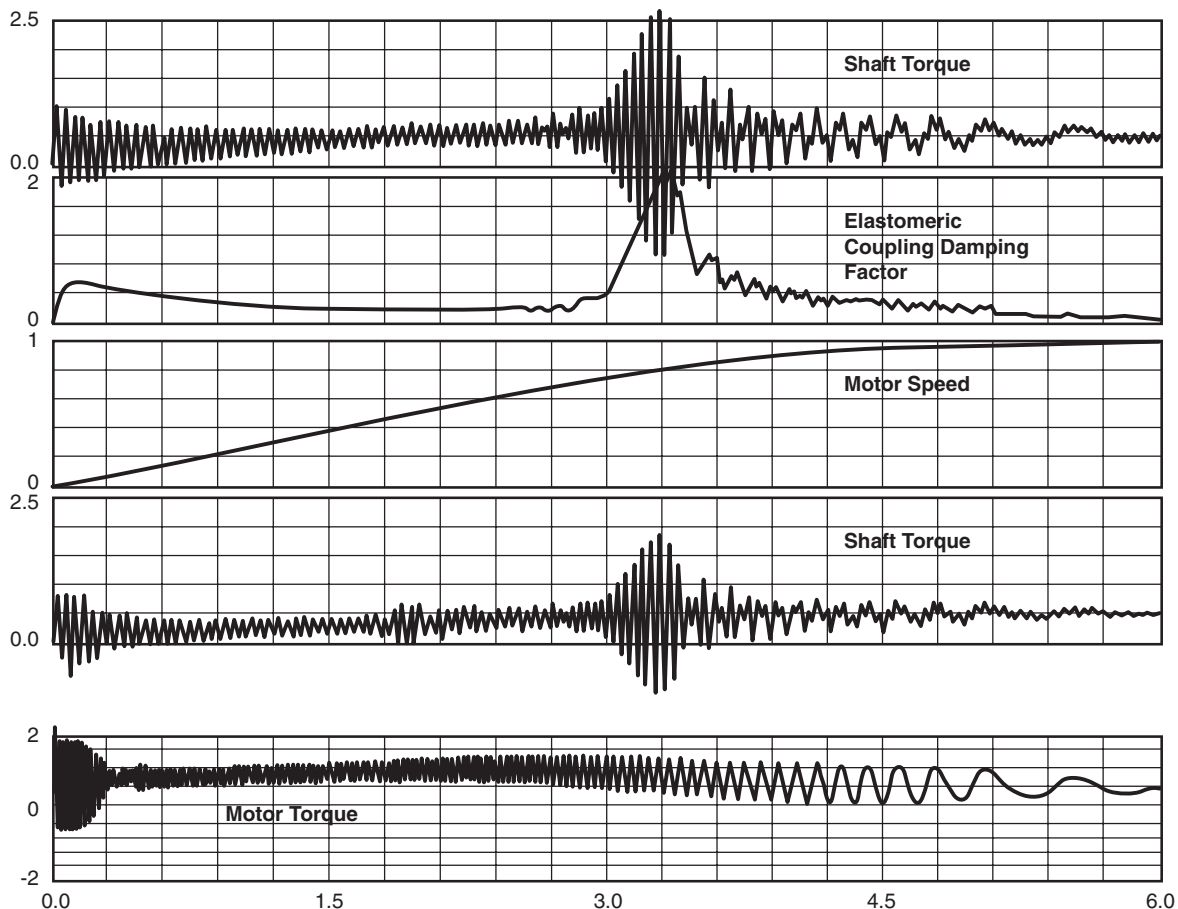


Figure 4-39-1—Plot of Synchronous Motor Transient Response Analysis with Motor Torque Shaft Torques, Motor Speed and Torque Dependent Damping of an Elastomeric Coupling

7. Sohre, J.S., "Transient Torsional Criticals of Synchronous Motor-Drive, High Speed Compressor Units," ASME Paper No. 66-FE-22, June 1965.
8. Thames, P.B. and Heard, T.C., "Torsional Vibrations in Synchronous Motor-Geared Compressor Drives," AIEE Paper No. 59-657, Dec. 1959, pp. 1053 – 1056.
9. Mruk, G.K., "Compressor Response to Synchronous Motor Startup", 7th Turbomachinery Symposium Proceedings, pp. 95 – 101, 1978.

4.4.5 Transfer Matrix (Holzer) Method

4.4.5.1 General Description

The Transfer Matrix (Holzer) Method is best described as a method in which the output oscillating torque is calculated at one end of the train given an input oscillating torque at the other end of the train. The undamped torsional natural frequencies of the train may be calculated by noting that the magnitude of the calculated oscillating torque at the free end of the train becomes zero when the frequency of the oscillating torque matches a train natural frequency. In mathematical terms, the condition of torsional natural frequency (within a specified torque residual error) is defined as follows:

$$T_N = \sum_{i=1}^N \frac{I_i \omega^2 A_i}{g_c} = 0 \quad (4-24)$$

where

T_N = torque residual, N-m (in.-lbf),

I_i = i^{th} polar moment of inertia, kg-m² (lbm-in.²),

ω = frequency of oscillation, rad/s,

A_i = i^{th} shaft section coefficient,

g_c = Gravitational constant, 1.0 kg-m/N-s² (386 lbm-in./lbf-s²).

The convergence limit for a typical transfer matrix routine is to within ± 0.01 Hertz of the actual analytical value at natural frequency. Instead of using the magnitude of the torque residual at the end of each iteration as the convergence dependent variable, most codes search for the torque residual's crossover points on the frequency axis to within the specified tolerance limit. This method is used because for all modes above the first several (which are typically controlled by the coupling torsional stiffnesses) the slope of the torque residual curve becomes very steep and may result in excessive computer iteration time if a residual torque magnitude convergence routine is employed. Since the frequencies of interest are generally several hundred CPM or larger, the error in the

calculated frequency is less than $\pm 0.01\%$ regardless of the magnitude of the torque residual.

4.4.5.2 Limitations of Analysis

4.4.5.2.1 Subsystem Natural Frequency

A common occurrence in the torsional response of a rotor train is the presence of a subsystem natural frequency. This condition will yield an additional torsional natural frequency in the train analysis. However, upon closer inspection of the rotor mode shapes, it can be seen that such a frequency does not represent a true system phenomenon but, rather, is a characteristic frequency of an isolated part of the train. This subsystem natural frequency is essentially uncoupled in nature from the remainder of the system and, as such, is not a true train natural frequency. However, this frequency still represents a potentially significant vibration mode of interest in that, given the required excitation input, an undesirable resonant condition could exist. Additionally, inspection of the residual torque curve indicates that a normal cross-over point exists for a subsystem natural frequency with a finite slope at $T_N = 0$. The following are examples of such a condition:

- a. Exciter assemblies.
- b. Multiple-gear systems, multiple branches.
- c. Discontinuous systems.

4.4.5.2.2 Tuned Oscillator

Most systems yield several characteristic modes that do not represent actual resonant conditions and, as such, are of no concern to the vibrations engineer or designer. The problem lies in identifying these specific frequencies and thereby eliminating them from the remaining resonant modes of interest. These particular frequencies represent a system phenomenon whereby a part of the system is responding to the dynamics of the remainder of the system in the capacity of a tuned oscillator or vibration absorber and, therefore, does not represent a potentially resonant condition. These frequencies can be extracted by close inspection of the torque residual curve at their respective cross-over points. Tuned oscillators do not exhibit normal cross-over points in that the slope becomes infinite and the curve becomes asymptotic to the tuned oscillator frequency, with $T_N = \pm \infty$ on one side of the cross-over and $T_N = \pm \infty$ on the opposite side (Figures 4-39-2). Extracting these modes can be difficult and must be done with caution. It is especially significant to recognize that tuned oscillators exist and that the Holzer technique will yield their frequencies as if they were true natural frequencies. Pre-dominance of these frequencies can be found in more complicated systems, especially multi-branch or multi-gear systems.

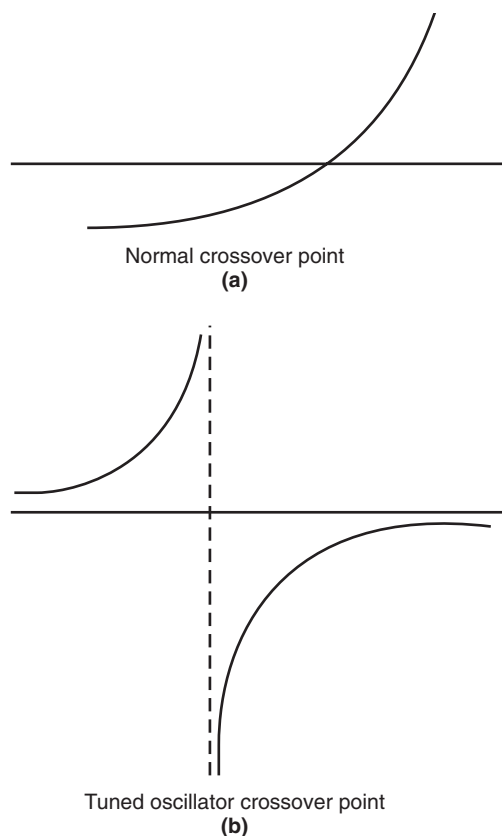


Figure 4-39-2—Crossover Points on Torque Residual Curves

4.5 TORSIONAL EXCITATION SOURCES FROM ROTATING MACHINERY

4.5.1 Continuous Sources

There are several potential sources of torsional excitation from rotating machinery. Fortunately most of these are of a small magnitude that will not create torsional excitation. Tables of potential excitations with associated frequencies and magnitudes can be found in Table 5 of Reference [1] and Tables 1 and 4 of Reference [2]. Details of these excitations are elaborated in the references and the material which follows.

4.5.1.1 Centrifugal Compressors

Centrifugal compressors are not normally considered significant sources of torsional excitation within a system. References [1] and [2] discuss the magnitude and frequency associated with torsional excitation from a centrifugal compressor. The authors recommend that an excitation of 1% of the operating torque be used for synchronous frequency excitation and 0.5% of operating torque be used for non synchronous frequencies which must be defined.

A transient torsional excitation may be created by the surge of a centrifugal compressor, however it is very difficult to quantify the frequency and magnitude associated with surge. Since surge can lead to lateral vibration, overheating and

excessive bearing loads, particularly thrust bearings, surge is protected from occurring by anti-surge control systems.

Sub-synchronous vibration associated with stall cells has the potential to develop torque variations within a compressor, however the magnitudes and frequencies of these torque variations can not be quantified. Stall may result in lateral vibration that would alert users to its presence.

4.5.1.2 Steam Turbines

The potential torsional magnitude of steam turbines are similar to those of centrifugal compressors as identified in Reference [1]. The excitations are normally a function of nozzle or blade passing frequency.

4.5.1.3 Gearing

The potential magnitude of torsional excitation from high quality gearing is quite low. Reference [1] identifies 1% or less of rated torque. The excitation frequency is reported to occur at one to two times rotational frequency, of either the gear or the pinion, and gear mesh frequency. It should be noted that badly worn gearing can cause excitations many times the magnitudes defined for high quality gearing. There is no known method to calculate the excitation magnitude as a function of the AGMA quality level.

Gear units have some unique characteristics that must be considered when discussing their torsional vibration characteristics. Lateral vibrations and torsional vibrations are normally not related; however, in gear units there is a relationship between these two very different types of machinery vibrations. The compound angle created by the gear tooth helix and pressure angles will result in torque variations due to variations in radial displacement, such as displacement due to unbalance, conversely, torque variations will result in radial and axial force variations. Torque is transmitted from one shaft to another in a gear set via radial forces acting between the gear teeth. As a result of this interaction there will be mean tooth forces that are a function of the average torque transmitted by the shafts, and fluctuating tooth forces that are the result of variations in the torque or varying radial vibration. The bearings supporting the shafts have significant radial loads as a result of these tooth forces. This relationship between torque and radial load can cause torsional vibrations and radial vibrations to interact as noted above.

The relationship between torque tooth load and radial bearing load means that torsional vibration can impact the design of the gear teeth and the shaft support bearings. In the presence of an alternating torque a significant consideration is the selection of the direction of rotation of the gear unit to load the various bearings in the most favorable way. The weight of the rotating assemblies and the direction of load from the gear teeth can increase or reduce the bearing loads. Large torque fluctuations can cause the radial bearing load to change load vector orientation. The shafts can actually rise and fall in the bearing clearance as a result of radial loads developed by alternating torque.

All gear teeth are subject to cyclic stress loading during normal operation as gear teeth enter and leave the gear mesh. These cyclic stresses result in the eventual failure of the gear teeth from fatigue. This fatigue failure can be designed to occur after so many cycles of operation that the design gear life is longer than the expected life of the machinery train. However, torsional vibration can cause reversals in shaft torque or large variations with low mean torque. This torsional vibration can cause the teeth to separate. Impact load associated with teeth separating and then re-contacting can significantly increase the tooth stresses and thus reduce the life of the gear teeth. Even without tooth separation or impact due to torque reversal, cyclic stresses associated with torsional vibration will reduce the number of cycles to tooth failure. A good rule of thumb is that variations in shaft torque, i.e. torsional vibration, should not exceed 30% of the mean transmitted torque during any mode of operation. Torsional impact loads from connected machinery, for instance compressor surge, can excite a torsional transient resonance and cause significant increase in gear teeth stresses. Transient torsional loads during synchronous motor start-ups are another case of tooth loading that can reduce the life of a gear set.

During operation gear teeth are in contact with one another with only a very thin film of oil between the tooth flanks. Therefore, proper gear tooth geometry is essential for smooth transmission of motion from one shaft to the other. The profile of the gear flank and proper match between gear teeth along the face width are important in insuring even stress distribution on the gear teeth, but tooth spacing errors are the most significant contributor to the torsional response effects of the gear tooth errors. Such gear tooth spacing errors normally increase the stress on the gear teeth and most gear rating formulas include a “dynamic factor” to account for these loads. The dynamic factor is a function of the gear accuracy and the peripheral speed of the gear teeth. It assumes the connected train is free from significant torsional response. Gear spacing errors are broken into two broad categories, tooth-to-tooth and total accumulated. Both have an effect on the gear stress but the accumulated errors occur closer to shaft speeds and are more likely to effect torsional vibrations. The large mass of the gear and pinion shafts limit the amount of forced torsional vibrations transmitted to the shafts and connected machinery from gear tooth errors.

For information on tooth accuracy refer to ANSI/AGMA ISO 1328 -1 & -2 and ISO TR 10064 part 1 through part 4. These documents specify accuracy grades and measurement techniques but do not specify accuracy requirements for various applications. It is generally recognized that high speed gears should have an accuracy grade of 5 or better. API 613, Fifth Edition specifies an accuracy grade of 4 or better. Note that gears with accuracy grades better than 3 are extremely difficult and expensive to manufacture. When speeds are low accuracy grades of 6 or less may be used. Gear teeth are manufactured to tight tolerances, and mechanical damage during handling must be avoided. Gear sets operate as pairs of shafts

so the accuracy of gear teeth on individual shafts is only as good as the support structure, housing, bearings, and foundation, which support the shafts.

API 613 and API 677 are the American Petroleum Institute Standards on gear unit requirements. For more detail on gear terminology and gear rating, refer to the American Gear Manufacture Association standards such as ANSI/AGMA 1010-E95 for terminology on wear and failure of gear teeth, ANSI/AGMA 2001-C95 for fundamental rating methods for gear teeth, ANSI/AGMA 6010-F97 for rating of enclosed gear units, and ANSI/AGMA 6011-H98 for rating of enclosed high speed gear units.

4.5.1.4 Excitation from Constant Speed Induction Motors

Excitation from direct connected induction motors at operating speed are quite low. Reference [1] identifies 1% of output torque as a magnitude for the line frequency and 0.5% for twice line frequency. Reference [2] identifies potential excitation equal to the number of magnetic poles times the rotational speed.

The most serious torsional excitations result from premature breaker reclosure or electrical faults. Transient excitation may also occur during initial energization of the motor. These excitations are transient in nature and are discussed in 4.5.2. It should be recognized that most potential excitations occur at one or two times line frequency. For this reason it is prudent to avoid system natural frequencies of one and two times electrical line frequency for motor driven equipment.

4.5.1.5 Electric Motors Driven by Variable Frequency Drives

VFD applications for induction motors, and to a lesser extent synchronous motors, have become more prevalent as the cost of the VFDs have been reduced and the technology has improved (Reference [3]). The application of VFDs has generated a potential for torsional vibration (Reference [4]). All VFDs convert alternating line current (AC), 50 or 60 HZ, to direct current, (DC), and reinvert the DC to variable frequency AC current. The AC-DC-AC conversion adds excitation frequencies to the system. These frequencies have a practical application range from approximately 20% of line frequency to line frequency, or even super synchronous frequency that is greater than the incoming line frequency, depending upon how the VFD is designed. In the rectification and inversion process, harmonics of the drive output frequency are created. These harmonics occur at integer multiples of the drive output frequency referred to as harmonic distortion. In addition there is a potential of integer multiples of the difference between line frequency and the VFD output frequency which is referred to as inter harmonic distortion (Reference [5]).

The potential for torsional vibration occurs at relatively low speeds for harmonic distortion. Typical first mode tor-

sional natural frequencies of single body compressor trains are usually 30 Hz or less. The lowest harmonic of a VFD is usually six times the output frequency. Therefore a potential for torsional vibration exists at 5 Hz drive output frequency or less than 10% of the rated line frequency. Higher order harmonics would occur at a drive output frequency lower than this. Therefore the potential for torsional vibration is transient in nature as these speeds are accelerated through during start-up or decelerated through during shutdown. At such low drive output frequencies the mean torque applied to the drive train components is usually quite low, and therefore, the mean stress in drive train components is low, however, if the harmonic distortion has an electrical circuit resonance that creates a relatively high percent of rated torque then the transient torque can be substantial. In this case typical compressor trains often have a magnification factor at the first resonance of 10 times or greater.

The problem of inter harmonic distortion is a far greater concern as the nature of the equation

$$f_e = C_1 (f_l - f_{do}) \quad (4-25)$$

where

f_e = Excitation frequency, Hz,

C_1 = A constant associated with the VFD design,

f_l = Line frequency, Hz,

f_{do} = Drive output frequency, Hz.

indicates that the frequency required to excite a 1st mode torsional frequency will occur at a drive output frequency close to input line frequency. Values of C_1 have been identified to be 6 or 12 for Current Source Inverter drives, Reference [5]. A value of 18 has also been associated with C_1 . Therefore as the drive output frequency approaches the line frequency the excitation frequency reduces and again has the potential to excite the same torsional modes as during the low speed acceleration phase. The potential for severe torsional vibration associated with inter harmonic distortion occurs at speeds normally above 80% of rated speed, where the mean torque is much higher and operation sustained for long periods. Inter-harmonic distortion above 80% then becomes a concern for high cycle fatigue, References [5] and [6]. A methodology for analyzing systems with VFDs was presented in Reference [7].

In addition to the potential for harmonic and inter harmonic distortion there is also the potential for torsional excitation from speed control feedback loops within the VFD controls. If the drive is equipped with a control scheme that measures the speed of the driven equipment and compares the measurement to the set point drive output frequency, there is the possibility that the feed back control correction frequency could coincide with a torsional frequency of the driven equipment. Once the controller correction frequency and the sys-

tem mechanical torsional frequency coincide there is a potential for significant torsional vibration.

One of the insidious traits of torsional vibration in a VFD system is that one may not be aware of its existence until the system fails. Direct driven equipment usually have few outward indications of high torsional vibration. Mechanical systems that have a gear may give outward indications of gear vibration if the magnitude of torsional vibration is very large relative to the mean torque. Under these conditions "clattering" of the gear teeth may be heard as the gear teeth oscillate from a loaded to an unloaded condition. This clattering of teeth may also be heard at low speed during slow speed acceleration when the mean torque is very low.

In addition to mechanical concerns for power transmission components there are also electrical concerns as the harmonics sent by the drive to the motor result in frequencies that add an additional heat load to the motor stator. The motor and VFD package should be very closely coordinated to insure compatibility. Also, the location of the motor relative to drive is very important as the impedance of the interconnecting cables can influence the magnitude and frequency of resonant electrical circuits. The length of the cabling influences the impedance upstream of the VFD. This impedance is important since it affects the terminal voltage at the VFD itself. If the terminal voltage at the VFD is not within the VFD design specifications the harmonics can be magnified. There is also a concern about harmonic distortion passing backward from the VFD to the electrical system feeding the VFD. These harmonics are usually isolated by the use of an isolation transformer.

The design of VFDs has vastly improved through the 1990s. Most of the early application selections were Current Source Inverter (CSI) drives. These systems were designed to supply an AC frequency that was a modified sine wave consisting of 6 or 12 steps per cycle. Recent technology improvements in high power transistors has enabled the use of Pulse Width Modulated (PWM) drives to power levels of 3000 horsepower. The PWM drive creates an AC waveform to the motor that is a sine wave composed of 1500 – 4000 steps per cycles thus producing a wave form very close to that of a sine wave. In addition the frequencies of the harmonic content are so high as to not be a cause for concern regarding the excitation of torsional natural frequencies.

4.5.1.6 Screw Compressors

Rotary screw compressors are high speed positive displacement compressors. As a result of the compression process there is potential for torsional excitation to exist from the screw compressor. The primary frequency of this pulsation would be the lobe passing frequency of the compressor. There is no defined torsional excitation magnitude and no published torsional excitation measurements of screw compressor torsional excitation. If one were to approximate a magnitude of torsional excitation it would be reasonable to assume that a relationship exists between the dynamic pressure pulsations

present in the discharge passage of the compressor and the absolute pressure level in the discharge plenum. Historically a magnitude of 10% of the rated torque has been assumed for a variable speed screw compressor. The 10% is equally distributed on the male and female rotors and phased according to the modal displacement when the system is analyzed.

4.5.1.7 Reciprocating Engines and / or Compressors

The torsional excitation associated with reciprocating machinery is identified in 4.3.6.

4.5.1.8 Excitation from Generators

Large transient torques are not expected during normal operation of a synchronous generator. However, several faults can occur that lead to the creation of a large torque pulsation over a brief time span. These faults can come from two distinct and different sources. The first source is a short circuit in the three phase lines with each other or to ground that produce a line-to-ground and line-to-line faults. The second fault source can be produced during the synchronization of the generator with the power grid. As with short circuits, the synchronization errors can be either three phase or single phase.

The existence of fault torques is well known. However, accurate prediction of fault conditions is difficult especially for extended periods of time following the fault. While the initial fault may be a single incidence, it can be followed by a cascading of events each making predictions more inaccurate and unreliable. H.S. Kirschbaum [8] 1945, developed a series of equations describing several fault conditions in a synchronous generator. The generator was considered an "ideal" synchronous machine. Other assumptions included a uniform air gap and symmetrical windings.

Examples of the torques produced for two of the fault conditions are plotted on Figures 4-40 and 4-41. Although the three-phase synchronizing torque has roughly the same peak torque level as the line-to-line short circuit torque, its components are of a single frequency (fundamental) and largely unidirectional. This applied torque will produce higher shaft stresses and thus more low cycle fatigue damage. Fortunately, these torque levels shown are for a synchronization error of 45°. With current technology, this is very conservative. Synchronization errors are expected to be less than 10° given today's electronic controls.

4.5.2 Transient Excitation

4.5.2.1 Asynchronous Starting Of Synchronous Motors

Synchronous motors are normally used for higher horsepower applications where their operation with leading or lagging or unity power factors are used to balance the power

factor in a plant. Probably the reason that they are not more widely applied is the fact that synchronous motors develop significant torsional oscillation from the moment they are energized until the field is applied and the motor is synchronized to the line frequency. While this starting cycle is very short, under 30 seconds, every time the motor is started the torsional excitation is so strong that the shafting material may yield when torsional resonance is excited by the motor. Fortunately, due to the large size of the motor, they are not started very frequently. After the initial commissioning of the plant, these large motors are usually started only a few times a year. It is possible to design systems driven by a synchronous motor for 1000 or more starts which may amount to 20 or more years of service. Starting a system once a week for 20 years would accumulate 1040 starts.

The torsional excitation developed by a synchronous motor will occur at two times the slip frequency when the motor operates in the asynchronous starting mode until the field is applied and the motor rotor is synchronized to line frequency. Slip frequency is the difference between the line frequency in the stator minus the rotational speed of the rotor. Thus at 0 rpm with the motor energized the slip frequency will be equal to line frequency and zero when the motor is synchronized. This means that the excitation frequency will be two times the line frequency when the motor is energized and reduce linearly with speed until the field is applied at which time the torsional oscillations disappear. Therefore the motor has the potential to excite torsional natural frequencies anywhere between 0 and 100 Hz for 50 Hz electrical systems and 0 to 120 Hz for 60 HZ electrical systems.

Synchronous motor drives are often used for high horsepower centrifugal compressor applications. Such systems normally are excited by torsional oscillations that occur at the motor for the 1st torsional natural frequency. Higher modes are normally not excited in such systems. Usually the 1st torsional natural frequency is 30 Hz or less for such a system. Therefore, excitation of the 1st torsional mode at 30 Hz will occur at 25% slip or 75% rated speed for a 60 Hz electrical system. The following equation will identify the motor speed at which torsional excitation could excite a torsional frequency when the system torsional natural frequencies and the line frequency are known.

$$N_{cr} = N_s \left(1 - \left(\frac{f_n}{2f_e} \right) \right) \quad (4-26)$$

where

N_{cr} = Motor rotational speed at which torsional resonance occurs, rpm,

N_s = Synchronized motor rotational speed, rpm,

f_n = Torsional natural frequency, Hz,

f_e = Electrical line frequency, Hz.

4.5.2.1.1 Solid Pole Synchronous Motors Versus Laminated Pole Variations in Torsional Excitation

Recent trends have been to use solid pole synchronous motors rather than laminated pole designs. This trend to smaller higher speed synchronous motors results in a cost reduction from the standpoint of equipment cost for the motor and associated gearing. However, this trend has unfortunately made the problem of torsional vibrations with synchronous motor drives more pronounced. Unfortunately mechanical stress limitations constrain laminated pole designs from operating speeds greater than those associated with 6-pole machines, that is 1200 rpm for a conventional 60 Hz electrical system. The pulsation magnitude in the air gap torque from a solid pole synchronous motor is significantly larger than that of a laminated pole design. The motor designer of a laminated design pole had many design liberties in the design of the amortiser windings of the synchronous motor poles but this is not the case for the solid pole design. Also the older designs that utilized slip rings had the ability to alter the design of the exciter discharge resistor. That magnitude of variation of the discharge resistor, is no longer an option with self excited solid state exciters. Therefore some of the older laminated pole designs could be manufactured so that the peak torque developed for a typical single body geared compressor train would not exceed 5 times rated torque. Unfortunately similar designs with solid pole synchronous motors made now easily reach 8 – 10 times rated torque. Reference [9] identifies a uniform method for calculating and measuring torque pulsations that occur during starting for synchronous motors.

4.5.2.1.2 Methods to Minimize Magnitudes of Transient Torsional Vibrations For Systems With Synchronous Motors

One of the more common methods to reduce the magnitude of transient torsional vibration is to introduce damping into the system. Elastomeric couplings are the item most often introduced into a system. Other methods would be to increase the rate of acceleration. Since a high rate of acceleration is desirable to either avoid accumulating multiple equal magnitude peak torque cycles or to minimize the magnitude of the peak torque by accelerating through resonance as quickly as possible, then anything that can be done to increase the rate of acceleration should be considered. One way to achieve this is to reduce the magnitude of the connected load on the motor during starting. With a compressor system this is accomplished by throttling the system to minimum flow, or decreasing the system pressure level. Reducing the connected load allows more of the air gap torque to be available to accelerate the system inertia to synchronous speed. Other methods have also been used to reduce torsional

vibrations. One method actually reduces the motor voltage so that the system passes through resonance with lower voltage then switches to a higher voltage to accelerate to synchronization. Such systems may be difficult to design. Even though the motor torque is proportional to the square of the voltage the actual torque may be reduced but the number of cycles at high torque may be increased per start. The pros and cons must be evaluated through a low cycle fatigue analysis of the system to see which design offers more service life. Also it may be difficult to design a system with a torsional frequency high enough so that the system can pass through a torsional resonance at a lower operating speed to make this concept more feasible.

4.5.2.2 Breaker Reclosures of Electric Motors

Breaker reclosure is a term used to describe the interruption and reapplication of electrical power to an induction electric motor. The discussion that follows pertains only to induction motors. It is not recommended to attempt reclosure of synchronous motors as reclosure transient torques have been reported to be as high as 30 – 40 times rated torque (Reference [12]). Breaker reclosure can occur when the electric power supply is interrupted by faults in the power system such as lightening during thunder storms, faults in transformers or switching power on the electric power supply grid. These interruptions of electric power supply can, if the conditions are correct, develop high levels of instantaneous transient torques. These torques can be as high as 15 – 20 times (Reference [10] and [11]) the rated torque of the electric motor if the duration of the interruptions and the load characteristics of the driven equipment occur to maximize the transient torque. Reclosure torques are often reverse in direction. Observing reverse failures in keys, coupling hubs, etc. can be a tell-tale symptoms pointing to damage caused by excessive torque caused by a breaker reclosure.

When the power is removed from an induction motor a residual magnetic flux remains within the motor. The period of time that it takes to reduce the residual motor voltage to 36.8% of rated voltage is referred to as the motor open circuit time constant (Reference [10]). As a result of this residual flux the motor will self generate a terminal voltage that will rotate with the motor rotor. The generated frequency will be equal to the ratio of (instantaneous motor speed divided by the rated motor speed) times line frequency. Therefore, if power is reapplied prior to decay of the self generated voltage, the reapplied voltage will have frequency components of the self generated voltage and line voltage. As a result of this broad frequency spectrum there is significant potential of exciting a torsional natural frequency, especially torsional natural frequencies below line frequency. As the voltage reduces with the motor speed, there is a phase shift between the self generated voltage and the line frequency. If the power is reapplied to the motor prior to the

decay of the residual voltage, the effective voltage seen by the motor is the vector sum of the residual voltage magnitude and the reapplied line voltage with the associated phase angle between the residual voltage and the line voltage. In the worst case the residual voltage may not have decayed below rated voltage and be 180 degrees out of phase with the line voltage. If the electrical power is reapplied to the motor under the condition where the residual voltage is the rated motor voltage and 180 degrees out of phase with the line voltage the effective voltage seen by the motor is 200% of the rated voltage. Since the motor torque is proportional to the square of the applied voltage, the motor is capable of developing 400% rated torque. However, when the motor is deenergized, the driver and driven equipment decelerate. The rate of deceleration is a function of the level of power absorbed by the driven equipment and the amount of stored energy in the rotating inertia of the equipment train. If the motor is reenergized after a time duration and the rate of deceleration during this time has been such that the speed of the motor is at a location where the motor torque is a maximum on its speed torque curve, then when the motor is reenergized, the motor will develop a torque upon restarting that is the maximum shown on the speed torque curve if the effective motor voltage is identical to the voltage upon which the speed torque curve was created. However, during a breaker reclosure the effective voltage can be much higher than normal starting voltage. If the condition of the residual voltage is equal to the line voltage and 180 degrees out of phase with the line voltage, and the equipment has slowed to a point where the starting torque of the motor would normally be 200% – 250% of rated torque, then the torque developed by the motor during reapplication of electrical power could be 8 – 10 times the rated torque. Any torsional resonance in the system could amplify this magnitude. Torsional resonance can account for transient torques that exceed the potential torque of 8 – 10 times the motor rated torque. Torques of this magnitude will create stress in the power transmission components, such as shafting, couplings, gearing etc. that can plastically deform components or exceed the ultimate strength of the material in these components and cause failure (Reference [10]).

The protection recommended by motor manufacturers is to avoid the reapplication of power until the residual voltage is 25% – 30% of the motor rated voltage (Reference [13]). NEMA Standard MG1 includes developed recommendations for breaker reclosure (Reference [14]). As a practical rule motor vendors recommend the voltage should not be reapplied until a period of two open circuit time constants has elapsed between the time when the power is interrupted and the power is reapplied.

It should also be also mentioned that any capacitors at the motor terminals used for power factor correction will increase the value of the open circuit time constant. The motor vendor should be advised of any capacitors in the motor circuit.

4.5.2.3 Faults of Electric Motors and Generators

Torsional natural frequencies of systems with motors and generators can be excited by steady state unbalanced phase loading or by transient fault conditions due to phase shorts.

Transient torsional excitation can be created by short circuit conditions described as:

- a. A three-phase short circuit is a short between all three phases of a three phase motor or generator that will develop a maximum electromagnetic torque at electrical line frequency.
- b. A two-phase short circuit is a short between any two of the three phases of a three phase motor or generator. This short will develop excitation at electrical line frequency and twice line frequency.
- c. A single phase to ground short circuit is a short between any one of the three phases of a three phase motor or generator directly to ground. This short will develop excitation at electrical line frequency and twice line frequency
- d. A two phase to ground short circuit is a short between any two of the three phases of a three phase motor or generator directly to ground. This short will develop excitation at electrical line frequency and twice line frequency.

Steady state torsional excitation due to unbalanced electrical loads can occur if the individual phase loads of a three phase motor or generator are not balanced. The usual cause is the addition of a single phase load addition to a balanced three phase load. This condition results in a steady state excitation at twice line frequency.

The above fault conditions are rarely analyzed for motor drives. The electrical switch gear must detect such faults so rapidly so as not to endanger the motor or connected machinery, however as a precaution it is prudent to avoid system torsional natural frequencies at one and two times electrical line frequencies.

4.5.2.4 Synchronization of Generators

Large transient torsional excitations can occur if the frequency and phase of the generator is not properly synchronized when it is are connected to the existing grid. Electrical switch gear is provided for generators to avoid improper synchronization to the line.

4.5.3 References

1. J. C. Wachel and Fred R. Szenasi, "Analysis of Torsional Vibrations in Rotating Machinery," 22nd Turbomachinery Symposium Proceedings, 1993 Pages 127 – 151.
2. Mark A. Corbo and Stanley B. Malanoski, "Practical Design against Torsional Vibrations," 25th Turbomachinery Symposium Proceedings, 1996 Pages 189 – 223.

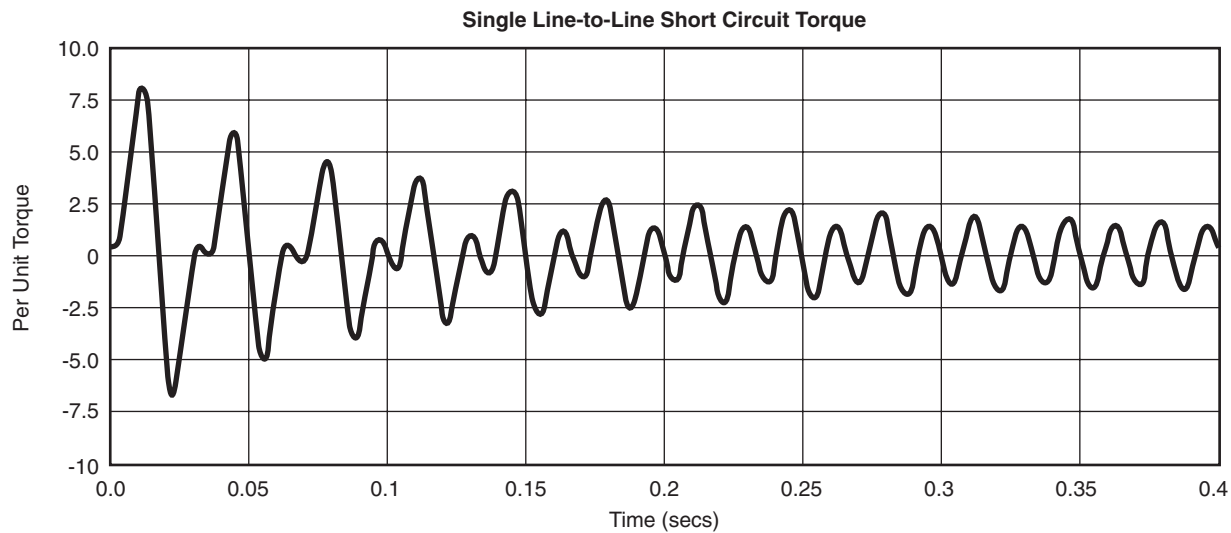


Figure 4-40—Transient Torque Associated with a Single Line to Line to Line Fault

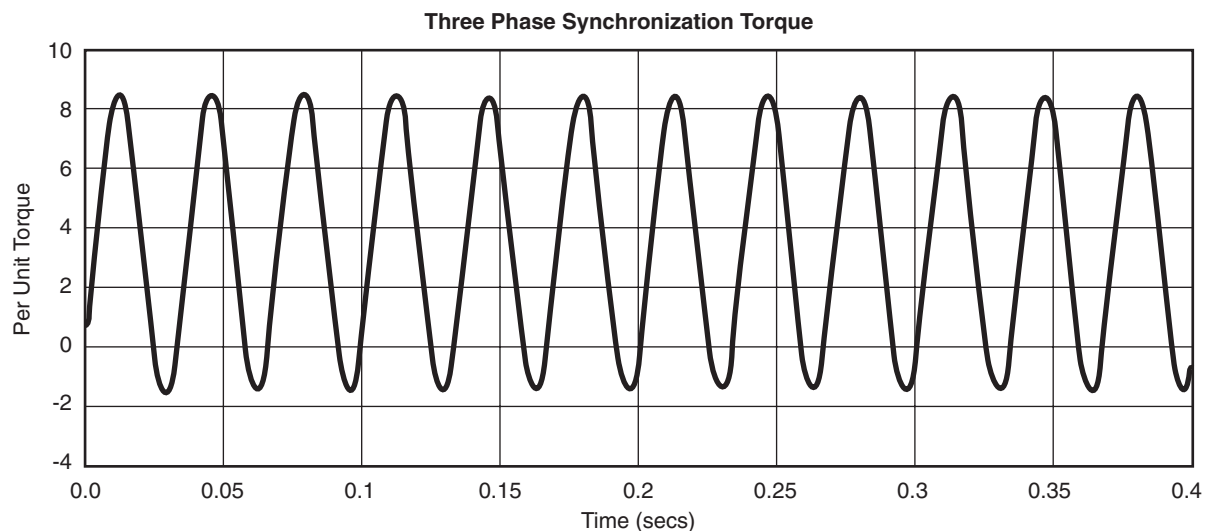


Figure 4-41—High Cycle Fatigue for Continuous Excitation Sources

3. Lucien Terens and Andrej Grgic, "Applying Variable Speed Drives with Static Frequency Converters to Turbomachinery," 25th Turbomachinery Symposium Proceedings, September 17–19, 1996 Pages 35–46.

4. David J. Sheppard, "Torsional Vibration Resulting from Adjustable-Frequency AC Drives," IEEE Transactions on Industry Applications, Volume 24, No. 5, September/October 1988.

5. James Hudson, "Lateral Vibration Created by Torsional Coupling of a Centrifugal Compressor System Driven by a Current Source Drive for a Variable Speed Induction Motor,"

21st Turbomachinery Symposium Proceedings, September 28–October 1, 1992 Pages 113–124.

6. Harley Tripp, Don Kim and Robert Whitney, "A Comprehensive Cause Analysis of a Coupling Failure Induced by Torsional Oscillations in a Variable Speed Motor," 22nd Turbomachinery Symposium Proceedings, September 14–16, 1993 Pages 17–24.

7. James Hudson, "Selection, Design, and Field Testing of a 10,500 Horsepower Variable Speed Induction Motor Compressor Drive," 25th Turbomachinery Symposium Proceedings, September 17–19, 1996 Pages 25–34.

8. Kirschbaum, H. S., "Transient Electrical Torques of Turbine Generators During Short Circuits and Synchronizing," *Electrical Engineering Transactions*, Vol 64, February 1945, pps 65 – 70.
9. IEEE Standard 1255-2000, *Guide for the Evaluation of Torque Pulsations During Starting of Synchronous Motors*.
10. Bob Brozek, "Induction motor open circuit time constant," General Dynamics Publication.
11. Gerald Mruk and John Halloran, "Torques due to electrical reclosures for induction motor driven centrifugal compressors", *Vibration Institute Proceedings, Twelfth Annual Meeting*, May 25 – 27, 1988.
12. J.C. Das, "Effects of Momentary Voltage dips on the Operation of Induction and Synchronous Motors," *IEEE Transactions on Industry Applications* Volume 26 Number 4 July/ August 1990.
13. Roger H. Daugherty, "Bus Transfer of AC Induction Motors, A Perspective," IEEE paper number PCIC-89-07.
14. G.W. Bottrell, "Fast Bus-Transfer Techniques for Maintaining Full Plant Protection," IEEE Paper number PCIC-89-08.

4.6 FATIGUE ANALYSIS

4.6.1 High Cycle Fatigue for Continuous Excitation Sources

If the undamped torsional natural frequency analysis indicates an interference between an undamped torsional natural frequency and a shaft rotative speed or other potential excitation mechanism, and the train design cannot be altered sufficiently to remove the resonant interference, then a damped torsional response and vibratory stress analysis must be performed to ensure that rotor shafts and couplings are not overstressed. Potential areas of vibratory stress concentrations are couplings and shaft ends. Results generated from the damped torsional response and vibratory stress analysis may indicate that shaft ends must be re-sized to safely accommodate the high levels of vibratory stress resulting from operation close to a torsional natural frequency. Figure 4-42 displays a typical plot of calculated oscillatory stresses versus the reference frequency (low speed shaft). The two peaks present in this plot indicate excitation of the first and second train torsional natural frequencies by 1 and 2 times operating speed torque pulsations, respectively.

Calculated stresses will be governed by assumptions regarding the level of available torsional damping as well as overall expected torque excitation levels at given frequencies.

These key parameters are normally set by mutual consent of both the purchaser and the vendor and are based on experience, measurement, and/or published literature. A comprehensive reference on torsional fatigue can be found in Reference [1]. Reference [2] discusses the calculation of shaft stress, stress concentrations and material fatigue stress limitation guidelines applicable to high cycle fatigue. Reference [3] also discusses shaft stress and presents the results of calculations on a Goodman diagram.

4.6.2 Low Cycle Fatigue for Transient Excitation

The discussion in 4.4.2 relates to the steady state forced synchronous torsional response analysis. In some instances, it becomes necessary to analyze the time-transient characteristics of the system torsional response, requiring a more elaborate computer code. A transient torsional analysis is generally accomplished with a system model that is a reduced version of the model used to calculate the torsional undamped natural frequencies. The reduced model of the system is used to minimize the computer time required to perform the numerical solution of the torsional equations of motion during unit transient events such as start up and fault conditions. The frequency and the mode shapes resulting from the system model of reduced scope should be compared to the full model results prior to proceeding with the transient analysis. Usually the reduction in model scope does not adversely affect the results. With the case of a synchronous motor drive or other motor driven systems, where the transient excitation is the result of an electrical excitation originating in the motor, the first mode is usually the only significant model excited.

A transient analysis is often required for the following cases:

- a. A synchronous motor/generator that undergoes an asynchronous start-up.
- b. A synchronous or induction motor that experiences a short-circuit transient fault condition or a synchronizing and/or switching transient (single/multiple reclosure).
- c. A variable speed motor drive.

Variable speed motor drives may require a transient torsional analysis because some variable frequency drive designs may result in high-level transient torque pulsations at the beginning of the unit start.

Machinery trains with synchronous motor drivers that undergo asynchronous unit starts require a transient torsional analysis to determine train response during unit start. This time-transient analysis, for the full period of train acceleration to normal running speed (synchronizing speed), is normally calculated for both full and reduced synchronous motor terminal voltage unless a complete electrical supply system and electrical motor circuit model is used. Figure 4-43 presents a typical plot from a transient torsional analysis.

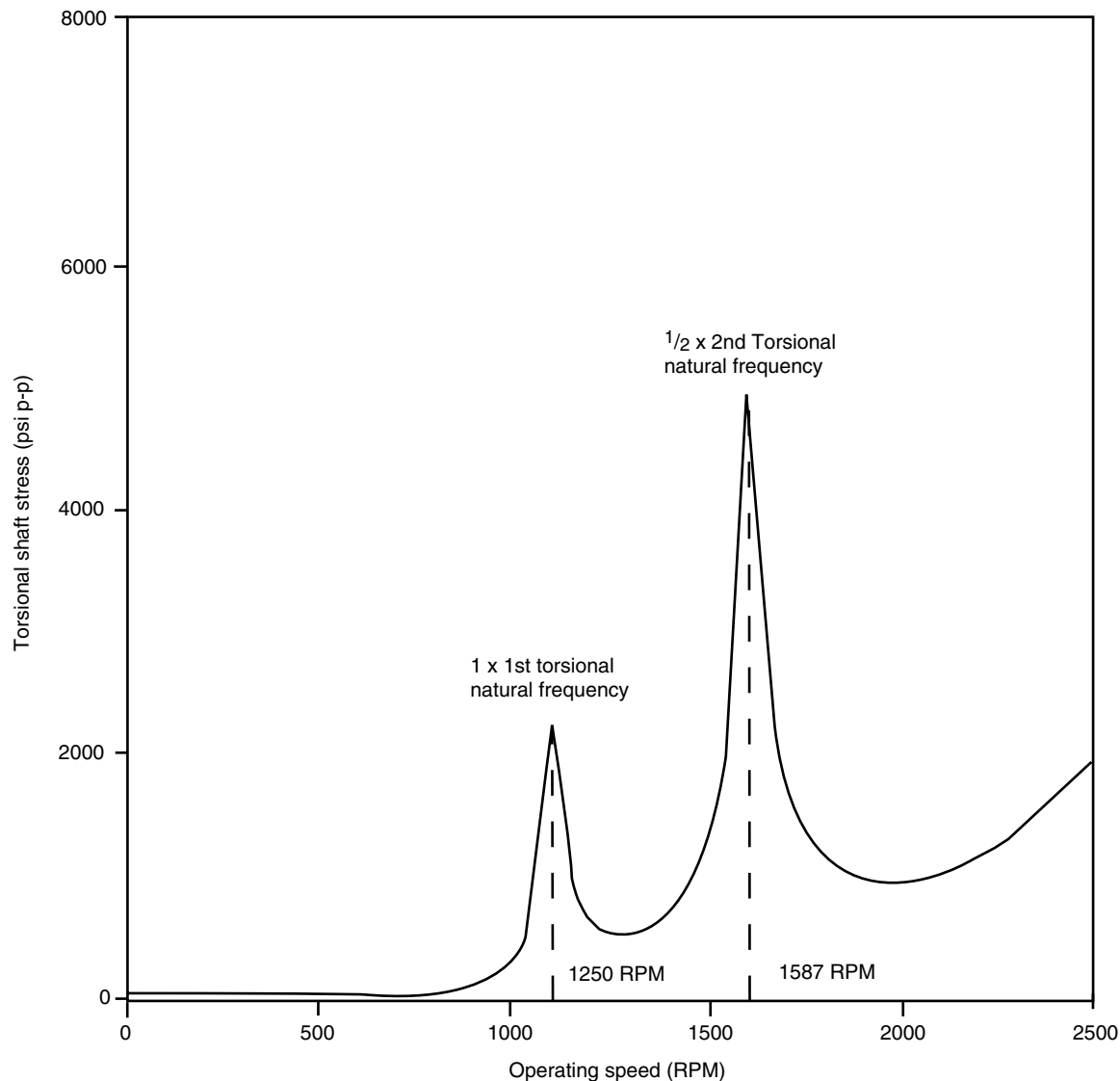


Figure 4-42—Plot of a Shaft Operating Stress as a Function of Shaft Operating Speed

Since the pulsating component of synchronous motor torque changes linearly in frequency from 2 times electric line frequency at 0% speed to 0 Hertz at 100% speed, and achieves a maximum amplitude at approximately 80% – 95% speed (Figure 4-38), all system torsional natural frequencies will be excited below 120 Hz for 60-Hertz AC or 100 Hz for 50-Hertz systems. Typically, amplification of the second and higher modes is minimal and not of any great concern. The primary concern is the degree of amplification of the motor pulsating torque component upon traversal of the system fundamental (first) torsional mode. Preferably, judicious component selection early in a design project will allow adequate sizing to account for the transients torques that will be developed by the system. When transient vibration characteristics are problematic, special couplings such as elastomeric cou-

plings and other damper or isolator couplings, may be used to reduce the transient torque pulsations.

Transient analysis of synchronous motor driven systems is more important in today's environment where 4-pole synchronous motors are often applied. The 4-pole design are usually solid pole as opposed to the laminated pole designs used on 6-pole synchronous motors. The laminated pole design offers the motor designer the opportunity to modify the pole design to minimize oscillating motor torque, an option that is not available when solid pole construction is used. Figure 4-44 is a speed torque curve for a laminated pole design.

A representative speed-torque curve for a solid pole motor is presented in Figure 4-45.

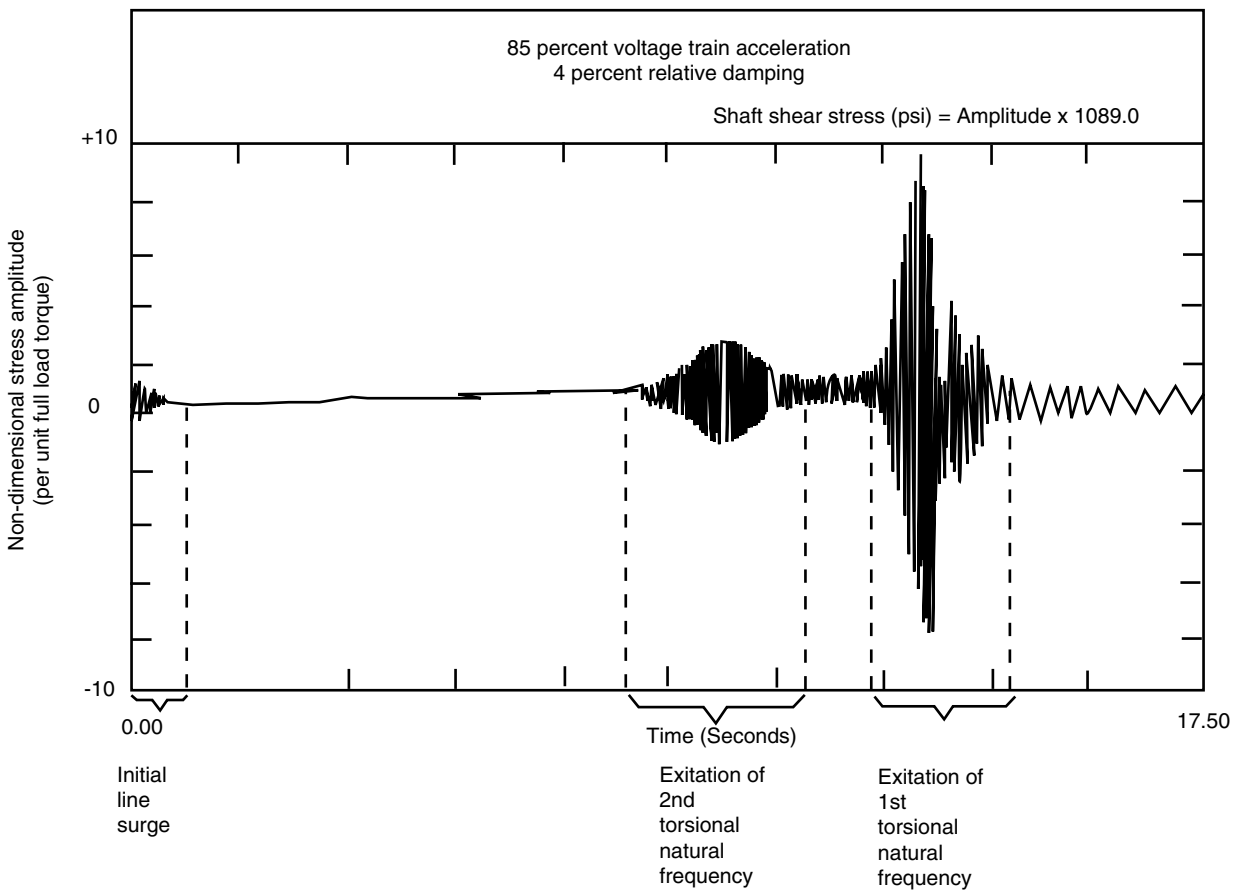


Figure 4-43—Transient Torsional Simulation of a Synchronous Motor-Driven Compressor Train

The principal results of the transient torsional analysis are given in terms of the following:

- Maximum vibratory torque response in shafting.
- Maximum alternating shear stress in shafting.

Maximum oscillating torque for a synchronous motor can be as high as 1.0 – 1.5 times full load torque. Also, when a train torsional natural frequency is traversed during startup the maximum oscillating torque encountered by shaft ends can be as high as 5 – 10 times the full load torque. Such levels of torque may mandate the use of larger couplings, larger shafting and increased torque capacity gearing than would otherwise be required. Care should be exercised in the use of non keyed coupling attachments to avoid slippage of coupling(s) during periods of high transient torque.

Although the calculated peak torque response levels on unit starts can be below the design limits for the train components, it is sometimes necessary to calculate the life of the components relative to low-cycle fatigue life to ensure the design integrity of the installation. For this analysis, the areas

of highest stress, typically the machinery shaft ends and coupling spacer components are investigated.

The basic concept of a fatigue life calculation is that each cycle of a torque signature dissipates a finite amount of the usable life of the shaft. Therefore, by counting the number and magnitude of stress cycles occurring at each torque level, the cumulative damage of each torque signature can be measured. This method of damage assessment calculates the expected number of complete torque signatures, that is the number of starts for the train, prior to the onset of fatigue failure.

If the calculated maximum number of train starts predicted by fatigue calculations is exceeded by an estimate of the expected number of number of train starts over the expected life of the train components, then this number represents a mechanical design constraint that may require redesign of some system components.

Refer to Reference [2] for a description of the low cycle fatigue analysis that uses the concepts of elastic plastic design for low cycle fatigue where stresses exceed the infinite fatigue life limits or even exceed the yield strength of the material.

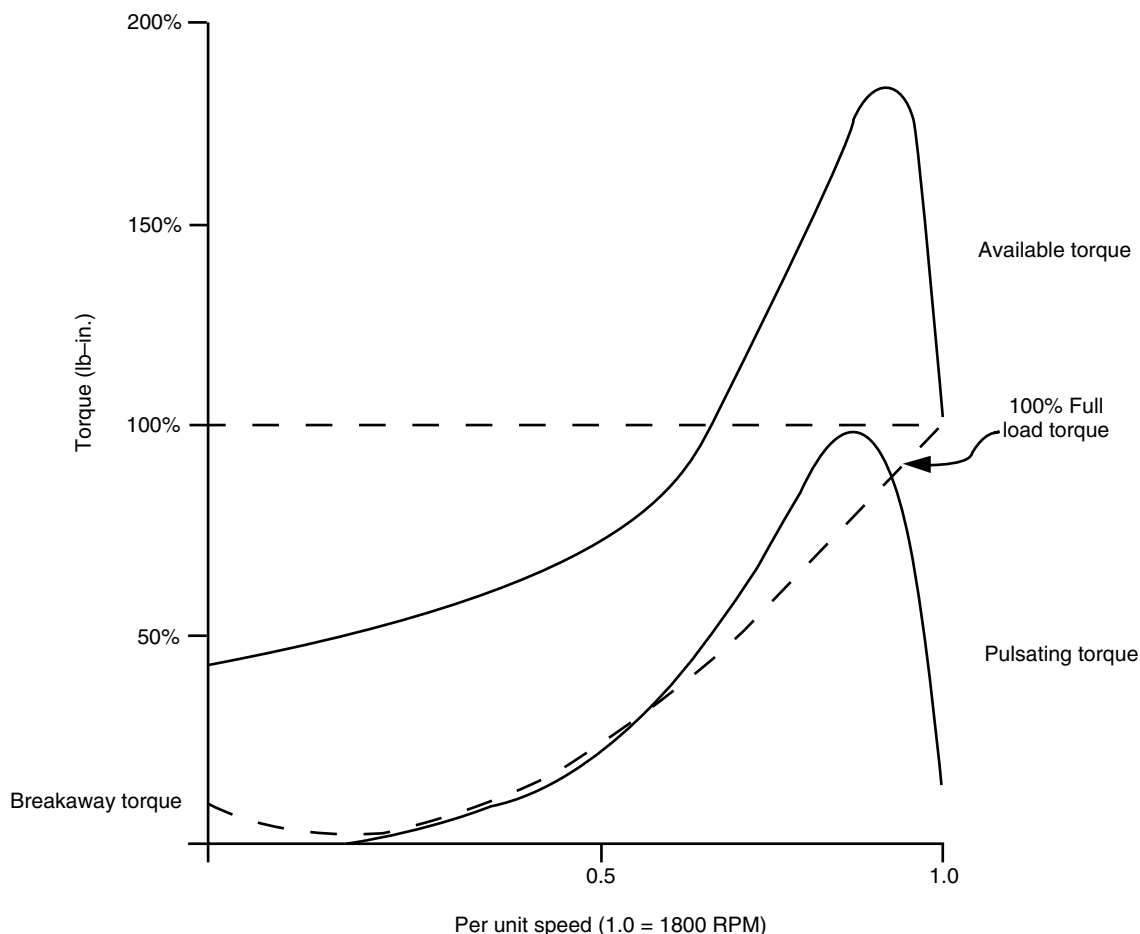


Figure 4-44—Typical Speed Torque Curve for a Synchronous Motor with Laminated Pole Construction

4.6.3 References

1. Stuart H. Loewenthal, Lewis Research Center, Cleveland, Ohio. "Design of Power Transmitting Shafts," NASA Reference Publication 1123 1984.
2. J. C. Wachel and Fred R. Szenasi, "Analysis of Torsional Vibrations in Rotating Machinery," 22nd Turbomachinery Symposium Proceedings, 1993 Pages 127 – 151.
3. Mark A. Corbo and Clifford P. Cook, "Torsional Vibration Analysis of Synchronous Motor Driven Turbomachinery," 29th Turbomachinery Symposium Proceedings, September 18 – 21, 2000 Pages 161 – 176.

4.7 CONTENTS OF A TORSIONAL REPORT

4.7.1 Reports For Systems That Do Not Have Conflicts With Operating Conditions And Torsional Frequencies

The report should contain data that describes the type of machinery being analyzed. Reference information that will enable the reader to determine the origin of the data used to

model the system such as coupling drawing numbers and revisions, driver mass elastic drawing number and revision, gear mass elastic drawing number, if applicable, with drawing number and revision and driven equipment reference data must be included. The report should contain a sketch of the equipment train. The report should contain a summary of the natural frequencies calculated for the system. The summary should include all the frequencies from 0 CPM through 125% of the highest rotor speed or two times the electrical line frequency whichever is greater. The report should contain a Campbell Diagram that includes the calculated natural frequency and lines that identify the speed range from 0 rpm to trip speed of all the rotors in the system. The diagram will show all known torsional excitations for the system being analyzed. The plot will identify the operating speed range of the equipment. In the event that none of the system natural frequencies conflicts with the equipment operating speed range then a statement shall be made that no conflicts exist between the torsional frequencies and the equipment operating speed range and known excitations.

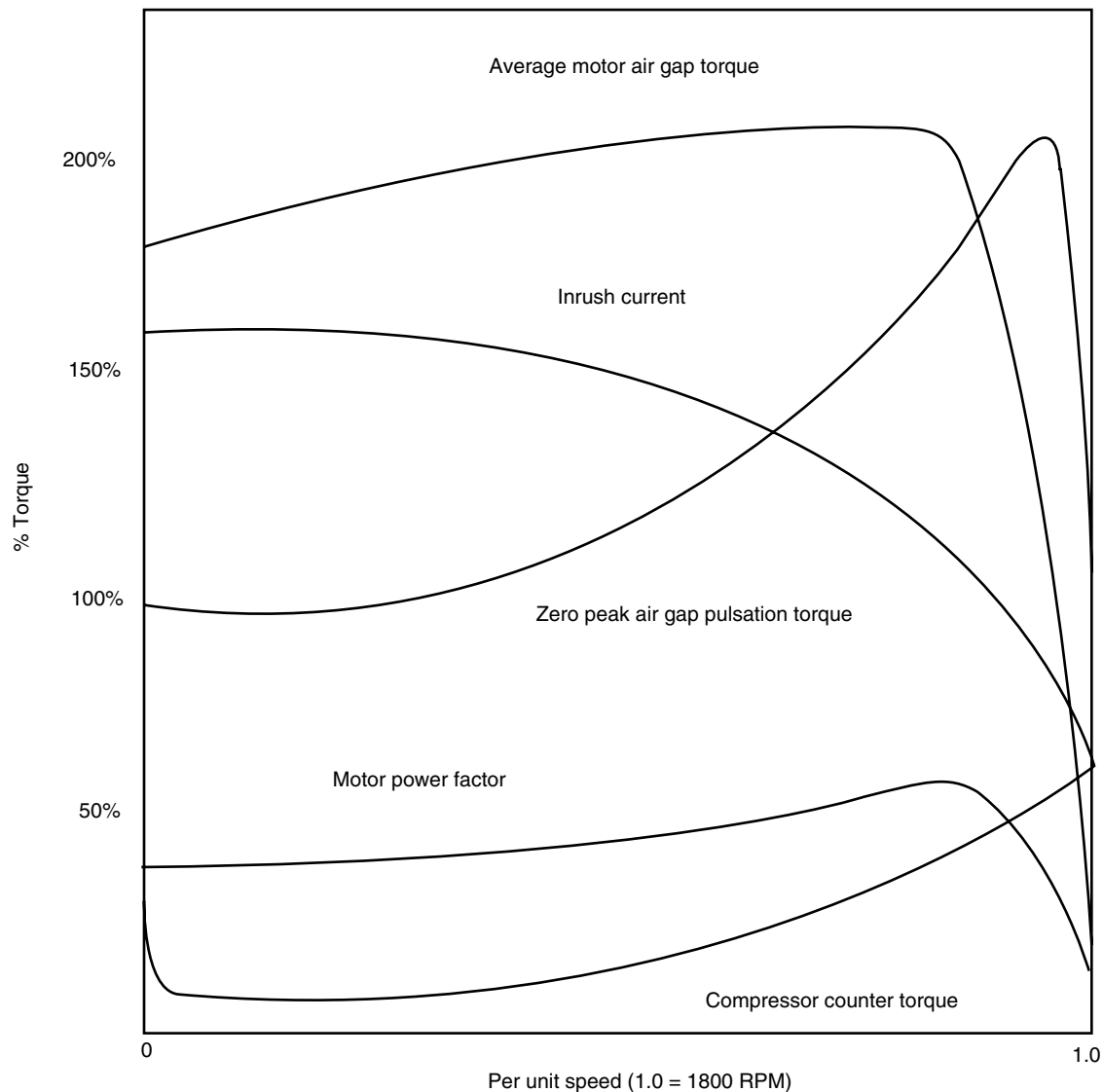


Figure 4-45—Typical Speed Torque Curve for a Synchronous Motor with Solid Pole Construction

4.7.2 Reports for Systems That Do Have Conflicts with Operating Conditions And Torsional Frequencies

In the event that a system torsional natural frequency, which can not be detuned, does not have the required separation between a known excitation or operating speed range the following shall be performed in addition to the requirements of 4.7.1.

a. When the modal displacement is distributed throughout the entire system then a response analysis shall be conducted with the known excitation applied at the source of origin within the equipment train. If a source of excitation can not be defined or the excitation is defined to be less than 2% of

rated torque then a response analysis is not required. The response of the system shall be identified throughout the system. A fatigue analysis, similar to that identified in 4.6.1 shall be conducted to verify the suitability of the design. The report shall contain the results of the response analysis and any fatigue calculations performed.

b. For the torsional natural frequency where the model displacement is distributed within one item of equipment within a system, then an investigation must be done to determine if that piece of equipment can develop an excitation at the natural frequency where a conflict exists. If no such excitation can be identified, no further investigation is required. The report shall state the degree to which this was investigated.

4.7.3 Reports for Systems That Have Transient Phenomena

For systems that have known torsional excitation which can excite a system torsional frequency in a transient manner, such as the start up of synchronous motor driven trains, or where fault conditions such as short circuit conditions for electric motors or breaker reclosure of electric motors, a transient analysis shall be conducted. The report shall contain a definition how the mechanical system is modeled and a description of the excitation mechanism and how its magnitude and frequency is determined. If the excitations are less than 2% of rated torque, such as might occur with a system driven by a variable speed drive, an analysis similar to that described in 4.7.2 may be conducted. If the analysis determines that the system response to excitation is unsuitable based on a high cycle fatigue analysis (see 4.6.1), then a more complex transient analysis shall be conducted to determine the stress history over a 20 year equipment life. The report shall contain a description of how the excitation was determined for the system and the various factors used in the analysis. Refer to 4.6.2 for details of a low cycle fatigue analysis.

4.8 FIELD TESTING TO DETERMINE TORSIONAL RESPONSE

4.8.1 Testing for Torsional Natural Frequencies

The exact location of an assembled train's torsional natural frequencies may be determined during start-ups through torsional testing. Occasionally torsional testing is performed when calculations indicate interference between a torsional natural frequency and an operating speed or some other potential torsional vibration problem. Testing for train torsional natural frequencies may be accomplished by measuring the torque transmitted through a shaft section or by measuring the absolute value of angular vibrations at a specific location. A torsiograph is an instrument that is used to measure the relative angular displacement between two points on a train. The relative angular displacement between two closely spaced points on a rotating element is directly proportional to the torque transmitted by the shaft section between the two points. A torsiograph or other torque-measuring devices should be placed, when possible, in areas of the train where the oscillating torques will be amplified for all torsional modes of concern. It may not be possible to select one location that is suitable to detect all torsional modes. The location must be accessible, such as a coupling or shaft end. The relative amplitude of the oscillating torques for each torsional mode of concern may be determined at any axial location by evaluating the slope of the undamped train torsional mode shapes.

Alternately, absolute torsional vibration displacements may be indirectly measured by attaching a ring with many equally sized, equally spaced optical or electrical (for exam-

ple, notches) targets to one of the rotating elements in the train. An optical pick-up or displacement probe monitoring the target surface then generates many discrete electrical pulses during each shaft revolution. If significant torsional vibrations occur at the target ring, then the electrical pulses generated by the keyphasor probe will not be evenly spaced. Signal processing equipment converts the uneven pulse spacing into torsional (angular) displacements. The target rings should not be placed (if possible) near torsional node points for torsional modes of concern. Note that gear teeth might provide an adequate set of electrical targets for a noncontacting displacement probe as long as the gear mesh is not a node for the torsional mode(s) in question.

4.8.2 Field Measurements Methods

4.8.2.1 Testing Using Strain Gage Measurement

A strain gage bridge can be mounted on the shaft or more typically on the coupling spool piece. The strain gage will measure the strain in the shaft for a given torque load. If the rotor system is operating at constant torque load, the output from the strain gage will remain at a constant value. If a torsional forcing function is manifest on the rotor system, the rotor system will respond with instantaneous torque changes at the frequency of the torsional forcing function. The magnitude of the change in strain energy is dependent upon the magnitude of the forcing function and the torsional spring rate of the rotor system. If the frequency of the torsional forcing function is close to a torsional natural resonance (particularly the first mode), large and potentially destructive torque oscillations can occur.

The output signal from the strain gauge can be measured in one of two ways:

1. A slip ring assembly can be mounted on the rotor and a signal cable can be attached to an appropriate data acquisition system. Slip ring applications are limited by the rotating speed of the rotor. Typical applications are for machine speeds less than 5000 rpm. They are also prone to wear. Therefore, they are limited life devices, suitable for short term testing.
2. Another and more permanent technique is the use of wireless telemetry to transmit the output signal to a receiver and the data acquisition system. The telemetry circuits can be bonded directly to the rotor with fiberglass laminations. A stationary device can transmit power to the telemetry circuit by electrical inductive coupling. This approach provides a long term measurement installation.

4.8.2.2 Torsional Displacement Measurement

A measurement of torsional oscillations in degrees peak to peak can also be made using the following methods:

A precision manufactured toothed wheel can be mounted on the coupling spool piece or a free end of the rotor if

available. The number of teeth on the wheel will determine the resolution of the measurement. Typically the minimum number of teeth required for an accurate measurement is 60 teeth. Two proximity probes observing the teeth on the wheel and mounted 180 degrees apart must be utilized for this measurement. Two probes are necessary to cancel out any radial vibration of the toothed wheel. The output from the probes will be a series of voltage pulses as the teeth pass by the probe tips. If there is constant torque and constant angular velocity, the frequency will be the tooth passing frequency. If torsional oscillations begin to occur, this frequency will be modulated. Refer to Figure 4-46. Suitable instrumentation can be used to detect this modulation, yielding torsional velocity. This signal can be integrated to yield torsional displacement in degrees peak to peak at the frequency of the torsional oscillations.

Infrared or laser transducers can also be used by observing an epoxy bonded tape wrapped around a coupling spool piece. The tape has a photo etched pattern (bar code) that simulates a toothed wheel. The same measurement process is used as described with the toothed wheel.

The accuracy and resolution of a torsional displacement measurement depends to a large degree on the manufacturing accuracy of the mechanical measurement media. For example, if a proximity probe/gear or laser/tape media are selected, the following calculations must be made.

Example:

Assume a 6-in. diameter gear or tape with 60 gear teeth or 60 tape bars is to be utilized.

- Circumference = $6 \times 3.1416 = 18.85$ in.
- Gear or bar spacing = $18.85 / 60 = 0.3142$ in. (this the spacing from the leading edge of a tooth or bar to the leading edge of the next tooth or bar)
- Degree spacing = $18.85 / 360 = 0.0526$ in./degree
- For torsional applications, a resolution to 0.1 degrees pp is required. Therefore, the required accuracy to manufacture the gear teeth or bar spacing is:
- Spacing accuracy = $0.0526 \times 0.10 = 0.00526$ in. or 5.26 mils.

Note: Gear teeth should be manufactured as straight cut parallel sided teeth; i.e. no gear profile.

- Figures 4-47 and 4-48 are typical installation examples.

4.8.2.3 Measurement Of Synchronous Motor Air Gap Torque

This test technique is not a measurement of torsional vibration, but rather a measurement of the excitation mechanism that drives the torsional vibration. Section 4.5.2.1 describes the excitation developed by a synchronous motor. This paragraph will describe test methods used to measure this excita-

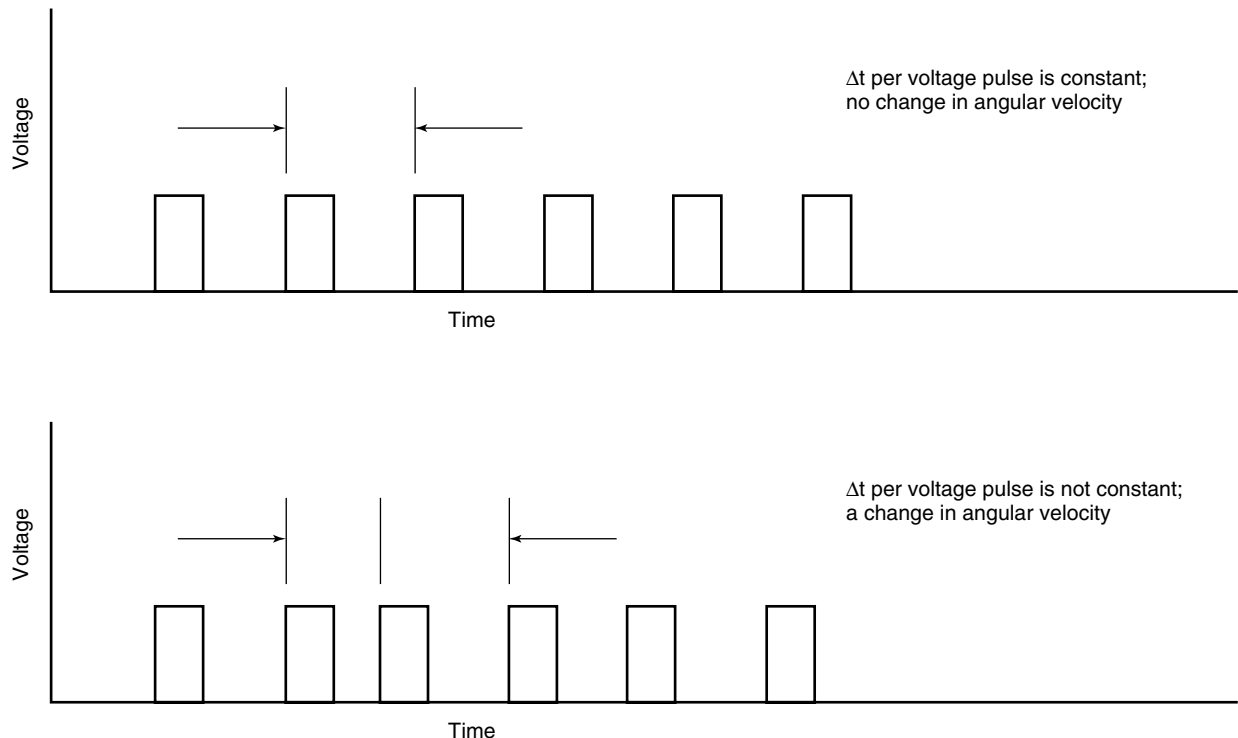


Figure 4-46—Displacement Measurement Considerations

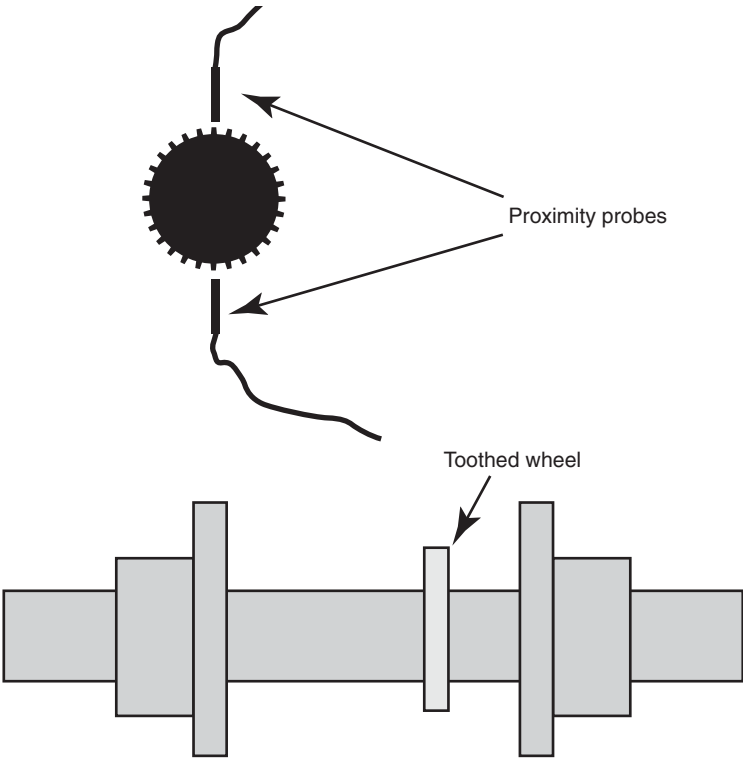


Figure 4-47—Torsional Measurements Using a Toothed Wheel and Sensors

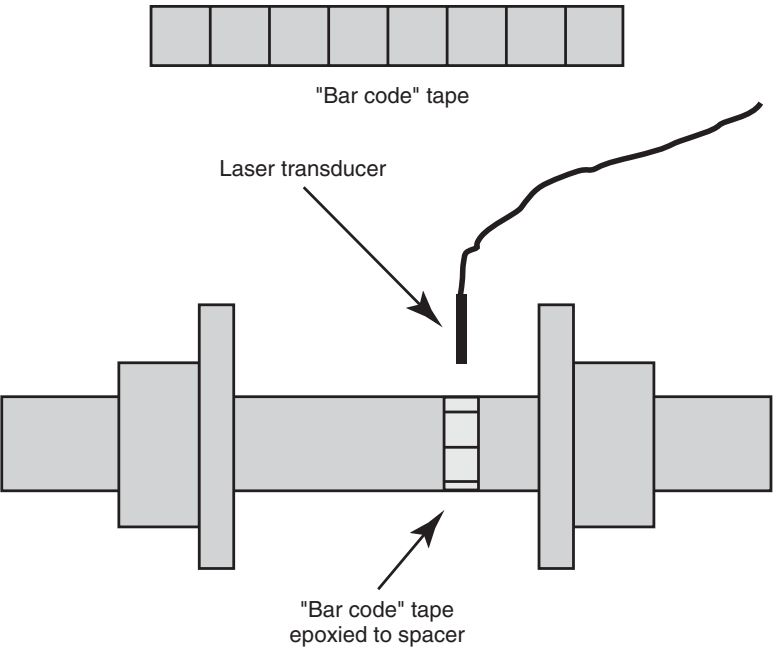


Figure 4-48—Torsional Vibration Measurements with a Laser

tion. Since the magnitude of torsional excitation is strongly dependant on actual motor terminal voltage the verification of the magnitude of the excitation should be seriously considered if a decision is made to measure the magnitude of the system torque during resonance. This technique can also be used on a shop floor motor test to verify the prediction of the torsional excitation of a synchronous motor.

If the motor terminal voltage and motor current at the motor terminals are accurately measured with precision current and potential transformers and these inputs fed into a Hall effect watt transducer the electrical power to the motor can be easily measured. The accuracy of these measurements are obviously dependant upon the accuracy of the measurement instruments. Due to the high efficiency of electric motors the measured air gap power at the motor terminal will be converted to 96% – 98% of the actual rotor torque. The trace from the watt transducer will not only identify the magnitude of the air gap torque but the frequency and variation in the magnitude of this torque as well. Reference [1] identifies a uniform method for calculating and measuring torque pulsations that occur during starting for synchronous motors.

4.8.2.4 References

1. IEEE Standard 1255-2000, *Guide for the Evaluation of Torque Pulsations During Starting of Synchronous Motors*.

4.9 TORSIONAL–LATERAL VIBRATION COUPLING

If the torsional vibration in a geared system is large enough, the torsional vibration may create lateral vibration in parts of the system. The vibration is usually non synchronous in nature. The reverse condition of the lateral vibration causing torsional vibration has not been documented. The lateral vibration usually occurs in the lightest gear element, the pinion. The lateral vibration of the pinion is created by non uniform torque transmitted through the gear. The torque is resolved into tangential, radial and axial forces at the gear mesh. It is the non-synchronous forces, when superimposed upon the gear reaction forces associated with the mean torque load, that create the vibration. The phenomenon of torsional lateral coupling has been documented in References [1] through [3]. These forces may be transient, as with torsional vibration associated with the starting of a synchronous motor, or transients developed during operation (Reference [3]), or continuous excitation created by a variable speed drive (References [1] and [2]). The spectrum of the vibration can provide information as to the source of the problem, Reference [1].

4.9.1 References

1. James Hudson, “Lateral Vibration Created by Torsional Coupling of a Centrifugal Compressor System Driven by a Cur-

rent Source Drive for a Variable Speed Induction Motor,” 21st Turbomachinery Symposium Proceedings, 1992, pp. 113 – 124.

2. Harley Tripp, Don Kim and Robert Whitney, “A Comprehensive Cause Analysis of a Coupling Failure Induced by Torsional Oscillations in a Variable Speed Motor,” 22nd Turbomachinery Symposium Proceedings, 1993, pp. 17 – 24.

3. Martin L. Leonhard, Ulrich Kern and Klaus Reischl, “Electric Power Supply Instabilities Exciting Torsional and Lateral Vibrations of an Integrally Geared Turbocompressor”, 30th Turbomachinery Symposium Proceedings, 2001, pp. 49 – 55.

4.10 API DOCUMENT PARAGRAPHS ON TORSIONAL VIBRATION

4.10.1 Standard Paragraphs from R22

Torsional Analysis

- **SP6.8.6.1** For motor-driven units and units including gears, units comprising three or more coupled machines (excluding any gears), or when specified, the vendor having unit responsibility shall ensure that a torsional vibration analysis of the complete coupled train is carried out and shall be responsible for directing any modifications necessary to meet the requirements of SP6.8.6.2.through SP6.8.6.6.

SP6.8.6.2 Excitation of torsional natural frequencies may come from many sources which may or may not be a function of running speed and should be considered in the analysis. These sources shall include but are not limited to the following:

- a. Gear characteristics such as unbalance, pitch line runout, and cumulative pitch error.
- b. Cyclic process impulses.
- c. Torsional transients such as start-up of synchronous electric motors and generator phase-to-phase or phase-to-ground faults.
- d. Torsional excitation resulting from electric motors, reciprocating engines, and rotary type positive displacement machines.
- e. Control loop resonances from hydraulic, electronic governors, and variable frequency drives
- f. One and two times line frequency
- g. Running speed or speeds.
- h. Harmonic frequencies from variable frequency drives.

SP6.8.6.3 The torsional natural frequencies of the complete train shall be at least 10% above or 10% below any possible excitation frequency within the specified operating speed range (from minimum to maximum continuous speed).

SP6.8.6.4 Torsional natural frequencies at two or more times running speeds shall preferably be avoided or, in systems in which corresponding excitation frequencies occur, shall be shown to have no adverse effect.

SP6.8.6.5 When torsional resonances are calculated to fall within the margin specified in SP6.8.6.3 (and the purchaser and the vendor have agreed that all efforts to remove the critical from within the limiting frequency range have been exhausted), a stress analysis shall be performed to demonstrate that the resonances have no adverse effect on the complete train. The assumptions made in this analysis regarding the magnitude of excitation and the degree of damping shall be clearly stated. The acceptance criteria for this analysis shall be mutually agreed upon by the purchaser and the vendor.

SP6.8.6.6 In addition to the torsional analyses required in SP6.8.6.2 through SP6.8.6.5, the vendor shall perform a transient torsional vibration analysis for synchronous motor driven units, variable frequency motors, and turbine generators sets. The acceptance criteria for this analysis shall be mutually agreed upon by the purchaser and the vendor.

4.10.2 Paragraphs from API 617 7th Edition

SP2.6.7 Torsional Analysis

- **SP2.6.7.1** For motor-driven units and units including gears, units comprising three or more coupled machines (excluding any gears), or when specified, the vendor having unit responsibility shall ensure that a Torsional vibration analysis of the complete coupled train is carried out and shall be responsible for directing any modifications necessary to meet the requirements of 2.6.7.2 through 2.6.7.6.

SP2.6.7.2 Excitation of torsional natural frequencies may come from many sources which may or may not be a function of running speed and should be considered in the analysis. These sources shall include but are not limited to the following:

- a. Gear characteristics such as unbalance, pitch line runout, and cumulative pitch error.
- b. Cyclic process impulses.
- c. Torsional transients such as start-up of synchronous electric motors and generator phase-to-phase or phase-to-ground faults.
- d. Torsional excitation resulting from electric motors, reciprocating engines, and rotary type positive displacement machines.
- e. Control loop resonance from hydraulic, electronic governors, and variable frequency drives.
- f. One and 2 times line frequency.
- g. Running speed or speeds.

h. Harmonic frequencies from variable frequency drives.

SP2.6.7.3 The torsional natural frequencies of the complete train shall be at least 10% above or 10% below any possible excitation frequency within the specified operating speed range (from minimum to maximum continuous speed).

SP2.6.7.4 Torsional natural frequencies at two or more times running speeds shall preferably be avoided or, in systems in which corresponding excitation frequencies occur, shall be shown to have no adverse effect.

SP2.6.7.5 When torsional resonances are calculated to fall within the margin specified in SP2.6.7.3 (and the purchaser and the vendor have agreed that all efforts to remove the critical from within the limiting frequency range have been exhausted), a stress analysis shall be performed to demonstrate that the resonances have no adverse effect on the complete train. The assumptions made in this analysis regarding the magnitude of excitation and the degree of damping shall be clearly stated. The acceptance criteria for this analysis shall be mutually agreed upon by the purchaser and the vendor.

SP2.6.7.6 In addition to the torsional analyses required in SP2.6.7.2 through SP2.6.7.5, the vendor shall perform a transient torsional vibration analysis for synchronous motor driven units, using a time-transient analysis. The requirements of SP2.6.7.6.1 through SP2.6.7.6.4 shall be followed.

SP2.6.7.6.1 In addition to the parameters used to perform the torsional analysis specified in SP2.6.7.1, the following shall be included:

- a. Motor average torque, as well as pulsating torque (direct and quadrature axis) vs. speed characteristics.
- b. Load torque vs. speed characteristics.
- c. Electrical system characteristics effecting the motor terminal voltage or the assumptions made concerning the terminal voltage including the method of starting, such as across the line, or some method of reduced voltage starting.

SP2.6.7.6.2 The analysis shall generate the maximum torque as well as a torque vs. time history for each of the shafts in the compressor train. Note: The maximum torques shall be used to evaluate the peak torque capability of coupling components, gearing and interference fits of components such as coupling hubs. The torque vs. time history shall be used to develop a cumulative damage fatigue analysis of shafting, keys and coupling components.

SP2.6.7.6.3 Appropriate fatigue properties and stress concentrations shall be used.

SP2.6.7.6.4 An appropriate cumulative fatigue algorithm shall be used to develop a value for the safe number of starts. The safe number of starts shall be as mutually agreed by the purchaser and vendor.

Note: Values used depend on the analytical model used and the vendor's experience. Values of 1000–1500 starts are common. API Std 541 requires 5000 starts. This is a reasonable assumption for a motor since it does not add significant cost to the design. The driven equipment, however, would be designed with overkill to meet this requirement.

Example: 20-year life, 1 start/week = 1040 starts. Equipment of this type normally would start once every few years rather than once per week. A reasonable number of starts should therefore be specified.

SECTION 5—BALANCING OF MACHINERY

5.1 SCOPE

This tutorial is directed toward both manufacturers and users of machinery built to API standards. However, the information presented generally applies to all rotating equipment. The purpose of the tutorial is to present the requirements for dynamic balancing, the reasoning behind these requirements, and the balancing techniques necessary to achieve these requirements. The information contained in this tutorial is applicable to rotors undergoing routine service, repair, or re-rating, as well as new rotors. Sections 5.5 and 5.6 are non-annotated excerpts from the API Standard Paragraphs, SP6.8.8 on vibration and balancing.

5.2 INTRODUCTION

5.2.1 Definition of Terms

Resonance is the condition when the frequency of a harmonic (periodic) forcing function coincides with a natural frequency of the structure (rotor system.) Critical speeds and other resonant conditions of concern are those with an amplification factor (AF) equal to or greater than 2.5. When a rotor accelerates or decelerates through this speed region(s), the observed vibration characteristics may include one or both of the following: (a) a peak in the 1X vibration amplitude and (b) a change in the phase angle.

5.2.1.1 balanced condition: A condition where the mass centerline (principal inertial axis) approaches or coincides with the rotor rotational axis, thus reducing the lateral vibration of the rotor and the forces on the bearings, at once per revolution frequency (1X).

5.2.1.2 balancing: A procedure for adjusting the radial mass distribution of a rotor so that the mass centerline (principal inertial axis) approaches or coincides with the rotor rotational axis, thus reducing the lateral vibration of the rotor due to unbalanced inertia forces and forces on the bearings, at once-per-revolution frequency (1X).

5.2.1.3 bow: A shaft deflection, other than gravitational deflection, such that the geometric shaft centerline is not straight and will affect balancing. Other conditions, such as thermal warpage, can impart a semi-permanent or permanent deflection (bow) to the rotor. This bow may be three-dimensional (corkscrew). Rotor bow can be determined by measuring the shaft relative displacement along its length in V blocks. (See 5.2.1.17 for the definition of sag, i.e., gravitational deflection. Sag does not affect balance.)

5.2.1.4 calibration: A test during which known values of the measured variable are applied and the resulting output readings are verified or justified.

5.2.1.5 calibration weight: A weight of known magnitude that is placed on the rotor at a known location in order to measure the resulting change in machine vibration (1X vector) response. In effect, such a procedure calibrates the rotor system (a known input is applied, and the resultant output is measured) for its sensitivity to unbalance. Calibration weight is sometimes called trial weight.

5.2.1.6 eccentricity: The extent to which the center of a perfect circle, which is the best fit to the surface in question, deviates from the true centerline of the shaft.

5.2.1.7 cylindricity (out-of-roundness): The variation of the outer diameter of a shaft surface when referenced to the true geometric centerline of the shaft.

5.2.1.8 electrical runout: A source of error on the output signal of a proximity probe transducer system resulting from non-uniform electrical conductivity/resistivity/permeability properties of the observed material shaft surface. The non-uniform properties may result from scratches, rust, engravings, or stencil marks. Electrical runout is a change in the proximity probe output signal that does not result from a probe gap change.

5.2.1.9 heavy spot: A term used to describe the position of the unbalance vector at a specified lateral location (in one plane) on a rotor.

5.2.1.10 high spot: The term used to describe the response vector of the rotor shaft due to an unbalance force.

5.2.1.11 unbalance (imbalance): A measure that quantifies how much the rotor mass centerline is displaced from the centerline of rotation (geometric centerline) resulting from an unequal radial mass distribution on a rotor system. Unbalance is usually given in either gram-centimeters or ounce-in.

5.2.1.12 influence vector: The synchronous vibration response vector divided by the calibration weight vector (trial weight vector) at a particular shaft rotative speed. The influence vector represents the transfer function between vibration response and unbalance force.

5.2.1.13 once-per-revolution mark: A location on the shaft circumference that is monitored by a phase reference transducer. The mark provides indication of a once-per-revolution occurrence (rpm.) The mark can be a keyway, a key, a hole or slot, or a projection.

5.2.1.14 mechanical runout: A source of error on the output signal of a proximity probe transducer system. It is sensed by a probe gap change that does not result from shaft dynamic motion. Common sources include out-of-round shafts, dents, eccentricity and flat spots.

5.2.1.15 non-symmetric (Asymmetric) rotor: A rotor whose cross-section has two different geometric second area moments of inertia. When rotated at any angle about its geometric center, it may not appear the same unless returned to its original orientation; for example, an elliptical cross-section, a rotor with a keyway, or a rotor section with a crack.

5.2.1.16 orbit: The dynamic path of the shaft centerline displacement motion as it vibrates during shaft rotation at a particular radial plane.

5.2.1.17 sag: Rotor deflection that is due to gravitational loading of a rotor. The sag is also the natural shape of the rotational axis as it rotates. Sag is not a factor in balancing. (See 5.2.1.3 for the definition of bow. Bow is a deflection of the rotor that does affect balance.)

5.2.1.18 synchronous component: The portion of a vibration signal that has a frequency equal to the shaft rotational frequency (1X).

5.2.2 Fundamentals of Balancing

5.2.2.1 Introduction

Achieving a balanced condition for a rotating assembly is a fundamental element in maximizing machinery reliability. If all other considerations are equal, the level of vibration produced by machinery is directly proportional to the unbalance of the assembly, i.e., the lower the unbalance, the lower the vibration. Lower vibrations produce lower forces and stresses on the rotating assemblies, bearings, and support systems, which increases machinery reliability.

Unbalance of rotating machinery parts is the most common cause of equipment vibration. The API Subcommittee on Mechanical Equipment has, therefore, developed equipment standards for allowable unbalance levels to minimize the effect of unbalance on overall equipment vibration. Precision dynamic balance of rotating machinery is required to ensure that the equipment performs with minimal vibration on both the vendor test stand and in the field.

The low value of unbalance required by the API standards provides the owner with some margin for in-service rotor erosion and fouling, bearing wear, oil system degradation. This conservatism in balancing increases the availability of the machinery.

5.2.2.2 Derivation of Forces Due to Unbalance

In an ideal rotor, the mass centerline (principal inertial axis) is coincidental with the rotational axis. If installed in bearings with common centerlines, the shaft would rotate without unbalance forces or vibration. In real rotors, the two axes are not coincidental. A real rotor would rather rotate around its mass centerline but cannot because it is constrained by the bearings. The forces due to the unbalance are constrained by the bearings and result in a displacement of the

mass center of the rotor, which creates the vibration in the shaft.

An analysis of a simple rotor system will illustrate the dominant influences, which produce rotor forces due to unbalance. Consider a rotor, turning with an angular velocity ω (radians/unit time) that has an unequal distribution of mass about its centerline. Further assume that the amount of unequal mass distribution can be represented as a single mass located at a distance r from the centerline of the shaft. This is an example of a rotor with simple static unbalance. The basic equation for forces due to rotation of a shaft assembly is:

$$F = U\omega^2 \quad (5-1)$$

where

F = centripetal force,

U = unbalance,

ω = rotational speed.

The force generated due to a rotor's unbalance can be shown by the following equation:

For SI units:

$$F = U \times 10^{-6} \left(\text{RPM} \frac{2\pi}{60} \right)^2 \quad (5-2)$$

where

F = radial force generated due to the unbalance of the rotating assembly (N),

RPM = maximum continuous speed of the rotating assembly (rpm),

U = the unbalance of the rotating assembly (g-mm).

For Customary units:

$$F = U \times 1.77 \left(\frac{\text{RPM}}{1000} \right)^2 \quad (5-3)$$

where

F = radial force generated due to the residual unbalance of the rotating assembly (lbf),

RPM = maximum continuous speed of the rotating assembly (rpm),

U = the unbalance of the rotating assembly (oz-in.).

This relationship illustrates two important characteristics of rotors with unbalance. The Force F varies linearly with the location and size of the unequal mass distribution but with the square of the shaft rotative speed. This explains why a particular U , for an 1800 rpm rotor, produces acceptable unbalance forces and vibration while the identical U , for a 10,800 rpm

rotor, is unacceptable. The forces are 36 times as great for the higher speed rotor!

These forces can be significant for relatively small amounts of unbalance. For example, a rotor with a residual unbalance of only 4320 gram-millimeters (6 ounce-in.) running at 10,800 rpm will generate a force due to unbalance of over 500 Newtons (1103 pounds).

Most rotors covered by the API Standards do not have simple static unbalance. However, the fundamental issues regarding their unbalance follow the basic issues described above.

5.2.3 Units for Expressing Unbalance

The amount of unbalance in a rotating assembly is normally expressed as the product of the unbalance weight (for example, grams and ounces) and its distance from the rotating centerline (such as millimeters and in.). Thus, the units for unbalance are generally gram-millimeters, ounce-in., gram-in., and so forth. For example, ten gram-millimeters of unbalance would equate to a heavy spot on a rotor of one gram located at a radius of ten millimeter from the rotating centerline.

Figure 5-1 illustrates this example of unbalance expressed as the product of weight and distance.

5.2.4 Types of Unbalance

The various types of unbalance can be understood by describing the relationship between a rotor's mass centerline (principal inertial axis) and its rotational axis. If these two axes are coincidental, the rotor has zero unbalance and is con-

sidered perfectly balanced. The limits of unbalance contained in the various API Standards are real world values, which if achieved, result in acceptable machinery reliability. The following sections provide a description of various unbalance conditions as determined by a typical low speed balance stand.

5.2.4.1 Static Unbalance

Static unbalance is the balance condition where the principal inertial axis is offset a parallel distance ' r ' from the rotor rotational axis (Figure 5-2). This locates the Center of Gravity (CG) away from the axis of the rotational. Static unbalance can be corrected in either of two methods. In the first method, a correction weight can be located directly 180° opposite the unbalance, (CG) and at the appropriate radius from the rotor centerline to equal the unbalance (gm-cm). In the second method, the weight is divided and distributed to each end of the rotor. The location of the weights must remain in line with the weight location of the first method, i.e., 180° opposite the CG of the rotor. Most rotors contain some static unbalance, but other types as well, necessitating a more involved balancing procedure than described above.

5.2.4.2 Couple Unbalance

A 'couple,' in static force analysis, is the application of equal forces, applied about the CG of a body, in opposite directions (Figure 5-3). Rotor couple unbalance is the balance condition where the mass centerline (principal inertial axis) intersects the rotor rotational axis and this intersection is also

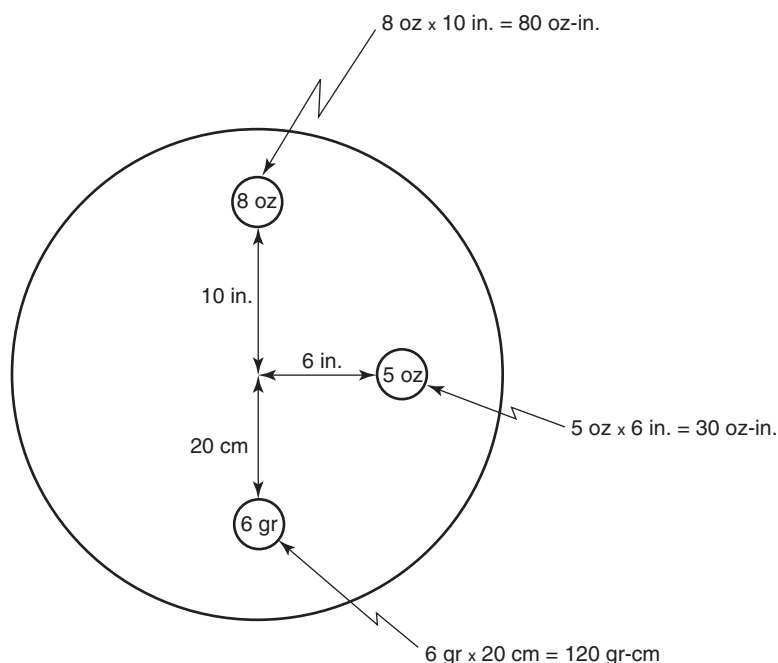


Figure 5-1—Unbalance Expressed as the Product of Weight and Distance

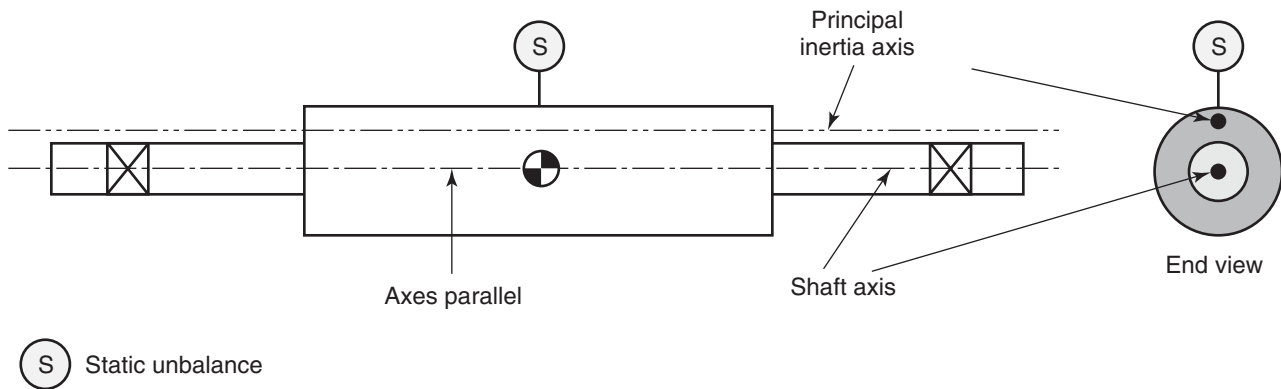


Figure 5-2—Static Unbalance

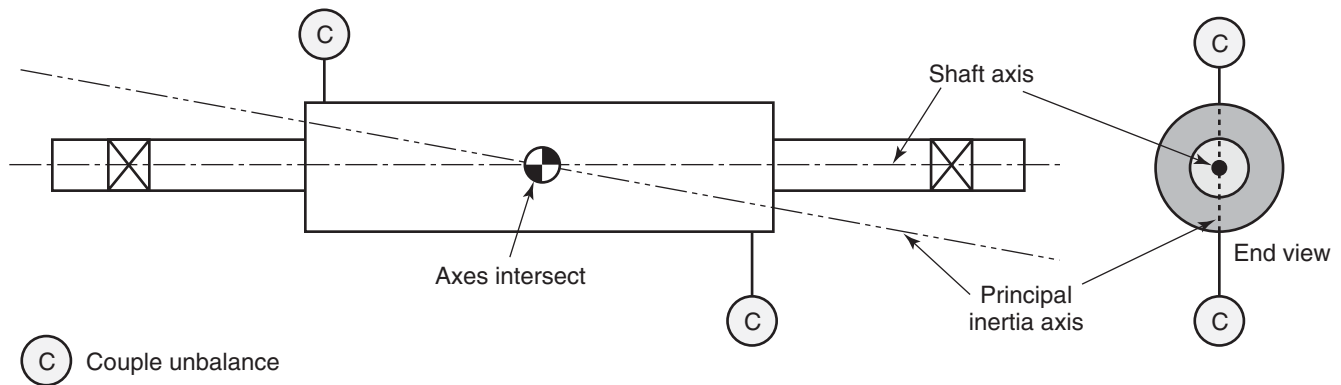


Figure 5-3—Couple Unbalance

the CG. A rotor with couple unbalance will have no static unbalance (the CG lies on the rotor rotational axis), but, if rotated, the opposing forces produce vibration in the bearings. Couple unbalance must be addressed by making weight corrections in the same axial plane of the unbalance at each end of the rotor, i.e., 180° apart. Most rotors contain some couple unbalance, as well as other types of unbalance, necessitating a more involved balancing procedure than described above.

5.2.4.3 Quasi-static Unbalance

Quasi-static unbalance is the balance condition where the mass centerline (principal inertial axis) intersects the rotor rotational axis, but not at the CG of the rotor (Figure 5-4). This condition is a combination of static and couple unbalance wherein the static component lies in a plane that also contains the couple unbalance. This type of unbalance is not common. Like couple unbalance, quasi-static unbalance must also be addressed by making weight corrections in a minimum of two planes.

5.2.4.4 Dynamic Unbalance

Dynamic unbalance is the balance condition where the mass centerline (principal inertial axis) does not intersect either the rotor rotational axis or the CG of the rotor, as shown in Figure 5-5. This condition is a combination of static and couple unbalance wherein the static component lies in an axial plane different from one of the couple unbalance forces. This type of unbalance is common. Like couple unbalance, dynamic unbalance must also be addressed by making weight corrections in a minimum of two planes.

5.2.5 Causes of Unbalance

There are many reasons for unbalance in a rotor. The most common causes of rotor unbalance are the following:

- a. *Non-homogeneous material:* On occasion, rotors with cast components such as pump impellers, will have blow holes or sand traps which result from the casting process. This condition can also be caused by porosity in the rolled or forged material for shafting and impeller disks. These areas are

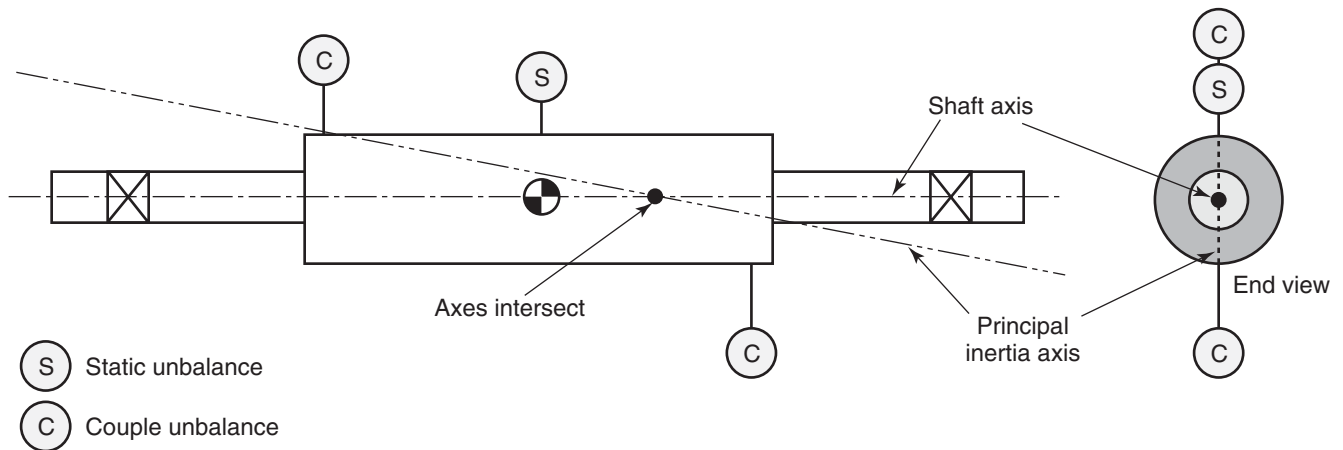


Figure 5-4—Quasi-static Unbalance

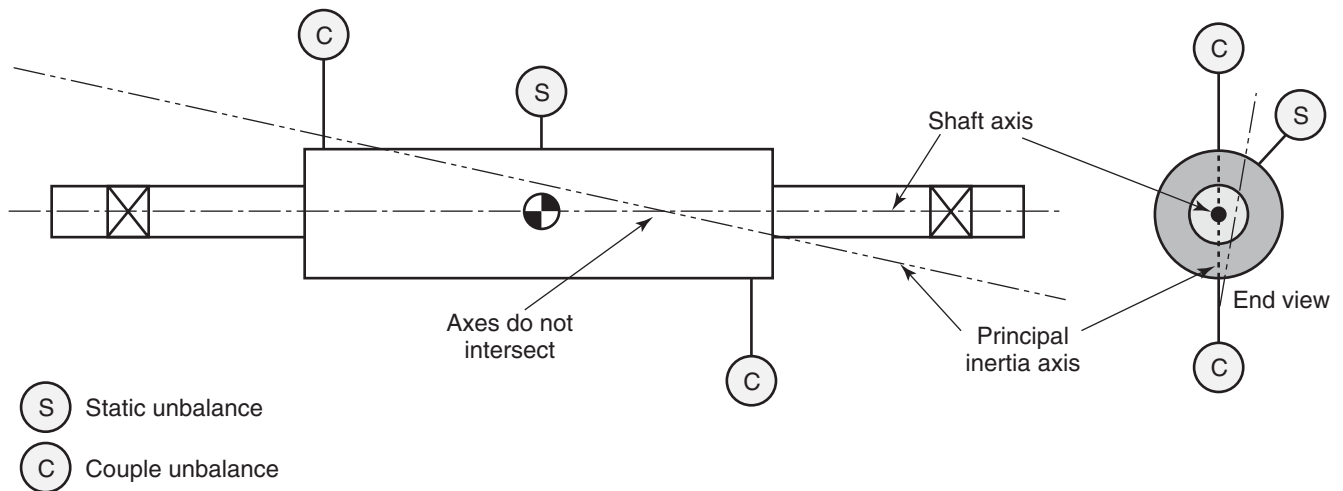


Figure 5-5—Dynamic Unbalance

undetectable through visual inspection. Nonetheless, the void created may cause a significant unbalance.

b. *Eccentricity*: This exists when the geometric centerline of a rotating assembly does not coincide with the axis of rotation.

c. *Lack of rotor symmetry*: This is a condition that can result from a casting core shift as in a pump impeller.

d. *Distortion*: Although a part may be reasonably well balanced following manufacture, there are many influences that may serve to alter its original balance. Common causes of such distortion include stress relief and thermal distortion. Impellers that have been fabricated by welding can have internal stresses. Any part that has been shaped by pressing, drawing, bending, extruding, and welding without stress relief, will naturally have high internal stresses. Therefore all such components should be stress relieved prior to balancing. If the rotor or component parts are not stress relieved prior to balancing, they may undergo stress relief naturally over a

period of time, and as a result, the rotor may distort slightly to take a new shape, thus altering the rotor balance.

Distortion that occurs with a change in temperature is called thermal distortion. Although all metals expand when heated, most rotors, due to minor imperfections and uneven heating, will expand unevenly causing distortion. This distortion is quite common on machines that operate at elevated temperatures (that is, induced draft boiler fans and steam turbines). For this reason steam turbine shafting is often subjected to a heat stability test. Thermal distortion can also be induced by uneven cooling such as occurs in a steam turbine rotor after a trip. For this reason, turning gears are often employed in large turbine driven trains.

e. *Stacking errors*: Slight variations in mounting or cocking a shrink-fit disk or impeller on its shaft may result in unbalance. This can also result from the stack-up of machining tolerances in a rotating assembly or from unaccounted for keys or other missing components.

f. *Bent rotor shaft:* This condition can occur when a rub causes a yield of the shaft material due to thermal effects. This shifts the entire rotor off-center from the axis of rotation. However, rotors that have experienced a hard rub in service may only have a 'kinked' shaft. In this instance, the entire rotor may not be off-center and the unbalance can be corrected.

g. *Corrosion, erosion, or deposits:* Many rotors, particularly those involved in material handling processes, are subjected to corrosion, erosion, abrasion, deposit buildup, and wear. If the corrosion or wear does not occur uniformly, unbalance will result. In some applications, deposits on rotor/blade surfaces can accumulate and/or be removed unevenly causing unbalance.

h. *Eccentric mounting of balanced components:* Items such as couplings and dry gas seal rotors are balanced as individual items and contain their own residual unbalance. However, they are not added to a rotor, during the balancing procedure, to determine the effect of their unbalance on the entire assembly. This effect is more significant on small rotors as compared to large rotors.

The distribution of these unbalances along the length and circumference of the rotor will be more or less random (see Figure 5-6). The unbalances presented in Figure 5-6 are identified by the component. For example, the source of the shaft unbalance may be machining errors and/or bow. The impeller/stage unbalance may be created by stacking errors and/or eccentric mounting and may be either static and/or couple unbalance. As noted in 5.2.4, low speed balance machines are able to resolve these unbalances into a combination of static and couple unbalances. This is made possible since the low speed balance machine treats the rotor as a rigid body. The extent to which this holds true during operation determines

the need for flexible body balancing (operating-speed balancing).

In summary, all of the preceding causes of unbalance can exist to some degree in a rotor. However, the vector summation of all unbalance can be considered as a concentration at a point called the heavy spot. Balancing is thus the technique for determining the amount and location of this heavy spot so that an equal amount of weight can be removed at this location, or an equal amount of weight added 180° opposite of the heavy spot.

5.2.6 API Standard Balance Specifications

Balancing denotes the attempt to improve the mass distribution of a rotating assembly such that the assembly rotates in its bearings with minimal unbalance forces and acceptable vibration amplitudes. This goal, however, can be achieved only to a certain degree; even after careful balancing of a given rotor is completed, the rotor will still retain a certain degree of unbalanced mass distribution known as residual unbalance.

The API Standard Paragraphs specifications for residual unbalance were originally adopted from the US Navy, Bureau of Ships Standards.

For SI units, use the following equation:

$$U = 6350 \frac{W}{N} \text{ (g-mm)} \quad 5-4$$

For Customary units, use the following equation:

$$U = 4 \frac{W}{N} \text{ (oz-in.)} \quad 5-5$$

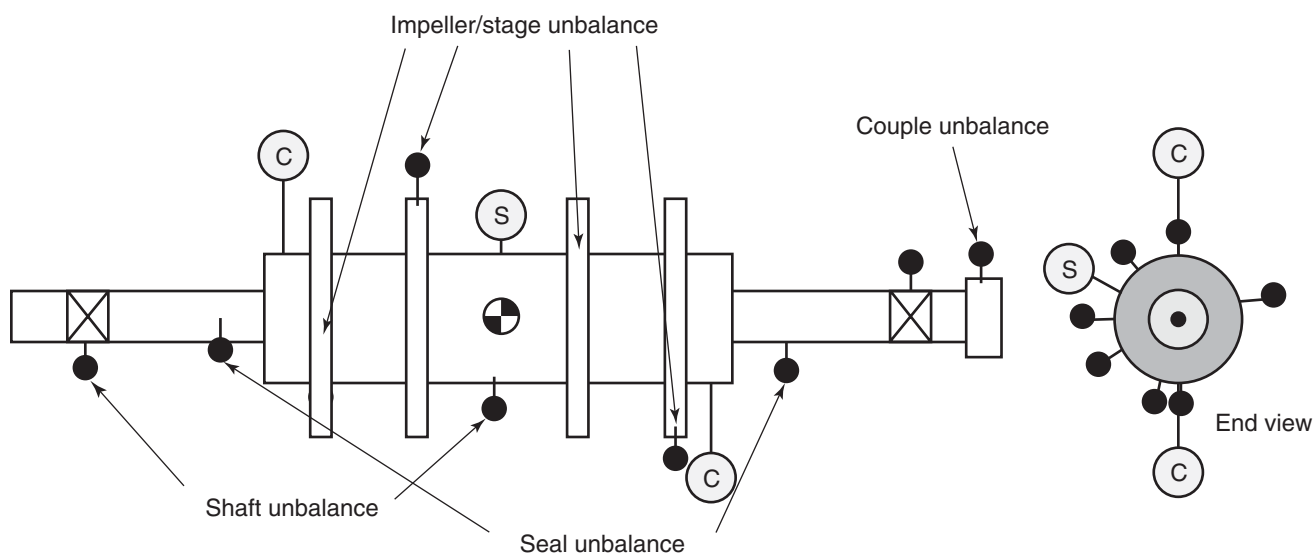


Figure 5-6—Unbalance Distribution Resolution

where

U = maximum allowable residual unbalance for each correction plane. The tolerance for each plane is based on the static weight supported at each end of the rotor,

W = bearing journal static weight at each end of the rotor. W is expressed in pounds for customary units or kilograms for metric units. Note that for relatively uniform rotors, W represents $1/2$ the total rotor weight,

N = maximum continuous speed of the rotor in revolutions per minute (Note: Not the balance speed).

The API Standard Paragraphs for residual unbalance provide an achievable unbalance level that will minimize the effect of rotating unbalance on overall vibration level. It is important to remember that a rotor's vibration level and residual unbalance are two separate measurements used to achieve the same end: a smooth running machine.

5.2.7 Balancing Tolerances

The present-day state of the art in balancing technology is such that it is not uncommon for high-speed turbomachinery rotors to operate with shaft vibration levels of 12.5 microns (0.5 mils) or less. Achieving vibration levels this low requires sound balance practices and tight manufacturing and residual unbalance tolerances. In establishing balance tolerances, there is always a trade-off between what is practically feasible and what is economical.

There have been a number of balancing tolerances developed over the years; a few of these are: ISO Standards (International Standards Organization), VDI Standards (Society of German Engineers), ANSI Standards (American National Standards Institute), and the Military Standards (MIL-STD-167). All of these standards share a common objective of developing a smoother running machine. In the final analysis, however, all balancing standards specify an allowable eccentricity, or offset weight distribution, from the rotating centerline.

The ISO Standard is another commonly referenced balancing standard. The ISO Standard provides a series of rotor classifications as a direct plot of residual unbalance per unit of rotor mass versus service speed (see Figure 5-7). For the ISO specification, turbomachinery rotors are assigned the Grade of 2.5. The ISO Grade 2.5 equates to an API upper limit allowable unbalance of about $15W/N$ and a lower limit of about $6W/N$. This range has been found to be unsatisfactory for most turbomachinery applications. To achieve the same allowable residual unbalance level as the $4W/N$ API Standard would require an ISO Grade of 0.7. This comparison can be graphically illustrated as shown in Figure 5-8.

Although the API $4W/N$ balance tolerance is significantly tighter than that of ISO Grade G-2.5, this tighter tolerance is just as easy for an experienced balancing machine operator to achieve and requires little additional time.

As written, the API balance tolerance ($4W/N$) has no boundaries (can approach zero as speed increases.) It should be recognized that there exists a finite lower limit of a balance machine's ability to determine residual unbalance. The practical limit of new shop balance machines is approximately 5 microinches new but only 10 microinches during normal use. Therefore, the smallest unbalance measurable in a balance machine is:

$$U_{limit} = c \times SW \times 16 \times 10^{-6} \quad (5-6)$$

where

W = rotor mass, kg (lbm),

S = balance machine sensitivity, μmm ($\mu\text{in.}$),

U_{limit} = unbalance (oz-in.),

c = constant, 1000 (16).

Typical values of S range from 5 to 10 $\mu\text{in.}$ (microinches). The API unbalance tolerance ($4W/N$) and machine unbalance limit (U_{limit}) using a sensitivity of 10 $\mu\text{in.}$ can be plotted as unbalance versus speed. This is shown in Figure 5-9.

As can be seen, the API tolerance cannot be reached at operating speeds of the rotor above 25,000 rpm for a balance machine with a sensitivity of 10 microinches.

5.3 BALANCING MACHINES

5.3.1 General

In choosing a balancing machine for a given rotor, care must be taken to ensure that the rotor weight is matched to the balancing machine capability and will be of sufficient sensitivity to provide good residual unbalance data. In other words, is the balancing machine capable of providing the unbalance tolerance required?

The balancing machine drive system must also be of sufficient horsepower to bring the rotor up to the desired balance speed. This is of particular importance with large steam turbine and centrifugal fan rotors.

There are two basic types of balancing machines, namely soft-bearing and hard-bearing machines. The term hard or soft refers to the support system used in these machines, not to the type of bearings employed. Figure 5-10 illustrates the applicable speed ranges for hard-bearing and soft-bearing balancing machines [3]. With regard to the bearings, balance machine anti-friction support rollers should not have a diameter that is within $\pm 5\%$ of the diameter of the rotor journal. This is to prevent the roller variations (eccentricity and out-of-roundness) from masking the rotor vibration readings.

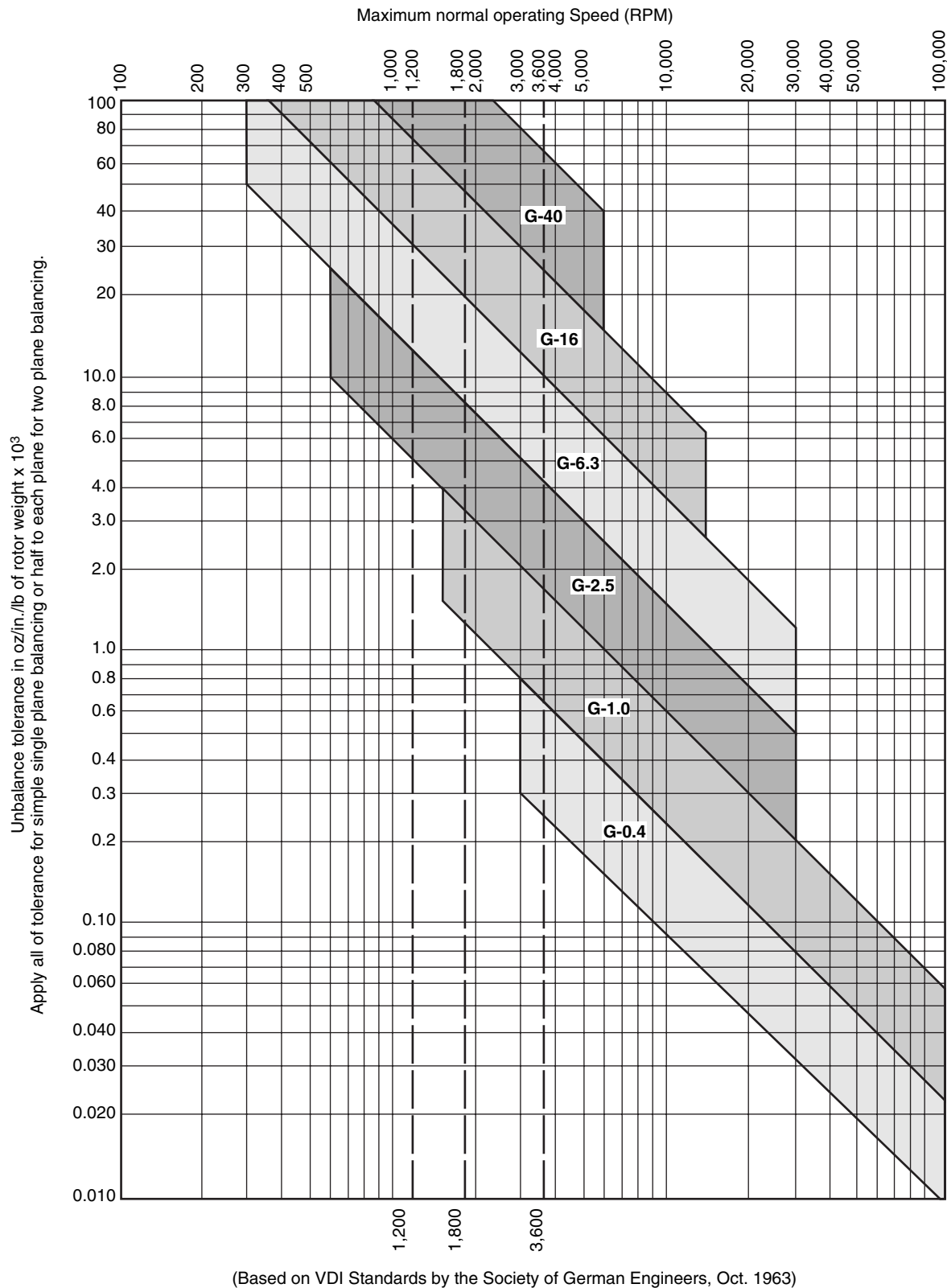


Figure 5-7—ISO Unbalance Tolerance Guide for Rigid Rotor

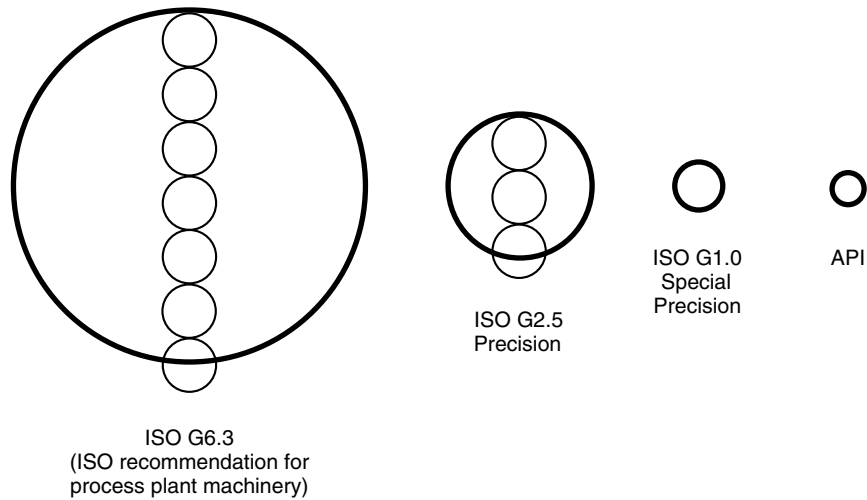


Figure 5-8—Shaft Centerline Unbalance Orbits (Based on ISO and API Standards)

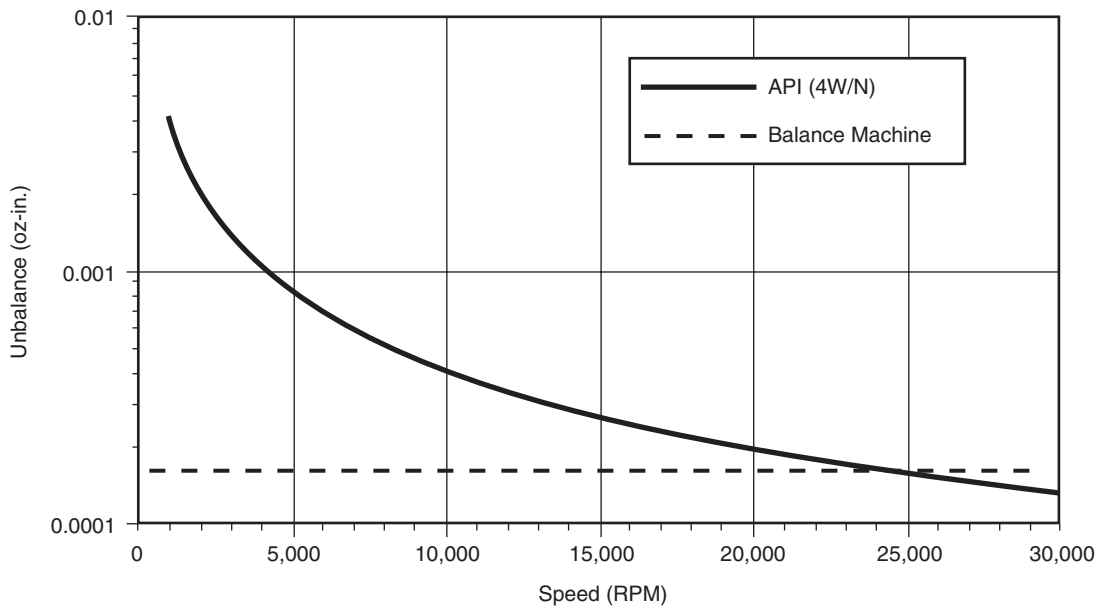


Figure 5-9—Unbalance Versus Speed for API Limits and Balance Machine Limit (Calculated at $W = 1$ pound)

5.3.2 Soft-Bearing Balancing Machines

The soft-bearing balancing machine design employs a flexible spring support system on which the workpiece is mounted. The 1st natural frequency of a soft-bearing support system (including the rotating assembly to be balanced) is very low, so actual balancing is done above this system's natural frequency. The unbalance in the rotor results in an unrestrained vibratory motion in the support system. This motion is normally measured with velocity transducers mechanically connected to the support system.

With soft-bearing balancing machines, different types of rotors of the same weight will produce different displace-

ments of the vibration pickups, depending upon the configuration of the rotors to be balanced. The signals coming from the vibration pickups are dependent not only on the unbalances and on their positions, but also on the masses and moments of inertia of the rotor. The methods employed in a soft-bearing balancing machine are similar to those found in field balancing.

The residual unbalance can be obtained only after calibrating the measuring devices to the rotor being balanced using test masses that constitute a known amount of unbalance. Therefore, this type of balancing machine is generally used for production applications in which many identical components are successively balanced.

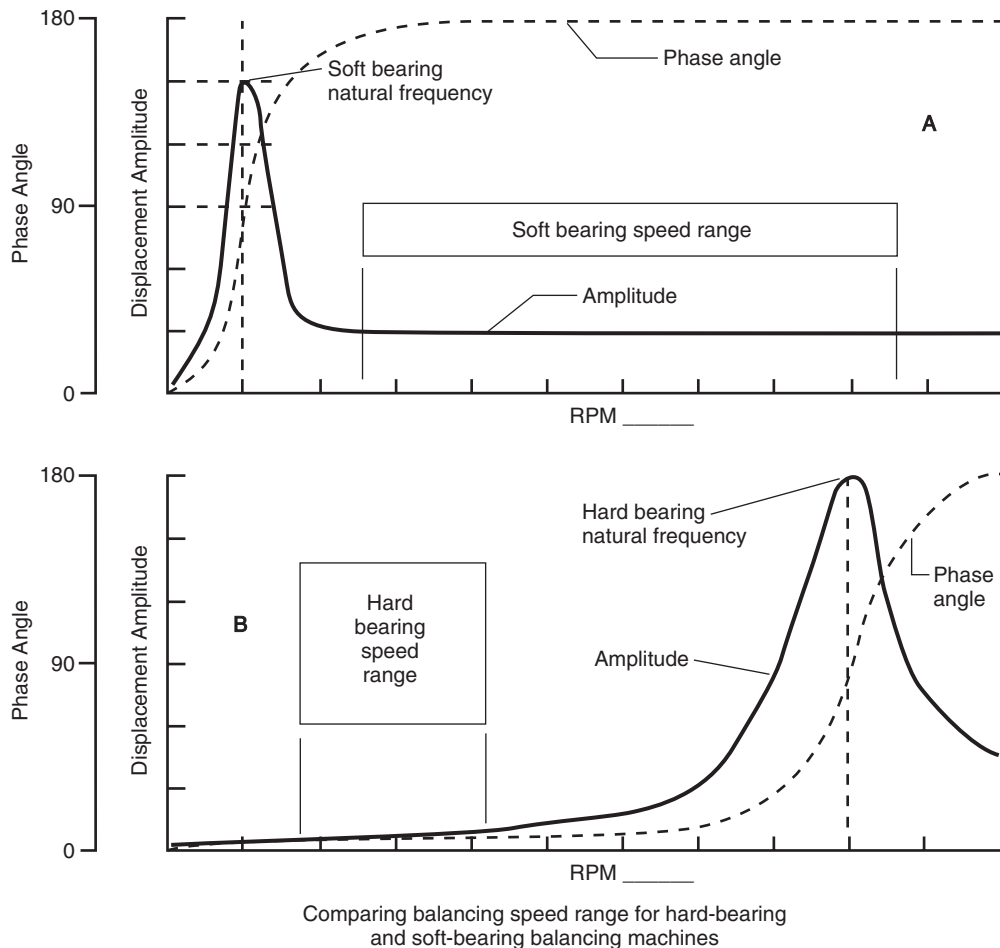


Figure 5-10—Applicable Speed Ranges for Hard-bearing and Soft-bearing Balancing Machines

5.3.3 Hard-bearing Balancing Machines

Hard-bearing balancing machines are essentially the same as soft-bearing machines except that the supports are much stiffer. This greater stiffness causes the natural frequency of the balancing machine's rotor bearing system to be well above the balancing speed. A hard-bearing balancing machine also accepts a wider range of rotor weights and configurations without requiring re-calibration.

This type of balancing machine measures rotor unbalance using strain-gauge transducers and correlates the unbalance to a force. Also, the strain-gauge transducer's readouts are proportional to the rotor unbalance. Since the readout of hard-bearing machines is unbalance force and not vibration of a spring force system, the readout will be close to the amount of actual unbalance, in a properly calibrated machine. The force a specific unbalance develops at a specific speed is always the same, regardless of the physical attributes of the rotor. Restated, the force is not influenced by the bearing mass, rotor weight, rotor configuration, rotor moment of inertia, or windage oscillations from the rotating workpiece.

5.3.4 Balancing Machine Drives

5.3.4.1 General

Balancing machines typically employ one of three different drive configurations to spin the rotating assembly. These drive mechanisms include the direct end drive, the wrap-around belt drive, and the tangential belt drive.

5.3.4.2 Direct-end Drive

The direct-end drive includes a drive shaft with a universal joint (U-joint) connection to the rotor. It is typically used with rotors that have large moments of inertia or high windage losses. This drive design will transmit high torque forces for fast acceleration and safe braking. To attach the drive shaft, a rotor end must be prepared to accept the U-joint directly or must be fitted with an adaptor hub. With this design, the drive system becomes a part of the rotor and must be considered in the balancing accuracy of the system. Before this type of drive can be used to accurately balance a workpiece, the U-joint assembly, itself, must be balanced. The desired end

result is to be able to rotate the U-joint assembly 180° in relation to the workpiece without any variance in the balancing machine readout. To confirm this level of unbalance, the following procedure can be utilized. After the addition of the first component(s), rotate the driveshaft 180° and check the residual unbalance. If the unbalance value changes and exceeds the values allowed in 5.2.6, the driveshaft is not balanced or the pilot fit of the shaft is incorrect. The error must be corrected before the balancing can proceed.

5.3.4.3 Wrap-Around Belt Drive

A wrap-around belt drive works very well for rotors weighing less than 2250 kg (5000 lbs) and with at least one smooth surface. For this drive configuration, 2250 kg (5000 lbs) is approximately the maximum rotor weight that will allow adequate torque transmission to bring the rotor up to the required balance speed. A 180° wrap is required to provide adequate torque to rotate the rotor and keep the applied torque in the vertical plane of the balancing machine pedestal. A belt drive of this type is considerably more accurate than a direct-coupled end drive in that the drive mechanism does not influence the workpiece balance.

5.3.4.4 Tangential Belt Drive

A tangential belt drive, either under the rotor or in an over-arm configuration, is frequently used in smaller capacity, high-volume-production oriented balancing machines for rotors weighing less than 450 kg (1,000 lbs). This type of drive configuration is used to bring the rotor up to the required balancing speed. The drive arm is then moved away from the rotor and the unbalance data is collected.

5.3.5 Balancing Machine Pitfalls

A few other points concerning balancing machines, regardless of drive type, are worth noting. One is to avoid using a machine with anti-friction support bearings having diameters that are equal to the journals of the workpiece. In this instance, any imperfection that results in non-concentricity of the outer race will be interpreted as unbalance by the balancing machine electronics.

In addition, since unbalance force varies as the square of the rotor speed, a balancing speed range that the balancing machine manufacturer recommends to achieve the desired sensitivity should be chosen and maintained from the start to the finish of the job. The balance speed chosen is of particular importance on steam and gas turbine rotors where the stage buckets must be seated (due to centrifugal force) in their blade-root attachments in order to achieve repeatable balance data.

Balancing machines with a belt drive have also been known to introduce residual magnetism into the workpiece from friction and slippage between the belt and the work-

piece. The residual magnetism levels of the workpiece should always be checked after using this type of balancing machine, and the workpiece degaussed if necessary. The gauss level of the proximity probe area should not exceed 2 gauss as specified by API 670.

5.4 BALANCING PROCEDURES

5.4.1 General

The balancing machine calibration must be verified prior to starting the balancing procedure. Balancing machines should be capable of providing the location (separation) of the balance planes, the dynamic unbalance, and the static/couple unbalance. Balance machine bearings should be located on a surface machined to the same runout tolerance of the actual machine journals. Rotors with temporary bows should be run until the initial readings are stable. The records of the balancing procedure should include the initial and final values of the unbalance.

Prior to making final balance corrections, the balance machine operator should verify the proposed correction by using trial weights of clay. This step is recommended to ensure the balance machine indicates the desired level of residual unbalance has been achieved.

Final balance corrections are made in either of two methods, removal of weight or the addition of weight. Both of these methods may be utilized in the process of balancing. Weight may be removed by either grinding or drilling. Care should be exercised so that the components are not damaged or weakened in the process. If weight is added, it is done by rigidly affixing the weights to the components. This may be done by the use of bolts, set screws, or pinning. Balance weights must be compatible with the component material and suitable for the operating environment. For example, this may require the balance weights to be made from material that has corrosion resistance equal to or greater than the item being balanced.

Occasionally, rotors to be balanced include previously balanced ancillary component assemblies, e.g., couplings. If these assemblies contain balance weights, the weights should not be altered in the process of balancing the rest of the rotor. See 5.2.5h for the potential impact to the residual unbalance if properly balanced components are eccentrically mounted on a rotor.

5.4.2 Component Balancing

5.4.2.1 Introduction

On flexible shaft rotors (those that operate above the first critical speed), it is vital to multi-plane dynamically balance all of the major components, individually, before assembly. Major components include the shaft, balancing drum, and the impellers. The components shall be balanced to the same tolerance as is required for the complete assembly. If the rotor is fully assembled without this step, there is no way to know

exactly what contribution each component part is making to the total measured unbalance vector. In addition, if a large unbalance exists in one of the major components within the rotor, the rotor shaft may flex at this point during high-speed operation and cause significant damage to the rotating and stationary parts.

5.4.2.2 Mandrel Requirements

Each major rotor component must be individually balanced on a precision ground mandrel. (Note that expanding mandrels are not acceptable for this purpose.) The mandrel shall have a surface finish roughness that does not exceed $0.4\text{ }\mu\text{m}$ ($16\text{ }\mu\text{in.}$) R_a . The mandrel shall also have no measurable eccentricity when assessed by an indicator graduated in $2.5\text{ }\mu\text{m}$ (0.0001 in.). The mandrel mass should not exceed 25% of the mass of the component to be balanced.

The balance mandrel should be ground between centers to assure concentricity of all diameters throughout its length as well as to assure a good smooth surface finish. After grinding, the mandrel must be precision balanced. A trial bias weight may be used to raise the observed residual unbalance readout of the balancing machine. The desired balance result is such that no matter at what angular location the bias weight is added, the unbalance readout is always the same. In this case the residual unbalance of the precision mandrel is as close to zero as possible.

5.4.2.3 Component Preparation and Mounting

After each component is mounted on its mandrel, the axial and radial runouts may be checked to ensure that the mounted impeller or hub is not cocked on its mandrel prior to component balancing. If components are not phase-referenced marked, zero phase shall be taken as the component keyway, locking pin, or key block. If the components are not keyed or do not have a reference point, zero phase shall be permanently identified for use during the assembly balancing procedure.

Mandrels typically do not have keyways. When components that have keyways are to be mandrel-balanced, the keyway should be filled with an inside-crowned half key or an equivalent compensating correction should be added to the component so that a proper balance can be achieved.

5.4.2.4 Special Considerations

Major components, e.g., turbine disks or impellers, may receive a static balance if the component has a balance plane separation that makes dynamic balance impractical.

5.4.3 Low-Speed Balancing Techniques

For rotors operating between the first and second critical speed, there are two principal balancing techniques and each addresses static, couple, and quasi-static unbalance.

a. The first technique is a low-speed progressive-stack balance as described in 5.4.4. In this method, no more than two major components are added at a time. The static and couple unbalance of the assembly is established at each step and the appropriate correction is made to the last two added components (two plane balance).

b. The second technique is an operating speed balance of a complete rotor that has been initially slow-speed balanced as a complete rotor. In the low-speed balance step, a three-plane balance procedure is followed. In this procedure, it is preferred to compensate 30% – 60% of the static component from the center plane, Schenck [1]. The remainder of the correction is divided between the two end planes. This 3-plane procedure should also be used for other rotors such as those that require a re-balance after assembly, based on guidelines in 5.4.5.

5.4.4 Progressive Component Stack Balancing

5.4.4.1 Introduction

Progressive or stack balancing is used to counteract the introduction of unbalance into a rotor by the following two paths.

a. The most common introduction of unbalance into a rotor occurs when previously balanced components are added to the rotor. This occurs in two primary ways. The first cause is the eccentricity between the mandrel and the component and the shaft and the component is different. The second cause is the phase orientation of the mandrel high side to the shaft high side is not duplicated.

b. Components with unequal stiffness in all planes, such as those with single keyways, may deform when shrunk onto the rotor shaft. For such components, considerable deformation and resultant unbalance can occur between mandrel balancing using a light shrink fit and stack balancing on the job shaft with a heavy shrink fit.

5.4.4.2 Balance Procedure

Progressive balancing is a procedure that requires several distinct steps of balancing. It is accomplished by adding no more than two major components for each balance step. Balance corrections are made to the elements added in each step. Component axial and radial runouts should be checked against mandrel runouts, as each component is stacked. In general, the stacked component runouts should match those runouts recorded with the components on the mandrel.

As each rotor component is stacked into position an inspection must be made to verify the components are properly fitted to the main rotor. Common reasons for an unbalance being introduced include the improper mounting or eccentricity of a component or the shift of a component (impeller) due to the relaxation of an interference fit. Trim

balancing of the complete assembly, if required, is done as necessary to achieve the balance tolerance.

5.4.4.3 Index Balancing

Index balancing is a technique employed during low speed balancing to identify the unbalance attributable to components of an assembly. The process involves indexing (turning) of one component (or part of an assembly) with respect to the other during the balance procedure. Vector math is used to identify the unbalance of each of the two components or assemblies. The process is described both graphically and vectorially below.

Index balancing is commonly used in the following situations:

- Low speed balancing involving tooling or arbors that will not accompany the component in the assembly (Ex: The balancing of impellers that require an arbor to be placed on the low speed stand.); and,
- The balance of sub-assemblies or components making an assembly that may not remain together during use. (Ex: Pipeline operators that change impellers in an overhung compressor to meet flow demands.)

In the first situation, it is desirable to correct the impeller for unbalance attributable to the impeller only and not due to unbalance from the arbor or its fit. In the second case, an assembly balance where components may be replaced (without rebalancing) does not guarantee that the new assembly will remain in balance. The individual components or sub-assemblies must be corrected independently.

These situations arise since fits and changes in relative angular position between components may create unbalance. As one component is replaced, the newer component may have variations in the fit in different locations and amounts within the tolerance. Removal and installation of a component may also lead to a different relative angular position with respect to the rest of the assembly through error or inability to

measure the orientation. If an assembly balance is used in the original configuration, an implied assumption is made that the fits and the angular position will always remain the same.

A simple example is provided to show how fit eccentricities will cause unbalance. Take for example a shaft with an overhung fit location (see Figure 5-11). The fit location is eccentric to the centerline of the bearings by an amount, e . The eccentric shaft section has a weight of m . A component of weight, M , is to be installed on the shaft. Assuming that the component is balanced with a perfect fit bore, the resulting unbalance produced by the fit eccentricity would be:

$$U = (m + M) e \quad 5-7$$

Balancing these components as an assembly with balance planes located on the component and the right end of the shaft, a correction of U/r would be made to the component at radius, r (see Figure 5-12).

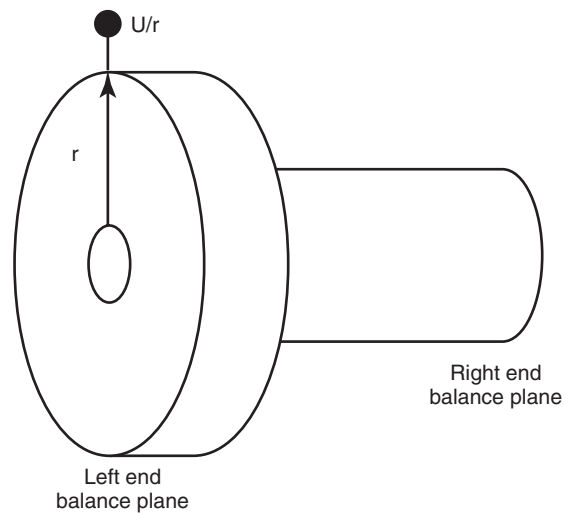


Figure 5-12—Unbalance Correction to Fit Eccentricity

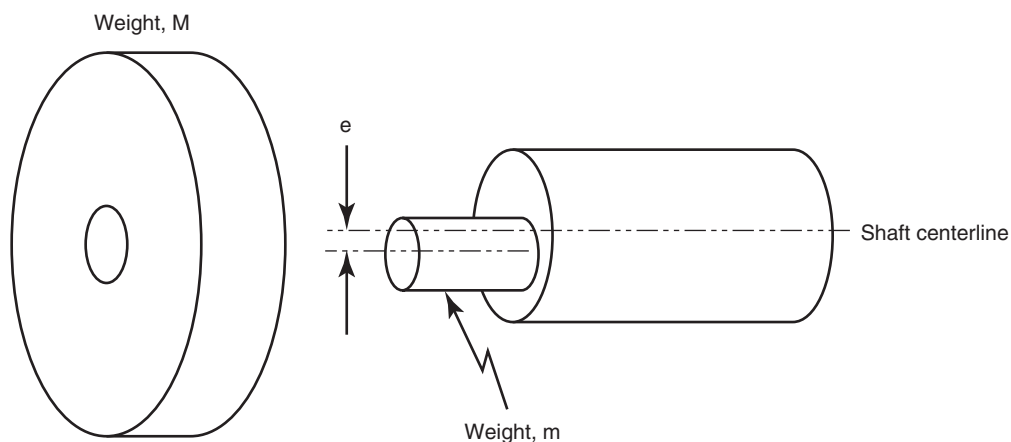


Figure 5-11—Fit Eccentricity Related Unbalance

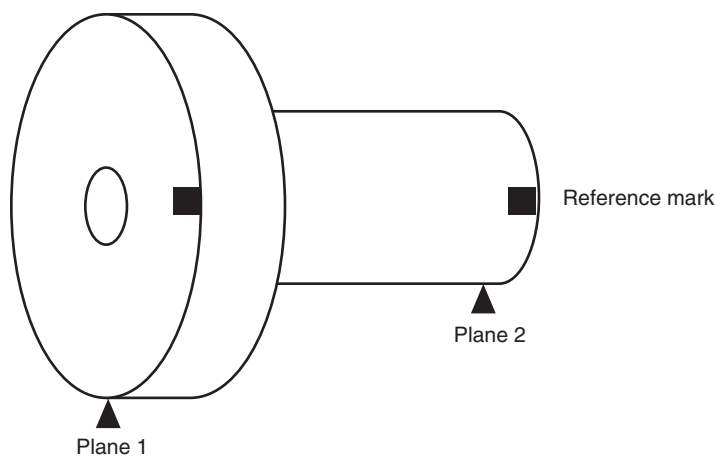
However, should the component be mis-installed rotated 180° , the correction would also be turned and would cause an unbalance of $2U$. Additionally, if the component was replaced with an identically perfect component, the correction would be lost altogether. The correct balance procedure in this case is to make the correction on the left end of the shaft since it was the shaft's fit that created the unbalance originally. Then subsequent mis-installation and replacement of the component would not cause unbalance problems.

The key to the simple example above is identifying which component is the cause of what percentage of the unbalance identified in the low speed balance machines. This cannot be achieved by balancing the pieces separately as is commonly done. Keep in mind that if the shaft was balanced on its own, a correction of only $U = m\varepsilon$ would be made at the left end since the component weight of M would not be present.

If the component in the example above also had an unbalance, u , the low speed balance machine would read a total unbalance level as the vector sum of u and U at the left end balance plane. As noted, the successful balance procedure would then correct the component unbalance, u , on the component and the shaft unbalance, U , on the shaft. Index balancing achieves this separation.

Keeping with the same example, a step-by-step index balance procedure will be performed. A graphical and vectorial description of each step will be shown.

The component (impeller) and the shaft are assembled and an arbitrary 0° reference mark is made. The assembly is placed in the low speed balance machine (low speed stand) and readings are taken at the impeller and far end of the shaft (see Figure 5-13).



The readings taken are \vec{R}_{11} at plane 1 and \vec{R}_{21} at plane 2. (The subscripts denote plane number first and then index step second.) These vectors are comprised of the vector sum of the impeller unbalance \vec{u}_1 and the shaft unbalance \vec{U}_1 also both vector quantities. In our simplistic example, the impeller will be treated as a thin disk. In that case, the impeller unbalance contribution to the plane 2 readings is insignificant. (The impact of this will be highlighted later.) Thus, the reading at plane 1 can be expressed as $\vec{R}_{11} = \vec{u}_1 + \vec{U}_1$. The plane 2 reading is solely comprised of shaft unbalance, \vec{U}_2 , \vec{R}_{11} and \vec{R}_{21} should be recorded at this point.

The next step is removal and indexing of the impeller 180° relative to the shaft. The assembly should be placed in the stand and readings taken (see Figure 5-14).

Since the impeller has been turned 180° relative to the shaft, the unbalance readings taken at plane 1 can now be expressed as $\vec{R}_{12} = -\vec{u}_1 + \vec{U}_1$. The unbalance readings at plane 2 remain unchanged per our simplifying assumption. Vectorially, \vec{R}_{11} and \vec{R}_{12} are shown in Figure 5-15. At this stage, the vector quantities \vec{u}_1 and \vec{U}_1 are still unknown.

Through vector manipulation the following statements are true:

$$\vec{R}_{12} + \vec{R}_{11} = 2\vec{U}_1 \quad (5-8)$$

$$\vec{R}_{11} - \vec{R}_{12} = 2\vec{u}_1 \quad (5-9)$$

Notice that by either adding or subtracting the two readings taken during the procedure, the unbalance attributable to either piece is identifiable. This permits correction of the

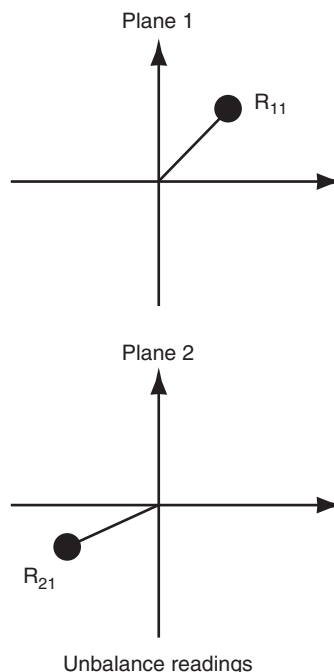


Figure 5-13—Initial Reading of the Index Balancing Method

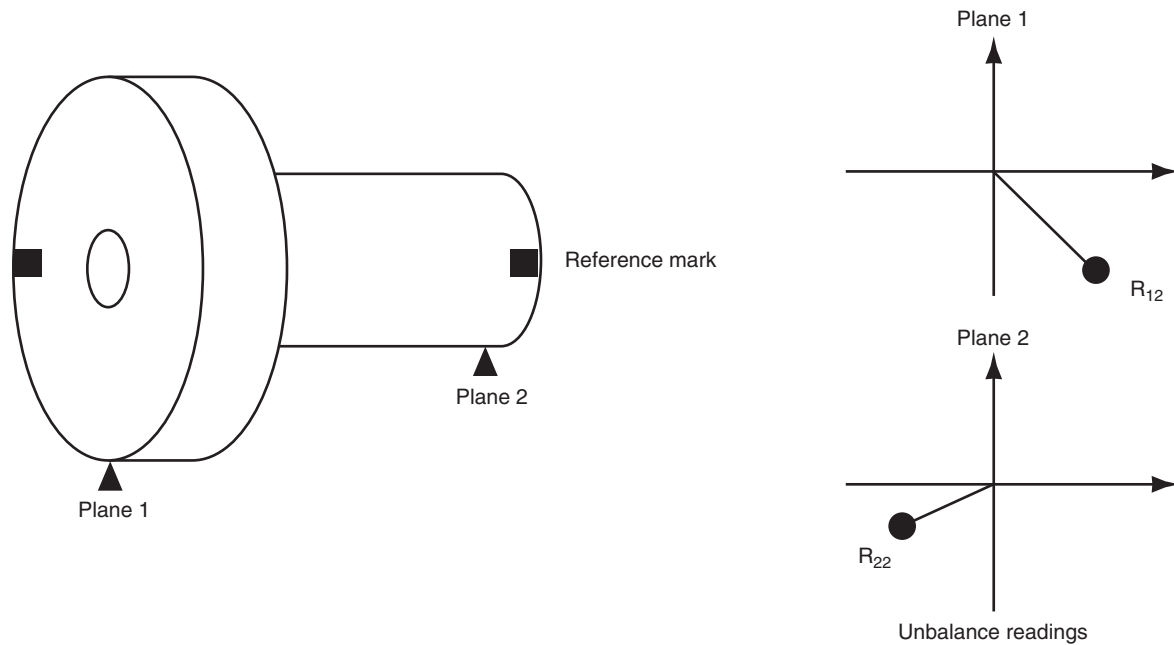


Figure 5-14—Indexed Component Relative to the Shaft

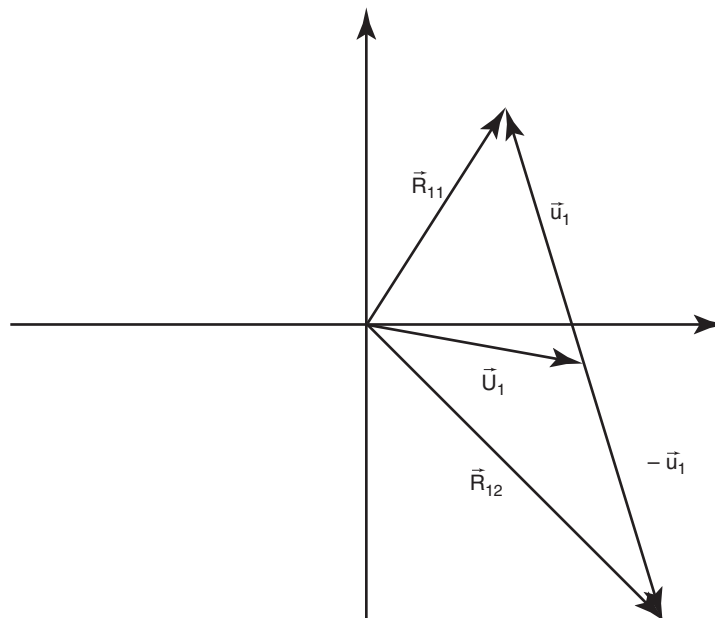


Figure 5-15—Vector Representation of R_{11} and R_{12}

impeller and the shaft by the amounts identified in the equations. Graphically, these vector manipulations are shown in Figure 5-16.

Once these corrections are made to the corresponding parts, the process can be repeated to ensure that balance tolerances have been met. Most low speed balance machines have software that automates this process and performs the vector subtraction internally.

The assumption was made early on that the component could be balanced using one plane (its $L/D \ll 1.0$). If two planes were needed to balance the component or subassembly (the impeller in our example), the balance planes during the indexing procedure would be set for the locations as required on that part. Since the shaft or remaining part may not share those balance planes, the shaft (unbalance attributable to that part) would be ignored during these runs. After

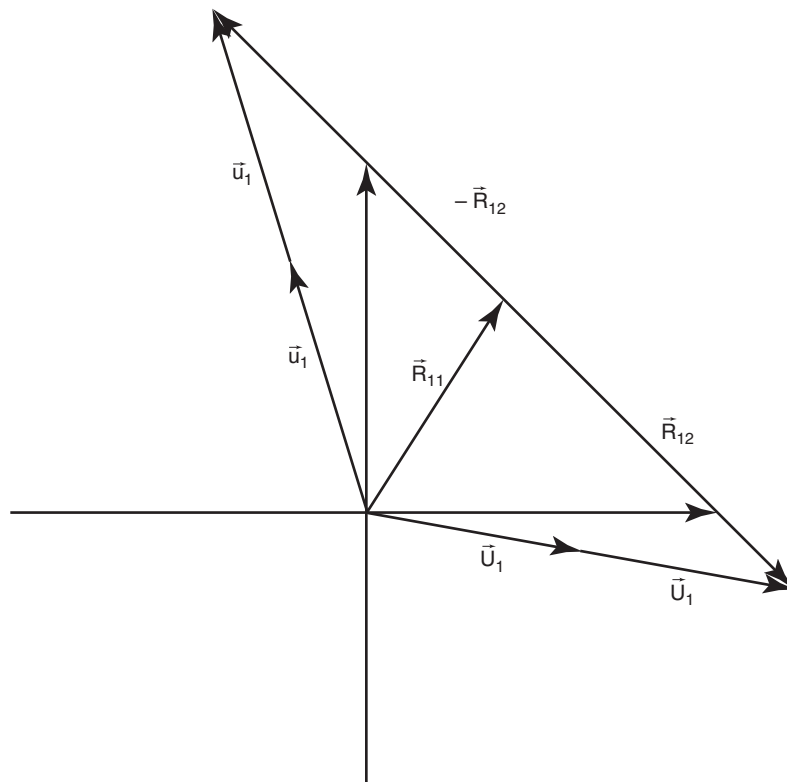


Figure 5-16—Results of Adding and Subtracting Vectors R_{11} and R_{12}

completing the index balance of the first component (impeller in our example), the planes would be reset to those needed to balance the remaining component or subassembly (shaft in our example.) The index balance procedure would then be repeated but now the unbalance attributable to the impeller would be ignored.

Note: That since the impeller was previously balanced, its unbalance levels should be within tolerance.

Finally, literature is available concerning the index balance method. Implementation of the method without automated software is shown in Reference [5].

5.4.5 Operating-speed Balancing

5.4.5.1 Introduction

The balancing of flexible rotors (rotors that operate above their first critical speed) at their operating speed has become a more acceptable practice in the turbomachinery industry in recent years. This practice is a dramatic change from the time when all rotors were low speed balanced and operating speed balancing was seen as an expensive, unproven technology. Operating speed balancing requires measuring dynamic forces at the bearings, at operating speed and with bearings that closely simulate the actual rotor/bearing dynamics. This technique is especially useful where bending deflections, at

operating speed magnify the forces that are present due to the residual unbalance remaining from a slow speed balance.

5.4.5.2 Applications of Operating-speed Balancing

There are conditions where operating-speed balancing should be considered as the balancing procedure. They include:

- Rotors, which have exhibited high vibration as they pass through their critical speeds.
- Rotors, which accelerate slowly through their critical speeds (ie. gas turbines).
- Rotors, which are running on or near a critical speed.
- Rotors, which are very sensitive to unbalance.
- Rotors for equipment in extremely critical services.
- Rotors going to inaccessible locations, such as offshore.
- Very long, flexible rotors.
- Places where a critical rotor cannot be run in its intended casing prior to installation.

ISO Standard 5406 provides a classification system for balancing of rotors. They are:

- **Class 1:** Rigid rotors.
- **Class 2:** Rotors, which cannot be considered rigid but can be balanced in a low speed balance machine. (Most API turbomachinery.)
- **Class 3:** Rotors, which cannot be balanced in a low-speed balancing machine and which require high speed balancing techniques.
- **Class 4:** Rotors which could be placed into Classes 1, 2, or 3, but which have, in addition, one or more components, which are flexible or are flexibly attached.
- **Class 5:** Rotors, which could be placed into Class 3, but for some reason, e.g., economy, are balanced for only one speed.

Using the above classification, new rotors in most API turbomachinery would be placed into Class 2. These Class 2 rotors would be candidates for receiving an operating speed balance for conditions b, e, and h, as described in 5.2.5. Likewise, existing rotors in service would be likely to receive an operating speed balance for conditions a, c, d, and g.

5.4.5.3 Operating-Speed Balancing Procedure

The contract rotor dynamics analysis should be available prior to attempting an operating-speed balance. This analysis will provide information about the predicted rotor mode shape as it passes through its resonant frequencies and about the best location for balance weights to minimize rotor vibration.

Note since the stiffness and mass of the balancing machine bearing pedestals may vary significantly from actual field installation, the critical speeds as observed in the balancing machine may differ significantly from that observed when the rotor is run in the field.

In the operating speed balancing process, incremental rotor assembly and balance for Class 1 or 2 rotors is not required. Instead, a preliminary three-plane, low-speed balance is required to limit the initial rotor response (see 5.4.3). The final corrections are then made following operating speed measurements.

In this procedure, a rotor is completed assembled for the balancing procedure. The assembly should include thrust collars with locking collars and any auxiliary such as power take-off gears, overspeed trip assemblies, and tachometer rings for governor overspeed switches. In most cases, the facility drive coupling and adapter is adequate to insure the rotor mode shape is simulated at operating speed. Note, the pedestal stiffness may depress the second resonant frequency. In some cases, the job-coupling hub with moment simulator may be required, especially for the outboard ends of drive-through machines. The balance of the rotor is checked at low speed. (Bypassing of this procedure could result in serious

damage to the rotor and/or operating-speed balancing machine.) Engineering judgment and operator experience is then used to determine if any corrections need to be made prior to running the rotor at operating speed.

The rotor and balancing machine pedestal supports are placed in a vacuum chamber to reduce the power required to turn the rotor at higher speeds and to reduce heating from windage. Specially-manufactured oil film design bearings or job bearings are generally necessary to perform the balancing since the high speeds require journal bearings rather than the anti-friction type used in low-speed balancing machines. The more closely the bearings used in the balancing machine match the job bearings, the more closely the response of the rotor in the balance machine will match the expected response of the rotor in field.

Proper conditioning of the rotor workpiece to remove all bows and distortion prior to operating-speed balancing is essential. This conditioning is accomplished by spinning the rotor up and down in speed until the unbalance readout and phase angle becomes stabilized. This process may also require the application of heat to the rotor during the spinning process. The time required for this stabilization will vary widely from rotor to rotor.

Once the stable rotor is at operating speed, corrections can be made to the rotor, often in more than two planes, to achieve the desired levels of unbalance.

5.4.5.4 Balancing Tolerance

The velocity acceptance criteria for operating-speed balancing, with maximum pedestal stiffness at all speeds, measured on the pedestals is dependent on the magnitude of the force transmitted from the rotor to the bearings. The velocity criterion is also highly dependent upon the pedestal stiffness. For example, pedestals with low stiffness can depress the second resonant frequency so that it is near the operating speed. This may cause the rotor response to be accentuated. In this situation, a lower velocity criterion would be required to achieve a properly balanced rotor.

For Class 2 rotors, the pedestal velocity should be optimized at the first critical speed and at the maximum continuous speed. The velocity should be limited to the value that will result in the transmitted force to be 0.2 'g', i.e., 10% of the rotor weight to each pedestal at maximum continuous speed. At the first resonant frequency, the velocity should be limited to the value that will result in the transmitted force to be 0.5 'g'.

If the test setup has depressed the second resonant frequency so that it is within 20% of the operating speed, the tolerance can be increased to 0.5 'g'. The rationale for this approach results from the fact the second critical speed will be much higher in the installed situation and the rotor response will be significantly decreased. In this special situation, additional screening factors may be required.

The following example will demonstrate the relationship between the velocity criteria, pedestal stiffness, and the balance tolerance.

Assume a balance tolerance of 0.2 'g'. Further assume the rotor weighs 2000 lb (1000 lb per pedestal) and operates at 10,000 rpm (167 Hz). If the velocity (V) of the bearing pedestal is 1.0 mm/sec RMS, then the displacement of the pedestal is

$$\text{Peak Displacement} = \frac{1.414V}{2\pi f} = \frac{1.414(1.0)}{2(3.14)(166.7)} \quad (5-10)$$

$$\text{Peak Displacement} = 0.00135 \text{ mm} (0.000053 \text{ in.})$$

where

V = velocity of the bearing pedestal.

Two common pedestal stiffness values are $5.6 \times 10^8 \text{ N/m}$ ($3.2 \times 10^6 \text{ lb/in.}$) and $1.33 \times 10^9 \text{ N/m}$ ($7.6 \times 10^6 \text{ lb/in.}$). From the relationship,

$$\text{Force N (lbf)} = \text{Displacement m (in.)} \times \text{Stiffness N/m (lbf/in.)} \quad (5-11)$$

And, for the pedestal stiffness of $5.6 \times 10^8 \text{ N/m}$ ($3.2 \times 10^6 \text{ lb/in.}$),

$$\text{Force N (lbf)} = 1.35 \times 10^{-6} \text{ m} (0.000053 \text{ in.}) \times 5.6 \times 10^8 \text{ N/m} (3.2 \times 10^6 \text{ lb/in.}) = 756 \text{ N} (170 \text{ lbf}) \quad (5-12)$$

Or, for the pedestal stiffness of $1.33 \times 10^9 \text{ N/m}$ ($7.6 \times 10^6 \text{ lb/in.}$),

$$\text{Force N (lbf)} = 1.35 \times 10^{-6} \text{ m} (0.000053 \text{ in.}) \times 1.33 \times 10^9 \text{ N/m} (7.6 \times 10^6 \text{ lb/in.}) = 1795.5 \text{ N} (400 \text{ lbf}). \quad (5-13)$$

In this case, the velocity criteria of 1.0 mm/sec is appropriate for the pedestal stiffness of $3.2 \times 10^6 \text{ lb/in.}$ but is inadequate for the pedestal stiffness of $7.6 \times 10^6 \text{ lb/in.}$ For the latter case, the velocity criteria should be 0.5 mm/sec.

The relationship between balancing machine pedestal stiffness, rotor weight and operating speed for one manufacturer is shown in Table 5-1.

Note: Pedestal stiffness is intentionally lower than normal machinery supports in order to have good balancing sensitivity. The mass of the pedestals also affects the rotor support system natural frequencies. These values are approximate and care must be used to remain within limits set by manufacturer of the pedestals. There may be pedestal stiffening available to increase the stiffness values. A particular balance facility may have pedestals that only cover part of the speed range, are not able to accommodate rotor lengths or outside diameter, or do not have required bearings to fit inside the pedestals for a particular application.

5.4.5.5 Advantages of Operating Speed Balancing

Operating speed balancing can provide a rotor with less vibration from the remaining unbalance distribution, and therefore, a rotor that is less sensitive to additional unbalance that might be acquired during operation. In variable speed applications, this benefit could allow the process flexibility of safely operating the machine at a higher speed, which would be closer to the second critical speed.

5.4.6 Keys and Keyways

Keys and keyway clearances are areas that are often overlooked and yet critical to a precision balance job. All keys should have a top clearance of 0.05 mm – 0.15 mm (0.004 in. – 0.006 in.). Excessive top key clearance will allow the key to move radially outward during operation, resulting in a change in unbalance. Conversely, insufficient (or zero) top key clearance may prevent the wheel from properly seating on the shaft. A tall key will distort the wheel bore, resulting in a change in unbalance.

During progressive component stack balancing, all empty shaft single keyways must be filled with half-keys to ensure that unbalance due to unfilled keyways is not compensated for in trim balancing stacked components.

5.4.7 Residual Unbalance Test

After completion of the final balancing of the rotating assembly, and before removing the rotor from the balancing machine, a residual unbalance test should be performed to verify that the residual unbalance of the rotor is within the $4W/N$ tolerance. This test is performed to ensure that the balancing machine readout is correct because balancing machine calibration shift and operator error can occur.

Table 5-1—Relationship Between Balancing Machine Pedestal Stiffness, Rotor Weight and Operating Speed (for one manufacturer)

Pedestal Size	Typical Pedestal Stiffness Range		Typical Rotor Weight Range		Typical Speed Range
	Customary Units	SI Units	Customary Units	SI Units	
	lb/in. $\times 10^6$	N/ μm	lb	kg	
SMALL	1.5 – 2.0	250 – 350	100 – 5, 500	45 – 2,500	20,000
MEDIUM	2.5 – 4.5	450 – 800	500 – 28,000	225 – 12,700	12,000
LARGE	5.5 – 10.0	1,000 – 1,800	1,500 – 110,000	680 – 50,000	6,000

The API Residual Unbalance Test, as shown in 5.4.11, leaves no doubt as to the amount and location of the assembled rotor's residual unbalance.

This test is accomplished by adding a known trial weight to the rotor in six equally spaced radial positions in each balance machine readout plane. The trial weight and radius is selected so that approximately two times the $4W/N$ residual unbalance tolerance (four times $4W/N$ for soft bearing balancing machines) is produced. The trial weight should first be positioned at the heavy spot on the rotor (if known) to assist in selecting the proper readout scale on the balancing machine. The heavy spot location on the rotor is then considered as the zero point on the rotor for the polar plot.

The rotor is then run up to test speed and the balancing machine amplitude and trial weight location is measured and recorded on polar graph paper. (Note that the data to be recorded on the polar plot is balancing machine amplitude versus the angular location of the trial weight, not the balancing machine phase angle). This test is repeated for all trial weight positions in each balance plane of the rotor. Each plane's polar plot of balancing machine amplitude versus the trial weight location should approximate a true circle that encircles the center of the polar plot. If the plot does not approximate a true circle and/or encircle the center of the polar plot, then either the residual unbalance is in error due to inadequate sensitivity of the balancing machine, the trial weight is smaller than the residual unbalance indicating that the rotor is not balanced correctly, or a balancing machine fault exists (i.e., a faulty pickup).

Careful placement of the known unbalance at the correct radius at each interval is essential for this test.

The polar point plotted for run-test number one should repeat at the end of the test indicating that the balancing machine is reading out consistently. A balancing machine that will not read out consistently for two identical runs cannot be used to determine true residual unbalance.

For rotors that are balanced at operating speed, the residual unbalance test is not applicable. The unbalance distribution, due to the optimization of the first critical and operating speed conditions, can result in low-speed readings that exceed the $4W/N$ criteria. An alternative test would be to perform a Check Balance per 5.4.8. To conduct this test, the final unbalance readings from a low speed balancing machine should be recorded along with an identified phase reference and then compared to the readings obtained following the operating speed balancing.

5.4.8 Check Balancing

Once a rotor has been balanced in accordance with the above outlined procedures, further balancing should not be required. Far too often rotors that have been properly balanced to the correct tolerances are removed from storage for check balancing prior to their installation. During this check

balancing procedure it is possible that the rotor will be found to be out of tolerance and, therefore, will be re-balanced.

Unfortunately, what the balancing machine operator does not realize is that he or she has just balanced out a temporary rotor bow resulting from long-term horizontal storage of the rotor. Also, very small temperature differences between the top and bottom of a horizontally stored rotor can contribute to a temporary bow. (The above two reasons are the primary reasons that rotors are stored vertically.) This temporary bow, after installation into the machine, may straighten itself after being placed into operation and thus become unbalanced, resulting in excessive vibration.

A rotor that has been properly stack-component balanced and documented as such should never be re-balanced prior to its installation unless obvious damage or other sound justification is apparent. If the check balance of a rotor prior to its installation reveals an out-of-tolerance residual unbalance condition, then a thorough inspection of the rotor should be performed and additional data (that is, rotor runout maps) should be measured and recorded to ascertain the problem with the rotor. If the problem cannot be located and resolved, then the rotor should be totally disassembled and re-stack component balanced as previously specified.

5.4.9 Field Balancing

In some cases, field balancing has been found to be necessary. This is typical of very large steam turbines (over 50 MW) and for field-erected equipment that does not lend itself to shop balancing. This, however, should be considered as a last resort for high-speed rotors.

Field balancing attempts to correct for the combined effect of misalignment, seal rubs, foundation resonance, and rotor unbalance. This approach does not address the true cause of the excitation forces on the rotor. Generally, only end-plane balance corrections are available, which further limits the effectiveness of this balancing method.

While field balancing has been done successfully, it has a fairly high failure rate in rotors with multiplane correction points and may not correct the problem despite the best of efforts.

5.4.10 References

1. "Aspects of Flexible Rotor Balancing," Third Edition, 1980, Schenck Trebel, Deer Park, New York.
2. "Fundamentals of Balancing," Third Edition, April 1990, Schenck Trebel, Deer Park, New York.
3. "Dynamic Balancing Handbook Form #2049", October 1990, IRD Mechanalysis, Inc., Columbus, Ohio.
4. Brown, R.N., 1997, "Compressors—Selection and Sizing", Gulf Publishing Company.
5. Wowk, V., *Machinery Vibration: Balancing*, 1994, McGraw-Hill Professional.

5.5 STANDARD PARAGRAPHS ON BALANCING

SP6.8.8 Vibration and Balancing

SP6.8.8.1 Major parts of the rotating element, such as the shaft, balancing drum and impellers, shall be individually dynamically balanced before assembly, to ISO 1940 Grade G1 or better. When a bare shaft with a single keyway is dynamically balanced, the keyway shall be filled with a fully crowned half key, in accordance with ISO 8821. Keyways 180° apart, but not in the same transverse plane, shall also be filled. The initial balance correction to the bare shaft shall be recorded. The components to be mounted on the shaft (impellers, balance drum etc.), shall also be balanced in accordance with the “half-key-convention” as described in ISO 8821.

SP6.8.8.2 Unless otherwise specified, the rotating element shall be sequentially multiplane dynamically balanced during assembly. This shall be accomplished after the addition of no more than two major components. Balancing correction shall only be applied to the elements added. Minor correction of other components may be required during the final trim balancing of the completely assembled element. In the sequential balancing process, any half-keys used in the balancing of the bare shaft (see SP6.8.8.1) shall continue to be used until they are replaced with the final key and mating element. On rotors with single keyways, the keyway shall be filled with a fully crowned half-key. The weight of all half-keys used during final balancing of the assembled element shall be recorded on the residual unbalance work sheet (see Appendix B). The maximum allowable residual unbalance per plane (journal) shall be calculated as follows:

In SI units:

$$U_{\max} = 6350 W/N \quad (9a)$$

In Customary units:

$$U_{\max} = 4 W/N \quad (9b)$$

where

U_{\max} = Residual unbalance, in g-mm (oz-in.),

W = Journal static weight load, in kilograms (lb.),

N = Maximum continuous speed (rpm).

- **SP6.8.8.3** When specified, completely assembled rotating elements shall be subject to high speed (at speed) balancing in lieu of a sequential low speed balancing (6.8.8.2). When the vendor’s standard balance method is by high speed balancing in lieu of a sequential low speed balancing and high speed balancing is not specified, it may be used with the pur-

chaser’s approval. The high speed balance shall be in accordance with 6.8.8.4.

SP6.8.8.4 When the complete rotating element is to be high speed balanced (see SP6.8.8.3), the rotor shall be supported in bearings of the same type and with similar dynamic characteristics as those in which it will be supported in service. The final check balance shall be carried out at maximum continuous speed. Before making any corrections (unless it is necessary to improve the initial balance in order to be able to run the rotor at high speed), the rotor shall be run, in the balancing machine at trip speed for at least 5 minutes, to allow seating of any shrunk-on components.

SP6.8.8.5 Unless otherwise specified, the vibration acceptance criteria for high speed balancing, with maximum pedestal stiffness at all speeds, measured on the bearing cap shall be as follows:

- For all speeds above 3000 rpm; it shall not exceed the “greater” of 7400/ N mm/sec (291/ N in./sec) or 1 mm/sec (0.039 in./sec) where N is the speed in revolutions per minute.
- For all speeds less than 3000 rpm; it shall not exceed 2.5 mm/sec (0.098 in./sec).

Note: This residual unbalance is at all speeds (includes any criticals) and the force from this residual unbalance is ≤ 0.079 gs.

- **SP6.8.8.6** When specified, a rotor that is to be high speed balanced, shall first receive a sequential low speed balance as specified in SP6.8.8.2.
- **SP6.8.8.7** For a rotor that has been low speed sequentially balanced (SP6.8.8.2) and when specified for rotors that are high speed balanced (SP6.8.8.3), a low speed residual unbalance check shall be performed in a low speed balance machine and recorded in accordance with the residual unbalance work sheet (see Appendix B).

Note: This is done to provide a reference of residual unbalance and phase for future use in a low speed balance machine.

SP6.8.8.8 During the shop test of the machine, assembled with the balanced rotor, operating at its maximum continuous speed or at any other speed within the specified operating speed range, the peak-to-peak amplitude of unfiltered vibration in any plane, measured on the shaft adjacent and relative to each radial bearing, shall not exceed the following value or 25 microns (1 mil), whichever is less:

In SI units:

$$A_1 = 25.4 \sqrt{\frac{12,000}{N}} \quad (10a)$$

In Customary units:

$$A_1 = \sqrt{\frac{12,000}{N}} \quad (10b)$$

where

A = Amplitude of unfiltered vibration, μm (mil) true peak to peak,

N = Maximum continuous speed, (rpm).

At any speed greater than the maximum continuous speed, up to and including the trip speed of the driver, the vibration shall not increase more than $12.7 \mu\text{m}$ (0.5 mil) above the maximum value recorded at the maximum continuous speed.

Note: These limits are not to be confused with the limits specified in SP6.8.3 for shop verification of unbalanced response.

SP6.8.8.9 Electrical and mechanical runout shall be determined by rotating the rotor through the full 360° supported in V blocks at the journal centers while measuring runout with a

non-contacting vibration probe and a dial indicator at the centerline of each probe location and one probe-tip diameter to either side.

DISCUSSION: It should be pointed out that the rotor runout determined from SP6.8.8.9 generally will not be reproduced when the rotor is installed in a machine with hydrodynamic bearings. This is due to pad orientation on tilt pad bearings and effect of lubrication in all journal bearings. The rotor will assume a unique position in the bearings based on the slow roll speed and rotor weight.

SP6.8.8.10 Accurate records of electrical and mechanical runout for the full 360° at each probe location shall be included in the mechanical test report.

SP6.8.8.11 If the vendor can demonstrate that electrical or mechanical runout is present, a maximum of 25% of the test level calculated from Equation 6 or 6.4 microns (0.25 mil), whichever is greater, may be vectorially subtracted from the vibration signal measured during the factory test.

5.6 STANDARD PARAGRAPHS ON DYNAMICS

SP6.8 DYNAMICS

SP6.8.1 General

Note: Refer to API Publ 684 *Tutorial on the API Standard Paragraphs Covering Rotor Dynamics and Balancing: An Introduction to Lateral Critical, Stability, and Train Torsional Analysis and Rotor Balancing*.

SP6.8.1.1 In the design of rotor-bearing systems, consideration shall be given to all potential sources of periodic forcing phenomena (excitation) which shall include, but are not limited to, the following sources:

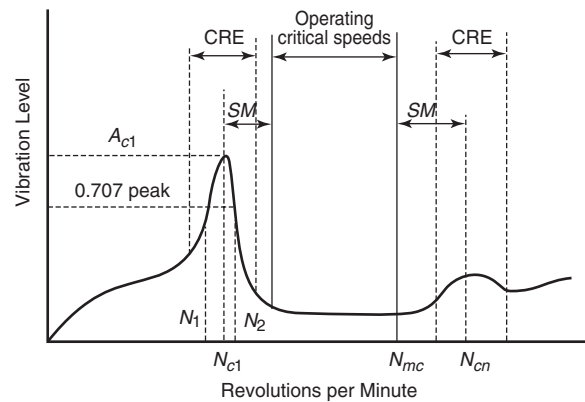
- Unbalance in the rotor system.
- Oil-film instabilities (whirl).
- Internal rubs.
- Blade, vane, nozzle, and diffuser passing frequencies.
- Gear-tooth meshing and side bands.
- Coupling misalignment.
- Loose rotor-system components.
- Hysteretic and friction whirl.
- Boundary-layer flow separation.
- Acoustic and aerodynamic cross-coupling forces.
- Asynchronous whirl.
- Ball and race frequencies of rolling element bearings.
- Electrical line frequency.

Note 1: The frequency of a potential source of excitation may be less than, equal to, or greater than the rotational speed of the rotor.

Note 2: When the frequency of a periodic forcing phenomenon (excitation) applied to a rotor-bearing support system coincides with a natural frequency of that system, the system will be in a state of resonance. A rotor-bearing support system in resonance may have the magnitude of its normal vibration amplified. The magnitude of amplification and, in the case of critical speeds, the rate of change of the phase-angle with respect to speed, is related to the amount of damping in the system.

SP6.8.1.2 For the purposes of this standard, resonant conditions of concern are those with an amplification factor (AF) equal to or greater than 2.5 (see Figure SP-6).

SP6.8.1.3 Resonances of structural support systems that are within the vendor's scope of supply and that affect the rotor vibration amplitude shall not occur within the specified operating speed range or the specified separation margins (SM) (see SP6.8.2.10). The effective stiffness of the structural support shall be considered in the analysis of the dynamics of the rotor-bearing-support system (see SP6.8.2.4d).



- N_{c1} = Rotor first critical, center frequency, cycles per minute
- N_{cn} = Critical speed, nth
- N_{mc} = Maximum continuous speed
- N_1 = Initial (lesser) speed at $0.707 \times$ peak amplitude (critical)
- N_2 = Final (greater) speed at $0.707 \times$ peak amplitude (critical)
- $N_2 - N_1$ = Peak width at the half-power point
- AF = Amplification factor
- $$= \frac{N_{c1}}{N_2 - N_1} \quad (1)$$
- SM = Separation margin
- A_{c1} = Amplitude at N_{c1}
- A_{cn} = Amplitude at N_{cn}

Note: The shape of the curve is for illustration only and does not necessarily represent any actual rotor response plot.

Figure SP-6—Rotor Response Plot

Note: Resonances of structural support systems may adversely affect the rotor vibration amplitude.

- SP6.8.1.4** The vendor who is specified to have unit responsibility for the complete drive train shall communicate the existence of any undesirable running speeds in the range from zero to trip speed. A list of all undesirable speeds from zero to trip shall be submitted to the purchaser for his review and included in the instruction manual (see Annex B of the applicable chapter).

Note: Examples of undesirable speeds are those caused by the rotor lateral critical speeds, system torsionals, and blading modes.

SP6.8.2 Lateral Analysis

SP6.8.2.1 Critical speeds and their associated AF s shall be determined by means of a damped unbalanced rotor response analysis.

SP6.8.2.2 The location of all critical speeds below the trip speed shall be confirmed on the test stand during the mechanical running test (see SP6.8.3.1). The accuracy of the analytical model shall be demonstrated (see SP6.8.3).

SP6.8.2.3 Prior to carrying out the damped unbalanced response analysis, the vendor shall conduct an undamped

analysis to identify the undamped critical speeds and determine their mode shapes located in the range from 0% – 125% of trip speed. Unless otherwise specified, the results of the undamped analysis shall be furnished. The presentation of the results shall include:

- a. Mode shape plots (relative amplitude vs. axial position on the rotor).
- b. Critical speed-support stiffness map (frequency vs. support stiffness). Superimposed on this map shall be the calculated system support stiffness, horizontal (k_x), and vertical (k_y) (see Figure SP-7).

Note: For machinery with widely varying bearing loads and/or load direction such as overhung style machines, the vendor may propose to substitute mode shape plots for the undamped critical speed map and list the undamped critical speed for each of the identified modes.

SP6.8.2.4 The damped unbalanced response analysis shall include but shall not be limited to the following:

Note: The following is a list of items the analyst is to consider. It does not address the details and product of the analysis which is covered in SP6.8.2.7 and SP6.8.2.8.

a. Rotor masses, including the mass moment of coupling halves, stiffness, and damping effects (for example, accumulated fit tolerances, fluid stiffening and damping).

b. Bearing lubricant-film stiffness and damping values including changes due to speed, load, preload, range of oil temperatures, maximum to minimum clearances resulting from accumulated assembly tolerances, and the effect of asymmetrical loading which may be caused by gear forces, side streams, eccentric clearances, etc.

c. For tilt-pad bearings, the pad pivot stiffness.

d. Support stiffness, mass, and damping characteristics, including effects of frequency dependent variation. The term “support” includes the foundation or support structure, the base, the machine frame and the bearing housing as appropriate. For machines whose bearing support system stiffness values are less than or equal to 3.5 times the bearing oil film stiffness values, support stiffness values derived from modal testing or calculated frequency dependent support stiffness and damping values (impedances) shall be used. The vendor shall state the support stiffness values used in the analysis and the basis for these values (for example, modal tests of similar rotor support systems, or calculated support stiffness values).

Note 1: The support stiffness should in most cases be no more than 8.75×10^5 N/mm (5×10^6 lb/in.).

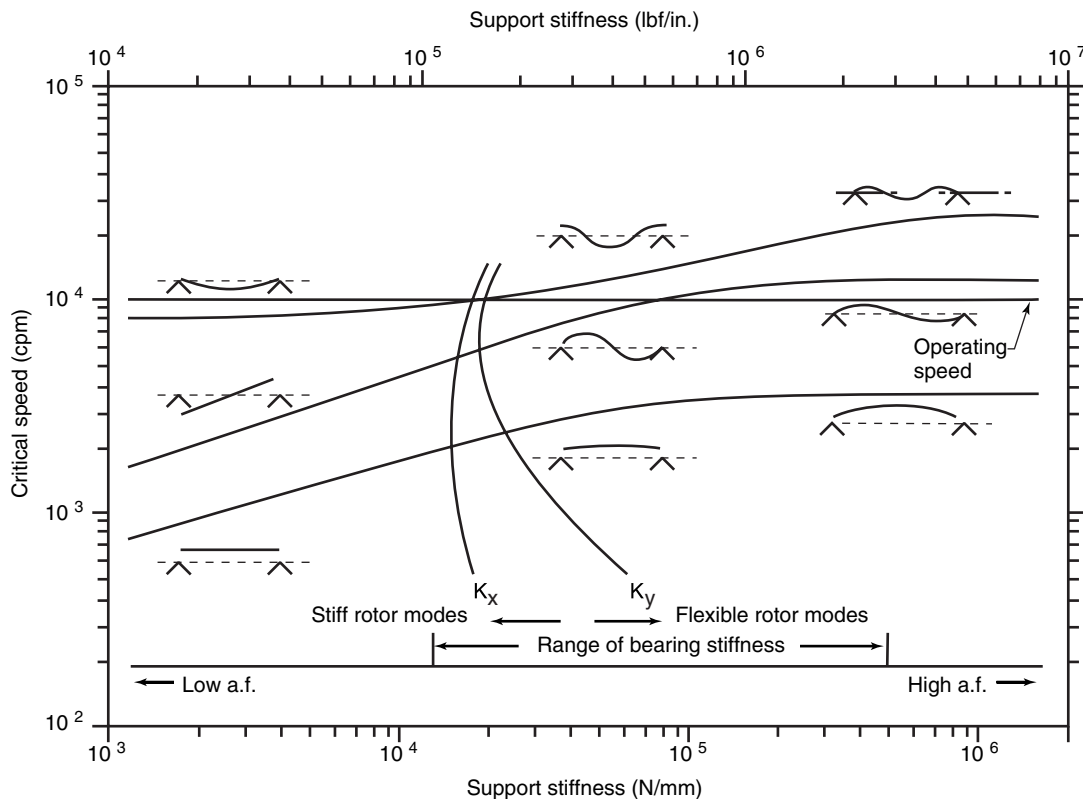


Figure SP-7—Undamped Critical Speed Map

Note 2: Guidelines are used to define whether or not bearing support stiffness should be considered. While modal testing of the actual bearing support system would be preferred, an analytical analysis (such as FEA) is permitted.

e. Rotational speed, including the various starting-speed detents, operating speed and load ranges (including agreed upon test conditions if different from those specified), trip speed, and coast-down conditions.

f. The influence, over the operating range, of the hydrodynamic stiffness and damping generated by the casing shaft end seals.

g. The location and orientation of the radial vibration probes which shall be the same in the analysis as in the machine.

h. Squeeze film dampers.

SP6.8.2.5 In addition to the damped unbalanced response analysis requirements of SP6.8.2.4, for machines equipped with rolling element bearings, the vendor shall state the bearing stiffness and damping values used for the analysis and either the basis for these values or the assumptions made in calculating the values.

- **SP6.8.2.6** When specified, the effects of other equipment in the train shall be included in the damped unbalanced response analysis (that is, a train lateral analysis shall be performed).

Note: In particular, this analysis should be considered for machinery trains with rigid couplings.

SP6.8.2.7 A separate damped unbalanced response analysis shall be conducted for each critical speed within the speed range of 0%–125% of trip speed. Unbalance shall analytically be placed at the locations that have been determined by the undamped analysis to affect the particular mode most adversely. For the translatory (symmetric) modes, the unbalance shall be based on the sum of the journal static loads and shall be applied at the location of maximum displacement. For conical (asymmetric) modes, an unbalance shall be added at the location of maximum displacement nearest to each journal bearing. These unbalances shall be 180 degrees out of phase and of a magnitude based on the static load on the adjacent bearing. Figure SP-8 shows the typical mode shapes and indicates the location and definition of U for each of the shapes. The magnitude of the unbalances shall be 4 times the value of U as calculated by Equations 2a or 2b.

In SI units:

$$U = 6350 W/N \quad (2a)$$

or 254 μm mass displacement, whichever is greater.

In U.S. Customary units:

$$U = 4 W/N \quad (2b)$$

or 10 mils mass displacement, whichever is greater.

where

U = input unbalance for the rotordynamic response analysis in g-mm (oz-in.),

N = maximum continuous operating speed, rpm,

W = journal static load in kg (lbm), or for bending modes where the maximum deflection occurs at the shaft ends, the overhung mass (that is the mass of the rotor outboard of the bearing) in kg (lbm) (see Figure SP-8).

Note: The limits on mass displacement are in general agreement with the capabilities of conventional balance machines, and are necessary to invoke for small rotors running at high speeds.

SP6.8.2.7.1 For rotors where the impellers are cantilevered beyond the journal bearings, unbalance shall be added at the impellers and components such as locknuts, shaft end seals and the coupling for the case of the non-integrally geared rotors. Each mode that is less than 125% of trip speed shall be analyzed. The modes shall be calculated at minimum and maximum support stiffness and in the case of integrally geared rotors include the change in support stiffness resulting from minimum to maximum torque transmitted through the gearing. The unbalance shall be located at or close to the component center of gravity and phased to create maximum synchronous response amplitude.

SP6.8.2.7.2 For rotors which are between bearing designs, unbalance shall be added at the impellers and major rotor components such as balance drums and couplings. The unbalance shall be located at or close to the component center of gravity and phased to create maximum synchronous response amplitude.

SP6.8.2.8 As a minimum, the unbalanced response analysis shall produce the following:

Note: The following is the list of analysis details and identifies the deliverables. The items to be considered in the analysis were identified in SP6.8.2.4.

- Identification of the frequency of each critical speed in the range from 0% – 125% of the trip speed.
- Frequency, phase and response amplitude data (Bode plots) at the vibration probe locations through the range of each critical speed resulting from the unbalance specified in SP6.8.2.7.
- The plot of deflected rotor shape for each critical speed resulting from the unbalances specified in SP6.8.2.7, showing

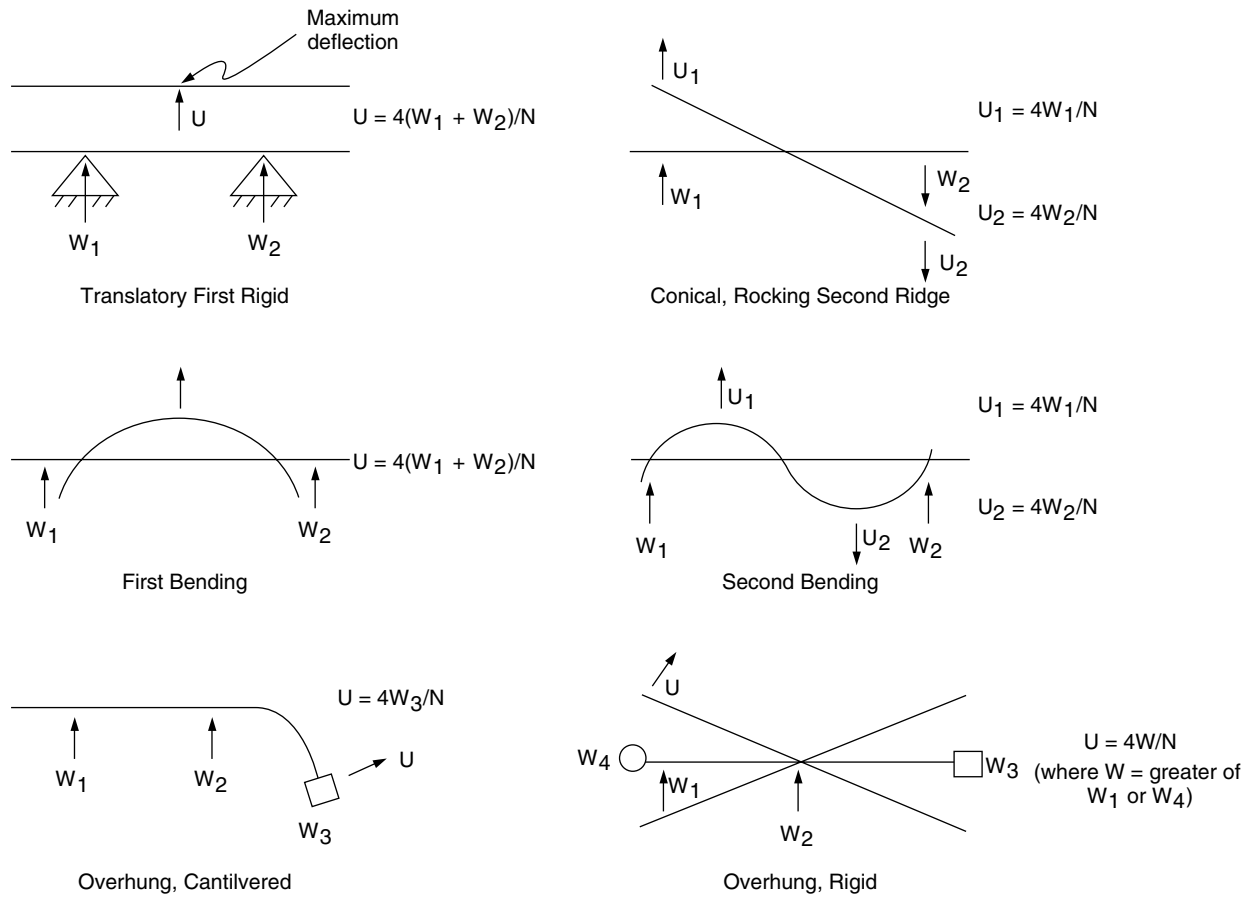


Figure SP-8—Typical Mode Shapes

the major-axis amplitude at each coupling plane of flexure, the centerlines of each bearing, the locations of each radial probe, and at each seal throughout the machine as appropriate. The minimum design diametral running clearance of the seals shall also be indicated.

d. Additional Bode plots that compare absolute shaft motion with shaft motion relative to the bearing housing for machines where the support stiffness is less than 3.5 times the oil-film stiffness.

SP6.8.2.9 Additional analyses shall be made for use with the verification test specified in SP6.8.3. The location of the unbalance shall be determined by the vendor. Any test stand parameters which influence the results of the analysis shall be included.

Note: For most machines, there will only be one plane readily accessible for the placement of an unbalance; for example, the coupling flange on a single ended drive machine, or the impeller hub or disk on an integrally geared machine, or expander-compressors. However, there is the possibility that more planes are available such as axial compressor balance planes, or on through drive compressors. When this occurs, and there is the possibility of exciting other criticals, multiple runs may be required.

SP6.8.2.10 The damped unbalanced response analysis shall indicate that the machine will meet the following *SM*:

- If the *AF* at a particular critical speed is less than 2.5, the response is considered critically damped and no *SM* is required.
- If the *AF* at a particular critical speed is 2.5 or greater and that critical speed is below the minimum speed, the *SM* (as a percentage of the minimum speed) shall not be less than the value from Equation SP-A3 or the value 16 which ever is less.

$$SM = 17 \left(1 - \frac{1}{AF - 1.5} \right) \quad (3)$$

- If the *AF* at a particular critical speed is equal to 2.5 or greater and that critical speed is above the maximum continuous speed, the *SM* (as a percentage of the maximum continuous speed) shall not be less than the value from Equation 4 or the value of 26 which ever is less.

$$SM = 10 + 17 \left(1 - \frac{1}{AF - 1.5} \right) \quad (4)$$

SP6.8.2.11 The calculated unbalanced peak-to-peak amplitudes (see SP6.8.2.8b) shall be multiplied using the correction factor calculated from Equation 5. The correction factor shall have a value greater than 0.5.

$$CF = \frac{A_1}{A_{4X}} \quad (5)$$

where

CF = correction factor,

A_1 = amplitude limit, calculated using Equations 6a or 6b in μm (mils) peak to peak,

A_{4X} = peak-to-peak amplitude at the probe location per requirements of SP6.8.2.8, item b, in μm (mils) peak to peak.

In SI units:

$$A_1 = 25.4 \sqrt{\frac{12,000}{N}} \quad (6a)$$

In Customary units:

$$A_1 = \sqrt{\frac{12,000}{N}} \quad (6b)$$

where

N = maximum continuous operating speed, in rpm.

SP6.8.2.12 The calculated major-axis, peak-to-peak, unbalanced rotor response amplitudes, corrected in accordance with SP6.8.2.11 at any speed from zero to trip speed shall not exceed 75% of the minimum design diametral running clearances throughout the machine (with the exception of floating-ring seal locations). For machines with abraidable seals, the response amplitude to the running clearance shall be mutually agreed.

Note: Running clearances may be different than the assembled clearances with the machine shutdown.

SP6.8.2.13 If the analysis indicates that the *SMs* still cannot be met or that a non-critically damped response peak falls within the operating speed range and the purchaser and vendor have agreed that all practical design efforts have been exhausted, then acceptable amplitudes shall be mutually agreed upon by the purchaser and the vendor, subject to the requirements of SP6.8.3.3.

- **SP6.8.2.14** When specified, in addition to the other requirements of SP6.8.2, the lateral analysis report shall include the following:

a. Dimensional data of the bearing design in sufficient detail to enable calculations of stiffness and damping coefficients.

b. Shaft geometry with sufficient detail to model the shaft including the location of bearing centerlines and mounted components.

c. The weight, polar and transverse moments of inertia and center of gravity of the impellers, balance piston, shaft end seals and coupling(s) with sufficient detail to conduct an independent analysis of the rotor.

d. The input model used for the vendors analysis.

e. The support stiffness used in the analysis and its basis.

SP6.8.3 Unbalanced Rotor Response Verification Test

SP6.8.3.1 An unbalanced rotor response test shall be performed as part of the mechanical running test (Note: See Section of the applicable chapter), and the results shall be used to verify the analytical model. The actual response of the rotor on the test stand to the same arrangement of unbalance and bearing loads as was used in the analysis specified in SP6.8.2.9 shall be the criterion for determining the validity of the damped unbalanced response analysis. To accomplish this, the requirements of SP6.8.3.1.1 through SP6.8.3.1.6 shall be followed.

SP6.8.3.1.1 During the mechanical running test (Note: See Section of the applicable chapter), the amplitudes and phase angle of the shaft vibration from zero to trip speed shall be recorded. The gain of any analog recording instruments used shall be preset before the test so that the highest response peak is within 60% – 100% of the recorder's full scale on the test unit coast-down (deceleration).

Note: This set of readings is normally taken during a coastdown, with convenient increments of speed such as 50 rpm. Since at this point the rotor is balanced, any vibration amplitude and phase detected should be the result of residual unbalance and mechanical and electrical runout.

SP6.8.3.1.2 The location of critical speeds below the trip speed shall be established.

SP6.8.3.1.3 The unbalance which was used in the analysis performed in SP6.8.2.9, shall be added to the rotor in the location used in the analysis. The unbalance shall not exceed 8 times the value from Equations 2a or 2b.

SP6.8.3.1.4 The machine shall then be brought up to the trip speed and the indicated vibration amplitudes and phase shall be recorded using the same procedure used for SP6.8.3.1.1.

SP6.8.3.1.5 The corresponding indicated vibration data taken in accordance with SP6.8.3.1.1 shall be vectorially subtracted from the results of this test.

Note: It is practical to store the residual unbalance vibration measurements recorded in the step at SP6.8.3.1.1 and by use of computer code perform the vectorial subtraction called for in this paragraph at each appropriate speed. This makes the comparison of the test results with the computer analysis of SP6.8.2.9 quite practical. It is necessary for probe orientation be the same for the analysis and the machine for the vectorial subtraction to be valid.

SP6.8.3.1.6 The results of the mechanical run including the unbalance response verification test shall be compared with those from the analytical model specified at SP6.8.2.9.

SP6.8.3.2 The vendor shall correct the model if it fails to meet either of the following criteria:

a. The actual critical speeds determined on test shall not deviate from the corresponding critical speeds predicted by analysis by more than 5%. Where the analysis predicts more than one critical speed in a particular mode (due, for example, to the bearing characteristics being significantly different horizontally and vertically or between the two ends of the machine), the test value shall not be lower than 5% below the lowest predicted value nor higher than 5% above the highest predicted value.

Note: It is possible, particularly on electric motors, that the vertical and horizontal stiffness are significantly different and the analysis will predict two differing critical speeds. Should the operating speed fall between these critical speeds, these two critical speeds should be treated separately, as if they resulted from separate modes.

b. The actual major axis amplitude of peak responses from test, including those critically damped, shall not exceed the predicted values. The predicted peak response amplitude range shall be determined from the computer model based on the four radial probe locations.

SP6.8.3.3 If the support stiffness is less than 2 times the bearing oil film stiffness, the absolute vibration of the bearing housing shall be measured and vectorially added to the relative shaft vibration, in both the balanced (see SP6.8.3.1.1) and in the unbalanced (see SP6.8.3.1.3) condition before proceeding with the step specified in SP6.8.3.1.6. In such a case, the measured response shall be compared with the predicted absolute shaft movement.

SP6.8.3.4 Unless otherwise specified, the verification test of the rotor unbalance shall be performed only on the first rotor tested, if multiple identical rotors are purchased.

SP6.8.3.5 The vibration amplitudes and phase from each pair of x-y vibration probes shall be vectorially summed at each vibration response peak after correcting the model, if required, to determine the maximum amplitude of vibration. The major-axis amplitudes of each response peak shall not exceed the limits specified in SP6.8.2.12.

SP6.8.4 Additional Testing

SP6.8.4.1 Additional testing is required (see SP6.8.4.2) if from the shop verification test data (see SP6.8.3) or from the damped, corrected unbalanced response analysis (see SP6.8.3.3), it appears that either of the following conditions exists:

a. Any critical response which fails to meet the *SM* requirements (see SP6.8.2.10) or which falls within the operating speed range.

b. The clearance requirements of SP6.8.2.12 have not been met.

Note: When the analysis or test data does not meet the requirements of the standard, additional more stringent testing is required. The purpose of this additional testing is to determine on the test stand that the machine will operate successfully.

SP6.8.4.2 Unbalance weights shall be placed as described in SP6.8.2.7; this may require disassembly of the machine. Unbalance magnitudes shall be achieved by adjusting the indicated unbalance that exists in the rotor from the initial run to raise the displacement of the rotor at the probe locations to the vibration limit defined by Equations 6a or 6b (see SP6.8.2.11) at the maximum continuous speed; however, the unbalance used shall be no less than twice or greater than 8 times the unbalance limit specified in SP6.8.2.7, Equations 2a or 2b. The measurements from this test, taken in accordance with SP6.8.3.1.1 and SP6.8.3.1.2, shall meet the following criteria:

a. At no speed outside the operating speed range, including the *SM*, shall the shaft deflections exceed 90% of the minimum design running clearances.

b. At no speed within the operating speed range, including the *SM*, shall the shaft deflections exceed 55% of the minimum design running clearances or 150% of the allowable vibration limit at the probes (see SP6.8.2.11).

SP6.8.4.3 The internal deflection limits specified in SP6.8.4.2 items a and b shall be based on the calculated displacement ratios between the probe locations and the areas of concern identified in SP6.8.2.12 based on a corrected model, if required. Actual internal displacements for these tests shall be calculated by multiplying these ratios by the peak readings from the probes. Acceptance will be based on these calculated displacements or inspection of the seals if the machine is opened. Damage to any portion of the machine as a result of this testing shall constitute failure of the test. Minor internal seal rubs that do not cause clearance changes outside the vendor's new-part tolerance do not constitute damage.

SP6.8.5 Level I Stability Analysis

SP6.8.5.1 A stability analysis shall be performed on all centrifugal or axial compressors and/or radial flow rotors except those rotors whose maximum continuous speed is below the first critical speed in accordance with SP6.8.2.3, as calculated on rigid supports. For this analysis, the machine inlet and discharge conditions shall be at either the rated condition or another operating point unless the vendor and purchaser agree upon another operating point.

Note: Level I analysis was developed to fulfill two purposes: first, it provides an initial screening to identify rotors that do not require a more detailed study. The approach as developed is conservative and not intended as an indication of an unstable rotor. Second, the Level I analysis specifies a standardized procedure applied to all manufacturers similar to that found in SP6.8.2. (Refer to 3.12 for a detailed explanation.)

SP6.8.5.2 The model used in the Level I analysis shall include the items listed in SP6.8.2.4 together with the effects of squeeze film dampers where used.

SP6.8.5.3 All components shall be analyzed using the mean values of oil inlet temperature and the extremes of the operating limits for clearance to produce the minimum log decrement.

SP6.8.5.4 When tilt pad journal bearings are used, the analysis shall be performed with synchronous tilt pad coefficients.

SP6.8.5.5 For rotors that have quantifiable external radial loading (e.g., integrally geared compressors), the stability analysis shall also include the external loads associated with the operating conditions defined in SP6.8.5.1. For some rotors, the unloaded (or minimal load condition) may represent the worst stability case and should be considered.

SP6.8.5.6 The anticipated cross coupling, Q_A , present in the rotor is defined by the following procedures:

a. For centrifugal compressors:

The parameters in Equation 7 shall be determined based on the specified operating condition in SP6.8.5.1.

$$q_a = \frac{(HP)B_c C}{D_c H_c N} \left(\frac{\rho_d}{\rho_s} \right) \quad (7)$$

Equation 7 is calculated for each impeller of the rotor. Q_A is equal to the sum of q_A for all impellers.

b. For axial flow rotors:

$$q_a = \frac{(HP)B_t C}{D_t H_t N} \quad (8)$$

Equation 8 is calculated for each stage of the rotor. Q_A is equal to the sum of q_A for all stages.

SP6.8.5.7 An analysis shall be performed with a varying amount of cross coupling introduced at the rotor mid-span for between bearing rotors or at the center of gravity of the stage or impeller for single overhung rotors. For double overhung rotors, the cross coupling shall be placed at each stage or impeller concurrently and should reflect the ratio of the anticipated cross coupling, q_A , calculated for each impeller or stage.

SP6.8.5.8 The applied cross coupling shall extend from zero to the minimum of:

- A level equal to 10 times the anticipated cross coupling, Q_A .
- The amount of the applied cross coupling required to produce a zero log decrement, Q_0 . This value can be reached by extrapolation or linear interpolation between two adjacent points on the curve.

SP6.8.5.9 A plot of the calculated log decrement, δ , for the first forward mode shall be prepared for the minimum and maximum component clearances. Each curve shall contain a minimum of five calculated stability points. The ordinate (y axis) shall be the log decrement. The abscissa (x-axis) shall be the applied cross coupling with the range defined in SP6.8.5.8. For double overhung rotors, the applied cross coupling will be the sum of the cross coupling applied to each impeller or stage.

A typical plot is presented in Figure SP-9. Q_0 and δ_A are identified as the minimum values from either component clearance curves.

SP6.8.5.10 Level I Screening Criteria:

a. For centrifugal compressors:

If any of the following criteria apply, a Level II stability analysis shall be performed:

- $Q_0/Q_A < 2.0$.
- $\delta_A < 0.1$.
- $2.0 < Q_0/Q_A < 10$ and CSR is contained in Region B of Figure SP-10.

Otherwise, the stability is acceptable and no further analyses are required.

b. For axial flow rotors:

If $\delta_A < 0.1$, a Level II stability analysis shall be performed. Otherwise, the stability is acceptable and no further analyses are required.

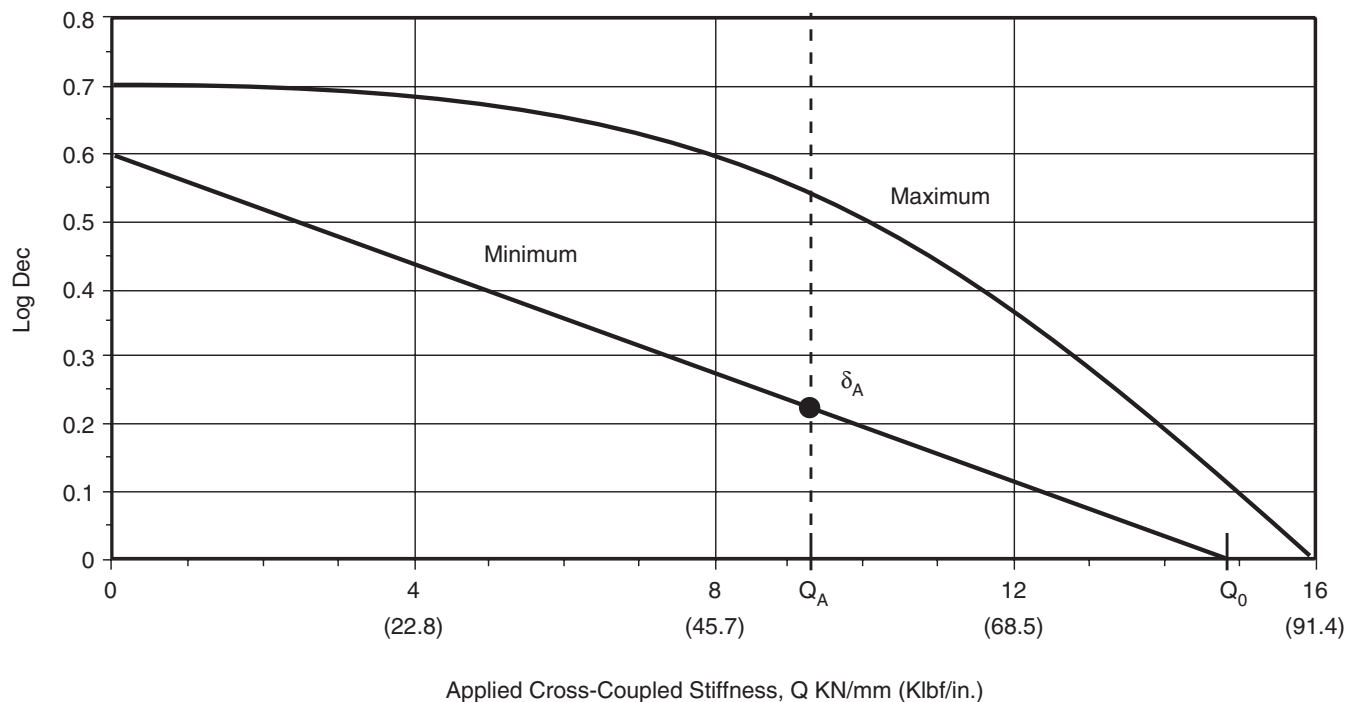


Figure SP-9—Typical Plot of Applied Cross-Coupled Stiffness vs. Log Decrement

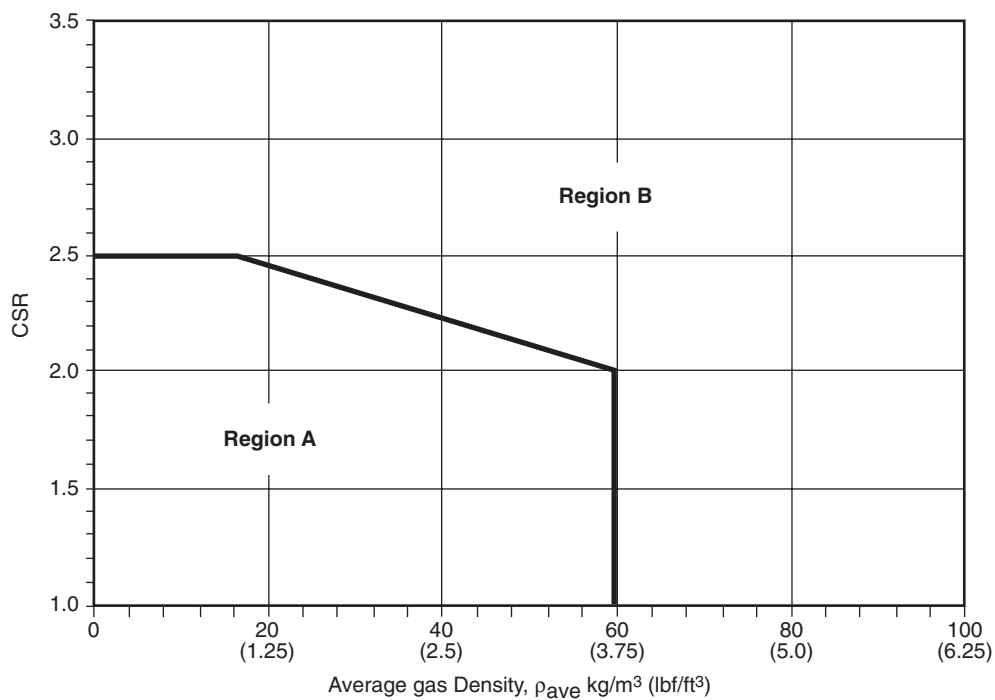


Figure SP-10—Level I Screening Criteria

SP6.8.6 Level II Stability Analysis

SP6.8.6.1 A Level II analysis, which reflects the actual operating behavior of the rotor, shall be performed as required by SP6.8.5.10.

SP6.8.6.2 The Level II analysis shall include the dynamic effects from all sources that contribute to the overall stability of the rotating assembly as appropriate. These dynamic effects shall replace the anticipated cross coupling, Q_A . These sources may include, but are not limited to, the following:

- Labyrinth seals.
- Balance piston.
- Impeller/blade flow.
- Shrink fits.
- Shaft material hysteresis.

It is recognized that methods may not be available at present to accurately model the destabilizing effects from all sources listed above. The vendor shall state how the sources are handled in the analysis.

SP6.8.6.3 The Level II analysis shall be calculated for the operating conditions defined in SP6.8.5.1 extrapolated to maximum continuous speed. The modeling requirements of SP6.8.5.2, SP6.8.5.4 and SP6.8.5.5 shall also apply. The component dynamic characteristics shall be calculated at the extremes of the allowable operating limits of clearance and oil inlet temperature to produce the minimum log decrement.

SP6.8.6.4 The frequency and log decrement of the first forward damped mode shall be calculated for the following conditions (except for double overhung machines where the first two forward modes must be considered):

- Rotor and support system only (basic log decrement, δ_b).
- For the addition of each group of destabilizing effects utilized in the analysis.
- Complete model including all destabilizing forces (final log decrement, δ_f).

SP6.8.6.5 Acceptance Criteria

The Level II stability analysis shall indicate that the machine, as calculated in SP6.8.6.1 through SP6.8.6.3, shall have a final log decrement, δ_f , greater than 0.1.

SP6.8.6.6 If after all practical design efforts have been exhausted to achieve the requirements of SP6.8.6.5, acceptable levels of the log decrement, δ_f , shall be mutually agreed upon by the purchaser and vendor.

Note: This stability analysis section represents the first uniform methodology specified for centrifugal compressors, steam turbines and axial and/or radial flow rotors. The analysis method and the acceptance criteria specified are unique in that no manufacturer has used these exact methods to evaluate the susceptibility of their equipment to subsynchronous instability. When these requirements are included within a specification, all manufacturers are expected to analyze their rotors accordingly. However, it should be recognized that other analysis methods and continuously updated acceptance criteria have been used successfully since the mid-1970s to evaluate rotordynamic stability. The historical data accumulated by machinery manufacturers for successfully operated machines may conflict with the acceptance criteria of this specification. If such a conflict exists and a vendor can demonstrate that his stability analysis methods and acceptance criteria predict a stable rotor, then the vendor's criteria should be the guiding principle in the determination of acceptability.

Symbols

$$B_c = 3,$$

$$B_t = 1.5,$$

$$C = 9.55 (63),$$

$$D_c = \text{Impeller diameter, mm (in.)},$$

$$D_t = \text{Blade pitch diameter, mm (in.)},$$

$$H_c = \text{Minimum of diffuser or impeller discharge width per impeller, mm (in.)},$$

$$H_t = \text{Effective blade height, mm (in.)},$$

$$\text{HP} = \text{Rated power per stage or impeller, Nm/sec. (HP)},$$

$$\text{CSR} = \text{Critical speed ratio is defined as:}$$

$$\text{CSR} = \frac{\text{maximum continuous speed}}{\text{first undamped critical speed on rigid support (FCSR)}}$$

$$N = \text{Operating speed, rpm},$$

$$Q_A = \text{Anticipated cross coupling for the rotor, KN/mm (Klbf/in.) defined as:}$$

$$Q_A = \sum_{i=1}^S q_{Ai}$$

$$Q_0 = \text{Minimum cross coupling needed to achieve a log decrement equal to zero for either minimum or maximum component clearance,}$$

$$q_A = \text{Cross coupling defined in Equation 7 or 8 for each stage or impeller, KN/mm (Klbf/in.)},$$

$$S = \text{Number of stages or impellers,}$$

$$\delta_A = \text{Minimum log decrement at the anticipated cross coupling for either minimum or maximum component clearance,}$$

δ_b = Basic log decrement of the rotor and support system only,

δ_f = Log decrement of the complete rotor support system from the Level II analysis,

ρ_d = Discharge gas density per stage or impeller,

ρ_s = Suction gas density per stage or impeller,

ρ_{ave} = Average gas density across the rotor, kg/m³ (lb/ft³).

Definitions

Stability analysis is the determination of the natural frequencies and the corresponding logarithmic the damped rotor/support system using a complex eigenvalue analysis.

Synchronous tilt pad coefficients are derived from the complex frequency dependent coefficients with the frequency equal to the rotational speed of the shaft.

Stage refers to an individual turbine or axial compressor blade row.

Hysteresis or internal friction damping causes a phase difference between the stress and strain in any material under cyclic loading. This phase difference produces the characteristic hysteric loop on a stress-strain diagram and thus, a destabilizing damping force.

Minimum clearance for a tilt pad bearing occurs at the maximum preload condition. These can be calculated using the following formulas:

For minimum clearance at maximum preload:

$$\text{Preload}_{\max} = 1 - \frac{\text{Bearing Radius}_{\min} - \text{Shaft Radius}_{\max}}{\text{Pad Bore}_{\max} - \text{Shaft Radius}_{\max}}$$

$$\text{Bearing Clearance}_{\min} = \text{Bearing Radius}_{\min} - \text{Shaft Radius}_{\max}$$

For maximum clearance at minimum preload:

$$\text{Preload}_{\min} = 1 - \frac{\text{Bearing Radius}_{\max} - \text{Shaft Radius}_{\min}}{\text{Pad Bore}_{\min} - \text{Shaft Radius}_{\min}}$$

$$\text{Bearing Clearance}_{\max} = \text{Bearing Radius}_{\max} - \text{Shaft Radius}_{\min}$$

SP6.8.7 Torsional Analysis

SP6.8.7.1 For motor-driven units and units including gears, units comprising three or more coupled machines (excluding any gears), or when specified, the vendor having unit responsibility shall ensure that a torsional vibration analysis of the complete coupled train is carried out and shall be

responsible for directing any modifications necessary to meet the requirements of SP6.8.7.2 through SP6.8.7.6.

SP6.8.7.2 Excitation of torsional natural frequencies may come from many sources which may or may not be a function of running speed and should be considered in the analysis. These sources shall include but are not limited to the following:

- Gear characteristics such as unbalance, pitch line runout, and cumulative pitch error.
- Cyclic process impulses.
- Torsional transients such as start-up of synchronous electric motors and generator phase-to-phase or phase-to-ground faults.
- Torsional excitation resulting from electric motors, reciprocating engines, and rotary type positive displacement machines.
- Control loop resonance from hydraulic, electronic governors, and variable frequency drives.
- One and 2 times line frequency.
- Running speed or speeds.
- Harmonic frequencies from variable frequency drives.

SP6.8.7.3 The torsional natural frequencies of the complete train shall be at least 10% above or 10% below any possible excitation frequency within the specified operating speed range (from minimum to maximum continuous speed).

SP6.8.7.4 Torsional natural frequencies at two or more times running speeds shall preferably be avoided or, in systems in which corresponding excitation frequencies occur, shall be shown to have no adverse effect.

SP6.8.7.5 When torsional resonances are calculated to fall within the margin specified in SP6.8.7.3 (and the purchaser and the vendor have agreed that all efforts to remove the critical from within the limiting frequency range have been exhausted), a stress analysis shall be performed to demonstrate that the resonances have no adverse effect on the complete train. The assumptions made in this analysis regarding the magnitude of excitation and the degree of damping shall be clearly stated. The acceptance criteria for this analysis shall be mutually agreed upon by the purchaser and the vendor.

SP6.8.7.6 In addition to the torsional analyses required in SP6.8.7.2 through SP6.8.7.5, the vendor shall perform a transient torsional vibration analysis for synchronous motor driven units, using a time-transient analysis. The requirements of SP6.8.7.6.1 through SP6.8.7.6.4 shall be followed.

SP6.8.7.6.1 In addition to the parameters used to perform the torsional analysis specified in SP6.8.7.1, the following shall be included:

- a. Motor average torque, as well as pulsating torque (direct and quadrature axis) vs. speed characteristics.
- b. Load torque vs. speed characteristics.

Electrical system characteristics effecting the motor terminal voltage or the assumptions made concerning the terminal voltage including the method of starting, such as across the line, or some method of reduced voltage starting.

SP6.8.7.6.2 The analysis shall generate the maximum torque as well as a torque vs. time history for each of the shafts in the compressor train.

Note: The maximum torques shall be used to evaluate the peak torque capability of coupling components, gearing and interference fits of components such as coupling hubs. The torque vs. time history shall be used to develop a cumulative damage fatigue analysis of shafting, keys and coupling components.

SP6.8.7.6.3 Appropriate fatigue properties and stress concentrations shall be used.

SP6.8.7.6.4 An appropriate cumulative fatigue algorithm shall be used to develop a value for the safe number of starts. The safe number of starts shall be as mutually agreed by the purchaser and vendor.

Note: Values used depend on the analytical model used and the vendor's experience. Values of 1000 – 1500 starts are common. API Std 541 requires 5000 starts. This is a reasonable assumption for a motor since it does not add significant cost to the design. The driven equipment, however, would be designed with overkill to meet this requirement. Example: 20-year life, 1 start/week = 1040 starts. Equipment of this type normally would start once every few years rather than once per week. A reasonable number of starts should therefore be specified.

SP6.8.8 Vibration and Balancing

SP6.8.8.1 Major parts of the rotating element, such as the shaft, balancing drum and impellers, shall be individually dynamically balanced before assembly, to ISO 1940 Grade G1 or better. When a bare shaft with a single keyway is dynamically balanced, the keyway shall be filled with a fully crowned half key, in accordance with ISO 8821. Keyways 180 degrees apart, but not in the same transverse plane, shall also be filled. The initial balance correction to the bare shaft shall be recorded. The components to be mounted on the shaft (impellers, balance drum, etc.), shall also be balanced in accordance with the "half-key-convention," as described in ISO 8821.

SP6.8.8.2 Unless otherwise specified, the rotating element shall be sequentially multiplane dynamically balanced during

assembly. This shall be accomplished after the addition of no more than two major components. Balancing correction shall only be applied to the elements added. Minor correction of other components may be required during the final trim balancing of the completely assembled element. In the sequential balancing process, any half-keys used in the balancing of the bare shaft (see SP6.8.8.1) shall continue to be used until they are replaced with the final key and mating element. On rotors with single keyways, the keyway shall be filled with a fully crowned half-key. The weight of all half-keys used during final balancing of the assembled element shall be recorded on the residual unbalance worksheet (see Annex 1B). The maximum allowable residual unbalance per plane (journal) shall be calculated as follows:

In SI units:

$$U_{max} = 6350W/N \quad (9a)$$

or 254 μm of mass eccentricity, whichever is greater.

In U.S. Customary units:

$$U_{max} = 4W/N \quad (9b)$$

or 10 mils of mass eccentricity, whichever is greater.

where

U_{max} = residual unbalance, g-mm (oz-in.),

W = journal static weight load, kilograms (lb),

N = maximum continuous speed, rpm,

Mass eccentricity = Unbalance/Weight =
[$U/1000W$ ($U/16W$)].

SP6.8.8.2.1 When the vendors standard assembly procedures require the rotating element to be disassembled after final balance to allow compressor assembly (i.e., stacked rotors with solid diaphragms and compressor/expanders), the vendor shall, as a minimum, perform the following operations:

- a. To ensure the rotor has been assembled concentrically, the vendor shall take runout readings on the tip of each element (impeller or disc). The runout on any element shall not exceed a value agreed upon between the purchaser and the vendor.
- b. The vendor shall balance the rotor to the limits of SP6.8.8.2, Equations 9a or 9b.
- c. The vendor shall provide historic unbalance data readings of the change in balance due to disassembly and reassembly. This change in unbalance shall not exceed 4 times the sensitivity of the balance machine. For this purpose, balance machine sensitivity is 254 μm (10 mils) maximum.

d. The vendor shall conduct an analysis in accordance with SP6.8.2, to predict the vibration level during testing, using an unbalance equal to that in item b, plus 2 times the average change in balance due to disassembly and reassembly as defined in item c. The results of this analysis shall show that the predicted vibration at design speed on test shall be no greater than 2 times the requirements of SP6.8.8.8.

e. After the rotor has been reassembled in the compressor case, the vibration during testing shall meet the limits as shown in SP6.8.8.8.

Note: Trim balancing in the compressor case may be done to achieve this level.

- **SP6.8.8.2.1.1** When specified, the vendor shall record the balance readings after initial balance for the contract rotor. The rotor shall then be disassembled and reassembled. The rotor shall be check balanced after reassembly to determine the change in balance due to disassembly and reassembly. This change in balance shall not exceed that defined in SP6.8.8.2.1c.
- **SP6.8.8.3** When specified, completely assembled rotating elements shall be subject to operating-speed (at speed) balancing in lieu of a sequential low speed balancing (see SP6.8.8.2). When the vendor's standard balance method is by operating-speed balancing in lieu of a sequential low speed balancing and operating speed balancing is not specified, it may be used with the purchaser's approval. The operating-speed balance shall be in accordance with SP6.8.8.4.
- **SP6.8.8.4** When the complete rotating element is to be operating-speed balanced (see SP6.8.8.3), the rotor shall be supported in bearings of the same type and with similar dynamic characteristics as those in which it will be supported in service. The final check balance shall be carried out at maximum continuous speed. Before making any corrections (unless it is necessary to improve the initial balance in order to be able to run the rotor at high speed), the rotor shall be run, in the balancing machine at trip speed for at least 5 min., to allow seating of any shrunk-on components.
- **SP6.8.8.5** Unless otherwise specified, the vibration acceptance criteria for operating-speed balancing, with maximum pedestal stiffness at all speeds, measured on the bearing cap shall be as follows:
 - a. For speeds above 3000 rpm: it shall not exceed the greater of $7400/N$ mm/sec. ($291 N/\text{in.}/\text{sec.}$) or 1 mm/sec. ($0.039 \text{ in.}/\text{sec.}$), where N is the speed in rpm.
 - b. For all speeds less than 3000 rpm: it shall not exceed 2.5 mm/sec. ($0.098 \text{ in.}/\text{sec.}$).

Note: This residual unbalance is at all speeds (includes any criticals), and the force from this residual unbalance is dependant on the pedestal stiffness and the measure velocity.

- **SP6.8.8.6** A rotor that is to be operating-speed balanced shall, when specified, first receive a sequential low speed balance as specified in SP6.8.8.2.
- **SP6.8.8.7** For a rotor that has been low speed sequentially balanced (see SP6.8.8.2), and when specified for rotors that are high-speed balanced (see SP6.8.8.3), a low speed residual unbalance check shall be performed in a low speed balance machine and recorded in accordance with the residual unbalance worksheet (see Annex 1B).

Note: This is done to provide a reference of residual unbalance and phase for future use in a low speed balance machine.

SP6.8.8.8 During the mechanical running test of the machine, assembled with the balanced rotor, operating at its maximum continuous speed or at any other speed within the specified operating speed range, the peak-to-peak amplitude of unfiltered vibration in any plane, measured on the shaft adjacent and relative to each radial bearing, shall not exceed the following value or $25.4 \mu\text{m}$ (1 mil), whichever is less:

In SI units:

$$A_1 = 25.4 \sqrt{\frac{12,000}{N}} \quad (10a)$$

In U.S. Customary units

$$A_1 = \sqrt{\frac{12,000}{N}} \quad (10b)$$

where

A = amplitude of unfiltered vibration, μm (mil) true peak-to-peak,

N = maximum continuous speed, rpm.

At any speed greater than the maximum continuous speed, up to and including the trip speed of the driver, the vibration level shall not increase more than $12.7 \mu\text{m}$ (0.5 mil) above the maximum value recorded at the maximum continuous speed.

Note: These limits are not to be confused with the limits specified in SP6.8.3 for shop verification of unbalanced response.

SP6.8.8.9 Electrical and mechanical runout shall be determined by rotating the rotor through the full 360 degrees supported in V blocks at the journal centers while continuously recording the combined runout with a non-contacting vibration probe and measuring the mechanical runout with a dial indicator at the centerline of each probe location and one probe-tip diameter to either side.

Note: The rotor runout determined above generally may not be reproduced when the rotor is installed in a machine with hydrodynamic bearings. This is due to pad orientation on tilt pad bearings and effect of lubrication in all journal bearings. The rotor will assume a unique position in the bearings based on the slow roll speed and rotor weight.

SP6.8.8.10 Accurate records of electrical and mechanical runout, for the full 360 degrees at each probe location, shall be included in the mechanical test report (see SP6.8.3.1.1).

SP6.8.8.11 If the vendor can demonstrate that electrical or mechanical runout is present, a maximum of 25% of the test level calculated from Equation 6 or 6.4 mm (0.25 mil), whichever is greater, may be vectorially subtracted from the vibration signal measured during the factory test. Where shaft treatment such as metallized aluminum bands have been applied to reduce electrical runout, surface variations (noise) may cause a high frequency noise component which does not have an applicable vector. The nature of the noise is always additive. In this case, the noise shall be mathematically subtracted.



American Petroleum Institute 2005 Publications Order Form

Effective January 1, 2005.

API Members receive a 30% discount where applicable.

The member discount does not apply to purchases made for the purpose of resale or for incorporation into commercial products, training courses, workshops, or other commercial enterprises.

Available through Global Engineering Documents:

Phone Orders: 1-800-854-7179 (Toll-free in the U.S. and Canada)

303-397-7956 (Local and International)

Fax Orders: 303-397-2740

Online Orders: www.global.ihs.com

Date: _____

☐ **API Member** (Check if Yes)

Invoice To (☐ Check here if same as "Ship To")

Name: _____

Title: _____

Company: _____

Department: _____

Address: _____

City: _____

State/Province: _____

Zip/Postal Code: _____

Country: _____

Telephone: _____

Fax: _____

E-Mail: _____

Ship To (UPS will not deliver to a P.O. Box)

Name: _____

Title: _____

Company: _____

Department: _____

Address: _____

City: _____

State/Province: _____

Zip/Postal Code: _____

Country: _____

Telephone: _____

Fax: _____

E-Mail: _____

Quantity	Product Number	Title	SO★	Unit Price	Total

☐ **Payment Enclosed** ☐ **P.O. No.** (Enclose Copy) _____

☐ **Charge My Global Account No.** _____

☐ **VISA** ☐ **MasterCard** ☐ **American Express** ☐ **Diners Club** ☐ **Discover**

Credit Card No.: _____

Print Name (As It Appears on Card): _____

Expiration Date: _____

Signature: _____

Subtotal

Applicable Sales Tax (see below)

Rush Shipping Fee (see below)

Shipping and Handling (see below)

Total (in U.S. Dollars)

★ To be placed on **Standing Order** for future editions of this publication, place a check mark in the **SO** column and sign here:

Pricing and availability subject to change without notice.

Mail Orders – Payment by check or money order in U.S. dollars is required except for established accounts. State and local taxes, \$10 processing fee*, and 5% shipping must be added. Send mail orders to: **API Publications, Global Engineering Documents, 15 Inverness Way East, M/S C303B, Englewood, CO 80112-5776, USA.**

Purchase Orders – Purchase orders are accepted from established accounts. Invoice will include actual freight cost, a \$10 processing fee*, plus state and local taxes.

Telephone Orders – If ordering by telephone, a \$10 processing fee* and actual freight costs will be added to the order.

Sales Tax – All U.S. purchases must include applicable state and local sales tax. Customers claiming tax-exempt status must provide Global with a copy of their exemption certificate.

Shipping (U.S. Orders) – Orders shipped within the U.S. are sent via traceable means. Most orders are shipped the same day. Subscription updates are sent by First-Class Mail. Other options, including next-day service, air service, and fax transmission are available at additional cost. Call 1-800-854-7179 for more information.

Shipping (International Orders) – Standard international shipping is by air express courier service. Subscription updates are sent by World Mail. Normal delivery is 3-4 days from shipping date.

Rush Shipping Fee – Next Day Delivery orders charge is \$20 in addition to the carrier charges. Next Day Delivery orders must be placed by 2:00 p.m. MST to ensure overnight delivery.

Returns – All returns must be pre-approved by calling Global's Customer Service Department at 1-800-624-3974 for information and assistance. There may be a 15% restocking fee. Special order items, electronic documents, and age-dated materials are non-returnable.

***Minimum Order** – There is a \$50 minimum for all orders containing hardcopy documents. The \$50 minimum applies to the order subtotal including the \$10 processing fee, excluding any applicable taxes and freight charges. If the total cost of the documents on the order plus the \$10 processing fee is less than \$50, the processing fee will be increased to bring the order amount up to the \$50 minimum. This processing fee will be applied before any applicable deposit account, quantity or member discounts have been applied. There is no minimum for orders containing only electronically delivered documents.

There's more where this came from.

The American Petroleum Institute provides additional resources and programs to the oil and natural gas industry which are based on API® Standards. For more information, contact:

- | | |
|---|--|
| • API Monogram® Licensing Program | Phone: 202-962-4791
Fax: 202-682-8070 |
| • American Petroleum Institute Quality Registrar (APIQR®) | Phone: 202-962-4791
Fax: 202-682-8070 |
| • API Spec Q1® Registration | Phone: 202-962-4791
Fax: 202-682-8070 |
| • API Perforator Design Registration | Phone: 202-962-4791
Fax: 202-682-8070 |
| • API ISO/TS 29001 Registration | Phone: 202-962-4791
Fax: 202-682-8070 |
| • API Training Provider Certification Program | Phone: 202-682-8490
Fax: 202-682-8070 |
| • Individual Certification Programs | Phone: 202-682-8064
Fax: 202-682-8348 |
| • Engine Oil Licensing and Certification System (EOLCS) | Phone: 202-682-8516
Fax: 202-962-4739 |
| • API PetroTEAM™ (Training, Education and Meetings) | Phone: 202-682-8195
Fax: 202-682-8222 |

Check out the API Publications, Programs, and Services Catalog online at www.api.org.



Helping You Get
The Job Done Right.®

Additional copies are available through Global Engineering Documents at (800) 854-7179 or (303) 397-7956

Information about API Publications, Programs and Services is available on the World Wide Web at: <http://www.api.org>



**American
Petroleum
Institute**

1220 L Street, Northwest
Washington, D.C. 20005-4070
202-682-8000

Product No. C68402